Biomechanics and Gait Analysis

Nick Stergiou

Biomechanics and Gait Analysis

Biomechanics and Gait Analysis

Nick Stergiou
Department of Biomechanics, University of Nebraska at Omaha,
Omaha, NE, United States

ACADEMIC PRESS
An imprint of Elsevier

Academic Press is an imprint of Elsevier
125 London Wall, London EC2Y 5AS, United Kingdom
525 B Street, Suite 1650, San Diego, CA 92101, United States
50 Hampshire Street, 5th Floor, Cambridge, MA 02139, United States
The Boulevard, Langford Lane, Kidlington, Oxford OX5 1GB, United Kingdom

Notices
Knowledge and best practice in this field are constantly changing. As new research and experience broaden our understanding, changes in research methods, professional practices, or medical treatment may become necessary.

Practitioners and researchers must always rely on their own experience and knowledge in evaluating and using any information, methods, compounds, or experiments described herein. In using such information or methods they should be mindful of their own safety and the safety of others, including parties for whom they have a professional responsibility.

To the fullest extent of the law, neither the Publisher nor the authors, contributors, or editors, assume any liability for any injury and/or damage to persons or property as a matter of products liability, negligence or otherwise, or from any use or operation of any methods, products, instructions, or ideas contained in the material herein.

British Library Cataloguing-in-Publication Data
A catalogue record for this book is available from the British Library

Library of Congress Cataloging-in-Publication Data
A catalog record for this book is available from the Library of Congress

ISBN: 978-0-12-813372-9

Publisher: Mara Conner
Acquisitions Editor: Fiona Geraghty
Editorial Project Manager: Lindsay Lawrence
Production Project Manager: Nirmala Arumugam
Cover Designer: Victoria Pearson

Typeset by MPS Limited, Chennai, India

Dedication

This book is dedicated to my mentors and all those people who helped me become the person I am.

Contents

List of Figures

List of Contributors

Barry T. Bates
University of Oregon, Eugene, OR, United States

James T. Cavanaugh
University of New England, Portland, ME, United States

Janet S. Dufek
University of Nevada Las Vegas, Las Vegas, NV, United States

Aaron D. Likens
University of Nebraska at Omaha, Omaha, NE, United States

Douglas A. Rowen
University of Nebraska at Omaha, Omaha, NE, United States

Luis M. Silva
University of Nebraska at Omaha, Omaha, NE, United States

Andreas Skiadopoulos
University of Nebraska at Omaha, Omaha, NE, United States

Nick Stergiou
University of Nebraska at Omaha, Omaha, NE, United States

Jorge M. Zuniga
University of Nebraska at Omaha, Omaha, NE, United States

Preface

When you start on your journey to Ithaca, then pray that the road is long, full of adventure, full of knowledge. Do not fear the Lestrygonians and the Cyclopes and the angry Poseidon. . .

Always keep Ithaca fixed in your mind. To arrive there is your ultimate goal

From the poem "Ithaca" by Konstantinos Kavafis (1863–1933) who was an Egyptiote Greek poet, journalist, and civil servant.

Success in science is not easy. A scientist has to face many adversities, exactly like Odysseus, the hero of Homer's epic poem the Odyssey, on his trip to Ithaca. The road to success will be laid with many Lestrygonians and Cyclopes. The sea will be rarely calm, and you may feel that Poseidon is always angry with you. However, the biomechanist has to face even more adversities than Odysseus, more adversities than other scientists, that make success even more difficult to achieve. This arises from the fact that biomechanics is a new science that the public does not fully understand. When I started at university in 1996, the term was not even in existence. The course that I was asked to teach was called "applied kinesiology." It was I who changed its name to biomechanics a few years later to better reflect what was being taught. Just recently, I have seen the term being used in the scientific journal *Science* to describe a discipline and related articles. Often, I found myself describing my career under a different professional title (i.e., ergonomist and engineer) to help the other person to understand what I do. Even in the American Society of Biomechanics, we are not just members of the society, but we also declare where we come from (i.e., kinesiology and engineering). Despite its obscurity, biomechanics increasingly contributes many benefits to everyday life. A good example is the plethora of gait analysis laboratories found in hospital around the world. Gait analysis laboratories provide instrumental information regarding movement disorders in terms of diagnosis, treatment, progression of interventions, proper selection of an intervention, etc. The knowledge provided by these laboratories is exclusively based on biomechanics. Many of my former students work in gait analysis laboratories or perform gait analysis evaluations on their jobs, almost daily.

Therefore the first goal of this book was to assist readers to better understand my discipline, which I have served and loved for more than 30 years now. Of note is that I drive frequently on my vacations in Greece by the birthplace of the great Aristotle, who was born about an hour away from my hometown. The next time that I will do so, I will be able to stop by and, while I pay my respects, I could say to the father of our discipline that, through this book, I have done a small part in further building on his initial efforts. The second goal was to enhance communication between biomechanics and one of its major applications, namely, gait analysis. Many times, as we move from theory and education to practice, information is lost. This book makes an effort to bridge this gap and better assist the professionals and practitioners of gait analysis to better understand their scientific realm, as it relates to biomechanics. It also provides them with an arsenal of knowledge tools to improve their invaluable work. This is why every chapter has numerous examples that translate knowledge to the application of gait analysis.

The organization of our book is as follows.

The first chapter is an Introduction to Biomechanics. For the reader, it is Biomechanics 101. We define biomechanics as the study of forces that act on a body and the effects they produce. We describe how, in biomechanics, we study movement because we want to understand the underlying mechanisms of movement and to improve our understanding of the acquisition and regulation of skill. However, the uniqueness of biomechanics, as an area of study, evolves not from the unique body of knowledge but from the uniqueness of the questions we ask relative to understanding human movement. In this chapter, we also provide a historical perspective, as biomechanics can trace its origins to Aristotle who wrote the first textbook in biomechanics, but during the 20th century biomechanical research witnessed a scientific explosion fueled by the availability of appropriate technology. As such, it has influenced applications in industrial, medical, and other practical areas. Biomechanics evolved as a necessary science-based method for the study of human and animal movement.

In the second chapter, we present Basic Biomechanics. Completing Biomechanics 101 entitles you now to move to Biomechanics 201. In this chapter we cover the basic principles of biomechanics. We discuss the anatomical and mechanical principles that provide the basis for understanding and analyzing the various forms of human movement. We don't intend to replace, with a single chapter, the large volume of biomechanics textbooks that have been published mostly for undergraduate courses. However, we want to introduce the reader to a fundamental understanding on how to develop the ability to link the structure of the human body with its function from a biomechanical perspective.

In the third chapter, we move beyond the basic principles of biomechanics and cover various special topics. This is Advanced Biomechanics or, in our reader's curriculum, Biomechanics 301. We continue our journey into the understanding of anatomical and mechanical principles, and we take a closer look at analyzing the various forms of human movement through various examples and problems from biomechanics research.

Our beloved Stickman is the topic of our fourth chapter. The Stickman lives in every biomechanics laboratory. He is a "simple" man that is generated in biomechanical processing software. In this chapter, we offer Biomechanics 401, and, because our reader is now a senior, we use the Stickman as a model to overview selected aspects of human movement and performance in order to gain an appreciation of their complex interactions. We wish to assist the reader in developing skills in conceptual thinking and reasoning.

The fifth chapter focuses on a topic that is a common source of errors in biomechanics; filtering and smoothing. This was even acknowledged by the great David Winter, one of the modern pillars of our discipline, in terms of a book on signal processing. This chapter marks a departure from core courses of our sequence in biomechanics. The rest of our chapters will complete our reader's curriculum with other fundamental courses. One is a solid understanding on Fourier transform, data sampling, spectral leakage, noise, digital filtering, smoothing, and time series processing. We strongly believe that biomechanists and gait analysts must understand the basic concepts of digital processing in order to be responsible users of commercial equipment and software.

In the sixth chapter, we revisit a classic as we provide a protracted summary of McMahon's (1984) text entitled *Muscles, Reflexes, and Locomotion*. This text has educated several generations of biomechanists. Thus revisiting this foundational text allows our reader to reconnect with the classics and develop a strong historical background to the research performed in biomechanics. It is important that we educate ourselves, both in breadth and in depth. The reader will also note that, despite not being updated since the 1980s, the material we summarize broaches a number of topics with strong contemporary appeal, including coordination dynamics and robotics. The scope of McMahon's book and his clear mastery of deep topics such as mathematics, biology, and mechanics of animal locomotion are difficult to summarize within the pages of a single chapter. In many instances, we refer the reader to the original text for richer historical context and more in-depth treatments of difficult topics. Although the content of the book is exceptional, many important scientific discoveries have been made in the time since this book was last published. Therefore, when possible and space allows, we point the reader to recent discoveries made in the intervening years.

Next, we cover the basic principles of gait analysis. In the seventh chapter, we discuss gait as a skill, along with the definition of motor skill, more generally; we define gait analysis; present the periods and the phases of gait; and identify the most important spatiotemporal parameters to evaluate during gait analysis. We explore two special cases, the first being step width and lateral stepping, and the second being stride/step time and gait variability; and we examine the determinants of gait. In addition, we present a few more advanced principles with respect to modeling, such as the dynamic walking method and the inverted pendulum.

Starting with Chapter 8, Gait variability: a theoretical framework for gait analysis and biomechanics, and continuing with Chapter 9, Coordination and control: a dynamical systems approach to the analysis of human gait and Chapter 10, A tutorial on fractal analysis of human movements, we provide the reader with a theoretical foundation and plenty of tools to ask important questions in the gait analysis laboratory and to supplement evaluations with essential knowledge of human movement variability. My mentor, Barry Bates, considers variability in human movement as one of the great mysteries of biomechanics and one domain that deserves much more attention in the laboratory. Thus in the eighth chapter we view gait as a variable and necessarily adaptable behavior. We quantify gait variability in terms of its amount and complexity, two distinct yet complementary facets of human gait that are associated with the health status of the performer, their stage of learning, the demands of a particular walking task, and the environmental conditions in which walking occurs. We also present measures of gait variability derived from theoretical assumptions about motor control that could provide rehabilitation professionals with a new generation of gait assessment tools and intervention approaches for clinical populations with walking limitations.

In the ninth chapter, we present the application of dynamical systems theory to the study of human movement and gait analysis. Our efforts focus on presenting both theory and practical suggestions regarding the analysis and interpretation of results. Moreover, we have demonstrated a major benefit in applying dynamical systems theory to human gait—simplicity. Our intention in constructing this chapter is to facilitate research in those domains, as we feel there is much revolutionary science yet to come from applying dynamical systems theory to the analysis of gait. Furthermore, we strongly advocate the use of this powerful investigative approach by scientists and clinicians that work in gait analysis laboratories or utilize gait analysis to understand the effects of various pathologies on human gait.

Moving into the tenth chapter, we present an introduction to fractal analysis of human movement data. Our approach avoids heavy mathematics and

confusing jargon. Instead, we present the material in plain language and take care to define terms unique to fractal theory and analyses. To that end, we present basic ideas related to fractal theory and translate those ideas to fractal characteristics typical of human movement variability. In addition, we present an in-depth tutorial on one of the most common methods of fractal and multifractal analysis. We supplement our presentation with two complete examples demonstrating how to use these techniques in laboratory studies. We believe that our presentation will provide gait analysts and biomechanists with an easy way to implement fractal analysis into their research and practice.

Finally, we finish with the view to the future as, in the eleventh chapter, we provide a brief introduction to the utilization of 3D printing as an effective biotechnology for biomechanists and gait analysts to supplement their research in the laboratory. This is a special area from which we expect tremendous growth in the future. This chapter presents applications of 3D printing for lower and upper extremity applications, anatomical modeling for surgical planning, fracture castings, and the development of upper extremity exoskeletons for stroke patients. Practical information about the creation of a 3D printing research laboratory on a budget is also provided. We also review the current FDA recommendations of 3D-printed medical devices, such as those covered by a recently published FDA guidance document. Finally, we discuss the main limitations of these techniques, and we describe future perspectives of this technology.

This book could have not been possible without the contributions of my coauthors. My previous research associates, Dr. Louis Silva and Dr. Aaron Likens, my current research associate, Dr. Andreas Skiadopoulos, my previous students, Mr. Douglas Rowen, Dr. Jorge Zuniga, and Dr. James Cavanaugh, and my mentors, Dr. Barry Bates and Dr. Janet Dufek. They all worked hard to fulfill all my idiosyncrasies regarding this book, but, at the same time, they have been a fantastic academic family that I will cherish forever.

At this point, a disclaimer needs to be made regarding the significant financial support that I have received over the years from several agencies. The NIH, NASA, US Department of Education (NIDRR), NSF, VA, Nebraska Research Initiative, and many others, have consistently provided funds for my work and allowed me to progress with financial stability over the years. I am particularly grateful to the NIH and NIGMS for a COBRE P20GM109090 grant that I have recently received that supported the writing of this book.

In closing, I would like to acknowledge that during my life I have faced, more than once, adversity and disappointment. Such times have also been aplenty in my career and in the development, not only of this book, but also of the investigation of a novel area of research such as biomechanics that is

different from traditional approaches. In these times, there is one certainty, that solace is needed around you to overcome even the highest of obstacles. This is why I am eternally grateful for my parents, Jesus and Vaya, my brother, Dimitris and his family, my "academic" parents, Barry and Janet, my mentors over the years starting with the late George Rontogiannis, my "American" parents, Ruth and Bill Scott and the entire Scott family, my friends and collaborators, my Elsevier friends Fiona and Lindsay and particularly my students for their love, support, and constant encouragement. In particular, I am grateful to my research associate and dear friend Dr. Aaron Likens, who not only coauthored several chapters of this book but even read and provided comments for almost every other chapter.

CHAPTER 1

Introduction to biomechanics

Nick Stergiou
University of Nebraska at Omaha, Omaha, NE, United States

Elsewhere we have investigated in detail the movement of animals after their various kinds, the differences between them, and the reasons for their particular characters (for some animals fly, some swim, some walk, others move in various other ways); there remains an investigation of the common ground of any sort of animal movement whatsoever.

The opening sentence from the book *On the Motion of Animals by Aristotle* (384–322 BCE).

CONTENTS

1.1 Introduction

I define biomechanics as the study of the forces that act on a body and the effects they produce. Bates suggested that biomechanics is an intersection of biology, physiology, anatomy, physics, mathematics, and chemistry to solve difficult problems in medicine and health (Bates, 1991). Hay described biomechanics as the science that examines the forces acting upon and within a biological structure and the effects produced by such forces (Hay, 1973). Alt referred to biomechanics as the science that investigates the effect of internal and external forces on human and animal bodies in movement and at rest (Alt, 1967). These descriptions and definitions communicate the essential relationship of the organisms and mechanics found in biomechanics and identify biomechanics as a science. However, is biomechanics a science or an application?

Some investigators and academicians suggest that biomechanics is the application of physics and mathematics on biological problems. I fervently disagree with this notion and strongly believe that biomechanics is a science. A science is an area of study that deals with understanding, predicting, and explaining phenomena within a content domain. In biomechanics, we study movement because we want to understand the underlying mechanisms of

Biomechanics and Gait Analysis. DOI: https://doi.org/10.1016/B978-0-12-813372-9.00001-4

movement and to improve our understanding of the acquisition and regulation of skill. However, the uniqueness of biomechanics as an area of study evolves not from a unique body of knowledge but from the uniqueness of the questions we ask relative to understanding human movement (Bates, 1991). We use techniques and methods from other scientific disciplines, such as physics and engineering, and relate them to human movement. In biomechanics we complement mechanical assessments with biological interpretations (Higgins, 1985).

The study of movement involves the explanation and understanding of the structural and functional mechanisms underlying human performance in all of its presentations, from fundamental motor skills to demanding exercise. Higgins (1977) proposed that skill is a movement that allows an organism to respond or act effectively within the environment and to integrate past and present. To become skillful requires mastery of the redundant degrees of freedom (Bernstein, 1967). These degrees of freedom, *or constraints*, are morphological, biomechanical, environmental, and task specific (Higgins, 1977). The study of these constraints is required to explain and understand the underlying mechanisms of movement. Thus we have to approach movement from an interdisciplinary approach. Movement, as a very broad phenomenon, appears in many different forms such as play, dance, sport, work, and daily-living activities. This is why a biomechanist cannot study meaningful questions without adequate preparation in areas such as motor control, physics, physiology, mathematics, computer science, and engineering.

1.2 The history of biomechanics

1.2.1 A trip down the memory lane

The history of biomechanics can be traced back to the ancient Greeks (Nigg & Herzog, 1994). Aristotle (384–322 BCE) was the first to examine and write about complex movements, such as running and walking. In his book *On the Motion of Animals*, the first biomechanical textbook, he said that the animal that moves makes its change of position by pressing against that which is beneath it. Hence, athletes jump farther if they have the weights in their hands than if they have not, and runners run faster if they swing their arms, for in extension of the arms there is a kind of leaning upon the hands and wrists. Archimedes (287–212 BCE) was the first to examine floating bodies and their movements in water. Hippocrates (460–370 BCE) advocated that man should base observations on and draw conclusions only from what is perceived through the senses. Galen (CE 131–201) was the physician of the gladiators. He developed anatomical descriptions and the present-day terminology in use in many biological science fields.

During the Renaissance, Leonardo Da Vinci (1452–1519) examined the structure and function of the human body in a variety of movements and Vesalius (1514–64) laid the foundation of modern anatomy. Following in their footsteps, another group of scientists contributed heavily to the growth of biomechanics. Galileo Galilei (1564–1642) studied the action of falling bodies and provided the basis for the mechanical analysis of movement. Alfonso Borelli (1608–79) was a student of Galileo. He examined muscular movement and mechanical principles. His work *De Moto Animalium* combined the sciences of mathematics, physics, and anatomy. The year the world lost Galileo it gained Sir Isaac Newton (1642–1727), who developed his famous mechanical laws, and was the founder of calculus, statistics, and dynamics. The contribution of this time period to biomechanics included Newtonian mechanics, which provided us with a theory for mechanical analysis, and an improvement in science through development of the process of theory and experimentation.

During the 19th century the contribution to biomechanics included the foundation of electromyography, the development of measuring techniques to examine the kinematics and kinetics of movement, and the beginning of the use of engineering principles in biomechanical analysis. Wilhelm Eduard Weber (1804–91) published the *Mechanism of walking in mankind* which was a study, undertaken in conjunction with his younger brother, Eduard Friedrich Weber (1806–71). In this study the Weber brothers investigated the influence of gravity on limb movements in walking and running and were the first to study the path of the center of gravity during movement. Eadweard Muybridge (1830–1904) studied animal (horses) and human locomotion and was the first to use multiple cameras to capture motion in stop-motion photographs. He also developed a device, the zoopraxiscope, to project motion pictures and he produced over 100,000 images of animals and humans in motion. Étienne-Jules Marey (1830–1904) used various photographical methods to examine movement. He believed that movement was the most important of all human functions and he described it graphically for biological research in his publications *Du mouvement dans les fonctions de la vie* and *Le Mouvement*.

These early examples of photographic techniques would develop into the motion capture used in modern cinema and biomechanics. During the 20th century biomechanical research influenced applications in industrial, medical, and other practical areas, and biomechanics evolved as a necessary science-based method in the study of human and animal movement.

Jules Amar (1879–1935) collected extensive experimental data during various physical activities, including load bearing. Amar attempted to quantify muscular output, creating tools to measure different types of effort using the

techniques described by Marey. He summarized the physiological aspects related to industrial work in his famous book *The Human Motor*. This book was translated into English in 1920 and established the standards for human engineering in the United States and Europe. In this book, he explained the scientific qualities and important consequences of the physiology of work, and helped to organize the basis of an experimental science pilot for the workforce.

Nikolai Aleksandrovich Bernstein (1896–1966) examined walking, running, and jumping, and laid the foundation for the study of motor control and coordination. He used cyclographic techniques to track human movement. His work became known to Western scientists in the 1960s, when his seminal book *The Co-ordination and Regulation of Movements* was translated into English from Russian. Bernstein was the first to address the question of how the central nervous system is capable of adequately controlling the many degrees of freedom of the musculoskeletal system. This question is known as the "Bernstein problem" in the movement sciences.

Christian Wilhelm Braune (1831–92) was encouraged by the work of Marey to produce experimental and anatomical studies of human gait. His work was published in the book *Der Gang des Menschen* [cowritten with physiologist Otto Fischer (1861–1917)]. The methodology of gait analysis used by Braune and Fischer essentially remains the same today.

Later, A.V. Hill (1886–1977) investigated efficiency and energy cost in human movement, while W.O. Fenn (1893–1971) published the first biomechanical works in the exercise and sport science literature regarding cinematographical analysis of sprint running (Fenn, 1929, 1931).

In the 1960s the term "biomechanics" began to appear with more frequency in the literature. Biomechanics finally became a graduate specialization, being first established at Indiana University and Penn State University. Richard Nelson developed a laboratory for biomechanical research at Penn State in 1966, which was the first to be identified as using the term biomechanics (Atwater, 1980). His first graduates were Doris Miller and Charles Dillman. Charles Dillman went to the University of Illinois to establish a biomechanics program. In 1967, and about the same time, John Cooper developed a similar laboratory at the University of Indiana. The first graduate of this program was Barry Bates who developed the biomechanics program at the University of Oregon, and the author/editor of this book is one of his students. From these pioneer programs and their graduates many programs around the country were developed. Others with tremendous contributions to the development of biomechanics around the United States include James Hay (University of Iowa), Stanley Plagenhoef (University of Massachusetts), and Carol Widule (Purdue University).

The period from 1966 to the present has been an era of great growth in biomechanics. It has included the development of a number of new societies, journals, and professional meetings. In the United States, the First North American meeting in biomechanics was organized by John Cooper at Indiana University in 1970 (Cooper, 1971). We also had the First International Seminar on Biomechanics, Zurich, Switzerland, in 1967 and the origination of the *Journal of Biomechanics* in 1968 (Wilkerson, 1997). Furthermore, the Fourth International Seminar on Biomechanics was held at Penn State University in 1973 (Bates, 1974), marking the founding of the International Society of Biomechanics. In 1975 the Fifth International Seminar in Biomechanics in Jyvaskyla, Finland, marked the conceptualization of the American Society of Biomechanics, which was founded the following year in Chicago, Illinois (Wilkerson, 1997).

In 1982 the International Society for Biomechanics in Sport was founded at San Diego, California (Terauds, 1982). More recently, an international electronic mail communication list called BIOMCH-L (Biomechanics-List) was established at the University of Calgary, Canada, to help biomechanists from all over the world to get closer than ever before, in order to exchange ideas, problems, information, etc. (Bogert & Gielo-Perczak, 1992). In 2016, the first Department of Biomechanics was created at the University of Nebraska at Omaha by Nick Stergiou. This is the first academic department of its kind that both conducts biomechanics research and offers degree programs in biomechanics; namely a Bachelor of Science in Biomechanics, and graduate programs. The department is housed in the Biomechanics Research Building, which is also the first building in the world dedicated exclusively to research in biomechanics, opening its doors in 2013.

1.2.2 Archimedes: an early biomechanist

Archimedes was a great inventor, mathematician, and engineer of the ancient times. He was born in Syracuse, the largest Greek settlement in Sicily and a colony of Corinth, around 287 BCE. Tradition says that he did both his "undergraduate and graduate" work at Alexandria which was the best "university" at that time. His "mentor" was probably a disciple of Euclid, another famous Greek mathematician. Following his education he returned to his hometown, which was then a thriving metropolis, and spent the rest of his life there.

To achieve funding for his research, he applied to the local national science foundation, in other words, to his king, Hiero. As with all funding agencies, he had to convince Hiero of the soundness of his research. His research at that time was on pure mechanics as he invented levers and their laws, and the pulley. Therefore in front of his king, he used some of his pilot data.

He said: "Give me a place to stand on, and I will move the Earth." Of course, he was referring to the way levers can assist humans to move objects many times larger than themselves. In his "grant proposal," he included a demonstration of a system of levers that was capable of moving a ship fully loaded with passengers and freight.

Using his initial funding he discovered, among other things, that every object has a center of gravity, and he also developed the principle of buoyancy. It is interesting to note how he discovered this principle. King Hiero asked him to evaluate a new royal crown for which he had provided solid gold to a goldsmith. The King was suspicious that the goldsmith had added silver to the crown and kept some of the gold for himself. This project was out of Archimedes' line of research and the famous Greek had a hard time with it. After many pots of coffee and hard work in the laboratory, he decided to take a bath. He noticed that the full bath overflowed when he lowered himself into it, and realized that he could measure the crown's volume by the amount of water it displaced. From his extensive research on volume, he knew that since he could measure the crown's volume, all he had to do was to discover its weight in order to calculate its density and hence its purity. Archimedes was so delighted with his discovery that he ran out into the busy streets of Syracuse naked shouting "Eureka!," which in old Greek meant "I have found [it]!"

In another such story, King Hiero was unable to empty rainwater from the hull of one of his ships. The king called upon Archimedes for assistance. Archimedes created a machine with a hollow tube containing a spiral that could be turned by a handle at one end. When the lower end of the tube was placed into the hull and the handle turned, water was carried up the tube and out of the ship. This machine is known as the Archimedes Screw and it is still used as a method of irrigation in developing countries.

Archimedes spent a great deal of his research endeavors exploring theoretical mathematics. He realized that in this way he could publish many manuscripts and quickly develop a strong curriculum vita to support his grant proposals. He invented the method of exhaustion, an early form of integration, to identify the area of figures bounded by curved lines or surfaces. This method is characterized as a proponent of calculus. Using this method, he estimated the value of pi (π). He obtained this information by inscribing and circumscribing a circle with a 96-sided regular polygon. Archimedes also proved that the volume of an inscribed sphere is two-thirds the volume of a circumscribed cylinder. He requested that this formula/diagram be inscribed on his tomb!

Archimedes also had some problems with plagiarism. As he wrote in the preface to one of his books, he used to send his latest theorems (but without

giving proofs) to some journals with high impact factors at Alexandria. Some of the mathematicians there claimed the results as their own. Therefore, Archimedes in his book wrote that on one occasion, when he sent them theorems, he included two which were false "so that those who claim to discover everything, but produce no proofs of the same, may be confuted as having pretended to discover the impossible."

Another major funding source for Archimedes was the army, who supported his work on mechanics and for whom he designed several machines to defend Syracuse against the Romans. He developed huge cranes, which could pull enemy ships out of the water, twist them around, and then abruptly dump them back in the water. He also designed catapults that were capable of throwing heavy rocks at the enemy. Finally, he engineered a system of mirrors that reflected and focused the sun's rays on enemy ships to set them on fire.

Unfortunately, when the Romans finally broke the siege in 212 BCE, a tragic end was awaiting Archimedes. He was busy working on a problem, drawing diagrams on the sand, and had not realized that the city had been taken. A Roman soldier unexpectedly approached him and accidently stood on his diagrams. Archimedes snapped at him saying "Me mu tus Keklus tarate," meaning "Don't disturb my circles!" The Roman soldier did not speak Greek and thought that Archimedes had cursed him, and so, enraged, the soldier drew his sword and killed him.

Archimedes' work affects what biomechanists now do on a daily basis, working with levers, hydrostatics, pi, and many other of his discoveries and theorems. There is so much of him in each and every one of us regarding a love for science and discovery.

1.3 Areas of biomechanical inquiry: examples of diverse and unique questions in biomechanics

Using very similar techniques, biomechanists work in a variety of different areas. Five areas of biomechanical inquiry are described: developmental biomechanics, exercise biomechanics, rehabilitative biomechanics, occupational biomechanics, and forensic biomechanics.

1.3.1 Developmental biomechanics

Biomechanical research in human development focuses on evaluating essential movement patterns across the human life span. Individuals of different ages are examined while performing a variety of daily-living motor skills. The activities can then be quantified, described, and analyzed. Biomechanical analysis is specifically important in quantifying the development of motor

skills and movement patterns such as walking, kicking, jumping, throwing, and catching. Research in this area has resulted in the characterization of typical activity patterns for each age group. These patterns can then be compared to an individual's performance to determine his or her level of ability at any age. This type of analysis has been performed for a variety of daily-living activities across the human life span, including ascending and descending stairs, raising from and lowering to a different level (such as a chair or bed), lifting and carrying objects, pushing and pulling objects, and working with short- and long-handled implements. Again, the evaluation and quantification of each type of activity at a variety of ages allows comparisons to be made between ages, and makes it possible to evaluate an individual's skill or ability in a specific activity at a particular age.

Biomechanists have used high-speed camera systems and force platforms to capture and analyze slight movement changes in young children. The data from these devices have assisted biomechanists in objectively examining movements such as body sway during sitting and standing, and/or the range of motion at the joints during walking. These results are then shared with pediatricians and pediatric physical therapists to accurately evaluate developmental motor milestones during infancy and childhood. In particular, such objective biomechanical measurements are used to evaluate therapies for children with developmental movement disorders (e.g., global developmental delay, cerebral palsy, and Down's syndrome). A specific example of biomechanical research in this area is the work by Stergiou and colleagues at the University of Nebraska on children with cerebral palsy and the development of independent sitting. Sitting offers additional opportunities for object exploration, play, and social engagement. The achievement of sitting coincides with important milestones in other developmental areas, such as social engagement with others, understanding of spatial relationships, and the use of both hands to explore objects. These milestones are essential skills necessary for play behavior. Our biomechanical studies have led to the development of a perceptual motor intervention that can significantly improve the sitting skill, supporting further improvements in overall function and quality of life.

Another great example in this area is the research by Delp and colleagues at Stanford University, where work on the biomechanics of walking has led to the development of the free software OpenSim, which is now used by scientists around the world to model humans and animals and to understand how they move. In particular, it is used extensively to help orthopedic surgeons to develop models in order to plan surgery to improve the walking capabilities of children with cerebral palsy.

Biomechanical research has also examined the other end of the developmental spectrum, namely the aging process. Activity levels and working capacity are

diminished in older adults; aspects of physiological and motor performance, such as reaction time, movement time, muscle strength, and flexibility, are also reduced with age. Biomechanical analysis is commonly used to assess movement changes in older adults in order to identify the causes of slips, trips, and falls that the older adult population experiences. Recently the American Physical Therapy Association recognized walking speed as the sixth vital sign of overall health, something made possible by the work of several biomechanists. In addition, biomechanists strive to develop biomedical devices that can improve the quality of life for older adults, prevent injury, and quantify the best treatment approaches for restoring diminished balance and other motor abilities. A very good example of such a biomedical device is the ankle exoskeleton, and the work of Malcolm and colleagues (Malcolm et al., 2018).

1.3.2 Exercise biomechanics

In the area of exercise, biomechanical research has focused on postures and movement patterns that minimize the risk of injury during physical activity and improve performance. Among the contributions of biomechanics are the development of exercise machines for improving strength, endurance, flexibility, and speed; the development of new exercise modes, such as plyometrics and isokinetics, to improve performance; the design of exercise and sports equipment to minimize injuries; and the development of exercise and sport techniques to optimize performance. A very good example of a contribution in the area of exercise biomechanics is the development of the clap skate. The clap skate is a type of ice skate used in speed skating and was developed at the Faculty of Human Movement Sciences of the Vrije Universiteit of Amsterdam. A young biomechanist, Gerrit Jan van Ingen Schenau, started working on a hinged speed skate in 1979 and created his first prototype in 1980, finishing his PhD thesis on the subject in 1981. The whole idea was based on the premise that a skater would benefit from the extended movement with the skate on the ice, allowing the calf muscles to partake longer in the skate movement. Eventually it was found that the speed gain was due to the point of rotation being moved from the tip of the skate to the hinge, facilitating the transfer of power to the ice. The clap skate was first used in the 1984 skating season, taking a while for the idea to be recognized by others. Eventually it was used by the Dutch women's national team in 1996 with great success. The idea was soon copied widely, leading to numerous world records in the following seasons, including the 1998 Winter Olympics in Nagano, Japan.

The design of sport footwear is an example of the use of biomechanics to improve performance and reduce injury. Until the beginning of the 1970s, changes in the design of sport shoes were based on the subjective

observations of athletes and coaches. Because the movements of the lower extremities were too fast to be evaluated with the naked eye, or even standard film cameras, a new technology needed to be developed. High-speed cinematography and videography was a welcome invention allowing for detailed examination of the movement of the foot and leg while in contact with the ground during walking or running. Today, advanced technology such as digital video camera systems are used to capture movements in sports that are extremely fast, such as the golf swing and the baseball pitch.

Currently, most biomechanical shoe research is directed toward the cushioning and stability of the sport shoe. Some other important considerations in shoe design are the flexibility and density of the sole as well as the weight, durability, and breathability of the upper part of the shoe. Using the techniques previously described, biomechanists analyze the demands of a specific sport (e.g., basketball or volleyball) in relation to the shoes that are designed for that sport. This research has changed the design of all sport shoes.

Examples of biomechanists' involvement with the development of exercise equipment for improving strength and endurance can be found in stair-stepping machines and exercise bicycles. Biomechanists have evaluated posture and the ability to produce force, while reducing the potential for injury, on each of these devices. The result has been the evolution of both the stair-stepping machine and the exercise bicycle. These devices are now more comfortable and easier to use, while still providing safe and effective resistance for improving strength and endurance.

An example of the use of biomechanics to improve sport performance can be found in the golf-swing analysis now available from many professionals who teach golf. With a high-speed video camera and speed-measuring device, the golf instructor can determine a player's position and movement throughout the golf swing. The speed and path of the golf club head, as well as the speed and path of the ball after contact, can also be determined. These data provide the instructor with the information necessary to pinpoint the actions of the player that resulted in the path of the golf ball. By adjusting the player's actions, the instructor can alter the path of the ball and perhaps improve performance. This type of analysis can be helpful to the beginner as well as the highly skilled player.

1.3.3 Rehabilitative biomechanics

Biomechanical research also involves studying the movement patterns of people with injury or disability. Biomechanists analyze movement changes after injury and determine the specific movement abnormality. This information is crucial for clinicians, especially physical therapists and athletic

trainers, when developing an appropriate rehabilitation protocol for individuals to relearn motor skills after an injury.

Biomechanical research in the area of rehabilitative biomechanics led to the development of exercises and exercise equipment to train injured individuals back to preinjury functioning; the development of assistive devices such as canes, crutches, walkers, and orthotics; and the development of rehabilitative devices such as prostheses and wheelchairs. By using objective biomechanical measurements obtained through equipment such as goniometers, handheld dynamometers, and force transducers, biomechanists can determine the effectiveness of those assistive and rehabilitative devices and provide professional opinion to help physicians and therapists improve their usage.

An example in rehabilitative biomechanics is the study of the effects of peripheral artery disease (PAD) on gait patterns (Chen S, Pipinos, Johanning, Radovic, Huisinga, Myers, & Stergiou, 2008; Huisinga, Pipinos, Stergiou, & Johanning, 2010; Myers et al., 2015). PAD is a progressive disease that limits patients' ambulation due to intermittent pain in the leg muscles and cramping pain induced by movement (i.e., walking). Rehabilitative biomechanists can determine specific abnormalities in the joint movement patterns of the patients' legs. The effects of pharmacotherapy, conservative treatment, and surgical treatment then can be evaluated by biomechanically monitoring these abnormalities. Patients with multiple sclerosis are another group that can benefit from rehabilitative biomechanics. As a progressive neurological disorder that results in a high incidence of gait disturbance, multiple sclerosis can be studied with biomechanics to determine specific gait impairments and to develop rehabilitation techniques that address the problems identified (Wurdeman, Huisinga, Filipi, & Stergiou, 2010, 2013).

1.3.4 Occupational biomechanics

Biomechanical research often focuses on providing a safer environment for the worker. The development of better safety equipment (e.g., helmets, shin guards, and footwear) to protect the body from impacts and collisions with objects is an important area of biomechanical research. In addition, the development of safer or more mechanically efficient tools, improvements in the designs of transportation modules (e.g., airplanes, trains, boats, automobiles, and motorcycles), and the decrease in occupational injury have involved major contributions by biomechanists to various work environments.

As with other areas of biomechanical inquiry, biomechanists are involved in legal cases involving industrial design and safety. For example, a biomechanist was asked to determine the factors that contributed to two nail-gun

accidents. The issues assessed included the adequacy of the design of the nail-gun relative to human performance capabilities and the expected use patterns. The adequacy of machine design relative to safety when cleaning and operating the nail-gun was also a concern. Site and product examination, coupled with an analysis of human perceptions and expectations, suggested that the design was unsafe and a contributing cause of the accidents.

Product liability is another area in which biomechanists may be asked to testify. This area is illustrated with some real examples. There was one case in which a woman playing softball severely injured her ankle when she slid while wearing an improperly designed shoe. The biomechanical analysis demonstrated, within a reasonable degree of probability, that the specific injuries were caused by improper shoe design, even though the slide was properly executed. In another case, the possible causes of a knee injury while playing golf were evaluated to determine the likelihood that poorly designed shoes were the cause.

To reduce the incidence of occupational injury, biomechanists objectively evaluate working performance and develop optimal environments. For example, biomechanists have examined proficiency in robotic assistive surgery by measuring the joint range of motion and the muscle activation of the surgeons' upper extremities during surgical procedures (Judkins, Oleynikov, & Stergiou, 2009; Narazaki, Oleynikov, & Stergiou, 2006). Biomechanists have also investigated the effects of environmental factors, for example, distractions in the operating room (Siu, Suh, Mukherjee, Oleynikov, & Stergiou, 2010; Suh et al., 2010), on robotic assistive surgical performance, muscle effort, and fatigue. Biomechanical data have been used to develop an advanced surgical training program (Suh, Mukherjee, Oleynikov, & Siu, 2011) that optimizes surgeon performance and minimizes tissue injury in a variety of surgical operations.

1.3.5 Forensic biomechanics

Biomechanical research in this area is related to questions that arise in legal situations. Forensic biomechanists are invited to analyze evidence, clarify some of the most important issues, and facilitate the decisions of the jury. In most cases, biomechanists provide forensic investigations, technical reports, and expert testimony for a broad range of human performance-related incidents involving personal injury. For example, a biomechanist was asked to determine which of two occupants involved in a fatal auto accident was driving. Vehicle and site inspection data and an evaluation of the occupants' injuries were incorporated into the analysis to show that the driver was likely to have

been the one thrown from the car during the accident. In another case, an analysis and evaluation were performed to determine the potential effects of lap belt and shoulder harness restraint systems on the injuries suffered by a passenger in a car accident. Various forces on the spine were calculated to demonstrate the differential effects of the restraint systems and body positions. A number of cases involving low-speed, rear-end impacts were also evaluated. Such case evaluations typically use computer simulations to estimate movement and forces on the head and neck. In addition, biomechanical analyses are conducted on the system designs to determine their adequacy.

In another case, a biomechanist was asked to determine the possible causes of a fall that occurred when a victim was descending a stairway. The primary issue for investigation was whether small deviations in riser heights and tread slopes could sufficiently alter performance such that a fall resulted. The biomechanical evaluation, however, suggested the fall resulted from other factors.

Evaluations also have been performed to determine whether poorly designed and constructed shoes can cause a slip-and-fall accident. The ensuing site and product examination verified that the shoe construction was poor, such that, over time, deterioration took place, resulting in a product that was hazardous when worn on selected surfaces. A fall from a kitchen stool being used on a linoleum surface was also investigated. A biomechanical evaluation of the stool–surface system showed that a typical movement by the user was sufficient to cause the stool to slide, resulting in the fall.

1.4 A quick look into the future of biomechanics

In the future, biomechanics will influence many professional domains in order to understand fundamental movement in sports, exercise, medicine, robotics, biology, gaming, and occupational science. We will have many more departments of biomechanics across the world and degrees in biomechanics will be as common as those in biology or physics. Biomechanists will continue making significant contributions to physiology and medicine, developing theoretical models to understand the forces that act on human and animal bodies and the effects that they produce.

Biomechanical experimentation utilizing various measurements and tools will investigate human movement from infants to older adults and from healthy to pathological populations. Biomechanists will design exoskeletons and robots using 3D printed technology and harnessing human and animal movement studies. New and innovative techniques and analyses in

biomechanics—for example, nonlinear analysis of human movement variability (Stergiou, 2004)—will be used extensively to study performance. For example, the Center for Research in Human Movement Variability specializes in this type of innovative research (http://www.unomaha.edu/college-of-education/cobre/). By using advanced mathematical algorithms, biomechanists will be able to understand human movement variability in a novel fashion. Such approaches will expand our understanding of human movement in many biomechanical applications, especially in clinical areas.

Human movement will also be studied to a greater extent using virtual reality that is portable and easy to use. The use of virtual reality takes biomechanical research beyond the laboratory settings to simulating actual environments from which natural human movement responses can be detected. As new research technologies continue to emerge, wireless transmission will have a major impact on biomechanics. Using wireless systems, research activities normally conducted in laboratories can be expanded outside the laboratory to enable a larger range of human activity to be monitored. In sports and exercise research, increasing emphasis is being placed on obtaining accurate measures to determine the outcomes of various training protocols. Computer modeling, simulation, and virtual reality can be used to evaluate a training protocol that is designed to enhance athletic performance. For example, an athlete can practice specific movements in virtual reality to gain a cognitive edge. Such advanced biomechanical methodologies can optimize performance and further improve the design of training programs. In the future, successful training in sports and exercise will rely on both computer technology and various biomechanical measurements of movement, as well as specific individually designed models.

In clinical settings, biomechanical approaches and methods will commonly be used by physicians, physical therapists, and other specialists. The goals will be to examine pathological human movement and develop more effective treatments for patients in order to regain their quality of life by using motion analysis and gait evaluations that can be conducted away from the laboratory with inexpensive wireless technology. This technology will also be incorporated into standard clinical examinations in hospitals to increase the precision of clinical diagnoses.

In occupational science, biomechanically designed environments will be the norm. The architectural focus will slowly shift toward a realization that the interface between the human and the machine is very important. Thus biomechanists will need to work with engineers and architects to design more biologically sound workplace layouts that are safe and that will improve productivity.

In sum, biomechanics is a discipline which is on the rise. The forefathers of biomechanics should be proud of where we are now, but the future is even brighter. The final chapter of this book also provides a specific case for the tremendous possibilities that biomechanics has to offer to society.

References

Alt, F. (1967). *Advances in bioengineering and instrumentation*. New York: Plenum Press.

Atwater, A. E. (1980). Kinesiology/biomechanics: Perspectives and trends. *Research Quarterly in Exercise and Sport, 51*, 193–218.

Bates, B. T. (1974). The fourth international seminar on biomechanics. *Journal of Health, Physical Education, and Recreation, 45*, 69–70.

Bates, B. T. (1991). The need for an interdisciplinary curriculum. In *Third national symposium on teaching kinesiology and biomechanics in sports proceedings* (pp. 163–166). Ames, IA.

Bernstein, N. (1967). *The coordination and regulation of movement*. New York: Pergamon Press.

Bogert, T. V., & Gielo-Perczak, K. (Eds.), (1992). Letter to the Editor: BIOMCH-L: An electronic mail discussion forum for biomechanics and movement science. *Journal of Biomechanics, 25*, 1367.

Chen, S.J., Pipinos, I., Johanning, J., Radovic, M., Huisinga, J.M., Myers, S.A., & Stergiou N. (2008). Bilateral claudication results in alterations in the gait biomechanics at the hip and ankle joints, *Journal of Biomechanics 41*, 2506–2514.

Cooper, J. M. (1971). *Selected topics on biomechanics*. Chicago, IL: Athletic Institute.

Fenn, W. O. (1929). Mechanical energy expenditure in sprint running as measured in moving pictures. *American Journal of Physiology, 90*, 343–344.

Fenn, W. O. (1931). A cinematographical study of sprinters. *Science Monthly, 32*, 346–354.

Hay, J. G. (1973). *Biomechanics of sports techniques*. Englewood Cliffs, NJ: Prentice Hall.

Higgins, J. R. (1977). *Human movement: An integrated approach*. St. Louis, MO: Mosby.

Higgins, S. (1985). Movement as an emergent form: Its structural limits. *Human Movement Science, 4*, 119–148.

Huisinga, J. M., Pipinos, I. I., Stergiou, N., & Johanning, J. M. (2010). Treatment with pharmacological agents in peripheral arterial disease patients does not result in biomechanical gait changes. *Journal of Applied Biomechanics, 26*, 341–348.

Judkins, T. N., Oleynikov, D., & Stergiou, N. (2009). Electromyographic response is altered during robotic surgical training with augmented feedback. *Journal of Biomechanics, 42*(1), 71–76.

Malcolm, P., Galle, S., Van den Berghe, P., & De Clercq, D. (2018). Exoskeleton assistance symmetry matters: unilateral assistance reduces metabolic cost, but relatively less than bilateral assistance. *Journal of Neuroengineering and Rehabilitation, 15*(1), 74.

Myers, S. A., Huben, N. B., Yentes, J. M., McCamley, J. D., Lyden, E. R., Pipinos, I. I., & Johanning, J. M. (2015). Spatiotemporal changes posttreatment in peripheral arterial disease. *Rehabilitation Research and Practice, 2015*, 124023.

Narazaki, K., Oleynikov, D., & Stergiou, N. (2006). Robotic surgery training and performance: Identifying objective variables for quantifying the extent of proficiency. *Surgical Endoscopy, 20* (1), 96–103.

Nigg, B. M., & Herzog, W. (1994). *Biomechanics of the musculoskeletal system*. New York: John Wiley & Sons.

Siu, K. C., Suh, I. H., Mukherjee, M., Oleynikov, D., & Stergiou, N. (2010). The impact of environmental noise on robot-assisted laparoscopic surgical performance. *Surgery*, *147*(1), 107–113.

Stergiou, N. (2004). *Innovative analyses of human movement*. Champaign, IL: Human Kinetics Publishers.

Suh, I., Mukherjee, M., Oleynikov, D., & Siu, K. C. (2011). Training program for fundamental surgical skill in robotic laparoscopic surgery. *The International Journal of Medical Robotics and Computer Assisted Surgery*, *7*(3), 327–333.

Suh, I. H., Chien, J. H., Mukherjee, M., Park, S. H., Oleynikov, D., & Siu, K. C. (2010). The negative effect of distraction on performance of robot-assisted surgical skills in medical students and residents. *The International Journal of Medical Robotics and Computer Assisted Surgery*, *6*(4), 377–381.

Terauds, J. (1982). *Biomechanics in sports: Proceedings of the international symposium of biomechanics in sports*. Del Mar, CA: Academic Press.

Wilkerson, J. D. (1997). Biomechanics. In J. D. Massengale, & R. A. Swanson (Eds.), *The history of exercise and sport science* (pp. 321–365). Champaign, IL: Human Kinetics.

Wurdeman, S. R., Huisinga, J. M., Filipi, M., & Stergiou, N. (2010). Multiple sclerosis affects the frequency content in the vertical ground reaction forces during walking. *Clinical Biomechanics*, *26*(2), 207–212.

Wurdeman, S. R., Huisinga, J. M., Filipi, M., & Stergiou, N. (2013). Multiple sclerosis alters the mechanical work performed on the body's center of mass during gait. *Journal of Applied Biomechanics*, *29*(4), 435–442.

Suggested readings

Adrian, M. J., & Cooper, J. M. (1995). *Biomechanics of human movement* (2nd ed.). New York: McGraw-Hill.

Alexander, R. M. (1992). *The human machine*. New York: Columbia University Press.

Chaffin, D. B., Andersson, G. B. J., & Martin, B. J. (1999). *Occupational biomechanics* (3rd ed.). New York: John Wiley & Sons.

Hall, S. J. (2018). *Basic biomechanics* (8th ed.). New York: McGraw-Hill Education.

McCaw, S. (2014). *Biomechanics for dummies*. New York: John Wiley & Sons.

McGinnis, P. M. (2013). *Biomechanics of sport and exercise* (3rd ed.). Champaign, IL: Human Kinetics Publishers.

Nordin, M., & Frankel, V. H. (2012). *Basic biomechanics of the musculo-skeletal system* (4th ed.). Philadelphia, PA: Lippincott Williams & Wilkins.

Stergiou, N. (2016). *Nonlinear analysis for human movement variability*. Boca Raton, FL: CRC Press.

Stergiou, N. (2019). *Advice for the novice investigator: Examples taken from movement sciences*. Boca Raton, FL: CRC Press.

CHAPTER 2

Basic biomechanics

Aaron D. Likens and Nick Stergiou
University of Nebraska at Omaha, Omaha, NE, United States

We build too many walls and not enough bridges.

Sir Isaac Newton (1642–1727)

CONTENTS

2.1 Introduction

In the first chapter, we defined biomechanics as the study of the forces that act on a body and the effects they produce. Biomechanics is essentially two words combined into one (Fig. 2.1); "bio" which in Greek means "life," and "mechanics" which again in Greek means "the study of machines." Thus a direct translation from Greek is "the study of living machines."

If, on the first day of an introductory biomechanics class, you ask the students: what is more complex, bio or mechanics, they always answer mechanics? This is because they think that mechanics, which involves physics and mathematics, is more difficult than anatomy and physiology. However, it is exactly the opposite. Bio is very complex. Just consider how little we know about the brain or the myriad of the degrees of freedom that are involved in even the simplest movements. Thankfully, mechanics applies some rules to the complexity of the bio and help us to understand and explain its intricacies. Mechanics is a branch of physics that asks questions and solves problems pertaining to the actions of forces on mechanical systems. Dr. Barry Bates, a well-respected biomechanist from the University of Oregon, used to say: "Things in life you can't avoid: death and taxes. Things in movement you can't avoid: gravity and friction." In this saying, he wanted to emphasize how mechanics rules the way we move. Many times he also said that if you don't know the answer to a question pertaining to a movement, then just say gravity. Ninety percent of the time, you will be correct! Again, this stresses the importance of mechanics in dictating the way we move. Conversely, complexity in bio is so pervasive that, when large changes occur, they completely

Biomechanics and Gait Analysis. DOI: https://doi.org/10.1016/B978-0-12-813372-9.00002-6

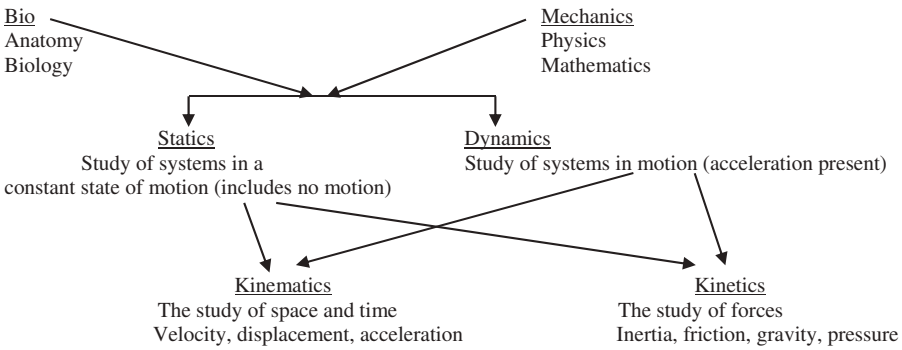

FIGURE 2.1
Schematic of the basic concepts in biomechanics.

throw off our limited models and calculations. What would happen if we, as humans, suddenly acquired an additional knee joint? Just consider how adding this single degree of freedom may affect the way we walk.

Mechanics is divisible into two disciplines: statics and dynamics (Fig. 2.1). Statics is defined as the study of systems in a constant state of motion (including no motion). Dynamics is defined as the study of systems in motion (acceleration is present). They can be further subdivided into kinetics and kinematics, where kinetics is the study of forces and kinematics the study of time and space (Fig. 2.1). These divisions allow us to better analyze movement, as we will see in later sections.

2.2 Analysis of movement

A famous physiologist called Sir Charles Scott Sherrington (1857–1952; Nobel Prize in Physiology in 1932) once stated that "all man can do is move" (Sherrington, 1951). Dr. Bates modified this statement as "all man can do is apply force." This is a perspective from a biomechanist, as opposed to a physiologist. A synthesis of those ideas resembles the following: "all man can do is apply force in order to move things."

A natural question is: why do we *want* to move? We move because we want to solve a problem, simple or complex. Thus movement is a problem-solving method. For example, we want to transport ourselves from point A to point B, or we want to transfer an object from point A to point B, etc. But, what is the best way or the proper solution to solve a problem to accomplish a goal? Biomechanists analyze movement to answer this question in many different contexts.

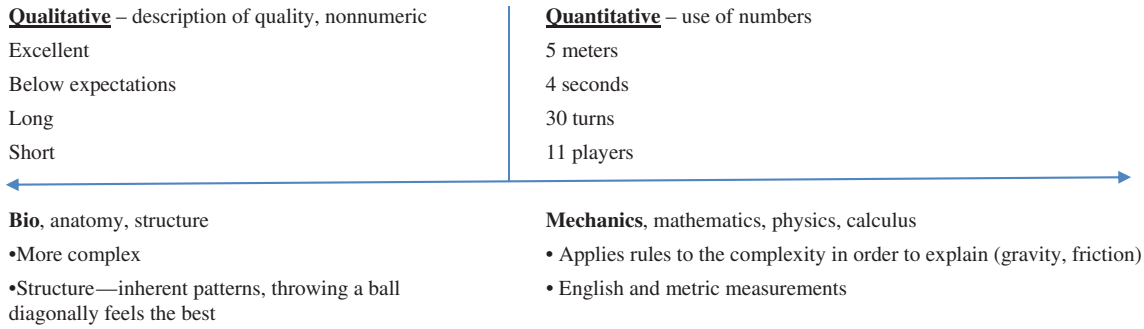

FIGURE 2.2
Qualitative versus quantitative analysis of movement.

Analysis of movement can be performed qualitatively or quantitatively (Fig. 2.2). Qualitatively, we describe the "quality" of movement (i.e., good, bad, long, heavy). It is a nonnumeric analysis. A qualitative analysis requires no instrumentation and is performed on a daily basis. It also tends to be based more on the knowledge of bio in terms of anatomy and physiology. For example, knowing the arrangement of muscle fibers in terms of their pennation angle allows us to understand why a movement is performed in a certain way (i.e., diagonally). This is because we understand how the muscles wrap around the bones, pulling and spinning them. Understanding that the knee joint cannot extend beyond 180 degrees provides us with a structural constraint to allow us a description of the movements of the legs.

In comparison, a quantitative analysis is numerical and usually requires instrumentation. This type of analysis requires one to measure, count, and understand the rules that dictate the movement under study. Quantitative methods tend to be more precise and are generally based on knowledge of mechanics. For example, gravity being one of our favorite "answers" allows us to explain why a person hops on the moon instead of walking.

In the analysis of movement, biomechanists work closely with others that are interested in movement such as clinicians, coaches, therapists, and prosthetists. They will all:

1. Describe/manipulate/observe movement.
2. Conceptualize movement.
3. Internalize movement.
4. Practice movement.

Communication with these groups requires a common language, which is the focus of the next section.

2.3 Basic terminology for analyzing movement

Because our intention is to analyze movement, we need a "language," a terminology, to speak about the body, the movement, and the musculoskeletal system. This basic terminology allows us to communicate with other professionals who are also interested in movement. To that end, we have listed below the most important terms, reflecting both the bio and mechanics, that are necessary to keep in mind when analyzing movement.

2.3.1 Basic bio terms/concepts

Let us start with the anatomical reference position. This is the neutral position, which is considered the starting position for all body segment movements. In the anatomical reference position, you are facing forward; all body parts are facing forward (including your hands) with feet slightly apart. With respect to this position, we have the following identifications regarding locations of body parts:

1. Superior—closer to the head;
2. Inferior—farther away from the head;
3. Anterior—toward the front of the body;
4. Posterior—toward the back of the body;
5. Medial—toward the midline of the body;
6. Lateral—away from the midline of the body;
7. Proximal—closer to the trunk (the knee is proximal to the ankle);
8. Distal—away from the trunk (the wrist is distal to the elbow).

There are three imaginary cardinal planes that transect the body and describe the location of structures or the direction of movements. These are called the anatomical reference planes. Movement within each plane occurs around the corresponding axis of rotation that is perpendicular to the plane.

The anatomical reference planes and the corresponding axes are:

1. Sagittal plane (or anteroposterior plane) with the mediolateral axis
   a. Divides the body vertically into left and right;
   b. Contains all forward and backward movement. Movements that occur mostly on this plane are walking, running, cycling, etc.
2. Frontal plane (or coronal plane) with the anteroposterior axis
   a. Divides the body vertically into front and back;
   b. Contains lateral movements. Movements that occur mostly on this plane are jumping jacks, abduction, lateral stepping, etc.
3. Transverse plane (or horizontal plane) with axis the longitudinal
   a. Divides the body into top and bottom;
   b. Contains horizontal movements. Movements that occur mostly on this plane are spinning, pirouettes, vertical jumping, etc.

We should mention here that most human movements do not occur strictly in one plane. Furthermore, the three planes intersect at a single point when in anatomical reference. This point is the center of mass (COM).

Movement occurs in the following forms:

1. Linear or translation: movement along a line which may be straight or curved.
   a. If the line is straight, it is called rectilinear.
   b. If the line is curved, it is called curvilinear.
2. Angular: rotation around a central imaginary line called the axis of rotation.
   a. The axis of rotation is perpendicular to the plane of rotation and passes through the center of rotation. If the axis passes through the body's COM, the body is said to rotate upon itself, or spin.
3. General movement: comprised of both linear and angular components.
   a. Human and animal movements are mostly of general motion.

Movements with respect to the joints, the anatomical reference position, and the planes are as follows. In the sagittal plane, we have the following movements: flexion, extension, hyperextension, foot dorsiflexion, and plantarflexion.

1. Flexion is when the segment moves away from the anatomical reference position.
2. Extension is when the segment returns to the anatomical reference position.
3. Dorsiflexion is when the foot moves toward the leg.
4. Plantarflexion is when the foot moves toward the ground.

In the frontal plane, we have the following movements: abduction, adduction, lateral flexion, elevation and depression of the shoulder girdle, ulnar and radial deviation, and eversion and inversion.

1. Abduction is when the segment moves away from the midline of the body.
2. Adduction is when the segment returns to midline.
3. Lateral flexion is a sideways rotation of the trunk.
4. Elevation is the superior movement of the shoulder girdle.
5. Depression is the inferior movement of the shoulder girdle.
6. Ulnar deviation is the rotation of the wrist toward the radius (thumb side).
7. Radial deviation is the rotation of the wrist toward the ulna (little finger side).
8. Eversion is the movement toward the medial aspect as the foot rolls in.

9. Inversion is the movement toward the lateral aspect as the foot rolls out.
10. Pronation of the foot—combines eversion, abduction, and dorsiflexion.
11. Supination—combines inversion, adduction, and plantarflexion.

In the transverse plane movements, we have the following movements: left and right rotation, medial and lateral rotation, pronation and supination, horizontal adduction and abduction.

1. Left and right rotations of the head, neck, and trunk.
2. Medial and lateral rotations of the hip.
3. Pronation and supination of the forearm. Pronation is the movement of the hand to turn the palm posteriorly. The opposite is supination.
4. Horizontal abduction and adduction with the arm or the thigh at 90 degrees of flexion.

We should mention here that, with respect to the anatomical reference position, all body segments are considered to be positioned at 0 degrees.

An effective method that brings together all the above in terms of analyzing a movement, is the phases of movement (Hay & Reid, 1988). This method could be the first step anytime that you are faced with a movement-related analysis problem that you need to solve. Basically, the first step is to divide the entire movement/task into its respective phases of motion. For example, the stance phase of running (when the foot is on the ground) can be divided into the following phases: loading phase (from heel contact to mid-support) and propulsive phase (mid-support to toe-off). The next step (using the analysis rubric in Fig. 2.3) is to identify the starting position of each joint, the joint actions that occur during the phases, as well as the appropriate plane and axis.

2.3.2 Basic mechanics terms/concepts

As in the previous section, here we provide basic terminology for studying mechanics. We begin with the simpler terms and slowly move to more complex concepts.

1. Mass is the quantity of matter contained in a body.
   a. Units: SI system uses kg; English system uses slug.
2. Inertia is the tendency of a body to resist a change in its state of motion; inertia is resistance to acceleration.
   a. Inertia is Newton's first law.
   b. Inertia is unitless, although the amount of inertia a body possesses is directly proportional to its mass. More mass means more resistance and more difficulty in changing the position of a body.

		Phase I (Up)				Phase II (Down)			
Joint	Start position	Movements	Plane	Axis	Intermediate position	Movements	Plane	Axis	End position
Neck	Anatomical	None			Anatomical	None			Anatomical
Trunk	Anatomical	None			Anatomical	None			Anatomical
Shoulder	Anatomical	Flexion	Sagittal	M-L	Flexed	Extension	Sagittal	M-L	Anatomical
Elbow	Flexed	Extension	Sagittal	M-L	Extended	Flexion	Sagittal	M-L	Flexed
Radioulnar	Pronated	None			Pronated	None			Pronated
Wrist	Hyperextended	None			Hyperextended	None			Hyperextended
Fingers	Extended	None			Extended	None			Extended
Hip	Anatomical	None			Anatomical	None			Anatomical
Knee	Anatomical	None			Anatomical	None			Anatomical
Ankle	Plantarflexed	None			Plantarflexed	None			Plantarflexed
Toes	Hyperextended	None			Hyperextended	None			Hyperextended

FIGURE 2.3

The phases of movement method (Hay & Reid, 1988) is implemented here using an analysis rubric with the push-up. This movement has two phases—up (lifting) and down (lowering). This is a very simple movement with two phases. If we have a more complex movement (i.e., gait), there may be more phases that extend the rubric. In addition, movements may occur in more planes and these movements can be incorporated within the same boxes along with their corresponding planes and axes. The purpose of this method is to make you think about the movement you are analyzing and organize your thoughts in an effective manner within this rubric. This preliminary step could provide you with a solid foundation in terms of your movement analysis. M-L, medio-lateral.

3. Force is a push or a pull on a body.
   a. Forces are vectors and as such are characterized by their magnitude, direction, and point of application.
4. Force is mass times acceleration ($F = ma$).
   a. This equation is practically the definition of biomechanics: the study of the forces (F) applied on a body (m) and the effects (a) that they produce. Force is the cause and movement is the effect.
   b. This is Newton's second law.
   c. Units: SI system uses Newton (N or Nt); English system uses pound (lb).
5. Weight is the force of gravity, that is, the gravitational force the Earth exerts on a body.
   a. Weight is a force and does not directly measure mass.
   b. Weight acts toward the center of the Earth.
   c. A vector applied downwards.
   d. $F = ma$ is translated to $Wt = mg$ or weight is mass times acceleration due to gravity.
   e. Acceleration of gravity (g) units: SI system uses -9.8 m/s^2; English system uses -32 ft/s^2; where the negative sign indicates direction.
   f. Units are the same as the force units; N and lb.
6. A free body diagram is a sketch or a graphical illustration that provides a visualization of all applied forces, movements, and resulting reactions on a body in a given condition (Fig. 2.4). Weight is assumed to act on a body's center of gravity (COG).
7. Pressure is the amount of force acting over a given area.
   a. It is calculated as pressure = force/area.
   b. Units: SI system uses N/m^2 or Pascal (Pa) or N/cm^2; English system uses lb/in^2 or psi.
   c. Real life example: Why does it hurt so much if a person that wears spiked heels steps on you on the busy New York subway? Let us assume that the spiked heel area is around 5 cm^2. If this person weighs 150 pounds (667 N), then the pressure that would be applied on your foot is 133 N/cm^2. However, if the person was more considerate of your foot and was wearing a sport shoe with a much larger heel area (e.g., 180 cm^2), then the pressure would drop significantly and would be only 4 N/cm^2. A biomechanist always checks the type of shoes people wear in a subway!

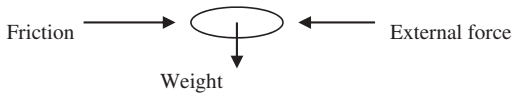

FIGURE 2.4
A very simple free body diagram.

8. Volume is the space occupied by a body.
   a. Space has three dimensions—height, length, and width. Therefore a unit of volume is height times length times width.
   b. Units: SI system uses cm^3 or m^3 or liter (L) which is equal to 1000 cm^3; English system uses in^3 or ft^3 or quart which is equal to 57.75 in^3.
   c. Real life example: The shot put and the softball have roughly the same volume but have substantially different weights.
9. Density is mass per unit of volume.
   a. It is denoted by the Greek letter rho (ρ). It is calculated as ρ = mass/volume.
   b. Units: SI system uses kg/m^3
   c. Units: English system uses $slugs/ft^3$ but pound-mass per cubic foot (lbm/ft^3) is often used. Note that there is a difference between pound-force (lbf) and pound-mass (lbm). Slugs can be multiplied by 32.2 for a rough value in pound-mass (lbm).
   d. Real life example: The shot put has a much greater density than the softball but have substantially different weights.
10. Torque is the rotary effect of a force or a force that produces rotation.
   a. Torque is calculated as the product of force and d, where d is the perpendicular distance from the axis of rotation to the force's line of action.
   b. Units: SI system uses Newton-meter (Nm or Ncm); English system uses pound-foot (lbf·ft.).
   c. Real life example: If you plot torque versus joint angle, then your graph will be an inverted U. As the body segment moves through its range of motion, the perpendicular distance between the axis of rotation (the center of the joint) and the force's line of action (the long axis of the muscle) increases and then decreases. Maximum torque occurs when this distance is also at its maximum. Regarding the joint angle, this maximum occurs at the "sticking" point, the point where you fail a lift during weight lifting. If you can pass this point, then you can complete the lift.
11. Impulse is force multiplied by time, that is, the duration over which a force is applied.
   a. It is calculated as J or Imp = $F\Delta t$
   b. Since force is a vector quantity, impulse is also a vector in the same direction.
   c. Units: SI system uses Newton-second (Ns); English system uses pound-second (lbf.s)
   d. Real life example: In golf, one usually applies a very large force (a golf swing) for a very short duration during a golf shot producing high impulse. This is why, in golfing, this is often described as the club giving the ball an *impulse*.

12. Forces acting on bones can be considered as different types of mechanical loads. These load types are listed and defined below:
    a. Compression forces are pressing or squeezing forces directed axially through a body. Such forces create problems on our musculoskeletal system during running and at impact with the ground.
    b. Tension forces are pulling or stretching forces directed axially through a body. Such forces create problems on our musculoskeletal system during throwing and at ball release.
    c. Shear forces are directed parallel to a surface. These forces create problems in our joints due to improper foot plants or improper playing turfs.
    d. Compression and tension are axial forces while shear is a torsional force. Our bones are designed quite well to deal with axial forces. However, this is not the case with torsional forces (Nordin & Frankel, 1989). This is why torsional forces generate more injuries during movement, especially in sports.
    e. Axial forces are pure compression or tension. Bending forces are complex loadings, involving both axial forces. Torsion forces are shear, rotational forces.
    f. Acute injuries or acute mechanical loading are the application of a single force of sufficient magnitude to cause injuries. In vitro investigations explore the strength of biomaterials and biological structures to identify their limits during such loading.
    g. Repetitive injuries or repetitive mechanical loading are the application of a subacute load or a force that is usually of relatively low magnitude but is applied for a long period of time.
    h. Real life example: Stergiou, Bates, and James (1999) demonstrated that, during running, proper coordination between subtalar joint pronation/supination and knee joint flexion/extension via tibial rotation is important to attenuate ground reaction impact forces. They found that running at faster speeds and over obstacles of greater heights produce increases in these forces and differences between rearfoot and knee angular velocities. The higher the obstacle and the faster the speed, the greater the forces and the greater the velocity differences. The velocity differences between the actions of the subtalar and the knee joint, which in essence capture the antagonistic nature of their relationship, indicate increased and opposite rotational forces at the two ends of the tibia. Importantly, these velocity differences produced a significant high correlation with an independent clinical evaluation of the participating subjects regarding their susceptibility to injury. The authors suggested that a possible mechanism responsible for

various running injuries could be lack of coordination between subtalar and knee joint actions that leads to repetitive improper loading on the lower extremity. The authors also suggested that an evaluation of this mechanism may have potential for predicting runners with susceptibility to injury.

13. Stress is the distribution of force within a body and is quantified as force divided by the area over which the force acts. This is similar to pressure, but pressure represents force that is external to the body, whereas stress represents internal force distribution that results from external application of a force.
    a. Stress is calculated as a quotient of a force divided by an area.
    b. Real life example: Many students use backpacks to carry their possessions (e.g., their precious books) as they walk around campus. What is the compressive stress of the spine? If the vertical surface area of the lumbar 1 to lumbar 2 (L1−L2) disc is 20 cm^2 and the student weighs 125 pounds (556 N), then the stress on L1−L2 is as follows: stress = $(556 \times 0.45)/20 = 12.5$ N/cm^2. We multiply by 0.45 as L1−L2 will support only that portion of our body and not the entire body. Now let us consider carrying a heavy backpack that weighs 40 pounds (178 N). Our calculations are modified as follows: stress = $[(556 \times 0.45) + 178]/20 = 21.4$ N/cm^2. The backpack almost doubles the stress on our spine and lower back.

2.4 Basic bio considerations

Our next step in establishing the fundamentals needed to analyze movement is to describe the basic bio-related elements of the neuromusculoskeletal system. Therefore we have listed below the most important terms and principles regarding the anatomical components that interact effectively to produce movement.

2.4.1 Basic biomechanics of bones

There is a total of 206 bones in the human body. These bones are designed to fulfill three roles:

1. Protection. They protect many of our vital organs, such as the brain and lungs.
2. Provide the body with a rigid framework. To understand this architectural role, just consider a building where there are no beams or a frame.

3. Provide the ability to use levers. We use levers continuously to accomplish movements. Using levers, a relatively rigid object can be made to rotate about an axis as a result of a force.

Due to these roles and the stresses (compression, tension, shear) they have to withstand, there are four different types of bones:

1. Short. These bones are mostly shock absorbers. Examples are the carpals and the tarsals.
2. Flat. The primary tasks of these bones are (a) to protect organs and soft tissue and (b) provide sites of attachments for muscle and ligament. Examples are the scapulae, sternum, ribs, patellae, and skull.
3. Irregular. These bones are of different shape to fulfill a variety of special needs. Examples are the vertebrae, sacrum, coccyx, and maxilla.
4. Long. The primary task of these bones is to form the framework of our skeleton. Examples are the femur and tibia.

Much of the development of the formation of the bones is determined genetically. However, the environment and the forces that act on the bones throughout life have a major effect. These changes that occur throughout the lifespan and are unrelated to normal growth and development, are described by Wolff's law. Wolff's law, developed by the German anatomist and surgeon Julius Wolff (1836–1902) in the 19th century, states that a healthy bone will adapt to the loads under which it is placed (Wolff, 1986). Bones place or displace themselves in the direction of functional forces and increase or decrease their size, shape, and density to reflect the amount of functional forces. The bone modeling and remodeling that Wolff's law describes are controlled by the bone cells, the osteocytes. The osteocytes trigger the actions of osteoclasts and osteoblasts that are typically in balance with each other.

Numerous sports-related examples indicate that if loading on a particular bone increases, the bone will remodel itself over time to become stronger (i.e., hypertrophy) in order to resist this type of loading. In a classic study conducted by Jacobsen, Beaver, Grubb, Taft, and Talmage (1984), the bone mineral content of tennis players, swimmers, and age-matched controls revealed the effect of the level and distribution of the forces applied due to the specific sport. The swimmers and tennis players had greater bone mineral density and bone width at the distal locations than the matched controls. Interestingly, the metatarsal bone mineral density was 9% higher in the swimmers and 22% in the tennis players. However, at the lumbar vertebrae only the tennis players had higher bone mineral density (by 11%) than the controls. The interplay of gravity, buoyancy, and sport specificity is certainly a major factor in these results. In an earlier study, Nilsson and Westlin (1971) compared top-level athletes from different sports regarding the bone mineral content of their femur. They found that weightlifters had the greatest

bone density, followed by throwers, runners, and soccer players. However, swimmers were not significantly different from matched controls, underlining the importance of weight-bearing activities in causing hypertrophy in the lower extremities. Similarly, a great number of studies have demonstrated bone atrophy when there is a substantial decrease in weight-bearing activities. In general, if the loading on a bone decreases (e.g., no exercise, no movement, reduced gravity), the bone will atrophy and become less dense and weaker. This reduction in bone density is called osteopenia. Rates of bone loss can approach 1% per week when people spend time in space, live a sedentary life, or are immobilized due to bed rest, casting after a sports-related injury, or pathologies such as paraplegia and muscular dystrophy (Abramson & Delagi, 1961; Andersson & Nilsson, 1979; Berg, Eiken, Miklavcic, & Mekjavic, 2007; Rodríguez-Gómez et al., 2018; Smith et al, 2014; Walton & Warrick, 1954). Implants that are used for stress protection can also cause bone loss (Roesler, 1987).

From the above examples, it is obvious that a major factor responsible for bone configuration throughout life is actually gravity. Modern life that has people sit for long periods of the day or working jobs that have minimal lifting may significantly impact bone health. Therefore it seems critical that one implements weight-bearing activities in daily physical activity regimens, and weight training should be incorporated in most exercise prescriptions that do not involve sufficient bone loading. Such actions may prevent later in life osteopenia that may likewise evolve into osteoporosis. This disorder involves decreased bone mass and minerals and decreased bone strength (Handout on Health: Osteoporosis. NIH Publication No. 14-5158, 2014). Weakened bones increase the risk of fractures (bone breaks). Osteoporosis is the most common reason for a fractured bone among older adults, including predominantly the vertebrae, the forearm bones, and the hip joint articulating bones (Golob & Laya, 2015). Proper diet, smoking abstinence, and weight-bearing physical activity (specifically strength training throughout life) are commonly cited as ways to prevent this disorder (Handout on Health: Osteoporosis. NIH Publication No. 14-5158, 2014).

Fractures are disruptions of continuity in a bone that result from improper loading. An interesting category of fractures is the so-called stress fractures that result from repetitive, low-magnitude, loading force. Stress fractures are common in sports such as basketball, running, and volleyball. In Chapter 3, Advanced biomechanics, we discuss how movement variability could be useful in preventing stress fractures by distributing forces in a slightly different way when we execute the same movement over multiple repetitions, such as in running. This may involve the use of different pairs of shoes, even of the same brand and model between days, different routines, and several other strategies.

2.4.2 Basic biomechanics of joints

The anatomical make-up of the joints of the human body dictate human movement capabilities. Therefore joints can be classified based on movement as follows:

1. Synarthroses (in Greek "syn" means together and "arthrosis" means joint). These are joints that connect the bones in an extremely tight fashion in order to better absorb forces. Examples are the joints between the skull bones (also called sutures) and the joints between the tibia and fibula (also called syndesmoses).
2. Amphiarthroses (in Greek "amphi" means on both sides and "arthrosis" means joint). These joints are similar to the synarthroses but also allow more movement. Examples are the joints between the vertebral and pubic symphysis (also called symphyses).
3. Diarthroses or synovial (in Greek "dia" means through and "arthrosis" means joint). They are also called synovial because the connection between the bones is lubricated by synovial fluid which is engulfed by the articular capsule that surrounds the joint. The surfaces of the articulating bones are covered with articular cartilage, a protective layer of connective tissue, and often include soft cartilaginous discs between the bones, such as knee menisci. This design allows for better distribution of loads, decreased stress, and decreased wear and tear of the bones by reduced friction. The coefficient of friction of the articular cartilage is one of the lowest of contact-bearing surfaces and has been reported to range from 0.001 to 0.03 (Ateshian & Mow, 2005). In comparison, de Koning, de Groot, and van Ingen Schenau (1992) developed special skates to measure the ice frictional forces during speed skating and found the mean coefficients of friction for the straights and curves to be, respectively, 0.0046 and 0.0059. Interestingly, McCann, Ingham, Jin, and Fisher (2009) have shown that the removal of the meniscus at a specific synovial joint, the knee, significantly increased the coefficient of friction between the cartilage surfaces from 0.02 to 0.05 as a result of the increased contact pressure.

The synovial joints are designed to allow many different types of movement capabilities. This is why we have six different types of these joints:

1. Gliding. These joints permit movement in one plane and in the form of sliding. Examples are the joints between the tarsal and carpal bones and those between the vertebrae.
2. Hinge. These joints permit movement in one plane (the sagittal) and around the mediolateral axis. Examples are the elbow and the ankle and their flexion and extension movements.

3. Pivot. These joints permit movement in one plane (the transverse) and around the longitudinal axis. An example of this joint is the radioulnar.
4. Condyloid. These joints permit biaxial movement and allow flexion/extension, abduction/adduction, and circumduction. Examples of this joint are the metacarpophalangeal joints of the fingers.
5. Saddle. These are also biaxial permitting movement joints, similar to the condyloid joints, but allow for even more movement. An example of this joint is the carpometacarpal joint of the thumb.
6. Ball and socket. These are triaxial joints that allow for maximum movements in all three planes. Examples are the hip and the shoulder.

The above classification of the synovial joints is based not only on the movement capabilities of the joints but, as the names imply, they are related to the anatomical architecture of the articulating bones. Besides this architecture, the amount of movement allowed by a joint is determined by the extensibility of the involved muscles and ligaments, the elasticity of the articular capsule, and the elasticity of the other surrounding tissues (i.e., skin). Importantly, ligaments, capsules, tendons, muscle membranes, and skin are all composed of connective tissue (collagen elastic fibers). Thus we mention here a few things about the elastic properties of connective tissue (Martin, Burr, & Sharkey, 1998). These are defined by the load–deformation or stress–strain relationship (Fig. 2.5). When human connective tissue is subjected to a load/stress, it will deform (this deformation is also called strain). The relationship between load and deformation is initially linear or proportional to the load and obeys the general Hooke's law. This is known as the

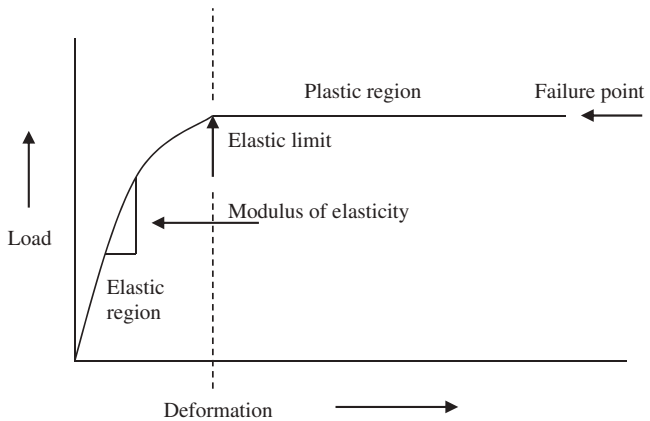

FIGURE 2.5
The load–deformation or stress–strain relationship.

elastic region (Fig. 2.5). In this region, the deformed tissue will return to its original shape when the load is removed. The slope of the elastic region is the Young's modulus of elasticity. At higher loads a tissue may become stressed beyond its elastic limit and this may be expressed as an injury of the tissue (e.g., tendinopathy). If we continue loading the tissue, we will enter further into the plastic region where the tissue will be permanently deformed. The majority of chronic overuse injuries are the result of such tissue damage. Eventually, the tissue reaches a failure point where it ruptures and requires surgery to be treated (Fig. 2.5). Tendons and ligaments can be deformed to 5%–7% without damage (Martin et al., 1998). The maximum deformation that a ligament or tendon can withstand before rupture is around 12%–15%. However, significant damage to the collagen fibers can occur before complete rupture. Regarding the modulus of elasticity values, here are two examples. The human patellar tendon value is 660 ± 266 MPa (Johnson et al., 1994) and the tibialis anterior tendon is about 1200 MPa (Maganaris & Paul, 1999). Pathology and aging may affect the mechanical properties of tendons. For example, the modulus of the human patellar tendon of individuals that are 29–50 years old is 660 ± 266 MPa. However, it decreases to 504 ± 222 MPa for individuals that are 64–93 years old (Johnson et al., 1994). Proper conditioning of the connective tissue through stretching and quality warm-up that increases the temperature of the elastic fibers in order to be able to withstand higher loads, are ways to stay within the elastic region of the load–deformation curve.

The amount of movement that is allowed by a joint is described by the range of motion of the joint or the joint flexibility. Range of motion is measured as the angle of the allowable movement of a joint, and this is accomplished using tools such as goniometers, electrogoniometers, the Leighton flexometer, and video recordings. In terms of joint flexibility, we can identify static flexibility, which is based on the passive movement of the joint (e.g., by another person), and dynamic flexibility, which is achieved actively (e.g., by muscle contraction). Therefore distinguishing between static and dynamic flexibility is important when we measure range of motion. In addition, we should consider several other factors that can affect our measurements such as aging, temperature, and injury, but also other environmental factors such as taping, bracing, and shoes. Importantly, there are certain neural sensory organs that can also affect range of motion such as the Golgi tendon organ and the muscle spindles. The Golgi tendon organ, which is located in the junction between the tendon and the muscle fibers, is a sensory receptor that detects tension. It relaxes or inhibits stretched muscles and develops tension in the antagonist muscles. Thus it is considered our "friend" when we are stretching in a slow fashion, allowing for a greater range of motion. The muscle spindle is located parallel to and within the muscle fibers. It develops

tension of the stretched muscle by initiating the stretch reflex and relaxes the antagonist muscles. It is considered our "enemy" during stretching because it could inhibit movement if we stretch too fast.

2.4.3 Basic biomechanics of muscles

Muscles produce forces to move the bones via the joints. There are about 650 muscles making up 40%–45% of total body weight (Poole, 1986). There are about 75 pairs of muscles responsible for movement and posture, while the rest are involved in eye control and swallowing. There are four behavioral properties for all muscle tissues (skeletal, cardiac, and smooth):

1. Contractility. The ability of the muscle to shorten.
2. Extensibility. The ability of the muscle to lengthen.
3. Elasticity. The ability of the muscle to return to its normal or resting length after it has been either shortened or lengthened.
4. Irritability. The ability of the muscle to receive and respond to a stimulus (nerve innervation or external force).

From a mechanical standpoint, these properties are described by the A.V. Hill muscle model (Fig. 2.6). According to this model, the muscle comprises the parallel elastic component (PEC) which is the muscle membranes that are passively stretched when the muscle changes length, the series elastic component (SEC) which is the tendons that store energy when the muscle is stretched, and the contractile component which is the muscle fibers (i.e., the myofilaments). The stretch–shortening cycle, where an eccentric contraction is followed immediately by concentric contraction, takes full advantage of these properties by allowing the development of fast and forceful movements in throwing, jumping, running, etc. (Alexander, 2002a, 2002b; Hof & van den Berg, 1986; Roberts, Marsh, Weyand, & Taylor, 1997).

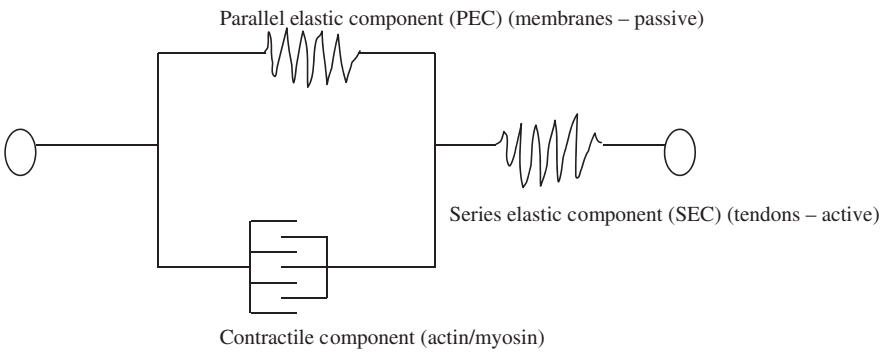

FIGURE 2.6
The A.V. Hill muscle model (Gasser & Hill, 1924; Shadmehr & Arbib, 1992).

Muscle contraction is defined as the tension-developing response of a muscle to a stimulus. Muscle contractions are classified according to velocity:

1. Isometric. The tension developed does not result in any movement and velocity is equal to zero since the resistance is equal to the tension.
2. Isotonic. The tension developed results in movementand velocity is variable through the range of motion.
3. Isokinetic. The tension developed results in movement, but the velocity is constant through the range of motion (this is accomplished through the use of an isokinetic dynamometer).

Muscle contractions can also be classified according to the length of the muscle or whether the muscle works with or against an external force that generates the movement (i.e., gravity):

1. Concentric. The muscle shortens to accomplish the movement which is performed by overcoming an external force (e.g., gravity) as in the upward phase of an elbow curl.
2. Eccentric. The muscle lengthens to control the movement, which is performed by relying upon an external force to perform the movement, for example, gravity as in the downward phase of an elbow curl. Someone may argue that this movement could also be accomplished by completely relaxing the involved muscles but such an approach will result in a very abrupt movement, possibly causing an injury.

We should also mention that the distinction of eccentric or concentric could be given to the overall phase of a movement. For example, during a push-up the downward phase is the eccentric phase. Thus the sum of our muscular contractions has an eccentric controlling result. Understanding the type of contractions that are performed during a movement will allow for a better analysis.

All the above can be brought together in the force–velocity relationship graph (Fig. 2.7). This graph demonstrates that muscles can resist/control fast eccentric actions by producing almost twice the maximum isometric force (Alexander, 2002a, 2002b). We also observe that, concentrically, as velocity decreases, we produce more force (using mostly the contractile component of Hill model's; Fig. 2.8), but movement becomes more difficult, as in lifting a heavier and heavier weight in an elbow curl. This trend continues to the point that we cannot move anymore; velocity is zero as in an isometric contraction. However, eccentrically, as velocity increases, we can produce more force because now muscles act in a different fashion and utilize our PEC and SEC more for controlling movement (Fig. 2.8). Increased use of the elastic muscle components comes at a lower energetic cost, as eccentric muscle action can produce high workloads at lower oxygen uptake levels than the same loads produced concentrically (Asmussen, 1952). However, we pay an

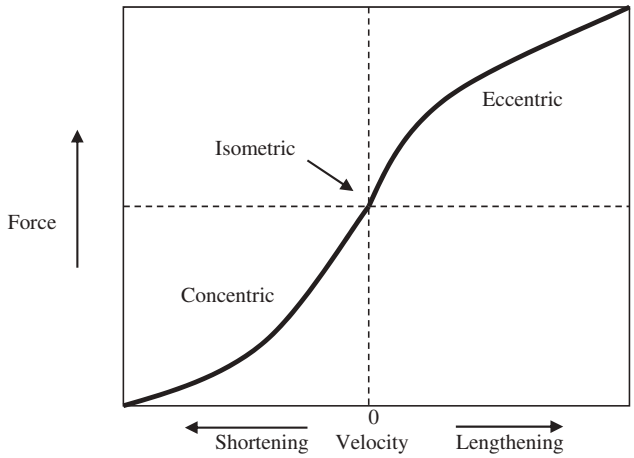

FIGURE 2.7
The force–velocity relationship graph.

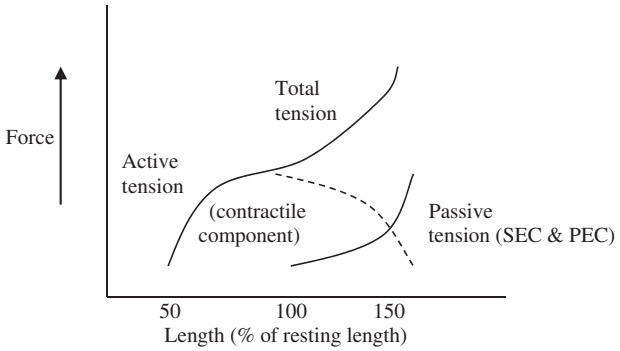

FIGURE 2.8
The force–length relationship graph.

injury cost for these higher forces produced eccentrically, because the muscles become more vulnerable to injury due to overstretching (Stauber, 2004). For example, in sprinting, hamstring injuries are common during the swing phase, possibly resulting from the high hip eccentric joint moment produced during this phase.

Muscle contractions also have an interesting relationship with the angle of movement, that is, the joint's range of motion (Fig. 2.9). This relationship is dictated purely by mechanics and the fact that joint torque is the product of the force produced by the contracting muscle and the perpendicular distance in meters from the line of action of the muscle force to the axis of rotation

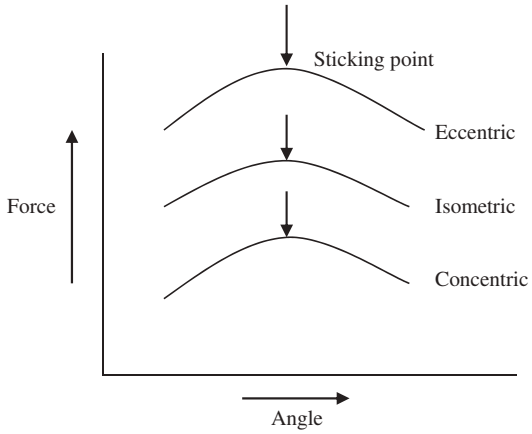

FIGURE 2.9
The force–angle relationship graph.

(joint center). This perpendicular distance changes as the segments move through the range of motion. For example, in an elbow curl the largest distance will be at 90 degrees. In addition, the rotary component of the force will be the largest at this point. If you are lifting a weight, the downwards torque produced by this weight will also be the greatest at this point. At the same time, your anatomical structure has optimized its function so you are also at your highest upwards torque production point to overcome the weight. However, if you fail to lift, it will also be right at this "sticking point" where the weight being lifted is at its maximum torque production point (Fig. 2.9). This interplay between mechanics and anatomical structure is an essential consideration in the analysis of movement.

Muscle roles may also vary in terms of their involvement in the performed joint movement. Understanding their different roles during a movement will allow for a better analysis. The muscles can be classified according to these roles as follows:

1. Agonist. This is the primary muscle or muscles that cause movement, for example, the biceps brachii in an elbow curl.
2. Antagonist. This is the muscle or muscles that work opposite to the agonist by slowing or stopping movement, for example, the triceps in an elbow curl.
3. Stabilizer. These are muscles that stabilize the joint in order to perform the movement, for example, the deltoids in an elbow curl.
4. Neutralizer. These are muscles that eliminate unwanted action produced by some other force, for example, the pronator teres which counteract supination of the forearm in an elbow curl.

The above classification becomes difficult though, when considering that many muscles cross more than one joint. Thus they could be involved in the movement of more than one joint. This is also important because the amount of tension developed in any muscle is consistent throughout its length. Therefore these muscles will affect movement simultaneously at all of the joints they cross. The classification of muscles according to the number of joints they cross, is as follows:

1. Monoarticular. These muscles cross just one joint, for example, from the shoulder joint: the two flexor muscles, pectoralis major and anterior deltoid, and the two extensor muscles, teres major and posterior deltoid.
2. Biarticular. These muscles cross two joints, for example, from the shoulder and elbow joints: the biceps brachii long head and triceps branchii long head.
3. Multiarticular. These muscles cross more than two joints, for example, the flexor digitorum superficialis that crosses the elbow, wrist, metacarpophalangeal joints, and interphalangeal joints and acts to flex all those joints.

Let us illustrate this with a few examples of how function is affected due to this anatomical characteristic of the muscles. For our first example, consider making a fist with your wrist flexed and your wrist in the anatomical position. This allows you to appreciate the multiarticularity of the finger flexors. For our second example, we will examine how the hip and knee joint function. The rectus femoris, as a biarticular muscle, flexes the hip and extends the knee, while the hamstrings (except the popliteus), being also biarticular, extend the hip and flex the knee. Due to this anatomical configuration, the range of motion of the flexion of the hip with the knee extended is 90 degrees. However, with the knee flexed, the range of motion increases to 120 degrees. On the opposite, extension of the hip with the knee extended is 20 degrees. However, with the knee flexed, it is only 10 degrees. How does this affect movement? Take running for an example. During the swing phase, by flexing your knee, you can get more hip flexion and thus longer strides. These tradeoffs reflect very important characteristics of the muscles that need to be considered carefully when performing movement analysis.

The quantitative method used to evaluate the function of the muscles during a movement is electromyography (EMG), which provides data on muscle activity. An electromyograph records electrical changes that occur in a muscle before, during, or after contraction. This electrical activity can be captured, amplified, filtered, and recorded as an indication of muscle activity or fatigue during a performance.

From a qualitative perspective, we can use some preliminary steps to EMG. Earlier in this chapter an effective qualitative method was described that could

be used to preliminarily analyze a movement, called the phases of movement (Hay & Reid, 1988; Fig. 2.3). As the next step to analyze a movement, you can use your bio based knowledge to describe the movement that occurs for a specific activity. You can think of the muscle group that controls the movement and indicate the type of muscular contraction that occurs (e.g., concentric or eccentric). For example, if we consider the elbow joint in a forearm curl with a weight, then the analysis reveals that the movement is an elbow flexion performed by the elbow joint flexors acting in a concentric contraction. The next step could be to list the muscles that are part of the group that perform this movement. For example, as elbow flexors one would list:

1. Biceps brachii—PM (primary);
2. Brachialis—PM;
3. Brachioradialis—PM;
4. Pronator teres—Asst (assists);
5. Flexor carpi radialis—Asst;
6. Flexor carpi ulnaris—Asst;
7. Palmaris longus—Asst;
8. Flexor digitorum superficialis—Asst.

These preliminary steps, along with the phases of movement, permit a better understanding of the movement under investigation. Armed with this knowledge, the researcher is much better prepared to enter the biomechanics and/or gait analysis laboratory and to ask better, more specific quantitative questions that require expensive and sophisticated equipment such as EMG.

2.5 Basic mechanics considerations

Following the presentation of the basic bio considerations of the neuromusculoskeletal system, we continue with the description of the mechanics-related fundamentals needed to analyze movement. Therefore we have listed below the most important mechanical terms and principles necessary for efficient movement analysis.

2.5.1 Linear kinematics

As mentioned above, kinematics is a subfield of mechanics that deals with the study of the time and space in which a movement occurs (Fig. 2.1). When the movement under study is linear or translational, then we are talking about linear kinematics. The most important terms and principles of linear kinematics are the following.

1. Position (p) is the location of an object in space.
2. Displacement is the change in position ($\Delta p = p_f - p_i$) of an object (final position−initial position). It is a vector quantity and informs us about

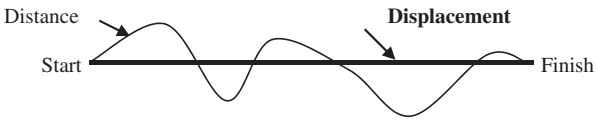

FIGURE 2.10
The distance—displacement relationship.

how far and in which direction we moved. The units of displacement are m, cm, km, in, ft, mi.

3. Distance is the length of the path traveled (Fig. 2.10). It is a scalar quantity and thus informs us only about how far we moved. The units are the same as displacement. For example: In a 400 m track and field race around the stadium what is the distance covered? 400 m. What is displacement? 0 m. In a 100 m race what is the distance covered? 100 m. What is the displacement? 100 m.
4. Velocity is the rate of change in position with respect to time ($v = \Delta p/\Delta t = (p_f - p_i)/(t_f - t_i)$) or displacement over time. It is a vector quantity and informs us about how fast and in which direction we moved. The units of velocity are m/s, km/h, mi/h, ft/s. For example: Why, when we walk at the airport, is our velocity higher when we use the moving walkways? This is because our velocity and the one of the moving belt are added as vectors. What is our velocity when we walk on the treadmill? It is actually zero since the vector of our velocity is subtracted by the equal vector of the treadmill's belt.
5. Speed is the rate of change in distance with respect to time (speed = distance/time). It is a scalar quantity and informs us only about how fast we move. The units are the same as in velocity. For example: In a 400 m track and field race around the stadium, what is the speed if the athlete finished in 50 s? 8 m/s. What is the velocity? 0 m/s.
6. Acceleration is the rate of change in velocity with respect to time ($a = \Delta a/\Delta t = (v_f - v_i)/(t_f - t_i)$). It is a vector quantity and informs us about how fast the velocity is changing. The units of acceleration are: m/s/s or m/s^2, ft/s/s, ft/s^2. Acceleration may be negative or positive based on the direction of movement (by convention, movement to the right is regarded as the positive direction and left is the negative direction) and direction of the change in velocity. If acceleration is negative, velocity may be either increasing in a negative direction or decreasing in a positive direction.

   Acceleration in terms of aeronautics has also been measured with the unit G. This unit is a dimensional representation of the magnitude of acceleration, expressed as a ratio of the magnitude of the measured acceleration to the magnitude of the acceleration of gravity.

Because acceleration is a vector quantity, having properties of both magnitude and direction, the capital letter G is used to mean that only magnitudes are being compared. Using this unit, human responses to sustained G have been reported (Parker & West, 1973). For 6–9 Gs, we have increased chest pain and pressure; breathing difficulty, with shallow respiration from position of nearly full inspiration; further reduction in peripheral vision, increased blurring, occasional tunneling, great concentration to maintain focus; occasional lacrimation; body, legs, and arms cannot be lifted at 8 G; head cannot be lifted at 9 G. For 9–12 Gs, we have severe breathing difficulty; increased chest pain; marked fatigue; loss of peripheral vision, diminution of central acuity, lacrimation. Finally, for 15 Gs we have extreme difficulty in breathing and speaking; severe chest pain; loss of tactile sensation; recurrent complete loss of vision (Parker & West, 1973).

7. Velocity is the slope of the trajectory of movement generated when you plot the position over time (Fig. 2.11). Therefore by observing such a trajectory we can make inferences about the related velocity. For example, when the position–time trajectory moves upwards, velocity (the slope) is positive; when it moves downwards, velocity (the slope) is negative; when it changes directions, velocity (the slope) is zero; when it changes from being concave (concave downward) to convex (concave upward) or vice versa, then you have an inflection point and velocity (the slope) is maximum or minimum. This knowledge has multiple benefits: (a) if you plot a hypothetical position–time

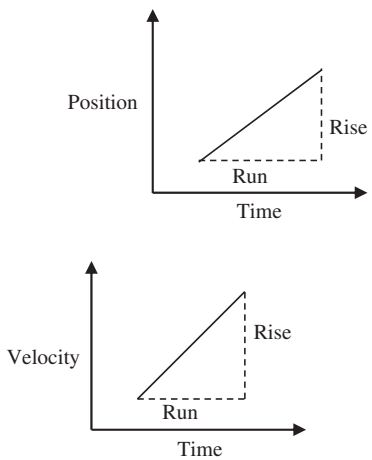

FIGURE 2.11

The slope of the position over time graph is velocity (slope–rise/run = Δposition/Δtime = velocity). Similarly, the slope of the velocity over time graph is acceleration (slope–rise/run = Δvelocity/Δtime = acceleration).

trajectory to model the movement under question, you can also plot velocity on the same graph to further evaluate your model; (b) you can plot the velocity without actually calculating it, providing a qualitative evaluation of how fast the movement occurs, possibly saving time at certain situations in the laboratory; (c) you can perform a rough evaluation, if you calculated velocity correctly through your computer program; and (d) you can perform again a rough evaluation of your smoothing (over- or undersmoothing) at the velocity level.

All the above is also true for acceleration, given that acceleration is the slope of the trajectory of movement generated when you plot the velocity over time. We can also consider position, velocity, and acceleration together, if we plot them over the same time *x*-axis (Fig. 2.12). From this perspective, when position changes direction and the velocity is zero, then acceleration will be at a maximum or minimum depending on whether velocity went, respectively, from negative to positive or positive to negative. Similarly, when position is at an inflection point and velocity is at a maximum or a minimum, acceleration will be at zero. This knowledge allows all the above-mentioned benefits but now while also considering all three quantities together. Thus this method provides a powerful tool to think first about the movement we want to analyze. We can plot and model it before we enter the laboratory to have an overall understanding of what to expect. We can do so for the entire body by considering the COM or for a certain segment or a joint. Furthermore, we can also check our calculations and smoothing. In terms of acceleration, this method provides a rough estimate of the forces acting on

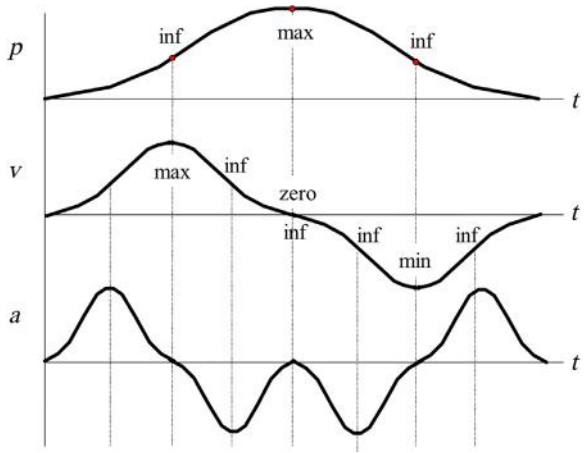

FIGURE 2.12

The position, velocity, and acceleration, plotted together versus the corresponding time using the concept of slopes. Source*: Modified from an original figure provided by Dr. Timothy R Derrick from Iowa State University.*

the body because acceleration times mass equals force. However, mass is a constant and thus the acceleration trajectory configuration will not be affected by this multiplication. Importantly, forces are almost directly related to injuries and thus when acceleration is at a maximum or a minimum (minimum is only because of the sign—consider the absolute value in this case), there exists a greater chance of injury.

2.5.1.1 Special case of linear kinematics: projectiles

Projectile motion is a form of curvilinear translation experienced by an object or a body that is projected near the Earth's surface and moves along a curved path under only the effect of gravity (the effect of air resistance is considered negligible). Basically, anything projected in the air, including the human body, is a projectile and subject to projectile properties. A body in free fall is also considered under this category.

We observe numerous types of projectiles in sports but also in daily activities. Obvious examples are the long jump or basketball, but running is also an activity wherein the human body is projected. Basketball, discus throwing, and shot-putting are activities where an external object is projected. Pole-vaulting and diving are activities where the projectile is assisted by an additional force.

We analyze projectiles in terms of the vertical and horizontal velocities of the projected object (Fig. 2.13). Horizontal and vertical components of velocity are independent and they are estimated using Pythagoras theorem and/or computational methods from simple trigonometry. Based on these, vertical velocity is computed as the product of the resultant velocity times the sine of

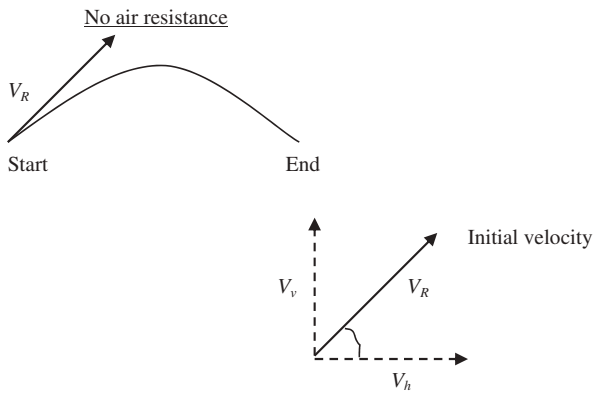

FIGURE 2.13

We analyze projectiles in terms of the vertical and horizontal velocities of the projected object.

the angle of release [$V_v = V_R \times (\sin \theta)$] and horizontal velocity is computed as the product of the resultant velocity times the cosine of the angle of release [$V_h = V_R \times (\cos \theta)$]. Thus important factors affecting projectiles are the initial velocity (V_R) and the angle of release (θ) as well as gravity. We should also note here that projection height (if there is a difference between release height and landing height) will also affect the projectile.

Gravity will influence vertical velocity at a constant rate. Air resistance will influence horizontal velocity. If we neglect air resistance, then we have a constant horizontal velocity and the corresponding vertical acceleration will be zero. The influence of gravity is quite important because, without gravity, there would be no projectile curve; with gravity, the trajectory of the projectile, the flight path, is a parabola. This is because gravity constantly decreases the initial upward vertical velocity reaching zero at the apex of the flight path. After this point gravity constantly increases the downward vertical velocity. Because we have neglected air resistance, the projectile's trajectory is a perfect parabola divided into two equal parts by the apex of the projectile. If we have a horizontal velocity which is larger ($\cos \theta$ is large) than the vertical velocity ($\sin \theta$ is small), then we have a longer distance and a straighter trajectory with a flatter parabola. If we have a vertical velocity which is larger ($\sin \theta$ is large) than the horizontal velocity ($\cos \theta$ is small), then we will have less distance and a sharper parabola.

Because the only influencing factor is gravity and gravity is constant, we can solve projectile problems using the laws of constant acceleration. These laws were derived by Galileo (Galileo Galilei, 1638; Settle, 1961) and are as follows, where a = gravity and $d = \Delta p$ = displacement:

1. $v_{\text{final}} = v_{\text{initial}} + at$ (velocity − time equation; 1st equation of motion)
   Velocity is directly proportional to time when acceleration is constant.
2. $d = v_{\text{initial}}t + \frac{1}{2}at^2$ (position − time equation: 2nd equation of motion)
   Displacement is proportional to time squared when acceleration is constant.
3. ${v_{\text{final}}}^2 = {v_{\text{initial}}}^2 + 2ad$ (velocity − position equation; 3rd equation of motion)
   Displacement is proportional to velocity squared when acceleration is constant.

For projectiles, these equations can be slightly modified based on the problem we are trying to solve, as follows. For the horizontal velocity, there is no acting acceleration and the equations become:

1. $v_{\text{final}} = v_{\text{initial}}$
2. $d = v_{\text{initial}}t$
3. ${v_{\text{final}}}^2 = {v_{\text{initial}}}^2$

Therefore if the initial horizontal velocity is 18 m/s and flight time is 3 seconds, then displacement (how far the projected object traveled) is equal to 54 m.

For a free fall, such as when an object is dropped from a static position, the initial horizontal velocity is zero and the equations become:

1. $v_{final} = at$
2. $d = \frac{1}{2}at^2$
3. $v_{final}^2 = 2ad$

Therefore if you drop an object from 0.5 m, then it will take 0.32 seconds to land.

If we are trying to identify the maximum height reached, then vertical velocity at the apex of the parabola is zero and the equations become:

$$0 = v_{initial} + at$$
$$d = v_{initial}t + \frac{1}{2}at^2$$
$$0 = v_{initial}^2 + 2ad$$

Therefore if the initial vertical velocity is equal to 20 m/s, then the object will reach a height of 20.4 m.

In sports, projectiles are common. In the track and field event of long jump, mechanics dictates that the optimal angle of takeoff is between 42 and 44 degrees, for both men and women. This is for velocities at takeoff above 8 m/s, such as those accomplished for world records. However, the typical angle of takeoff is between 17 and 24 degrees, which is what bio allows us to do. Two historic men's world records are the one by Bob Beamon in 1968 at Mexico and the other by Mike Powell in 1991 in Tokyo. The first was 8.90 m and was accomplished with a takeoff velocity of 9.6 m/s and a takeoff angle of 24.0 degrees. This world record was achieved at an altitude of 2240 m and with a favorable wind of 2.0 m/s. The second was 8.95 m and was accomplished with a takeoff velocity of 9.8 m/s and a takeoff angle of 23.2 degrees. This world record was achieved at sea level and with a favorable wind of 0.3 m/s. Let us compare these two world records with the jump performed by Carl Lewis, which is the third best ever but did not give him a world record. His jump was 8.87 m in 1991 and in Tokyo (the 1991 World Championships in Tokyo was truly incredible as a battle between Powell and Lewis). This jump was accomplished with a speed of 10.0 m/s and a takeoff angle of 18.7 degrees. Therefore we can observe very interesting individual differences (or strategies as will be discussed in Chapter 3: Advanced biomechanics). A higher takeoff velocity results in decreases in takeoff angle because control of momentum to accomplish the jump becomes much more

difficult. In general, long jumpers try to maintain their velocity in favor of controlling the takeoff angle because velocity is the most important factor in projection.

The respective values of these two parameters vary considerably in other sports. In the high jump, using the Fosbury flop, the takeoff angle was reported as between 40 and 48 degrees, while using the old-fashioned straddle technique produces angles between 42 and 53 degrees (Dapena, 1980). In discuss throwing the takeoff angle was reported to be 35−38.5 degrees (Terauds, 1975). In pitching, the fast ball velocity at release was reported at 35.1 m/s and the curve ball velocity at release at 28.2 m/s (Elliott, Grove, & Thurston, 1986).

2.5.2 Angular kinematics

When the movement under study is rotational, this involves angular kinematics. The most important terms and principles of angular kinematics are the following.

1. Angle. An angle is composed of two lines that intersect at a point called a vertex and is used to designate the measure of a rotation. Most human movements involve the rotation of bones around the joint centers or axes of rotation. Thus for the human body, joint centers form the vertices of body segment angles. The relative angle is the angle formed by the longitudinal axes of adjacent body segments. In other words, the angle formed between two articulating bones. The absolute angle is the angle formed by the longitudinal axis of one body segment with respect either to the horizontal or the vertical axes. The units are degrees or radians. In biomechanics we use tools such as goniometers, electrogoniometers, and most frequently kinematic analysis through video recordings (Fig. 2.14). In kinematic analysis, cameras are used to capture the movement of markers that are placed at certain body locations and/or anatomical landmarks. Subsequently, simple trigonometry is used to calculate the relative and absolute angles in question (Fig. 2.15).
2. Angular displacement is the change in angular position. It is analogous to linear displacement. It is calculated as $\Delta\theta = \theta_{\text{final}} - \theta_{\text{initial}}$. It is an angular vector quantity and informs us about how much rotation we have and in which direction this rotation occurs. If a segment rotates counterclockwise, then it has a positive value, represented by a vector pointing upwards. If a segment rotates clockwise, then it has a negative value, represented by a vector pointing downwards. To help us identify these relationships, we use the right hand rule where the curled fingers

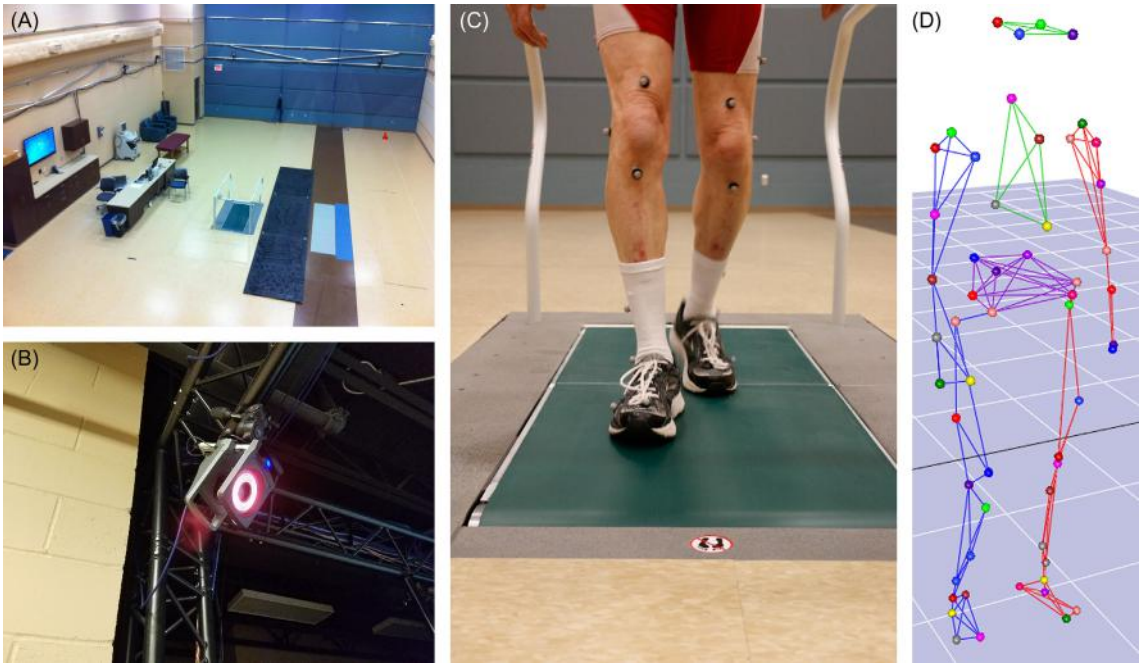

FIGURE 2.14

(A) One of the gait analysis laboratories at the Biomechanics Research Building. (B) A closer look to one of the cameras. (C) A subject with markers placed on them. (D) A computer model of a subject with the markers.

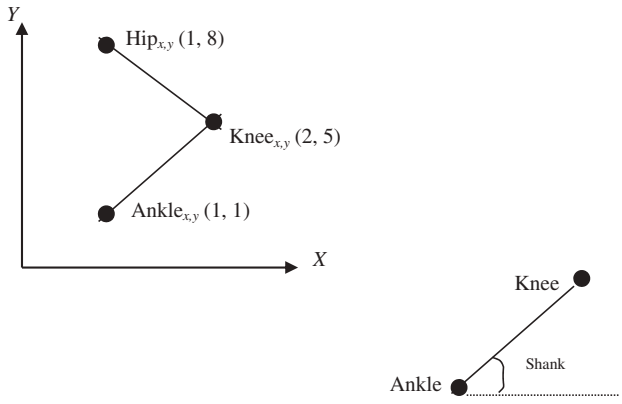

FIGURE 2.15

Angles are analyzed from video recordings. We start with certain coordinates as we see below. Let us assume that we want to calculate the absolute angle of the shank with respect to the horizontal. Using trigonometry for each segment, we get the following summarized formula: tan θ_{shank} = (y proximal−y distal)/(x proximal−x distal) = y knee−y ankle/x knee−x ankle = (5−1)/(2−1) = 4/1 = 3 = inverse tan(4) = 76 degrees.

of the right hand point in the direction of the rotation, while the direction of the vector coincides with the direction of the extended thumb. The units are degrees or radians.

3. Angular distance (φ) is the length of the angular path taken. It is analogous to linear distance. The units are the same as displacement. For example, if a segment rotates counterclockwise for 40 degrees and then clockwise for 20 degrees, then the angular distance is 60 degrees while the angular displacement is 20 degrees.
4. Angular velocity is the rate of change in the angular position ($\omega = \Delta\theta/\Delta t$ or $\omega = \theta_{final} - \theta_{initial}/time_{final} - time_{initial}$). It is analogous to the linear velocity. It is a vector quantity and informs us about how fast the angle is changing and in which direction the rotation occurred. Positive values indicate a counterclockwise rotation, while negative values indicate a clockwise rotation. The units are degrees/s or rad/s. Values of 2320 degrees/s and 7240 degrees/s were found for elbow extension and internal rotation, respectively, in Major League baseball pitchers, while values of 1900–2200 degrees/s were found for the rotating racket during the tennis serve of professional male tennis players (Elliott, 1989; Fleisig, Barrentine, Zheng, Escamilla, & Andrews, 1999).
5. Angular speed is the rate of change in angular distance with respect to time ($s = \varphi/t$). It is a scalar quantity and informs us only about how fast the angle is changing. It is analogous to the linear speed. The units are the same as in velocity.
6. Angular acceleration is the rate of change in angular velocity ($\alpha = \Delta\omega/\Delta t$ or $\alpha = \omega_{final} - \omega_{initial}/time_{final} - time_{initial}$). It is analogous to the linear acceleration. The units are degrees/s^2 or rad/s^2. Human movement rarely involves constant angular velocity or constant angular acceleration. An exception is isokinetic contractions where angular velocity stays constant through the use of an isokinetic dynamometer.
7. The linear and angular motion of a rotating object are related since $d = r\theta$ (linear displacement = radius of rotation × angular displacement). Based on this, the farther away the point of interest in the rotating object is from the axis of rotation, the larger the linear displacement (Fig. 2.16). This extends at the velocity ($v = r\omega$; linear velocity = radius of rotation × angular velocity) and the acceleration level ($a = \alpha r$; linear velocity = radius of rotation × angular acceleration). This is why golfers select a 3-iron golf club over a 9-iron and little leaguers use longer and lighter bats—to send the ball farther away.
8. A very interesting way that angular kinematics has been used in the literature is for the examination of the dynamical systems theory tenets in human movement and specifically human movement coordination. You will read more on this in Chapter 9, Coordination and control: a

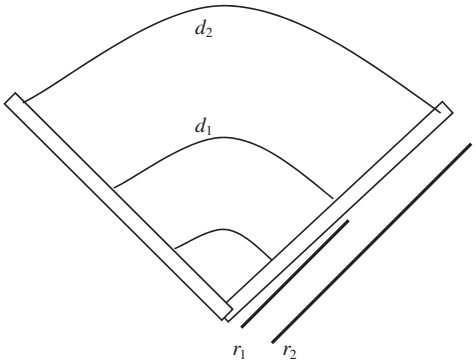

FIGURE 2.16

Linear displacement is the product of radius of rotation and angular displacement ($d = r\theta$). Thus the farther away is the point of interest in the rotating object from the axis of rotation ($r2 > r1$), the larger the linear displacement ($d2 > d1$). The angular displacement θ is the same for all rotating points.

dynamical systems approach to the analysis of human gait. However, we should mention here that a similar approach has also been utilized by Stergiou and his research group to understand how coordination and running injuries may be connected. Initially, Stergiou et al. (1999) showed that a possible mechanism responsible for various running injuries could be lack of coordination between subtalar and knee joint actions. Specifically, they found that speed changes and obstacle heights produced increases in ground reaction impact forces and differences between rearfoot and knee angular velocities. The higher the obstacle and the faster the running speed, the greater the impact forces and the greater the velocity differences. They also observed a change in the rearfoot angle curve from the traditional unimodal (one minimum) to a bimodal (two minimums) parabolic configuration. The appearance of the second minimum was attributed to a lateral deviation of the tibia as a rebound effect due to the increased impact forces with the ground. The velocity differences between the actions of the subtalar and the knee joint, which in essence capture the antagonistic nature of their relationship, produced the highest correlation with a clinical evaluation of the participating runners. In a follow-up study (Stergiou, Jensen, Bates, Scholten, & Tzetzis, 2001), they investigated intralimb coordination during running over a level surface and over obstacles of three different heights. They used the phasing relationships between the foot and leg motions in the frontal plane, and the shank and thigh motions in the sagittal plane to compare patterns of coordination. The behavioral patterns of these segments were studied under changing task demands using analysis

techniques from dynamical systems theory. They found that increases in obstacle height resulted in significant changes in impact forces and more in-phase relationships between the segments during early-stance. They mentioned that since impact forces increased significantly, the observed coordination changes might be at-risk movement patterns predisposing runners to injury. Finally, Kurz and Stergiou (2004) and Kurz, Stergiou, Buzzi, and Georgoulis (2005) extended this work with studies intended to investigate the effect of the anterior cruciate ligament reconstruction and footwear on coordination dynamics during running.

2.5.3 Linear kinetics

As mentioned above, kinetics is a subfield of mechanics that deals with the study of forces (Fig. 2.1). In Section 2.3.2, we have already, albeit briefly, identified several important terms and principles of linear kinetics such as force, weight, inertia, pressure, and impulse. Here we further discuss some of these terms and principles, while adding a few more.

1. Newton laws of motion (Isaac Newton, Cohen, & Whitman, 1726). These fundamental relationships of modern mechanics are listed below as written by Sir Isaac Newton.
   a. Constant state—law of inertia. "Every body persists in its state of being at rest or of moving uniformly straight forward, except insofar as it is compelled to change its state by force impressed." This law defines inertia, which is the resistance of an object to changes in motion. Inertia is unitless, but the amount of resistance varies directly with the mass of the object. This law is also known as the conservation of momentum because when an object is in motion, its resistance to change in motion is determined by its velocity as well as its mass. Momentum is the mass of an object multiplied by the velocity ($p = mv$).
   b. Cause effect—law of acceleration. "The alteration of motion is ever proportional to the motive force impressed; and is made in the direction of the right line in which that force is impressed." This law describes the equation of force ($F = m \times a$ where F is the cause and a is the effect).
   c. Action reaction—law of reaction. "To every action there is always opposed an equal reaction: or the mutual actions of two bodies upon each other are always equal, and directed to contrary parts." The force platform is used to measure the ground reaction forces which are created from our exertion of forces against the ground during walking or running (Fig. 2.17).

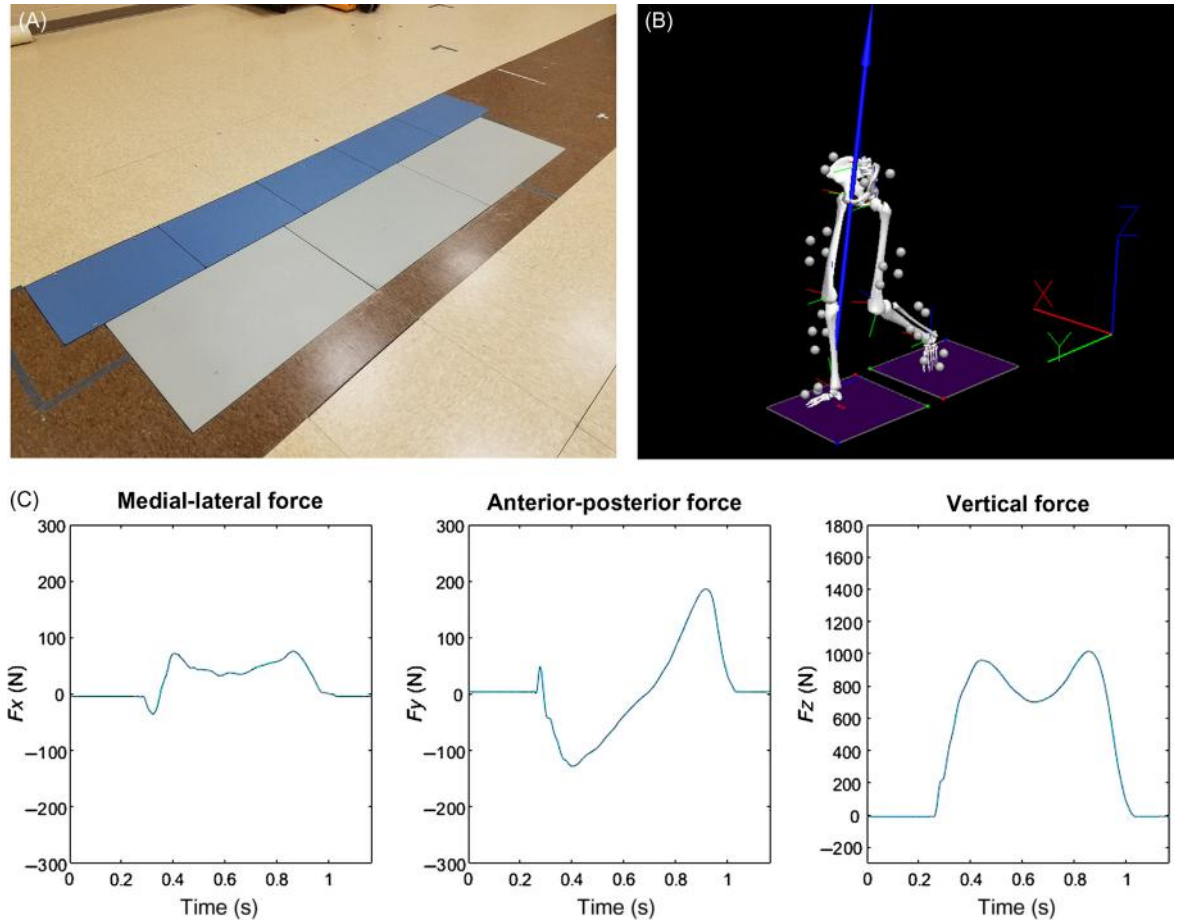

FIGURE 2.17

A subject is stepping on force platforms like those shown installed on the ground of a gait analysis laboratory at the Biomechanics Research Building (see Fig. 2.14A). (A) A closer look at these force platforms. (B) A visual 3D generated model of the subject with the resultant ground reaction force vector identified in blue. (C) The three separate components of the resultant ground reaction force vector during walking.

d. We will consider as a fourth Newton's law the law of gravitation. "All bodies are attracted to one another with a force proportional to the product of their masses and inversely proportional to the distance between them." This law describes the gravitational equation where $F = G\ (m_1 \times m_2/d^2)$; G is a constant (6.67×10^{-11} N-m^2/kg^2), m_1 and m_2 are masses of the bodies, d is the distance between these two bodies. Due to this law, we would expect differences in the force of gravity between locations at the equator and the poles. Heiskanen (1955) showed that the world record for the javelin throw is equivalent to 15.75 cm farther at Melbourne (the 1956 Olympic Games were at Melbourne) than at Helsinki (the 1952 Olympic Games were at Helsinki).

2. Friction is the force acting at the area of contact between two surfaces in the direction opposite to that of motion or motion tendency. Practically, the friction force always opposes motion, and in order to have movement, the applied force must be greater than the friction force. If there is no applied force, then there is no friction and no motion. If the applied force is equal to the friction force, then again we have no motion. The friction force that is equal to the maximum applied force that does not result in motion is called the maximum static friction. After this critical point, the applied force is larger than the friction force and motion occurs (Fig. 2.18). The coefficient of static friction is a number representing an index of the interaction between the two surfaces. It is calculated from $F_s = \mu_s \times R$, where μ_s is the coefficient of friction, F_s is the maximum static friction force, and R is the normal force which is perpendicular to the surface and equivalent to the weight of the object (or at least the vertical component of the weight force) that is being moved by the applied force. We can also calculate a dynamic μ in a similar fashion from the dynamic area of the curve (Fig. 2.18), however the static μ will be larger than the dynamic μ as the maximum static friction force is larger

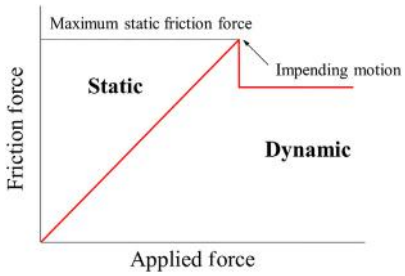

FIGURE 2.18
The relationship between applied force and friction force.

than the dynamic friction force. In addition, as we can see from the equation, the greater the magnitude of μ, the greater the force necessary to overcome friction. In Section 2.4.2 we discussed the values of the coefficient of friction at the synovial joints as being one of the lowest of contacting bearing surfaces and has been reported to range from 0.001 to 0.03 (Ateshian & Mow, 2005).

3. The impulse–momentum relationship describes the effects of a force over a period of time. Practically, in $F = m \times a$ we substitute $\Delta v/\Delta t$ for acceleration and we have $F \times \Delta t = m \times \Delta v$. Momentum is $m \times \Delta v$ and is described as the quantity of motion than an object possesses. A static object has no momentum. Conservation of momentum states that in the absence of external forces, the total momentum of a given system remains constant ($mv_{\text{before}} = mv_{\text{after}}$). Impulse is the $F \times \Delta t$ or the product of a force and the time interval over which the force acts and an impulse causes a mass to change its velocity. In Fig. 2.17, we can estimate impulse as the area under the curve since the y-axis is force and the x-axis is time. In particular, from Fig. 2.17C and the anterior–posterior force curve, we can calculate a negative braking impulse from the first part of the stance phase of walking and a positive propelling impulse from the second part. By knowing both braking and propelling impulses, as well as the mass of the subject, we can estimate the change in velocity between the two walking phases. If the two are the same, then the subject does not lose any horizontal velocity during this stance phase. If the braking impulse is larger than the propelling (as in the case of overstriding), then the subject's horizontal velocity decreases. Similarly, we can estimate the impulse from the vertical and the mediolateral curves. Importantly, changes in body mechanics (i.e., changes in knee flexion) will affect these ground reaction forces and subsequently will affect impulse.
4. Work is a force applied over a given distance ($W = F \times d$). The units are Nm or Joules (J). If an athlete has a weight of 580 N and runs a distance of 100 m, then the work produced is 58,000 J. From this example, it is obvious that a larger athlete will have to produce more work. Further, and based on the work equation, positive work is found when the force is applied in the same direction as the motion. As mentioned in Section 2.4.3, this corresponds with concentric contractions. On the other hand, negative work is found when the force is applied in the opposite direction of the motion. This corresponds to eccentric contractions.
5. Power is the rate of work production. It is calculated as work over time ($P = W/\Delta t$). The units are Joules/s or Watts. It is completely different if an athlete that has a weight of 580 N runs a distance of 100 m in 10 seconds or in 20 seconds. In the first case, power will be equal to

5800 W and in the second 2900 W. The power equation can also be modified to relate power with force and velocity ($P = W/\Delta t = F \times \Delta p/\Delta t = F \times \Delta v$; thus $P = F \times \Delta v$). Therefore power can be positive or negative depending on whether F and v are in the same direction (force is applied in the direction of motion; positive power) or in opposite directions (force is applied opposite to the direction of motion; negative power). This means that positive power indicates that energy is being generated as in concentric contractions. On the other hand, negative power indicates that energy is being absorbed as is the case in eccentric contractions.

6. Energy is the capacity to perform work. The unit of energy is Joules. There are two basic forms of energy.
   a. Kinetic energy (KE) is the energy that an object possesses due to its motion. It is calculated as $KE = \frac{1}{2}mv^2$. If there is no velocity, then there is no motion and thus no kinetic energy.
   b. Potential energy (PE) is the energy held by an object due to its position relative to other objects. From a gravitational standpoint, PE is calculated as the product of the weight of the object (the force of gravity) and the height (h; distance) of the object from the Earth [$PE = Fh = (mg)h = mgh$]. If the object is released from that height, the energy is transformed into KE. Elastic potential energy is the PE of an elastic object (e.g., a bow or a spring) that is deformed under stress. It is generated by a force that tries to restore the deformed object to its original form. If the stretch is released, the energy is transformed into KE. Elastic PE is also called strain energy (SE) and is calculated as $SE = \frac{1}{2}kx^2$ where k is a spring constant related with the stiffness of the spring, and x is the distance of deformation. SE is utilized continuously within our bodies as tendons, ligaments, muscles, and other tissues are stretched. For example, a recent study by Stearne et al. (2016) investigated how SE stored in the arch each time the foot comes into contact with the ground during running is affected if you restrict the arch with a rigid insole. They found that blocking arch compression causes your energy efficiency during a run to decrease by up to 6%.
7. Conservation of mechanical energy: In physics and chemistry, the law of conservation of energy states that the total energy of an isolated system remains constant and is conserved over time. This is the law of conservation of energy and means that energy can neither be created nor destroyed, it can only be transferred from one form of energy to another. For example, chemical energy is converted to KE when a walker uses chemical energy provided within his/her body to accelerate his/her body to a chosen walking speed. Furthermore, in walking we have a continuous interplay between KE and PE as the COG moves up

and down. During single-leg support during walking, the COG is at a maximum height and energy is stored in a form of PE, which is then transferred to KE as we come down toward the double-leg support. During double-leg support, the COG is a minimum height and KE is used to move the body back up again to single-leg support. In downhill skiing, PE is transferred from the starting position (maximum height at the top of the hill or mountain) to KE as the skier makes her way down the hill. At the end position, KE and velocity are at a maximum (minimum height at the bottom of the hill or mountain). In order for the skier to stop, unpacked snow is used to increase friction and transfers this kinetic energy to thermal energy. Another interesting example of conservation (and thus transfer) of energy is bipedal hopping locomotion which is used by some hopping species, such as red kangaroos, to keep constant (or even decrease) the amount of energy expended as speed increases (Dawson & Taylor, 1973; Kram & Taylor, 1990; McGowan & Collins, 2018). This ability of red kangaroos has been attributed to their ability to store and return elastic SE from their "Achilles tendons" (Alexander & Vernon, 1975). Importantly, the amount of elastic SE stored and returned increases with increasing speed while muscular work remains constant (Biewener, Konieczynski, & Baudinette, 1998). The amount of energy returned from the tendons accounts for almost 50% of the energy required for steady-speed hopping (Alexander & Vernon, 1975; Biewener et al., 1998).

8. Impact is a large force applied over a short time interval when two or more bodies collide. Such collisions are common in sports but also in daily activities such as when we run and collide with the ground with every step. We can consider two categories of collisions:
   a. Inelastic collisions where there is a total loss of system velocity, such as when a shot imbeds itself in a muddy field.
   b. Elastic collisions where the two bodies bounce apart. In these collisions, there is always a deformation and a restoration of the configuration (i.e., size and shape) of the colliding bodies. In these situations, the elasticity of the colliding bodies (the ability to resist a distorting force and to return to the original configuration when that force is removed; see also Fig. 2.5) is very important. The composition of these materials, in terms of both materials and arrangement, affects their elasticity. The coefficient of restitution (COR) describes the elasticity of the colliding bodies. It is a unitless constant and ranges from 0 to 1, where 1 would be a perfectly elastic collision where velocities before and after the collision will be equal (all KE is conserved). A perfectly inelastic collision has a coefficient of 0, and can be calculated as $\text{COR} = (v_b - v_a)/(u_a - u_b)$, where v_a is the velocity of the colliding object A after impact, v_b is the velocity of the

other colliding object B after impact, u_a is the initial velocity of object A before impact, and u_b is the initial velocity of object B before impact. This equation is derived if we consider KE before and after the collision. If we examine the case where an object is dropped from rest onto a horizontal surface, then we can consider PE before and after the collision. Then COR can be calculated by dividing the bounce height by the drop height (COR = bounce height/drop height). The International Table Tennis Federation has ruled that a valid table tennis ball should bounce up 24–26 cm when dropped from a height of 30.5 cm on to a standard steel block. This gives an acceptable table tennis ball COR of 0.89–0.92 (ITTF International Table Tennis Federation, 2009). For a leather basketball bouncing on a hard linoleum floor with concrete underneath, the COR should be 0.81–0.85 (American Physical Society Press Release, 2006). In another example from the track and field area regarding collisions, we mentioned above (Section 2.5.1) that two of the three longest long jumps of all time (Powell 8.95 m world record and the Lewis 8.87 m jump) took place at the same competition, the 1991 World Championships in Tokyo. In addition, in the 100 m race, six men ran under 10 seconds and this was the first time that had happened. After the championships ended, it was found that the surface of the track and the runways was extremely hard. This especially benefited sprinters and jumpers because impacts with the ground resulted in more elastic collisions and higher CORs. It was decided that future tracks and runways that had this level of hardness would be considered invalid by the IAAF.

2.5.4 Angular kinetics

As mentioned above, kinetics is a subfield of mechanics that deals with the study of forces (Fig. 2.1). In Section 2.3.2 we have identified briefly an important term in angular kinetics, namely torque. Here, we expand our discussion on torque and further present several more terms and principles.

1. Torque or moment of force is the angular equivalent of linear force. It is a force that produces a rotary effect and is calculated as the product of this force and is represented by d, where d is the perpendicular distance from the axis of rotation to the force's line of action ($T = Fd_{\perp}$). This perpendicular distance is called the moment arm. The units used are Nm, Ncm, and lbf·ft (see Section 2.3.2). Torque is a vector and thus has magnitude and direction. By convention, if the torque produces a counterclockwise effect, then it has a positive value. If the torque produces a clockwise effect, then it has a negative value.

2. Joint torque. When a muscle develops tension, it produces torque at the joint(s) it crosses. This joint torque develops because the force created by the muscle tension acts at a distance from the joint's axis of rotation. As the joint angle changes, changes also occur in the moment arm which directly affects the muscle torque generated (Section, 2.3.2). Only the perpendicular component of the resultant force will produce rotation. This is because the other orthogonal force component has a perpendicular distance equal to zero as its line of action goes directly through the joint axis. The perpendicular force component is calculated as the product of the resultant force and the sine of the angle at which the muscle pulls. In sum, the torque created by the muscle depends on the size of the muscle force, the angle at which the muscle pulls, and the distance that the muscle attaches away from the joint axis.
3. A lever is a simple machine where a rigid bar-like structure is pivoting around a fulcrum (Fig. 2.19). It consists of two forces, the effort and the resistance, which act around the fulcrum or the axis. The perpendicular distance from the line of action of the effort force to the axis is called the effort arm. The perpendicular distance from the line of action of the resistance force to the axis is called the resistance arm. The musculoskeletal system functions as a system of levers, where the bone is the rigid bar, the joint is the axis of rotation, the weight of the segment is the resistance, and the muscles supply the effort. There are three classes of levers (Fig. 2.19): (1) first class where the fulcrum

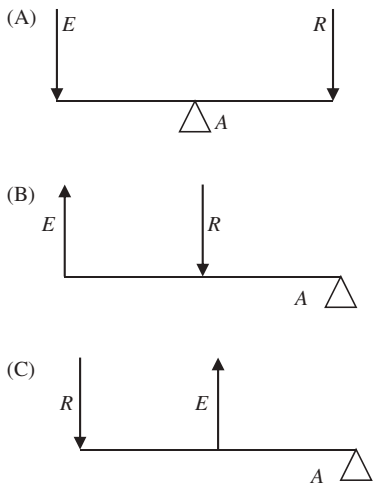

FIGURE 2.19

The three classes of levers. (A) First class where the fulcrum or axis is between the effort and the resistance. (B) Second class where the resistance is between the axis and the effort. (C) Third class where the effort is between the resistance and the axis.

or the axis is between the effort and the resistance; (2) second class where the resistance is between the axis and the effort; and (3) third class where the effort is between the resistance and the axis. An important concept regarding levers is the mechanical advantage which is the ratio of the effort arm to the resistance arm. If the mechanical advantage is 1, then the lever simply redirects the applied effort. If the mechanical advantage is greater than 1, then the lever acts to increase the effort. If the mechanical advantage is less than 1, then the lever acts to increase the speed and the range of motion based on the principles discussed in Section 2.5.2, part 7 (see also Fig. 2.16). Examples of the different classes of levers are as follows. For first class levers, we have the seesaw, crowbar, scissors, overhead elbow extension, etc. For this class, the mechanical advantage varies and can be less than, equal to, or greater than 1. For second class levers, we have the wheelbarrow, nutcracker, bottle opener, push-up, etc. For this class the mechanical advantage is always greater than one and this is why levers in this class are called force multiplier levers. For third class levers, we have tweezers, the hammer, elbow flexion, knee extension, shoulder extension, etc. Most of the levers in the human body are third class, as we mostly prioritize speed and range of motion over effort. For this class the mechanical advantage is always less than 1 and this is why the levers in this class are called speed multiplier levers.

4. Equilibrium is the situation where the sum of the forces and the sum of the moments acting upon a body are both equal to zero. This situation arises when the body is in a stationary state or a state of static equilibrium. This state is described by the following equations: (a) $\Sigma F = 0$ and (b) $\Sigma T = 0$. Using equilibrium, we can also define two more terms. Stability could be defined as the resistance to disruption of equilibrium. Balance could be defined as the ability to control equilibrium.
5. COM is the point around which the body's mass is equally distributed. If we consider gravity, then we define the COG as the point around which the sum of the torques produced by the weights of the body segments is equal to zero. COM and COG have been used interchangeably in the biomechanics literature. Because on Earth we cannot escape from gravity, COG is probably the better descriptor for biomechanical investigations. A common method to identify the COG is the segmental method (Clauser, McConville, & Young, 1969; Dempster, 1955; Miller & Morrison, 1975). This method uses video recordings to calculate first the COGs of the body segments and then the COG of the whole body. The study of the COG can provide us with a general understanding of what the entire human body is doing. For example, the study of the COG of the human body has revealed

that in infants the COG is located at about two-thirds of the thoracic region of the spine (due to their enormous head with respect to the rest of the body), while in adults it is located at the end of the lumbar region of the spine. This difference results in having tremendous problems with maintaining stability and balance as an infant. To better understand this, consider if your COG as an adult is at two-thirds of your thoracic region. This would be almost equivalent to having a table strapped on your head. Now consider how difficult it could be to walk like that. To demonstrate the effect of gravity in the movements of infants, Thelen, Fisher, and Ridley-Johnson (1984) placed infants in water. They demonstrated that infants were able to perform well coordinated steps in water. In another example, using the Fosbury flop in the track field event of high jumping, an athlete can clear the bar while his/her body's COG remains as much as 20 cm below it, while in the straddle technique, the COG of the athlete has to clear the bar (Dapena, 1980). Therefore generating the same kinetic energy on the ground, you can achieve higher heights even though the potential energy will be the same.

6. Moment of inertia is the angular equivalent to linear inertia. It is defined as the resistance to angular motion and is dependent on the mass distribution around the axis of rotation. The more closely mass is distributed to the axis of rotation, the easier it is to rotate. For example, it is much easier to swing a flexed leg than an extended leg during walking. For a point-like mass, the moment of inertia about an axis is given by $I = mr^2$, where r is the distance of the point from the axis and m is the mass. For an extended rigid body, the moment of inertia is just the sum of all the small pieces of mass multiplied by the square of their distances from the axis in rotation. In this case, we can use as a distance the radius of gyration, which is the distance from the axis of rotation to a point where the body's mass could be concentrated without altering its rotational characteristics. Then the moment of inertia equation can be modified as $I = mk^2$, where k is the radius of gyration. The radius of gyration is often expressed as a proportion of the segment's length and thus the moment of inertia equation can be further revised to $I = m(rl)^2$, where r is the radius of gyration as a proportion of the length of the segment and l is the length of the segment. The unit of the moment of inertia is kg-m^2. Due to the fact that the moment of inertia is highly depended upon r (which is even squared), rotation around the different anatomical axes of the human body will have a completely different moment of inertia. Body positioning will also have a large effect, where an extended position will increase the moment of inertia. For example, performing a rotation in the transverse plane and around the longitudinal axis with the arms extended doubles the magnitude of the

moment of inertia (from 1.0–1.2 to 2.0–2.5 kg-m^2; Hochmuth, 1984). Performing a whole-body rotation in the frontal plane and around the anteroposterior axis results in much higher moment of inertia values in comparison to the transverse plane (12.0–15.0 to 2.0–2.5 kg-m^2; Hochmuth, 1984).

7. Newton's laws of angular motion. These are the equivalent laws of linear motion, and are listed as written by Hay and Reid (1988).
   a. The angular form of Newton's first law is as follows. "A rotating body will continue to turn about its axis of rotation with constant angular momentum unless a torque is exerted upon it." Angular momentum is the rotational equivalent of linear momentum. It is calculated as $H = I \times \omega$, where I is the moment of inertia and ω is the angular velocity. The unit of angular momentum is kg-m^2/s. This law is also known as the principle of conservation of angular momentum as the total angular momentum of a closed system remains constant. We see multiple examples of this principle in human movements. For example, a figure skater increases rotational speed around the longitudinal axis by decreasing the moment of inertia by drawing in their arms and legs. In this fashion the figure skater conserves angular momentum. We observe the same in a diver who makes a rotation around the mediolateral axis. Immediately after leaving the board, the diver makes a rotation by tucking the body into a fully flexed position which decreases the moment of inertia but increases rotational speed to accomplish the rotation quickly. Then the diver extends fully the body by increasing the moment of inertia and decreasing the angular velocity, allowing them to enter the water.
   b. The angular form of Newton's second law is as follows. "The rate of change of angular momentum of a body is proportional to the torque causing it and takes place in the direction in which the torque acts." This law is the equivalent of the linear $F = ma$. Therefore torque can also be expressed as the product of the moment of inertia and angular acceleration ($T = I\alpha$).
   c. The angular form of Newton's third law is as follows. "For every torque that is exerted by one body on another, there is an equal and opposite torque exerted by the second body on the first." This law is the equivalent of the linear action–reaction. For example, in the long jump the athlete rotates the legs and arms in such a fashion as to counter the movement of the trunk. This results in a more favorable position during landing.
8. For the linear terms of work, energy, and power, there are angular equivalents. These are calculated as follows. Angular impulse is Tt; angular work is $T\Delta\theta$; angular kinetic energy is $\frac{1}{2}I\omega^2$; and angular power is $T\omega$.

9. Inverse dynamics is a method for computing forces and torques based on the kinematics of a body and the body's mass and moment of inertia (Winter, 2009). In gait analysis, inverse dynamics is used to compute internal moments and forces at the joints of the lower extremities using measurements of the motion of the segments and external forces such as ground reaction forces under certain assumptions. The equations of dynamic equilibrium are used to accomplish this task. These equations for a two-dimensional solution are: $\Sigma F_x - ma_x = 0$; $\Sigma F_y - ma_y = 0$; $\Sigma T - I\alpha = 0$.

2.6 Summary and concluding remarks

In this chapter we have covered the basic principles of biomechanics. We have discussed the anatomical and the mechanical principles which provide the basis for understanding and analyzing the various forms of human movement. Our goal was not to replace, with a single chapter, the large volume of biomechanics textbooks that have been published mostly for undergraduate courses. However, we wanted to introduce the reader to a fundamental understanding on how to develop the ability to link the structure of the human body with its function from a biomechanical perspective.

References

Abramson, A. S., & Delagi, E. F. (1961). Influence of weight-bearing and muscle contraction on disuse osteoporosis. *Archives of Physical Medicine and Rehabilitation*, *42*, 147–151.

Alexander, R. M. N. (2002a). *Principles of animal locomotion*. Princeton University Press.

Alexander, R. M. N. (2002b). Tendon elasticity and muscle function. *Comparative Biochemistry and Physiology. Part A, Molecular and Integrative Physiology*, *133*(4), 1001–1011.

Alexander, R. M. N., & Vernon, A. (1975). The mechanics of hopping by kangaroos (Macropodidae). *Journal of Zoology*, *177*, 265–303.

American Physical Society Press Release. (2006). UT Arlington Physicists question new synthetic NBA basketball. Retrieved from https://web.archive.org/web/20110130152540/http://aps.org/about/pressreleases/20061028.cfm.

Andersson, S. M., & Nilsson, B. E. (1979). Post-traumatic bone mineral loss in tibial shaft fractures treated with a weight-bearing brace. *Acta Orthopedica Scandinavia*, *50*(6 Pt 1), 689–691.

Asmussen, E. (1952). Positive and negative muscular work. *Acta Physiologica Scandinavica*, *28*, 364–382.

Ateshian, G. A., & Mow, V. C. (2005). Friction, lubrication, and wear of articular cartilage and diarthrodial joints. In V. C. Mow, & R. Huiskes (Eds.), *Basic orthopaedic biomechanics and mechano-biology* (pp. 447–494). Philadelphia: Lippincott Williams & Wilkins.

Berg, H. E., Eiken, O., Miklavcic, L., & Mekjavic, I. B. (2007). Hip, thigh and calf muscle atrophy and bone loss after 5-week bedrest inactivity. *European Journal of Applied Physiology*, *99*(3), 283–289.

Biewener, A. A., Konieczynski, D. D., & Baudinette, R. V. (1998). In vivo muscle force-length behavior during steady-speed hopping in tammar wallabies. *Journal of Experimental Biology, 201*, 1681–1694.

Clauser, C. E., McConville, J. T., & Young, J. W. (1969). *Weight, volume, and center of mass of segments of the human body (AMRL Technical Report 69-70)*. Wright-Patterson Air Force Base, OH: Aerospace Medical Research Laboratories.

Dapena, J. (1980). Mechanics of translation in the Fosbury Flop. *Medicine and Science in Sports and Exercise, 12*, 37–44.

Dawson, T. J., & Taylor, C. R. (1973). Energetic cost of locomotion. *Nature, 244*, 47–49.

de Koning, J. J., de Groot, G., & van Ingen Schenau, G. J. (1992). Ice friction during speed skating. *Journal of Biomechanics, 25*(6), 565–571.

Dempster, W. T. (1955). *Space requirements for the seated operator (WADC Technical Report 55-159)*. Wright-Patterson Air Force Base, OH: Wright Air Development Center.

Elliott, B. C. (1989). Tennis strokes and equipment. In C. L. Vaughan (Ed.), *Biomechanics of sport*. Boca Raton, FL: CRC Press.

Elliott, B. C., Grove, J. R., & Thurston, B. (1986). A three-dimensional cinematographic analysis of the fastball and curveball pitches in baseball. *Journal of Sports Biomechanics, 2*, 20–28.

Fleisig, G. S., Barrentine, S. W., Zheng, N., Escamilla, R. F., & Andrews, J. R. (1999). Kinematics and kinetic comparison of baseball pitching among various levels of development. *Journal of Biomechanics, 32*(12), 1371–1375.

Galileo Galilei. (1638). *Two new sciences*, Leiden; Translated by Henry Crew and Published by Martino Fine Books in 2015.

Gasser, H. S., & Hill, A. V. (1924). The dynamics of muscular contraction. *Proceedings of Royal Society of London, 96*, 398–437.

Golob, A. L., & Laya, M. B. (2015). Osteoporosis: screening, prevention, and management. *The Medical Clinics of North America, 99*(3), 587–606.

Handout on Health: Osteoporosis. NIH Publication No. 14-5158, 2014. Retrieved from on 1-13-2020 from <https://web.archive.org/web/20150518091922/http://www.niams.nih.gov/health_info/Osteoporosis/default.asp>.

Hay, J. G., & Reid, J. G. (1988). *Anatomy, mechanics, and muman Motion*. Englewood Cliffs, NJ: Prentice Hall.

Heiskanen, W. A. (1955). The Earth's gravity. *Scientific American, 193*, 164–165.

Hochmuth, G. (1984). *Biomechanics of athletic movement*. Berlin: Sportverlag.

Hof, A. L., & van den Berg, J. W. (1986). How much energy can be stored in human muscle elasticity? *Human Movement Science, 5*(2), 107–114.

Isaac Newton. (1726). In I. B. Cohen, & A. Whitman (Eds.), *The mathematical principles of natural philosophy - philosophiae naturalis principia mathematica* (3rd ed.). Berkeley, CA: University of California Press. (1999).

ITTF International Table Tennis Federation (2009). *The ball (version for 40mm balls)*. Technical Leaflet T3. Lausanne, Switzerland.

Jacobsen, P., Beaver, W., Grubb, S., Taft, T., & Talmage, R. (1984). Bone density in women: college athletes and older athletic women. *Journal of Orthopedic Research, 2*, 328–332.

Johnson, G. A., Tramaglini, D. M., Levine, R. E., Ohno, K., Choi, N. Y., & Woo, S. L. (1994). Tensile and viscoelastic properties of human patellar tendon. *Journal of Orthopedic Research, 12*(6), 796–803.

Kram, R., & Taylor, C. R. (1990). Energetics of running: a new perspective. *Nature, 346*, 265–267.

Kurz, M. J., & Stergiou, N. (2004). Does footwear affect ankle coordination strategies? *Journal of the American Podiatric Medical Association*, *94*(1), 53–58.

Kurz, M. J., Stergiou, N., Buzzi, U. H., & Georgoulis, A. D. (2005). The effect of anterior cruciate ligament reconstruction on lower extremity relative phase dynamics during walking and running. *Knee Surgery Sports Traumatology Arthroscopy*, *13*(2), 107–115.

Maganaris, C. N., & Paul, J. P. (1999). In vivo human tendon mechanical properties. *Journal of Physiology*, *521*, 307–313.

Martin, R. B., Burr, D. B., & Sharkey, N. A. (1998). *Mechanical properties of ligament and tendon. Skeletal tissue mechanics*. New York: Springer.

McCann, L., Ingham, E., Jin, Z., & Fisher, J. (2009). Influence of the meniscus on friction and degradation of cartilage in the natural knee joint. *Osteoarthritis and Cartilage/OARS, Osteoarthritis Research Society*, *17*(8), 995–1000.

McGowan, C. P., & Collins, C. E. (2018). Why do mammals hop? Understanding the ecology, biomechanics and evolution of bipedal hopping. *Journal of Experimental Biology*, *221*, jeb161661.

Miller, D. I., & Morrison, W. E. (1975). Prediction of segmental parameters using the Hanavan human body model. *Medicine and Science in Sports and Exercise*, *7*(3), 207–212.

Nilsson, B. E. C., & Westlin, N. E. (1971). Bone density in athletes. *Clinics in Orthoepdic Related Research*, *77*, 179–182.

Nordin, M., & Frankel, V. H. (Eds.), (1989). *Basic biomechanics of the musculoskeletal system*. Philadelphia, PA: Lea & Febiger.

Parker, J. F., & West, V. R. (1973). *Bioastronautics data book*. Washington, DC: NASA Scientific and Technical Information Office.

Poole, R. M. (Ed.), (1986). *The incredible machine*. Washington, DC: National Geographic Society.

Roberts, T. J., Marsh, R. L., Weyand, P. G., & Taylor, C. R. (1997). Muscular force in running Turkeys: The economy of minimizing work. *Science (New York, N.Y.)*, *275*(5303), 1113–1115.

Rodríguez-Gómez, I., Mañas, A., Losa-Reyna, J., Rodríguez-Mañas, L., Chastin, S. F. M., Alegre, L. M., … Ara, I. (2018). Associations between sedentary time, physical activity and bone health among older people using compositional data analysis. *PLoS One*, *13*(10), e0206013.

Roesler, H. (1987). The history of some fundamental concepts in bone biomechanics. *Journal of Biomechanics*, *20*(11-12), 1025–1034.

Settle, T. B. (1961). An experiment in the history of science. *Science (New York, N.Y.)*, *133*(3445), 19–23.

Shadmehr, R., & Arbib, M. A. (1992). A mathematical analysis of the force-stiffness characteristics of muscles and the role of reflexes in control of a single joint system. *Biological Cybernetics*, *66*, 463–477.

Sherrington, C. S. (1951). In Gifford Lectures (Ed.), *Man on his nature* (2nd ed.). Cambridge: Cambridge University Press, at Edinburgh.

Smith, S. M., Zwart, S. R., Heer, M., Hudson, E. K., Shackelford, L., & Morgan, J. L. (2014). Men and women in space: bone loss and kidney stone risk after long-duration spaceflight. *Journal of Bone Mineral Research*, *29*(7), 1639–1645.

Stauber, W. T. (2004). Factors involved in strain-induced injury in skeletal muscles and outcomes of prolonged exposures. *Journal of Electromyography and Kinesiology*, *14*(1), 61–70.

Stearne, S. M., McDonald, K. A., Alderson, J. A., North, I., Oxnard, C. E., & Rubenson, J. (2016). The foot's arch and the energetics of human locomotion. *Scientific Reports*, *6*, 19403.

Stergiou, N., Bates, B. T., & James, S. L. (1999). Asynchrony between subtalar and knee joint function during running. *Medicine and Science in Sports and Exercise*, *31*(11), 1645–1655.

Stergiou, N., Jensen, J. L., Bates, B. T., Scholten, S. D., & Tzetzis, G. (2001). A dynamical systems investigation of lower extremity coordination during running over obstacles. *Clinical Biomechanics*, *16*, 213–221.

Terauds, J. (1975). Some release characteristics if international discus throwing. *Track and Field Quarterly Review*, *75*, 54–57.

Thelen, E., Fisher, D. M., & Ridley-Johnson, R. (1984). The relationship between physical growth and a newborn reflex. *Infant Behavior and Development*, *7*, 479–493.

Walton, J. N., & Warrick, C. K. (1954). Osseous changes in myopathy. *British Journal of Radiology*, *27*(313), 1–15.

Winter, D. A. (2009). *Biomechanics and motor control of human movement*. Hoboken, NJ: John Wiley and Sons.

Wolff, J. (1986). *The law of bone remodeling (translation of the German 1892 edition)*. New York: Springer Publ.

Further readings

Adrian, M. J., & Cooper, J. M. (1995). *Biomechanics of human movement* (2nd ed.). New York: McGraw-Hill.

Alexander, R. M. (1992). *The human machine*. New York: Columbia University Press.

Basmajian, J. V., & De Luca, C. J. (1985). *Muscles alive: Their functions revealed by electromyography* (5th ed.). Baltimore, MD: Williams & Wilkins.

Chaffin, D. B., Andersson, G. B. J., & Martin, B. J. (1999). *Occupational biomechanics* (3rd ed.). New York: John Wiley & Sons.

Hall, S. J. (2018). *Basic biomechanics* (8th ed.). New York: McGraw-Hill Education.

McCaw, S. (2014). *Biomechanics for dummies*. New York: John Wiley & Sons.

McGinnis, P. M. (2013). *Biomechanics of sport and exercise* (3rd ed.). Champaign, IL: Human Kinetics Publ.

Nigg, B. M., & Herzog, W. (2007). *Biomechanics of the musculo-skeletal system* (3rd ed.). Hoboken, NJ: John Wiley & Sons.

Nordin, M., & Frankel, V. H. (2012). *Basic biomechanics of the musculo-skeletal system* (4th ed.). Philadelphia, PA: Lippincott Williams & Wilkins.

Whiting, W. C., & Zernicke, R. F. (2008). *Biomechanics of musculoskeletal injury* (2nd ed.). Champaign, IL: Human Kinetics.

CHAPTER 3

Advanced biomechanics

Barry T. Bates[1], Janet S. Dufek[2] and Nick Stergiou[3]
[1]University of Oregon, Eugene, OR, United States, [2]University of Nevada, Las Vegas, Las Vegas, NV, United States, [3]University of Nebraska at Omaha, Omaha, NE, United States

> No sensible person will deny that the works of Nature are in the highest degree simple, necessary and as economical as possible. Therefore, machines devised by mankind will doubtlessly likewise attain most success if they are as far as possible modelled on works of Nature.
>
> **Giovanni Alfonso Borelli (1608–79)**

CONTENTS

3.1 Injuries and biomechanics

Running injuries are presented as an example of how biomechanics has influenced neuromusculoskeletal problems. As is described below, biomechanics in general has allowed for fewer mistakes to be made in treating individuals just because of the general knowledge acquired through biomechanics research. However, the number of neuromusculoskeletal injuries has stayed fairly similar over the years, which is a point of great concern. There are several reasons for this and we outline some of them here. The proper application of the scientific method is another reason which can be found elsewhere (Stergiou, 2019).

3.1.1 Running injuries

Injury statistics for running have been documented by a number of people over the years. Regarding frequency of injuries among runners, several studies in the 1980s have reported values of around 50%; Koplan, Powell, Sikes, Shirley, and Campbell (1982) reported 35%, Lysholm and Wiklander (1987) 65%, Marti, Vader, Minder, and Abelin (1988) 46%, and Walter, Hart, McIntosh, and Sutton (1989) 48%. In the next decade these values remained the same, as van Mechelen (1992) reported 50% and Asplund and Tanner (2004) also reported 50%. Importantly, in a more recent review paper,

Biomechanics and Gait Analysis. DOI: https://doi.org/10.1016/B978-0-12-813372-9.00003-8

Nigg, Baltich, Hoerzer, and Enders (2015) stated that the frequency of running injuries has not changed over the past 40 years.

Common injuries in runners have been documented by several authors and include plantar fasciitis, stress fractures in the foot and the tibia, Achilles tendonitis, shin splints, iliotibial band syndrome, patellofemoral pain syndrome, ankle sprains, muscle pulls, and blisters (Arnold & Moody, 2018; Tenforde, Yin, & Hunt, 2016). It is interesting to note that in a study in 1978, James et al. stated that the primary cause (at 60%) of running injuries is training errors (James, Bates, & Osternig, 1978). Anatomic factors, shoes, and surfaces were identified as major components of training errors. In a later study, Hoeberigs (1992) identified high weekly mileage, previous injury, faster running speeds, and less running experience as important factors for running injuries. More recently, Brown (2013) documented as causes being a novice runner (inexperience), post injury (coming back too fast or trying too hard after an injury), and change or training error, as in James et al. (1978), mentioned previously. Regarding training errors, Brown included distance, intensity, and time; practically, too much, too hard, and too long. Other training errors were anatomic abnormalities and environmental factors such as shoes/surfaces/weather, similarly with the early James et al. (1978) study.

Regarding treatment modalities, in James et al. (1978) the following were identified:

- *Rest*—taking load off the system (at 47% of the cases);
- *Reduced mileage*—again taking load off the system (at 26% of the cases);
- *Orthotics*—a change of foot biomechanics (at 46% of the cases);
- *Shoe change/modification*—again a change of foot biomechanics (at 19% of the cases);
- *Medical intervention* (at 36% of the cases).

In sum, all the above demonstrate that since 1978 we have not witnessed any real change with respect to running injuries and injury prevention.

Some suggestions for injury avoidance, if we consider the running literature in general, are the following:

- *Warm up*—get the body ready for the upcoming loading and stress;
- *Avoid overtraining*—do not overstress the system with too much force and loading;
- *Follow the 10% rule*—do not change anything by more than 10% to allow the body to accommodate;
- *Wear proper footwear*—each person is different and this individuality needs to be respected;

- *Avoid specificity*—do not do the same thing every day but incorporate variations such as cross training.

We can offer some insights regarding running injuries. Injury is a function of change. Prevention and rehabilitation are a function of patience, and patience is a function of controlled change following the 10% rule discussed previously. When we consider injury as a function of change, we must also remember what we call the "Too" rule. In terms of change in training regimen, we must remember the five Too's: too much, too soon, too fast, too similar, and too different. Practically, vary your training but do not vary it "too" much: do not start doing things too quickly, do not change things too fast, do not overtrain, be careful of making change, and if you make a change follow the 10% rule.

At this point, we would like to address a very important question that our reader is certainly thinking. Why have we not seen a change in the percentage of running injuries with 40 years of study, especially in terms of biomechanics? Colonel John Stapp (1910–99), who was a US Air Force officer, flight surgeon, physician, biophysicist, and pioneer, in studying the effects of acceleration and deceleration forces on humans made the following statement: "This fifty-liter rawhide bag of gas, juices, jellies, gristle and threads movably suspended on more than 200 bones presided over by a cranium, seldom predictable and worst of all living, presents a challenge to discourage a computer into incoherence" (Stapp, 1971). Practically, this statement acknowledges the existence of many different factors that need to be considered when we study humans. It also seems logical that with all of these factors being able to vary, people will be different. Unfortunately, this very simple observation is largely ignored in biomechanical studies. Practically, biomechanics research investigates people not as individuals but as groups of individuals that are placed together in the same "bucket," or in other words, are grouped together in terms of statistics. This leads to the investigation of the "average performer" without this average performer resembling any of the individual performers. The end result of this statistical model is a group of average performers that all look identical, a group model. In reality, what should be the end result of the statistical model is information about each individual. This concept is typically ignored in biomechanics research. We do not believe that we can capture the complexity of humans in a generalized group model. This is truly evident when we consider that the human system feeds back on itself through continual experiences and changing perceptions (Bates, 1996). The group model and the data generated will give some information and concepts but will not really solve specific individual problems.

So how has biomechanics contributed so far in terms of running injuries? Two things need to be consider before we can answer this question. First is

the progression of scientific production and its delivery to the patient and second the steps of scientific inquiry as applied to this problem.

The progression of scientific production is shown in Fig. 3.1. The majority of scientists attempt to address problems relating to the biomechanics of running injuries by investigating groups of people (occasionally some of the scientists use individual models). This research work gave us science. From this science we have the production of general knowledge about how the system works and how things are affected regardless of whether group models are used. Next the practitioner needs to take this knowledge and treat individuals. This is primarily an art, as knowledge must be abstracted from these group models.

The steps of scientific inquiry are as shown in Fig. 3.2. The first two steps are *to describe* through descriptive experimentation that will hopefully allow us *to understand* or give us understanding especially at the application level for the podiatrist, the physical therapist, and others. Unfortunately, in biomechanics

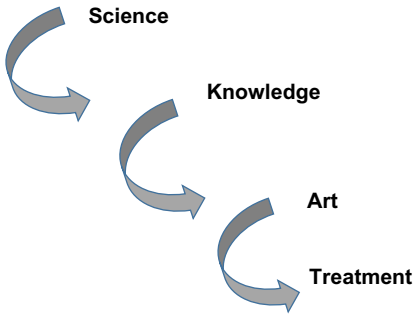

FIGURE 3.1
The progression of scientific production.

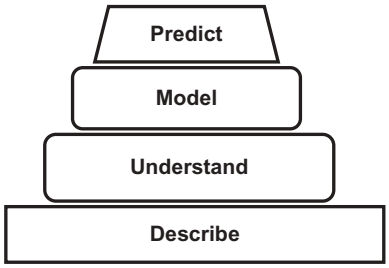

FIGURE 3.2
The steps of scientific inquiry.

many times we never go beyond this level. There are multiple reasons for this problem. One of them is that many scientists become too method-oriented. For example, how many more studies do we need on methods of placing markers or calibrating wearable technology devices? Many times, we praise a lifetime of study but truly what is really needed is not a lifetime but maybe a few months of systematic application of strong inference (Stergiou, 2019). Strong inference is an excellent model of scientific inquiry that emphasizes the need for alternative hypotheses (Platt, 1964).

The next step is *to model* or develop a general hypothesis of why running injuries occur and there are certainly some models in the literature. However, these models tend to describe the average person and not the individual (more in Section 3.2.1). Ultimately, we would like *to predict* outcomes and avoid injuries. However, even the development of models or general hypotheses has been difficult in biomechanics. We believe that this is due to a lack of application of strong inference as many scientists become too attached to their hypothesis and do not seek its disproof. However, as Platt (1964) states "a theory which cannot be mortally endangered cannot be alive." Always ask yourself what experiment will disprove your theory. When you go to a scientific meeting, ask the same question to other scientists. It will likely provoke very interesting discussions. On the other hand, being involved in science without a theory is similar to being lost in the middle of nowhere without a map. This is exactly why you need strong inference and its systematic application; to know where you are going in your scientific investigations. Therefore if we are going to propose a theory, we need to be able to propose experiments that will disprove this theory. Otherwise it is dogma. A good theory has two characteristics. It must (1) describe a large group of observations, and (2) provide predictions about the results of future observations (Hawking, 1998). Practically, a theory gives meaning to facts, just as a blueprint provides the structure that transforms stones into a house (Miller, 2002). If you have no theory or testable hypotheses, you just produce stones that lay around the yard.

Now let us get back to the really important question, how has biomechanics contributed so far in terms of running injuries? Biomechanics probably has allowed for fewer mistakes to be made in treating individuals just because of the general knowledge acquired through biomechanics research. We are not saying that biomechanics has not contributed, but we are saying that statistically we have the same number of injuries that we had 40 years ago. However, the treatment results have improved considerably because of the knowledge abstracted by the practitioners and transferred to treating individuals. Even though the knowledge provided to the practitioners is based on group statistics, practitioners utilize their skills to infer information at the

individual level in addition to using the information gathered directly from the patient at the time of visitation.

3.2 Biomechanical statistics

In this section, we will discuss certain aspects of statistics that are important to consider when someone performs investigations in biomechanics or evaluates biomechanics literature.

3.2.1 The single-subject approach for biomechanics and gait analysis

Let us initially consider the relationship between variability and strategy. Human movement variability can be described as the normal variations that occur in motor performance across multiple repetitions of a task (Stergiou, Harbourne, & Cavanaugh, 2006). Newell and Corcos (1993) stated that variability is inherent within and between all biological systems and is a result of interactions among the structural and functional characteristics of the system and the constraints imposed on motion. Because variability is an inherent component of movement both within and among individuals, one simply cannot replicate a movement pattern exactly given the various physical and environmental constraints surrounding the performance (Newell & Corcos, 1993).

Strategy, on the other hand, is a selected neuromusculoskeletal solution for the performance of a specific motor task (Bates, 1996). If we choose a particular strategy and we replicate it over multiple trials of the performance, then each of these trials will have inherent variability (intraindividual variability). Therefore strategy incorporates variability in each trial. For example, if we consider a specific strategy for flexing and extending our knee during walking (Fig. 3.3), we can observe a general configuration in our movement trajectory which includes two peaks (the second bigger than the first) with a valley between them. This strategy or self-selected neuromusculoskeletal solution for the performance of a motor task (i.e., walking) varies between and among trials or strides. This variability is clearly observed in the movement trajectories which do not perfectly overlap even though the general configuration always stays the same (Fig. 3.3). In Chapter 7, Coordination and control of gait, we also describe strategies as attractors and variability as the stability of the attractor using the dynamical systems theory approach.

To further understand the notion of strategy, we present some data from a biomechanical study in Fig. 3.4. In this experiment, we had five subjects landing under three different conditions (soft, normal, and stiff landings).

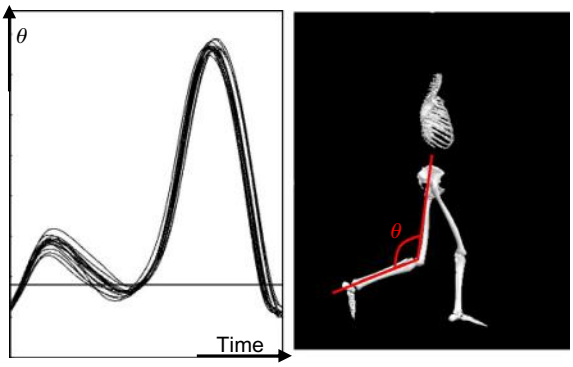

FIGURE 3.3
Here we can observe the strategy of the solution we selected to flex and extend our knee during walking. We also observe the variability from one trial to the next or from one stride to the next over this strategy, as the trajectories do not perfect overlap. Data are provided from the University of Nebraska Biomechanics Research Building database.

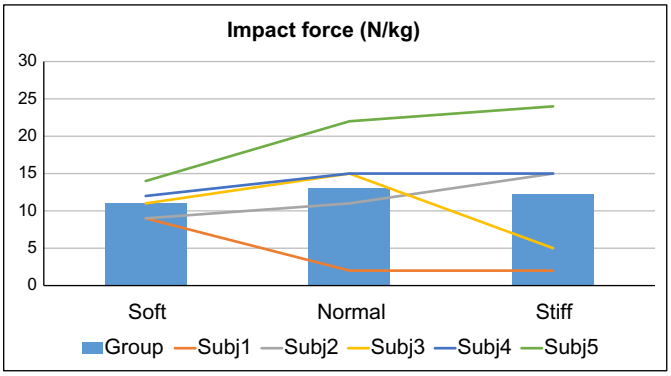

FIGURE 3.4
In this graph we observe impact ground reaction force data from three different landing conditions. It is evident that the group response reveals almost negligible differences between conditions, resulting in a lack of statistical significance in a group model. However, the five subjects have quite different responses. These individual responses are missed when all the subjects are group together. Data are provided from Dr. Barry Bates' personal database.

From a purely mechanical perspective, these three conditions are progressively more demanding, which allows us to hypothesize that the dependent variable, the impact ground reaction force, will increase. The group results are presented in bars, while the individual responses are presented in lines. It is evident that the group results/response reveals almost negligible differences between conditions, resulting in a lack of statistical significance for the group

model. However, the five subjects have quite different responses. Two of them use an accommodating strategy to the increasing mechanical demand by decreasing the impact force. The other three use an ignoring or acknowledging strategy by allowing the impact force to increase. Therefore the "average" person response, which is what we observe in the group results, is not the same as any of the individual responses. Statistically, the individual responses are compromised or missed when the subjects are grouped together.

Selection of a particular strategy can be voluntary or involuntary, but the execution of a strategy (to accomplish a task) results in a unique pattern of movement with its own pattern of intraindividual variability. Patterns of movement are constrained to respond to three peripheral sources of variation (constraints): mechanical or biomechanical, morphological, and environmental (Bernstein, 1967; Higgins, 1977). The intrasubject variability observed, as well as actual or real between-subject differences observed in human movement, is caused by these constraints. One critically important aspect of this constraint domain that influences strategy selection is related to the perceptions and experiences of the performer. For example, in response to the addition of ankle weights, a gymnast and a mountaineer would likely perceive the need to modify landing performance differently based on their past experiences relative to the weight of performance footwear, that is, slippers versus boots. Empirical evidence in support of individual strategies can be found in the research literature. Here we discuss selected examples across a variety of movement tasks and situations for illustrative purposes.

Bates, Osternig, and Mason (1979) identified unique performance characteristics among five elite runners that were initially masked using a group descriptive analysis approach. The "average" runner, as depicted by the mean data, did not resemble any of the individuals in the group. Dufek and Bates (1990), Dufek, Bates, Stergiou, and James (1995), and Dufek and Zhang (1996) examined the landing performance of elite volleyball players following execution of a blocking maneuver across the competitive season. The authors went on to create prediction models from kinematic variables during execution of the block that would predict landing impact forces. The results of their work, using both a group and an individual approach, produced group prediction models for forefoot and rearfoot landing force that were not representative of any of the individual volleyball players evaluated. The general (group) model was that of an "average" performer not representative of any single athlete participating in the study. Some additional individual strategy examples in the biomechanics literature can be seen in other studies (Cavanagh & Kram, 1989; Jensen & Phillips, 1991; Judkins, Oleynikov, &

Stergiou, 2008; Reinschmidt & Nigg, 1995; Simpson & Pettit, 1997; Stergiou & Scott, 2005).

Another area in which strategies can influence conclusions is that of learning and/or motor skill acquisition experiments. Schmidt, Treffner, Shaw, and Turvey (1992) stated that acquisition of motor skills involves the successive parameterization of a dynamical control structure in the direction of increasing stability. The authors went on to indicate that the intentional process of parameterization is itself dynamical. The process of motor skill acquisition is both dynamic and variable; therefore, it should be apparent that performance options exist for individual subjects and that when combined in a group analysis, these individual learning effects could be obscured. In their work, Schmidt et al. (1992) did identify two unique strategies for the acquisition of the interlimb movement pattern under investigation. Worringham (1993) also examined motor skill acquisition via the evaluation of spatial variability associated with complex arm movement tasks. Worringham made a priori awareness of subject differences clear, and in an attempt to gain statistical power in the experiment, the importance of avoiding any subject grouping was stressed. The author implied that the need to understand acquisition of the skill was possibly more important than incorporating traditional statistical treatment techniques during data analysis. Benzecri and Benzecri (in Loslever, 1993) further emphasized Worringham's point when they stressed the importance of developing one's model to fit the data rather than forcing one's data into a model. Loslever (1993) further suggested that it is often unreasonable to expect a single model to fit all subjects in a given study because of excessive between-subject variability that could result from individuals' use of unique strategies. Thus the author suggested that the model should be adjusted for each class of behavior identified, which in practice would require examination of subjects at a deeper level than as members of the group. Lastly, Schlaug, Knorr, and Seitz (1994) investigated intersubject variability of cerebral activation patterns during the acquisition of a complex sequential finger movement pattern. The results of group mean activation images illustrated some consistent task-specific activation sites in the brain; however, there was little or no spatial overlap of these patterns among subjects. The observed individual changes suggested a prominent inter- and intraindividual plasticity of cerebral activation patterns.

3.2.2 Bringing together running injuries and the single-subject approach

Impact forces have been implicated as a major cause of running injuries (James et al., 1978; van Mechelen, 1992). Protection of the body from excessive impact forces has been considered as one of the primary functions of

sport shoes (Bates, James, Osternig, & Sawhill, 1983; Nigg & Segesser, 1992). Two methods have been identified for evaluating the abilities of sport shoes to absorb these forces. These two methods are: (1) in vitro evaluation using impact testing equipment (Frederick, 1984) and (2) in vivo evaluation of individuals running across a force platform (Bates et al., 1983). Interestingly, the in vitro tests are always able to differentiate shoes in terms of their cushioning abilities, while a lack of correlation has been observed when in vitro results have been related with in vivo results (Frederick, 1984; Kaelin, Denoth, Stacoff, & Stuessi, 1985; Nigg, Bahlsen, Luethi, & Stokes, 1987). This lack of correlation has generally been attributed to kinematic adjustments brought about by adaptation mechanisms (Clarke, Frederick, & Cooper, 1983; Frederick, 1984; Kaelin et al., 1985; Nigg et al., 1987). This lack of relationship is contradictory to considerable anecdotal evidence in the medical/sports medicine profession, which suggests that improper footwear can cause injury and that a shoe change can in fact facilitate the healing process in some instances (Arnold & Moody, 2018; Becker, 1989; James et al., 1978; McKenzie, Clement, & Taunton, 1985; Tenforde et al, 2016).

As we suggested previously, these conflicting results could be due to intersubject variability that could result in false support for the null hypothesis (no observed differences; Fig. 3.4). Practically, subjects could be responding differentially to shoe conditions, that is, using different performance strategies, which can result in minimal or no observed condition effects (Bates, 1996). To address this issue, Bates and Stergiou (1996) performed a study that investigated the effects of individual response patterns on the results obtained from a more traditional and commonly accepted group analysis approach. In order to achieve their purpose, the experimental design used was a shoe condition by subjects nested in shoe hardness [Shoe Condition × (Subject × Shoe Hardness)] (Keppel, 1991). The factors of shoe hardness and shoe condition were determined from in vitro tests. Six production shoes from several manufacturers were selected and evaluated using an Impact Testing System (Exeter Research Inc.). Based upon these test results, shoes were assigned to the shoe condition and shoe hardness factors. The two softest shoes were identified as the soft shoe condition. The next two shoes in hardness were classified as the medium shoe condition, with the final two designated as the hard shoe condition. The shoes within each condition were categorized as soft or hard based upon the same tests. Furthermore, the dependent measures of ground reaction impact force and maximum knee flexion during stance were acquired through in vivo testing from 18 runners.

Bates and Stergiou (1996) used a single-subject procedure (Model Statistic: Bates, 1996; Bates, James, & Dufek, 2004) in addition to the group design. The Model Statistics technique was developed to take advantage of the repeated measures concept associated with within-subject experiments rather

than use an independent technique that lacks comparison sensitivity. On the assumption that the single-subject analyses would produce both statistically significant and nonsignificant responses to the shoe hardness conditions, the next step in the Bates and Stergiou (1996) analysis was to regroup the subjects based upon these results into two distinct groups for subsequent analyses. This second group evaluation employed a series of repeated measures ANOVA (Subjects × Hardness) analyses on the dependent variables for each of the two groups ($P < .05$). Finally, Bates and Stergiou performed a series of correlations for the dependent variables using the original group of 18 subjects and the two subgroups identified using the single-subject analyses.

The group ANOVA analyses resulted in no significant interactions between the two factors for the two dependent variables. Similar results of no significant differences were observed for the main effects of shoe condition. Significant differences ($P < .05$) were only identified between mean impact forces for the soft shoe condition and mean maximum knee flexion angles for the hard shoe condition. The single-subject analyses identified no significant ($P < .05$) impact force differences for eight subjects, while 10 subjects exhibited significant differences. Post hoc group analyses identified a relationship ($r = 0.6$) between in vitro and in vivo results for the 10-subject subgroup. Importantly, the correlation coefficient for the total group (18 subjects) was a nonsignificant 0.06. Bates and Stergiou (1996) also took a closer look at the 10 subjects that exhibited significant responses, which were distributed among the three shoe conditions with five, two, and three occurring in the soft, medium, and hard conditions, respectively. All significant results were in the expected direction, with the hard shoe producing greater values than the soft shoe. The eight nonsignificant responses were evenly distributed in both directions. The distribution of significant and nonsignificant individual responses, along with the directions and magnitudes of these responses, at least partially explained the outcome of the group analysis. The significant response distributions among the three shoe conditions also indicated that subjects were less likely to change their performance strategy (adapt) for shoes having the best cushioning properties. From these results it does not appear that adaptation within the temporal constraints of this type of experiment is a consistent and universal mechanism used by individuals as suggested by other researchers (Clarke et al., 1983; Kaelin et al., 1985; Nigg et al., 1987).

The differential response patterns observed by Bates and Stergiou (1996) seem perfectly reasonable since it is unlikely that individuals will come to an experimental setting with the same experiences and have the same perceptions of the environment (different shoes) which are necessary to produce the same performance adjustments. Given the vast number of possible influencing factors it is more likely than not that response strategies will occur

along a continuum from purely Newtonian, where the differences are completely ignored (impact forces values increase mechanically and predictably), to purely neuromuscular, where the system totally accommodates to the differences between conditions resulting in equal impact force values. A group by condition experiment simply dichotomizes and supports one of the extreme positions on the continuum depending upon the predominance of individual performances along the continuum and the researchers' ability to detect real differences of a certain magnitude, that is, statistical power relative to effect size. Evaluation of an individual subject dichotomizes performance about a point on the continuum in a similar manner.

Bates and Stergiou (1996) summarized that the ultimate goal of research is to gain a better understanding of the underlying mechanisms of performance, while the goal of an individual experiment should be to maximize the amount of information made available. The more complex less traditional designs could allow for the evaluation of the data from several different perspectives, which could provide additional insight into the interactive nature between performer response patterns and analysis technique. Subjects can and do respond differently to the same perturbation and these differential responses can compromise group analysis results. Since we are dealing with biomechanics, we should never ignore the "bio" component. Response patterns or strategies appear to lie on a continuum between purely Newtonian or mechanical and purely neuromuscular or accommodating (more on this matter in Chapter 4: Why and how we move: the Stickman story). Bates and Stergiou (1996) concluded in their results that although some adaptation is usually exhibited by most subjects, some of the previously reported nonsignificant differences between shoe conditions could have been the result of differential adaptation patterns and/or nonsufficient statistical power. These findings further suggest the need to modify the way we approach the study of some human performance problems, especially where individual results, such as injury and performance enhancement, are important.

3.3 Final considerations

A difficult task for most of us is changing the way we think. We feel more secure processing information in our traditional ways. We must be willing to try alternative approaches, or at least let others try them. The advancement of science is often dependent on alternative measurement procedures. It is important to remember that measurement is not neutral and that all measurement schemes lose more information than they gather, no matter how thorough and well-conceived they may be. In addition, we all have biases—we cannot "study anything separate from ourselves. Our acts of observation are part of the process that brings forth the manifestation of what we are

observing" (Wheatley, 1992, p. 36). We choose what we study and how we study it, including the experimental methods, the controls, the independent and dependent variables, and the analysis techniques. Since all outcomes are dependent on the state of the organism interacting with the environment at a specified moment in time, much information is lost forever. Furthermore, the data cannot be duplicated even through study replication. How then can we retrieve the data we lost when we went looking for the data we found? One way is to encourage as many research approaches as possible. In this way we maximize our chances of discovering variations of those lost data that might further our understanding of the underlying mechanisms and processes controlling human movement. Researchers using traditional group methodology are seeking "generalizability" and believe that this goal can be achieved as soon as all of the variables can be accounted for. Some system components and processes are undoubtedly generalizable within limited definable constraints, but as a total, self-actuated system, the "human" is seldom predictable (Stapp, 1971), making it unlikely that this complex system can be captured in a single generalized model. After all, the human system continuously feeds back on itself through experiences and the resulting changing perceptions. This fact—that we are complex, continuously changing interactive systems, each possessing "uniqueness"—not only justifies but sometimes also dictates the use of individual evaluations to better understand individual movement patterns.

3.3.1 Take home messages

Here are some take home messages for the biomechanists and the gait analysts that will read this book.

1. We are not suggesting you change the way you view/do your research but that you keep an open mind about the way others view/choose to do their research.
2. Be aware of strengths and limitations of various statistical procedures. Statistics is a "tool" to help scientists and not guide the way they do science like some commands written on stone.
3. Be aware of the bases and constraints influencing performance/movement and the possible effects on the best research approach.
4. To ultimately acknowledge the value of single-subject methodology for some research problems. At the end of the day clinicians do so every time they see a patient and perform a gait analysis for any clinical reason.

References

Arnold, M. J., & Moody, A. L. (2018). Common running injuries: Evaluation and management. *American Family Physician, 97*, 510–516.

Asplund, C., & Tanner, S. M. (2004). The runner. In R. B. Birrer, & F. G. O'Connor (Eds.), *Sports medicine for the primary care physician* (pp. 223–231). Boca Raton, FL: CRC Press.

Bates, B. T. (1996). Single-subject methodology: An alternative approach. *Medicine and Science in Sports and Exercise*, *28*, 631–638.

Bates, B. T., James, C. R., & Dufek, J. S. (2004). Single subject analysis. In N. Stergiou (Ed.), *Innovative analyses of human movement.* (pp. 3–28). Champaign, IL: Human Kinetics Publications.

Bates, B. T., James, S. L., Osternig, L. R., & Sawhill, J. A. (1983). An assessment of subject variability, subject-interaction, and the evaluation of running shoes using ground reaction force data. *Journal of Biomechanics*, *16*, 181–191.

Bates, B. T., Osternig, L. R., & Mason, B. R. (1979). Variations in velocity within the support phase of running. In J. Terauds, & G. Dales (Eds.), *Science in athletics.* (pp. 51–59). Del Mar, CA: Academic Press.

Bates, B. T., & Stergiou, N. (1996). Performance accommodation to midsole hardness during running. *Journal of Human Movement Studies*, *31*, 189–210.

Becker, N. L. (1989). Specific running injuries and complaints related to excessive loads–Medical criteria of the running shoe. In B. Segesser, & W. Pforringer (Eds.), *The shoe in sport* (pp. 16–25). London: Wolfe Publishing.

Bernstein, N. (1967). *Coordination and regulation of movement*. Oxford: Pergamon Press.

Brown, C. R. (2013). Common injuries from running. In J. B. Imboden, D. B. Hellmann, & J. H. Stone (Eds.), *Current diagnosis and treatment: Rheumatology* (3rd ed.). New York: McGraw-Hill.

Cavanagh, P. R., & Kram, R. (1989). Stride length in distance running: Velocity, body dimensions, and added mass effects. *Medicine and Science in Sports and Exercise*, *21*(4), 467–479.

Clarke, T. E., Frederick, E. C., & Cooper, L. B. (1983). Biomechanical measurement of running shoe cushioning properties. In B. M. Nigg, & B. A. Kerr (Eds.), *Biomechanical aspects of sport shoes and playing surfaces* (pp. 25–33). Calgary, AB: The University of Calgary Press.

Dufek, J. S., & Bates, B. T. (1990). The evaluation and prediction of impact forces during landings. *Medicine and Science in Sports and Exercise*, *22*(3), 370–377.

Dufek, J. S., Bates, B. T., Stergiou, N., & James, C. R. (1995). Interactive effects of group and single-subject response patterns. *Human Movement Science*, *14*, 301–323.

Dufek, J. S., & Zhang, S. (1996). Landing models for volleyball players: A longitudinal evaluation. *Journal of Sports Medicine and Physical Fitness*, *36*, 35–42.

Frederick, E. C. (1984). *Sport shoes and playing surfaces*. Champaign, IL: Human Kinetics.

Hawking, S. W. (1998). *A brief history of time*. London: Bantam.

Higgins, J. R. (1977). *Human movement: An integrated approach*. St. Louis, MO: C.V. Mosby.

Hoeberigs, J. H. (1992). Factors related to the incidence of running injuries. A review. *Sports Medicine*, *13*, 408–422.

James, S. L., Bates, B. T., & Osternig, L. R. (1978). Injuries to runners. *American Journal of Sports Medicine*, *6*, 40–50.

Jensen, J. L., & Phillips, S. J. (1991). Variations on the vertical jump: Individual adaptations to changing task demands. *Journal of Motor Behavior*, *23*(1), 63–74.

Judkins, T. N., Oleynikov, D., & Stergiou, N. (2008). Objective evaluation of expert performance during human robotic surgical procedures. *Journal of Robotic Surgery*, *1*(4), 307–312.

Kaelin, X., Denoth, J., Stacoff, A., & Stuessi, E. (1985). Cushioning during running—Material test contra subject test. In S. Perren, & E. Schneider (Eds.), *Biomechanics current interdisciplinary research* (pp. 651–656). Dordrecht: Martinus Nijhoff Publishers.

Keppel, G. (1991). *Design and analysis: A researcher's handbook*. Englewood Cliffs, CA: Prentice-Hall Inc.

Koplan, J. P., Powell, K. L., Sikes, R. K., Shirley, R. W., & Campbell, G. C. (1982). An epidemiological study of the benefits and risks of running. *Journal of the American Medical Association*, *248*, 3118–3121.

Loslever, P. (1993). Error and data coding in the multi-dimensional analysis of human movement signals. *Proceedings of the Institute of Mechanical Engineers*, *207*(2), 103–110.

Lysholm, J., & Wiklander, J. (1987). Injuries in runners. *American Journal of Sports Medicine*, *15*, 168–171.

Marti, B., Vader, J. P., Minder, C. E., & Abelin, T. (1988). On the epidemiology of running injuries. *American Journal of Sports Medicine*, *16*, 285–294.

McKenzie, D. C., Clement, D. B., & Taunton, J. E. (1985). Running shoes, orthotics, and injuries. *Sports Medicine*, *2*, 334–347.

Miller, P. H. (2002). *Theories of developmental psychology*. (4th ed.). New York: Worth Publishers.

Newell, K. M., & Corcos, D. M. (1993). Issues in variability and motor control. In K. M. Newell, & D. M. Corcos (Eds.), *Variability and motor control* (pp. 1–12). Champagne, IL: Human Kinetics.

Nigg, B. M., Bahlsen, H. A., Luethi, S. M., & Stokes, S. (1987). The influence of running velocity and midsole hardness on external impact forces in heel-toe running. *Journal of Biomechanics*, *20*, 951–960.

Nigg, B. M., Baltich, J., Hoerzer, S., & Enders, H. (2015). Running shoes and running injuries: Mythbusting and a proposal for two new paradigms: 'Preferred movement path' and 'comfort filter'. *British Journal of Sports Medicine*, *49*, 1290–1294.

Nigg, B. M., & Segesser, B. (1992). Biomechanical and orthopedic concepts in sport shoe construction. *Medicine and Science in Sports and Exercise*, *24*, 595–602.

Platt, J. R. (1964). Strong inference. Certain systematic methods of scientific thinking may produce much more rapid progress than others. *Science*, *146*(3642), 347–353.

Reinschmidt, C., & Nigg, B. M. (1995). Influence of heel height on ankle joint moments in running. *Medicine and Science in Sports and Exercise*, *27*(3), 410–416.

Schlaug, G., Knorr, U., & Seitz, R. J. (1994). Inter-subject variability of cerebral activations in acquiring a motor skill: A study with positron emission tomography. *Experimental Brain Research*, *98*, 523–534.

Schmidt, R. C., Treffner, P. J., Shaw, B. K., & Turvey, B. T. (1992). Dynamical aspects of learning an interlimb rhythmic movement pattern. *Journal of Motor Behavior*, *24*(1), 67–83.

Simpson, K. J., & Pettit, M. (1997). Jump distance of dance landings influencing internal joint forces: II. Shear forces. *Medicine and Science in Sports and Exercise*, *29*(7), 928–936.

Stapp, J. P. (1971). Closing remarks: The future. In *Symposium of biodynamic models and their applications*. AMRL_TR_71_29. Wright-Patterson Air Force Base, OH.

Stergiou, N. (2019). *Advice for the novice investigator: Examples taken from movement sciences*. Boca Raton, FL: CRC Press.

Stergiou, N., Harbourne, R. T., & Cavanaugh, J. T. (2006). Optimal movement variability: A new theoretical perspective for neurologic physical therapy. *Journal of Neurologic Physical Therapy*, *30*, 120–129.

Stergiou, N., & Scott, M. M. (2005). Baseline measures are altered in biomechanical studies. *Journal of Biomechanics*, *38*(1), 175–178.

Tenforde, A. S., Yin, A., & Hunt, K. J. (2016). Foot and ankle injuries in runners. *Physical Medicine and Rehabilitation Clinics of North America*, *27*, 121–137.

van Mechelen, W. (1992). Running injuries. A review of the epidemiological literature. *Sports Medicine*, *14*, 320–335.

Walter, S. D., Hart, L. E., McIntosh, J. M., & Sutton, J. R. (1989). The Ontario cohort study of running related injuries. *Archives of Internal Medicine*, *149*, 2561–2564.

Wheatley, M. J. (1992). *Leadership and the new science: Learning about organization from an orderly universe*. San Francisco, VA: Berrett-Koehler Publications.

Worringham, C. J. (1993). Predicting motor performance form variability measures. In K. M. Newell, & D. M. Corcos (Eds.), *Variability and motor control* (pp. 53–63). Champaign, IL: Human Kinetics.

CHAPTER 4

Why and how we move: the Stickman story

Barry T. Bates[1], Janet S. Dufek[2] and Nick Stergiou[3]
[1]University of Oregon, Eugene, OR, United States, [2]University of Nevada Las Vegas, Las Vegas, NV, United States, [3]University of Nebraska at Omaha, Omaha, NE, United States

CONTENTS

> The vain presumption of understanding everything can have no other basis than never having understood anything. For anyone who had ever experienced just once the perfect understanding of one single thing, and had truly tasted how knowledge is accomplished, would recognize that of the infinity of other truths he understands nothing.
>
> **Galileo Galilei (1564–1642)**

4.1 Briefly introducing Stickman

What we are interested in is why we move and how we move. To attack this problem, we will present the story of the Stickman. The title Stickman was given to the intellectual work presented in this chapter, by Dr. Bates' former students to honor his artistic abilities as displayed in Fig. 4.1. Importantly, we should note that Stickman and Stickwoman are essentially equal and all performance information will be equally applicable.

4.2 The Stickman's evolution of movement

Why should we study movement? First, to better understand the underlying processes and mechanisms of movement. In practice, how things work. Second, to enhance our knowledge regarding the acquisition and understanding of motor skills/movement patterns. Third, to better understand the facilitation of development at all performance levels from the physically challenged to the highly skilled.

In this section, we overview selected aspects of human movement performance and gain an appreciation of its complex interactions. These complex

Biomechanics and Gait Analysis. DOI: https://doi.org/10.1016/B978-0-12-813372-9.00004-X

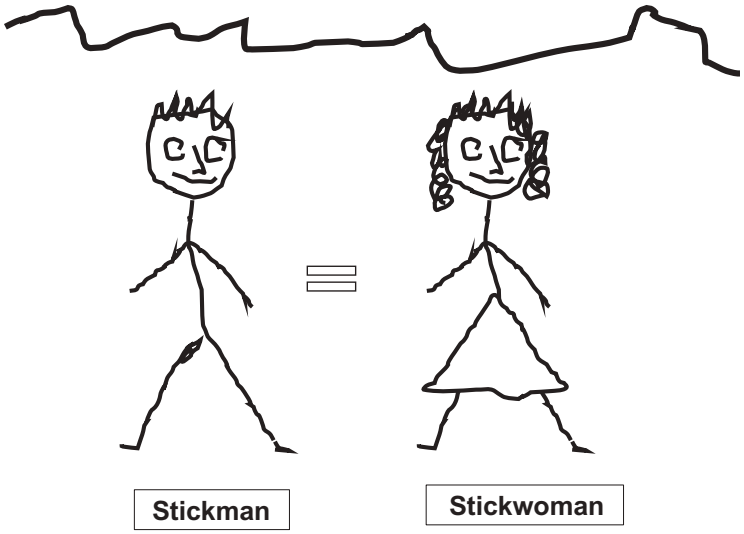

FIGURE 4.1
The Stickman and Stickwoman as drawn by Dr. Barry Bates. His artistic abilities are clearly displayed.

interactions vary and are quite different from individual to individual and in total they present a dilemma to Stickman in executing motor skills and movement patterns (Fig. 4.2).

To begin with we have to examine Stickman's similarities and differences with others. In more detail, the question becomes, "Are we unique or different?" We can examine this from several perspectives including:

1. anatomical structure;
2. functional capabilities (how the system completes its tasks);
3. individual experiences; and
4. individual goals.

The first two perspectives express the fact that we are essentially the same. There are minor differences but the general structure and capabilities of each individual are very similar. On the other hand, experiences and goals (perspectives 3 and 4) are mostly different among individuals and, therefore, they will influence various aspects of movement and human performance.

From this perspective, an overall conceptual model of Stickman as an individual is presented in Fig. 4.3. First, we need to consider the conscious thoughts, the mind. Second, within the mind we have the subconscious, an area that lies below the level of consciousness. It is always there and everything enters the subconscious, unless we consciously reject it. Third, is the command center that takes all the information and generates commands that

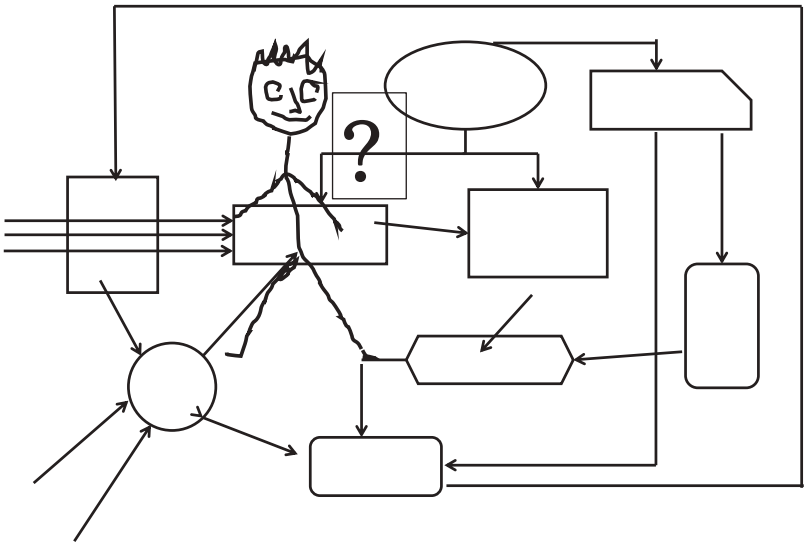

FIGURE 4.2
The complex interactions of human movement and performance present a dilemma to Stickman in executing motor skills.

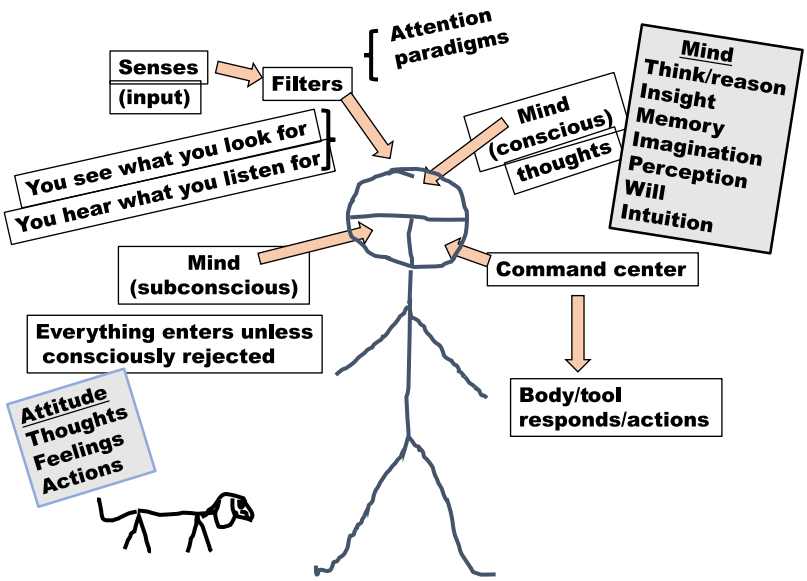

FIGURE 4.3
An overall conceptual model of the Stickman as an individual.

represent the tool, the body, and how it responds with appropriate actions. Obviously, the mind is not divided into parts as they are all interconnected, but this is a conceptual model as previously indicated. With respect to input, information is gained from the environment through the senses (hearing, sight, smell, taste, and touch). All information from the senses is subject to possible and potential filters, which are influenced by previous experiences, prior to entering the mind. In other words, you see what you look for and sometimes you miss things that you are not looking for, or you hear what you are listening for and miss other important information that may be in the environment. Factors that also affect the input information include the attention we pay and the paradigms we have developed from past experiences that influence what we are going to look for or listen to. Another aspect of the performance is attitude, which includes some of our thoughts, feelings, actions, and how they influence what we do and why we do it. Finally, it is the mind itself where we can identify some of the functions that are helpful and related and provide some unique advantages. Such functions include:

1. *Reason/think*: the ability to form in the mind, to determine, to relate.
2. *Insight*: the ability to override instinctive behavior.
3. *Memory*: the ability to store and retrieve information/experiences.
4. *Imagination*: the ability to form a mental image of something not present and never before experienced in reality, creative ability, and combining parts into a new whole.
5. *Perception*: the ability to interpret sensations based upon experience, intuitive cognition, and how we view things.
6. *Intuition*: the ability to have quick and ready insight, power of attaining direct knowledge/cognition without evident rational thought, and reference.
7. *Will*: the ability to have persistence, determination, power of control over one's emotions/actions.

Having examined a conceptual model of the performer, we next want to examine movement itself (Fig. 4.4). Movement consists of two fundamental components, time and space. This is a physics perspective. However, since we are interested in human movement we have to add the neuro-musculoskeletal system, the "bio," to these components. Finally, we need to consider what is happening in the real world and, thus, we have to add two forces that are always present that we can never avoid. One is gravity and the other is friction. A famous physiologist called Sir Charles Scott Sherrington (1857–1952; Nobel prize in physiology in 1932) once stated that "all man can do is move" (Sherrington, 1951). We believe that this is shortsighted and we would like to modify this as "all man can do is *apply force*." This is a perspective from a biomechanist as opposed to a physiologist. As an example

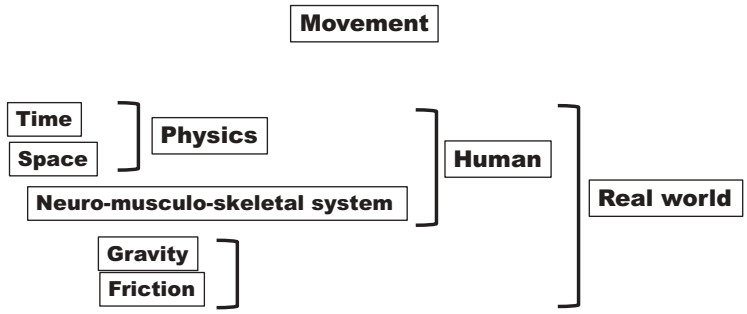

FIGURE 4.4
The components of movement.

to illustrate our perspective, we can be standing on the floor and we apply force to the floor, but there is no movement involved. So, force is applied, yet it does not result in movement (no disrespect meant to Sir Sherrington!).

A related statement was made by Colonel John Stapp (1910–99), who was a US Air Force officer, flight surgeon, physician, biophysicist, and pioneer in studying the effects of acceleration and deceleration forces on humans. He stated the following (Stapp, 1971): "This fifty-liter rawhide bag of gas, juices, jellies, gristle and threads movably suspended on more than 200 bones presided over by a cranium, seldom predictable and worst of all living, presents a challenge to discourage a computer into incoherence." This statement clearly describes the complexity of what we are as humans. In order to incorporate movement to this complexity, it is even more challenging.

So what are we from a movement perspective (Fig. 4.5)? We are creatures of experience. When we are born we have no experiences and nothing internal. However, we immediately start having experiences (many occur inside the womb as well) which are behavioral (movement) and cognitive (mind). These experiences form memories. Once we have memories, they allow us to have perceptions and expectations of what we may be facing in a future moment. The perceptions and expectations lead us to make assumptions about our environment, the world around us, and how are we going to interact with it. These assumptions allow us to pursue thoughts and actions (a task) in order to pursue our objectives. Once we have a thought or have carried out an action, it immediately becomes an experience that feeds back into the experiences that become memories and the whole process repeats itself.

Given this feedback loop, let us take a closer look at *task*. What is a task and what are the tasks that we are concerned with? We are concerned with

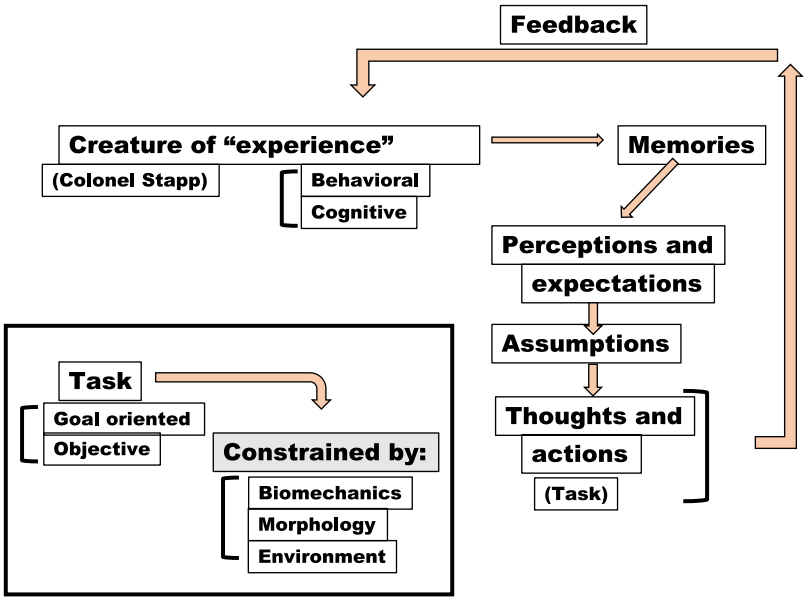

FIGURE 4.5
A schematic of what we are as humans from a movement perspective.

goal-oriented movements that are also objective. As such, reflexes are not part of this model. These tasks are constrained or limited by a number of factors. These factors are biomechanical (the laws of physics and motion), morphological (our total make up of body, mind, experiences, memories, etc.), and environmental (all the external information that we get through our sensory system) (Higgins, 1985).

Next we want to examine feedback from another perspective. The various phases from memories to perception to assumptions to thoughts, all require time which is indicated by ΔT (change in time) in Fig. 4.6. This means that when we are going to perform a movement, we have to deal with neuromuscular constraints that predispose us to what and when we can do something in a feedforward setting. Thus we are always in the process of projecting our thoughts and movements into the future and therefore there is always a chance for error. The better our memories and the better and more often we repeat something, the shorter these times (latencies) become and we get from memories to actions in much quicker time. The feedforward system leads us into living in a world where we always make assumptions and predictions relative to what we are doing and what we are going to do. Even with the feedforward system in place, once we complete an action it goes

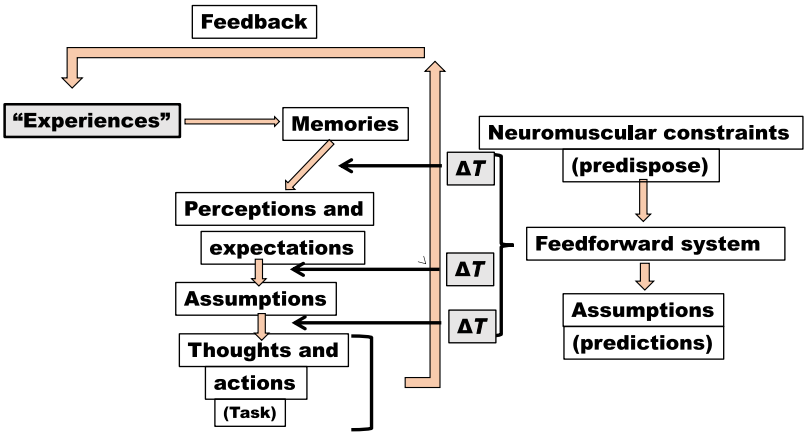

FIGURE 4.6
A schematic of our feedback system along with our feedforward system that allows for the generation and improvement of movement performance.

back into the feedback loop as another experience/memory resulting in shorter ΔTs with repetition.

4.3 The Stickman's performance of movement

As previously discussed, we are interested in goal-oriented movements that are also objective. These goal-oriented objective movements or tasks are constrained or limited by a number of factors. These factors are biomechanical (the laws of physics and motion), morphological (our total make up of body, mind, experiences, memories, etc.), and environmental (all information that we get through our sensory system) (Higgins, 1985). Let us examine these constraints in more detail.

Below we identify some specific factors that constrain our performance and that we should always be aware of:

1. Structure
   a. Anatomical
   b. Neuromuscular functions
2. Sensory motor development
3. Physiological regulation
4. Psychological stressors
5. Social factors
6. Mechanical stressors
7. Environmental considerations

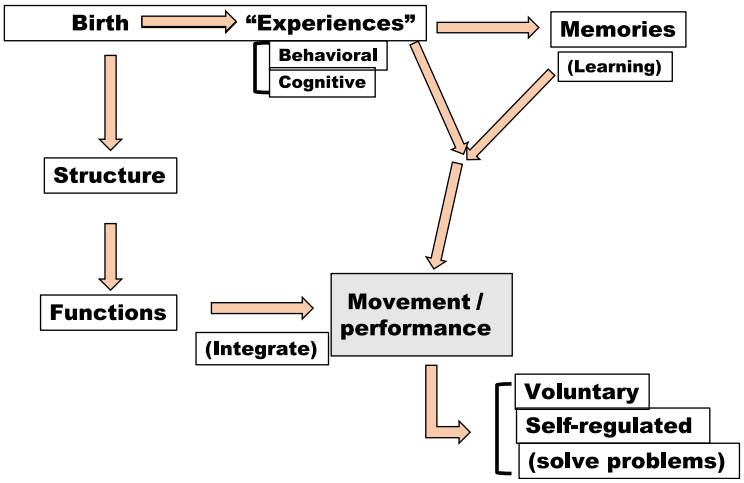

FIGURE 4.7
A motor development-based model of movement.

The task itself can also be viewed as a constraint. However, we prefer to view it as a problem and thus movement as a problem-solving process. This process starts at birth when we start acquiring experiences that form memories (Fig. 4.7). We start as infants with no experiences or memories but we have a basic structure which is inherent and has fundamental functions (see the first two bullets above). For example, the elbow or the shoulder can perform certain functions such as flexion–extension, rotation, and others. We use these fundamental functions to create the movement patterns that we are interested in performing, and we integrate these functions along with our experiences and memories into movement performance. However, we also have to consider time since the structure will be changing over time as a result of maturation, thus affecting functions which further influence movement.

Structure is a constraint that arises from a number of sources. First is the genetic bases which are very similar among all humans with slight individual uniquenesses. Second is a hardwired lever and pulley system consisting of muscles, bones, and connective tissue. Third are the innate reflexes that can affect goal-oriented movements. Finally, fourth is random patterns of the structure that have inherent characteristics or, in other words, certain movement patterns that exist in the body are predetermined by the structure. To better understand this last source, consider for example the so-called stepping reflex in infants (Thelen, 1986).

Structure, as we mentioned above, has certain fundamental functions. For example, joint rotations, flexions/extensions, and others. They are built into

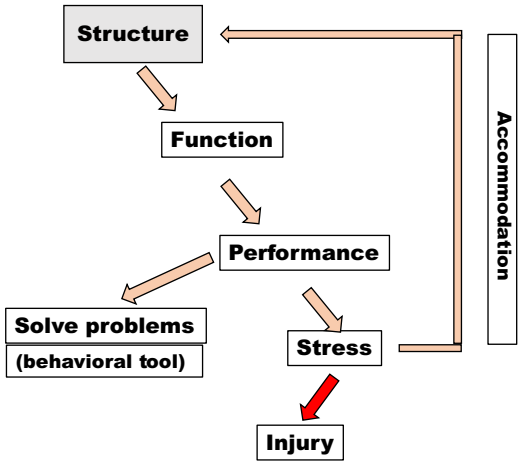

FIGURE 4.8
A model of injury as part of movement performance.

the system as functional components which allow us to create performances. We put together or combine these functional components to perform more complex movement patterns such as throwing. The parts, the functional components, are inherent and what we learn is how to combine them. This is a possible problem that we want to solve in order to perform throwing. Furthermore, when we perform a movement, the structure and the involved components are stressed. This stress results in feedback or accommodation to the structure, itself resulting in modifications. This is a continuous looping process. Different movements will also produce different modifications. If the system is overstressed, an injury can result (Fig. 4.8).

4.4 The Stickman learns how to move

Previously (Fig. 4.7), we stated that movement is a problem-solving process viewed as a voluntary-type action that is self-regulated or controlled by the individual. There are two possibilities for these types of movements, reactive, and proactive. As reactive, we consider movements that are not reflexes but are reflexive or conditioned reflexes. In other words, these are movements that we learned through continuous repetition or response to an external force perturbing the system (e.g., when a force tends to throw us off balance). As proactive we consider movements that are purposeful and skilled, which with practice can result in highly skilled performances. If we evaluate voluntary movement regarding how it is being performed, then we can infer

about the integration or character of movement which reflects its organizational status and the ability to resolve constraining factors.

Therefore learning how to perform movements is critical to solving problems. This learning process involves certain steps. The first step is to observe or describe the movement based on visual (show me) or auditory (tell me) information. There is also a possibility of imagining or creating the movement but this is usually only the case for extremely skilled individuals. This step involves the senses and the imagination. The second step is to conceptualize or understand the movement based on thinking and visualizing it in our memory. This step involves the mind. The third step is to internalize or translate the movement. This is where the movement transforms from an idea to a set of motor commands for the muscles to execute the movement. This step involves the motor cortex, the command center. The final step is to execute the movement. This step involves the neuro-musculo-skeletal system. After this step, a feedback loop starts where the entire process is repeated many times or practiced in order to become highly skilled at mastering the movement (Fig. 4.9).

Referring back to our simple model of experiences and memories in Fig. 4.7, we identified movement as a self-regulated voluntary action. Given our ability to self-regulate our actions, we are capable of choosing different solutions or strategies to accomplish a given task. A strategy is the self-selected neuro-musculo-skeletal response that we choose to solve a particular problem for the performance of a motor task. To better understand the notion of

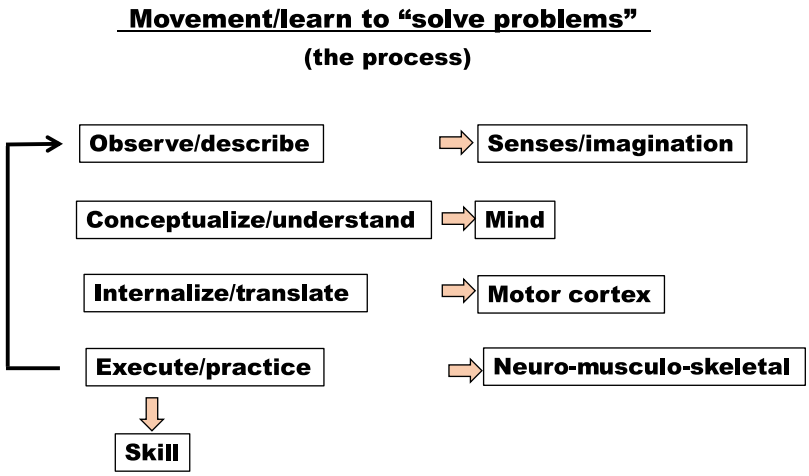

FIGURE 4.9
The process of learning a movement.

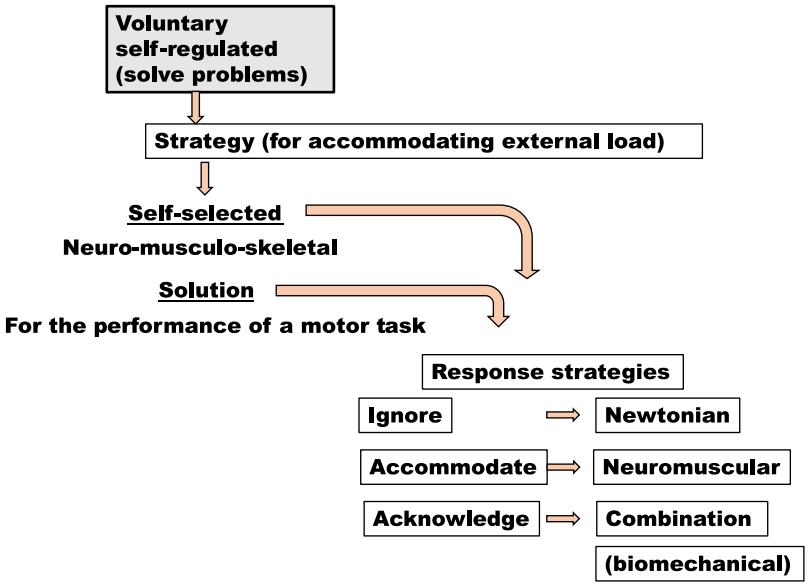

FIGURE 4.10

Further expanding the motor development-based model of movement in Fig. 4.7, we add strategies that produce individual differences in our responses during the performance of a motor task.

strategies, let us use as an example how we accommodate to an external load (Fig. 4.10). In particular, let us consider stepping off a three-foot platform. Doing so will result in a certain amount of ground reaction impact force when we land on the ground based upon our chosen neuro-musculo-skeletal response. Next, let us add weight in the form of a backpack and repeat the task. One extreme strategy would be to ignore this additional weight (using the same neuro-musculo-skeletal response) resulting in a Newtonian or mechanical response consistent with the laws of physics. In this situation the ground reaction impact force will be greater and equal to the previous force without the backpack plus the force generated by the added weight. Another extreme response would be to use a modified neuro-musculo-skeletal response (a different strategy) to fully accommodate to the extra weight (James, Atkins, Dufek, & Bates, 2014; James, Atkins, Yang, Dufek, & Bates, 2015; James, Bates, & Dufek, 2003; Nordin, Dufek, James, & Bates, 2017). In this situation we make perfect adjustments to the way the muscles work by producing a softer landing that results in keeping the ground reaction impact force equal to what it was without the backpack. In between these two extremes, there are an infinite number of possibilities of partially acknowledging the added weight, resulting in ground reaction forces between the two extremes. This is what happens most of the time and is accomplished by

using a combination of the previous two responses or a biomechanical response, which practically means that we use both bio and mechanics. Adjustments are made but they are not perfect and as indicated, the ground reaction forces will be greater than the neuromuscular but lesser than the Newtonian response.

Placing these responses on a graphical model (Fig. 4.11), we have on the *x*-axis the applied stressor (adding weight/load) and on the *y*-axis the external impact force (what happens to the impact force). The force can go from some lower limit to some upper limit. If we were to be fully accommodating or, in other words, to perfectly predict the load and its effect, we would have the same impact force as we had without the load. We can maintain this for a certain amount of time (*A* to *G*) until eventually we do not have any more ability for a neuromuscular response to fully accommodate. At the upper limit, which is *B* to *C*, there is a threshold which, if surpassed, and based upon the performer's structure, can eventually cause injury. At the lower limit, which is *E* to *D*, there is a threshold below which one cannot actually go and cannot accommodate any further. This results in a Newtonian response, which is a predictable response *A* to *F*, that immediately acknowledges the load. Such a response can happen along the fully accommodating

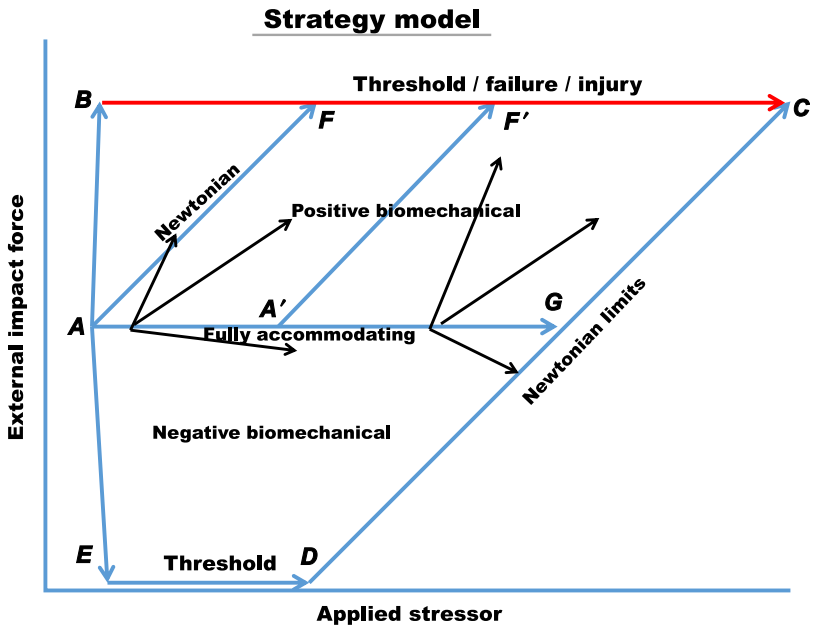

FIGURE 4.11
A graphical model of strategies.

continuum at any point indicated by A' to F'. Practically, this means that you are accommodating to a higher and higher applied stressor until you cannot do so anymore, resulting in a Newtonian response at this point (A'). However, there is a Newtonian limit because of one's structure. Above the A to G line or the fully accommodating response, we have a positive biomechanical response. Practically this means that the impact force is greater because one does not fully acknowledge the load and exhibits a lesser mechanical response on the outcome. Below the A to G line, we observe a negative biomechanical response because one overaccommodates due to possible concerns for the load. Importantly, and as it is identified by the three connected arrows, every time one executes the landing and has an experience, the whole model repositions itself as determined by the individual capabilities.

4.5 The Stickman's mechanics

In Section 4.2, Sherrington's statement "all man can do *is move*" was modified to "all man can do is *apply force*," which is a biomechanical perspective as opposed to a physiological perspective. As an example, we stated that one can be standing on the floor and we apply force to the floor but there is no movement involved.

Let us examine the term "apply force" in more detail. When we apply a force we have the cause (Fig. 4.12). This cause results in an effect but this effect is not always movement. The cause creates a change in state. Based on Newton's first law, the cause could maintain a steady state and that force can

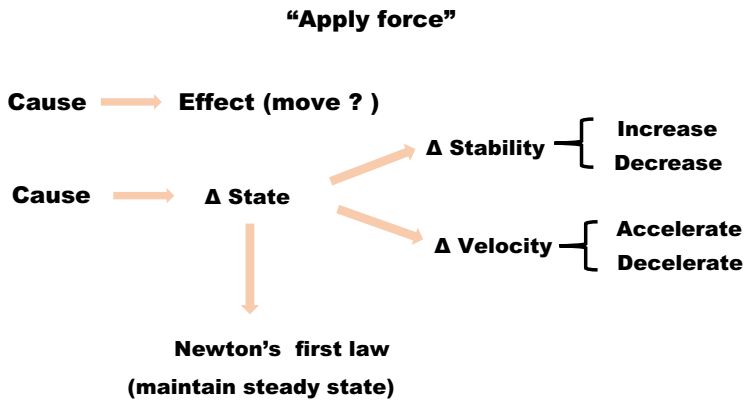

FIGURE 4.12
Applying forces do not always cause movement (Newton's first law). A change in velocity is required.

increase or decrease mechanical stability. For example, if we split our legs and put more force on our back leg, then we become more stable regarding a backward push; however, we are less stable regarding a forward push. Consider also lifting weights (e.g., a dead lift). If we have a weight on the floor and we try to pick it up but are unable, the result is a stable condition; even though the forces on our body increase and the forces between the weight and the floor decrease, there is no movement. There is only movement if we generate enough force to change the velocity and actually lift the weight. If we are able to lift the weight, initially we accelerate the weight as we apply sufficient force to lift the weight against gravity. However, our structure limits the amount of upward force we can produce and the weight begins to decelerate, eventually coming to a stop. Depending on what type of lift we are performing, the weight can come to a fixed stable position over the chest or the head or in the case that the lift was not completed could fall back on the ground.

When we apply forces, the cause and effect relationship can be examined through Newton's second law, the equation $F = ma$ and its rotational counterpart $T = I\alpha$ (Fig. 4.13). However, a problem occurs here because we really have forces that do not directly contribute to ma. This is due to energy in the form of deformation, heat, and sound being absorbed. All three take energy out of the system but they do so differentially based upon the characteristics of the object. For instance, when a golf club is hitting a golf ball, we can have different answers based upon which component is being analyzed (the club or the ball) since each of these variables has a different effect on the

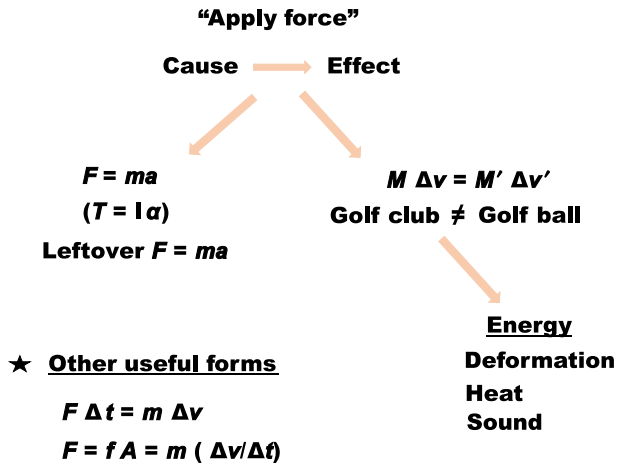

FIGURE 4.13
Applying forces through Newton's second law.

club and ball. As a result of this differential energy loss to the two objects the change in momentum ($M\Delta v$) of the objects are not equal. Consequently, if we evaluate the golf club and golf ball independently, the metal club head absorbs very little energy while the relatively soft golf ball absorbs considerably more energy, resulting in an observed inequality between the calculated momentums of the two objects. In another example, heading a highly inflated soccer ball or a softer soccer ball will result in great differences in terms of the duration of the impact, deformation of the ball, and the maximum contact force. Another useful form of Newton's second law equation is $F\Delta t = m\Delta v$, which can be used to evaluate various types of impacts as we examine the mechanics of different systems.

Applying forces can be viewed through the cause–effect–cause relationship (Fig. 4.14). For example, we have two objects like the golf club head (object 1) and the golf ball (object 2). Initially, we have a steady state 1 and a steady state 2 (Newton's first law). We apply a force $F1$ and $F2$ (Newton's second law) and what we know is that, in fact, $F1$ and $F2$ have to be opposite and equal based on Newton's third law. Therefore what happens when we bring these together, we have $m1a1$ equal to $m2a2$ and $m1(\Delta v1/\Delta t)$ equal to $m2$ $(\Delta v2/\Delta t)$. Practically, the two things that are going to be equal are $F1$ and $F2$ and the time of impact when the two objects make contact. Their effect on the individual objects is typically differential. Thus when we look at the outcomes they may appear to be different but they are not different because the energy loss is differential for the two objects. In our biomechanical

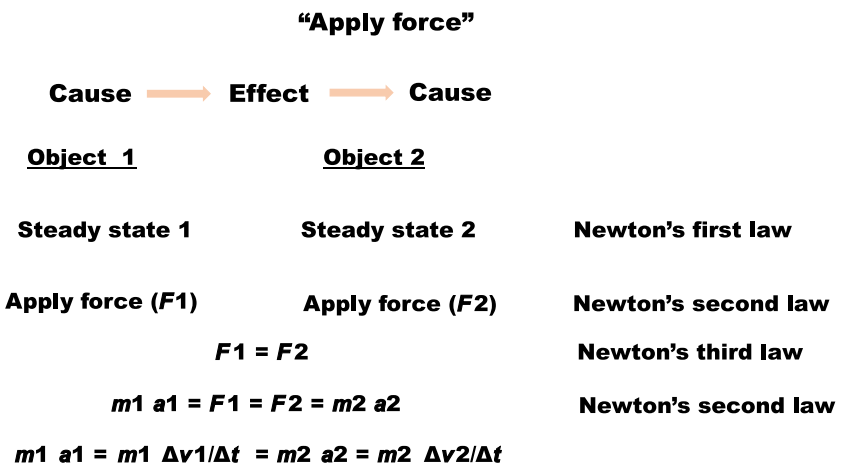

FIGURE 4.14

Another application of applying forces considering also Newton's third law.

experiments we have to be careful because usually we do not account for the energy loss and thus we have to be careful how we interpret the results.

When we apply forces we also have to consider impulse and momentum (Fig. 4.15). Impulse equals $F\Delta t$, momentum equals $m\Delta v$, and impulse equals momentum (force applied over time equals the observed movement). Thus we have $F\Delta t$ of an impact and if we increase F then, typically, under the same set of conditions, Δt will decrease during an impact like when a club hits a ball. However, in a push, something that is slow, Δt will increase independent of what happens to F, which can increase or decrease. Lastly, let us consider special forces with respect to applying forces (Fig. 4.16). Gravity is one such special force. If F is greater than W or the weight of the object, then the object will rise as when we lift weights. If F is lesser than W, then

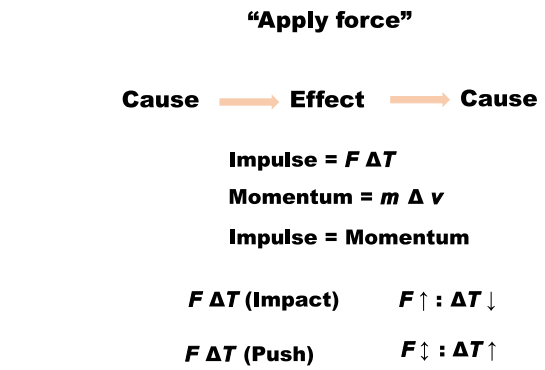

FIGURE 4.15
Applying forces with respect to impulse and momentum.

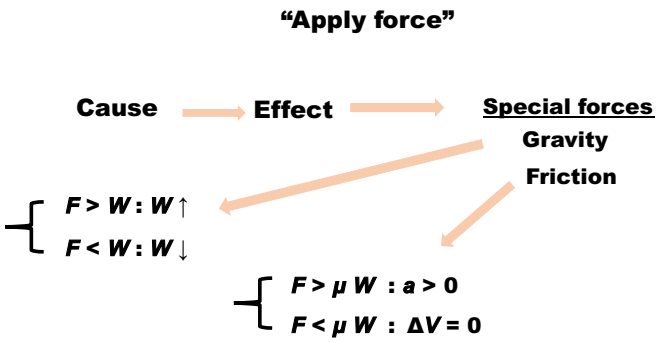

FIGURE 4.16
Applying forces with respect to the special forces with respect to gravity and friction.

the object will fall. Thus during a biceps curl we have to generate a greater F than the W of the object to successfully lift it. When we lower the object, we reduce the biceps F to less than W and the object falls due to gravity. The other special force is friction. If F is greater than the coefficient of friction multiplied by W, then the object is going to accelerate. If F is less than the coefficient of friction multiplied by W, then the object will not move.

4.6 The Stickman's goodbye

In this chapter we presented a very simple model, the Stickman, in order to study movement. The conceptual model of Stickman, as described in Fig. 4.3, helped us to understand how Stickman functions. We then presented several of the problems that Stickman must address regarding learning, mechanics, constraints, and the complex interactions between the various components. Stickman provides us with many different hypotheses to explore experimentally to further understand how and why we move. The reader is invited to visit Stickman often and rethink and reevaluate the hows and the whys of movement. Stickman and Stickwoman want to thank you for reading and thinking about these concepts. Stickdog simply says "Woof" to thank you for your interest.

References

Higgins, S. (1985). Movement as an emergent form: Its structural limits. *Human Movement Science*, *4*, 119–148.

James, C. R., Atkins, L. T., Dufek, J. S., & Bates, B. T. (2014). An exploration of load accommodation strategies during walking with extremity-carried weights. *Human Movement Science*, *35*, 17–29.

James, C. R., Atkins, L. T., Yang, H. S., Dufek, J. S., & Bates, B. T. (2015). Kinematic and ground reaction force accommodation during weighted walking. *Human Movement Science*, *44*, 327–337.

James, C. R., Bates, B. T., & Dufek, J. S. (2003). Classification and comparison of biomechanical response strategies for accommodating landing impact. *Journal of Applied Biomechanics*, *19*, 106–118.

Nordin, A. D., Dufek, J. S., James, C. R., & Bates, B. T. (2017). Classifying performer strategies in drop landing activities. *Journal of Sports Sciences*, *35*(18), 1858–1863.

Sherrington, C. S. (1951). *Man on his nature (Gifford Lectures, Edinburgh)* (2nd ed.). Cambridge: Cambridge University Press.

Stapp, J. P. (1971). Closing remarks: The future. In *Symposium of biodynamic models and their applications*. AMRL_TR_71_29. Wright-Patterson Air Force Base, OH.

Thelen, E. (1986). Treadmill-elicited stepping in seven-month-old infants. *Child Development*, *57*, 1498–1506.

CHAPTER 5

Power spectrum and filtering

Andreas Skiadopoulos and Nick Stergiou
University of Nebraska at Omaha, Omaha, NE, United States

Some parts of animals are simple, and these can be divided into like parts, as flesh into pieces of flesh; others are compound, and cannot be divided into like parts, as the hand cannot be divided into hands, nor the face into faces. Of these some are not only called parts, but members, such as those which, though entire in themselves, are made up of other parts, as the head and the leg, the hand and the entire arm, or the trunk; for these parts are both entire in themselves, and made up of other parts.

***The opening sentence from the first book of* The History of Animals**
by Aristotle (384–322 BCE)

CONTENTS

5.1 Introduction

Greeks in the ancient times used sundials to cast shadows, where the length of the shadow indicated the time of day. Much later, Galileo and Huygens developed the pendulum clock, which provided a much more precise indication of time. The outcome of these analog devices, that is, shadows and pendulum motions, are like sine waves when viewed across time—like those in Fig. 5.1—each one with its own period, amplitude, and phase. The first transformation of a time-domain signal to the frequency domain was performed by Galileo by measuring heart beats using a pendulum. He designed an instrument, known as the pulsilogium, which enabled the length of a pendulum to be adjusted for a fast or slow oscillation, corresponding to the frequency of a patient's pulse (Seeger, 1966, p. 5). It was an early medical device that used the amplitude of a time-domain wave to describe the frequency of heart beats! The Fourier series analysis was introduced much later. It was in the early 19th century, when the French mathematician Jean Baptiste Joseph, Baron de Fourier used, for the first time, the sums of periodic sine and cosine waves to represent more complex functions.

Biomechanics and Gait Analysis. DOI: https://doi.org/10.1016/B978-0-12-813372-9.00005-1

However, it was James Cooley and John Tukey, who in 1965 introduced the algorithm known as fast Fourier transform (FFT), which made it possible to perform quickly all the necessary operations of the Fourier transform (Cooley & Tukey, 1965). The introduction of the FFT radically changed many scientific disciplines. The Fourier transform is more than a description of how a signal is constructed from sinusoids. It is at the heart of many engineering disciplines, including the biomechanics of human movement. The aim of this chapter is to describe frequency domain analysis and demonstrate its major applications in biomechanics. Code to perform most of the analysis techniques described here via R software (R Core Team, 2018) is also provided.

5.2 A simple composite wave

A signal is an ordered sequence of numbers in time or space that describes the trends and variations of a quantity (Najarian & Splinter, 2012). In biomechanics, signals are mostly one-dimensional functions of time (i.e., time-series). A basic assumption is that a time-series inherently possesses dependence between adjacent observations (Myers, 2016). Therefore time-series analysis could reveal how a system evolves over time or changes over repetitions (Myers, 2016). All the information a signal conveys can be described in the time-domain and the frequency-domain. Neither of these domains extracts additional information about a signal. It is the same information, however, it is represented using different characteristics (Najarian & Splinter, 2012).

Fig. 5.1 illustrates the relationship between the time-domain and the frequency-domain of two periodic waves (Fig. 5.1A and B) and of their synthesis (Fig. 5.1C). In synthesis, two or more waves are added together to form a composite waveform (Peters & Williams, 1998). The wave W_A in Fig. 5.1A, describes the vertical displacement of point A as a function of time. Point A is located on the perimeter of the rotating disk A with radius OA equal to 1 m. Point A completes one full rotation every second, which corresponds to a frequency of 1 Hz with a magnitude of 1 m (Fig. 5.2A, power spectra). Similarly, wave W_B in Fig. 5.1B corresponds to the vertical displacement of point B as a function of time, which is located on the perimeter of the rotating disk B with radius OB = 1/3 m. Point B completes 23 cycles every second, which corresponds to a frequency of 23 Hz with a magnitude of 1/3 m (Fig. 5.2B, power spectra). The waveform W_{AB} in Fig. 5.1C corresponds to the vertical displacement of point B as a function of time. But now the waveform has been synthesized by adding together the previous two waves. Physically, disk B is attached to disk A with the center of rotation at point A. The two disks continue rotating as before, without any changes in their frequencies or radius. The resulting waveform is the vertical

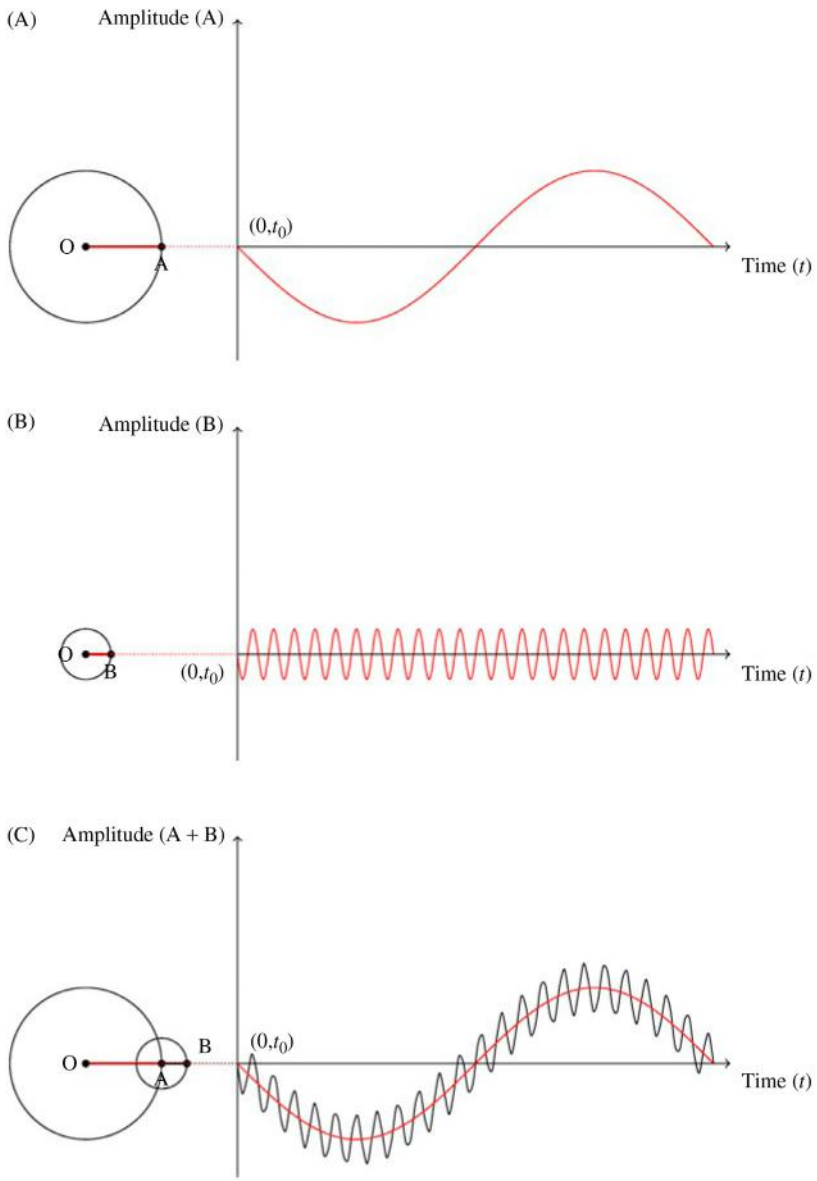

FIGURE 5.1

The vertical displacement of (A) point A (W_A) and of (B) point B (W_B) is plotted as a function of time t. The points A and B are located on the perimeters of disks A and B, respectively (radius of disk OA = 1 m and radius of disk OB = 1/3 m). Both disks are rotating clockwise with uniforms angular speeds. Disk A completes one cycle in 1 s (i.e., a frequency of 1 Hz), and disk B completes 23 cycles in 1 second (i.e., a frequency of 23 Hz). (C) When disk B is attached to disk A at point A without changing any of the previous characteristics, the vertical displacement of point B (W_{AB}) as a function of time (red signal) is now the sum (i.e., synthesis) of the displacements of point A (W_A) and point B (W_B).

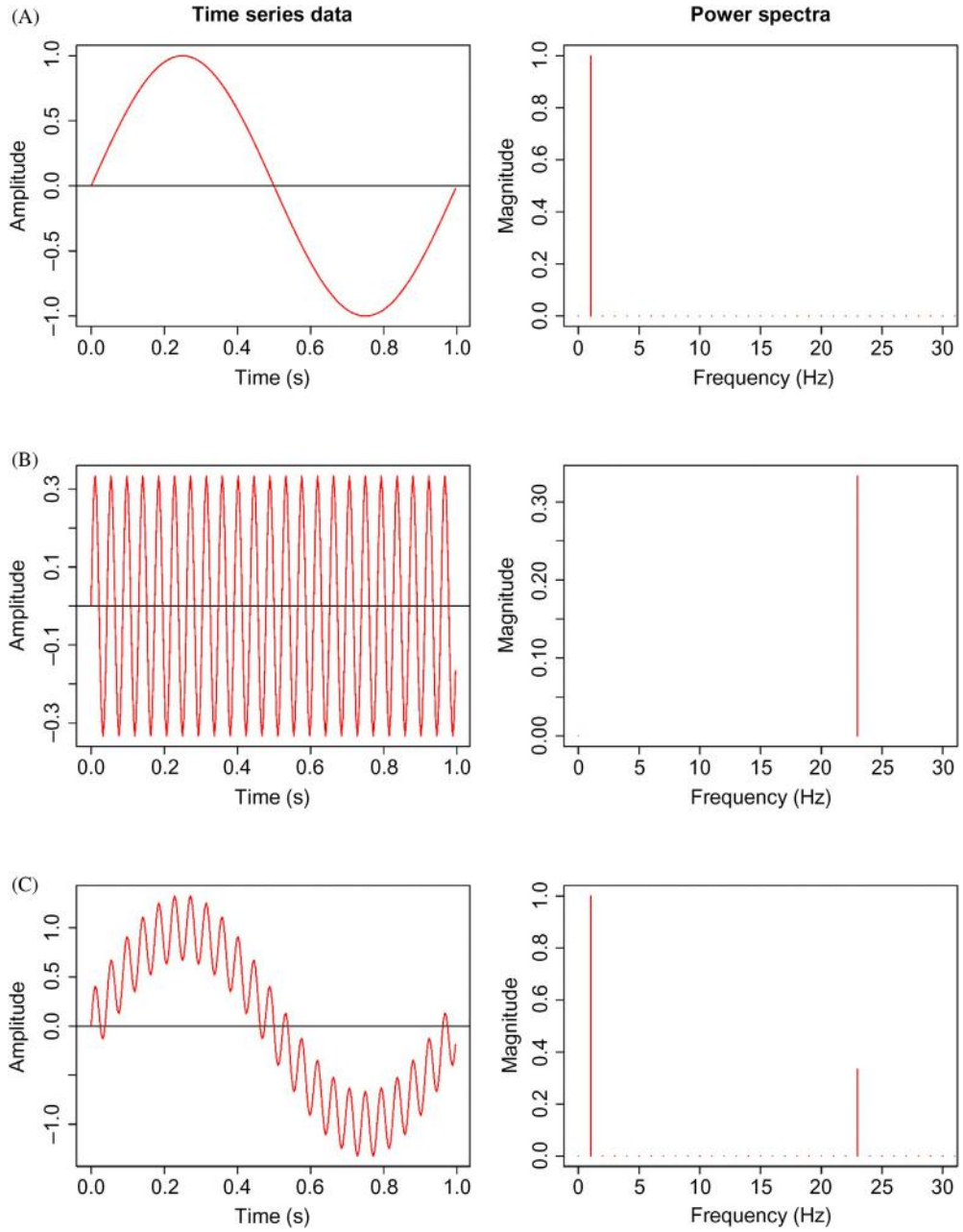

FIGURE 5.2

The time series data and the power spectra of the waves generated by the rotation of the disks in Fig. 5.1: (A) $W_A = \sin(\omega_0 t)$, (B) $W_B = 1/3\sin(23\omega_0 t)$, (C) $W_{AB} = \sin(\omega_0 t) + (1/3)\sin(23\omega_0 t)$, with $\omega_0 = 2\pi$ rad/s (i.e., $f_0 = 1$ Hz). The outcome of the Fourier transformation is a set of discrete harmonics at integer multiples of the fundamental frequency of the continuous signal. Wave A (W_A) has an amplitude of 1 m and rotates with a frequency of 1 Hz. W_A represents a paradigm for the data we want to collect. Wave B (W_B) has amplitude of 1/3 m and rotates with a frequency of 23 Hz. W_B represents a paradigm for noisy data superimposed to the signal. The composite waveform W_{AB} is used to demonstrate the superimposed noise in measurements.

displacement pattern of point B as a function of time relative to point O. It is the sum of the individual displacements of point A relative to point O and of point B relative to point A. Point B completes one cycle around point O every second, and 23 cycles around point A every second at the same time. Although it is difficult to see these details by observing the composite motion of waveform W_{AB} in the time domain (Fig. 5.2C, time series), in the frequency domain it is relatively easy (Fig. 5.2C, power spectra).

5.3 Spectral analysis

One way to describe the previous composite waveform W_{AB} mathematically is given by the following function:

$$W_{AB}(t) = \sin(\omega_0 t + \theta_1) + \frac{1}{3}\sin(23\omega_0 t + \theta_{23}) \tag{5.1}$$

where $\omega_0 = 2\pi f_0$ is the fundamental angular frequency in rad/s, and θ_1 and θ_{23} are the phase angles of the W_A and W_B sinusoids in radians (or rad for short), respectively. The unit of the fundamental frequency $f_0 = \omega_0/2\pi$ is the Hertz (or Hz for short), which is defined as one complete cycle per second. The amplitude of W_A is 1 m, and for W_B it is 1/3 m. The amplitude equals the radius of disks W_A and W_B in Fig. 5.1A and B. The position of a wave on the cycle at the instant we start to measure it is called phase (Peters & Williams, 1998). For example, the phase of all the waves in Fig. 5.1 is 0 rad (1 cycle $= 2\pi$ *rad*). It should be remembered that there are four characteristics of signals that are included in the sinusoids that represent the waveform W_{AB}:

- Frequency, denoted by f and measured in Hertz;
- Amplitude, denoted by A in the same units as the measured variable;
- Offset or 0*th* harmonic, denoted by a_0 in the same units as the measured variable;
- Phase angle, denoted by the Greek letter θ and measured in radians.

Any signal can be described using these characteristics. Thus, if we know these characteristics, then we can write the equation for the signal. For example, the following signal $x(t)$ (t in parenthesis indicates it is a function of time in seconds) incorporates these characteristics:

$$x(t) = a_0 + A\sin(2\pi f t + \theta) \tag{5.2}$$

and because $2\pi f = \omega$, the signal $x(t)$ can be rewritten as

$$x(t) = a_0 + A\sin(\omega t + \theta) \tag{5.3}$$

The frequency content of the periodic waveform $W_{AB}(t)$ is expressed in multiples of the angular frequency ω_0 (note the subscript 0). The angular frequency ω_0 (or equally the frequency $f_0 = \omega_0/2\pi$) is called the fundamental

frequency and its multiples are called harmonics (Peters & Williams, 1998). For example, the 23rd harmonic of the waveform W_{AB} has an angular frequency of $23\omega_0$ rad/s. Given the frequency components contained in a signal, the fundamental frequency is just the "greatest common divisor"—the largest divisor of all other numbers. Similarly, the fundamental period is the "least common multiple" of the individual periods of the components. For example, the fundamental frequency f_0 of W_{AB} is the greatest common divisor of $f_A = 1$ Hz, and $f_B = 23$ Hz, which is $f_0 = 1$ Hz.

In general, any continuous and periodic time-domain waveform is synthesized by adding together sinusoids whose frequencies are harmonically related (Peters & Williams, 1998). If the frequencies of the added sinusoids are not harmonically related, the composite signal is not periodic. For example, there is no greatest common divisor of two sinusoids with frequencies $3\pi/2$ and 2 Hz since π is an irrational number. Thus, the synthesis of these two sinusoids is not a periodic signal.

Let us denote a continuous time-domain waveform by $x(t)$ (t in parenthesis indicates it is a function of time in seconds). Any given periodic waveform $x(t)$ can be expressed as the sum of a series of sine and cosine waves (i.e., sinusoids). The sum of the individual amplitudes of the harmonics forms a Fourier series (Winter, 2009):

$$x(t) = a_0 + \sum_{k=1}^{\infty} a_k \cos(k\omega_0 t) + \sum_{k=1}^{\infty} b_k \sin(k\omega_0 t) \tag{5.4}$$

where $\omega_0 = 2\pi f_0 = 2\pi(1/T_0)$ is the fundamental angular frequency in rad/s with T_0 the time duration of a single period, t is the time in seconds, and a_k and b_k are the amplitude coefficients of the cosine and sine waves of the kth harmonic, respectively; a_0 is the amplitude of a cosine wave with zero frequency or the 0th harmonic. The frequency characteristics of the harmonics (frequency, phase, and magnitude) of any continuous and periodic waveform $x(t)$ are obtained by *harmonic analysis* (Winter, 2009). Harmonic analysis makes it possible to plot the magnitude (or the power) of each frequency present in a time-domain waveform against that frequency (Fig. 5.2, power spectra). The graphs created are called harmonic plots, spectral plots, or power spectrum plots (Peters & Williams, 1998; Winter, 2009). Similarly, it is possible to plot phase against frequency. The Fourier synthesis makes it possible to compose a waveform in the time-domain by adding together the individual amplitudes and phases of a given range of frequencies (Peters & Williams, 1998; Winter, 2009).

Depending on the type (time-continuous, digital, or time-discrete) and properties (periodic or aperiodic/random) of the waveform, four varieties of the Fourier analysis and corresponding synthesis techniques can be applied (Gaydecki, 2005):

1. The *Fourier series* is applied to describe continuous and periodic signals.
2. The *Fourier transform* is applied to describe continuous and aperiodic/random signals.
3. The *discrete Fourier series* (also called *discrete Fourier transform*) is applied to digital and periodic or aperiodic/random signals.
4. The *discrete-time Fourier transform* (the discrete-time equivalent of the Fourier transform) is applied to periodic or aperiodic/random sampled signals.

5.4 Fourier series

For a given period T, the Fourier coefficients (α_k and b_k) of the kth harmonic ($k > 0$) of any waveform $x(t)$, with amplitude A_k and phase θ_k, are calculated using the following Fourier series analysis equations [Eqs. (5.5–5.7)] (Winter, 2009):

$$a_k = \frac{2}{T}\int_0^T x(t)\cos(k\omega_0 t)dt \tag{5.5}$$

$$b_k = \frac{2}{T}\int_0^T x(t)\sin(k\omega_0 t)dt \tag{5.6}$$

and for $k = 0$ the 0th harmonic is obtained by the following equation:

$$a_0 = \frac{1}{T}\int_0^T x(t)dt \tag{5.7}$$

For reconstruction of the $x(t)$ waveform the following equations [Eqs. (5.8 and 5.9)] are used (Winter, 2009):

$$A_k = \sqrt{a_k^2 + b_k^2} \tag{5.8}$$

$$\theta_k = \tan^{-1}\left(\frac{b_k}{a_k}\right) \tag{5.9}$$

There is no particular reason why both a cosine and a sine wave are used to synthesize the waveform $x(t)$, and not only a sine wave. Because of the trigonometric property $\cos(\theta) = \sin\big(\theta + (\pi/2)\big)$, the sinusoids of Eq. (5.4) could be a set of sines only. If the phase of a sine function is shifted by $\pi/2$, then it would match that of a cosine function. Thus, the synthesis Eq. (5.4), by means of simple trigonometric manipulations and the help of Eqs. (5.7–5.9) can also be written as follows:

$$x(t) = a_0 + \sum_{k=1}^{\infty} A_k \sin(k\omega_0 t + \theta_k) \tag{5.10}$$

Any given periodic waveform $x(t)$ can also be expressed as a series of exponential functions (Gaydecki, 2005; Peters & Williams, 1998). There is a

mathematical equivalence between trigonometric and exponential functions. By using Euler's/De Moivre's formulae (Gaydecki, 2005; Peters & Williams, 1998):

$$\cos(k\omega_0 t) \pm j\sin(k\omega_0 t) = (\cos(\omega_0 t) \pm j\sin(\omega_0 t))^k = e^{\pm jk\omega_0 t} \tag{5.11}$$

that holds for any real number $\omega_0 t$ and integer k, the following relationships are derived, which relate the sine and cosine waves to exponential functions:

$$\begin{aligned} \cos(k\omega_0 t) &= \frac{e^{jk\omega_0 t} + e^{-jk\omega_0 t}}{2} \\ \sin(k\omega_0 t) &= \frac{-j\left(e^{jk\omega_0 t} - e^{-jk\omega_0 t}\right)}{2} \end{aligned} \tag{5.12}$$

where $j = \sqrt{-1} \Rightarrow j^2 = -1$ is the imaginary unit. These exponential functions are complex numbers, which are made from "real" and "imaginary" parts. The application of the complex mode is simple as soon as one becomes familiar with the imaginary unit j. Thus, the sine and cosine functions of Eq. (5.4) can be described in the complex mode, as well. The complex exponential expression of the trigonometric form of the Fourier series synthesis given by Eq. (5.4) is presented by the following equation (Gaydecki, 2005):

$$x(t) = a_0 + \sum_{k=1}^{\infty} a_k \left(\frac{e^{jk\omega_0 t} + e^{-jk\omega_0 t}}{2}\right) - jb_k \left(\frac{e^{jk\omega_0 t} - e^{-jk\omega_0 t}}{2}\right) \Rightarrow \cdots \Rightarrow x(t) = \sum_{k=-\infty}^{\infty} X[k] e^{jk\omega_0 t} \tag{5.13}$$

It is interesting to note that in the complex mode there are "real" and "imaginary" Fourier coefficients and both negative and positive frequencies. The "real" coefficients give the cosine terms, and the "imaginary" coefficients give the sine terms (Peters & Williams, 1998). The magnitude spectrum of the negative frequencies is the mirrored magnitude spectrum of the positive frequencies, while the coefficients of the "real" component exhibits even symmetry, and the coefficients of the "imaginary" component exhibits odd symmetry respecting the frequency axis. The negative frequencies are a mathematical artifact without any physical meaning that are necessary to compute the Fourier series when the complex form is used (Gaydecki, 2005). Going back to Eq. (5.13), the following complex quantity can be defined (Gaydecki, 2005):

$$X[k] = \begin{cases} \frac{1}{2}(a_k - jb_k), & k > 0 \\ \frac{1}{2}(a_k + jb_k), & k < 0 \\ a_{0,} & k = 0 \end{cases} \tag{5.14}$$

where the following relationship holds true:

$$\left|\frac{1}{2}\left(a_k - jb_k\right)\right| = \left|\frac{1}{2}\left(a_k + jb_k\right)\right| = \frac{A_k}{2} \tag{5.15}$$

and by substituting Eqs. (5.5) and (5.6) into a_k and b_k in Eq. (5.14, for $k > 0$), and applying Euler's/De Moivre's formulae, Eq. (5.16) can be derived, which corresponds to the exponential formula for the harmonic analysis (Gaydecki, 2005):

$$X[k] = \frac{1}{T}\int_0^T x(t)e^{-jk\omega_0 t}dt \tag{5.16}$$

The outcome of Eq. (5.16) represents the two-sided frequency spectrum, where the frequency content of a real periodic signal is expressed in multiples of the fundamental frequency $f_0 = \omega_0/2\pi$ (Winter, 2009).

5.5 Discrete Fourier analysis

Biomechanics deals with digital signals since the processing is performed with computers after sampling, quantizing, and transforming analog signals to digital numbers. Therefore, the discrete Fourier series (from now on referred to as *discrete Fourier transform* or DFT) is used to find the frequency spectra of the digital waveforms. In practice, only the DFT is used in digital signal processing, because by definition both the magnitude and time vectors of a signal are comprised of discrete values. The DFT calculates the magnitude and phase of the harmonics components of the digital and periodic or aperiodic/random waveform. The outcome of the DFT is a discrete spectrum. If the signal is periodic the amplitude of each of the harmonics is plotted, while for aperiodic/random signals the spectrum is defined by the lowest and highest frequencies (Winter, 2009).

Data processing requires a major assumption to be satisfied. Since we are dealing with digital time-varying signals, prior to the analysis of any digital signal it must be ensured that the Nyquist–Shannon sampling theorem has not been violated. The following section is devoted to this important issue.

5.5.1 Data sampling

The sampling frequency needs to be high enough to capture the dynamics of the quickest changes in the system of interest. The Nyquist–Shannon sampling theorem states that the sampling rate should be greater than twice the highest frequency of the analog signal in order to be able to reconstruct it without any loss of information. This means that the minimum frequency at which you need to sample in order to have a chance of obtaining periodic dynamics is twice the frequency of the fastest dynamics (Myers, 2016). The highest frequency presented in the signal is called the Nyquist frequency.

Therefore, if an analog waveform contains frequencies up to 5 Hz, it would be possible to reconstruct it if it is sampled at least at 10 Hz. This is the minimum acceptable sampling frequency for this signal. Sampling with a frequency less than twice the Nyquist frequency, for example when the previous waveform is sampled at 1.95 times the Nyquist frequency ($1.95 \times 5 = 9.75$ Hz), results in an error called *aliasing* of the signal's components (Fig. 5.3). Violation of the Shannon–Nyquist sampling theorem will

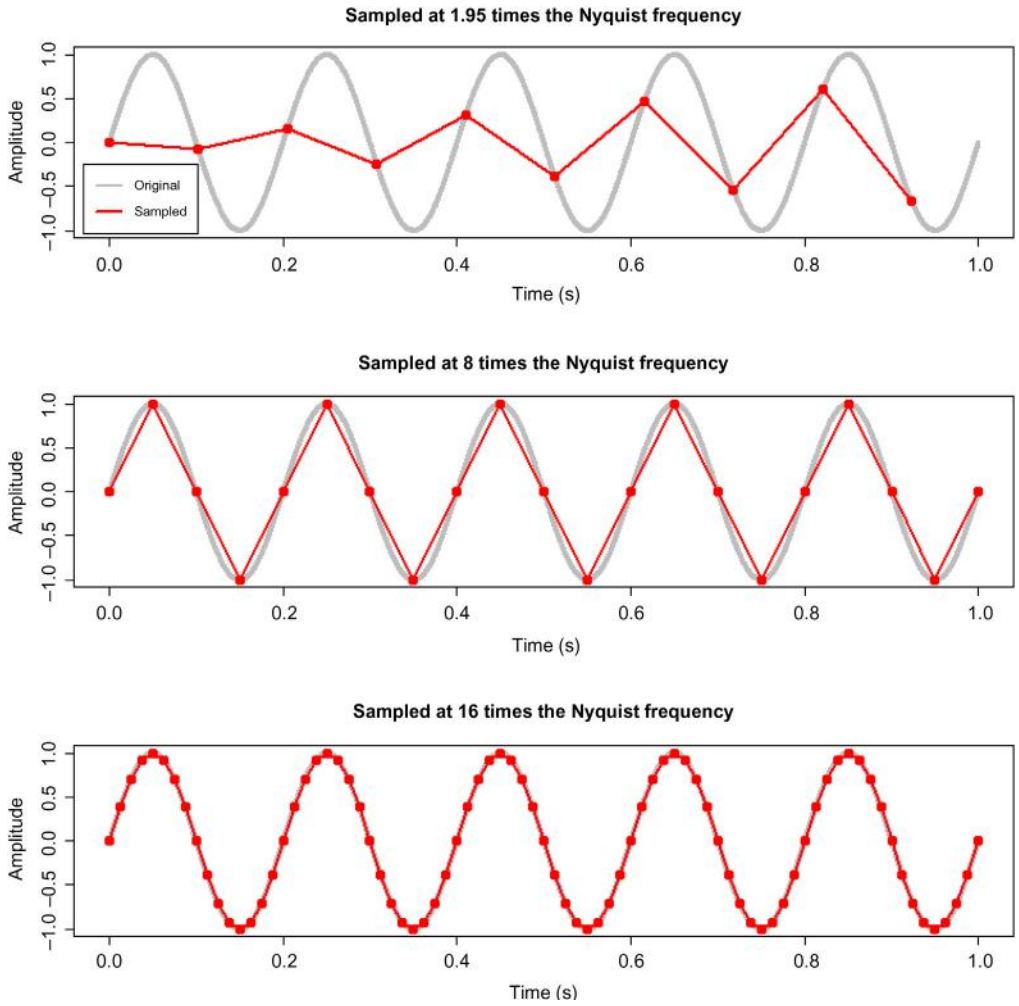

FIGURE 5.3

A signal with Nyquist frequency 5 Hz, sampled at different sampling rates. A lower sampling frequency than the Nyquist frequency results in aliasing, and the original signal cannot be reconstructed. 16 times higher sampling frequency reconstructs the signal with more detail.

Table 5.1 Examples with recommended minimum sampling frequencies.

Movement	System	Sampling frequency (Hz)
Balance	Video	50
Balance	Force plates	50
Walking	Video	50–100
Walking	Force plates	200–500
Running—sprinting	Video	100–200
	Force plates	1000
Javelin throwing	Video	200–300
	Force plates	1000
Muscle contraction	Electromyographic (EMG)	≥ 1000

introduce false lower frequencies into the sampled signal that equal the difference between the sample frequency and the true signal frequency (Winter & Patla, 1997). For example, according to the previous example, sampling at 9.75 Hz will introduce an aliasing frequency of 4.75 Hz. To avoid aliasing, it should be also checked that the analog-to-digital converters of the acquisition systems are furnished with antialiasing low-pass filters at their inputs to *ensure* that the sampling theorem is not violated. The DFT would incorrectly represent the frequency components of any signal that were sampled, violating the sampling theorem, and the inverse discrete Fourier transform (IDFT) would not be able to accurately represent the original signal.

In biomechanics, the sampling rate should be at least 10 times greater than the Nyquist frequency of the signal. The highest frequencies that occur during walking are less than 12 Hz. For example, a 50-Hz camera would probably be sufficient for recording walking data to examine knee joint kinematics (Vaughan, Davis, & O'Connor, 1999). However, this frequency will not be high enough to investigate the kinematics of more dynamic activities such as javelin throwing (Table 5.1) (Bartlett, Müller, Lindinger, Brunner, & Morriss, 1996; Brunt, Liu, Trimble, Bauer, & Short, 1999; Cavanaugh et al., 1999; Dingwell & Cavanagh, 2001; Ferdjallah, Harris, & Wertsch, 1999; Önell, 2000). A 50–100 Hz sampling rate should be satisfactory for kinematics data. However, kinetic data measured by force platforms should be sampled at frequencies greater than 500 Hz because of the impacts that are present at heel strike.

How can we decipher what the highest frequency in our data is? The Nyquist frequency of a waveform with unknown frequency characteristics can be estimated by recording the waveform using a very high sampling rate (i.e., oversampling), and then calculating the highest harmonic of the recorded signal using the DFT. However, when analyzing real biomechanical signals (e.g., kinematics data) it is not as straightforward to find the highest harmonic,

because the higher harmonics of the signal are overlapped with noise. However, since kinematics signals have more power at lower frequencies, the DFT can be used to find at which harmonic the cumulative power spectrum (i.e., the cumulative percentage of the power spectrum from the lowest-to-higher harmonics) exceeds ~99% of the total power spectrum of the signal (see Section 5.9, Table 5.6). This harmonic represents the highest frequency in the signal, and the sampling rate should be about 10 times higher than its frequency. If it is not possible to sample at that rate, it must be ensured that the sampling rate will not to be less than four times this frequency (Winter & Patla, 1997). For example, for clinical stabilometry in quiet standing, the sampling rate of the force platform should be at least 50 Hz, although most of the power at the center of the pressure signal lies within 3–5 Hz (Scoppa, Capra, Gallamini, & Shiffer, 2013).

Since the sampling rate refers to the number of samples per second, it defines the *temporal resolution* of the digital time-domain waveform. For example, when a signal is sampled at $f_{sr} = 20$ Hz, the temporal resolution is $t_r = 1/f_{sr} = 0.05$ seconds, while sampling at rate $f_{sr} = 40$ Hz, the temporal resolution is 0.025 seconds. When increasing the sampling rate it is not only the temporal resolution that increases, but also the signal-to-noise ratio (SNR), however this depends on the quality of the system (Woltring, 1995). Hence, if data are oversampled, more measurement noise could be introduced (Myers, 2016). The sampling rate must not violate the sampling theorem in order to avoid aliasing, but it could be greater than twice the Nyquist frequency (Furnee, 1989; Woltring, 1995, 1984). The formula of Lanshammar (1982a, 1982b) [see Eq. (5.35) in Section 5.9] can be used to discover how the noise changes with oversampling. However, it should be remembered that if data are undersampled, the entire signal is not captured.

The duration of the record length is related to the *frequency resolution* of the data. The frequency resolution refers to the number of frequency components that can be discriminated, and is determined by the number of data points in the digital signal. An experimentally collected biomechanical digital signal of length N has $(N/2) + 1$ frequency components; there are $(N/2) + 1$ equally spaced Fourier components from 0 Hz up to the Nyquist frequency, and the spacing between the Fourier components (i.e., frequency bins) is $\Delta f = F_s/N$ (Broch, 1990). Zero padding (i.e., add zeros at the end of the time series) is an artificial way to increase the frequency resolution. It is interesting to note that according to the sampling theorem the maximum frequency (f_{max}) that can be present in the signal is $f_{max} = F_s/2 = k_{max} \times f_0$, where k_{max} is the maximum harmonic. Because, $f_0 = 1/T_0 = 1/NT_s = F_s/N$, then $F_s/2 = k_{max} \times f_0 = k_{max} \times F_s/N$. Thus, $k_{max} = N/2$. This means that the number of harmonics is dependent on the number of sample values.

The duration of the record length is also related to the *frequency precision*, and is decided by the lowest frequency present in the signal or the lowest frequency to be analyzed. If the lowest frequency component of the signal to be recorded is unknown, trial-and-error data collection at different recording lengths is needed in order to discover the lowest frequency (Winter, 2009). For example, sampling for 60 seconds at 10 Hz the lowest harmonic that can be plotted is at $1/60 = 0.017$ Hz, and the highest is at 5 Hz. For example, if we limit the recording length to 60 seconds it will not be possible to capture frequencies lower than 0.017 Hz.

5.5.2 The discrete Fourier transform

We are going to use the digital form of Eq. (5.4) to synthesize a digital waveform, and the digital form of Eqs. (5.5) and (5.6) to compute the $k = N/2$ harmonics. The trigonometric form of the IDFT is given by:

$$x[n] = a_0 + \sum_{k=1}^{N/2} \left(\alpha_k \cos\left(\frac{2\pi kn}{N}\right) + b_k \sin\left(\frac{2\pi kn}{N}\right) \right) \tag{5.17}$$

and the Fourier coefficients of the kth harmonic (magnitude and phase) are calculated by Eqs. (5.18) and (5.19) given the digital equivalents of Eqs. (5.5) and (5.6) (Broch, 1990; Gaydecki, 2005; Winter, 2009). Therefore the trigonometric form of the DFT is given by:

$$a_k = \frac{2}{N} \sum_{n=0}^{N-1} x[n] \cos\left(\frac{2\pi kn}{N}\right) \tag{5.18}$$

$$b_k = \frac{2}{N} \sum_{n=0}^{N-1} x[n] \sin\left(\frac{2\pi kn}{N}\right) \tag{5.19}$$

and the 0th harmonic is given by:

$$a_0 = \frac{1}{N} \sum_{n=0}^{N-1} x[n] \tag{5.20}$$

We can make Eqs. (5.17), (5.18), and (5.19) more general by using N data (Gaydecki, 2005). Therefore

$$x[n] = \sum_{k=0}^{N-1} \left(\alpha_k \cos\left(\frac{2\pi kn}{N}\right) - b_k \sin\left(\frac{2\pi kn}{N}\right) \right) \tag{5.21}$$

and

$$a_k = \frac{1}{N} \sum_{n=0}^{N-1} x[n] \cos\left(\frac{2\pi kn}{N}\right) \tag{5.22}$$

$$b_k = -\frac{1}{N}\sum_{n=0}^{N-1} x[n]\sin\left(\frac{2\pi kn}{N}\right) \tag{5.23}$$

The equivalent exponential form of Eqs. (5.21), (5.22), and (5.23) can be derived using Euler's/De Moivre's formulae (Gaydecki, 2005). The following formula of the IDFT is used to synthesize a signal, and transform it from the frequency domain to the time domain:

$$x[n] = \sum_{k=0}^{N-1} X[k]e^{\left(\frac{j2\pi kn}{N}\right)} \tag{5.24}$$

and the following formula of the DFT is used for the harmonic analysis:

$$X[k] = \frac{1}{N}\sum_{n=0}^{N-1} x[n]e^{\left(\frac{-j2\pi kn}{N}\right)} \tag{5.25}$$

in which, N is the number of data points in the digital signal x, and $X[k]$ are the Fourier coefficients.

To reduce the number of calculations needed for the estimation of the Fourier coefficients, the FFT developed by Cooley and Tukey is used (Cooley & Tukey, 1965). With the FFT algorithm, the number of computational steps is reduced from N^2 to $N\log_2 N$.

As we have seen previously, the sampling frequency is a critical consideration when dealing with time series data. It is a measure of how often data samples are acquired, and thus sampling frequency F_s multiplied by the length of time that you sampled t, gives the number of data points in your time series ($N = F_s \times t$). As is explained in Section 5.5.3, when recording a biomechanical signal, it is assumed most of the time that the fundamental period T_0 is equal to the time duration of recording t. Let us assume that a digital signal $x[n]$ is obtained after sampling an analog signal $x(t)$; its nth data point is the $n \times T_s$ sample of the analog signal ($x[n] = s(n \times T_s)$), where T_s is the sampling interval in seconds. The digital signal $x[n]$ represents a discrete series of n sample values that are equally spaced at T_s seconds apart. Let us consider that the digital signal $x[n]$ is also periodic, with fundamental period $T_0 = 2\pi/\omega_0$ seconds and fundamental frequency $f_0 = 1/T_0$ and was sampled at $F_s = 1/T_s$ Hz resulting at n equally spaced samples with $0 \le n \le N-1$, where $N = F_s \times T_0$. Let us now obtain the DFT of the periodic digital waveform W_B with $f_B = 23$ Hz that was sampled at $F_s = 60$ Hz ($T_s = 1/60$ seconds) (Fig. 5.2A, time series data). The waveform was recorded for a time interval of $t = 1$ second, which corresponds to $N = 60$ data points:

$$W_B[n] = \frac{1}{3}\sin(23\omega_B n T_s) \tag{5.26}$$

Using the DFT function in Eq. (5.25), we obtain its Fourier transformation. Because the digital waveform W_B is a sine function, the "imaginary" part should give the signal's magnitude (at the frequency of 23 Hz). Similarly, the Fourier transformation of the digital waveform W_A with $f_A = 1$ Hz that was sampled at $F_s = 60$ Hz ($T_s = 1/60$ seconds) and recorded for a time interval of $t = 1$ second is obtained (Fig. 5.2B, time series data):

$$W_A[n] = \sin(\omega_A n T_s) \tag{5.27}$$

Let us add the waveforms W_A and W_B together. Thus, the digital translation of the continuous signal

$$W_{AB}(t) = \sin(\omega_0 t) + \frac{1}{3}\sin(23\omega_0 t) \tag{5.28}$$

is the waveform:

$$W_{AB}[n] = \sin(2\pi f_0 n T_s) + \frac{1}{3}\sin(2\pi 23 f_0 n T_s) \tag{5.29}$$

The Fourier transformation of the sum of the two digital waveforms W_{AB} is also the sum of their Fourier transforms (Fig. 5.2C, power spectra). Based on the previous two paragraphs we will get an "imaginary" magnitude of 1 m at a frequency of 1 Hz, and an "imaginary" magnitude of 1/3 m at a frequency of 23 Hz. The peak in the power spectra corresponds to the frequency of the wave function in the time series (Fig. 5.2A and B). The time series W_{AB}, that is a sum of two wave functions, has two peaks, corresponding to the two frequencies which were added together (Fig. 5.2C, power spectra). Tables 5.2–5.4 show the Fourier coefficients of the W_A, W_B, and W_{AB} waveforms, respectively.

Table 5.2 The Fourier transform coefficients of the signal $W_B[n] = (1/3)\sin(2\pi 23 n T_s)$ (only 5 of the 30 Fourier coefficients that surround the frequency of 23 Hz are shown).

$(1/3)\sin(2\pi 23 n T_s)$		
Sampling rate = 60 Hz		
Frequency (Hz)	**Fourier coefficients**	**Magnitude**
21	0.0000−0.0000i	0.0000
22	0.0000−0.0000i	0.0000
23	0.0000−0.3333i	0.3333
24	0.0000−0.0000i	0.0000
25	−0.0000−0.000i	0.0000

At the frequency of 3 Hz we expect an "imaginary" value of 0.333 and a real value of 0.

Table 5.3 The Fourier transform coefficients (only the first 5 of the 30 Fourier coefficients are shown) of the signal $W_A[n] = \sin(2\pi n T_s)$.

$\sin(2\pi n T_s)$		
Sampling rate = 60 Hz		
Frequency (Hz)	**Fourier coefficients**	**Magnitude**
0	0.0000−0.0000i	0.0000
1	0.0000−1.0000i	1.0000
2	0.0000−0.0000i	0.0000
3	0.0000−0.0000i	0.0000
4	0.0000−0.0000i	0.0000

At the frequency of 1 Hz we expect an "imaginary" value of 1 and a real value of 0. At the frequency of 0 Hz, the 0th harmonic is presented.

The reason we use the Fourier transform is to separate the sine and cosine functions of the recorded time series data, so we are able to see which frequencies are contributing most to the data just by examining the peak positions. If the peak corresponding to 1 Hz is very high, then it is likely that there is a 1-Hz component in the times series data. Knowing that the 23-Hz component of the signal is the highest frequency of interest, we know it would need a sampling frequency of at least 46 Hz (2×23 Hz $= 46$ Hz) to capture it, but something more like 230 Hz (10×23 Hz $= 230$ Hz) would allow us to define it better. For real experimentally obtained biomechanical time series determining the highest frequency of the signal is a bit tricky because real signals rarely are band-limited, and thus there is not a clear cutoff point.

5.5.3 Spectral leakage

Because the signals are sine waves, it is the "imaginary" parts of the Fourier coefficients that give us the magnitude of the sinusoids in the original signal. For example, for the W_A waveform the value of the "imaginary" part at the frequency of 1 Hz is the magnitude of the first harmonic (Table 5.2). Clearly, the composite waveform W_{AB} shows us the corresponding Fourier coefficients at the appropriate places (i.e., at the frequencies of 1 and 23 Hz) (Table 5.4).

Let us reanalyze the waveform W_{AB}, but now the waveform will be recorded for a time interval of $t = 1.3$ seconds, which corresponds to $N = 78$ data points. By observing the frequency resolution of the waveform, $\Delta f = F_s/N \cong 0.77$ Hz, we can see that the frequency bins are not centered with the frequency of the first harmonic (1 Hz) and with the frequency of the 23rd harmonic (23 Hz). Thus, the DFT spreads the energy of the harmonics over the adjacent frequency bins (Fig. 5.4A). This is called spectral

Table 5.4 The Fourier transform coefficients of the signal $W_{AB}[n] = (1/3)\sin(2\pi 23nT_s) + \sin(2\pi nT_s)$.

$(1/3)\sin(2\pi 23nT_s) + \sin(2\pi nT_s)$		
Sampling rate = 60 Hz		
Frequency (Hz)	**Fourier coefficients**	**Magnitude**
0	0.0000−0.0000i	0.0000
1	**0.0000−1.0000i**	**1.0000**
2	0.0000−0.0000i	0.0000
3	0.0000−0.0000i	0.0000
4	0.0000−0.0000i	0.0000
5	0.0000−0.0000i	0.0000
6	0.0000−0.0000i	0.0000
7	0.0000−0.0000i	0.0000
8	0.0000−0.0000i	0.0000
9	0.0000−0.0000i	0.0000
10	0.0000−0.0000i	0.0000
11	0.0000−0.0000i	0.0000
12	0.0000−0.0000i	0.0000
13	0.0000−0.0000i	0.0000
14	0.0000−0.0000i	0.0000
15	0.0000−0.0000i	0.0000
16	0.0000−0.0000i	0.0000
17	0.0000−0.0000i	0.0000
18	0.0000−0.0000i	0.0000
19	0.0000−0.0000i	0.0000
20	0.0000−0.0000i	0.0000
21	0.0000−0.0000i	0.0000
22	0.0000−0.0000i	0.0000
23	**0.0000−0.3333i**	**0.3333**
24	0.0000−0.0000i	0.0000
25	0.0000−0.0000i	0.0000
26	0.0000−0.0000i	0.0000
27	0.0000−0.0000i	0.0000
28	0.0000−0.0000i	0.0000
29	0.0000−0.0000i	0.0000
30	0.0000−0.0000i	0.0000

At the frequency of 1 Hz we expect an "imaginary" value of 1 and a real value of 0, and at the frequency of 3 Hz we expect an "imaginary" value of 0.333 and a real value of 0.

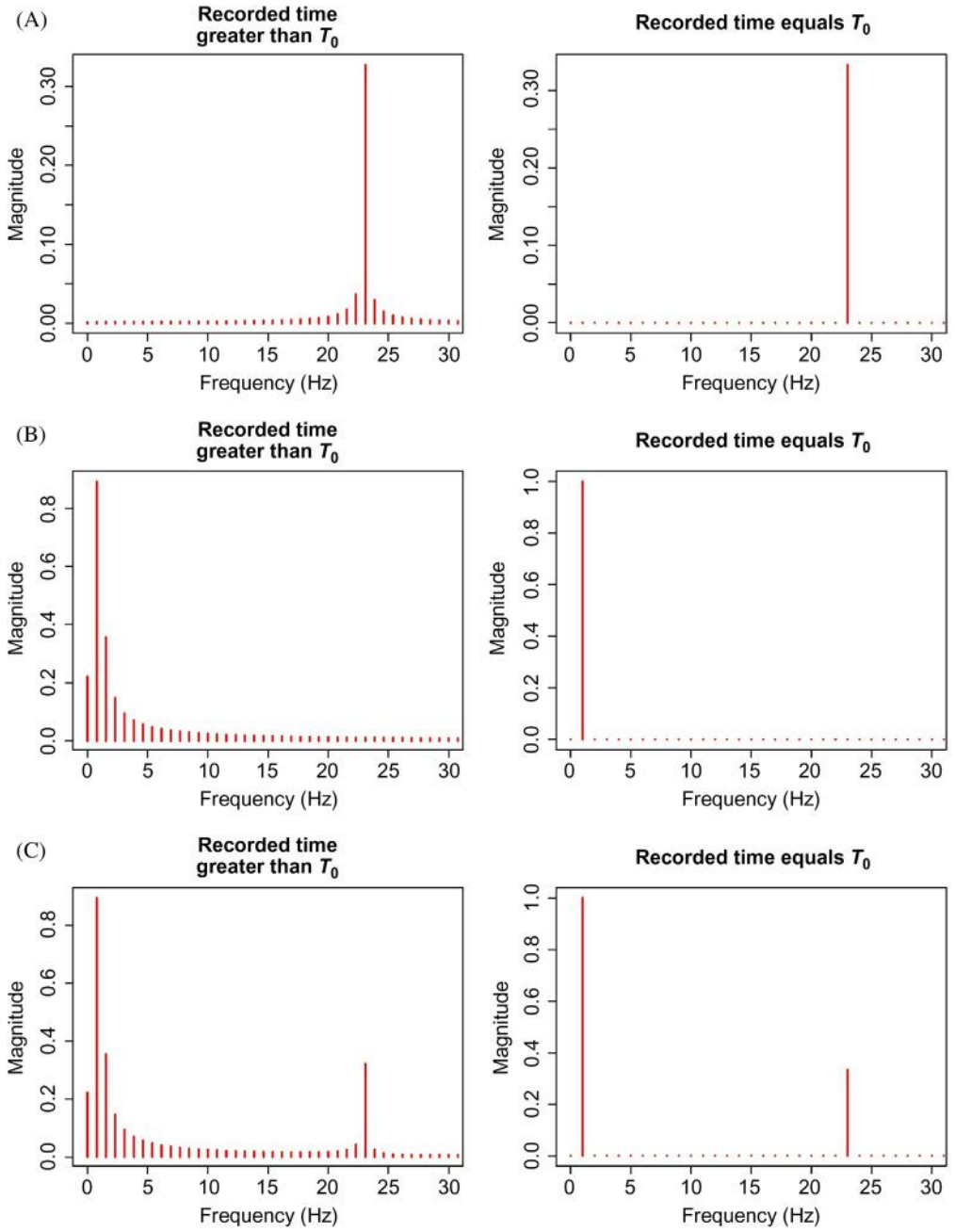

FIGURE 5.4

The frequency domain of the digital periodic waveforms (A) $W_A = \sin(\omega_0 t)$, (B) $W_B = 1/3\sin(23\omega_0 t)$, (C) $W_{AB} = \sin(\omega_0 t) + (1/3)\sin(23\omega_0 t)$, with $\omega_0 = 2\pi$ rad/s ($f_0 = 1$ Hz) are represented by bars located at the different harmonics. The harmonics are calculated as multipliers of the fundamental frequency f_0 and are measured in Hertz. The length of the bars is the absolute value of the amplitude of each harmonic. When the recorded time t is not equal to the period T_0 of the waveforms (or an integer multiple of it), the energy of the harmonic is leaked over adjacent frequency bins.

leakage (Broch, 1990). However, the spectral leakage is not present when the recorded time t is equal to the fundamental period T_0 of the waveform W_{AB} (Fig. 5.4A). In general, if the recorded time is not matched to an integer multiplier of the signal's fundamental period, we get spectral leakage. Similarly, the frequency spectrum of the waveforms W_A (Fig. 5.4B) and W_{AB} (Fig. 5.4C) have leakage when the recorded time is greater than the fundamental period T_0, but not an integer multiplier of T_0.

The cause of the leakage—or equally of the noncentered frequency bins—is the assumption that the input digital signal to the DFT is a periodic signal with fundamental period T_0 that has been recorded for a time interval of one period T_0 or in n integer multiples of the fundamental period nT_0. If this were true, there would not be any discontinuities of the recirculated signal at the instant between one period and the next (Fig. 5.5C). Therefore, any digital signal, periodic or not, when continuously recirculated represents an artificial periodic signal with an infinite period (Broch, 1990). However, to prevent spectral leakage, we must ensure not only that the end of the signal is connected to its beginning (something that could be true for both periodic and aperiodic/random signals), but also that the slopes at the starting and stopping instants of the repeated signal are equal (most times it is not true for aperiodic or random signals) (Broch, 1990). Violation of these assumptions leads to spectral leakage.

A solution to reduce spectral leakage is to taper the digital signal by a window function before the DFT takes place (Broch, 1990). The cosine bell window function (Hann window) can be used because it tapers the data to zeroes at both edges of the window and improves circularity. Tapering the digital waveform before transformation results in smoother edges. However, the magnitude of the harmonics should be corrected when a tapered window function is used. When a Hann window (Eq. (5.30)) is applied before a N-point DFT takes place, the magnitude should be multiplied by a factor of 2 to compensate for its $1/2$ reduction prior to transformation.

$$w(n) = \frac{1}{2}\left(1 - \cos\frac{2\pi n}{N}\right) \tag{5.30}$$

where $n = 0,\ldots, N-1$. When the direct Fourier transform is applied to short duration and transient signals, a rectangular window function is recommended instead of the Hann window function (Broch, 1990). In practice this means using the DFT "as it is," since a rectangular window is used by default (because we assume periodic digital signals). Table 5.5 shows the Fourier coefficients of the aperiodic and windowed version of the W_{AB} waveform. The use of the Hann window reduces the spectral leakage and dramatically improves the accuracy of the Fourier coefficients for the W_{AB} waveform (Fig. 5.6). Vignette 5.1 contains the code to perform DFT with Hann window in R programming language.

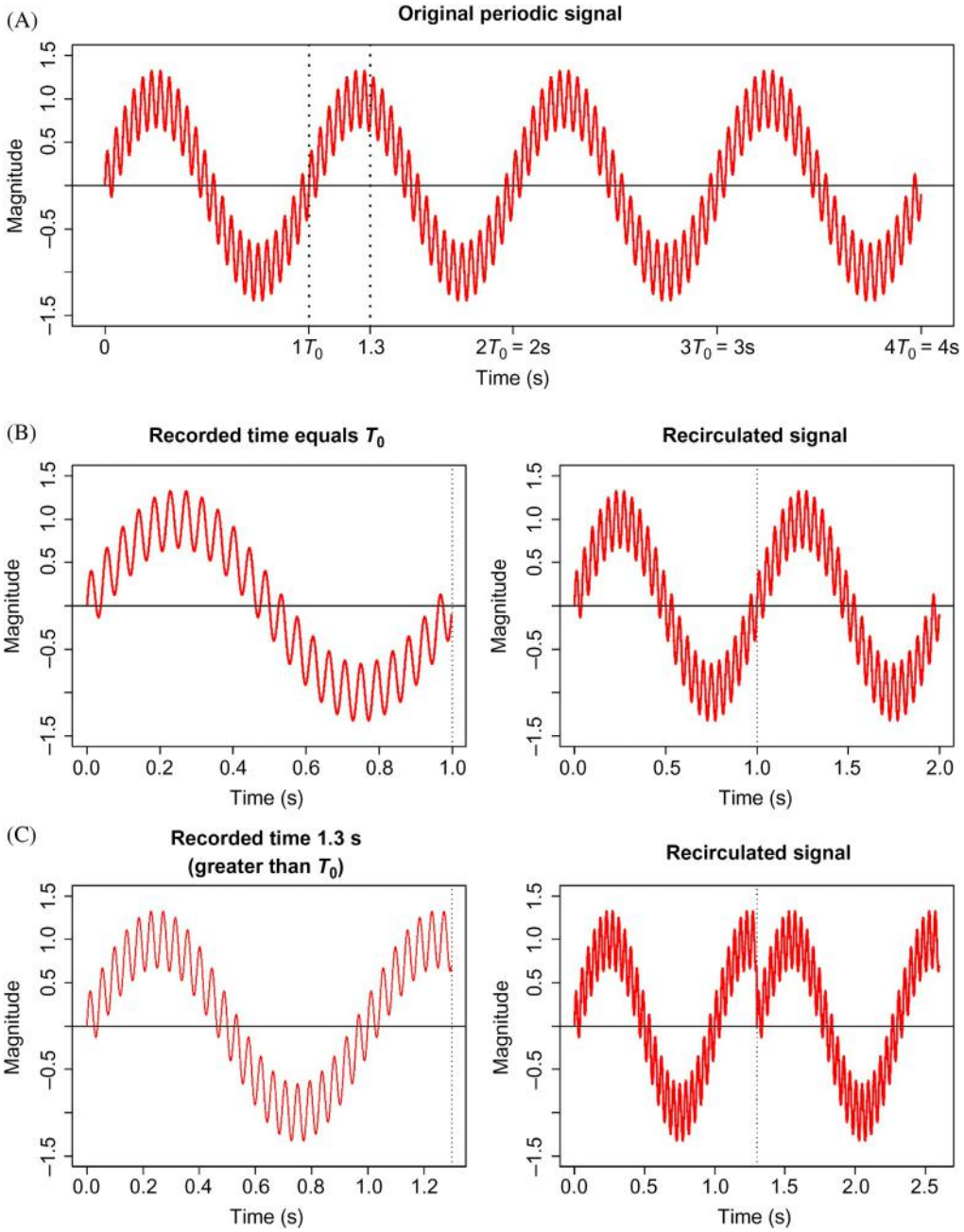

FIGURE 5.5

(A) Signal to be recorded. (B) An example in which periodic waveforms have circular continuity because the recorded time equals to their period T_0. (C) An example in which periodic waveforms do not have circular continuity because the recorded time is different to their period T_0. The sudden gaps at the end of the repeated waves provoke leakage in the frequency domain.

Table 5.5 The Fourier transform coefficients of the signal $W_{AB}[n] = (1/3)\sin(2\pi 23nT_s) + \sin(2\pi nT_s)$ with length of record not an integer multiple of fundamental frequency T_0, after multiplying it with the Hann window.

$(1/3)\sin(2\pi 23nT_s) + \sin(2\pi nT_s)$				
Sampling rate = 60 Hz				
	Nonwindowed signal		**Windowed signal**	
Frequency (Hz)	**Coefficients**	**Magnitude**	**Coefficients**	**Magnitude**
0.000	0.21981 + 0.0000i	0.21981	−0.3017203 + 0.0000000i	0.3017203
0.769	**0.77538−0.4388i**	**0.89092**	**0.7315891−0.5916975i**	**0.9409190**
1.538	0.24415 + 0.2620i	0.35813	−0.6114851 + 0.3842783i	0.7222076
2.308	−0.08376 + 0.1241i	0.14972	0.0687426−0.0406503i	0.0798623
3.077	−0.04751 + 0.0844i	0.09688	0.0130162−0.0076151i	0.0150801
3.846	−0.03289 + 0.0647i	0.07258	0.0047415−0.0027355i	0.0054740
4.615	−0.02543 + 0.0527i	0.05849	0.0022814−0.0012733i	0.0026127
5.385	−0.02108 + 0.0445i	0.04923	0.0012884−0.0006799i	0.0014567
6.154	−0.01832 + 0.0385i	0.04266	0.0008073−0.0003936i	0.0008981
6.923	−0.01645 + 0.0340i	0.03775	0.0005435−0.0002391i	0.0005938
7.692	−0.01511 + 0.0304i	0.03395	0.0003853−0.0001491i	0.0004131
8.462	−0.01413 + 0.0275i	0.03092	0.0002835−0.0000937i	0.0002986
9.231	−0.01338 + 0.0251i	0.02845	0.0002142−0.0000583i	0.0002220
10.000	−0.01279 + 0.0231i	0.02641	0.0001649−0.0000350i	0.0001686
10.769	−0.01232 + 0.0214i	0.02469	0.0001283−0.0000195i	0.0001297
11.538	−0.01192 + 0.0200i	0.02325	0.0001000−0.0000093i	0.0001004
12.308	−0.01160 + 0.0187i	0.02201	0.0000773−0.0000027i	0.0000774
13.077	−0.01131 + 0.0176i	0.02096	0.0000584 + 0.0000009i	0.0000584
13.846	−0.01106 + 0.0167i	0.02006	0.0000418 + 0.0000021i	0.0000418
14.615	−0.01082 + 0.0160i	0.01929	0.0000262 + 0.0000009i	0.0000263
15.385	−0.01060 + 0.0153i	0.01865	0.0000107−0.0000033i	0.0000112
16.154	−0.01038 + 0.0149i	0.01812	−0.0000064−0.0000114i	0.0000131
16.923	−0.01014 + 0.0145i	0.01772	−0.0000271−0.0000261i	0.0000377
17.692	−0.00988 + 0.0144i	0.01746	−0.0000553−0.0000526i	0.0000763
18.462	−0.00958 + 0.0145i	0.01737	−0.0000986−0.0001029i	0.0001425
19.231	−0.00918 + 0.0150i	0.01755	−0.0001752−0.0002084i	0.0002722
20.000	−0.00861 + 0.0160i	0.01818	−0.0003371−0.0004670i	0.0005760
20.769	−0.00768 + 0.0182i	0.01978	−0.0007870−0.0012919i	0.0015128
21.538	−0.00583 + 0.0234i	0.02410	−0.0029731−0.0058937i	0.0066011
22.308	0.00011 + 0.0411i	0.04114	0.0723069 + 0.1775939i	0.1917495
23.077	**−0.11246−0.3058i**	**0.32581**	**−0.0998025−0.3157871i**	**0.3311828**
23.846	−0.02036−0.0227i	0.03051	0.0317413 + 0.1383479i	0.1419424
24.615	−0.01599−0.0096i	0.01865	0.0006574 + 0.0045333i	0.0045807
25.385	−0.01445−0.0052i	0.01535	0.0000730 + 0.0012260i	0.0012282
26.154	−0.01369−0.0031i	0.01403	−0.0000162 + 0.0005029i	0.0005031
26.923	−0.01324−0.0019i	0.01338	0.0000348 + 0.0002491i	0.0002516
27.692	−0.01297−0.0012i	0.01302	0.0000382 + 0.0001345i	0.0001398
28.462	−0.01281−0.0007i	0.01282	0.0000381 + 0.0000722i	0.0000816
29.231	−0.01272−0.0003i	0.01272	0.0000374 + 0.0000319i	0.0000492
30.000	−0.00897 + 0.0000i	0.00897	0.0000262 + 0.0000000i	0.0000262

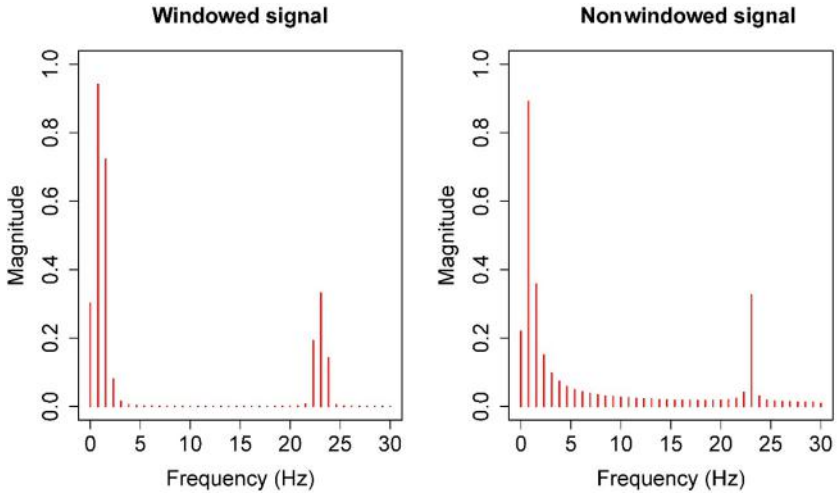

FIGURE 5.6

The Hann window reduces the spectral leakage of the digital periodic waveform in the frequency domain. The spectral plot of the waveform without tapered by a window function and without leakage is presented in Fig. 5.4C.

VIGNETTE 5.1

The following vignette contains a code in R programming language that performs the DFT from Eq. (5.25).

```
DFT = function(tseries, fs) {
    # tseries: the times series to transform
    # fs: the sampling frequency
    x = tseries
    N = length(x)
    f = seq(0, N - 1) * fs/N
    if ((N%%2) == 0) {
        f[-c(1:N/2)] = f[-c(1:N/2)] - fs  # even
    } else {
        f[-c(1:(N + 1)/2)] = f[-c(1:(N + 1)/2)] - fs  # odd
    }
    f = f[f >= 0]  # only positive f
    y = c(matrix(0, length(x), 1))
    time = seq(from = 0, to = (N - 1), by = 1)/N
    for (fi in c(1:N)) {
        sine_wave = exp(c(-(0+1i) %*% 2 %*% pi %*% (fi - 1)) * time)
        xx = sine_wave * x
        y[fi] = sum(xx[1:length(xx)])/N
    }
    y[1] = y[1]/sqrt(2)
    y[length(f)] = y[length(f)]/sqrt(2)
    magnitude = 2 * abs(y[1:length(f)])
    power = 2 * (abs(y[1:length(f)]))^2
    results = list(frequency = f, magnitude = magnitude,
    power = power, coefficients = 2 * y[1:length(f)])
}
```

(*Continued*)

VIGNETTE 5.1 (Continued)

The following vignette contains a code in R programming language that performs the DFT from Eq. (5.25) with Hann window from Eq. (5.30).

```
window_hanning = function(N){
  nn = N
  np = (2*pi*seq(from = 0, to = (nn- 1), by = 1))/nn
  w = .5*(1 - cos(2*pi*(1:nn)/(nn)))
  results = list(w = w)
}

DFTwindow = function(tseries, fs){
  # tseries: the times series to transform
  # fs: the sampling frequency
  x = tseries
  N = length(x)
  w = window_hanning(N)
  f = seq(0,N-1)*fs/N
  if ((N %% 2) == 0) {
    f[-c(1:N/2)] = f[-c(1:N/2)]-fs
  } else {
    f[-c(1:(N+1)/2)] = f[-c(1:(N+1)/2)]-fs
  }
  f = f[f>=0] # only the positive f
  y = c(matrix(0,length(x),1))
  time = seq(from = 0, to = (N - 1), by = 1)/N
  for (fi in c(1:N)) {
    sine_wave = exp(c(-1i %*% 2 %*% pi %*% (fi - 1))*time)
    xx = sine_wave*x*w$w
    y[fi] = sum(xx[1:length(xx)])/N
  }
  y[1] = y[1]/sqrt(2)
  y[length(f)] = y[length(f)]/sqrt(2)
  magnitude = 2*2*abs(y[1:length(f)])
  power = 2*2*(abs(y[1:length(f)]))^2
  results = list(frequency = f, magnitude = magnitude, power = power,coeff
icients = 2*2*y[1:length(f)])
}
```

Until now we have not made any distinction between aperiodic and random signals. This is because random signals are aperiodic. However, not all aperiodic signals are random. Periodic signals, and some aperiodic, can be described directly with mathematical treatment of the time function $x(t)$, thus these signals are called deterministic. Any random signal can only be described by means of statistical methods, because its function changes continuously with time without repeating itself exactly (Broch, 1990). Random signals whose statistical properties (mean and variance) do not vary in time are called stationary in the broader sense, whereas random signals whose

statistical properties vary in time are called nonstationary (Broch, 1990). The Hann window is recommended when the DFT is applied to random stationary digital signals (Broch, 1990; Cohen, 2014).

5.6 Stationarity and the discrete Fourier transform

When the digital random signal is stationary, the joint probability distribution does not change over time. This means that the statistics of the signal (mean and variance), and their frequency structure are unchanged over different time periods. A stationary digital signal in which the mean and variance of any recording of the signal across time equals the ensemble average is called *ergodic*. Many signals in biomechanics can be modeled as stationary and ergodic signals [e.g., electromyographic (EMG)]. The ergodicity and stationarity are very practical assumptions. When the time series is ergodic the ensemble averaging can be replaced by time averaging. This means that the statistical properties of an ordered sequence of random variables in time are the same as the statistical properties of a random variable measured many times at a certain time instant.

The Birkhoff–Khinchin ergodic theorem formulates the interchangeability of time averages and ensemble averages. Myoelectric signals are considered ergodic under conditions of sustained isometric contractions (Kleissen & Zilvold, 1994). This means that the statistical behavior of the EMG signal in a period of recording represents the ensemble average of many recordings under the same conditions. Thus, one EMG recording is sufficient to analyze a random EMG signal.

For stationary random signals, the frequency characteristics of magnitude and phase are not meaningful, thus the mean square spectral densities [power spectrum density (PSD)] are utilized. The PSD of an ergodic digital signal is based on the DFT, and is called a periodogram (Fig. 5.7). The power spectral density is estimated as the magnitude of its Fourier transform squared:

$$\left|X[k]\right|^2 = \frac{1}{N}\left|\sum_{n=0}^{N-1} x[n]e^{\left(\frac{-j2\pi kn}{N}\right)}\right|^2 \tag{5.31}$$

From the Wiener–Khinchin theorem the PSD can also be estimated from the autocorrelation (or autocovariance) function, and is called a correlogram. The autocorrelation function is the Pearson product moment correlation of a time series with itself after phase shifting one of the series forward or backward in time (Winter & Patla, 1997). The autocovariance is the normalized (by the variance) autocorrelation. The Wiener–Khinchin theorem relates the autocorrelation function to the power spectral density via the DFT. The

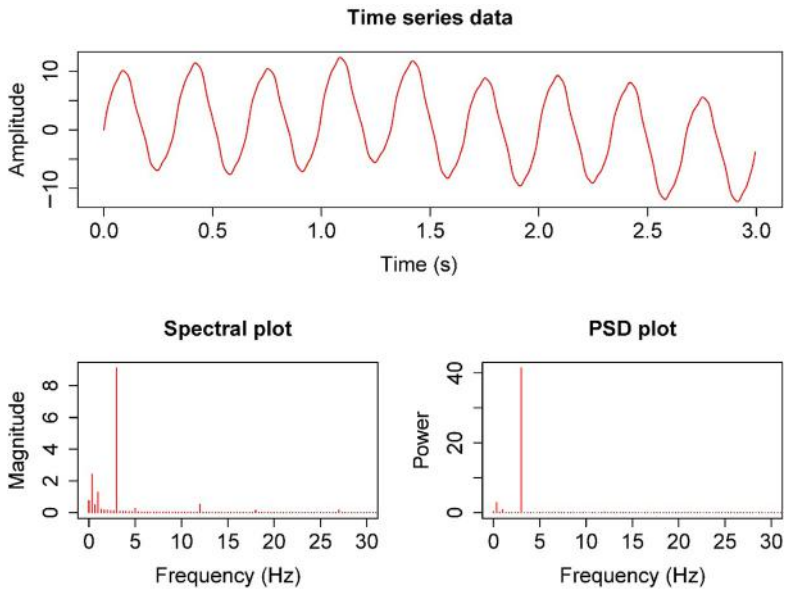

FIGURE 5.7

Spectral and power spectrum density (PSD) plots of a digital time series data.

theorem applies to stationary and, by extension, ergodic signals. Thus, the PSD function is mathematically defined as the DFT of the autocorrelation function:

$$|X[k]|^2 = \frac{1}{N}\sum_{m=0}^{N-1} r_{xx}[m]e^{\left(-\frac{j2\pi km}{N}\right)} \tag{5.32}$$

With r_{xx} the autocorrelation function and m the lag interval:

$$r_{xx}[m] = \sum_{n=0}^{N-1} x[n][n+m] \tag{5.33}$$

Recently, an alternative technique was introduced for the detection of periodicities in dynamical systems based on recurrence plots (Zbilut & Marwan, 2008). The recurrence plot-based Fourier transform links recurrence quantification with spectral analysis through the Wiener−Knichin theorem, since the autocovariance function can be obtained through the recurrence plot. The recurrence plot was introduced by Eckmann, Kamphorst, and Ruelle (1987) to visualize m-dimensional phase space trajectory through a two-dimensional representation of its recurrences (Webber & Marwan, 2015). The extension of Fourier-based techniques to nonlinear and nonstationary processes, where dynamics reside in higher dimensional spaces, give additional power to this mathematical tool.

Sometimes the DFT is used to analyze nonstationary signals. There are two main limitations when the DFT is used with nonstationary signals: power appears at frequencies that were not present in the original signal, and the time-varying changes to the frequency components in the original signal cannot be localized. This is because the DFT is used to analyze a signal in terms of basic periodic sinusoidal functions of different frequencies summed over the signal. Thus, the DFT cannot provide information about the time localization of the individual frequency components of the nonstationary signal because it is assumed that the sinusoidal basic functions with the different frequencies are spread equally over the summed signal (Peters & Williams, 1998). When the stationarity assumption is violated, the frequency domain of the signal cannot be analyzed with the DFT. Sometimes, time and frequency characteristics are combined into the joint time–frequency domain. This is necessary when the time-series to analyze is not stationary (Najarian & Splinter, 2012; Peters & Williams, 1998).

The results obtained from the DFT do not show the time-varying changes of the frequency components that are presented in the nonstationary signal. The DFT always provides one-dimensional information; the power spectrum of the frequency components. There is no information regarding the time localization of the individual frequency components. In stationary signals, all of the individual frequency components are spread equally over the signal. However, the information a nonstationary signal conveys is localized in time since the individual frequency components are not spread equally over time. In order to know when the frequencies are presented in a nonstationary signal, an alternative method must be performed, such as the short-time Fourier transform (Najarian & Splinter, 2012; Peters & Williams, 1998).

5.7 Short-time discrete Fourier transform

We have seen that spectral leakage is reduced by tapering the digital signal by a window function before the DFT takes place. A generalization of this technique is the short-time discrete Fourier transform (STDFT). A sliding window isolates short-time parts of the signal before the discrete Fourier transformation takes place. The STDFT provides two-dimensional information: the frequencies at each sliding window as a function of the time. Thus, the STDFT is a time–frequency extension of the discrete Fourier transformation (Peters & Williams, 1998).

The STDFT localizes the power spectra of the frequencies on short-time windows of the digital signal, where it is assumed that the digital signal is stationary. The windowed signal is tapered by a window function before the transformation takes place. The Hann window is recommended

(Cohen, 2014). The window function can be applied to any segment of the signal. However, care must be taken to ensure that the window function tapers all the data of the segment, especially when it is used at the beginning and end of the signal. Practically, some data could be collected before or after the time period being analyzed. After tapering, these extra data can be removed. All of the other issues of the DFT also apply to the STDFT.

By increasing the time window, the frequency resolution and precision increase (Cohen, 2014). However, by increasing the time window the time intervals are made longer, and the time precision decreases. Thus, localization in time of an individual frequency (i.e., time precision) is limited by the length of the window function (Peters & Williams, 1998). Therefore, the choice of the window's length influences both the time precision and the frequency resolution and precision. Shorter windows provide more time precision but less frequency resolution precision, and longer windows provide less time precision but better frequency resolution precision. The duration of the window should also be long enough to capture at least one cycle of the desired frequency component that we want to analyze. There is a tradeoff between time precision and frequency precision that is addressed by the *uncertainty principle*. By using a time window that tapers one cycle of the desired frequency, the time precision increases at the expense of frequency precision (Fig. 5.8). Successive windows can be overlapped. With overlapping the time precision is improved, and there are no zeroed data between time windows resulting from tapering (Cohen, 2014). Moreover, time–frequency plots become smoother (Fig. 5.8C).

Spectral analysis is a very powerful tool for finding periodic components in time-series data. There are a number of software programs that can be used to perform spectral analysis (R software is one of them), but there are many subtleties not discussed here, such as detrending and zero-padding (Beard, 2011; Huang et al., 1998; Percival & Walden, 2009; Prabhu, 2017; Stoica & Moses, 1997) that are needed for more in-depth spectral analysis. See Percival and Walden (2009) for a more detailed discussion of spectral analysis.

The DFT can be used to analyze only stationary signals because it cannot give information about the time localization of individual frequencies if the signal is nonstationary. To know where or when the frequencies are presented in a nonstationary signal, time–frequency methods should be used. The windowed, STDFT is an example of a time–frequency analysis technique with a similar mathematical definition to the DFT. It belongs to Cohen's class of time–frequency distributions together with the Wigner–Ville and Choi–Williams distributions (Cohen, 1989; Giakas, 2004). However, the STDFT provides constant time and frequency resolution. With wavelets multiresolution analysis can be performed. The wavelet transforms are a

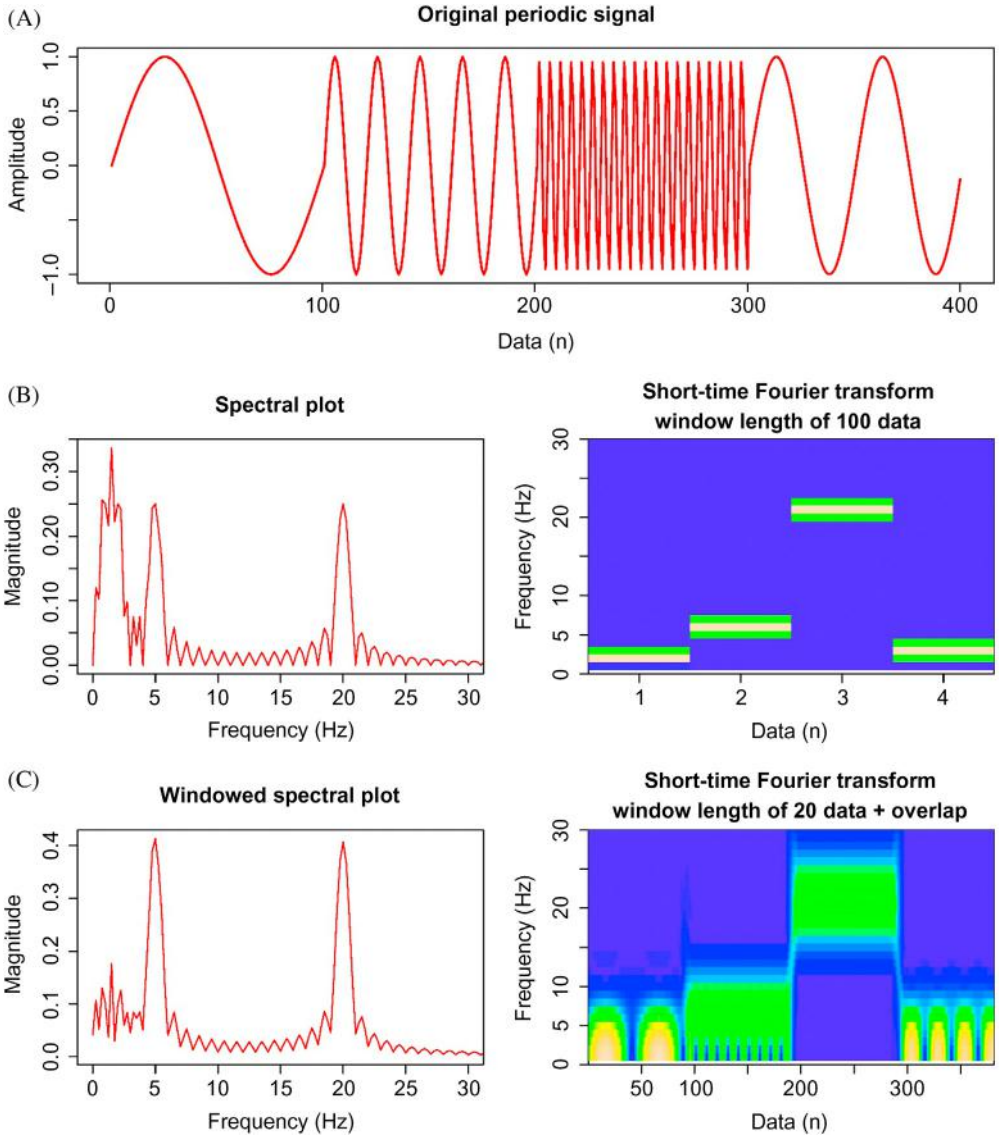

FIGURE 5.8

(A) Signal to be recorded. (B) Discrete Fourier transform (DFT) and (C) short-time discrete Fourier transform (STDFT) of a nonstationary signal. Only the time–frequency analysis provides time localization of the frequency components of the signal. However, to achieve a good time localization, narrow windows are needed at the expense of blurring the frequency domain. In contrast, wider windows provide precision in the frequency domain.

time–frequency analysis technique, that analyze a signal according to a scale and not according to their frequency (Cohen, 2014; Peters & Williams, 1998). To achieve time–frequency localization the sinusoidal basic functions used in the Fourier transform are replaced by some other functions that are more localized in time (e.g., scaling functions—wavelets) (Peters & Williams, 1998).

5.8 Noise

The errors declared by the measurement system's manufacturer are not the errors that a specific measurement system exhibits during an experiment, but rather are the limits of the errors that a measurement system could have during an experiment in an ideal environment. These errors are associated with the specific properties of the measurement system and are assessed by the manufacturer. In general, modern measurement systems fulfill the performance requirements necessary for optimal registration of any type of human movement. However, additional errors arise while conducting an experiment or after recording, during the data analysis. Errors originate from the degradation of the equipment over time, from previous bad usage, improper maintenance, suboptimal laboratory conditions and setup, and lack of user skill (Bartlett, 2007; Challis, 2007; Chiari, Croce, Leardini, & Cappozzo, 2005; Hunt, 1998; Lees & Lake, 2007; Medved, 2001). Any cable malfunction, electrical and electronic faults, improper experimental setup, temperature and humidity variations, or vibrations from the supporting structure can alter the accuracy and precision characteristics provided by the manufacturer (Bartlett, 2007; Calderita, Bandera, Bustos, & Skiadopoulos, 2013; Challis, 2007; Chiari et al., 2005; Hunt, 1998; Lees & Lake, 2007; Medved, 2001). Consequently, tests should be conducted before the experiment takes place in order to verify that the performance specifications of the measurement systems in the current laboratory conditions are in conformance with the measurement accuracy and precision stated by the manufacturer. Such tests can also verify that the system maintains its performance characteristics during operation in the experimental procedure and that the performance characteristics are adequate for the ongoing experiment, that is, experimental reliability.

What is accurate for one experimental procedure might be approximate for another. For a simplified ad hoc test of the performance properties of the measurement system, spot-checks can be done in the laboratory to verify that equipment fulfills the requirements of accuracy and precision. Measurement accuracy is defined as the closeness of agreement between a measured quantity value and a true quantity value of a measurand (i.e., the quantity intended to be measured) (ISO-JCGM 200, 2008), and is often limited by

calibration errors. Measurement precision is defined as the closeness of the agreement between measured values obtained by replicate measurements on the same or similar objects under specified conditions (ISO-JCGM 200, 2008), and is associated with random errors. Measurement errors are due to systematic [i.e., component of measurement error that in replicate measurements remains constant or varies in a predictable manner (ISO-JCGM 200, 2008)] and/or random errors [i.e., component of measurement error that in replicate measurements varies in an unpredictable manner (ISO-JCGM 200, 2008)]. Ideally, instrumental systems should not have any inherent sources of systematic error. Systematic errors can be corrected by compensation methods (calibration, filters, etc.). Operators can also introduce systematic errors. In contrast, many sources of random measurement error are inherent to the equipment. Therefore the output signal of the measurement system is always distorted by a random error, meaning that there is no correlation between the error at one data point and the error at another data point. This random error is called random noise or white noise. In general, noise in biomechanical signals is a random signal superimposed over the true recorded biomechanical signal. The superimposed noise is often modeled as white Gaussian noise. A characteristic of white Gaussian noise is that data points are uncorrelated from each other in the time domain, and they have a Gaussian distribution with zero mean. The *rnorm* function in R software can be used to generate a white Gaussian noise signal (i.e., a sequence of independent and identically distributed random variables). Unlike true biomechanical signals, noise signal has low-amplitude but high-frequency components.

Random noise can have many colors! White noise has a flat power spectrum over its frequency components, the same as white light. Using digital filters, it is possible to change the distribution of the power spectrum of the frequency components and produce other types of random noise, the so-called colored noises (e.g., red noise, pink noise, etc.). In general, the spectrum of the noises follows a $1/f^{\beta}$ power-law decay; for white noise $\beta = 0$, while for the other noises $\beta \neq 0$. A characteristic of the white Gaussian noise spectrum is that it can be reduced by increasing the sampling rate. This is because by increasing the sampling rate the white noise power spreads over a larger frequency band, improving the quality of the signal (i.e., the SNR) (Lanshammar, 1982a, 1982b; Teulings & Maarse, 1984; Woltring, 1995). Teulings and Maarse (1984), have derived the required oversampling ratio, defined as the factor that the actual sampling frequency f should be higher than its minimum sampling rate (i.e., twice the Nyquist frequency f_N):

$$\frac{f}{f_N} > \frac{1}{2k+1}\left(\frac{f_N}{f_0}\right)^{2k}\frac{\mathrm{SNR}_k}{\mathrm{SNR}} \tag{5.34}$$

where f_0 is the fundamental frequency, and SNR_k is the desired residual signal-to-noise ratio of the kth time derivative after noise reduction. The quality of the recorded signal is defined by the SNR, which is the ratio that is obtained by dividing the true signal mean amplitude with the standard deviation of the noise.

Even with careful design of the experimental setup to reduce all noise sources as much as possible, some noise will always be superimposed over the true—recorded—signal. Sometimes, the quality of the obtained time series data can be compromised by the presence of 60 Hz noise in North American and 50 Hz noise in European main power. If the collected time series are EMG signals (normally acquired at sampling rates at or above 1000 Hz), which contains most of their power in the range of 30−100 Hz, it is extremely difficult to separate the 50 Hz noise (or 60 Hz) from the real data without losing substantial information from the EMG signal (Myers, 2016).

Experimentally, noise can be quantified by measuring (i.e., recording) a constant signal. For example, the recorded signal from an unloaded force platform (center of pressure, forces, or moments) should be zero, but it is not because of the random noise inherent to the equipment (Skiadopoulos & Gianikellis, 2014). Following the definition of precision [i.e., the closeness of agreement between measured values obtained by replicate measurements on the same or similar objects under specified conditions (ISO-JCGM 200, 2008)], random noise can also be measured when a known measurand is recorded several times and the true value is subtracted from the measured value. For example, by measuring the standard deviation of an intermarker distance with a motion capture system it is possible to calculate the random error of the recorded system (Chiari et al., 2005). Equally the coefficient-of-variation can be used, which is obtained by dividing the standard deviation of the noise with the true signal mean amplitude. The higher the SNR is, or the lower the coefficient-of-variation is, the higher the quality of the recorded signal will be.

In any experiment, there will always be concerns about measurement error, or contamination of what you are trying to measure with other information that you are not trying to measure. Often the assumption is made that the noise is white Gaussian noise. Remember that the trace of a digital time series, experimentally collected after sampling, always conveys data and noise. Noise is a signal itself, which does not convey any useful information and should be removed or attenuated.

5.9 Data filtering

Experimentally collected digital signals convey information and noise (i.e., unwanted data). Digital filtering is used to deal with the experimental noise

that contaminates our signal of interest. Filtering comes from the analogy to light, where a colored filter allows only certain wavelengths of light to pass. In human movement, any operation that changes the data by reducing or amplifying certain components in either the time or frequency domain is considered filtering. Another common term for filtering is "smoothing," which usually refers to a way of forcing the data to fit a polynomial or a spline model (Woltring, 1995).

With differentiation of displacement data with respect to time the velocity (first derivative with respect to time) and acceleration (second derivative with respect to time) can be calculated. This process preferentially amplifies higher frequencies; the amplitude of the first derivative increases linearly with the number of the harmonic (e.g., the amplitude of the first derivative of the second harmonic is twice as high as that of the fundamental, whereas the first derivative of the 23rd harmonic is 23 times higher), while the amplitude of the second derivative is proportional to the *square* of the number of the harmonic (e.g., the amplitude of the second derivative of the second harmonic is four times higher than that of the fundamental, whereas the second derivative of the 23rd harmonic is 23^2 times higher) (Winter, 2009). Fig. 5.9 shows the amplification of the amplitude of the components of the W_{AB} signal after differentiation. The amplification of the 23rd harmonic of W_{AB}, especially at the second derivative, clearly masks the amplitude of the first harmonic.

The amplification of higher harmonics with differentiation is a serious problem in the analysis of biomechanical time series because, as discussed previously, it is not easy to separate the noisy part from the real data. Fig. 5.10 presents the power spectra of the first derivative (i.e., angular velocity) and second derivative (i.e., angular acceleration) of the angular displacement time-series data of the elbow joint collected by Pezzack, Norman, and Winter (1977) and modified by Lanshammar (1982a). The power spectral density of the angular velocity and acceleration demonstrate the problem created by the noise at the higher frequencies of the signal after differentiation (Giakas, 2004). Every time a differentiation with respect to time take place, the noise increases relative to the signal. Therefore, time-series data must be filtered to remove the noise superimposed over the true biological signal (Myers, 2016). In general, the data are filtered before any numerical differentiation is applied. However, since differentiators and low-pass filters are both linear operators, there will be no difference if the position signal or its derivatives are filtered first (Winter & Patla, 1997). In practical terms, current filtering techniques cannot remove all noise from the time series data, thus velocity signals are noisier than position signals and acceleration signals are noisier than velocity signals. We can use the formula of Lanshammar (1982a, 1982b), to assess the quality of the differentiated data:

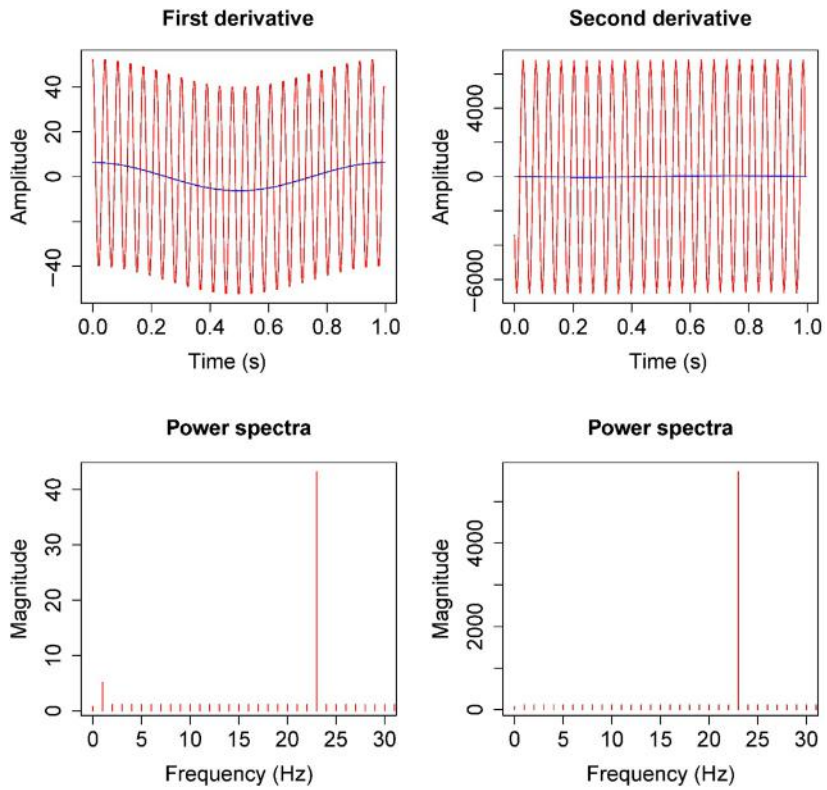

FIGURE 5.9

The first derivative (velocity) and the second derivative (acceleration) of W_{AB}, previously presented in Fig. 5.2C. The blue line is the first derivative of the W_A signal. Compare the oscillations with Fig. 5.2C. Note the dramatic increase of the high-frequency (W_B) component of the signal W_{AB}.

$$\sigma_k^2 = \sigma^2 \tau \frac{\omega_b^{2k+1}}{\pi(2k+1)} \tag{5.35}$$

where σ_k^2 is the noise variance; kth order derivative; σ^2 is the noise variance in the raw data; τ is the sampling interval; ω_b is the band-limit of the signal.

The term $\sigma^2\tau$ has been used to evaluate the measurement quality of motion capture systems (Furnee, 1989; Woltring, 1995, 1984). However, it can be used to assess the measurement quality of any recorded system (Furnee, 1989; Woltring, 1984). Small values of $\sigma^2\tau$ correspond to a less noisy system.

Fourier-based digital filters and polynomials or spline functions are commonly used to remove noise. A common type of smoothing is curve fitting, using polynomials of different orders or Fourier series. In these methods, the

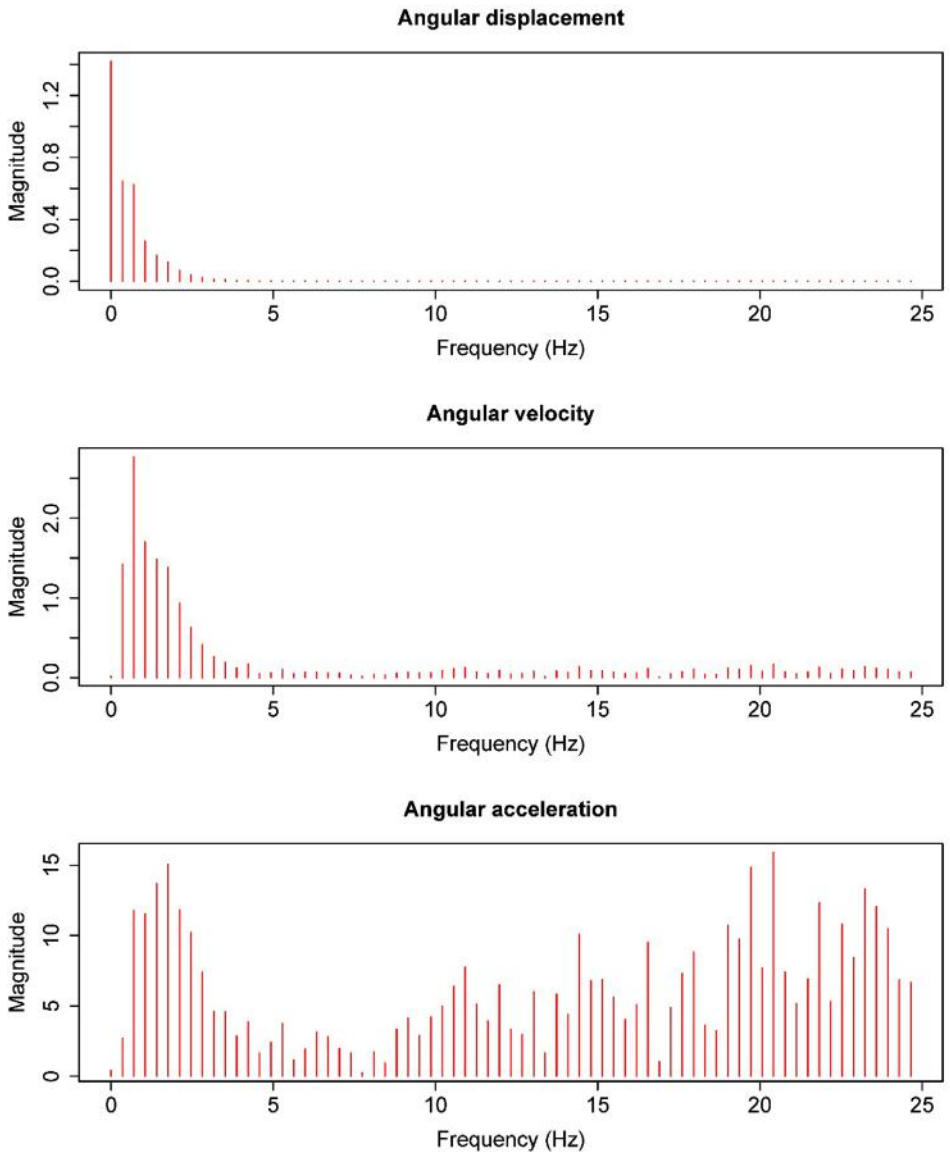

FIGURE 5.10

The power spectrum of the Lanshammar data (1982) and of its two first derivatives. The power of the higher frequency band increases dramatically, especially at the second derivative.

data are forced to fit a certain mathematical model. This is a poor method because there is limited control over what data are included or excluded, so it is likely that true data will be removed. An improved methodology that is an extension of the idea of using polynomials for smoothing is to use

splines. A spline function consists of a number of low-order polynomials that are pieced together. By using spline functions, we can differentiate (because splines are polynomials) but also smooth the data at the same time. Quintic-order natural splines are the most popular for biomechanics applications (Giakas, 2004; Myers, 2016). The software package GCVSPL developed by Woltring (1986) uses natural splines and is widely used in biomechanics. It can be downloaded from the International Society of Biomechanics website (https://isbweb.org/software/sigproc.html). Natural splines of *m*th order behave like an *m*th order double Butterworth filter (Woltring, de Lange, Kauer, & Huiskes, 1987) when the superimposed noise is white.

Another type of smoothing is digital filtering. By using Fourier-based digital filters, it is possible to change the distribution of the power spectrum of the frequency components of the signal. The operation used to change the coefficients of specific frequency components is called the transfer function. The type of transfer function determines which frequencies are filtered. The transfer function of the filter can be presented as a function of frequency: passband, transition band, and stopband (Giakas, 2004; Myers, 2016). A passband preserves the specified frequency components, a transition band progressively decreases the power of the frequency components covered, and the stopband removes all remaining frequencies (Myers, 2016). In human movement biomechanics we frequently use the lowpass to remove the high-frequency noisy part of the kinematic data, and the band-pass filter to remove the higher and lower frequencies of the EMG data. To remove the 60 Hz (or 50 Hz in Europe) main power contamination, a notch filter can be used (Fig. 5.11) (Giakas, 2004). Of course, a low-pass or a high-pass filter can be combined with a notch filter if necessary. One can select which frequencies to be removed by choosing the cutoff frequency (or cutoff frequencies for bandpass filters). The cutoff informs the filter to keep or remove previous or subsequent frequencies. There are also different algorithms that can be implemented to correctly filter the data. Two of the most common implementations of this technique are the Butterworth filter and the critically damped filter (Winter, 2009). The algorithms use the selected cutoff and contain different bands depending on what type of data are being smoothed. The most widely used filter to attenuate the high-frequency noise in biomechanical signals is the fourth-order low-pass filter proposed by Winter (2009).

The greatest challenge, however, is the selection of an appropriate cutoff frequency. When we use a high cutoff frequency, the filtered signal is close to the original raw signal because more frequency components are allowed to pass. We do not know if the additional frequency components allowed with a higher cutoff frequency are part of the signal or of the noise (or of both).

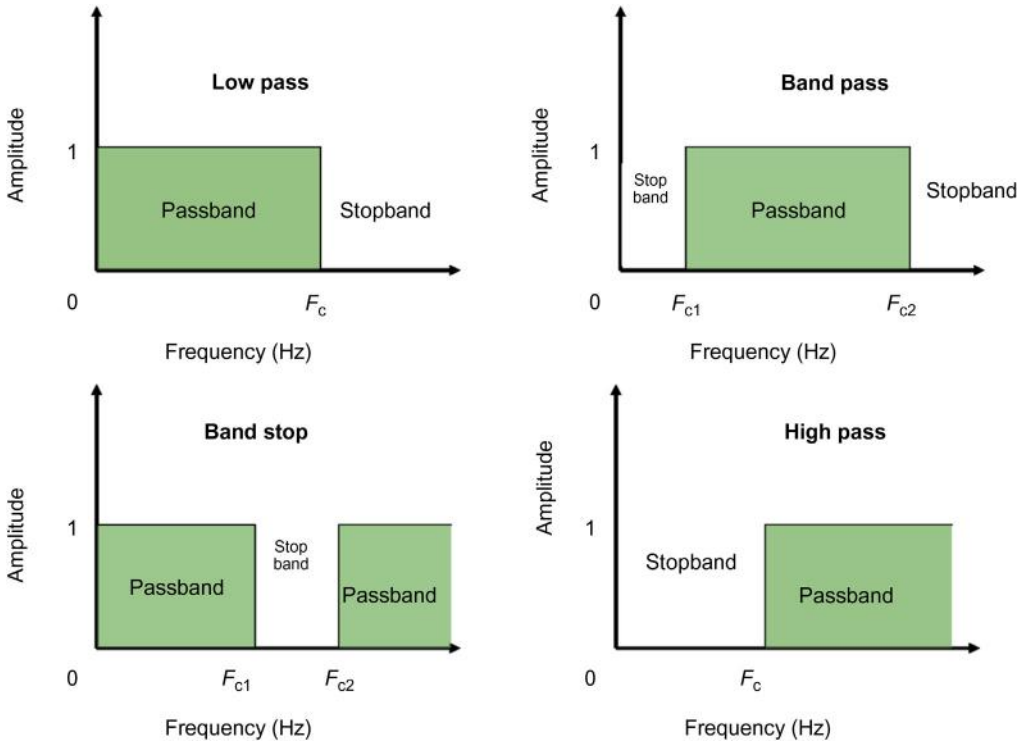

FIGURE 5.11

There are four types of filters, although in human movement we frequently use the lowpass for kinematic data filtering and the band pass for EMG data filtering. The type chosen depends on the frequencies that we want to eliminate. To eliminate the higher frequencies we use a low-pass filter, to eliminate the lower frequencies we use a high-pass filter, to remove frequency components at the central part of the power spectrum we use a band-stop filter, to keep central frequency components and remove the components at the lowest and the highest band of the spectrum we use a band-pass filter. In the low-pass and high-pass filters *Fc* indicates the cutoff frequency. In the band-stop and band-pass filters *Fc*1 and *Fc*2 define a range in the frequency spectrum to keep or remove specific frequency bands.

On the other hand, a lower cutoff frequency could eliminate useful frequency components that are part of the true signal. Therefore, the cutoff frequency must be carefully selected to remove only (as much as possible) the noise superimposed on the true biological signal. For example, Fig. 5.12 presents the angular displacement time series data of the elbow joint collected by Pezzack et al. (1977) and modified by Lanshammar (1982a) filtered with three different cutoff frequencies (Giakas, 2004). By increasing the cutoff frequency, more harmonics are used to reconstruct the time series data, and the reconstructed signal gets closer to the raw data.

Stergiou, Bates, and James (1999) published a paper on the mechanisms of running injuries. In their paper, they found that the inappropriate usage of a

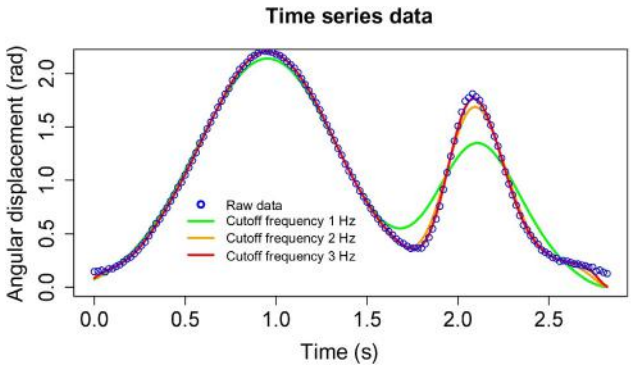

FIGURE 5.12

The angular displacement time-series data of the elbow joint collected by Pezzack et al. (1977) and modified by Lanshammar (1982a) filtered with the fourth-order zero-phase-shift low-pass filter from Eq. (5.37) at three different cutoff frequencies (1, 2, and 3 Hz). A higher cutoff frequency will "push" the reconstructed signal toward the raw signal. The cutoff frequency of 3 Hz provides an acceptable reconstruction of the angular displacement data.

cutoff frequency in the biomechanics of running literature results in very "smooth" rearfoot angle data even when impact forces have increased dramatically, and this impact should have been reflected in the angular data. Specifically, Stergiou et al. (1999) examined the asynchrony between subtalar and knee joint angular movement during running. They found that the rearfoot angle is described by a bimodal curve as opposed to the unimodal curves presented in the literature (Stergiou & Bates, 1997). The bimodal nature of this curve was more pronounced with higher impact forces (i.e., running on a harder surface, at faster speeds, or over higher obstacles) (Stergiou et al., 1999). Importantly, the presence of a bimodal rearfoot angle curve was related to the function of the knee; the more pronounced was the bimodality of the rearfoot angle curve, the higher was the asynchrony between the knee and the ankle. This was shown by the authors to be strongly related to susceptibility to running injuries. The observation of bimodal rearfoot angle curves with higher impact forces during running was made possible by the authors only after careful selection of an appropriate cutoff frequency. Cutoff frequencies below 15 Hz attenuated severely the high-frequency component of the signal. Interestingly, even though in the literature a sampling frequency of 180–200 Hz is recommended based on spectra analysis, the cutoff frequencies used currently remain around 6 Hz or even lower. Therefore it is not surprising that many authors suggest that we are still uncertain as to how runners become injured! Inappropriate biomechanics in terms of data analysis has lead to inappropriate conclusions and confusion in the literature that has propagated through the years.

Table 5.6 Contribution of frequencies to the overall power spectrum (PS) and power spectral density (PSD) of the data shown in Fig. 5.7.

Harmonic #	Frequency (Hz)	PS (%)	CPS (%)	PSD (%)	CPSD (%)
1	0.333	14.41	14.40	6.43	6.43
2	0.667	3.00	17.40	0.28	6.71
3	1.000	7.72	25.10	1.85	8.55
4	1.333	1.31	26.40	0.05	8.61
5	1.667	1.10	27.60	0.04	8.64
6	2.000	1.01	28.60	0.03	8.68
7	2.333	1.03	29.60	0.03	8.71
8	2.667	1.34	30.90	0.06	8.76
9	3.000	54.17	85.10	90.83	99.59
10	3.333	0.38	85.50	0.00	99.60
11	3.667	0.03	85.50	0.00	99.60
12	4.000	0.10	85.60	0.00	99.60
13	4.333	0.14	85.80	0.00	99.60
14	4.667	0.17	85.90	0.00	99.60
15	5.000	1.34	87.30	0.06	99.65
16	5.333	0.12	87.40	0.00	99.65
17	5.667	0.14	87.50	0.00	99.65
18	6.000	0.14	87.70	0.00	99.65

Therefore it is important to select a cutoff frequency that will preserve most of the data of interest. Usually an optimization method is used, or sometimes a cutoff frequency that maintains 99% of the data is chosen (Table 5.6). The roll-off is the steepness of the filter response in the transition between bands (from passband to stopband). The steepness of the slope changes with the filter order. As the order is increased, the sharpness of the slope is increased and vice versa. The fourth-order low-pass filter proposed by Winter (2009) behaves well for biomechanical data. The effect of the order is mainly visible at the second derivative (i.e., acceleration data). For example, Fig. 5.13 presents vertical acceleration data from Vaughan (1982) filtered with the low-pass filter proposed by Winter (2009) with different orders (Giakas, 2004). By increasing the order, oscillations are introduced to the signal. The time series data should be equal to $g = -9.81$ m/s (gravitational acceleration) but it is not. At both edges the filter introduces errors; at the start past unfiltered data are need and at the end feature unfiltered data are needed. At the second derivative this problem is very obvious. The best solution is to collect additional data before and after the desired signal, however, extrapolation techniques have been suggested if this is not possible (Giakas, Baltzopoulos, & Bartlett, 1997; Smith, 1989; Vint & Hinrichs, 1996).

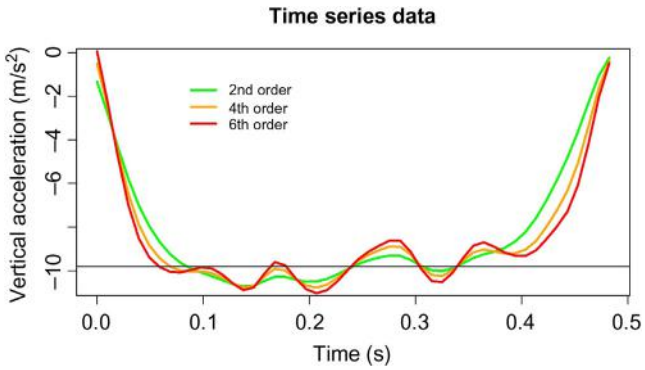

FIGURE 5.13

The calculated acceleration of a free-falling ball as recorded by Vaughan (1982) after being filtered with a Butterworth digital filter (cutoff frequency 4 Hz). The acceleration should be equal to the gravitational acceleration (-9.8 m/s^2), but it appears not to be. This graph demonstrates the effect of the order of the filter. The increase in order from two to four and then to six introduces unwanted oscillations in the acceleration pattern. The problem of a nonconstant acceleration around the area of -9.84 m/s^2 is more evident at the edges.

The optimal cutoff frequency for the low-pass digital filter can be found by residual analysis (Winter, 2009), and for the smoothing splines by applying a generalized cross-validation (GCV) (Woltring, 1986). The residual analysis compares the residuals between filtered and raw signals over a range of different cutoff frequencies, and the cutoff frequency that minimizes both signal distortion and noise that passes the filter is chosen. GCV defines the optimal cutoff frequency as the lowest frequency for which the residual noise is white.

Digital filtering is performed only with equidistantly sampled, uniformly weighted data. Although biomechanical time series are rarely nonequidistant, it is very common that the noise superimposed over the true signal is not uniformly weighted. Instead, the noise could be a nonstationary signal whose joint probability distribution changes when shifted in time (e.g., not the same moments). Therefore an alternative method to the Fourier-based digital filtering for removing the noise superimposed over a biomechanical signal is the smoothing splines method with the implementation of a GCV procedure (Woltring, 1986). Compared to the Fourier-based digital filters, the smoothing splines techniques can also remove noise from nonequidistantly sampled and nonuniformly weighted data (i.e., nonstationary noise signals) (Woltring, 1986), while, for example, the Butterworth filter can be performed only on equidistantly sampled and uniformly weighted data (i.e., stationary noise signals).

It is important to remember that research questions drive our time-series data analysis. Therefore, it is recommended to avoid digital filtering if the true dynamics of the system need to be captured (Myers, 2016). The Fourier-based filters are not designed for, and are not recommended to be used on,

data that will subsequently be analyzed using nonlinear techniques (Myers, 2016), because they will alter the nonlinear dynamics of the time series (Rapp, Albano, Schmah, & Farwell, 1993; Theiler & Eubank, 1993). Nonlinear filters are not recommended to be used on data that will subsequently be analyzed using nonlinear techniques because the underlying dynamics can be distorted (Kantz & Schreiber, 2004). Their use with experimentally collected time-series data is somewhat tricky as we cannot know the nature of the underlying behavior that we try to investigate by reconstructing a state space (Myers, 2016). Moreover, filtering the time series can alter the embedding dimension (a parameter also used to reconstruct the state space) and can influence calculations of the time lag and others (Myers, 2016).

5.10 Practical implementation

As suggested by Winter (2009), to cancel the phase shift of the output signal relative to the input that is introduced by the second-order filter, the once-filtered data has to filtered again, but this time in the reverse direction. However, at every pass the −3dB cutoff frequency is pushed lower, and a correction is needed to match the original single-pass filter. This correction should be applied once the coefficients of the fourth-order low-pass filter are calculated. Nevertheless, it should be also checked whether functions of closed source software use the correction factor. If they have not used it, the output of the analyzed signal will be distorted. The format of the recursive second-order filter is given by Eq. (5.36) (Winter, 2009):

$$y_k = \alpha_0 x_k + \alpha_1 x_{k-1} + \alpha_2 x_{k-2} + \beta_1 y_{k-1} + \beta_2 y_{k-2} \tag{5.36}$$

where y are the filtered output data, x are past inputs, and k the kth sample. The coefficients $\alpha_0, \alpha_1, \alpha_2, \beta_1$, and $\beta 2$ for a second-order Butterworth low-pass filter are computed from Eq. (5.37) (Winter, 2009):

$$\begin{aligned}
\omega_c &= \frac{\tan\left(\frac{\pi f_c}{f_s}\right)}{C} \\
K_1 &= \sqrt{2}\omega_c \\
K_2 &= \omega_c^2 \\
K_3 &= \frac{\alpha_1}{K_2} \\
\alpha_0 &= \frac{K_2}{1 + K_1 + K_2} \\
\alpha_1 &= 2\alpha_0 \\
\alpha_2 &= \alpha_0 \\
\beta_1 &= K_3 - \alpha_1 \\
\beta_2 &= 1 - \alpha_1 - K_3
\end{aligned} \tag{5.37}$$

where, ω_c is the cutoff angular frequency in rad/s, f_c is the cutoff frequency in Hz, and f_s is the sampling rate in Hz. When the filtered data are filtered again in the reverse direction to cancel phase-shift, the following correction factor to compensate for the introduced error should be used:

$$C = (2^{\frac{1}{n}} - 1)^{\frac{1}{4}} \tag{5.38}$$

where $n \geq 2$ is the number of passes. For a single-pass $C = 1$, and no compensation is needed. For a dual pass, ($n = 2$), a compensation is needed, and the correction factor should be applied. Thus, the ω_c term from Eq. (5.37) is calculated as follows:

$$\omega_c = \frac{\tan\left(\frac{\pi f_c}{f_s}\right)}{(2^{\frac{1}{2}} - 1)^{\frac{1}{4}}} = \frac{\tan\left(\frac{\pi f_c}{f_s}\right)}{0.802} \tag{5.39}$$

A systematic error is introduced to the signal if the correction factor is not applied. Therefore, remember to check any algorithm before using it. Let us check the correctness of the fourth-order low-pass filter that was built previously in R language. Vignette 5.2 contains the code to perform Winter's (2009) low-pass filter in R programming language. Because the filter needs two past inputs (two data points) to compute a present filtered output (one data point), the time-series data to be filtered (the raw data) should be padded at the beginning and at the end. Additional data are usually collected before and after the period of interest.

1. The first step is to create a sine (or equally a cosine) wave with known amplitude and known frequency. Vignette 5.3 is used to synthesize periodic digital waves. Let us create a simple periodic sine wave $s[n]$ with the following characteristics:
   a. Amplitude $A = 1$ unit (e.g., 1 m);
   b. Frequency $f = 2$ Hz;
   c. Phase $\theta = 0$ rad;
   d. Shift $a_0 = 0$ unit (e.g., 0 m).

   Let us choose an arbitrary fundamental period $T_0 = 2$ seconds, which corresponds to a fundamental frequency of $f_0 = 1/T_0 = 0.5$ Hz. Now, knowing the fundamental frequency, the fourth harmonic that corresponds to a sine wave with frequency of $f = 2$ Hz will be chosen. The periodic sine wave $s[n]$ will be sampled at $Fs = 40$ Hz ($T_s = 1/40$ seconds) (i.e., 20 times the Nyquist frequency, $f_N = 2$ Hz). The sine wave will be recorded for a time interval of $t = 2$ s, which corresponds to $N = 80$ data points. Thus, and because $\omega_0 = 2\pi f_0$, we have:

   $$s[n] = \sin(2\omega_0 n T_s)$$

   which means that the fourth harmonic has frequency $f = 2$ Hz. Fig. 5.14A shows the sine wave created. The first and last 20 data points can be considered as extra points (padded). Additional data at

VIGNETTE 5.2

The following vignette contains a code in R programming language that performs the fourth-order zero-phase-shift low-pass filter from Eq. (5.37).

```
WinterLowPassFilter = function(raw, sr, n, fc) {
  # sr = sampling frequency
  # n = number of passes
  # fc = cut-off frequency
  signal = raw
  # Correction factor for number of passes required
  # Correction factor
  cf = (2^(1/n) - 1)^0.25
  # Angular cutoff frequency
  omega_c = 2 * pi * fc
  # Adjusted angular cutoff frequency
  omega_ac = tan(omega_c/(2 * sr))
  # Corrected-adjusted angular cutoff frequency
  omega_cac = omega_ac/cf
  # Required Coefficients
  k1 = sqrt(2) * omega_cac
  k2 = omega_cac^2
  a0 = k2/(1 + k1 + k2)
  a1 = 2 * a0
  a2 = a0
  k3 = a1/k2
  b1 = k3 - a1
  b2 = 1 - a1 - k3
  # CHECK = a0 + a1 + a2 + b1 + b2
  # Single low-pass Butterworth filter in forward direction
  FilteredData = matrix(0, length(signal), 1)
  for (i in c(1:length(signal))) {
    if (i >= 3) {
      FilteredData[i] = a0 * signal[i] + a1 * signal[i - 1] + a2 * signal[
i - 2] + b1 * FilteredData[i - 1] + b2 * FilteredData[i - 2]
    } else if (i == 2) {
      FilteredData[i] = a0 * signal[i] + a1 * signal[i - 1] + b1 * Filtere
dData[i - 1]
    } else {
      FilteredData[i] = a0 * signal[i]
    }
  }
  # Second low-pass Butterworth Filter in the reverse direction
  # reverse the order of the filtered data
  signal = FilteredData[seq(length(FilteredData), 1)]
  FilteredData = matrix(0, length(signal), 1)
  for (i in c(1:length(signal))) {
    if (i >= 3) {
      FilteredData[i] = a0 * signal[i] + a1 * signal[i - 1] + a2 * signal[
i - 2] + b1 * FilteredData[i - 1] + b2 * FilteredData[i - 2]
    } else if (i == 2) {
      FilteredData[i] = a0 * signal[i] + a1 * signal[i - 1] + b1 * Filtere
dData[i - 1]
    } else {
      FilteredData[i] = a0 * signal[i]
    }
  }
  # reverse the order of the second-pass filtered data
  signal = FilteredData[seq(length(FilteredData), 1)]
}
```

VIGNETTE 5.3

The following vignette contains a code in R programming language that synthesizes periodic waveforms from sinusoids.

```
Fourier.Series = function(A.components, harmonics, phase.components, fs, T, t)
{
  # harmonics = harmonics of the signal; c(1,...,n) with n = integer
  # A.components = Amplitude of the harmonics; c(A1,A2,...,An) with A = real
positive
  # fs = sampling rate (Hz); should not violate sampling theorem; fs > 2*F0*n
with F0 the fundamental frequency and n the number of the harmonics
  # T = Fundamental period (seconds)
  # t = Recorded time (seconds)
  F0 = 1/T # Fundamental frequency (Hz)
  omega0 = 2*pi*F0 # Fundamental angular frequency (rad/sec)
  T0 = seq(from = 0, to = T-(1/fs), by = 1/fs) #  Time vector of T (seconds)
  ts = seq(from = 0, to = t-(1/fs), by = 1/fs) #  Time vector of t (seconds)
  signal_T0 = sapply(T0, function(t) sum(A.components*sin(harmonics*omega0*t
+ phase.components)))
  signal_ts = sapply(ts, function(t) sum(A.components*sin(harmonics*omega0*t
+ phase.components)))
  results = list(T0 = T0, ts = ts, s_T0 = signal_T0, s_ts = signal_ts,F0 = F0)

}
```

the beginning and end of the signal are needed for the next steps because the filter is does not behave well at the edges. Thus, the signal of interest starts at 0.5 seconds and ends at 1.5 seconds, which corresponds to $N = 40$ data points.

2. An extra, but not mandatory, step is to interpolate the created sine wave in order to increase the temporal resolution of the created signal (Fig. 5.14B). Of course, when a digital periodic signal is created from scratch, like we are doing using the R code in the vignettes, we can easily sample the signal at higher frequencies. However, if we want to use real biomechanical time series data, that have already been collected, a possible way to increase its temporal resolution is by using the Whittaker–Shannon interpolation formula. With the Whittaker–Shannon interpolation a signal is up-sampled with interpolation using the *sinc()* function (Yaroslavsky, 1997):

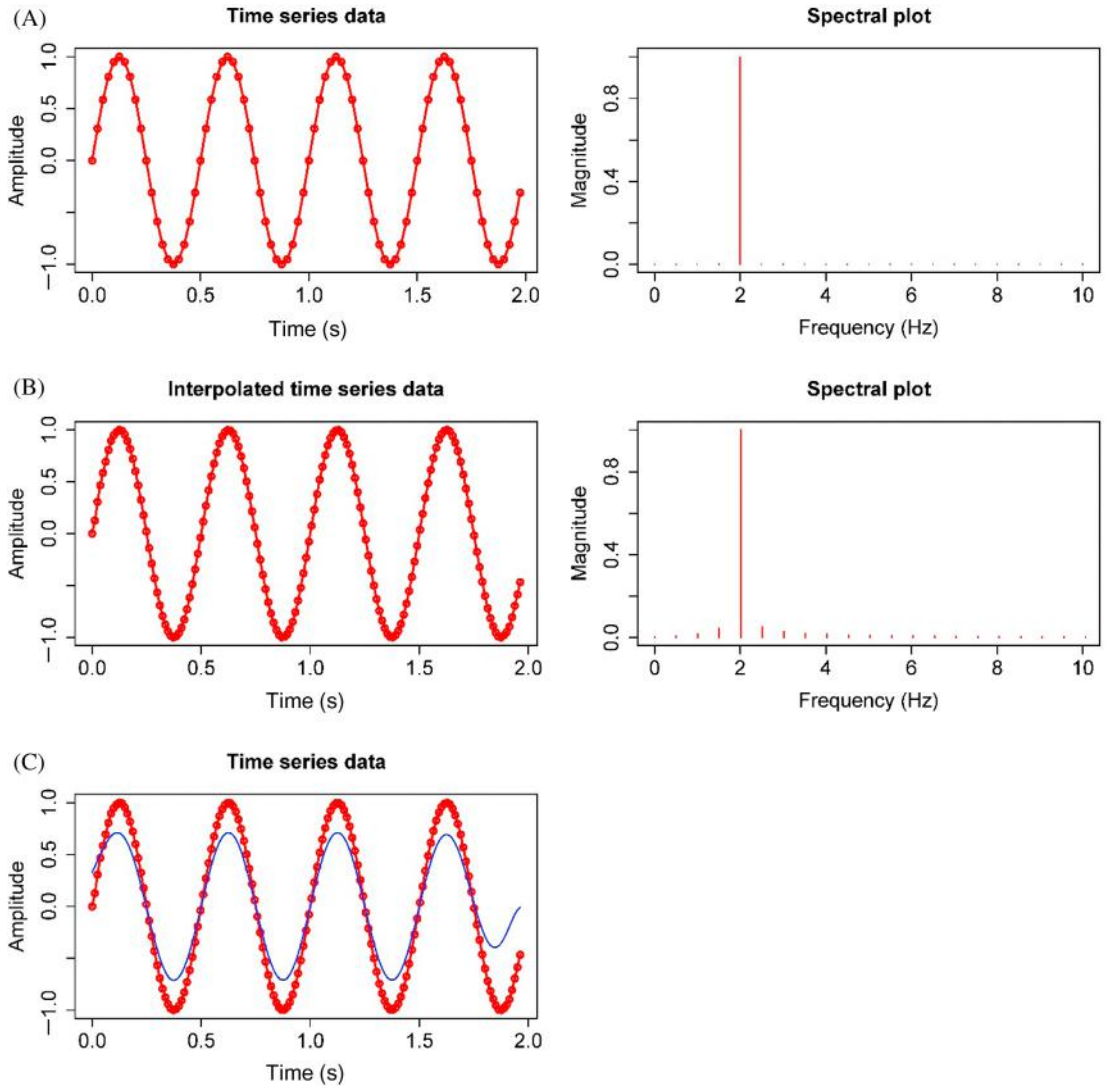

FIGURE 5.14

(A) Example of a low-pass filter (cutoff frequency = 2 Hz) applied to a sine wave sampled at 40 Hz, with amplitude equal to 1 m, and frequency equal to 2 Hz. (B) The signal interpolated by a factor of 2, and filtered with cutoff frequency equal to the frequency of the sine wave (cutoff frequency = 2 Hz). (C) Since the amplitude of the filtered signal has been reduced by a ratio of 0.707, the low-pass filter correctly attenuated the signal. The power spectra of the original and reconstructed signal are shown.

VIGNETTE 5.4

The following vignette contains a code in R programming language that runs the normalized discrete *sinc()* function, and the Whittaker–Shannon interpolation function.

```
sinc = function(x) {
  n = which(x == 0)
  if (identical(n, integer(0))) {
    y = sin(pi * x)/(pi * x)
  } else {
    y = sin(pi * x)/(sin((pi * x)/length(x))) * length(x)
    y[[n]] = 1
  }
}
WhittakerShannonInterpolation = function(y, m, sr) {
  # y = signal
  # m = increased by m integer
  # sr = sampling rate
  u = seq(0, length(y) - 1, length = length(y) * m)
  yp = matrix(0, length(u), 1)
  x = seq(from = 0, to = length(y) - 1, by = 1)
  for (i in seq(from = 1, to = length(u), by = 1)) {
    yp[[i]] = sum(y * sinc((x - u[i])))
  }
  t = seq(0, (1/sr) * (length(y) - 1), length = m * length(y))
  results = list(t = t, n = u, Interpolated = yp)
}
```

$$s(x) = \sum_{n=0}^{N-1} \alpha_n \frac{\sin\left(\pi\left(\frac{x}{\Delta x} - n\right)\right)}{N\sin\left(\pi\left(\frac{x}{\Delta x} - n\right)/N\right)} \tag{5.40}$$

The Whittaker–Shannon interpolation formula can be used to increase the temporal resolution after removing the "white" noise from the data. Without filtering, the interpolation results in a noise level equal to that of the original signal before sampling (Marks, 1991). However, the interpolation noise can be reduced by both oversampling and filtering the data before interpolation (Marks, 1991). An alternative, and efficient, method is to run the DFT, zero-pad the signal, and then take the IDFT to reconstruct it. Vignette 5.4 can be used to increase the temporal resolution by a factor of 2, which corresponds to a sampling frequency of 80 Hz.

3. The third step is to filter the previously created sine wave with the fourth-order zero-phase-shift low-pass filter, setting the cutoff

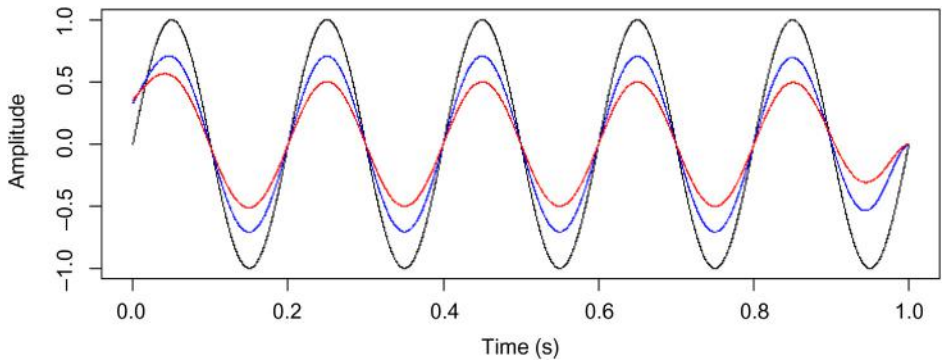

FIGURE 5.15

Example of a recursive low-pass filter applied to a sine wave with amplitude equal to 1 m and cutoff frequency equal to the frequency of the sine wave. Since the amplitude of the filtered signal has been reduced by a ratio of 0.707, the low-pass filter correctly attenuated the signal. However, the function without the correction factor reduced the amplitude by nearly one-half (0.51), indicating that the coefficients need correction.

frequency equal to the sine wave frequency $f = 2$ Hz. Vignette 5.2 is used for step 3. To cancel any shift (i.e., a zero-phase-shift filter) $n = 2$ passes must be chosen. The interpolated signal has a sampling rate of 80 Hz.

4. The fourth step is to investigate the frequency response of the filtered sine wave. The frequency response of the Butterworth filter is given by Eq. (5.41)

$$\left|\frac{A_{\text{out}}}{A_{\text{in}}}\right| = \frac{1}{\sqrt{\left(1+\frac{f_s}{f_{3\text{dB}}}\right)^{2n}}} \tag{5.41}$$

where the point at which the amplitude response, A_{out}, of the input signal, $s[n]$, with frequency, f, and amplitude, A_{in}, drops off by 3dB and is known as the cutoff frequency, $f_{3\text{dB}}$. When the cutoff frequency is set equal to the frequency of the signal ($f_{3\text{dB}} = f$), the ratio should be equal to 0.707, since:

$$\left|\frac{A_{\text{out}}}{A_{\text{in}}}\right| = \frac{1}{\sqrt{2}} \approx 0.707 \tag{5.42}$$

Fig. 5.14C shows the plots of the filtered and interpolated sine wave. Since the ratio of the maximum value of the filtered sine wave to the original sine wave ratio = 0.707, the created fourth-order zero-phase-shift low-pass filter works properly. Without the correction factor the amplitude reduces nearly to half (0.51), indicating that the coefficients of the filter needed correction. Fig. 5.15 also shows an erroneously filtered signal. You can try to create Fig. 5.15 by yourself.

The same procedure should be applied to check whether the output of the functions from closed source software used the correction factor or not. For example, using the *library(signal)* of the R computational software, if x is the vector that contains the raw data, then using *butter()* the Butterworth coefficients can be generated.

5.11 Conclusion

It is important to remember that the research question should drive our time-series data analysis. In addition, remember to consider the following:

- *Sampling frequency*: Sample at 10 times the Nyquist frequency. The Nyquist frequency within the data is determined with spectral analysis.
- *Noise*: Optimize the SNR.
- *Filtering and smoothing*: Be very cautious in filtering data intended to use for nonlinear analysis. If filtering must be done, find a cutoff frequency using optimization techniques. Do not copy previous methodologies without critique. Every biomechanical time series is unique. Filtering digital time series data based on a Fourier transform is a very common method of data manipulation for many types of linear analyses.
- *Algorithms*: Always check that they are doing what they are supposed to do. Study how software algorithms work before using them. Conduct simulation studies to ensure that everything is working properly. Visually check your data again and again.

References

Bartlett, R. (2007). *Introduction to sports biomechanics: Analysing human movement patterns*. New York: Routledge.

Bartlett, R., Müller, E., Lindinger, S., Brunner, F., & Morriss, C. (1996). Three-dimensional evaluation of the kinematic release parameters for javelin throwers of different skill levels. *Journal of Applied Biomechanics, 12*, 58–71.

Beard, J. K. (2011). *The FFT in the 21st century: Eigenspace processing*. New York, London: Springer.

Broch, J. T. (1990). *Principles of experimental frequency analysis*. New York: Elsevier Applied Science. Elsevier Science Publishers.

Brunt, D., Liu, S.-M., Trimble, M., Bauer, J., & Short, M. (1999). Principles underlying the organization of movement initiation from quiet stance. *Gait and Posture, 10*, 121–128.

Calderita, L. V., Bandera, J. P., Bustos, P., & Skiadopoulos, A. (2013). Model-based reinforcement of kinect depth data for human motion capture applications. *Sensors, 13*, 8835–8855.

Cavanaugh, J. T., Shinberg, M., Ray, L., Shipp, K. M., Kuchibhatla, M., & Schenkman, M. (1999). Kinematic characterization of standing reach: Comparison of younger vs. older subjects. *Clinical Biomechanics, 14*, 271–279.

Challis, H. J. (2007). *Data processing and error estimation. Biomechanical evaluation of movement in sport and exercise, The British Association of Sport and Exercise Sciences Guide* (pp. 129–152). Oxon: Taylor & Francis.

Chiari, L., Croce, U. D., Leardini, A., & Cappozzo, A. (2005). Human movement analysis using stereophotogrammetry: Part 2: Instrumental errors. *Gait and Posture*, *21*, 197–211.

Cohen, L. (1989). Time-frequency distributions—A review. *Proceedings of the IEEE*, *77*, 941–981.

Cohen, M. X. (2014). *Analyzing neural time series data: Theory and practice*. Cambridge: The MIT Press.

Cooley, J. W., & Tukey, J. W. (1965). An algorithm for the machine calculation of complex Fourier series. *Mathematics of Computation*, *19*, 197–301.

Dingwell, J. B., & Cavanagh, P. R. (2001). Increased variability of continuous overground walking in neuropathic patients is only indirectly related to sensory loss. *Gait and Posture*, *14*, 1–10.

Eckmann, J.-P., Kamphorst, S. O., & Ruelle, D. (1987). Recurrence plots of dynamical systems. *Europhysics Letters (EPL)*, *4*, 973–977.

Ferdjallah, M., Harris, G. F., & Wertsch, J. J. (1999). Instantaneous postural stability characterization using time-frequency analysis. *Gait and Posture*, *10*, 129–134.

Furnee, E. H. (1989). *Advances in TV/computer motion monitoring. Images of the twenty-first century. Proceedings of the annual international engineering in medicine and biology society* (pp. 1053–1054). Seattle, WA: IEEE.

Gaydecki, P. (2005). *Foundations of digital signal processing: Theory, algorithms and hardware design*. London: Institution of Electrical Engineers.

Giakas, G. (2004). Power spectrum analysis and filtering. In N. Stergiou (Ed.), *Innovative analyses of human movement* (pp. 223–258). Champaign, IL: Human Kinetics.

Giakas, G., Baltzopoulos, V., & Bartlett, R. M. (1997). Improved extrapolation techniques in recursive digital filtering: A comparison of least squares and prediction. *Journal of Biomechanics*, *31*, 87–91.

Huang, N. E., Shen, Z., Long, S. R., Wu, M. C., Shih, H. H., Zheng, Q., . . . Liu, H. H. (1998). *The empirical mode decomposition and the Hilbert spectrum for nonlinear and non-stationary time series analysis. Proceedings of the Royal Society A: Mathematical, Physical and Engineering Sciences* (454, pp. 903–995).

Hunt, A. (1998). *Guide to the measurement of force*. London: The Institute of Measurement and Control.

ISO-JCGM 200. (2008). International vocabulary of metrology—Basic and general concepts and associated terms (International Vocabulary of Metrology, VIM). JCGM 200:2008.

Kantz, H., & Schreiber, T. (2004). *Nonlinear time series analysis* (2nd ed.). Cambridge: Cambridge University Press.

Kleissen, R. F. M., & Zilvold, G. (1994). Estimation uncertainty in ensemble averaged surface EMG profiles during gait. *Journal of Electromyography and Kinesiology*, *4*, 83–94.

Lanshammar, H. (1982a). On practical evaluation of differentiation techniques for human gait analysis. *Journal of Biomechanics*, *15*, 99–105.

Lanshammar, H. (1982b). On precision limits for derivatives numerically calculated from noisy data. *Journal of Biomechanics*, *15*, 459–470.

Lees, A., & Lake, M. (2007). *Force and pressure measurements. Biomechanical evaluation of movement in sport and exercise, The British Association of Sport and Exercise Sciences Guide* (pp. 53–76). Oxon: Taylor & Francis.

Marks, R. J. I. (1991). *Introduction to Shannon sampling and interpolation theory*. New York: Springer-Verlag.

Medved, V. (2001). *Measurement of human locomotion*. Boca Raton, FL: CRC Press.

Myers, S. (2016). Time series. In N. Stergiou (Ed.), *Nonlinear analysis for human movement variability* (p. 405). CRC Press.

Najarian, K., & Splinter, R. (2012). *Biomedical signal and image processing* (2nd ed.). Boca Raton, FL: Taylor & Francis/CRC Press.

Önell, A. (2000). The vertical ground reaction force for analysis of balance? *Gait and Posture*, *12*, 7–13.

Percival, D. B., & Walden, A. T. (2009). *Spectral analysis for physical applications*. Cambridge: Cambridge University Press.

Peters, T. M., & Williams, J. (1998). *The Fourier transform in biomedical engineering*. Boston, MA: Birkhäuser.

Pezzack, J. C., Norman, R. W., & Winter, D. A. (1977). An assessment of derivative determining techniques used for motion analysis. *Journal of Biomechanics*, *10*, 377–382.

Prabhu, K. M. M. (2017). *Window functions and their applications in signal processing*. Boca Raton, FL: CRC Press.

R Core Team, 2018. R: A language and environment for statistical computing. R Foundation for Statistical Computing, Vienna.

Rapp, P. E., Albano, A. M., Schmah, T. I., & Farwell, L. A. (1993). Filtered noise can mimic low-dimensional chaotic attractors. *Physical Review E*, *47*, 2289–2297.

Scoppa, F., Capra, R., Gallamini, M., & Shiffer, R. (2013). Clinical stabilometry standardization: Basic definitions—Acquisition interval—Sampling frequency. *Gait and Posture*, *37*, 290–292.

Seeger, R. J. (1966). *Curious students. Men of physics: Galileo Galilei, his life and his works* (pp. 3–6). Pergamon Press.

Skiadopoulos, A., & Gianikellis, K. (2014). Random error propagation analysis in center of pressure signal. In *5th IEEE RAS/EMBS international conference on biomedical robotics and biomechatronics* (pp. 632–637). Sau Paulo: IEEE.

Smith, G. (1989). Padding point extrapolation techniques for the butterworth digital filter. *Journal of Biomechanics*, *22*, 967–971.

Stergiou, N., & Bates, B. T. (1997). The relationship between subtalar and knee joint function as a possible mechanism for running injuries. *Gait and Posture*, *6*, 177–185.

Stergiou, N., Bates, B. T., & James, S. L. (1999). Asynchrony between subtalar and knee joint function during running. *Medicine and Science in Sports and Exercise*, *31*, 1645.

Stoica, P., & Moses, R. L. (1997). *Introduction to spectral analysis*. Upper Saddle River, NJ: Prentice Hall.

Teulings, H.-L., & Maarse, F. J. (1984). Digital recording and processing of handwriting movements. *Human Movement Science*, *3*, 193–217.

Theiler, J., & Eubank, S. (1993). Don't bleach chaotic data. *Chaos: An Interdisciplinary Journal of Nonlinear Science*, *3*, 771–782.

Vaughan, C. L. (1982). Smoothing and differentiation of displacement-time data: An application of splines and digital filtering. *International Journal of Bio-Medical Computing*, *13*, 375–386.

Vaughan, C. L., Davis, B. L., & O'Connor, J. C. (1999). *Dynamics of human gait*. Cape Town: Kiboho Publishers.

Vint, P. F., & Hinrichs, R. N. (1996). Endpoint error in smoothing and differentiating raw kinematic data: An evaluation of four popular methods. *Journal of Biomechanics*, *29*, 1637–1642.

Webber, C. L., & Marwan, N. (Eds.), (2015). *Recurrence quantification analysis: Theory and best practices (Understanding complex systems)*. Cham: Springer.

Winter, D. A. (2009). *Biomechanics and motor control of human movement*. Hoboken, NJ: Wiley.

Winter, D. A., & Patla, A. E. (1997). *Signal processing and linear systems for the movement sciences*. Waterloo, ON: Waterloo Biomechanics.

Woltring, H. J. (1984). *Chapter Ib: On methodology in the study of human movement. Advances in psychology* (pp. 35–73). Elsevier.

Woltring, H. J. (1986). A Fortran package for generalized, cross-validatory spline smoothing and differentiation. *Advances in Engineering Software (1978), 8*, 104–113.

Woltring, H. J. (1995). *Smoothing and differentiation techniques applied to 3D data. Three-dimensional analysis of human movement* (pp. 79–99). Champaign, IL: Human Kinetics.

Woltring, H. J., de Lange, A., Kauer, J. M. G., & Huiskes, R. (1987). Instantaneous helical axis estimation via natural, cross-validated splines. In G. Bergmann, R. Kölbel, & A. Rohlmann (Eds.), *Biomechanics: Basic and applied research: Selected proceedings of the fifth meeting of the European Society of Biomechanics*, September 8–10, 1986, Berlin, F.R.G *(Developments in Biomechanics)* (pp. 121–128). Dordrecht: Springer.

Yaroslavsky, L. P. (1997). Efficient algorithm for discrete sinc interpolation. *Applied Optics, 36*, 460.

Zbilut, J. P., & Marwan, N. (2008). The Wiener–Khinchin theorem and recurrence quantification. *Physics Letters A, 372*, 6622–6626.

CHAPTER 6

Revisiting a classic: *Muscles, Reflexes, and Locomotion* by McMahon

Douglas A. Rowen, Aaron D. Likens and Nick Stergiou
University of Nebraska at Omaha, Omaha, NE, United States

CONTENTS

In this way, preserving the most balanced judgements ever tendered about the nature of space and time, he explained what had always been a source of great wonder until then — how the past may visit the present.

From the novel *Loving Little Egypt* by Thomas A. McMahon (1943–99) who wrote the book we revisit in this chapter.

6.1 Introduction

This chapter is based upon a similarly titled book by Thomas A. McMahon (1984) which is commonly used in universities for classes on biomechanics. McMahon (1943–99) was a professor of Applied Mechanics and Biology at Harvard University. This book, *Muscles, Reflexes, and Locomotion* (McMahon, 1984), is considered a classic on the mathematics, biology, and mechanics of animal locomotion. Although the content of the book is exceptional, many important scientific discoveries have been made in the time since this book was last published. This chapter revisits and updates McMahon's work to include more recent discoveries.

This chapter is organized into nine sections, corresponding to each of the nine original chapters in McMahon (1984). The first five sections describe fundamental aspects of muscle mechanics and function (Sections 6.2–6.6). The next two sections synthesize the literature about muscle interaction with the brain and body through reflexes and neural control (Sections 6.7 and 6.8). The final sections discuss the mechanics of locomotion and contemporary use of robotics to simulate such motion (Sections 6.9 and 6.10).

Biomechanics and Gait Analysis. DOI: https://doi.org/10.1016/B978-0-12-813372-9.00006-3

6.2 Fundamental muscle mechanics

This section covers the basics of muscle mechanics from early ideas of muscles to our current-day understanding. Much of the early knowledge originated from mechanical and electrical stimulation of single muscles, prepared outside of a body. This knowledge created a great basis for continuing research to expand upon the initial experiments. This was aided by improved technology, allowing more detailed experiments to determine further characteristics of muscles.

6.2.1 Early ideas about muscle mechanics

Many early scholars speculated about human and animal movement. Both Hippocrates and Aristotle shared the belief that tendons were the principal elements that caused the body to move. Erasistratus later suggested that air filled the muscles, causing them to shorten and produce movement. This pneumatic conceptualization of muscle activity was the foremost hypothesis of movement until the latter half of the 17th century (c.1660–70) when Jan Swammerdam and Francis Glisson conducted experiments on contracting muscles submerged in fluid. Their results showed that, when a muscle contracts, the volume of the fluid remains constant in both human and animal models. This means that, in contradiction to the pneumatic theory of muscle contraction, the muscle does not change in volume when contracted. These early results set the stage for many developments over the next four centuries, most notably those in the mid-20th century involving isolated muscles, the subject of the next section.

6.2.2 Isolated muscles

The early and middle 20th century produced some of the most important findings, to-date, related to muscle biomechanics. Those studies involved removing and mounting a single animal muscle onto a device that measured the tensile force produced by a muscle strand after exposure to electrical stimulation. The muscle's contractile response to applied stimulation was termed the *twitch* (Abbott & Ritchie, 1951). Repetitive stimulation produces not one but a series of twitches. Interestingly, when the interval between successive twitches is sufficiently brief, twitches fuse and produce a tension greater in magnitude than the originating twitch, a phenomenon called *tetanus* (see Fig. 6.1). *Tetanic fusion* occurs when increasing the rate of stimulation no longer produces a corresponding increase in force.

Following on from those original studies, Edman (1970) showed that there are multiple levels of tetanic fusion. Edman stimulated an isolated frog muscle to produce an incompletely fused tetanus. After the stimulus, the fiber

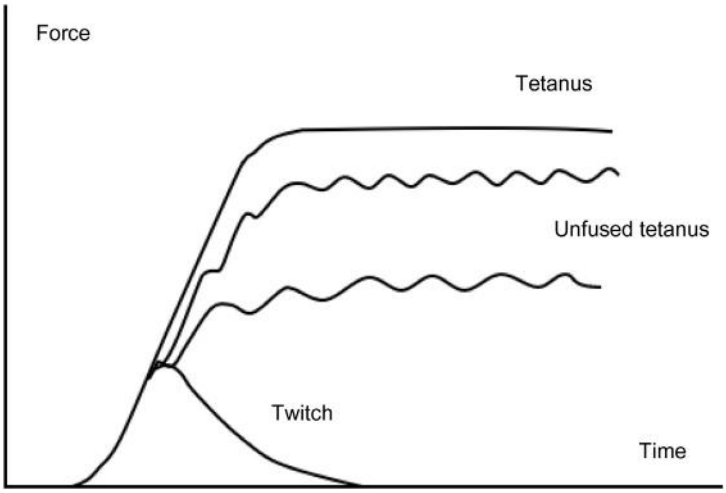

FIGURE 6.1

The force produced during a twitch, unfused tetanus, and tetanus. Source: *Recreated from McMahon, T. (1984).* Muscles, reflexes, and locomotion (Princeton paperbacks). *Princeton, NJ: Princeton University Press.*

was released to a new shorter isometric length. After the release, the fiber was stimulated again to create a series of peaks and troughs, *an unfused tetanus* (Fig. 6.1). By examining the isotonic shortening velocities at very light loads on frog muscles, Josephson and Edman (1998) found that the maximum shortening velocity was as much as 30% greater in the early part of the contraction than at the *tetanic plateau*, the region where the maximum force is produced during tetanus (the uppermost curve in Fig. 6.1). Those findings agreed with earlier predictions by Huxley (1957), namely, that maximum shortening velocity would be greater early in a contraction due to the actin-binding sites becoming activated and crossbridge connections being formed. These predictions by Huxley are explained in detail in Section 6.4.3. In brief, though, these studies demonstrated that the force of a muscle depends on the level of stimulation; however, other factors contribute to the amount of force a muscle can generate.

6.2.3 Force–velocity curves

The *force–velocity curve* refers to the graph of the relationship between the force and velocity of a muscle (Fig. 6.2). Understanding this curve also requires understanding the mechanical structure of muscle. Muscles can be represented through three main components: the *contractile component* (CE), the *series elastic component* (SE), and the *parallel elastic component* (PE) (Fig. 6.3). The CE acts similarly to a dashpot, a device for dampening shock

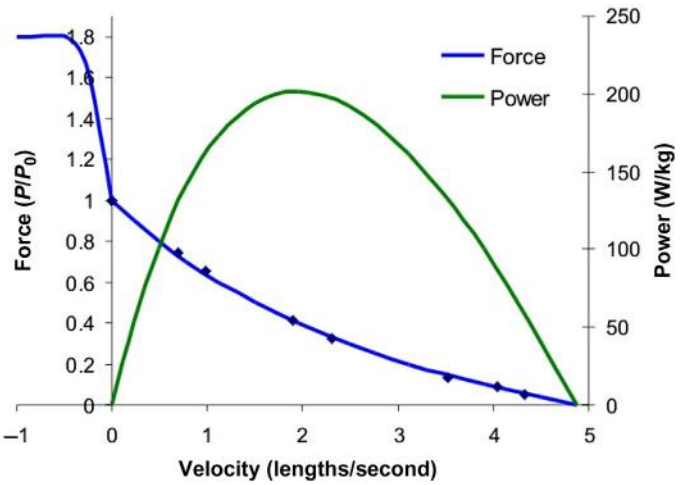

FIGURE 6.2
The force—velocity relationship in blue (Eq. 6.1) and the power—velocity relationship in green (Eq. 6.2). Maximum force is produced at zero velocity, while maximum power is produced at less than half of the maximum velocity. Source*: https://commons.wikimedia.org/wiki/File:Forcevelocity.jpg released into public domain.*

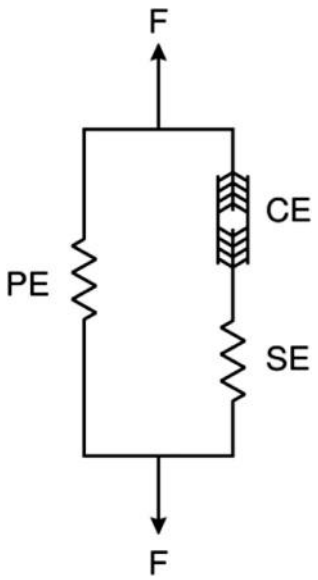

FIGURE 6.3
The mechanical structure of the muscle with the contractile component (CE), the parallel elastic component (PE), and the series elastic component (SE). Source*: https://commons.wikimedia.org/wiki/File:Hill_muscle_model.svg licensed under GNU Free Documentation License, Version 1.2.*

or vibration, while the elastic components are represented by springs. This muscle model is useful in describing basic interactions between the components and is used in simulations of movement (Arnold, Ward, Lieber, & Delp, 2009).

The CE is represented by a dashpot, meaning that it is damped and cannot change length instantaneously. The main evidence in support of this conceptualization is the observation that muscles shorten more rapidly against light weights than against heavy weights (Hill, 1938). Damping occurs because muscles produce less force when actively shortening than when contracting isometrically. The CE's inability to change length instantaneously means that any rapid shortening must be performed by the SE. When tension and elastic length are held constant, the CE is responsible for the muscle force (Lieber, Roberts, Blemker, Lee, & Herzog, 2017). Thus the CE represents the fundamental mechanical behavior of the muscle unit, while the elastic components influence the force, length, and speed of the muscle unit.

The SE provides force in quick, accelerative movements. This is apparent from research on independent muscle units (Galantis & Woledge, 2003), as well as from jumping movements performed by frogs and humans (Bobbert, 2001; Marsh & John-Alder, 1994). This elastic component is also important in energy dissipation, such as during a jump landing, because it absorbs energy through a rapid stretch, limiting the stretch to the CE (Konow & Roberts, 2015). Additionally, the elastic component may assist in the storage and return of energy in cyclic movements such as walking or running (Roberts, Chen, & Taylor, 1998), although the energetics of such energy storage may not be as beneficial as previously thought (Holt, Roberts, & Askew, 2014).

The CE's damping mechanism is responsible for an inverse relationship between force and shortening velocity (Fig. 6.2). Hill (1938) developed an equation (Eq. 6.1) which showed a hyperbolic relationship between force and velocity. This force–velocity curve has been shown to be the same for both isotonic and isovelocity shortening (Edman & Josephson, 2007). This relationship applies to a broad number of situations, even the superfast muscle fibers from toadfish, as the fibers produce a very low force (Rome et al., 1999). From the force–velocity equation, the power output is maximized when force and speed are between one-third and one-quarter of their maximum values (Eq. 6.2, Fig. 6.2). The speed of the shortening is responsible for the rate at which energy leaves the muscle, a process described in the next section.

$$(T + a)(v + b) = (T_0 + a)b \tag{6.1}$$

$$\text{Power} = Tv = \frac{v(b - T_o - av)}{(v + b)} \tag{6.2}$$

where T is the tension or force, v is velocity, a and b are constants, and T_0 is the maximum tension or tension at zero velocity.

6.2.4 Active and passive components

The elastic components involved in muscle contraction are further distinguishable as being either active or passive. Passive component properties are exposed when a muscle is stretched without any applied force. Fibrous elements of the muscle resist this stretching, resulting in an exponential increase in force as the muscle is stretched. This can be measured through a simple test in which the muscle is stretched to different lengths and the force is measured (Fig. 6.4). The active element results when the muscle is stimulated. The active element is more difficult to measure because of an inherent difficulty in separating actively produced force from passively produced force.

Length—tension curves can be used to identify how the active and passive components contribute to muscle tension at different lengths. The passive curve can be determined by the force needed to stretch a muscle at rest to a certain length, while the active component can be determined by calculating the difference between the tetanized and passive curves of the muscle (Fig. 6.4).

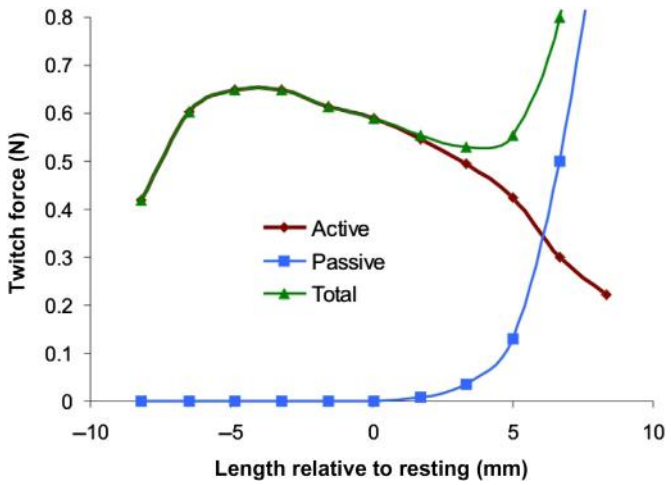

FIGURE 6.4

The length—tension curves of the tetanized (*green*) muscle and passive (*blue*) and active (*red*) components. The difference between the tetanized and passive curve determines the active elastic component of the muscle. Source*: https://he.wikipedia.org/wiki/%D7%A7%D7%95%D7%91%D7%A5:Lengthtension.jpg released into public domain.*

Jewell and Wilkie (1958, 1960) studied the active state model of the muscle, and observed that the tension of the muscle is reduced during the contraction period. This result established the skeletal muscle length dependency, as previous muscle models suggested that the active state time course was not length dependent (Aubert, Roquet, & Van der Elst, 1951). Other studies looked at the metabolic changes in muscle relaxation under fatigue (Edwards, Hill, & Jones, 1975) and the energetics of relaxation (Curtin & Woledge, 1974). These studies verified that the same length–tension relationship was applicable in multiple contexts. This relationship will be further investigated, along with newer findings, with respect to the sliding filament model, in Section 6.4.4.

6.2.5 Stress–strain relationship

The *stress–strain relationship* represents the behavior of a material as it is subjected to a load (Fig. 6.5). Fung (1967) found that many collagenous tissues from different parts of the body have the same nonlinear viscoelastic relationship between stress and strain. This is measured by determining the deformation caused by different applied forces. This stress–strain relationship is responsible for many of the passive components of the muscle.

A focus on the mechanical properties of soft tissues was continued with microstructural studies (Humphrey & Yin, 1987). Other studies tested different biological tissues, such as actin stress fibers, to determine that they also had similar characteristics with the other tissues that had been previously

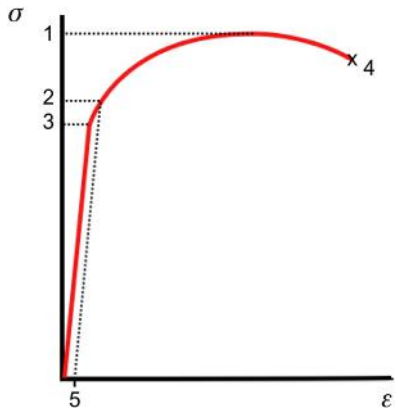

FIGURE 6.5

An example stress–strain relationship for a ductile material. Stress is represented on the *x*-axis and strain is on the *y*-axis. 1: Ultimate strength; 2: yield strength; 3: proportional limit stress; 4: point of rupture; 5: offset strain. Source: *https://commons.wikimedia.org/wiki/File:Stress_v_strain_Aluminum_2.png licensed under GNU Free Documentation License, Version 1.2.*

measured (Lu, Oswald, Hgu, & Yin, 2008). In addition, other methods of finding the stress–strain relation have been developed, although there are discrepancies in the Young's modulus between them. One such method that uses indentation to provide the elastic deformation provides consistently lower elasticity results when compared to the tensile force method (McKee, Last, Russell, & Murphy, 2011). Another technique of mechanical testing has emerged involving used isolated myocytes. Myocytes are the undifferentiated cells that ultimately become muscle cells. This method involves testing individual myocytes, which allows for finer testing because multiple areas within a muscle can be compared. With myocytes, both the passive and active mechanical properties can be determined (Louch, Sheehan, & Wolska, 2011). With dynamic loading, it has been shown that the bulk response is linear, while the dynamic shearing response shows an almost exponential growth of shear stress (Saraf, Ramesh, Lennon, Merkle, & Roberts, 2007). These studies allowed for further understanding of tissue characteristics to further improve muscle models.

Pinto and Fung (1973) showed that the same stress–strain relationship applied to papillary muscle of a rabbit heart. This test of the heart muscle was one of the earliest tests to examine the mechanical properties of the heart. Demer and Yin (1983) used a biaxial mechanical testing technique, one that provided force along two axes, that more closely represented in vivo loading conditions. Lin and Yin (1998) were able to apply the biaxial mechanical testing while supplying current to replicate the active state of the tetanized heart, further replicating in vivo conditions. Biaxial testing is still used to test the mechanical properties of the heart and has been adapted for use even in smaller animals, such as mice (Fomovsky & Holmes, 2010). Mechanical testing provides a method of determining the active and passive properties of muscles to improve understanding of how muscles respond to forces. Recent technological advances have allowed the process to more closely resemble the conditions the muscle experiences in the body.

6.2.6 Summary

The schematic representation of a muscle was introduced in the form of the SEs, PEs, and CEs. The characteristics of these components can be found through passive, tetanized, and quick twitch experiments. The model introduced in this section is a basic representation of a muscle, a template that can be used to resolve the redundancy of the physiological organ (Full & Koditschek, 1999). A template is the simplest model (least number of variables and parameters) that exhibits a targeted behavior, thus allowing for further study and understanding of the muscle in order to eventually comprehend its complex nature. Muscle models provide predictions about

how the muscle will respond in different scenarios. These scenarios can then be tested, and the muscle model can be updated to reflect the findings of the experiment.

6.3 Muscle heat and fuel

Helmholtz (1847) pioneered the study of muscle heat when he published a study showing that temperature increases in frog muscle when held in a sustained contraction. The relationship between the work done and the heat produced in a muscular contraction provides information about the biochemical nature of muscle contraction. The combined measurement of heat and work produced from a contraction can be used to determine the overall fuel used in the chemical reactions of a muscle. Thus by using these two measures, one could determine the necessary amount of *adenosine triphosphate* (ATP) needed to fuel a muscle. Muscles themselves only store enough ATP for about eight twitches (Margaria, 1976), so the supply of ATP necessary for sustained contractions must come from another source. When the ATP supply is exhausted, the supply of energy comes from the *phosphocreatine reservoir* (PCr) which, with an adequate oxygen supply, can provide enough energy for more than 10,000 muscle twitches. When the amount of oxygen present is not sufficient, as is the case with intense exercise, *anaerobic glycolysis* is performed in which glycogen is converted to *lactic acid*. Anaerobic glycolysis can be utilized for up to 600 twitches but results in a cumulative lactic acid buildup. We will further discuss this fundamental information below.

6.3.1 Heat production

Hill pioneered a rigorous study of muscle heat production. His work established both a knowledge base and a vocabulary for understanding and describing the relationship between muscle heat and fuel. Three forms of heat were discussed by Hill in relation to muscle contraction: resting heat, initial heat, and recovery heat. *Resting heat* is produced even when the muscles are not active, meaning that the contractile mechanism is linked to metabolic features, even at rest (Hill, 1940). Estimates of resting heat in frog muscle were measured to be about 0.0002 cal/g-min (Wilkie, 1954). *Initial heat* occurs during a contraction, while *recovery heat* is measurable for several minutes postcontraction. The magnitude of initial and recovery heat was found to be approximately equal, with the ratio ranging from 1.0 to 1.5 in frog muscles (Hill, 1938). Simultaneous measurements of oxygen consumption and heat production during recovery reveal almost identical time courses for those processes (Hill, 1940). This illustrates that recovery is an oxidative process, during which the muscle rebuilds the supply of PCr.

Stretching and contracting of a muscle result in an increase in heat and oxygen production (Wilkie, 1954). Wilkie (1968) also found that the difference in enthalpy of heat and oxygen between different types of muscle contractions was proportional to a drop in PCr. Additionally, there is a time delay for activation heat in frog muscles (Carlson & Wilkie, 1974). This time delay has also been found in other animal muscles, including rabbit cardiac muscle and mouse skeletal muscle (Constable, Barclay, & Gibbs, 1997; Gibbs, Loiselle, & Wendt, 1988). Wilkie's (1968) calculations were used as a basis for the physical parameters in finding a molecular model of muscle contraction (Duke, 1999). This model was used to provide the mechanical and thermodynamic properties of muscle shortening at the molecular level. More recently, in vivo studies of heat and ATP production have been used to test aerobic and anaerobic metabolism in humans during exercise (Krustrup, Ferguson, Kjær, & Bangsbo, 2003). Krustrup and colleagues showed that heat loss is lower in anaerobic ATP synthesis than in aerobic synthesis. Collectively, these studies showed that measuring heat loss during muscle activity is an accurate method of determining the amount of energy used by a muscle.

6.3.2 Activation heat

Hill (1953) proposed that, after a brief latency, the active state developed quickly based on three principal observations (McMahon, 1984):

1. The rapid ability of a muscle to bear a force equal to the tetanic tension after a quick stretch.
2. The very quick development of a shortening velocity approaching the maximum velocity when the muscle contracts against a light load.
3. The rate of heat production begins to increase 10–15 ms after a stimulus and can reach the maximum value before any tension is measured.

In tetanus, the activation heat is prolonged and is related to the length, but over time, as tetanus continues, the rate of heat production falls (Wilkie, 1968). Activation heat production begins quickly after a muscle is activated, and in most cases, heat production continues for the duration of the activation.

Woledge (1968) compared the rate of heat production in slow-twitch muscles (tortoises) to what was already known about fast-twitch muscles (i.e., frogs). In frogs, heat production declines slowly during tetanus, while active state tension remains the same (Wilkie, 1968). In tortoise muscle, both the rate of heat production and tension stay at constant and proportional levels during tetanus. This demonstrates that, for different muscle fiber types, the characteristics of heat production change. Other studies have looked at the

mechanical efficiency of energy conversion as well as the effect of fatigue on fast and slow muscles and the differences between the two muscle groups (Barclay, 1996). Barclay found that the maximum unfatigued efficiency was higher in slow-twitch muscles and that the slow-twitch muscle efficiency was more resistant to fatigue. These slow- and fast-twitch muscles have also been examined during gait in order to determine which muscle type seems more economical, based on a supply and demand concept (Usherwood, 2016). The tradeoff comes from the supply side, where contracting slow- and fast-twitch muscles requires differing amounts of energy but also differs in power output. This means that, during walking, the power from the slow- and fast-twitch muscles needs to match the demand of the gait requirements. This section has summarized how heat increased when muscle was activated; in the next section we look at differences in heat production for different kinds of contractions.

6.3.3 Shortening and lengthening heat

Fenn (1924) demonstrated that a muscle produces more heat when it shortens than when it contracts isometrically. This means that, in a shortening contraction, the energy needed to shorten increases by the amount of work done (Rall, 1982). Relatedly, Hill (1938) showed that the heat produced during shortening is proportional to the distance shortened through tetanic stimulation of the muscle. When a stimulated muscle is released, it shortens against a light load and produces more heat than would have been liberated if no shortening was allowed. That is, shortening muscle releases more energy, both because the muscle does external work and because it develops more heat. This phenomenon is known as the *Fenn effect* and is also observed in muscle lengthening.

Fenn (1924) also found that, in isolated muscles, when the muscle is forced to lengthen, heat production decreases. Even though work is being done to the muscle as it is forced to lengthen, the rate of heat production diminishes so that the heat deficits are proportional to the distance the muscle is stretched. In an isolated muscle, the constant of proportionality for lengthening was found to be around six times that of shortening (Abbott & Ritchie, 1951). Lengthening contractions exhibit a reduced energetic cost when compared to shortening contractions at the same force (Beltman, van der Vliet, Sargeant, & de Haan, 2004; Bigland-Ritchie & Woods, 1976). This has been shown directly during tapping through the use of magnetic resonance spectroscopy and a force clamp. These results supported the Fenn effect as more muscle effort is required when the muscle is shortening than when it is lengthening (Ortega et al., 2015).

6.3.4 Thermoelastic effects

In part, the cooling properties of stretched muscles are described by the *thermoelastic effect*, a change in temperature as the result of a strain or stretch. On the one hand, solid materials expand when they are heated and cool when they are stretched. On the other hand, rubber heats when it is stretched, with the increase in temperature resulting from restricted molecular movement. Muscle exhibits both solid and rubberlike properties, with resting muscle showing rubberlike thermoelastic properties for short muscle stretches, but normal thermoelastic properties during larger stretches. Active muscle displays normal thermoelasticity for all lengths, and, when the tension falls in an active muscle, heat is produced (Hill, 1953). In addition, when the tension rises, heat is absorbed (Gilbert & Matsumoto, 1976), and the energy liberated during an isometric contraction is greater than the heat production due to the thermoelastic effect (Woledge, 1963). The reverse can also be shown as, by heating a muscle in rigor, a decrease in tension is observed (Goldman, McCray, & Ranatunga, 1987). This result corresponds to Hill's (1953) early discovery that the thermoelectricity in active muscle is normal or nonrubberlike.

6.3.5 Lactic acid

As mentioned earlier (introduction to Section 6.3), anaerobic contraction of muscles produces a buildup of lactic acid. Muscles can contract many times, even when oxygen is absent, through the hydrolysis of glucose and the production of lactic acid in the muscle (Fletcher & Hopkins, 1907). Fletcher and Hopkins' finding showed that muscles can work without the presence of oxygen. During anaerobic muscle activity, the rate of recovery heat production was reduced even though the initial heat production did not change. This led to the conclusion that oxygen was not used in the production of force; however, it was used to build up energy. The lactic acid that forms in the muscle is only partially oxidized in the muscle with around 10% being absorbed. Lactic acid buildup takes more than 10 hours to disappear from muscle (Meyerhof, 1920).

Lactic acid buildup has been thought to be one of the potential causes of muscle fatigue due to acidosis (Fitts, 1994). However, this has recently been shown to not be the case as both the introduction of lactate (Dutka & Lamb, 2000) and low-pH environments (Westerblad, Bruton, & Lännergren, 1997) have resulted in minimal effects on contractions of skeletal muscle. In fact, lactic acid may even increase force in high-potassium ion environments through the inhibition of voltage-gated chloride channels (Bandschapp, Soule, & Iaizzo, 2012). Thus lactic acid buildup may actually be beneficial for maintaining muscle force during fatigued conditions.

6.3.6 Phosphates

ATP is the energy source that powers the body and muscles. Contractions of muscles are produced by splitting ATP into adenosine diphosphate (ADP) with a phosphate ion and the free energy that is used in muscle contractions. This reaction is highly regulated with a slight drop in the ATP concentration resulting in ADP combining with PCr to form more ATP. Even during intense exercise, where there is a tremendous increase in ATP demand, ATP levels remain relatively stable (Baker, McCormick, & Robergs, 2010). When oxygen is absent, the store of PCr found in the muscle is the only way to synthesize ATP (Carlson & Siger, 1960). Because ATP supply is highly regulated, measuring changes in ATP is difficult, except in cases of extreme fatigue when the PCr supply is almost depleted. However, if the muscle is removed and the enzyme for the reaction is inhibited, the contractile mechanism only has the ATP in the muscle to use for contractions and the removed muscles are only able to produce around eight twitches (Margaria, 1976).

6.3.7 Effects of exercise

The study of muscle during exercise has revealed insight into processes related to fatigue. For example, during light to moderate exercise, the PCr reservoir is the initial supply for replenishing the ATP that is used by the muscles (Saiki, Margaria, & Cuttica, 1967). Lactic acid concentration only rises slightly because there is a delayed oxidative response to keep up with the energy demand. Once the oxidative supply catches up with the energy demand caused by exercise, oxidative sources are used and there are no more increases in lactic acid concentration. Following the conclusion of exercise, the PCr supply must be built back up in a chemical process that involves oxygen, glycogen, and fatty acids. This is accomplished by producing excess ATP, which is used to produce and store PCr. This process of converting ATP to PCr is lengthy, requiring more than 30 minutes to replenish the PCr reservoir to capacity.

In heavy exercise, the lack of energy flow to the muscles causes the PCr levels to drop until they are almost exhausted (Jones, 1973). This is because the *maximum aerobic rate*, the peak point of oxidative energy flow, is not fast enough to keep up with the energy output. Isolated muscle experiments demonstrate this effect by stimulating a sustained tetanus over 45 seconds as seen in Fig. 6.6 (Jones, 1973). ATP levels tend to stay constant, even after the depletion of PCr; however, the concentration of lactic acid begins to rise after the contractile mechanism expends stored PCr (Fig. 6.6). Reduced tension and muscle fatigue also accompany increases in lactic acid concentration. When oxygen is unavailable during the recovery process, the buildup of PCr depends on anaerobic glycolysis, which restores PCr to near normal levels.

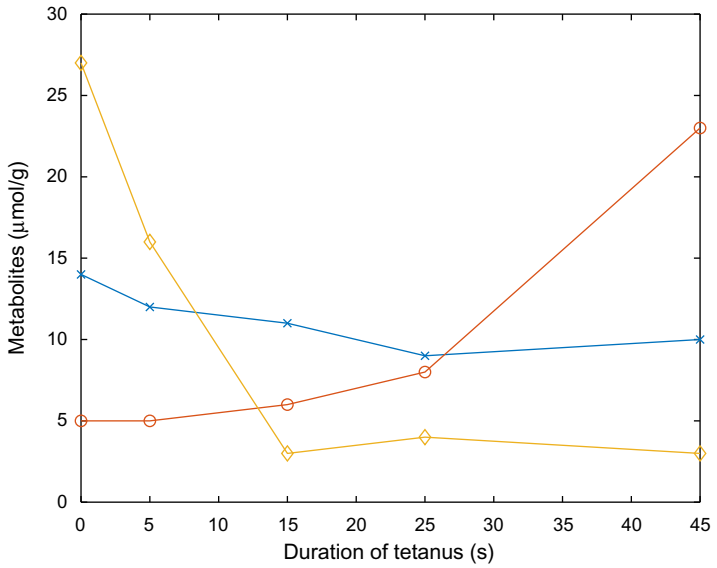

FIGURE 6.6

Concentrations of lactic acid (*red*, *circles*), adenosine triphosphate (ATP) (*blue*, *crosses*) and phosphocreatine (PCr) (*yellow*, *diamonds*) during sustained tetanus. It can be seen that the concentration of ATP stays about the same for the duration of tetanus while there is a decrease in PCr and an increase in lactic acid. Source*: Recreated from Jones, D. A. (1973). Combined techniques for studying the physiology and biochemistry of fatigue in the isolated soleus of the mouse. The Journal of Physiology*, 231, *68P–69P.*

Lactic acid's diminished role as a cause of fatigue has led researchers to consider a number of alternative mechanisms. Recent studies have investigated the relationship between the slowing of relaxation and metabolic factors, such as changes in pH and phosphorous metabolites (Cady, Elshove, Jones, & Moll, 1989). They found that hydrogen ion accumulation only partially explains the slow relaxation of fatigued muscles. Further work has demonstrated that the decrease in contractile strength found during fatigue is caused by altered kinetics in the crossbridges, which reduces the force output of each individual bridge (Edman & Lou, 1990). Jones (2010) investigated the slowing of the contracting properties of muscle due to fatigue and identified three factors: (1) a decrease in isometric force, which is caused by a reduction in the number of active crossbridges; (2) a slowing of the maximum shortening velocity; and (3) an increased curvature of the force–velocity relationship. These results show that a multitude of physiological responses are responsible for changes in muscle forces, and the slowing of contraction, due to fatigue.

The buildup of lactic acid depends on the duration of exercise, as seen in Fig. 6.6. The concentration of lactic acid in blood increases as a linear

function of exercise duration (Margaria, Cerretelli, di Prampero, Massari, & Torelli, 1963). To return the body to normal levels of lactic acid concentration, oxygen consumption also needs to be higher than normal. Interestingly, through training, athletes increase their oxygen consumption and delay the onset of excess lactic acid production. Additionally, when breathing pure oxygen, the peak aerobic work rate may increase (Margaria, Camporesi, Aghemo, & Sassi, 1972). Thus limitations in the maximum aerobic rate are caused by limited oxygen consumption during exercise.

Limiting the buildup of lactic acid, using a strategy that involves resting between intervals of strenuous running, could increase the total distance in which a person can run (Margaria, Oliva, di Prampero, & Cerretelli, 1969). With appropriate resting intervals, heavy exercise produces the same lactic acid concentration plateaus observed during light or moderate exercise. The key to this method is striking the correct balance between rest and exercise. Alternating sufficiently brief periods of running with sufficiently long periods of rest prevents activation of ATP synthesis by anaerobic glycolysis, and consequently, also prevents lactic acid buildup in muscle. By remaining in only a small lactic acid oxygen debt, individuals are able to repay that debt during rest through oxidative rephosphorylation, the typical method of ATP regeneration. This strategy proves useful to athletes as it provides a method of training through intervals that limits the amount of lactic acid buildup which could prevent fatigue (Margaria et al., 1972). This allows for the athletes to train for longer periods of time and to accomplish more during the training without muscle fatigue (Margaria et al., 1972).

Ferretti, Moia, Thomet, and Kayser (1997) studied the decrease of maximal oxygen consumption in endurance runners during hypoxia, which is a reduction in the amount of oxygen reaching the muscles. They found that there was a linear relationship between the maximum oxygen consumption during hypoxia and the shape of the oxygen equilibrium curve. Further research investigated the difference in maximum oxygen consumption in trained and untrained individuals using both in vitro and in vivo methods (Gifford et al., 2016). This study found that in untrained subjects, the maximum oxygen consumption is limited by mitochondrial demand even when there was an adequate oxygen supply. In subjects with training, they found that exercise training induces mitochondrial reserves, meaning that the trained subjects were limited by only their oxygen supply.

6.3.8 Summary

The study of heat and fuel, in muscles, has produced many important discoveries over the years. Muscle heat is a good measure of energy expenditure because when a muscle is used, it emits heat. The fuel for muscle

contractions comes from ATP which creates energy through a chemical reaction that removes a phosphate group from ATP. The amount of ATP is highly regulated in the body and the PCr reservoir is used to replenish ATP during aerobic conditions. During anaerobic conditions, a side product of the chemical reaction that yields ATP is also the production of lactic acid, which builds up in the muscles and may lead to fatigue. Lactic acid buildup can be avoided through proper exercise programs that involve interval training where the rest phase is used to replenish the ATP aerobically. Additionally, exercise can be used to increase the capacity to replenish ATP aerobically.

6.4 Contractile proteins

So far, we have described muscles and how they act as a strand or as a part of the body. This section looks at how muscle strands, and muscles as a whole, are organized on a microscopic level. The section concludes with how muscles contract and the *sliding filament model*, which will be more broadly examined in Section 6.5, along with its implications and limitations.

6.4.1 Organization of muscles

Muscles have characteristic organizations, whether considering an entire muscle or just a single muscle fiber. Individual muscles can either be arranged parallel to the long axis or obliquely, with respect to tendons (Fig. 6.7). This allows for muscles to function over the optimum part of their

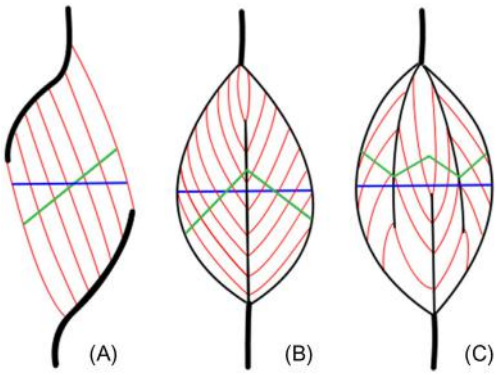

FIGURE 6.7

The different types of muscle organization. Unipennate muscles (A) have the tendon running along one side of the muscle fibers. In a bipennate muscle (B), the tendon passes up the center of the muscle and the fibers are attached on either side. Multipennate muscles (C) have tendon material approaching the belly of the muscle from both ends. Source: *https://commons.wikimedia.org/wiki/File:Fiederung.svg licensed under the Creative Commons Attribution-Share Alike 3.0 Unported license.*

length–tension curve (Gans & Gaunt, 1991). Examples of parallel muscles include skeletal muscles such as the sartorius muscle. The obliquely fibered muscles, otherwise known as pennate muscles, can be unipennate, bipennate, or multipennate, and are shown in Fig. 6.7. Examples of pennate muscles include the extensor digitorum longus, the rectus femoris, and the tibialis anterior (McMahon, 1984). An in-depth look at the individual muscle fibers is necessary to further understand their organization.

When an individual muscle is investigated under a microscope, it has a striated appearance (Fig. 6.8). Striation results from the division of muscles into sarcomeres, the smallest functional unit that still behaves like a muscle. Individual fibers are singular muscle cells that contain all the typical elements such as a nucleus and mitochondria, surrounded by a membrane and the sarcoplasm. Single fibers, in turn, also have a banded structure with two distinct bands being visible. The A-band has a higher concentration of proteins and is anisotropic to polarized light, while the I-band is isotropic. In the I-band, there is a structural membrane running through the entire muscle fiber that is called the Z-disk. The Z-disk is the divider between sarcomeres, as one sarcomere is the region contained between two adjacent Z-disks

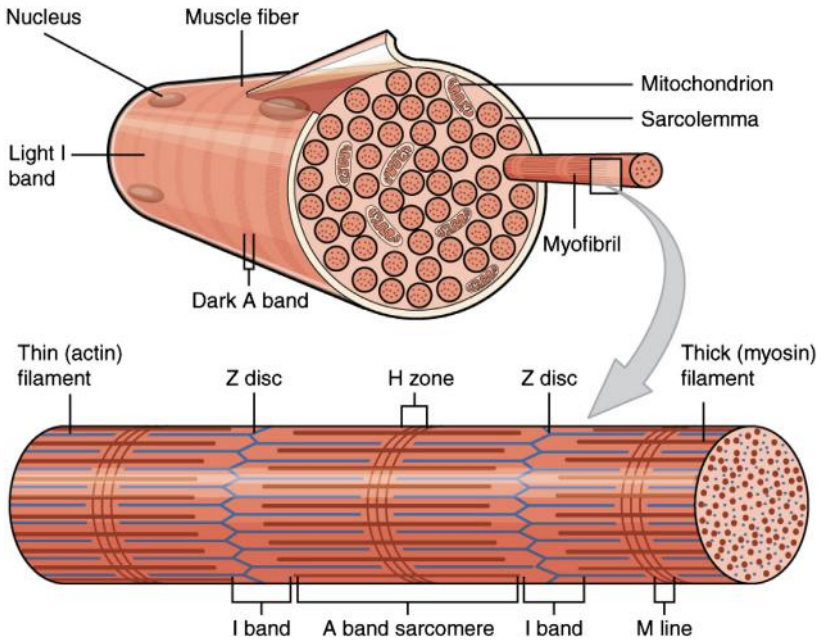

FIGURE 6.8

A schematic representation of a muscle fiber, and zoomed in as a myofibril. Source: *https://commons.wikimedia.org/wiki/File:1002_Organization_of_Muscle_Fiber.jpg licensed under the Creative Commons Attribution 4.0 International license.*

(Fawcett, 1968) (Fig. 6.8). By investigating muscles under the microscope, researchers were able to determine the basic structure of the sarcomere, however, other methods were needed to determine the proteins present in the sarcomeres.

6.4.2 Actin, myosin, and troponin

Contractile events were once thought to result from the solidification of proteins. This thinking originated from the isolation of a protein originally named myosin (Kühne, 1864). At that time, myosin was thought to be the only protein responsible for muscle contraction. Later experiments showed, however, that myosin was composed of several proteins. Straub (1942) separated myosin into two separate proteins, actin and myosin. Soon after, tropomyosin was also isolated (Bailey, 1948). Ebashi, Wakayabaya, and Ebashi (1971) studied tropomyosin and found that it was not a pure protein either and had three different components as opposed to the two previously identified, tropomyosin and troponin (Hartshorne & Mueller, 1968). This third component forms a complex with tropomyosin which acts as an inhibitory process within the muscle (Perry, Cole, Head, & Wilson, 1972). The role of troponin in the contractile activity is not completely understood; however, some explanations have been proposed. The first is that molecular changes to the calcium binding to the troponin could influence the behavior of the surrounding actin filaments (Perry, 2003). The second is that the role of troponin is to stabilize the actin filament and facilitate the transition of changes along the actin filament (Perry, 2003).

6.4.3 Sliding filament model

Once the actin and myosin filaments were identified, a model was developed to determine how these proteins interacted. The sliding filament model was proposed in 1954 and suggested that thick and thin filaments were arranged in parallel to the long axis of the muscle (Huxley & Niedergerke, 1954). When the muscle is shortened or lengthened, the two different types of filaments slide past one another. When these filaments overlap, they attach and form *crossbridges*. Development of this model followed from four fundamental findings:

1. Previous work using electron micrography showed that two sets of filaments exist (Huxley, 1953).
2. The thick filaments remain at a constant length during stretch (Huxley & Hanson, 1954).
3. The thick filaments are made of myosin and the thin filaments are made of actin (Hasselbach, 1953).

4. X-ray diffraction studies of resting muscles showed that the thick and thin filaments do not change length when the muscle is stretched (Huxley, 1957).

Further microscopy and X-ray diffraction have shown that the crossbridges are detached from the thin filaments in the presence of ATP (Fig. 6.9). When ATP is not present, and the muscle is in rigor, the crossbridges are angled at 45 degrees to the filament direction (Reedy, Holmes, & Tregear, 1965). Marston, Rodger, and Tregear (1976) showed the existence of a third state of the crossbridges, the others being detached or attached, in which they are attached but perpendicular to the filament axis in the presence of ATP analog adenosine 5-[β,γ-imido]triphosphate (AMPPNP). This third state increased rigor slightly at zero tension length and changed the muscle diffraction pattern and electron micrograph appearance (Marston et al., 1976). Later work showed that AMPPNP caused the release of rear crossbridges while inducing only small changes in shape and attachment angle (Reedy, Reedy, & Goody,

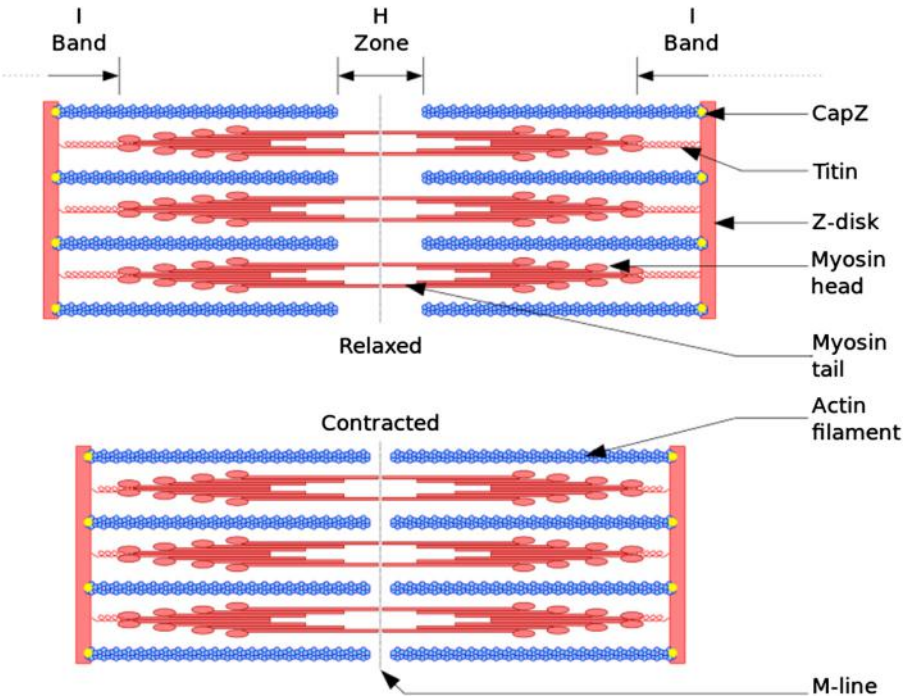

FIGURE 6.9

Schematic representation of the actin and myosin overlap during relaxed and contracted conditions. This representation is updated to include titin as a spring element connected to the myosin filaments. Source: *https://commons.wikimedia.org/wiki/File:Sarcomere.svg licensed under GNU Free Documentation License, Version 1.2.*

1987). Adding ethylene glycol to AMPPNP caused a reduction in muscle tension until a critical concentration when the muscles become stiff (Tregear et al., 1990). In addition, electron micrographs showed large numbers of crossbridges, with a variety of angles outside the thin-filament target zone (Schmitz, Reedy, Reedy, Tregear, & Taylor, 1997). X-ray diffraction studies by Wakabayashi et al. (1994) and Huxley, Stewart, Sosa, and Irving (1994) revealed that when a muscle is at full tension, the filaments themselves stretch very slightly under tension. Hence, imaging studies were essential as they provided more detailed information into how muscles and, specifically crossbridges, behave in real time during a variety of conditions.

6.4.4 Tension–length curves

Tension–length curves are also useful for examining how tension differs for different filament overlaps (Fig. 6.10). The developed tension in a muscle showed a nonlinear relationship with muscle length. This has been shown in microscope studies of single fibers, that is, the amount of filament overlap was different at the end of the fiber than at the middle of the fiber (Gordon, Huxley, & Julian, 1966; note that such nonlinearities exist everywhere within the function of the human body). Specifically, there exists a plateau when the filaments are sufficiently overlapped such that further overlap provides

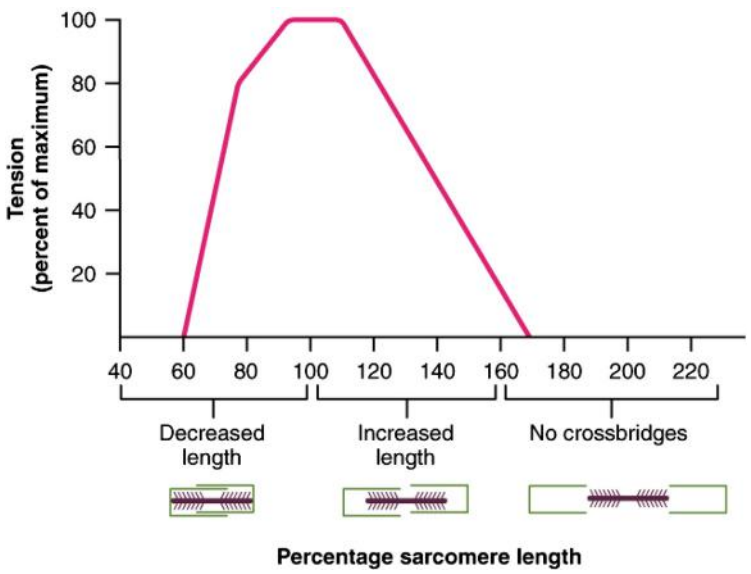

FIGURE 6.10

The tension–length curves of a single muscle fiber for different sarcomere lengths. Source: *https://commons.wikimedia.org/wiki/File:1011_Muscle_Length_and_Tension.jpg licensed under the Creative Commons Attribution 4.0 International license.*

no additional increase in tension. Additionally, when the sarcomere length was either too short or too long, the overlap was no longer active, and a progressive decrease of force was observed. Julian and Morgan (1979) found a permanent extra tension in which the tension plateau was found to be higher following an active stretch than during a fixed-end tetanus. They explained this phenomenon by reasoning that sarcomere lengths in a muscle fiber become very nonuniform under certain circumstances. The sarcomere nonuniformity is attributed to a few observations: force creep, or deformation in contractions produced at long sarcomere length (Edman & Reggiani, 1984), differences in force obtained when fibers are activated, and the kinetics of force development and relaxation (Edman & Flitney, 1982). More recently, studies with isolated myofibrils and single sarcomeres have confirmed the development of sarcomere nonuniformity (Rassier, Herzog, & Pollack, 2003). These results showed that the tensions found in sarcomeres were not consistent with varying amounts of overlap because muscle deformation and relaxation impacted the amount of tension present.

6.4.5 Sarcoplasmic reticulum

The *sarcoplasmic reticulum* is a membrane that runs along the filaments of the muscle and provides a source of calcium for the activation of muscles (MacIntosh, Gardiner, & McComas, 2006). The sarcoplasmic reticulum has a regular repeating pattern just like the repeating structure of the sarcomere. Hill (1949) showed that a substance released at the surface of the membrane would take too long to reach the middle and initiate muscle activation. However, the diffusion distance for calcium to get into the muscle fibers is quite small due to the sarcoplasmic reticulum. Ridgway and Gordon (1975) showed the rise and fall of calcium concentration in the sarcoplasm by using a protein isolated from jellyfish which gives off light when it binds to calcium ions. They measured this in barnacle fibers and found similar results to those previously found in frog muscle fibers (Rudel & Taylor, 1973). Baylor, Chandler, and Marshall (1983) found that after an initial rapid release of calcium, there is a longer maintained period of calcium intake. Calcium is released into the muscle by the sarcoplasmic reticulum where it diffuses to the thin filaments and binds to regulatory sites on troponin to activate muscle contraction (Baylor & Hollingworth, 2011). The sarcoplasmic reticulum provides the muscle with the source of calcium needed to contract.

6.4.6 Tropomyosin and troponin

Tropomyosin is a protein which, in combination with troponin, blocks the attachment sites for myosin crossbridges. Both proteins are necessary to allow calcium to work as the on–off switch for the actin–myosin

crossbridges. Tropomyosin, an alpha helix, lies in a groove between the two actin chains of the thin filament with one troponin molecule per seven actin molecules in a filament (Huxley & Brown, 1967). X-ray diffraction revealed that when calcium is released into the sarcoplasm, the troponin moves the tropomyosin chain aside and exposes an active site on the actin chain (Wakabayashi, Huxley, Amos, & Klug, 1975). This allows the actin–myosin cycle of attachment, force development, and detachment to occur. The cycling of this process continues as long as calcium is present in the muscle. At the conclusion of the muscle activity, the muscle relaxes by transporting calcium into the sarcoplasmic reticulum, allowing tropomyosin to reattach back and prevent any crossbridge attachment. The roles of troponin were mentioned previously in Section 6.4.2.

6.4.7 Titin

Titin, otherwise known as connectin, is a very large elastic protein that was separated from actin and myosin by Maruyama, Natori, and Nonomura (1976). It functions as an elastic spring that provides the passive stiffness of muscle (Granzier & Irving, 1995). Single titin molecules span half the sarcomere from the M-line to the Z-line (Furst, Osborn, Nave, & Weber, 1988). In the A-band, titin is attached with the thick filament, and could be used to control filament length (Whiting, Wardale, & Trinick, 1989). Because titin was not found until after the sliding filament model was developed, adjustments were necessary to account for the elastic element titin provides. These more recent adjustments are discussed in Section 6.5.9.

6.4.8 Summary

This section has reviewed muscle organization, both on the muscle level and on the fiber level. Muscles, as a whole, can be organized either parallel or pennate to the tendons, while individual muscle fibers can be broken down into sarcomeres. Using sarcomeres, it is possible to identify the essential role that actin and myosin play in the sliding filament theory. Following actin and myosin, several secondary proteins, and their roles in the sliding filament theory, were discovered. Specifically, these secondary proteins are troponin, which acts as an on–off switch, and titin, which acts as an elastic element. Additionally, the role that the sarcoplasmic reticulum plays in the release of calcium for muscle activation was discussed. The rest of this section focused on the sliding filament model and the tension–length curves that helped demonstrate how filament overlap impacted the force of the crossbridges. The next section discusses the sliding filament model in further detail as well as problems and updates to this influential model.

6.5 Sliding movement: Huxley's model revisited

The sliding filament model was introduced in Section 6.4.3. In this section, we provide more background on the model as well as its governing mathematical equations. Huxley (1957) introduced a mathematical model for the process of crossbridge attachment, detachment, and filament sliding. This model is remarkably general, predicting the Hill force–velocity curve, the discontinuity of the slope for lengthening, and the observation of muscle yielding at large velocities of stretch.

6.5.1 Other theoretical models

Before going into more detail about the sliding filament model, it is important to situate this model within the context of historically relevant alternatives. These earlier theories of muscle contraction were based on comparisons with other physical or physiological processes. An example of such a theory was that the muscle behaved like rubber and changed size when heated (Marey, 1874). These theories fell from favor, though, as scientists began to understand more about the biomechanics of muscle and its contraction. A more recent theory, suggested after the sliding filament model was introduced, was that a repulsive force is generated between filaments which causes muscle shortening by thickening the muscle (Elliott, Offer, & Burridge, 1976); however, this theory was soon discounted because fibers do not thicken when being shortened (Matsubara & Elliott, 1972). Another theory suggested that the actin–myosin filaments carry opposite electric charges that attract each other and cause an increase in overlap (Yu, Dowben, & Kornacker, 1970). This theory was contradicted because the actin–myosin filaments are able to overlap further than complete overlap (Huxley, 1979). Complete overlap would be the furthest overlap possible with the electrostatic theory. Additionally, another theory suggested that the muscle shortened by the thin filaments folding into the overlapping zone between thick and thin filaments (Podolsky, 1959); however, this has been disproved using electron microscopy, as the thin filaments slide inward during contraction (Huxley, 1964). To-date, no theoretical model has proven to be more predictive than the sliding filament model. Thus the sliding filament model is a fundamental concept used to describe muscle contraction today (Squire, 2016).

6.5.2 Evidence supporting independent force generators

Two important pieces of evidence suggest that crossbridges are discrete, independently acting, force generators (McMahon, 1984). The first is that isometric tetanic tension is proportional to the extent of actin–myosin overlap (Gordon et al., 1966; Granzier & Pollack, 1990; Morgan, Claflin, & Julian,

1991). This was shown by using a device to maintain a set length in a portion of a single fiber. Gordon et al. found that tetanic tension was directly proportional to the overlap between the actin and myosin and the number of active crossbridges (see Fig. 6.10). When muscle is stretched to a sarcomere length in which the actin–myosin overlap reaches zero—around 3.65 μm—the tension also goes to zero. This means that muscle force is only possible when there is an overlap of the actin and myosin.

The second piece of evidence concerning independent crossbridges is that the maximum shortening speed is independent of the actin–myosin overlap, at least within the range of where the thin filaments do not overlap one another and prohibit shortening (Huxley, 1964). Further experiments showed that the shortening peak tension during a twitch is the same as during tetanus (Edman, 1978) and that partially activated fibers have the same characteristics as fully activated fibers (Thames, Teichholz, & Podolsky, 1974). These two points of evidence suggest that actin–myosin crossbridges act as independent force generators, and that adding crossbridges in parallel increases tension without changing the speed of shortening. This means that the shortening seen in a muscle is caused by many cycles of crossbridges pulling during a single contraction. These two pieces of evidence were essential in detailing the sliding filament model.

6.5.3 Formulation of the model

At the time of development, Huxley's model needed to address several known properties related to muscles and their contraction (Huxley, 1957):

1. During shortening, the relationship between force and velocity is given by Hill's equation (Eq. 6.1; Hill, 1938).
2. There is a discontinuity of the force–velocity relationship at zero velocity (Katz, 1939).
3. Active muscle yields when the load exceeds about 1.8 times the isometric tension.
4. The Fenn effect shows a linear relationship between the total rate of energy liberation and tension (Fenn, 1924).
5. Muscle shortening should be based on the relative motion of sliding filaments because:
   a. The A-band width stays the same length during stretching and shortening.
   b. The A-band disappears when myosin is dissolved.
   c. The actin filaments run through different segments of the sarcomere than the myosin filaments.
6. Muscle energy liberation should be based on the splitting of high-energy phosphate.

With this knowledge in mind, Huxley proposed a model, acknowledging the following limitations (Huxley, 1957):

1. It applied to only the tension generated by the CE and ignored the PE.
2. It applied to only the plateau regions of the length–tension curve.
3. It assumed muscle was fully activated and did not change in the amount of activation over time.
4. It assumed the shortening velocity was fixed and that the tension was constant.
5. It assumed that each crossbridge went through a cycle of force development and detachment, although this assumption was later reconsidered.

These findings and assumptions created the foundation of the model, however, many details still needed to be determined. The next few parts of this section focus on the original equations used by Huxley (1957), beginning with a summary of the governing equations that describe the rate at which crossbridges attach and detach.

6.5.4 Attachment and detachment

At any point, the probability of any crossbridge being attached sits between zero and one. The representative first-order kinetic equation says that the fraction of attached bridges in the next increment of time depends upon the probability of attachment and the probability that some of the bridges will detach (see Eq. 6.3). The probability of both attachment and detachment depend upon the fraction of unattached fibers as well as a constant rate. The representative equation is given where $n(x)$ is the number of attached fibers, $f(x)$ is the attachment rate, and $g(x)$ is the detachment rate:

$$\frac{dn(x)}{dt} = [1 - n(x)]f(x) - n(x)g(x) \tag{6.3}$$

The constant rates are based upon the tendency of crossbridges to attach in a position where they contribute to a positive tensile force between the filaments. Due to this rate constant, the model predicts that the rate of detachment will be low unless the muscle shortens. This shortening allows for the crossbridges to complete their cycles and transfer energy from the elastic component to the outside load.

6.5.5 Crossbridge distribution for isotonic shortening

When muscles shorten at a constant force and speed, Eq. (6.3) can be rewritten as Eq. (6.4):

$$-v\frac{dn(x)}{dt} = f(x) - \big[f(x) + g(x)\big]n(x) \tag{6.4}$$

This equation is dependent on several conditions, and the constants can be solved based on these conditions:

$$x < 0: f(x) = 0; \quad g(x) = g_2 \tag{6.5}$$

$$0 \le x \le h: f(x) = f_1 \frac{x}{h}; \quad g(x) = g_1 \frac{x}{h} \tag{6.6}$$

$$x > h: f(x) = 0; \quad g(x) = g_1 \frac{x}{h} \tag{6.7}$$

where x is the displacement of the crossbridge, h is the finite range of the crossbridge, $f(x)$ is the attachment rate, $g(x)$ is the detachment rate, and g_1, g_2, f_1 are the attachment and detachment rate constants.

With these conditions applied back into the original equation, the crossbridge distributions for shortening can be summarized by:

$$x < 0: \quad n = \frac{f_1}{f_1 + g_1}\left[1 - e^{\frac{-\varnothing}{V}}\right] e^{\frac{2g_2 x}{sV}} \tag{6.8}$$

$$0 \le x \le h: n = \frac{f_1}{f_1 + g_1}\left[1 - e^{\left[\frac{x^2}{h^2} - 1\right]\frac{\varnothing}{V}}\right] \tag{6.9}$$

$$x > h: n = 0 \tag{6.10}$$

where

$$\varnothing = (f_1 + g_1)\frac{h}{s} \tag{6.11}$$

where s is the length of one sarcomere and V is the normalized rate of shortening in half-sarcomere lengths per second. These equations show that, as the muscle has higher shortening speeds, the number of attached crossbridges decreases while the developed force decreases more rapidly, as illustrated in Fig. 6.11.

6.5.6 Setting the constants

Huxley's model had nine rate constants. To determine important relationships between these constants, he used the known empirical relationships between tension, heat production rates, and shortening speed. Huxley used Hill's equations in their dimensionless form so that he did not have to set fixed values for those relationships. Huxley set values for three dimensionless groups composed of the original nine constants (Eqs. 6.12–6.14). The first (Eq. 6.12) was developed using the relationship between his constants and the maximum velocity when setting the tension equal to zero. The second and third relationships (Eqs. 6.13 and 6.14) were based upon the earlier discovery that the constant for shortening heat was similar to the constant found in force–velocity experiments (Hill, 1938). Huxley used the rate of

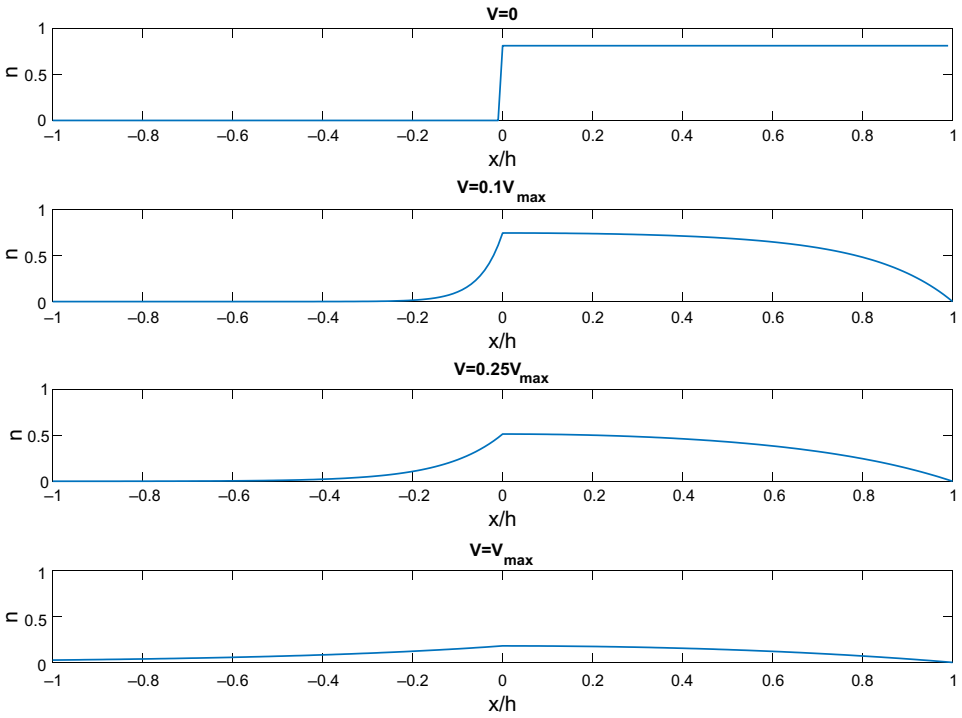

FIGURE 6.11

The percentage of attached crossbridges for different displacements. At zero shortening speed the number of crossbridges remains constant. As the speed of shortening increases, the number of attached crossbridges decreases for all displacements. Source*: Recreated from Huxley, A. F. (1957). Muscle structure and theories of contraction. Progress in Biophysics and* Biophysical Chemistry, 7*, 255–318.*

energy liberation along with tension and velocity to calculate the relationship between the other constants. When the rate of energy liberated and the force–velocity relationship are calculated, the results of the Huxley model are very similar to those calculated through Hill's equations. This was partly helped by the fact that Huxley chose parameters that matched the parameters from Hill's results

$$\frac{g_2}{f_1 + g_1} = 3.919 \tag{6.12}$$

$$\frac{g_1}{f_1 + g_1} = \frac{3}{16} \tag{6.13}$$

$$\frac{w}{e} = \frac{kh^2}{2e} = \frac{3}{4} \tag{6.14}$$

where k is the spring constant.

The equations for the sliding filament model (Hill, 1938) have been summarized previously in Section 6.5. For the rest of the section, we will discuss scenarios for which the model does not fit and how it was adapted to fit these scenarios.

6.5.7 Isotonic stretching

The preceding equations have all been applied to muscle shortening; however, the sliding movement model can also be applied to muscle stretching. When the muscle is being stretched, the crossbridge distribution includes a tail extending into a region with no attached bridges. The negative slope for the force–velocity curve for stretching was predicted to be larger than the negative slope for shortening. This discontinuity, at zero velocity, has previously been shown (Katz, 1939) and matched up with what the model predicted. This discontinuity also predicts the properties of muscle yielding, although the yielding force is larger than previously reported (Katz, 1939). In the model, yielding is caused by an increase in stretching speed. This means that the number of crossbridges available for attachment decreases and the force per crossbridge increases as the crossbridges are stretched.

6.5.8 Hill's revisions in heat production

In Hill's (1938) paper, he concluded that the thermal constant for shortening heat was independent of load, the speed of shortening, and the amount of work done. He did, however, notice that the extra heat produced by shortening was less at the highest speeds (see Fig. 6.12, black). This was later supported and shown to cause significant differences in heat production (Aubert, 1956). Hill later reexamined this concept and found that the constant of shortening heat was a function of shortening velocity and muscle tension (Hill, 1964; Fig. 6.12, blue). With this new information, the declining total rate of energy liberation is unable to be explained by the mathematical model (Chaplain & Frommelt, 1971). This newer result illustrated a serious problem with Huxley's (1957) model.

6.5.9 Reversible detachment

Huxley later revised his model based on the issues raise in Section 6.5.7 (Hill, 1964) to include a two-stage attachment process that explained the energy release during shortening (Huxley, 1973; Fig. 6.12, yellow). His updated model predicted that the rate of heat production would increase with increasing shortening speed because the rate of crossbridge cycling would also increase. For the model to show similar results to what Hill (1964) had shown with the rate of energy liberation, he assumed that, at larger displacements, the crossbridges could detach without ATP splitting

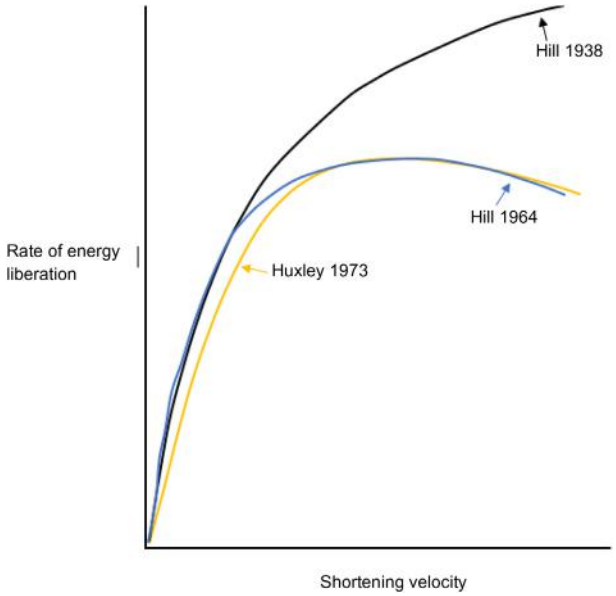

FIGURE 6.12
The rate of energy liberation comparison between Hill original (1938) and an updated (1964) model.

(Huxley, 1973). This modification to the model applied to the attachment process that occurred in two stages. The first stage of attachment permitted detachment without any energy use; the second stage of attachment was responsible for force development and behaved similarly to the Huxley's (1957) model. This two-stage attachment makes the attachment rate equation a second-order equation as opposed to the first-order equation in the original model. This means that the fraction of crossbridges that split ATP and release energy are proportional to the square of the time available for attachment, so the effect of greater shortening speeds is more profound using the updated model as depicted in Fig. 6.12. This change allowed for Huxley's (1973) model to match more closely with Hill's (1964) findings.

6.5.10 Problems and further updates of the model

Several problems have been raised with the sliding filament model since its inception. One such problem related to static instability emerges when many sarcomeres are arranged in series. *Static instability* means that any changes from resting length in the sarcomere will result in further changes in the direction of displacement. If some of the thick filaments are of different lengths and they are centered on the thin filaments, then the lengths of the filaments will be further amplified as the filaments overlap. Another issue is

that the tension plateau is found to be higher following an active stretch than during a fixed-end tetanus, even though the final end-to-end fiber length is the same. This is called the *permanent extra muscle tension* and has been observed in several studies (Edman, Elzinga, & Noble, 1976; Julian & Morgan, 1979). An addition to the sliding filament model that explains permanent tension is that the sarcomere lengths in a muscle fiber exhibit nonuniformity under certain circumstances (Julian & Morgan, 1979). That is, both permanent extra tension and tension creep observed in a fixed-end tetanus (Hill, 1953) provide support for the sliding filament model. The amplitude and duration of the creep phase in tension are greater at longer initial lengths of the muscle fiber because the sarcomeres have to contract further before reaching the plateau regions of the length–tension curve. This supports the theory that the end sarcomeres shorten at a higher velocity than the central ones, which causes the rise in velocity during the creep phase as the outside sarcomeres have a larger overlap than the central sarcomeres. These sarcomeres at the ends also play a role in active lengthening as they lengthen less than the central sarcomeres, promoting nonuniformity of the crossbridges.

Some additional problems have arisen since Huxley's (1973) amendment to his 1957 model, including the fact that it had difficulty predicting forces, energetics, and stiffness of muscles in eccentric contractions (Huxley, 1979). In addition, changes to the fundamental assumptions would be needed for prediction of residual force enhancement and depression using this method (Walcott & Herzog, 2008). However, including a spring element with variable stiffness, titin, to the crossbridge theory would allow for these problems to be corrected within the theory (Herzog, 1985).

There is an ongoing problem with the sliding filament model with respect to eccentric muscles, which are muscles that increase tension as they lengthen. Eccentric muscles act differently than the concentric muscles described by Huxley's theory, and they were included in the initial problems with the theory. In eccentric muscles, repeated use shows that the muscles become more compliant to strain because of the addition of sarcomeres in series (Butterfield, 2010). It has been speculated that titin plays a role in eccentric contractions and causes the force enhancement seen during the contraction (Hessel, Lindstedt, & Nishikawa, 2017). This means that these muscles would change activation over time and violate an assumption of the model.

More recently it has been shown that titin, a structural protein, in the sarcomere can vary stiffness by binding calcium or by phosphorylation (Labeit et al., 2003). In addition, titin may be able to bind to actin in the presence of activation, thus increasing stiffness (Herzog, Powers, Johnston, & Duvall, 2015). Due to these discoveries, a new three-filament model has been proposed with titin as the third filament that acts as modulated spring

(Schappacher-Tilp, Leonard, Desch, & Herzog, 2015). Herzog (2017) summarizes the future challenges of the crossbridge theory to be:

1. determining the role of nonactin–myosin-based force regulation;
2. verifying that titin binds to actin and determining the binding sites;
3. identifying any other structural proteins involved in force regulation; and
4. identifying if sarcomeres are the smallest independent contractile units in the muscle.

Addressing these challenges is at the forefront of muscle biomechanical research.

6.5.11 Summary

Originally, there were multiple theories on how muscles contracted, however, only Huxley's (1957, 1973) has withstood further testing. This section began with an explanation of how the model came to be and its original underlying assumptions. It then delved into some of the equations used by Huxley (1957) to describe the model. Though remarkably general, Huxley's (1957) model has proved to be inadequate in a number of contexts, a fate that befalls all modeling attempts. Failures to account for observed relationships between rates of energy expenditure and the shortening velocity (e.g., Hill, 1964), however, gave way to model improvements (Huxley, 1973) that recast the formation of actin–myosin crossbridges as a two-state process. With these improvements, Huxley's (1973) model remains just as influential today as ever, driving contemporary research on muscle biomechanics (Herzog, 2017).

6.6 Force development in the crossbridge

Quick changes in the length or force of tetanized muscles have been used to help further the knowledge of how single muscle fibers operate. These experiments, performed on even smaller time scales, were also useful in investigating the force dynamics of crossbridges for Huxley's updated model.

6.6.1 Early transients

Podolsky (1960) investigated what happened when a whole muscle, which was held and stimulated tetanically at constant length, was quickly released to an isotonic load. After the very rapid initial change in length due to the elastic element, the speed of shortening reached a very high and then a very low value before approaching the steady-state shortening velocity. This phenomenon could not be explained by Huxley's (1973) model or any other

mathematical model for muscles. Experiments with a single muscle fiber were able to complete a step change in muscle length in as little as 0.2 ms (Ford, Huxley, & Simmons, 1977). This result shows that the tension drop is synchronized with the change in length expected if the actin and myosin filaments were attached together with undamped springs. This also means that the elements of the muscle fiber that provide rapid elasticity resist a negative tension and do not go slack as the tension reaches zero. This cannot be attributed to either the actin or myosin filaments because when they are loaded under compression, they exhibit buckling.

6.6.2 Rapid elasticity and the series elastic component

Rapid elasticity, shown in the previous experiments (Ford et al., 1977; Section 6.6.1), is similar to the SE of a whole muscle, in the sense that they are both undamped springs that account for a fall in tension accompanied by a decrease in length. That is the limit of similarities, though, because rapid elasticity resists negative tension, the SE does not. Additionally, restretch of the rapid elasticity happens around 50 times faster than that of the elastic component due to the CE limiting elastic component stretch (Ford et al., 1977).

In rapid elasticity, the step length changes necessary to bring the tension to zero are the same for different fiber lengths. This means that, even when there are more crossbridges attached, the same sliding movement is sufficient to bring the force to zero (Ford, Huxley, & Simmons, 1981). Further research showed that the stiffness of the muscle fiber, which is proportional to the number of crossbridges attached, does not change proportionally with tension during the rapid recovery period (Ford, Huxley, & Simmons, 1974). This means that the number of attached crossbridges remains constant during rapid recovery. All this evidence points to the notion that the rapid elasticity resides within the crossbridges themselves.

As mentioned in Section 6.6.1, Ford et al. (1977) performed an experiment in which a single muscle fiber was subjected to a step change in length and found that it could be completed in 0.2 ms. Batters, Veigel, Homsher, and Sellers (2014) contend that that tension response to a step could be divided into four phases: (1) the initial elastic response during the step itself, (2) a rapid partial recovery toward the original tension, (3) a slowing or reversal of recovery, and (4) a slower return to original tension. Batters et al. further suggested that the displacement produced during a crossbridge attachment–detachment cycle is between 8 and 13 nm, providing additional evidence that there is instantaneous elasticity in the crossbridges. Additional work showed that, because only one-third to one-half of the crossbridges were attached during an isometric tetanus, the estimate of force per attached

crossbridges is about 8–12 pN as opposed to the 4 pN previously thought (Piazzesi, Lucii, & Lombardi, 2002). In brief, rapid elasticity experiments showed the muscle responds in less than 1 ms due to the elasticity present in the crossbridges.

6.6.3 Summary

Early quick twitch experiments were used to describe the force development and rapid length changes when muscles were released following stimulation. These experiments were related to force development in crossbridges in the context of the sliding filament model (Section 6.5) and found that there was a rapid elasticity in the muscle. Subsequently, comparisons were made between the rapid elasticity found in muscle experiments and the SE from Hill's muscle model. However, this rapid elasticity has been shown to reside in the crossbridges of the muscle so it could not be considered as the SE.

6.7 Reflexes and motor control

The preceding sections have focused on muscle contraction and muscle models. This section directs attention on how muscles are controlled within the body. Muscles are thought to be controlled by nerves that run through the spinal cord and into the brain. Muscles can also be controlled through reflexes which result in a mechanical behavior different than what would be observed either with a neural signal or in isolated muscle experiments like those first described in Section 6.2.

6.7.1 Organization of the motor control system

Most experiments that helped uncover the role that different brain regions played in motor control involved electronic stimulation to an area of interest or interruption of motor pathways. Multiple levels of control exert an influence on the motor system with different actions originating from various levels of a control hierarchy. Here we discuss the roles that specific brain regions play in motor control.

6.7.1.1 Spinal cord

The *spinal cord* is the lowest level of the central nervous system (Fig. 6.13). It plays a significant role in reflexes and simple actions, as well as the transmission of higher order signals to distal regions of the body. When the spinal cord is severed at the first vertebrae, animals still exhibit reflexes including the stretch and pain withdrawal reflexes (Hultborn, 2006). When these animals are placed on their feet, they can stand as the extensors of the limbs contract. Kittens can even walk on a treadmill following a spinal transection

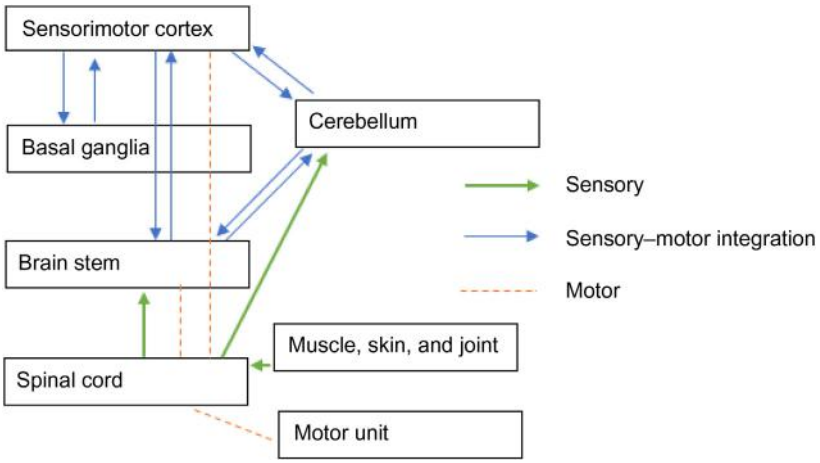

FIGURE 6.13

The organization of the central nervous system with arrows showing the connections between different regions of the brain. Source*: Recreated from McMahon, T. (1984).* Muscles, reflexes, and locomotion (Princeton paperbacks). *Princeton, NJ: Princeton University Press.*

when their body weight is supported. They are also able to change the speed at which their legs move in accordance with the speed of the treadmill (Grillner, 1975) and have exhibited airstepping, which refers to walk-like movements from the hindlimbs when held vertically in the air (Giuliani & Smith, 1985). Another classic example is that chickens can still run for a short period of time after their heads have been cut off. This shows that some features of locomotion are generated at the spinal cord level without input needed from higher levels of control.

6.7.1.2 Brain stem

The next level of the central nervous system is the *brain stem* (Fig. 6.13). The brain stem connects the higher brain regions to the spinal cord and consists of three main areas, the pons, the medulla, and the reticular formation. The pons acts a bridge between the sensorimotor cortex and the cerebellum and is involved in basic body functions such as chewing and breathing (Saladin, 2007). The medulla, or medulla oblongata, is the connection between the brain and the spinal cord and helps regulate physiologic processes (Magill, 2011). The reticular formation integrates sensory and motor information and can inhibit or amplify motor signals. The brain stem also plays a major role in the control of eye movements (Sparks, 2002). Animals with a transection in the midbrain show the same reflexes that were present in spinally severed animals, while also incorporating more elaborate motor activity. These

animals have the ability to right themselves when they are lying on their back or side, although these behaviors are dependent on a functioning otolith apparatus in the ear, which helps with sensations of the direction of gravity.

6.7.1.3 Sensorimotor cortex and basal ganglia

At the top level of the central nervous system lies the sensorimotor area of the cerebral cortex (Fig. 6.13). This area is devoted to the control and movement of limbs as well as receiving sensory information from the spinal cord. This region is important for the control of movement, especially for fine motor skills (Magill, 2011). The sensorimotor cortex plays a major role in motor learning and neuroplasticity (Francis & Song, 2011). This means that when the sensorimotor cortex is damaged or removed an animal has typical performance with respect to most motor functions but often lacks the ability to acquire new motor skills.

The basal ganglia are a group of structures in the upper brain stem that are important for motor control due to their numerous connections to the sensorimotor cortex. They receive information from the cerebral cortex and brain stem and send motor information to the brain stem (Magill, 2011). The basal ganglia also play an important role in the planning and initiation of movement (Lanciego, Luquin, & Obeso, 2012). Most of what is known about the function of the basal ganglia has been deduced from disturbances to human motor behavior accompanying disease. Parkinson's disease (PD) is one of the more common disorders that affects the basal ganglia, resulting in movement disorders such as bradykinesia, akinesia, and tremor (Magill, 2011).

6.7.1.4 Cerebellum

The cerebellum is in the posterior region of the brain near the brain stem (Fig. 6.13). This region plays a key role in the execution of smooth movements as damage to it leads to more clumsy movements (Ghez & Fahn, 1985; Magill, 2011). The cerebellum has roles in coordination, motor learning, postural control, balance reactions, and adapting gait to meet environmental demands (Kelly & Shanley, 2016). This region is a focus of incoming information including information about the length, force, and velocity of muscles and joint positions. Bard, Woolsey, Snider, Mountcastle, and Bromiley (1947) found that normal dogs subjected to the motion of a swing exhibited all the symptoms of human motion sickness, but dogs without a cerebellum appeared to be unaffected by motion sickness. Animals whose cerebellum has been removed have a nearly normal range of motor behavior, but their movements are awkward and clumsy, and they fall frequently

during running. The cerebellum performs a role of integration and smoothing of behaviors but does not produce movements itself.

6.7.2 Muscle fiber types

There have been three types of skeletal muscle fibers identified: fast glycolytic, fast oxidative glycolytic, and slow oxidative (Herbison, Jaweed, & Ditunno, 1982). These muscle fibers are typically identified through cross-sectional staining to reveal the presence of an oxidative enzyme involved in the aerobic process. The fast-glycolytic fibers show the least amount of staining and are the fastest performing of the groups of fibers. These fibers have a low density of mitochondria and blood capillaries and thus mainly rely on anaerobic mechanisms. The slow oxidative fibers show high levels of staining due to an abundance of oxidative enzymes. When compared to fast fibers, these muscles have a smaller diameter and produce greater resistance to fatigue. They are often used in muscles for near continuous activity such as flying in birds or swimming in fish (Jayne & Lauder, 1994; Johnston & Goldspink, 1973). The fast oxidative-glycolytic fibers are in between the two other groups of muscles in terms of staining. They are similar in speed to the fast-glycolytic fibers but contain more mitochondria and oxidative enzymes. These muscles are used in normal locomotion actions, while the fast-glycolytic fibers are used much less frequently (Scott, Stevens, & Binder–Macleod, 2001). Different muscle types are located throughout the body and combine together in different sizes to produce movement.

6.7.3 Motor units

An important aspect of the neuromuscular system is that a single motor neuron innervates many muscle fibers. This means that the stimulation of a single motor neuron causes hundreds, even thousands, of muscle fibers to contract. This connection between a motor neuron and all the target muscle fibers it stimulates is called a *motor unit*. Motor units can range from just a few fibers as observed in ocular muscles to over 2000 fibers, which is more typical for limb muscles (MacIntosh et al., 2006). When a stimulation is applied to a motor unit pathway, the small motor units will activate at low levels of a stimulus, but higher levels of stimulation are necessary to activate the larger motor units. This is known as the *size principle* (Henneman, Somjen, & Carpenter, 1965). Small motor units are typically made up of the slow muscle fibers as they are activated more often and need to be resistant to fatigue. Large motor units typically supply either type of the fast muscle fibers. These fibers are not required regularly but must produce high levels of speed and power for a short amount of time. As more force is needed for a task, larger and larger motor units are recruited to accomplish the task.

6.7.4 Muscle proprioceptors

For muscles to work properly, sensory feedback is necessary to provide feedback. Sensory receptors are very specialized, as different types of receptors are needed for each type of sensory feedback. The sensors with primarily motor functions are called proprioceptors (Tuthill & Azim, 2018). Proprioceptors include the sensory receptors in the skin and subcutaneous tissue that reflex motions depend on and the sensory receptors in and around joints to help stabilize them (MacIntosh et al., 2006). Joint receptors are important in locomotion, as reflexes can change based on the level of extension of the leg. Additional proprioceptors, such as the stretch receptors and the Golgi tendon organs, are also associated with muscles.

Stretch receptors, also called spindle organs, are found within most muscles of the body. These sensors measure length changes as well as the rate of change of the muscle (Suslak & Jarman, 2015). This makes spindle organs very important for reflex responses and coordination (MacIntosh et al., 2006). Spindle organs comprise two different types of intrafusal muscle fibers, the nuclear bag and the nuclear chain. Smaller muscles that are used for fine control have a high density of spindles; larger muscles have fewer spindles. These spindle organs signal to reset the muscle to its resting state.

The *Golgi tendon organ* is found in the tendon near the junction of tendon and muscle fibers. It responds to a tendon stretch, or a muscle contraction, by sending action potentials so that the muscle tension increases (Prochazka, Gillard, & Bennett, 1997). These sensory receptors send information to the brain and spinal cord to help control movement. Unlike the spindle organs, the Golgi tendon organs are not innervated by motor axons (MacIntosh et al., 2006). These proprioceptors provide information back to the muscles, spinal cord, and brain through axons.

6.7.5 Axons

Axons run from the brain through the spinal cord and into muscles and are used to connect the brain with muscles and motor units (Magill, 2011). The nerve axons which run away from the spinal cord and carry signals to the joints are *efferent axons*, whereas, the axons that carry information toward the spinal cord and brain are called *afferent axons*. The afferent nerve cells are found in the dorsal root ganglion between each vertebra. There are two groups of afferent nerves, Group I and Group II, based on the diameter of the axon. Group I fibers are larger and have higher conduction velocities. They typically bring information from the spindle or Golgi tendon organs. Group II fibers typically carry information from the spindle organs. The efferent motor neurons are found in the gray matter in the ventral root of the spinal cord. These are connected to the brain and other efferent neurons

through the surrounding white matter, which have long nerve fibers running up and down the spinal cord (Magill, 2011).

6.7.6 Reflexes

In some instances, axons send information to muscles based on feedback without any input from the brain (Fig. 6.14). This is the case during reflexes. A stretch reflex occurs when an activated muscle is stretched by an outside source; it contracts more forcefully than before the stretch. This is due to the spindle organs being stretched by the same amount as the muscle and signaling an increase in the firing rate of the muscle. A familiar example involves striking the patellar tendon from the front (McMahon, 1984). This produces a small stretch of the quadriceps, which is followed by the reflex kick of the quadriceps. This reaction happens quickly because it involves only one synapse. Other reflexes take longer because they require more synapses between the stimulus and response. For example, polysynaptic reflex circuits involve

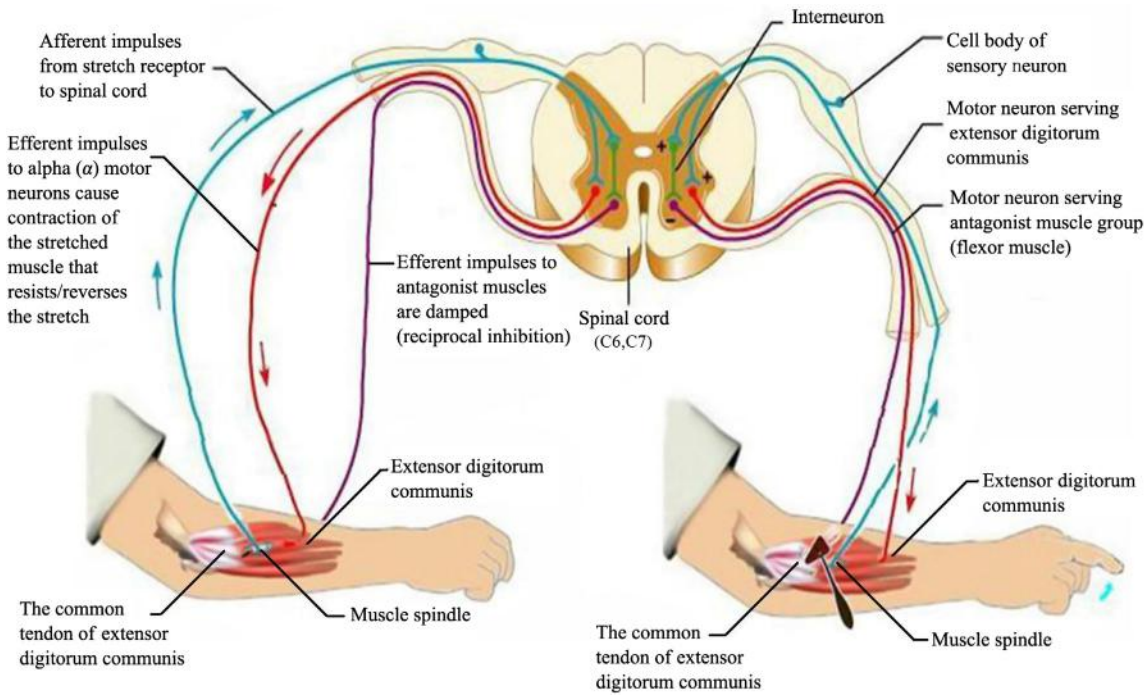

FIGURE 6.14

The muscle proprioceptors and the associated reflex pathway. Reflex pathways typically only involve the spinal cord and do not require any further central nervous system interaction. This specific illustration details the extensor digitorum reflex. Source: *https://commons.wikimedia.org/wiki/File:The_extensor_digitorum_reflex.jpg licensed under the Creative Commons Attribution-Share Alike 4.0 International license.*

multiple synapses in the spinal pathway. The crossed extension reflex, the response experienced when one steps on a nail, has a longer latency period because the synapses between many interneurons must be traveled.

In addition to the spindle organs, the tendon organs may play a role in control of muscle *reflex stiffness*. Originally, it was thought that the tendon organ served as the sensor in a reflex which turned off muscle activity when the force rose above safe levels. However, research has suggested that the tendon organs respond to less than 1 g of force (Houk, Singer, & Henneman, 1971), necessitating additional theorizing. A popular theory is that the ratio of force to muscle length is controlled and held at a constant value during the stretch reflex (Nichols & Houk, 1976). Nichols and Houk (1976) showed that the ratio of change in force to change in length was fixed at a constant value by the stretch reflex. This suggested that a skeletal muscle can present constant stiffness, even with large variations due to different portions of the length−tension curve.

Multiple studies have supported this idea with Hoffer and Andreassen (1978, 1981) measuring stiffness in cats with and without the reflex. This was accomplished by cutting the soleus nerve. At low force levels, the stiffness increased but plateaued at medium and high levels. In addition, Greene and McMahon (1979) were able to measure stiffness in humans by using a springboard and calculating the stiffness through a second-order coupled system based on the natural frequency resonance on the springboard. They found that stiffness increased by less than 10% as the weight increased, meaning that the muscles in the legs could be approximated as a spring with constant stiffness. Further research investigated stiffness for running on different surfaces and it was found that humans were able to change the leg stiffness based upon the stiffness of the surface on which they were running (Ferris, Louie, & Farley, 1998). Stiffness has also been used to investigate other parts of the body including the trunk, in which stiffness increases with the flexion angle (Granata, Rogers, & Moorhouse, 2005). These studies showed that stiffness is regulated by proprioceptors and reflexes in the body.

6.7.7 Tremor

Tremors and other neurological motor symptoms are useful in identifying how the neuromuscular system works. A *tremor*, defined as a rapid back-and-forth movement of a body part, is a motor phenomenon found both in normal individuals and as a pathological symptom (McAuley & Marsden, 2000). These tremors can be defined in two unique categories, physiological and pathological, each characterized by its own distinct frequencies. In pathological tremors, such as PD, the tremors are slower than would be seen through a stretch reflex pathway tremor.

Some cases of tremor can be attributed to the stretch reflex, mentioned in Section 6.7.6, as shown using electromyographic signal on the extensor muscle in the index finger (Lippold, 1970). This research showed that when a small tap was applied, the finger produced a series of low-amplitude oscillations before coming to rest. When a cuff was inflated on the arm, the oscillations were diminished. This shows that for low-amplitude motions, damping by the receptors was light enough to allow the oscillations to occur. Tremors were also investigated in the hand through the wrist extensor muscles in isotonic and isometric settings (Burne, Lippold, & Pryor, 1984). In the isotonic condition a peak at 8−12 Hz was observed, while the peak was absent in the isometric condition. These tremors have also been investigated for drug treatments as research has shown that the drug amitriptyline increased the central component of physiological tremor (Raethjen et al., 2001). Lakie, Vernooij, Osborne, and Reynolds (2012) have recently shown that the frequency spectrum of the tremor had a distinct peak at 8 Hz, while the spectrum was flat above 2 Hz, which shows the presence of resonance. Physiological tremors occur because the peripheral stretch reflex can be regarded as a negative-feedback loop (McAuley & Marsden, 2000).

6.7.8 Negative feedback and time delays

Negative feedback is a process in which the output of a system is fed back into the system to modulate it. Negative feedback usually tends to result in a reduction in the fluctuations of the output. When a time delay is present in the loop, or if the loop is underdamped, there is a possibility of oscillations specifically at a period twice that of the loop time (McAuley & Marsden, 2000). In the finger tremor considered in the previous paragraph, time delays in the control loops have been measured to be about 50 ms (Marsden, 1978). This would create physiological oscillations at 10 Hz, which is within the range of previous findings for finger tremor oscillations. In the body, Renshaw cells are responsible for the negative-feedback loop found in the reflex pathways (Roberts, 1978).

6.7.9 Renshaw Cells

Renshaw (1941) found that axons of motor neurons give off a branch in the gray matter of the spinal cord and this branch synapses with nerve cells close to the parent cells. These cell bodies, which have since been named Renshaw cells, send axons with inhibitory synapses to the parent motor neuron (Alvarez & Fyffe, 2007). These cells are responsible for the negative-feedback loops as the firing rates of the motor units for a muscle are generally lower than the firing rates of the spindle afferents from the same muscle (Roberts, 1978). Other evidence of the role in negative feedback comes from

decerebrated cats as Renshaw cells show rhythmic activity during locomotion even without sensory feedback (Rybak, Shevtsova, Lafreniere-Roula, & McCrea, 2006). Renshaw cells provide the mechanism behind negative-feedback loops in the stretch reflex pathways.

6.7.10 Summary

The motor control pipeline starts with reflexes at the spinal cord level and moves up to the highest levels at the cerebral cortex. Each level of the motor control system contributes to different movement and actions. Muscle proprioceptors and axons are used to communicate information from the brain to the muscles and vice versa. Reflexes make use of muscle proprioceptors to perform actions independently of the upper motor control system. Problems can arise from these reflex pathways such as tremors which result from a time delay present in the negative-feedback loop. Renshaw cells are responsible for the negative-feedback loop in human muscle. The hierarchical picture of motor control presented above positions neural mechanisms as central elements in the control of movement, which is the subject of the next section.

6.8 Neural control of locomotion

Animal locomotion has been studied by a broad range of researchers from any number of fields including neurobiology, physics, physiology, psychology, and zoology. Animals provide a great perspective on locomotion because of the variety of different strategies used. Unique morphologies (e.g., the number and positioning of legs) play a major role in limiting movement patterns; however, this section focuses on the neural aspects of controlling locomotion. Specifically, this section focuses on historical animal studies that have sought to localize neural underpinnings of locomotion by isolating neurophysiological components.

6.8.1 Gait comparisons

When it comes to animals, similar species often adopt similar locomotion patterns. This means that mammals move similarly to other mammals, while fish move similarly to other fish as well as amphibians and reptiles. Fish move by bending their vertebral column by contracting the muscles on one side of the body while keeping the muscles on the other side of their body relaxed. This produces a lag between the head and tail segments that makes the bending process—a wave—travel down the body. Faster locomotion requires the fish to increase the frequency of its tail beats which, in turn, corresponds to an increase in the speed of the bending wave (Grillner, 1975).

These rostral–caudal oscillations are also observed in amphibians which, when in water, swim essentially like fish. On land, they perform the same bending movements, which benefit their gaits by increasing step length (Gray, 1968). This wavelike behavior is far less pronounced in mammals, however, likely owing to the orientation of their limbs. In mammals, each limb is directly under the animal as opposed to sticking out to the side. The mammalian spinal column allows for twisting and bending in the lateral and vertical planes, but amphibians' and reptiles' spinal columns prevent twisting as well as flexion–extension. Interestingly, extension and flexion of the mammalian spinal column has putatively been preserved in sea mammals such as whales and dolphins (Grillner, 1975). However, our current discussions focus more on movement patterns on land.

There are two general categories classifying land walking, bipedal and quadrupedal gaits. In bipedal gait, the limbs operate, forming either an in-phase (hopping) or an alternate-phase (walking and running) pattern (see also Chapter 9: Coordination and control: a dynamical systems approach to the analysis of human gait, about these phasing relationships). Some animals, such as kangaroos, use the hopping technique to obtain high speeds at low energetic cost (Kram & Dawson, 1998). Walking entails periods of double support in which both feet are on the ground, followed by a single leg support phase in which one foot is swinging forward. Running, however, does not involve this double-support period, and during certain phases of the running gait cycle, both feet are off the ground.

Having two additional legs raises the number of possible quadrupedal gait strategies from three to six; however, only three of the six gait strategies are commonly observed: walking, trotting, and galloping. The six gait patterns can be identified by the duty factor and the relative phase (McGhee, 1968) (Table 6.1). The *duty factor* is the percentage of the stride cycle during which one foot is on the ground, while the *relative phase* represents the difference in cyclical phases of each foot while locomoting (Kurz & Stergiou, 2004). These four-legged gaits can be separated into alternate gaits, which do not use the spinal flexion extension, and in-phase gaits. Alternate gaits are typically used at low speeds, while in-phase gaits are used at high speeds (Alexander, 1977a). Alternate gaits are walking, where there is a quarter of a stride cycle between each foot strike; trotting, where the limbs at diagonal corners of the body work synchronously; and the rack, which is a variation of the trot used by camels and giraffes. The in-phase gaits are the canter, where the forefoot and a diagonal hindfoot strike the ground together; the transverse gallop, where a little delay occurs between the strike of the last hindfoot and the next forefoot; and the rotary gallop in which the sequence of footfalls goes around in a circle. These same interlimb coordination patterns have even been observed in cats with severed spinal cords on treadmills

Table 6.1 The duty factor and relative phase for the six types of quadrupedal gait.

Alternate gaits		**Walk**		**Trot**		**Rack**	
Duty factor		>0.5		0.3–0.5		0.3–0.5	
		L	R	L	R	L	R
Relative phase	Fore	0.00	0.50	0.00	0.50	0.00	0.50
	Hind	0.75	0.25	0.50	0.00	0.00	0.50

In-phase gaits		**Canter**		**Gallop (transverse)**		**Gallop (rotary)**	
Duty factor		0.3–0.5		<0.4		<0.4	
		L	R	L	R	L	R
Relative phase	Fore	0.00	0.80	0.00	0.80	0.00	0.80
	Hind	0.80	0.50	0.60	0.50	0.50	0.60

The reference foot for each gait is the left forefoot and the relative phase represents the percentage of the gait cycle by which each foot trails the reference foot.
Recreated from Alexander, R. M. (1977a). Terrestrial locomotion. In R. M. Alexander & G. Goldspink (Eds.), Mechanics and energetics of animal locomotion *(pp. 168–203). London: Chapman and Hall.*

(Forssberg & Grillner, 1973). So, what happens in insects that have more than four legs? Just like with four legs, there are a variety of interleg coordination patterns for six-legged insects (Ritzmann & Buschges, 2007). When each set of a hexapod's legs were amputated, it was found that the sensory information from the middle legs might be necessary for a regular hind leg stepping pattern (Grabowska, Godlewska, Schmidt, & Daun-Gruhn, 2012). The duty factor and relative phase allow for comparisons of gait in different animals and quantify all the possible gait patterns for four-legged animals. Once the amount of legs increases beyond four, the gait patterns remain similar to those of two- and four-legged animals.

6.8.2 Control of a single limb

With respect to the control of a single limb, we should mention the principle of *reciprocal inhibition*, which suggests that the stretch of extensor muscles inhibits the activity of flexor motor neurons, and vice versa (Crone, 1993). An upward force to the wrist deactivates the biceps during a cocontraction of the biceps and triceps muscles (Fig. 6.15, right). This principle originates in neural connections to the spinal cord that release an inhibitory transmitter substance. This can be shown in any joint of the body and is used to prevent muscles from competing with one another in the presence of an externally applied load. The body has a variety of reflexes that involve the spinal cord without use of higher processing centers (Crone, 1993).

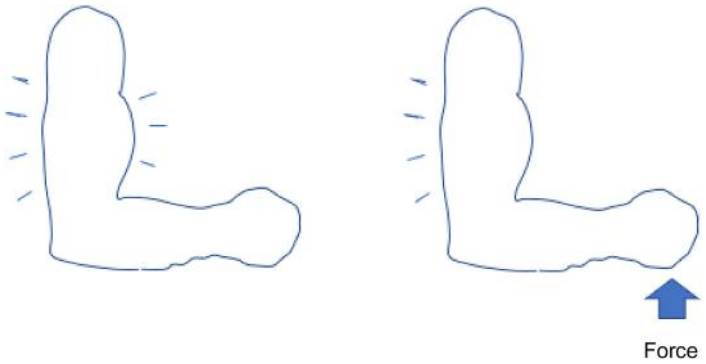

FIGURE 6.15

The principle of reciprocal inhibition: (*left*) cocontraction and (*right*) inhibition when a force is applied to the wrist. Source*: Recreated from McMahon, T. (1984).* Muscles, reflexes, and locomotion (Princeton paperbacks). *Princeton, NJ: Princeton University Press.*

6.8.3 Reflex reversal

Experiments with animals have been crucial in furthering our understanding of reflexes. If a cat is blindfolded and the upper surface of its paw touches the side of the table, it will lift its foot up and place it on the table. This reaction is called a *placing reaction* and is a spinal reflex observed even in kittens (Grillner, 1975). Despite having their spinal cord transected 1 week after birth, these kittens can walk on a treadmill when their body weight is supported. The placing reaction can be simulated in the kittens by touching or stimulating the top surface of the paw during treadmill walking. However, this reflex can only be activated when the foot is in the swing phase. During the stance phase, the reflex is reversed, and the limb shows extension as opposed to flexion. This reflex reversal can be seen when the animal is suspended in the air and there are no ground reaction forces. When pressure was applied to the bottom of the foot instead, the limb showed extension.

In humans, this reflex also is present during walking as the reflex changes from excitation of muscle during one phase of the gait cycle to inhibition at another part of the gait cycle (Duysens, Trippel, Horstmann, & Dietz, 1990). An example muscle that this can be seen in is the tibialis anterior, which is active from late stance through most of the swing phase and at the transition from swing to stance (De Serres, Yang, & Patrick, 1995). When a stimulus was applied to the tibialis anterior during the swing phase it produced a response. In contrast, when the stimulus was applied at the transition from swing to stance, the response was suppressed. This shows that even though the muscle was active at both points, it was performing very different roles (De Serres et al., 1995).

6.8.4 Mechanical oscillator

McMahon (1984) modeled this reflex reversal mechanism as a damped pendulum that produces self-sustained oscillations. Without some injection of energy (e.g., a stimulus), the oscillations would slow and stop, but with stimulation, the oscillations are able to continue indefinitely. In the pendulum system depicted in Fig. 6.16, the "stimulus" takes the form of a gas jet released when the pendulum opens an electrical contact meant to simulate a "receptor" in the nervous system. The stimulus is only effective if the pendulum is already in motion because the stimulus is not strong enough to start the pendulum from rest. This pendulum mimics the reflex reversal mechanism seen in each limb, although it cannot account for any interlimb coordination (McMahon, 1984).

Recently, mechanical oscillators have been used to improve stability in quasipassive robots. These quasipassive models use actuators and control to increase the stability when walking uphill or over level ground. In these quasipassive walkers, a mechanical oscillator is used to synchronize the period of lateral motion with the period of swing leg motion (Suzuki & Hachiya, 2008). This method can increase the environmental adaptability of a previously passive walker so that it can maintain stability across a variety of slopes

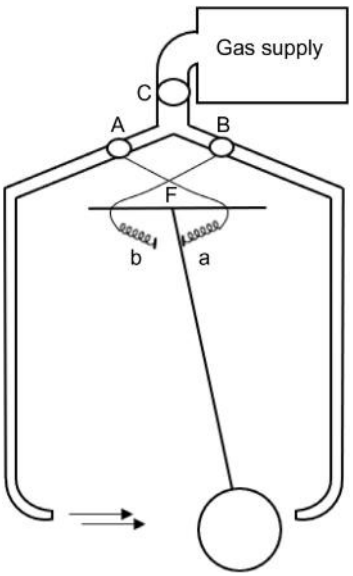

FIGURE 6.16

A mechanical oscillator based on reflex reversal. Source*: Recreated from McMahon, T. (1984).* Muscles, reflexes, and locomotion (Princeton paperbacks). *Princeton, NJ: Princeton University Press.*

(Cao, Suzuki, & Hoshino, 2014). Mechanical oscillators can be used to model the complex dynamics of gait.

6.8.5 Entrainment of frequency

Understanding interlimb coordination requires the concept of *entrainment*. Dutch astronomer Christian Huygens observed that when two pendulum clocks that have slightly different periods are placed on the same wall, they synchronize, assuming the wall is compliant enough to translate mechanical energy between the clocks (Willms, Kitanov, & Langford, 2017). McMahon (1984) illustrated the process of entrainment by analogy to a clock mechanism similar to that depicted in Fig. 6.16. Imagine that an external force shakes the entire enclosure left and right in a sinusoidal fashion. The external forcing causes the pendulum to swing with a period equivalent to the external force, even if the eigenfrequency of the pendulum is different from that of the external force. If the amplitude of the force is great enough, the pendulum will repeatedly open and close valves B and C. If valve A is also open—the conditions which would produce a self-sustained oscillation—then, the amplitude increases but the frequency does not. This phenomenon is known as *frequency entrainment*.

Huygens identified several conditions necessary for this form of synchronization (Willms et al., 2017). First, strength of coupling between oscillating components must be sufficient in order to produce entrainment. Placing Huygen's clocks farther apart on the wall weakens the coupling between them, and, at some critical distance, the coupling becomes effectively zero and the clocks will swing at their own natural frequencies. Second, the coupled oscillators need to have relatively similar natural frequencies. If starting from a state of entrainment, and one of the pendula is shortened with respect to the other, then at some point the clocks will once again tick at their own natural frequencies. Lastly, entrainment depends on the strength of internal forces of the clock (e.g., gas pressure in Fig. 6.16) and the strength of the external forcing function (Willms et al., 2017).

The range of relative frequencies the sinusoidal force may take, and still result in entrainment, is the *zone of entrainment* (Zalalutdinov et al., 2003). Continuing with the analogy of a sinusoidally forced clock, imagine the situation where the clock and external force have a constant frequency ratio (e.g., 1:1) such that the clock ticks once for each forcing cycle. If the shaking frequency is continuously lowered below the lower bound of the zone of entrainment, then the clock transitions back to its intrinsic frequency. Remarkably, though, lowering the frequency of the shaker further reveals additional zones of entrainment at 1/2, 1/3, ..., $1/n$ of the original entrainment range, a phenomenon known as *superharmonic entrainment*

(Eiswirth & Ertl, 1988). That is, in a 1:2 frequency ratio, the clock would cycle twice each time the external force cycles through its range of motion.

Far from a thought experiment, 1:*n* frequency entrainment has been repeatedly demonstrated in numerous experiments involving both bipedal and quadrupedal locomotion. Spinal cats have been observed to produce 1:2 (i.e., 1:*n* where $n = 2$) stepping patterns walking on a split treadmill where the belts are driven at different speeds (Grillner, 1975). Two times as many steps are taken on the faster belt than on the slower belt. Interestingly, the steps on the fast belt are not of equal duration because they are timed with the flexion and extension of the contralateral side (Grillner, 1975). Similar results have been reported across the literature and have implicated firing rates of Purkinje cells in the visual cortex in the appearance of superharmonic entrainment during split belt treadmill walking involving spinal cats (e.g., Yanagihara & Udo, 1994; Yanagihara, Udo, Kondo, & Yoshida, 1993). Similar results have been observed in humans and may have important clinical implications. For example, individuals who had cerebral stroke were able to adapt to the split belt similarly to healthy controls (Reisman, Wityk, Silver, & Bastian, 2007). However, some children with surgical hemidecortication showed disruption of this split belt adaption (Choi, Vining, Reisman, & Bastian, 2009).

Processes of coupling and entrainment are so prevalent in humans that they imply general mechanisms at work over virtually every temporal and spatial scale characteristic of human behavior (Amazeen, 2018). As noted, frequency entrainment is a defining feature of locomotion in animals (Grillner, 1975) and humans (Clark & Phillips, 1993; Kurz & Stergiou, 2002, 2004; Thelen, Ulrich, & Wolff, 1991), but entrainment characterizes many other forms of rhythmic coordination of the limbs, including the hands (Haken, Kelso, & Bunz, 1985), the wrists (Amazeen, Amazeen, & Turvey, 1998; Kugler & Turvey, 1987), and upper and lower extremities (Kelso & Jeka, 1992), just to name a few. Not limited to interlimb coordination, entrainment dynamics are common features of neural activity and describe the high-frequency collective behavior evident in neural oscillations (Buzsaki, 2006; Cohen, 2014, 2016; Tognoli & Kelso, 2009) and coordination across physiological subsystems (Amazeen, Amazeen, & Beek, 2001; Daffertshofer, Huys, & Beek, 2004). At a macroscale, features of entrainment are also evident in rhythmic and nonrhythmic forms of interpersonal coordination (Fine, Gibbons, & Amazeen, 2013; Fine, Likens, Amazeen, & Amazeen, 2015; Gorman, Amazeen, Crites, & Gipson, 2017; Likens, Amazeen, Stevens, Galloway, & Gorman, 2014; Schmidt, Carello, & Turvey, 1990; Stevens, Gorman, Amazeen, Likens, & Galloway, 2013). These latter instances, in which interpersonal entrainment produces patterns similar to those observed in intrapersonal entrainment, raise unanswered questions about the mechanism for coordination.

McMahon (1984) raised the hypothesis that entrainment observed in human locomotion (and, presumably other forms of coordination) may have originated the coordination of central pattern generators (CPGs; Grillner, 1975). CPGs are thought to be spinal neurons that, for example, alternate stimulating flexor and extensor motor neurons, without input from higher neural centers. The spinal cats that were discussed earlier in this section were taken as strong evidence of the existence of CPGs. This is an incredibly popular notion that still permeates contemporary motor control theory (Schmidt & Lee, 2011) as well as modern robotics (Aoi, Manoonpong, Ambe, Matsuno, & Worgotter, 2017). However, an early finding related to rhythmic interpersonal entrainment questions this hypothesis (Schmidt et al., 1990). In that study, participants were asked to coordinate the swinging of their legs, while maintaining particular relative phase patterns (e.g., 0 degree, 180 degrees). Remarkably, the observed dynamics between people were virtually identical to those observed within a person (Haken et al., 1985), questioning the role that CPGs play in interlimb coordination. Even more remarkably, just like Huygen's clocks, interpersonal entrainment requires some form of coupling in order for entrainment dynamics to emerge (Marmelat & Delignières, 2012; Richardson, Marsh, Isenhower, Goodman, & Schmidt, 2007). The implication is that CPGs may not be adequate descriptors of human locomotion.

6.8.6 Stimulated locomotion

When a cat, that has had its brain stem cut is suspended so that its feet do not touch the ground, is stimulated below the level of the cut, it will start walking (Grillner, 1975). At lower frequencies, the cat's limbs move in a pattern similar to walking in a normally functioning individual, but as the frequency of the stimulation is increased, so is the frequency of the stepping. At higher and higher frequencies and strengths of the signal, the gait becomes a trot and then switches to a gallop. Drugs have been discovered that show similar results to electrical stimulation of the pathways. L-DOPA, commonly used for PD, is used to increase the release of norepinephrine from descending neurons. L-DOPA was discovered by Nobel Prize winner Dr. Arvid Carlsson who showed in the 1950s that administering L-DOPA to animals with drug-induced Parkinson symptoms decreased the intensity of the animals' symptoms. This treatment was later extended to Parkinson patients by George Cotzias and his coworkers. The neurologist Oliver Sacks describes this treatment in human patients in his book *Awakenings*. This book was made into a well-known movie!

Other drugs, such as clonidine, have been shown to stimulate receptors or have been used to help stimulate walking in spinal cats. Specifically, clonidine facilitates hindlimb locomotor recovery following spinalization in

untrained cats by enhancing the excitability of central pattern generating spinal neurons that also participate in crossed extensor reflex transmission (Frigon, Johnson, & Heckman, 2012). These results show the presence of CPGs during walking as spinal animals could be able to display close to normal walking movements without input from the brain.

6.8.7 Legged vehicles

To demonstrate CPGs, researchers have turned to robot systems. The first legged vehicle to walk by itself under computer control was the "Phony Pony," built by Frank and McGhee at the University of California in 1966 (McGhee, 1966). A vehicle that was able to be rode was built at General Electric in 1968 and was controlled by a series of levers and by the rider's movements. These robotic models became more realistic and began to include the dynamic interactions of locomotion (Taga, Yamaguchi, & Shimizu, 1991). Quadruped robots achieved adaptive interlimb coordination by modeling CPGs with local sensory feedback (Maufroy, Kimura, & Takase, 2010). Fukuoka, Habu, and Fukui (2015) showed that these CPGs can be used at different speeds as a quadruped robot gait transitioned from a walk at slow speeds, to a trot at medium speeds, and a transverse gallop at high speeds.

Recent discoveries have thrown light onto the fact that gait is not periodic but exhibits stride-to-stride fluctuations that present long-range correlations (West & Scafetta, 2003). This, in turn, suggests that locomotion could be represented by a correlated stochastic version of a CPG as the oscillations of each limb cannot be described completely by cyclic repetitions (Scafetta, Marchi, & West, 2009). These super-CPGs, CPGs that employ long-range correlations, can reproduce both the fractal and multifractal properties of gait dynamics (West & Scafetta, 2003). These models show the importance of the nonlinear framework in analyzing and predicting human movement (see Chapter 8: Gait variability: a theoretical framework for gait analysis and biomechanics and Chapter 10: A tutorial on fractal analysis of human movements).

6.8.8 Summary

In this section, we have presented both historical and contemporary research on neural control of locomotion. Duty factor and relative phase identify characteristics of animal gait. Duty factor is a measure of how long each limb is on the ground, while relative phase is a measure of how much each leg lags behind the lead leg. This method allows comparison among the gaits of bipedal and quadrupedal animals. Through neural control, the muscles can be strategically inhibited through reflex reversal and reciprocal inhibition. Animals with a severed spinal cord show the ability to walk just using

reflexes without any input from the brain, provided that their body weight is supported. Studies of this nature developed the ideas of a CPG which controls gait at the level of the spinal cord. This led to the concept of entrainment, which describes how limbs act cooperatively to facilitate movement. CPGs have been updated over the years and were used in further models and robots to enhance our understanding of how they operate.

6.9 Mechanisms of locomotion

Walking and running are visually distinguishable by the fact that, during running, there are periods when both feet leave the ground. The question is: What are the mechanical specifics that lead to the qualitative differences between walking and running? The answer to this question hinges on basic ideas about the dynamics and energetics of walking and running, the subject of this section.

6.9.1 Motion-capture laboratories

Forceplates and motion-capture cameras represent essential tools in the study of the mechanics of locomotion (Fig. 6.17; see also Chapter 1: Introduction to biomechanics). A forceplate is an electronic "scale" which measures three-dimensional forces applied to it by a participant's foot. For a forceplate to be accurate, it needs to record at a high enough frequency, at least the Nyquist

FIGURE 6.17
The setup of a motion-capture laboratory at the University of Nebraska at Omaha with forceplates embedded into the treadmill. Cameras are seen attached to the wall (see boxes).

frequency which is twice the highest frequency present in the signal; give the same signal for a given force regardless of the location it is applied; and produce a low level of noise (see also Chapter 5: Power spectrum and filtering). In the past, forceplates were combined with high-speed cameras; however, the high-speed cameras have recently been replaced by infrared motion-capture cameras (Fig. 6.17). These laboratory essentials allow researchers to derive a wealth of information, including forces and moments about the various joints, the trajectories of joints, and the potential and kinetic energies of each of the limb segments.

During running and walking, forces are used to provide a calculated record of changes in the mechanical energy of the body's center of mass (Fig. 6.18). During walking, the changes in potential and kinetic energy are out of phase so that the amount of total energy changes very little over the course of the gait cycle (Gordon, Ferris, & Kuo, 2009; Kuo, 2007). During running, the changes in potential and kinetic energy are in phase leading to larger changes in total energy over the gait cycle (Segers, Aerts, Lenoir, & De Clerq, 2007). In walking, the mechanical energy of the body is somewhat conserved, while in running very little mechanical energy is conserved, although elastic energy

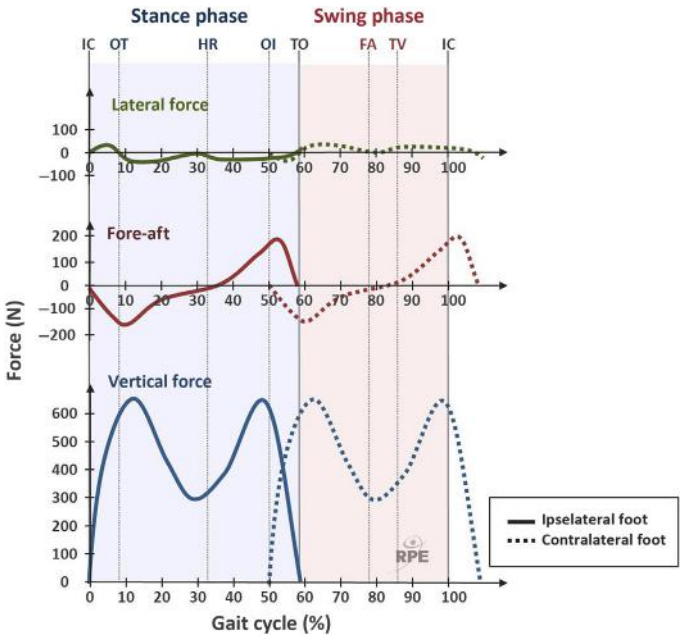

FIGURE 6.18

The force profiles generated while walking over a forceplate. Source: *https://commons.wikimedia.org/wiki/File:Bodenre.kr%C3%A4fte.jpg licensed under the Creative Commons Attribution-Share Alike 3.0 Unported license.*

provides most of the energy conservation during running (Gordon, Ferris, & Kuo, 2009).

6.9.2 Determinants of gait

Saunders, Inman, and Eberhart (1953) developed six determinants of normal gait that generally depend on one degree of freedom in the joints. These determinants were thought to reduce the vertical displacement of the body's center of mass. The six determinants were:

1. *Compass gait* is the movement of the pelvis through a series of arcs based upon the lengths of the legs.
2. *Pelvic rotation* allows for the rotation of the pelvis about the vertical axis.
3. *Pelvic tilt* is when the swing hip falls lower than the stance hip.
4. *Stance leg knee flexion* helps flatten out the arc of the pelvis.
5. *Plantar flexion of the stance ankle* is used to smooth the transition from double support to the swing phase.
6. *Lateral displacement of the pelvis* is the swaying back and forth as the hips alternate stance phase.

Using these six determinants, it is possible to minimize the vertical center of mass displacement. This would theoretically minimize the amount of energy needed for walking. Recent experiments have shown that some of the determinants, specifically, stance phase knee flexion (Gard & Childress, 1999), and pelvic rotation about the vertical (Kerrigan, Riley, Lelas, & Della Croce, 2001) and fore-aft axes (Gard & Childress, 1997) are not as effective in reducing the vertical center of mass displacement as previously thought. In fact, trying to minimize vertical displacement of the center of mass may increase metabolic energy expenditure (Ortega & Farley, 2005). Kuo (2007) recently calculated that maintaining a completely flat center of mass would more than double the metabolic cost of walking. Thus the six determinants theory may not be as useful in describing how humans minimize the metabolic cost of walking as previously thought.

6.9.3 Inverted pendulum walking

Another theory of walking is that the center of mass moves as if the stance leg represents an inverted pendulum (Cavagna, Saibene, & Margaria, 1963). This theory has been used to develop passive walkers that are able to maintain stability while walking down an incline. The cadence of these models is determined by the steepness of the slope, with steeper hills resulting in faster walking (McGeer, 1990). Simple models like these have been used to model surprisingly complex patterns entailed in human locomotion (Kurz, Judkins, Arellano, & Scott-Pandorf, 2008). This inverted pendulum of the stance leg

can be combined with the swing leg acting like a normal pendulum to describe the movement of both legs.

There is very little activity in the swing leg during walking at normal speed, with the only activation occurring at the beginning and end of the swing phase (Basmajian, 1976). The muscles activate during the double-support period, but for the swing phase, the muscles turn off and allow the leg to swing through like a jointed pendulum. This led to the ballistic model, as once the leg is in swing phase, only gravity acts upon it. The ballistic model has different vertical ground reaction forces and longer stride times than are seen during walking.

The inverted pendulum/ballistic model was then expanded to both walking and running for birds and quadrupedal animals (Cavagna, Heglund, & Taylor, 1977). Mochon and McMahon (1981) further expanded this model to include stance leg knee flexion, plantar flexion of the stance ankle, and pelvic tilt. Adding these gait determinants did little to change the variables of the ballistic model. With this model, a passive robot has been used to walk down gentle slopes using only gravity (McGeer, 1990). Buczek, Cooney, Walker, Concha, and Sanders (2006) challenged that the ballistic model does not use any joint power and is thus insufficient for the predictions of ground reaction forces and walking velocities. They found that the anterior ground reaction forces and velocities followed the ballistic model, but the vertical ground reaction forces did not until a telescoping action was applied using inverse dynamics. Thus the inverted pendulum may not provide a completely accurate model without including an elastic element to provide elastic energy storage.

6.9.4 Locomotion in reduced gravity

So how do these models work when gravity is reduced such as on the moon? Walking in reduced gravity results in a lower range of walking speeds than is typically found on Earth due to the changes in potential energy that are reduced along with gravity (McMahon, 1984). For the inverted pendulum model to work in a low-gravity environment, the swing phase time must increase substantially. When astronauts were on the moon, they took up a gait pattern that involved a series of small jumps. They could have jumped higher as the height of a maximal jump on the moon was calculated to be about 4 m (Margaria & Cavagna, 1972). The series of small jumps proved to be the most metabolically efficient in a reduced gravity environment.

By using body weight support, researchers can simulate reduced gravity locomotion. This method only works on the stance leg as the swing leg still experiences normal gravity (Sylos-Labini, Lacquaniti, & Ivanenko, 2014).

Research has shown that during running, using gaits that limited jumping height were energetically favorable (Polet, Schroeder, & Bertram, 2018). Additionally, the transition between walking and running happens more gradually in a reduced gravity environment (Ivanenko et al., 2011). The gait changes in a low-gravity environment are designed to reduce metabolic cost; however, this is accomplished with a much different gait pattern than is used in normal gravity environments.

6.9.5 Elastic storage of energy

In running, different energetics are in play, and conserving energy using the inverted pendulum is no longer important. Energy conservation during running comes from the elastic storage and release of energy. This is called the spring-mass model in which a massless spring is attached to a point mass (Blickhan, 1989). This model closely relates bouncing frequency and vertical displacement and requires only a few parameters to model the system. The landing velocity is important in being able to store elastic energy and influences contact time and hopping frequency.

The importance of the storage and release of elastic energy can be shown in kangaroos. Dawson and Taylor (1973) found that kangaroos were able to store energy through their tendons and return that energy at no cost to the point where an increase in hopping speed decreased metabolic cost. This is due in part to their large Achilles tendons. A dissected kangaroo had a tendon that was 1.5 cm in diameter and 35 cm in length (Dawson & Taylor, 1973). This is about three times longer than and twice as wide as the human Achilles tendon. More evidence showing the storage of elastic energy comes from a study where kangaroos hopped down a runway with a series of forceplates. It was found that two-thirds of the power required to lift and accelerate the center of mass during contact with the ground was provided through elastic energy (Cavagna et al., 1977). Muscles have shown spring-like recoil as they were stretched at different velocities of lengthening (Cavagna, Heglund, Harry, & Mantovani, 1994). Different titin isoforms in the muscles provide different stiffnesses, thus animals have different amounts of stiffness. In general, larger animals have more stiffness that smaller animals (Farley, Glasheen, & McMahon, 1993; Lindstedt, Reich, Keim, & LaStayo, 2002). This elastic storage of energy is most important during running as the mechanisms for the conservation of mechanical energy are minimal.

6.9.6 Cost of running

To compare the amount of energy needed to run in a variety of animals, a weight-dependent process is needed. This dimensionless analysis will be further presented in Section 6.10. The weight specific rate of oxygen

consumption is thought to be a linear function of speed for a multitude of animals (Taylor, Schmidt-Nielsen, & Raab, 1970). Taylor, Shkolnik, Dmi'el, Baharav, and Borut (1974) measured the rate of oxygen consumption of similar-sized cheetahs, gazelles, and goats running on a treadmill and found that the rate of oxygen consumption at a given speed was very similar for all the animals even though the distance from the center of mass to the pivot point was very different among the animals. Heglund and Taylor (1988) found that a variety of animals showed a similar ratio of maximum speeds compared to the minimum speed for a trot. Additionally, Heglund and Taylor found that the cost of locomotion is determined by the cost of activating muscles and the cost of generating a unit of force for a unit of time. Both of these factors increased with increasing stride frequency and stride length, meaning that with increasing stride frequency or length, there will be an increase in the cost of locomotion. Roberts et al. (1998) found that the metabolic cost of turkeys and dogs was also very similar even though turkeys used 2.5 times the muscle volume to generate a unit of force and took longer steps than dogs. In horses, adding a weight to the distal limb segments significantly increased metabolic cost and resulted in increased flexion of the hindlimb (Wickler, Hoyt, Clayton, Mullineaux, & Cogger, 2004). All these observations point to the idea that the cost of running is dependent on size, as similar-sized animals exhibit similar metabolic cost when they demonstrate completely different gait patterns.

6.9.7 Up- and downhills

Muscles both create and absorb energy. When a muscle absorbs mechanical energy, it produces negative work. The mechanical work done by the muscles in a step is estimated from the change in the average potential energy. This means that, when walking on level ground, the mechanical work done is approximately zero. When walking on a gradient, the sloped surface causes changes in the mechanical demands of locomotion as gravity either helps or hinders walking (Biewener & Daley, 2007). At large positive gradients, walking becomes like climbing a ladder, and the muscles are doing more work, since they need to increase the potential energy of the center of mass (Krause & Fischer, 2013; Roberts & Belliveau, 2005). When animals are walking or running up or down a steep enough hill, they are doing exclusively negative or positive work, respectively. On flat ground, the muscles of animals when walking or running are doing both positive and negative work in each step.

This contrasts when locomoting up or down a hill as the muscle do primarily positive or negative work, respectively. When animals walk up a hill, the velocity is decreased as a result of shorter steps and increased ground contact time (Birn-Jeffery & Higham, 2014). The shorter steps and increased ground

contact time have also been shown with humans on a treadmill (Leroux, Fung, & Barbeau, 2002). To facilitate these shorter steps, animals also adapt a more crouched posture when walking uphill (Foster & Higham, 2012). In contrast, when animals walk down a hill, forward velocity is also reduced, although this may be to increase stability (Birn-Jeffery & Higham, 2014). To prevent accelerating down the hill, animals use their legs as brakes resulting in an increase in ground reaction forces (Telhan et al., 2010). Additionally, muscle activity decreases when moving downhill (Crook, Wilson, & Hodson-Tole, 2010) as the decrease in potential energy accounts for some of the forward momentum. These studies showed that the body compensates for slopes by changing how the muscle activates.

6.9.8 Running with weights

When animals of various sizes underwent treadmill training while carrying various loads, it was found that the gait parameters were unaffected by the increase in load (Taylor, Heglund, McMahon, & Looney, 1980). This means that the force of the muscles involved must have increased an equivalent amount to the additional force carried. A similar relationship was observed with the oxygen consumption as the increase in load resulted in a similar increase in the rate of oxygen consumption. This means that the rate of oxygen consumption must be proportional to muscle tension, assuming all other things are equal. An increase in load is not equivalent to an increase in speed as when animals run faster changes in rates of muscle activations occur. Additionally, more muscle fibers and additional muscles are recruited at higher speeds, such as the iliocostalis lumborum, a muscle in the trunk of dogs, which is inactive for walking or trotting but activates for galloping (Taylor, 1978).

Similar results have been observed in humans. Increasing the weight carried increases the metabolic cost of walking, although the change in metabolic cost was not quite proportional to the amount of weight carried (Teunissen, Grabowski, & Kram, 2007). These studies have shown that body weight represents around 75% of the net cost of running (Teunissen et al., 2007). Additional research has shown running with increased load also increases leg stiffness (Silder, Besier, & Delp, 2015). This increased leg stiffness was accompanied by changes in kinematics including an increase in ground contact time and in hip and knee flexion. Increases in weight carried show increases in metabolic cost as well as leg stiffness to improve elastic energy return.

6.9.9 Summary

The mechanics of walking are typically measured in a laboratory setting using forceplates and motion-capture cameras. Through these methods, multiple

gait variables, such as joint angles and ground reaction forces, can be measured. The variables measured in the laboratory can then be used to create physical models of movement. For example, researchers have used the inverted pendulum as a model of walking and a spring mass as a model of running or hopping. During walking, the inverted pendulum model simulates the path of the center of mass over the course of a step. During running, the spring-mass model describes the storage and release of elastic energy. Similar to the Huxley (1973) model discussed in earlier sections, these models are also quite general, having been tested in various conditions, such as low gravity, on inclines, and with additional weight. Other generalities in locomotion are revealed by examining matters of scale.

6.10 Effects of scale

Animals of different sizes are capable of different things. Small animals' hearts beat faster, and they have a shorter lifespan. The effects of scale, therefore, have far-reaching consequences for the intrinsic activities of cells, as well as the performance of whole organisms. The key characteristic of locomotion is the conservation of energy, which is provided by potential energy during walking and elastic energy during running.

6.10.1 Dimensionless analysis

The study of scale is assisted by dimensionless analysis. This is because numbers without explicit scales can be used to compare two very different-sized variables. This results in fewer variables and the ability to directly compare variables across scales. Fundamental quantities are necessary to make variables dimensionless. These fundamental quantities are mass, length, and time. Using these quantities, dimensionless variables can be calculated. A specific biomechanical example is normalizing ground reaction forces by body weight (Mullineaux, Milner, Davis, & Hamill, 2006).

Another example of a dimensionless variable, the Reynolds number (Reynolds, 1883), is used to calculate air resistance and has been used to calculate the drag coefficient and other variables in a wind chamber. Pugh (1971) found that when subjects walk into the wind created by a wind tunnel fan, the rate of oxygen consumption increases directly with the square of the velocity. The same is true for the subject running, although the running lines bend over somewhat at the highest wind speeds, where the athlete changed his running style, leaning farther forward in order to keep from being blown backward. Heat and aridity also play a role in oxygen consumption during exercise (Nielsen, Strange, Christensen, Warberg, & Saltin, 1997). The role of heat and aridity can be shown in biking where higher body

temperatures, increased heat storage, and higher rating of perceived exertion were found during lower wind speeds (Saunders, Dugas, Tucker, Lambert, & Noakes, 2005). Saunders et al. also found that evaporation from the body increases with an increase in wind speed. In addition, heart rate is reduced, during biking, by around 7−11 beats/min for the first 15 minutes, when there is airflow present as opposed to when there is no airflow (Morrison, Cheung, & Cotter, 2014). These dimensionless parameters allow for direct comparisons between objects of different sizes.

Another such dimensionless number commonly found in the biomechanics literature is the Froude number (Alexander, 1991; Kramer & Sylvester, 2012; Steudel-Numbers & Weaver, 2006). Originally, the Froude number was used to determine the speed-to-length ratio of fluids and has been used in naval architecture to determine the resistance of objects moving through water. Alexander (1984) introduced the Froude number to characterize gait patterns by normalizing the velocity by gravity and leg length. This allowed for comparisons of gait regardless of the gravity or leg length (Vaughan & O'Malley, 2005). Alexander (1989) also found that the transition from walking to running occurs at a Froude value of around 0.5 and that animals with similar Froude numbers had similar gaits no matter the size of the animals.

6.10.2 Scaling by geometric similarity

Geometric similarity exists when two objects look exactly alike except for the fact that they are of different sizes. Hill (1950) discussed geometric similarity in animal performance. He observed that skeletal muscle strength is independent of body size as any muscle can develop the same amount of tension per cross section, whether it comes from a large or small animal. This means that the muscle shortening velocity is independent of body size, that maximum running speed is independent of body size, and that metabolic power for running at top speed is related to body weight. Heglund, Taylor, and McMahon (1974) investigated quadrupedal animals ranging from mice to horses running on a treadmill and measured kinematic parameters using photography. The stride frequency increased linearly with speed as the animals trotted, but when they changed to a gallop, the slope of the stride frequency and speed graph changed. Although each animal could double their speed when galloping, stride frequency changed by less than 10%. Pennycuick (1975) came to a similar result when studying animals ranging in size from a Thomson's gazelle to a giraffe (Fig. 6.19). These animals were observed from a stationary vehicle in the Serengeti National Park. They found that the stride frequencies chosen by the animals were confined to one relatively narrow range for walking and another narrow range for galloping. When the mean stride frequency for a gait was plotted against shoulder height, a power−law relationship emerged.

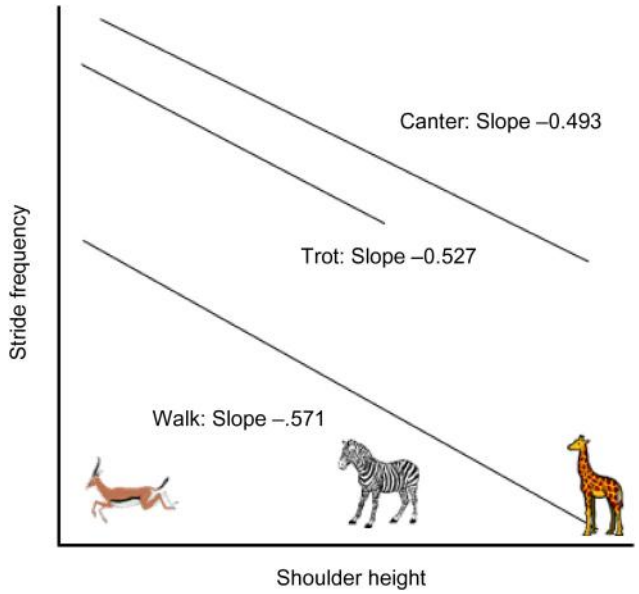

FIGURE 6.19

A log—log graph with stride frequency and shoulder height comparisons for different animals in Serengeti National Park. Source*: Recreated from Pennycuick, C. J. (1975). On the running of the gnu and other animals. The Journal of Experimental Biology, 63, 775—799.*

In terms of geometric similarity in humans, small deviations from isometry were found (Sylvester, Kramer, & Jungers, 2008). Alexander and Jayes claimed that animals also show similar deviations (Alexander & Jayes, 1983). They argued that since the animals were reasonably close to geometric similarity, in some of their dimensions, then geometric similarity could still be applied. However, in smaller populations, where only one species is analyzed, these small differences may become important (Kramer & Sylvester, 2009). This reasoning could describe differences seen in metabolic cost in humans that do not follow the Froude numbers (Kramer & Sylvester, 2012). In general, when studying large populations, the Froude number is still applicable, but the variability found in nature makes an exact relationship by geometric similarity across populations impossible.

6.10.3 The role of gravity and geometry

When gravity is considered into this scaling, it makes comparisons against different-sized animals difficult. This is due to the difficulties in keeping the models consistent when they contact the ground. If all the factors in muscles do not scale up in a linear fashion, then there would be a discrepancy as the

model is scaled up or down. To accomplish a scaled model, distortions need to occur in the geometry of the structure of the system so that the ratio of components stays the same (McMahon, 1984). This means that you need to change certain characteristics of the models so that the important variables remain the same. At times, the characteristic that needs to be distorted for the model to be accurate is the geometry. This is the case in animals, as many geometric distortions are needed to scale up or down complex biological systems.

To examine these characteristics in animals, experiments with reduced gravity were used. These experiments showed that even though animals had similar Froude numbers, the dynamic similarity, having all the characteristics of movement besides size equal, was not the same in reduced gravity (Bullimore & Donelan, 2008). Bullimore and Donelan showed that to exhibit dynamic similarity among species, four dimensionless parameters, not just the Froude number, must be equal. This same result has also been shown in humans as they do not exhibit dynamic similarity during running (Donelan & Kram, 2000). The Froude number provides a more accurate description during walking than running as elastic forces, which are not incorporated with the Froude number, play a major role during running.

6.10.4 Body proportions

One method of comparing different animals is by using body proportions such as height versus weight. This is referred to as allometry, which describes how animals change with size. These scaling relationships, when plotted on a log–log scale revealed linear trends (Gayon, 2000; Shingleton, 2010). For example, in primates, the log–log plot of chest circumference and body weight revealed a slope, or allometric exponent, of 0.37 (Stahl & Gummerson, 1967). Alexander (1977b) measured the lengths, diameters, and weights of the muscles, bones, and tendons in species of antelope ranging from 4.4 to 176 kg. He found that most of the bone lengths had allometric exponents near 0.25, many bone diameters had exponents near 0.37, and most muscles had cross-sectional areas whose allometric exponents were near 0.75. Later, Alexander, Jayes, Maloiy, and Wathuta (1979) measured the bones of 37 species representing a wide range of animals from shrews to elephants, and found that allometric exponents for limb bones were not well predicted by elastic similarity. In a comparison of mammals from mice to elephants, Prange, Anderson, and Rahn (1979) found in a multianimal study that skeletal mass is proportional to the 1.09 power of body mass. More recently there has been more discussion of the physiological and embryological mechanisms that act as proximate causes of allometry (Stern & Emlen, 1999). These studies demonstrated that the allometric exponent provided a

method to compare the scaling, or growth, of two different parts of an animal.

6.10.5 Metabolic power

It has long been known that oxygen requirements increase with increasing muscle force (Hartree & Hill, 1921). This can be applied to scaling as larger animals produce larger muscle forces and increased oxygen consumption. It was originally predicted that the allometry scaling between basal metabolic rate and mass would be two-thirds due to heat dissipation according to the surface to volume agreement (Ballesteros et al., 2018). However, results have shown that the scaling was closer to three-fourths (Bartels, 1982; Taylor et al., 1981). These results have been challenged because for masses less than 10 kg the expected exponent of two-thirds actually fits the data (Dodds, Rothman, & Weitz, 2001). Further challenges have been introduced when the basal metabolic rates exhibit curvature along the log–log scaling (Kolokotrones, Savage, Deeds, & Fontana, 2010). These studies raised questions into how predictive the metabolic rate is from allometric scaling.

6.10.6 Summary

The possible size range of animals makes comparison among different animal species difficult. For instance, it would be next to impossible to compare an elephant and a mouse without the use of scaling. Scaling is a process in which data are normalized to become unitless so that direct comparisons can be made. Specifically, scaling can be used to look at several features of gait discussed in Section 6.9 and provides a useful tool when multiple animal species are studied. Even in humans, scaling by weight or height is a method used to decrease subject-to-subject variability. This section specifically investigated scaling by geometric similarity and body proportions (for more detailed information on the role of size in biology see Bonner, 2006).

6.11 Conclusion

This chapter has provided a synopsis of one of the most fundamental works in the field of biomechanics, the classic textbook by McMahon titled *Muscles, Reflexes, and Locomotion*, which was originally published in 1984. Most of our current knowledge of muscles and reflexes comes from early work in the field of muscle physiology. With advances in technology, our knowledge has advanced as we have been able to build upon earlier research. This work, by Thomas McMahon, provided the basis for much of the work that the field of biomechanics has generated since it was last published. This text, in its scope and richness, will no doubt remain on the list of classic texts in

biomechanics for many years to come. We have only attempted here to revisit this old textbook and its richness by mentioning a few newer references and refocusing attention on some important issues for the newer generations of biomechanists and gait analysts. With respect to the old, comes progress to the new.

References

Abbott, B. C., & Ritchie, J. M. (1951). The onset of shortening in striated muscle. *Journal of Physiology, 113*, 336–345.

Alexander, R. M. (1977a). Terrestrial locomotion. In R. M. Alexander, & G. Goldspink (Eds.), *Mechanics and energetics of animal locomotion* (pp. 168–203). London: Chapman and Hall.

Alexander, R. M. (1977b). Allometry of the limbs of antelopes (Bovidae). *Journal of Zoology (London), 183*, 125–146.

Alexander, R. M. (1984). The gaits of bipedal and quadrupedal animals. *The International Journal of Robotics Research, 3*(2), 49–59.

Alexander, R. M. (1989). Optimization and gaits in the locomotion of vertebrates. *Physiological reviews, 69*(4), 1199–1227.

Alexander, R. M. (1991). Energy-saving mechanisms in walking and running. *The Journal of Experimental Biology, 160*, 55–69.

Alexander, R. M., & Jayes, A. S. (1983). A dynamic similarity hypothesis for the gaits of quadrupedal mammals. *Journal of Zoology, 201*, 135–152.

Alexander, R. M., Jayes, A. S., Maloiy, G. M. O., & Wathuta, E. M. (1979). Allometry of the limb bones of mammals from shrews (*Sorex*) to elephant (*Loxodonta*). *Journal of Zoology (Landon), 189*, 305–314.

Alvarez, F. J., & Fyffe, R. E. (2007). The continuing case for the Renshaw cell. *The Journal of Physiology, 584*(Pt 1), 31–45.

Amazeen, P. G. (2018). From physics to social interactions: Scientific unification via dynamics. *Cognitive Systems Research, 52*, 640–657.

Amazeen, P. G., Amazeen, E. L., & Beek, P. J. (2001). Coupling of breathing and movement during manual wheelchair propulsion. *Journal of Experimental Psychology: Human Perception and Performance, 27*(5), 1243.

Amazeen, P. G., Amazeen, E. L., & Turvey, M. T. (1998). Dynamics of human intersegmental coordination: Theory and research. In D. A. Rosenbaum, & C. E. Collyer (Eds.), *Timing of behavior: Neural, psychological, and computational perspectives* (pp. 237–259). Cambridge, MA: MIT Press.

Aoi, S., Manoonpong, P., Ambe, Y., Matsuno, F., & Worgotter, F. (2017). Adaptive control strategies for interlimb coordination in legged robots: A review. *Frontiers in Neurorobotics, 11*, 39.

Arnold, E. M., Ward, S. R., Lieber, R. L., & Delp, S. L. (2009). A model of the lower limb for analysis of human movement. *Annals of Biomedical Engineering, 38*(2), 269–279.

Aubert, X. (1956). *Le coup/age energetique de la contraction musculaire*. Brussels: Editions Arscia.

Aubert, X., Roquet, M. L., & Van der Elst, J. (1951). The tension-length diagram of the frog's sartorius muscle. *Archives Internationales de Physiologie, 59*, 239–241.

Bailey, K. (1948). Tropomyosin: A new asymmetric component of the muscle fibril. *The Biochemical Journal, 43*, 271–279.

Baker, J. S., McCormick, M. C., & Robergs, R. A. (2010). Interaction among skeletal muscle metabolic energy systems during intense exercise. *Journal of Nutrition and Metabolism*, *2010*, 905612.

Ballesteros, F. J., Martinez, V. J., Luque, B., Lacasa, L., Valor, E., & Moya, A. (2018). On the thermodynamic origin of metabolic scaling. *Scientific Reports*, *8*, 1448.

Bandschapp, O., Soule, C. L., & Iaizzo, P. A. (2012). Lactic acid restores skeletal muscle force in an in vitro fatigue model: Are voltage-gated chloride channels involved? *American Journal of Physiology Cell Physiology*, *302*(7), C1019–C1025.

Barclay, C. J. (1996). Mechanical efficiency and fatigue of fast and slow muscles of the mouse. *The Journal of Physiology*, *497*(3), 781–794.

Bard, P., Woolsey, C. N., Snider, R. S., Mountcastle, V. B., & Bromiley, R. B. (1947). Delineation of central nervous mechanisms involved in motion sickness. *Federation Proceedings*, *6*, 72.

Bartels, H. (1982). Metabolic rate of mammals equals the 0.75 power of their body weight. *Experimental Biology and Medicine*, *7*, 1.

Basmajian, J. V. (1976). The human bicycle. In P. V. Komi (Ed.), *Biomechanics* (Vol. 5-A). Baltimore, MD: University Park Press.

Batters, C., Veigel, C., Homsher, E., & Sellers, J. R. (2014). To understand muscle you must take it apart. *Frontiers in Physiology*, *5*, 90.

Baylor, S. M., Chandler, W. K., & Marshall, M. W. (1983). Sarcoplasmic reticulum calcium release in frog skeletal muscle fibres estimated from Arsenazo III calcium transients. *The Journal of Physiology*, *344*, 625–666.

Baylor, S. M., & Hollingworth, S. (2011). Calcium indicators and calcium signalling in skeletal muscle fibres during excitation–contraction coupling. *Progress in Biophysics and Molecular Biology*, *105*, 162–179.

Beltman, J. G. M., van der Vliet, M. R., Sargeant, A. J., & de Haan, A. (2004). Metabolic cost of lengthening, isometric and shortening contractions in maximally stimulated rat skeletal muscle. *Acta Physiologica Scandinavica*, *182*, 179–187.

Biewener, A. A., & Daley, M. A. (2007). Unsteady locomotion: Integrating muscle function with whole body dynamics and neuromuscular control. *The Journal of Experimental Biology*, *210*, 2949–2960.

Bigland-Ritchie, B., & Woods, J. J. (1976). Integrated electromyogram and oxygen uptake during positive and negative work. *The Journal of Physiology*, *260*, 267–277.

Birn-Jeffery, A. V., & Higham, T. E. (2014). The scaling of uphill and downhill locomotion in legged animals. *Integrative and Comparative Biology*, *54*(6), 1159–1172.

Blickhan, R. (1989). The spring-mass model for running and hopping. *Journal of Biomechanics*, *22*, 1217–1227.

Bobbert, M. (2001). Dependence of human squat jump performance on the series elastic compliance of the triceps surae: A simulation study. *Journal of Experimental Biology*, *204*, 533–542.

Bonner, J. T. (2006). *Why size matters: From bacteria to blue whales*. Princeton, NJ: Princeton University Press.

Buczek, F. L., Cooney, K. M., Walker, M. R., Concha, M. C., & Sanders, J. O. (2006). Performance of an inverted pendulum model directly applied to normal human gait. *Clinical Biomechanics*, *21*(3), 288–296.

Bullimore, S. R., & Donelan, J. M. (2008). Criteria for dynamic similarity in bouncing gaits. *Journal of Theoretical Biology*, *250*(2), 339–348.

Burne, J. A., Lippold, O. C., & Pryor, M. (1984). Proprioceptors and normal tremor. *The Journal of Physiology*, *348*, 559–572.

Butterfield, T. A. (2010). Eccentric exercise in vivo: Strain-induced muscle damage and adaptation in a stable system. *Exercise and Sport Sciences Reviews*, *38*, 51–60.

Buzsaki, G. (2006). *Rhythms of the Brain*. Oxford, UK: Oxford University Press.

Cady, E. B., Elshove, H., Jones, D. A., & Moll, A. (1989). The metabolic causes of slow relaxation in fatigued human skeletal muscle. *The Journal of Physiology*, *418*, 327–337.

Cao, Y., Suzuki, S., & Hoshino, Y. (2014). Uphill and level walking of a three-dimensional biped quasi-passive walking robot by torso control. *Robotica*, *34*(3), 483–496.

Carlson, F. D., & Siger, A. (1960). The mechano-chemistry of muscular contraction. I. The isometric twitch. *The Journal of General Physiology*, *44*, 33–60.

Carlson, F. D., & Wilkie, D. R. (1974). *Muscle Physiology*. Englewood Cliffs, NJ: Prentice-Hall.

Cavagna, G., Saibene, F., & Margaria, R. (1963). External work in walking. *Journal of Applied Physiology*, *18*, 1–9.

Cavagna, G. A., Heglund, N. C., Harry, J. D., & Mantovani, M. (1994). Storage and release of mechanical energy by contracting frog muscle fibres. *Journal of Physiology*, *481*(3), 689–708.

Cavagna, G. A., Heglund, N. C., & Taylor, C. R. (1977). Mechanical work in terrestrial locomotion: Two basic mechanisms for minimizing energy expenditure. *The American Journal of Physiology*, *233*(5), R243-R26 I.

Chaplain, R. A., & Frommelt, B. (1971). A mechanochemical model for muscle contraction. I. The rate of energy liberation at steady state velocities of shortening and lengthening. *Journal of Mechanochemistry and Cell Motility*, *1*, 41–56.

Choi, J. T., Vining, E. P., Reisman, D. S., & Bastian, A. J. (2009). Walking flexibility after hemispherectomy: Split-belt treadmill adaptation and feedback control. *Brain*, *132*, 722–733.

Clark, J. E., & Phillips, S. J. (1993). A longitudinal study of intralimb coordination in the first year of independent walking: A dynamical systems analysis. *Child Development*, *64*(4), 1143–1157.

Cohen, M. X. (2014). *Analyzing neural time series data: Theory and practice*. Cambridge, MA: MIT Press.

Cohen, M. X. (2016). Midfrontal theta tracks action monitoring over multiple interactive time scales. *NeuroImage*, *141*, 262–272.

Constable, J. K., Barclay, C. J., & Gibbs, C. L. (1997). Energetics of lengthening in mouse and toad skeletal muscles. *The Journal of Physiology*, *505*(1), 205–215.

Crone, C. (1993). Reciprocal inhibition in man. *Danish Medical Bulletin*, *40*(5), 571–581.

Crook, T. C., Wilson, A., & Hodson-Tole, E. (2010). The effect of treadmill speed and gradient on equine hind limb muscle activity. *Equine Veterinary Journal*, *42*, 412–416.

Curtin, N. A., & Woledge, R. C. (1974). Energetics of relaxation in frog muscle. *The Journal of Physiology*, *238*, 437–446.

Daffertshofer, A., Huys, R., & Beek, P. J. (2004). Dynamical coupling between locomotion and respiration. *Biological Cybernetics*, *90*(3), 157–164.

Dawson, T. J., & Taylor, C. R. (1973). Energetic cost of locomotion in kangaroos. *Nature*, *246*, 313–314.

De Serres, S. J., Yang, J. F., & Patrick, S. K. (1995). Mechanism for reflex reversal during walking in human tibialis anterior muscle revealed by single motor unit recording. *The Journal of Physiology*, *488*(1), 249–258.

Demer, L. L., & Yin, F. C. (1983). Passive biaxial mechanical properties of isolated canine myocardium. *The Journal of Physiology*, *339*, 615–630.

Dodds, P. S., Rothman, D. H., & Weitz, J. S. (2001). Re-examination of the 3/4 law of metabolism. *Journal of Theoretical Biology*, *209*, 9–27.

Donelan, J. M., & Kram, R. (2000). Exploring dynamic similarity in human running using simulated reduced gravity. *Journal of Experimental Biology*, *203*(16), 2405–2415.

Duke, T. A. J. (1999). Molecular model of muscle contraction. *Proceedings of the National Academy of Sciences of the United States of America*, *98*(6), 2770–2775.

Dutka, T. L., & Lamb, G. D. (2000). Effect of lactate on depolarization-induced Ca(2 +) release in mechanically skinned skeletal muscle fibers. *American Journal of Physiology Cell Physiology*, *278*(3), C517–C525.

Duysens, J., Trippel, M., Horstmann, G. A., & Dietz, V. (1990). Gating and reversal of reflexes in ankle muscles during human walking. *Experimental Brain Research*, *82*, 351–358.

Ebashi, S., Wakayabaya, T., & Ebashi, F. (1971). Troponin and its components. *Journal of Biochemistry*, *69*, 441–445.

Edman, K. A., & Flitney, F. W. (1982). Laser diffraction studies of sarcomere dynamics during 'isometric' relaxation in isolated muscle fibres of the frog. *The Journal of Physiology*, *329*, 1–20.

Edman, K. A., & Lou, F. (1990). Changes in force and stiffness induced by fatigue and intracellular acidification in frog muscle fibres. *The Journal of Physiology*, *424*, 133–149.

Edman, K. A., & Reggiani, C. (1984). Redistribution of sarcomere length during isometric contraction of frog muscle fibres and its relation to tension creep. *The Journal of Physiology*, *351*, 169–198.

Edman, K. A. P. (1970). The rising phase of the active state in single skeletal muscle fibres of the frog. *Acta Physiologica Scandinavica*, *79*, 167–173.

Edman, K. A. P. (1978). Maximum velocity of shortening in relation to sarcomere length and degree of activation of frog muscle fibers. *The Journal of Physiology*, *278*, 9P–10P.

Edman, K. A. P., Elzinga, G., & Noble, M. I. M. (1976). Force enhancement induced by stretch of contracting single isolated muscle fibers of the frog. *The Journal of Physiology*, *258*, 95P–96P.

Edman, K. A. P., & Josephson, R. K. (2007). Determinants of force rise time during isometric contraction of frog muscle fibres. *The Journal of Physiology*, *580*, 1007–1019.

Edwards, R. H., Hill, D. K., & Jones, D. A. (1975). Metabolic changes associated with the slowing of relaxation in fatigued mouse muscle. *The Journal of Physiology*, *251*, 287–301.

Eiswirth, M., & Ertl, G. (1988). Forced oscillations of a self-oscillating surface reaction. *Physical Review Letters*, *60*(15), 1526–1529.

Elliott, A., Offer, G., & Burridge, K. (1976). Electron microscopy of myosin molecules from muscle and non-muscle sources. *Proceedings of the Royal Society of London. Series B. Biological Sciences*, *193*(1110), 45–53.

Farley, C. T., Glasheen, J., & McMahon, T. A. (1993). *Running springs: Speed and animal size*, *Journal of Experimental Biology 185*, pp. 71–86.

Fawcett, D. W. (1968). The sporadic occurrence in cardiac muscle of anomalous Z bands exhibiting a periodic structure suggestive of tropomyosin. *The Journal of cell biology*, *36*(1), 266.

Fenn, W. O. (1924). The relation between the work performed and the energy liberated in muscular contraction. *The Journal of Physiology*, *58*, 373–395.

Ferretti, G., Moia, C., Thomet, J. M., & Kayser, B. (1997). The decrease of maximal oxygen consumption during hypoxia in man: A mirror image of the oxygen equilibrium curve. *The Journal of Physiology*, *498*(1), 231–237.

Ferris, D. P., Louie, M., & Farley, C. T. (1998). Running in the real world: Adjusting leg stiffness for different surfaces. *Proceedings of the Royal Society B: Biological Sciences*, *265*(1400), 989–994.

Fine, J. M., Gibbons, C. T., & Amazeen, E. L. (2013). Congruency effects in interpersonal coordination. *Journal of Experimental Psychology: Human Perception and Performance*, *39*(6), 1541–1556.

Fine, J. M., Likens, A. D., Amazeen, E. L., & Amazeen, P. G. (2015). Emergent complexity matching in interpersonal coordination: Local dynamics and global variability. *Journal of Experimental Psychology: Human Perception and Performance*, *41*(3), 723.

Fitts, R. H. (1994). Cellular mechanisms of muscle fatigue. *Physiological Reviews*, *74*(1), 49–94.

Fletcher, W. M., & Hopkins, F. G. (1907). Lactic acid in amphibian muscle. *The Journal of Physiology*, *35*(4), 247–309.

Fomovsky, G. M., & Holmes, J. W. (2010). Evolution of scar structure, mechanics, and ventricular function after myocardial infarction in the rat. *American Journal of Physiology-Heart and Circulatory Physiology.*, *298*, H221–H228.

Ford, L. E., Huxley, A. F., & Simmons, R. M. (1974). Mechanism of early tension recovery after a quick release in tetanized muscle fibres. *The Journal of Physiology*, *240*, 42P–43P.

Ford, L. E., Huxley, A. F., & Simmons, R. M. (1977). Tension responses to sudden length change in stimulated frog muscle fibers near slack length. *The Journal of Physiology*, *269*, 441–515.

Ford, L. E., Huxley, A. F., & Simmons, R. M. (1981). The relation between stiffness and filament overlap in stimulated frog muscle fibers. *The Journal of Physiology*, *311*, 219–249.

Forssberg, H., & Grillner, S. (1973). The locomotion of the acute spinal cat injected with clonidine i.v. *Brain Research*, *50*, 184–186.

Foster, K. L., & Higham, T. E. (2012). How forelimb and hind limb function changes with incline and perch diameter in the green anole, *Anolis carolinensis*. *The Journal of Experimental Biology*, *215*, 2288–2300.

Francis, J. T., & Song, W. (2011). Neuroplasticity of the sensorimotor cortex during learning. *Neural Plasticity*, *2011*, 310737.

Frigon, A., Johnson, M. D., & Heckman, C. J. (2012). Differential modulation of crossed and uncrossed reflex pathways by clonidine in adult cats following complete spinal cord injury. *The Journal of Physiology*, *590*(4), 973–989.

Fukuoka, Y., Habu, Y., & Fukui, T. (2015). A simple rule for quadrupedal gait generation determined by leg loading feedback: A modeling study. *Scientific Reports*, *5*, 8169.

Full, R. J., & Koditschek, D. E. (1999). Templates and anchors: Neuromechanical hypotheses of legged locomotion on land. *The Journal of Experimental Biology*, *202*(23), 3325–3332.

Fung, Y. C. B. (1967). Elasticity of soft tissues in simple elongation. *The American Journal of Physiology*, *213*, 1532–1544.

Furst, D. O., Osborn, M., Nave, R., & Weber, K. (1988). The organization of titin filaments in the half-sarcomere revealed by monoclonal antibodies in immunoelectron microscopy: A map of ten nonrepetitive epitopes starting at the Z line extends close to the M line. *The Journal of Cell Biology*, *106*, 1563–1572.

Galantis, A., & Woledge, R. C. (2003). The theoretical limits to the power output of a muscle–tendon complex with inertial and gravitational loads. *Proceedings of the Royal Society B: Biological Sciences*, *270*(1523), 1493–1498.

Gans, C., & Gaunt, A. S. (1991). Muscle architecture in relation to function. *Journal of Biochemistry*, *24*, 53–65.

Gard, S. A., & Childress, D. S. (1997). Effect of pelvic list on the vertical displacement of the trunk during normal walking. *Gait & Posture*, *5*, 233–238.

Gard, S. A., & Childress, D. S. (1999). The influence of stance phase knee flexion on the vertical displacement of the trunk during normal walking. *American Journal of Physical Medicine & Rehabilitation*, *80*, 26–32.

Gayon, J. (2000). History of the concept of allometry. *Integrative and Comparative Biology*, *40*(5), 748–758.

Ghez, C., & Fahn, S. (1985). The cerebellum. In E. R. Kandel, & J. H. Schwartz (Eds.), *Principles of Neural Science* (2nd ed., pp. 502–522). New York: Elsevier.

Gibbs, C. L., Loiselle, D. S., & Wendt, I. R. (1988). Activation heat in rabbit cardiac muscle. *The Journal of Physiology*, *395*, 115–130.

Gifford, J. R., et al. (2016). Symmorphosis and skeletal muscle $\dot{V}O_2$ max: In vivo and in vitro measures reveal differing constraints in the exercise-trained and untrained human. *The Journal of Physiology*, *594*(6), 1741–1751.

Gilbert, S. H., & Matsumoto, Y. (1976). A reexamination of the thermoelastic effect in active striated muscle. *The Journal of General Physiology*, *68*, 81–94.

Giuliani, C. A., & Smith, J. L. (1985). Development and characteristics of airstepping in chronic spinal cats. *The Journal of Neuroscience*, *5*(5), 1276–1282.

Goldman, Y. E., McCray, J. A., & Ranatunga, K. W. (1987). Transient tension changes initiated by laser temperature jumps in rabbit psoas muscle fibres. *The Journal of Physiology*, *392*(1), 71–95.

Gordon, A. M., Huxley, A. F., & Julian, F. J. (1966). The variation in isometric tension with sarcomere length in vertebrate muscle fibres. *Journal of Physiology*, *184*, 170–192.

Gordon, K. E., Ferris, D. P., & Kuo, A. D. (2009). Metabolic and mechanical energy costs of reducing vertical center of mass movement during gait. *Archives of physical medicine and rehabilitation*, *90*(1), 136–144.

Gorman, J. C., Amazeen, P. G., Crites, M. J., & Gipson, C. L. (2017). Deviations from mirroring in interpersonal multifrequency coordination when visual information is occluded. *Experimental Brain Research*, *235*(4), 1209–1221.

Grabowska, M., Godlewska, E., Schmidt, J., & Daun-Gruhn, S. (2012). Quadrupedal gaits in hexapod animals—inter-leg coordination in free-walking adult stick insects. *The Journal of Experimental Biology*, *215*(24), 4255–4266.

Granata, K. P., Rogers, E., & Moorhouse, K. (2005). Effects of static flexion–relaxation on paraspinal reflex behavior. *Clinical Biomechanics.*, *20*, 16–24.

Granzier, H. L., & Irving, T. C. (1995). Passive tension in cardiac-muscle-contribution of collagen, titin, microtubules, and intermediate filaments. *Biophysical Journal*, *68*, 1027–1044.

Granzier, H. L., & Pollack, G. H. (1990). The descending limb of the force–sarcomere length relation of the frog revisited. *Journal of Physiology, London*, *421*, 595–615.

Gray, J. (1968). *Animal locomotion*. London: Weidenfeld and Nicolson.

Greene, P. R., & McMahon, T. A. (1979). Reflex stiffness of man's antigravity muscles during kneebends while carrying extra weights. *Journal of Biomechanics*, *12*, 881–891.

Grillner, S. (1975). Locomotion in vertebrates: Central mechanisms and reflex interaction. *Physiological Reviews*, *55*, 247–304.

Haken, H., Kelso, J. A. S., & Bunz, H. (1985). A theoretical model of phase transitions in human hand movements. *Biological Cybernetics*, *51*(5), 347–356.

Hartree, W., & Hill, A. V. (1921). The regulation of the supply of energy in muscular contraction. *The Journal of Physiology*, *55*, 133–158.

Hartshorne, D. J., & Mueller, H. (1968). Fractionation of troponin into two distinct proteins. *Biochemical and Biophysical Research Communications*, *31*(1968), 647–653.

Hasselbach, W. (1953). Elektronenmikroskopische Untersuchungen an Muskelfibrillen bei totaler und partieller Extraktion des L-Myosins. *Zeitschrift für Naturforschung*, *8b*, 449–454.

Heglund, N. C., Taylor, C. R., & McMahon, T. A. (1974). Scaling stride frequency and gait to animal size: Mice to horses. *Science*, *186*, 1112–1113.

Heglund, N. C., & Taylor, C. R. (1988). Speed, stride frequency and energy cost per stride: how do they change with body size and gait? *Journal of Experimental Biology*, *138*(1), 301–318.

Helmholtz, H. (1847). *Ueber die Erhaltung der Kraft*. Berlin: Reimer.

Henneman, E., Somjen, G., & Carpenter, D. (1965). Excitability and inhibitability of motoneurons of different sizes. *Journal of Neurobiology*, *28*, 599–620.

Herbison, G. J., Jaweed, M. M., & Ditunno, J. F. (1982). Muscle fiber types. *Archives of Physical Medicine and Rehabilitation*, *63*(5), 227–230.

Herzog, W. (1985). Mechanisms of enhanced force production in lengthening (eccentric) muscle contractions. *Journal of Applied Physiology*, *116*(11), 1407–1417.

Herzog, W. (2017). Skeletal muscle mechanics: Questions, problems and possible solutions. *Journal of Neuroengineering and Rehabilitation*, *14*, 96.

Herzog, W., Powers, K., Johnston, K., & Duvall, M. (2015). A new paradigm for muscle contraction. *Frontiers in Physiology*, *6*, 174.

Hessel, A. L., Lindstedt, S. L., & Nishikawa, K. C. (2017). Physiological mechanisms of eccentric contraction and its applications: A role for the giant titin protein. *Frontiers in Physiology*, *8*, 70.

Hill, A. V. (1938). The heat of shortening and the dynamic constants of muscle. *Proceedings of. Royal Society B, London*, *126*, 136–195.

Hill, A. V. (1949). The onset of contraction. *Proceedings of Royal Society B, London*, *136*, 242–254.

Hill, A. V. (1950). The dimensions of animals and their muscular dynamics. *Science Progress*, *38*, 209–230.

Hill, A. V. (1953). Chemical change and mechanical response in stimulated muscle. *Proceedings of Royal Society B, London*, *141*, 314–320.

Hill, A. V. (1964). The effect of load on the heat of shortening of muscle. *Proceedings of Royal Society B, London.*, *159*, 297–318.

Hill, D. K. (1940). The anaerobic recovery heat production of frog's muscle at 0°C. *The Journal of Physiology*, *98*, 460–466.

Hoffer, J. A., & Andreassen, S. (1978). Factors affecting the gain of the stretch reflex and soleus muscle stiffness in premammillary cats. *Society for Neuroscience Abstracts*, *4*, 935.

Hoffer, J. A., & Andreassen, S. (1981). Regulation of soleus muscle stiffness in premammillary cats: Intrinsic and reflex components. *Journal of Neurophysiology*, *45*, 267–285.

Holt, N. C., Roberts, T. J., & Askew, G. N. (2014). The energetic benefits of tendon springs in running: Is the reduction of muscle work important? *Journal of Experimental Biology*, *217*(24), 4365–4371.

Hultborn, H. (2006). Spinal reflexes, mechanisms and concepts: From Eccles to Lundberg and beyond. *Progress in Neurobiology*, *78*, 215–232.

Houk, J. C., Singer, J. J., & Henneman, E. (1971). Adequate stimulus for tendon organs with observations on the mechanics of the ankle joint. *Journal of Neurophysiology*, *34*, 1051–1065.

Humphrey, J. D., & Yin, F. C. (1987). A new constitutive formulation for characterizing the mechanical behavior of soft tissues. *Biophysical Journal*, *54*, 563–570.

Huxley, A. F. (1957). Muscle structure and theories of contraction. *Progress in Biophysics and Biophysical Chemistry*, *7*, 255–318.

Huxley, A. F. (1973). A note suggesting that the cross-bridge attachment during muscle contraction may take place in two stages. *Proceedings of Royal Society B, London*, *183*, 83–86.

Huxley, A. F. (1979). *Reflections on muscle*. Liverpool: Liverpool University Press.

Huxley, A. F., & Niedergerke, R. (1954). Structural changes in muscle during contraction. Interference microscopy of living muscle fibres. *Nature*, *173*, 971–973.

Huxley, H. E. (1953). Electron microscope studies of the organization of the filaments in striated muscle. *Biochimica et Biophysica Acta*, *12*, 387–394.

Huxley, H. E. (1964). Structural arrangements and the contraction mechanism in striated muscle. *Proceedings of Royal Society B, London*, *160*, 442–448.

Huxley, H. E., & Brown, W. (1967). The low-angle X-ray diagram of vertebrate striated muscle and its 'behavior during contraction and rigor. *Journal of Molecular Biology*, *30*, 383–434.

Huxley, H. E., & Hanson, J. (1954). Changes in the cross-striations of muscle during contraction and stretch and their structural interpretation. *Nature*, *173*, 973–976.

Huxley, H. E., Stewart, A., Sosa, H., & Irving, T. (1994). X-ray diffraction measurements of the extensibility of actin and myosin filaments in contracting muscle. *Biophysical Journal*, *67*(6), 2411–2421.

Ivanenko, Y. P., Sylos-Labini, F., Cappellini, G., Macellari, V., McIntyre, J., & Lacquaniti, F. (2011). Gait transitions in simulated reduced gravity. *Journal of Applied Physiology*, *110*(3), 781–788.

Jayne, B. C., & Lauder, G. V. (1994). How swimming fish use slow and fast muscle fibers: Implications for models of vertebrate muscle recruitment. *Journal of Comparative Physiology A, Sensory, Neural, and Behavioral Physiology*, *175*, 123–131.

Jewell, B. R., & Wilkie, D. R. (1958). An analysis of the mechanical components in frog's striated muscle. *The Journal of Physiology*, *143*, 515–540.

Jewell, B. R., & Wilkie, D. R. (1960). The mechanical properties of relaxing muscle. *The Journal of Physiology*, *152*, 30–47.

Johnston, I. A., & Goldspink, G. (1973). A study of the swimming performance of the crucian carp *Carassius carassius* (L) in relation to the effects of exercise and recovery on biochemical changes in the myotomal muscles and liver. *Journal of Fish Biology*, *5*, 249–260.

Jones, D. A. (1973). Combined techniques for studying the physiology and biochemistry of fatigue in the isolated soleus of the mouse. *The Journal of Physiology*, *231*, 68P–69P.

Jones, D. A. (2010). Changes in the force–velocity relationship of fatigued muscle: Implications for power production and possible causes. *The Journal of Physiology*, *588*(16), 2977–2986.

Josephson, R. K., & Edman, K. A. P. (1998). Changes in the maximum speed of shortening of frog muscle fibres early in a tetanic contraction and during relaxation. *The Journal of Physiology*, *507*, 511–525.

Julian, F. J., & Morgan, D. L. (1979). Intersarcomere dynamics during fixed-end tetanic contractions of frog muscle fibres. *The Journal of Physiology*, *293*, 365–378.

Katz, B. (1939). The relation between force and speed in muscular contraction. *The Journal of Physiology*, *96*, 45–64.

Kelly, G., & Shanley, J. (2016). Rehabilitation of ataxic gait following cerebellar lesions: Applying theory to practice. *Physiotherapy theory and practice*, *32*(6), 430–437.

Kelso, J. A., & Jeka, J. J. (1992). Symmetry breaking dynamics of human multilimb coordination. *Journal of Experimental Psychology: Human Perception and Performance*, *18*(3), 645.

Kerrigan, D., Riley, P., Lelas, J., & Della Croce, U. (2001). Quantification of pelvic rotation as a determinant of gait. *Archives of Physical Medicine and Rehabilitation*, *82*, 217–222.

Kolokotrones, T., Savage, V., Deeds, E. J., & Fontana, W. (2010). Curvature in metabolic scaling. *Nature*, *464*, 753–756.

Konow, N., & Roberts, T. J. (2015). The series elastic shock absorber: Tendon elasticity modulates energy dissipation by muscle during burst deceleration. *Proceedings of the Royal Society B: Biological Sciences*, *282*(1804), 20142800.

Kram, R., & Dawson, T. J. (1998). Energetics and biomechanics of locomotion by red kangaroos (*Macropus rufus*). *Comparative Biochemistry and Physiology. Part B, Biochemistry and Molecular Biology*, *120*(1), 41–49.

Kramer, P. A., & Sylvester, A. D. (2009). Bipedal form and locomotor function: Understanding the effects of size and shape on velocity and energetics. *Paleoanthropology*, *2009*, 238–251.

Kramer, P. A., & Sylvester, A. D. (2012). Humans, geometric similarity and the Froude number: Is "reasonably close" really close enough? *Biology Open*, *2*(2), 111–120.

Krause, C., & Fischer, M. S. (2013). Biodynamics of climbing: Effects of substrate orientation on the locomotion of a highly arboreal lizard (*Chamaeleo calyptratus*). *The Journal of Experimental Biology*, *216*, 1448–1457.

Krustrup, P., Ferguson, R. A., Kjær, M., & Bangsbo, J. (2003). ATP and heat production in human skeletal muscle during dynamic exercise: Higher efficiency of anaerobic than aerobic ATP resynthesis. *The Journal of Physiology*, *549*(1), 255–269.

Kugler, P. N., & Turvey, M. T. (1987). *Information, natural law, and the self-assembly of rhythmic movement*. London: Routledge.

Kühne, W. (1864). *Untersuchungen über das Protoplasma und die Contractilität*. Leipzig: W. Engelmann.

Kuo, A. D. (2007). Choosing your steps carefully. *IEEE Robotics & Automation Magazine*, *14*(2), 18–29.

Kurz, M. J., Judkins, T. N., Arellano, C., & Scott-Pandorf, M. (2008). A passive dynamic walking robot that has a deterministic nonlinear gait. *Journal of Biomechanics*, *41*(6), 1310–1316.

Kurz, M. J., & Stergiou, N. (2002). Effect of normalization and phase angle calculations on continuous relative phase. *Journal of Biomechanics*, *35*(3), 369–374.

Kurz, M. J., & Stergiou, N. (2004). Applied dynamic systems theory for the analysis of movement. In N. Stergiou (Ed.), *Innovative analyses of human movement: Analytical tools for human movement research* (pp. 93–119). Champaign, IL: Human Kinetics.

Labeit, D., Watanabe, K., Witt, C., Fujita, H., Wu, Y., Lahmers, S., … Granzier, H. (2003). Calcium-dependent molecular spring elements in the giant protein titin. *Proceedings of National Academy of Sciences of the United States of America*, *100*(23), 13716–13721.

Lakie, M., Vernooij, C. A., Osborne, T. M., & Reynolds, R. F. (2012). The resonant component of human physiological hand tremor is altered by slow voluntary movements. *The Journal of Physiology*, *590*, 2471–2483.

Lanciego, J. L., Luquin, N., & Obeso, J. A. (2012). Functional neuroanatomy of the basal ganglia. *Cold Spring Harbor Perspectives in Medicine*, *2*(12), a009621.

Leroux, A., Fung, J., & Barbeau, H. (2002). Postural adaptation to walking on inclined surfaces: I. Normal strategies. *Gait & Posture*, *15*, 64–74.

Lieber, R. L., Roberts, T. J., Blemker, S. S., Lee, S., & Herzog, W. (2017). Skeletal muscle mechanics, energetics and plasticity. *Journal of Neuroengineering and Rehabilitation*, *14*, 108.

Likens, A. D., Amazeen, P. G., Stevens, R., Galloway, T., & Gorman, J. C. (2014). Neural signatures of team coordination are revealed by multifractal analysis. *Social Neuroscience*, *9*(3), 219–234.

Lin, D. H., & Yin, F. C. (1998). A multiaxial constitutive law for mammalian left ventricular myocardium in steady-state barium contracture or tetanus. *Journal of Biomechanical Engineering, 120*, 504–517.

Lindstedt, S. L., Reich, T. E., Keim, P., & LaStayo, P. C. (2002). Do muscles function as adaptable locomotor springs? *Journal of Experimental Biology, 205*, 2211–2216.

Lippold, C. J. (1970). Oscillation in the stretch reflex arc and the origin of the rhythmical, 8-12 c/s component of physiological tremor. *The Journal of Physiology, 206*, 359–382.

Louch, W. E., Sheehan, K. A., & Wolska, B. M. (2011). Methods in cardiomyocyte isolation, culture, and gene transfer. *Journal of Molecular and Cellular Cardiology, 51*, 288–298.

Lu, L., Oswald, S. J., Hgu, H., & Yin, F. C. (2008). Mechanical properties of actin stress fibers in living cells. *Biophysical Journal, 95*, 6060–6071.

MacIntosh, B., Gardiner, P., & McComas, A. (2006). *Skeletal muscle: Form and function* (2nd ed.). Champaign, IL: Human Kinetics.

Magill, R. A. (2011). *Motor learning and control: Concepts and applications*. New York: McGraw-Hill.

Marey, E. J. (1874). *Animal mechanism: A treatise on terrestrial and aerial locomotion*. New York: Appleton.

Margaria, R. (1976). *Biomechanics and energetics of muscular exercise*. Oxford: Clarendon Press.

Margaria, R., Camporesi, E., Aghemo, P., & Sassi, G. (1972). The effect of O_2 breathing on maximal aerobic power. *Pflügers Archiv für die gesamte Physiologie des Menschen und der Tiere, 336*, 225–235.

Margaria, R., & Cavagna, G. A. (1972). Biomechanics of exercise in reduced gravity. In *Proc. 4th "man in space" symposium*, Erevan, USSR.

Margaria, R., Cerretelli, P., di Prampero, P. E., Massari, C., & Torelli, G. (1963). Kinetics and mechanism of oxygen debt contraction in man. *Journal of Applied Physiology: Respiratory, Environmental and Exercise Physiology, 18*, 371–377.

Margaria, R., Oliva, R. D., di Prampero, P. E., & Cerretelli, P. (1969). Energy utilization in intermittent exercise of supramaximal intensity. *Journal of Applied Physiology: Respiratory, Environmental and Exercise Physiology, 26*, 752–756.

Marmelat, V., & Delignières, D. (2012). Strong anticipation: Complexity matching in interpersonal coordination. *Experimental Brain Research, 222*(1–2), 137–148.

Marsden, C. D. (1978). The mechanisms of physiological tremor and their significance for pathological tremors. Physiological tremor, pathological tremors and clonus. *Progress in Clinical Neurophysiology, 5*, 1–16.

Marsh, R. L., & John-Alder, H. B. (1994). Jumping performance of hylid frogs measured with high-speed cine film. *Journal of Experimental Biology, 188*, 131–141.

Marston, S. B., Rodger, C. D., & Tregear, R. T. (1976). Changes in muscle crossbridges when β, γ-imido-ATP binds to myosin. *Journal of Molecular Biology, 104*, 263–276.

Maruyama, K., Natori, R., & Nonomura, Y. (1976). New elastic protein from muscle. *Nature, 1976*(262), 58–59.

Matsubara, L., & Elliott, G. F. (1972). X-ray diffraction studies on skinned single fibers of frog skeletal muscle. *Journal of Molecular Biology, 72*, 657–669.

Maufroy, C., Kimura, H., & Takase, K. (2010). Integration of posture and rhythmic motion controls in quadrupedal dynamic walking using phase modulations based on leg loading/unloading. *Autonomous Robots, 28*, 331–353.

McAuley, J. H., & Marsden, C. D. (2000). Physiological and pathological tremors and rhythmic central motor control. *Brain, 123*(8), 1545–1567.

McGeer, T. (1990). Passive dynamic walking. *International Journal of Robotics Research, 9*, 62–82.

McGhee, R. B. (1966). Finite state control of quadruped locomotion. In *Proc. of second international symposium on external control of human extremities*, Dubrovnik, Yugoslavia.

McGhee, R. B. (1968). Some finite state aspects of legged locomotion. *Mathematical Biosciences*, *2*, 57–66.

McKee, C. T., Last, J. A., Russell, P., & Murphy, C. J. (2011). Indentation versus tensile measurements of Young's modulus for soft biological tissues. *Tissue Engineering. Part B, Reviews*, *17*, 155–164.

McMahon, T. (1984). *Muscles, reflexes, and locomotion (Princeton paperbacks)*. Princeton, NJ: Princeton University Press.

Meyerhof, O. (1920). Die Energieumwandlungen im Muskel. III. *Pflüger's Archiv für die gesamte Physiologie des Menschen und der Tiere*, *186*, 11.

Mochon, S., & McMahon, T. A. (1981). Ballistic walking: An improved model. *Mathematical Biosciences*, *52*, 241–260.

Morgan, D. L., Claflin, D. R., & Julian, F. J. (1991). Tension as a function of sarcomere length and velocity of shortening in single skeletal muscle fibres of the frog. *Journal of Physiology, London*, *441*, 719–732.

Morrison, S. A., Cheung, S., & Cotter, J. D. (2014). Importance of airflow for physiologic and ergogenic effects of precooling. *Journal of Athletic Training*, *49*, 632–639.

Mullineaux, D. R., Milner, C. E., Davis, I. S., & Hamill, J. (2006). Normalization of ground reaction forces. *Journal of Applied Biomechanics*, *22*(3), 230–233.

Nichols, T. R., & Houk, J. C. (1976). The improvement in linearity and the regulation of stiffness that results from actions of the stretch reflex. *Journal of Neurophysiology*, *39*, 119–142.

Nielsen, B., Strange, S., Christensen, N. J., Warberg, J., & Saltin, B. (1997). Acute and adaptive responses in humans to exercise in a warm, humid environment. *Pflugers Archiv*, *434*, 49–56.

Ortega, J. D., & Farley, C. T. (2005). Minimizing center of mass vertical movement increases metabolic cost in walking. *Journal of Applied Physiology*, *99*, 2099–2107.

Ortega, J. O., Lindstedt, S. L., Nelson, F. E., Jubrias, S. A., Kushmerick, M. J., & Conley, K. E. (2015). Muscle force, work and cost: A novel technique to revisit the Fenn effect. *The Journal of Experimental Biology*, *218*, 2075–2082.

Pennycuick, C. J. (1975). On the running of the gnu and other animals. *The Journal of Experimental Biology*, *63*, 775–799.

Perry, S. V. (2003). What is the role of tropomyosin in the regulation of muscle contraction? *Journal of Muscle Research and Cell Motility*, *24*, 593–596.

Perry, S. V., Cole, H. A., Head, J. F., & Wilson, F. J. (1972). *Localization and mode of action of the inhibitory component of the troponin complex*, *Cold Spring Harbor Symposia on Quantitative Biology 37*, pp. 251–262.

Piazzesi, G., Lucii, L., & Lombardi, V. (2002). The size and the speed of the working stroke of muscle myosin and its dependence on the force. *The Journal of physiology*, *545*(1), 145–151.

Pinto, J. G., & Fung, Y. C. (1973). Mechanical properties of the heart muscle in the passive state. *Journal of Biomechanics*, *6*, 597–616.

Podolsky, R. J. (1959). The chemical thermodynamics and molecular mechanism of muscular contraction. *Annals of the New York Academy of Sciences*, *72*, 522–537.

Podolsky, R. J. (1960). Kinetics of muscular contraction: The approach to steady state. *Nature*, *188*, 666–668.

Polet, D. T., Schroeder, R. T., & Bertram, J. E. A. (2018). Reduced gravity takes the bounce out of running. *Journal of Experimental Biology*, *13*, 221.

Prange, H. D., Anderson, J. F., & Rahn, H. (1979). Scaling of skeletal mass to body mass in birds and mammals. *The American Naturalist, 113*, 103–122.

Prochazka, A., Gillard, D., & Bennett, D. J. (1997). Positive force feedback control of muscles. *Journal of Neurophysiology, 77*(6), 3226–3236.

Pugh, L. G. C. E. (1971). The influence of wind resistance in running and walking and the mechanical efficiency of work against horizontal or vertical forces. *The Journal of Physiology, 213*, 255–276.

Raethjen, J., Lemke, M., Lindemann, M., Wenzelburger, R., Krack, P., & Deuschl, G. (2001). Amitriptyline enhances the central component of physiological tremor. *Journal of Neurology, Neurosurgery, and Psychiatry, 70*(1), 78–82.

Rall, J. A. (1982). Sense and nonsense about the Fenn effect. *The American Journal of Physiology, 242*, H1–H6.

Rassier, D. E., Herzog, W., & Pollack, G. H. (2003). Dynamics of individual sarcomeres during and after stretch in activated single myofibrils. *Proceedings of the Royal Society: Biological Sciences, 270*(1525), 1735–1740.

Reedy, M. C., Reedy, M. K., & Goody, R. S. (1987). The structure of insect flight muscle in the presence of AMPPNP. *Journal of Muscle Research and Cell Motility, 8*(6), 473–503.

Reedy, M. K., Holmes, K. C., & Tregear, R. T. (1965). Induced changes in orientation of the cross bridges of glycerinated insect flight muscle. *Nature, 207*, 1276–1280.

Reisman, D. S., Wityk, R., Silver, K., & Bastian, A. J. (2007). Locomotor adaptation on a split-belt treadmill can improve walking symmetry post-stroke. *Brain, 130*, 1861–1872.

Renshaw, B. (1941). Influence of discharge of motoneurones upon excitation of neighboring motoneurones. *Journal of Neurophysiology, 4*, 167–183.

Reynolds, O. (1883). An experimental investigation of the circumstances which determine whether the motion of water shall be direct or sinuous, and of the law of resistance in parallel channels. *Philosophical Transactions of the Royal Society, 174*, 935–982.

Richardson, M. J., Marsh, K. L., Isenhower, R. W., Goodman, J. R., & Schmidt, R. C. (2007). Rocking together: Dynamics of intentional and unintentional interpersonal coordination. *Human Movement Science, 26*(6), 867–891.

Ridgway, E. B., & Gordon, A. M. (1975). Muscle activation: Effects of small length changes on calcium release in single fibers. *Science, 189*, 881–884.

Ritzmann, R. E., & Buschges, A. (2007). Adaptive motor behavior in insects. *Current Opinion in Neurobiology, 17*(6), 629–636.

Roberts, T. D. M. (1978). *Neurophysiology of postural mechanisms*. London: Butterworths.

Roberts, T. J., & Belliveau, R. A. (2005). Sources of mechanical power for uphill running in humans. *Journal of Experimental Biology, 208*, 1963–1970.

Roberts, T. J., Chen, M. S., & Taylor, C. R. (1998). Energetic of bipedal running. II. Limb design and running mechanics. *Journal of Experimental Biology, 201*, 2753–2762.

Rome, L. C., et al. (1999). Trading force for speed: Why superfast crossbridge kinetics leads to superlow forces. *Proceedings of the National Academy of Sciences of the United States of America, 96*(10), 5826–5831.

Rudel, R., & Taylor, S. R. (1973). Aequorin luminescence during contraction of amphibian skeletal muscle. *The Journal of Physiology, 233*, 5P–6P.

Rybak, I. A., Shevtsova, N. A., Lafreniere-Roula, M., & McCrea, D. A. (2006). Modelling spinal circuitry involved in locomotor pattern generation: Insights from deletions during fictive locomotion. *The Journal of Physiology, 577*(Pt 2), 617–639.

Saiki, H., Margaria, R., & Cuttica, F. (1967). Lactic acid production in submaximal exercise. In R. Margaria (Ed.), *Exercise at altitude*. Amsterdam: Excerpta Medica.

Saladin, K. S. (2007). *Anatomy & physiology the unity of form and function*. Dubuque, IA: McGraw-Hill.

Saraf, H., Ramesh, K. T., Lennon, A. M., Merkle, A. C., & Roberts, J. C. (2007). Mechanical properties of soft human tissues under dynamic loading. *Journal of Biomechanics*, *40*(9), 1960–1967.

Saunders, A. G., Dugas, J. P., Tucker, R., Lambert, M. I., & Noakes, T. D. (2005). The effects of different air velocities on heat storage and body temperature in humans cycling in a hot, humid environment. *Acta Physiologica Scandinavica*, *183*, 241–255.

Saunders, J. B., Inman, V. T., & Eberhart, H. D. (1953). The major determinants in normal and pathological gait. *Journal of Bone and Joint Surgery*, *35A*, 543–558.

Scafetta, N., Marchi, D., & West, B. J. (2009). Understanding the complexity of human gait dynamics. *Chaos: An Interdisciplinary Journal of Nonlinear Science*, *19*(2), 026108.

Schappacher-Tilp, G., Leonard, T., Desch, G., & Herzog, W. (2015). A novel three-filament model of force generation in eccentric contraction of skeletal muscles. *PLoS One*, *10*(3), e0117634.

Schmidt, R. A., & Lee, T. D. (2011). *Motor control and learning: A behavioral emphasis* (5th ed.). Champaign, IL: Human Kinetics.

Schmidt, R. C., Carello, C., & Turvey, M. T. (1990). Phase transitions and critical fluctuations in the visual coordination of rhythmic movements between people. *Journal of Experimental Psychology: Human Perception and Performance*, *16*(2), 227–247.

Schmitz, H., Reedy, M. C., Reedy, M. K., Tregear, R. T., & Taylor, K. A. (1997). Tomographic three-dimensional reconstruction of insect flight muscle partially relaxed by AMPPNP and ethylene glycol. *The Journal of Cell Biology*, *139*(3), 695–707.

Scott, W., Stevens, J., & Binder-Macleod, S. A. (2001). Human skeletal muscle fiber type classifications. *Physical Therapy*, *81*(11), 1810–1816.

Segers, V., Aerts, P., Lenoir, M., & De Clerq, D. (2007). Dynamics of the body centre of mass during actual acceleration across transition speed. *Journal of Experimental Biology*, *210*, 578–585.

Shingleton, A. (2010). Allometry: The study of biological scaling. *Nature Education Knowledge*, *3*(10), 2.

Silder, A., Besier, T., & Delp, S. L. (2015). Running with a load increases leg stiffness. *Journal of Biomechanics*, *48*(6), 1003–1008.

Sparks, D. L. (2002). The brainstem control of saccadic eye movements. *Nature Reviews Neuroscience*, *3*, 952–964.

Squire, J. M. (2016). Muscle contraction: Sliding filament history, sarcomere dynamics and the two Huxleys. *Global Cardiology Science & Practice*, *2016*(2), e201611.

Stahl, W. R., & Gummerson, J. Y. (1967). Systematic allometry in five species of adult primates. *Growth*, *31*, 21–34.

Stern, D. L., & Emlen, D. J. (1999). The developmental basis for allometry in insects. *Development*, *126*(6), 1091–1101.

Steudel-Numbers, K., & Weaver, T. D. (2006). Froude number corrections in anthropological studies. *American Journal of Physical Anthropology*, *131*(1), 27–32.

Stevens, R., Gorman, J. C., Amazeen, P., Likens, A., & Galloway, T. (2013). The organizational neurodynamics of teams. *Nonlinear Dynamics, Psychology, and Life Sciences*, *17*(1), 67–86.

Straub, F.B. (1942). Actin. Studies of the Institute of Medical Chemistry University of Szeged 2, 3–15.

Suslak, T. J., & Jarman, A. P. (2015). Stretching the imagination beyond muscle spindles—stretch-sensitive mechanisms in arthropods. *Journal of Anatomy*, *227*(2), 237–242.

Suzuki, S., & Hachiya, M. (2008). Experimental study on stabilization of a three-dimensional biped passive walking robot. *Journal of the Society of Biomechanisms*, *32*(4), 239–246.

Sylos-Labini, F., Lacquaniti, F., & Ivanenko, Y. P. (2014). Human locomotion under reduced gravity conditions: Biomechanical and neurophysiological considerations. *BioMed Research International*, *2014*, 547242.

Sylvester, A. D., Kramer, P. A., & Jungers, W. L. (2008). Modern humans are not (quite) isometric. *American Journal of Physical Anthropology*, *137*, 371–383.

Taga, G., Yamaguchi, Y., & Shimizu, H. (1991). Self-organized control of bipedal locomotion by neural oscillators. *Biological Cybernetics*, *65*, 147–159.

Taylor, C. R. (1978). Why change gaits? Recruitment of muscles and muscle fibers as a function of speed and gait. *American Zoologist*, *18*, 153–161.

Taylor, C. R., Heglund, N. C., McMahon, T. A., & Looney, T. R. (1980). Energetic cost of generating muscular force during running: A comparison of large and small animals. *The Journal of Experimental Biology*, *86*, 9–18.

Taylor, C. R., Maloiy, G. M., Weibel, E. R., Langman, V. A., Kamau, J. M. Z., Seeherman, H. J., & Heglund, N. C. (1981). Design of the mammalian respiratory system. III. Scaling maximum aerobic capacity to body mass: Wild and domestic mammals. *Respiration Physiology*, *44*, 25–37.

Taylor, C. R., Schmidt-Nielsen, K., & Raab, J. L. (1970). Scaling of energetic cost of running to body size in mammals. *The American Journal of Physiology*, *219*, 1104–1107.

Taylor, C. R., Shkolnik, A., Dmi'el, R., Baharav, D., & Borut, A. (1974). Running in cheetahs, gazelles, and goats: Energy cost and limb configuration. *The American Journal of Physiology*, *227*, 848–850.

Telhan, G., Franz, J. R., Dicharry, J., Wilder, R. P., Riley, P. O., & Kerrigan, D. C. (2010). Lower limb joint kinetics during moderately sloped running. *Journal of Athletic Training*, *45*, 16–21.

Teunissen, L. P., Grabowski, A., & Kram, R. (2007). Effects of independently altering body weight and body mass on the metabolic cost of running. *Journal of Experimental Biology*, *210*, 4418–4427.

Thames, M. D., Teichholz, L. E., & Podolsky, R. J. (1974). Ionic strength and the contraction kinetics of skinned muscle fibers. *The Journal of General Physiology*, *63*, 509–530.

Thelen, E., Ulrich, B. D., & Wolff, P. H. (1991). Hidden skills: A dynamic systems analysis of treadmill stepping during the first year. *Monographs of the Society for Research in Child Development*, *56*(1), 1–98.

Tognoli, E., & Kelso, J. S. (2009). Brain coordination dynamics: True and false faces of phase synchrony and metastability. *Progress in Neurobiology*, *87*(1), 31–40.

Tregear, R. T., Wakabayashi, K., Tanaka, H., Iwamoto, H., Reedy, M. C., Reedy, M. K., … Amemiya, Y. (1990). X-ray diffraction and electron microscopy from Lethocerus flight muscle partially relaxed by adenylylimidodiphosphate and ethylene glycol. *Journal of Molecular Biology*, *214*(1), 129–141.

Tuthill, J. C., & Azim, E. (2018). Proprioception. *Current Biology*, *28*(5), R194–R203.

Usherwood, J. R. (2016). The muscle-mechanical compromise framework: Implications for the scaling of gait and posture. *Journal of Human Kinetics*, *52*, 107–114.

Vaughan, C. L., & O'Malley, M. J. (2005). Froude and the contribution of naval architecture to our understanding of bipedal locomotion. *Gait & Posture*, *21*(3), 350–362.

Wakabayashi, K., Sugimoto, Y., Tanaka, H., Ueno, Y., Takezawa, Y., & Amemiya, Y. (1994). X-ray diffraction evidence for the extensibility of actin and myosin filaments during muscle contraction. *Biophysical Journal*, *67*(6), 2422–2435.

Wakabayashi, T., Huxley, H. E., Amos, L. A., & Klug, A. (1975). Three-dimensional image reconstruction of actin-tropomyosin complex and actin tropomyosin-troponin 1-troponin T complex. *Journal of Molecular Biology*, *93*, 477–497.

Walcott, S., & Herzog, W. (2008). Modeling residual force enhancement with generic cross-bridge models. *Mathematical Biosciences*, *216*(2), 172–186.

West, B. J., & Scafetta, N. (2003). Nonlinear dynamical model of human gait. *Physical review E*, *67*(5), 051917.

Westerblad, H., Bruton, J. D., & Lännergren, J. (1997). The effect of intracellular pH on contractile function of intact, single fibres of mouse muscle declines with increasing temperature. *The Journal of Physiology*, *500*(1), 193–204.

Whiting, A., Wardale, J., & Trinick, J. (1989). Does titin regulate the length of muscle thick filaments? *Journal of Molecular Biology*, *205*, 263–268.

Wickler, S. J., Hoyt, D. F., Clayton, H. M., Mullineaux, D. R., Cogger, E. A., et al. (2004). Energetic and kinematic consequences of weighting the distal limb. *Equine Veterinary Journal*, *36*, 772–777.

Wilkie, D. R. (1954). Facts and theories about muscle. *Progress in Biophysics*, *4*, 288–324.

Wilkie, D. R. (1968). Heat, work, and phosphorylcreatine breakdown in muscle. *The Journal of Physiology*, *195*(1), 57–183.

Willms, A. R., Kitanov, P. M., & Langford, W. F. (2017). Huygens' clock revisited. *Royal Society Open Science*, *4*, 170777.

Woledge, R. C. (1963). Heat production and energy liberation in the early part of a muscular contraction. *The Journal of Physiology*, *166*, 211–224.

Woledge, R. C. (1968). The energetics of tortoise muscle. *The Journal of Physiology*, *197*, 685–707.

Yanagihara, D., & Udo, M. (1994). Climbing fiber responses in cerebellar vermal Purkinje cells during perturbed locomotion in decerebrate cats. *Neuroscience Research*, *19*, 245–248.

Yanagihara, D., Udo, M., Kondo, I., & Yoshida, T. (1993). A new learning paradigm: Adaptive changes in interlimb coordination during perturbed locomotion in decerebrate cats. *Neuroscience Research*, *18*, 241–244.

Yu, L. C., Dowben, R. M., & Kornacker, K. (1970). The molecular mechanism of force generation in striated muscle. *Proceedings of National Academy of Sciences of the United States of America*, *66*, 1199–1205.

Zalalutdinov, M., et al. (2003). Frequency entrainment for micromechanical oscillator. *Applied Physics Letters*, *83*, 3281.

Further reading

Elliott, G. F., Rome, E. M., & Spencer, M. (1970). A type of contraction hypothesis applicable to all muscles. *Nature*, *226*, 417–420.

Johnson, C., & Hull, M. L. (1988). Parameter identification of the human lower limb under dynamic, transient torsional loading. *Journal of Biomechanics*, *21*, 401–415.

Kelso, J. A., Holt, K. G., Rubin, P., & Kugler, P. N. (1981). Patterns of human interlimb coordination emerge from the properties of non-linear, limit cycle oscillatory processes: Theory and data. *Journal of Motor Behavior*, *13*(4), 226–261.

Martin, R. R., & Haines, H. (1970). Application of Laplace's law to mammalian hearts. *Comparative Biochemistry and Physiology*, *34*, 959–962.

Mogan, R., Fischer, R., & Bulbuliab, J. A. (2017). To be in synchrony or not? A meta-analysis of synchrony's effects on behavior, perception, cognition and affect. *Journal of Experimental Social Psychology*, *72*, 13–20.

Zivotofsky, A. Z., & Hausdorff, J. M. (2007). The sensory feedback mechanisms enabling couples to walk synchronously: An initial investigation. *Journal of Neuroengineering and Rehabilitation*, *4*, 28.

CHAPTER 7

The basics of gait analysis

Luis M. Silva and Nick Stergiou
University of Nebraska at Omaha, Omaha, NE, United States

> For man bends his legs convexly, a bird has his bent concavely; again, man bends his arms and legs in opposite directions, for he has his arms bent convexly, but his legs concavely. And a viviparous quadruped bends his limbs in opposite directions to a man's, and in opposite directions to one another; for he has his forelegs bent convexly, his hind legs concavely. Again, quadrupeds which are not viviparous but oviparous have a peculiar curvature of the limbs laterally away from the body. Again, why do quadrupeds move their legs criss-cross? We have to examine the reasons for all these facts, and others cognate to them; that the facts are such is clear from our Natural History, we have now to ask reasons for the facts. At the beginning of the inquiry we must postulate the principles we are accustomed constantly to use for our scientific investigation of nature, that is we must take for granted principles of this universal character which appear in all Nature's work. Of these one is that Nature creates nothing without a purpose, but always the best possible in each kind of living creature by reference to its essential constitution.
>
> **From the book on the Gait of Animals by Aristotle (384–322 BCE)**

CONTENTS

7.1 Introduction

This chapter covers basic principles of gait analysis. We discuss these principles in order to provide the basis for understanding and analyzing the fundamental skill of gait. Our goal is not to replace, with a single chapter, the significant number of gait analysis textbooks that have been published already, but to introduce the reader to a fundamental understanding on how to analyze gait from a biomechanical perspective. However, before we venture any further, we feel it is important to briefly discuss first the concept of skill. This is because gait, a manner of walking or moving on

Biomechanics and Gait Analysis. DOI: https://doi.org/10.1016/B978-0-12-813372-9.00007-5

foot according to the Merriam-Webster's Collegiate Dictionary (2003), is considered a skill that we master early in our lives and we use daily. What, though, is a skill?

7.2 The concept of skill

Merriam-Webster's Collegiate Dictionary (2003) includes three definitions for the word skill: (1) the ability to use one's knowledge effectively and readily in execution or performance, (2) dexterity or coordination, especially in the execution of learned physical tasks, and (3) a learned power of doing something competently: a developed aptitude or ability (i.e., language). Furthermore, Adams (1987), after reviewing the available literature, proposed that skill is: (1) a wide behavioral domain, (2) learned, and (3) a goal attainment that is dependent on motor behavior. Higgins (1977) proposed that skill is a movement that allows the organism to respond or act effectively within the environment and to integrate past and present information in order to appropriately move to achieve a particular goal. Furthermore, that author claimed that skill is usually the end product of practice and learning, it is goal directed, and the level of skill is determined by the degree of success in achieving a goal. From all the above definitions, we can see that it is critical to consider skill as both the consistency of outcome and performance. Higgins (1977) further emphasizes that skills are performed within different types of environments. Performing the same task in different spatially and temporally ordered environments will produce different movement outcomes. From the learning perspective, all the above definitions agree that the production of skill follows the order: movement, coordinated movement, skill. It is crucial, then, to consider the notion of coordinated movement.

Coordination has been defined by Berstein (1967) as the mastery of redundant degrees of freedom. Additionally, Bernstein suggested that a coordinated movement will exhibit homogeneity, integration, and structural unity. Homogeneity means that the movement components have little variation over trials. Integration means that movement is the combination of the neurophysiological system with the morphology and the environment. Finally, structural unity is the interrelation of different units within the nervous system. Bernstein's ideas led scientific research toward the importance of variability, which had been vastly ignored up to that point. However, variability is the essence of the notion of skill (Harrison & Stergiou, 2015; see also Chapter 8: Gait variability: a theoretical framework for gait analysis and biomechanics). Variability is introduced into the system from the constraints that dictate the system's behavior. The constraints are morphological, biomechanical, environmental, and task specific (Higgins, 1985). The morphological and biomechanical constraints define subsystems; integration

(as defined by Bernstein above) with the environmental and task specific constraints leads to a movement pattern. The idea of degrees of freedom is closely linked with the constraints. As morphological constraints, we define the anatomical, neurological, and structural characteristics of the system. All these characteristics introduce a tremendous number of degrees of freedom into the system. For example, walking involves the synchronized action of over 50 muscles, containing thousands of motor units and many other components. Each one of these structural components is a different degree of freedom that the system has to take into account in order to execute the specific movement. The biomechanical constraints introduce even more degrees of freedom because the system must function under the effects of gravity, friction, Newton's laws, etc.

Furthermore, environmental constraints are related to the spatial and temporal configuration of events in the world external to the system. Every environment is associated with a degree of predictability. Environments with a high degree of predictability are spatially and temporally certain (stable), while spatial and temporal uncertainty (unstable) characterizes an environment with a low degree of predictability. Gentile, Higgins, Miller, and Rosen (1975), based on environmental stability, classified skills as closed or open. As an example, in golf, the ball is always at the same spot, and you can easily predict that the ball will not change position prior to club contact. Thus, hitting a golf ball is a closed skill. On the other hand, in baseball batting, you don't have any idea where the ball is going to come. However, both closed and open skills can be further divided due to intertrial variability because we need to account for skills where a stable environment changes over time. As an example consider hitting a golf ball from a stationary tee, but in the next trial the height of the tee has been changed. Environmental constraints are closely linked to Bernstein's homogeneity notion of intertrial variability. Therefore environmental constraints introduce even more variability into the system, which must also account for the task-specific constraints. If we would like to scale variability in order of constraints, we start from biomechanical constraints which are the more predictable, to continue with those that are morphological, and then environmental. To summarize up to this point, in order to perform a movement, we have to account for all the above constraints that introduce variability (in terms of degrees of freedom) into the movement system. Mastery of this tremendous amount of degrees of freedom leads to coordinated movement.

A wonderful illustration of the degrees of freedom idea comes from the experiments of Arutyunyan, Gurfinkel, and Mirskii (1968, 1969) where they examined the coordination of movement in novice and expert pistol shooters. They found that novice shooters rigidly fixed their joints while shooting,

while experts braced the pistol by unlinking the arm joints and using muscle synergies. They concluded that the novice shooters decreased degrees of freedom in order to decrease variability and perform the task. However, as the individuals began to improve, the fixed degrees of freedom released to enable the system to perform a more coordinated movement, since now the system can master an even greater number of degrees of freedom. Similar results were found by Newell and his associates (McDonald, van Emmerik, & Newell, 1989; Newell & van Emmerik, 1989) when they evaluated movement coordination in handwriting and dart-throwing tasks. Therefore it seems obvious from the results of the above studies and the general findings from the motor learning literature, that practice produces coordinated movement and eventually a skill. With practice, variability decreases and eventually a skill evolves, which is the result of mastering the tremendous amount of degrees of freedom that are imposed by the constraints. The proper integration of all the subsystems leads to the appropriate movement pattern.

In motor learning, practice scheduling has received great attention. Theories have been developed like the closed-loop theory and the schema theory that are still a matter of debate (Adams, 1987). However, no one argues that specificity is one of the most important factors of practice. Specificity of practice means that what you practice is what you improve; however, the literature also supports transfer of specific practice because many motor skills share common components. That said, there are conflicting results regarding a highly skilled individual performing successfully in a wider range of motor tasks. Individual differences have been presented by Marteniuk (1974) as a logical explanation to these conflicting results. He stated that no method predicts how an individual will perform. This might by the reason that schema theory cannot be supported when tested with adult subjects (Van Rossum, 1990). It seems then that skill likely entails individual differences, which result from (1) genetics (structure), (2) developmental history, and (3) previous experiences. These individual differences coupled with the degrees of freedom that are imposed by the constraints are the reasons why a motor system can generate an apparently infinite number of trajectories that can be recognized as the same skill. Furthermore, this approach to skill explains the notion of talent and why some people can perform better than others, for example, Michael Jordan or Babe Ruth.

The environmental components as described above are critical during practice. When the task is open and presents intratrial variability (e.g., tennis), predicting the environment requires the development of a large variety of movements. A large repertoire allows you to choose among those that best suited for the current environment. However, based on the mathematical theory of chaos there are no closed tasks (Kurz, Stergiou, Heidel, & Terry Foster, 2005). This is demonstrated by the "butterfly effect" (Gleick, 1987), which is

the metaphorical example of the details of a tornado (how will be formed and where) being affected by minor perturbations such as the flapping of the wings of a distant butterfly a few weeks earlier. This was discovered by observations of continuous runs of a weather model with initial condition data that were rounded in a seemingly inconsequential manner. The model was failing to reproduce the results of runs with the unrounded initial condition data. Thus, a very small change in initial conditions had created a significantly different outcome (Gleick, 1987). Then, it can be hypothesized that experience, practice (and the resultant increase in releasing of degrees of freedom), and nonlinearity of life eventually lead to a greater degree of predictability, eliminating the possibility of having closed tasks (Cavanaugh, Kelty-Stephen, & Stergiou, 2017). There is practically a large number of available responses with enormous intrinsic flexibility. Additionally, we should not forget that the task will dictate these responses. The integration of all the subcomponents is influenced by the task. Thus, skill is the result of improved predictability of constraints along with the ability to integrate that information into the movement process (Harrison & Stergiou, 2015).

Finally, another view to skill and coordinated movement can be obtained from a dynamical systems perspective (see also Chapter 9: Coordination and control: a dynamical systems approach to the analysis of human gait), a theory that recognizes the importance of constraints. These constraints govern the organization of every movement. Under them, synergies are formed by the system, to produce autonomous control structures that are responsible for the execution of movement. These functional subsystems are called coordinative or dynamical control structures. Their production or self-organization is basically a road to equilibrium, stability, or steady states. From a learning perspective, it is necessary to know the laws that regulate a dynamical control structure or the conditions that produce a steady state. Bernstein, as we have already discussed, suggested the optimal management of degrees of freedom. Furthermore, it has been suggested that the acquisition of a new movement pattern by a system is a perceptual exploration of the dynamical work space of the control structure (see also Chapter 9: Coordination and control: a dynamical systems approach to the analysis of human gait). Physical examples like the pendulum can be used to model this notion. When an external force is applied on the pendulum, it will oscillate, before coming back to rest at its original equilibrium position. The time required to return to equilibrium can be viewed as the time to learn a specific skill. Every time that the pendulum swings, it loses some of its original energy (initial conditions).

Similarly, every time that we practice a task, we learn a little bit more, until we reach a plateau, a steady state, that is, the coordinated movement. The initial conditions are updated with every swing of the pendulum or every

time that we practice. However, changes in initial conditions can also result in bifurcations or discontinuities. A large enough external force can swing the pendulum in a highly variable way. Similarly, discontinuities have been witnessed on the learning process (Schmidt, Treffner, Shaw, & Turvey, 1992). These discontinuities will result in a transition to a new steady state, attractor, or behavior well. Eventually, the system will find its equilibrium by the self-organizing process described above. Variability can then be viewed as energy fluctuations that can push the system to a new threshold when they approach a critical threshold. Thus, learning of a new skill might be approached gradually or with bifurcations in the behavior. From the dynamical systems perspective variability is not an error but an essential part of the behavior (Stergiou & Decker, 2011; Stergiou, Harbourne, & Cavanaugh, 2006). Kelso and Ding (1993) questioned whether creativity is possible in the absence of variability.

In sum, dynamical systems theory provides an excellent explanation of the phenomena in terms of physical systems and attractor dynamics. Skill is viewed as an attractor and variability as energy fluctuations. Dynamical systems theory can also explain the infinite number of responses embedded in a skill in terms of the nonlinear behavior of the system (see also Chapter 9: Coordination and control: a dynamical systems approach to the analysis of human gait).

7.3 The skill of gait

Gait is a skill, defined here as the cyclic motion of lower and upper limbs that aims to move the body forward. A set of coordinated movements are used to locomote with the goal of moving from one point to another while supporting and transferring the weight of the body. As the body moves forward, one limb provides support while the other advances further to the next support position, and then the limbs alternate their roles as many times as intended. This sequence of movements results in a series of motion patterns performed by the joints forming a complex kinematic chain. For the joints to move, the muscles produce forces to pull the bones. This occurs under instructions from the nervous system which integrates multisensory information such as somatosensory (proprioceptive), visual, and vestibular sensations allowing constant adaptability (Nakazawa, Obata, & Sasagawa, 2012; Sugi, Kawana, & Nakamura, 2009; Takakusaki, 2017). If the analysis of these activities is based on a cause-and-effect approach, starting with the command from the brain to the forces derived from the contact of the foot with the ground, then it is called a *top-down* approach (Vaughan, Davis, & O'Connor, 1999). Based on such an approach, the control of gait is described as follows: (1) command initiation in the central nervous system; (2) diffusion of the

derived signal to the peripheral nervous system; (3) contraction of the muscles to generate forces; (4) application of the forces on the bones and generation of moments across joints; (5) regulation of forces and moments according to skeletal segments' anthropometry; (6) movement of the segments; and (7) generation of ground reaction forces. In this way, commands for gait are organized in the higher centers (cortex and basal ganglia) with assistance of the brain stem before being transmitted to the spinal cord. Contributions from the spinal cord also occur (Harkema, Dobkin, & Edgerton, 2000; Nakazawa et al., 2012). Gait is a multifaceted endeavor involving interaction of the positioning of bones, joint range of motion, neuromuscular activity, and mechanics (i.e., gravity and friction) that provide general rules for motion (Chambers & Sutherland, 2002).

Another approach to examine the control of gait is referred to as the inverse dynamics, where we start with the forces causing the movement and their immediate consequences in terms of movement (Vaughan et al., 1999). The inverse dynamics is a *bottom-top* approach. Control of gait is examined using dynamic equilibrium equations or equations of motion, based on multibody dynamic formulations, to determine reaction forces transmitted between segments and the net moments-of-force resulting from muscle activity (Silva & Ambrósio, 2002). To achieve these results, data are collected from different methodological setups such as image processing, floor sensors, and sensors placed on the body (Muro-de-la-Herran, García-Zapirain, & Méndez-Zorrilla, 2014).

7.3.1 Definition of gait analysis

Gait analysis can be defined as the set of procedures to observe, record, analyze, and interpret movement patterns performed as part of the skill of gait. The aims of gait analysis have been traditionally to gather information in order to understand control, improve performance, diagnose movement disorders, and evaluate treatment and rehabilitation programs. Clinical gait analysis can then be further defined as the process of recording and interpreting biomechanical measurements of gait to understand the effects of disease and dysfunction (Baker, Esquenazi, Benedetti, & Desloovere, 2016). Clinical gait analysis provides the methodology to identify impairments and functional limitations that contribute to disability during locomotion (Pirker & Katzenschlager, 2017). Perturbations in one of the systems that control gait, for example, neural, may be partially compensated by other structures and alter function leading to new adaptations and changes that are evaluated through clinical gait analysis (Jeng, Sandroff, & Motl, 2018; Sebastião, Bollaert, Hubbard, & Motl, 2018). Baker (2006) mentioned that the reasons for performing clinical gait analysis are (1) to diagnose the specific

disease/injury, (2) to assess the severity of a disease/injury, (3) to monitor the progress of an intervention, and (4) to predict the outcome of an intervention. Gait analysis could provide this kind of information acknowledging an effective rehabilitation management plan. To better perform gait analysis, the terminology used should be clear and consistent. To facilitate that goal, we start with the definition and description of the gait cycle (GC) and its phases.

7.4 Periods and phases of gait

A GC starts when one foot makes contact with the ground and ends when that same foot contacts the ground again. The GC can be broken down into periods and phases to determine normal and abnormal gait (Chambers & Sutherland, 2002; Levine, Richards, & Whittle, 2012). The reader is reminded that in Chapter 2, Basic biomechanics, we did something similar to anatomically examine the push-up (Chapter 2: Basic biomechanics; Fig. 2.3).

Most frequently, the GC is divided into two periods, stance and swing. The stance period is the time during which the foot is in contact with the ground. The swing period follows the stance period and is the time during which the same foot is in the air. The separation of the two periods is discerned by the toe-off. If one considers the location of the opposite or contralateral foot, then the stance period can be further divided into three subperiods. The initial double-leg support is the subperiod during which both feet are in contact with the ground. The single-leg support is the subperiod during which the opposite or contralateral foot is in the air. The terminal double-leg support is the subperiod during which both feet are again in contact with the ground (Perry & Burnfield, 2010). Normally, the stance period represents the first 60% of the GC and the swing the latter 40% (Blanc, Balmer, Landis, & Vingerhoets, 1999; Murray, Drought, & Kory, 1964). The initial double-leg support represents the initial 10% of the GC, the single-leg support is the next 40%, and the terminal double-leg support concludes the stance period with another 10% of the GC. Murray et al. (1964) found that the duration of successive periods of stance, swing, and double support are similar during the same walking trial and during repeated trials of the same subject. However, speed can affect these percentages with respect to the subperiods of stance, where increases in speed will decrease the double-leg support subperiods and increase single-leg support (Murray, Mollinger, Gardner, & Sepic, 1984). Eventually, if we keep moving faster and start running, the double-leg support subperiods will disappear. On the other hand, decreases in walking speed will have the exact opposite effect.

The GC can also be divided according to functional phases (Inman, Ralston, & Todd, 1981; Levine et al., 2012; Perry & Burnfield, 2010; Rose & Gamble, 2005). From this approach, we have the following phases:

1. Initial contact (0%–2% of the GC). Initial contact is the start of the loading response or of the weight acceptance. It is also the beginning of the stance period and the first part of the initial double-leg support period. During this phase we will also have the presence of any impact phenomena (Fig. 7.1) presented very early in the ground reaction forces.
2. Loading response (2%–12% of the GC). Loading response is the rest of the initial double-leg support period. During this phase, we continue and complete the task of weight acceptance. In terms of the anterior–posterior force, we have the minimum (or maximum) braking peak (Fig. 7.1). In terms of the anterior-posterior force, we have the presence of the minimum (or maximum) braking peak (Fig. 7.1).
3. Midstance (12%–31% of the GC). This is the first part of the single-leg support period. Stability is a major concern as the base of support will decrease significantly and the center of gravity will move to its highest point through leg extension. Kinetic energy transfers to potential energy. The end of this phase is distinguished by the occurrence of the "valley" or the local minimum of the vertical ground reaction force (Fig. 7.1).

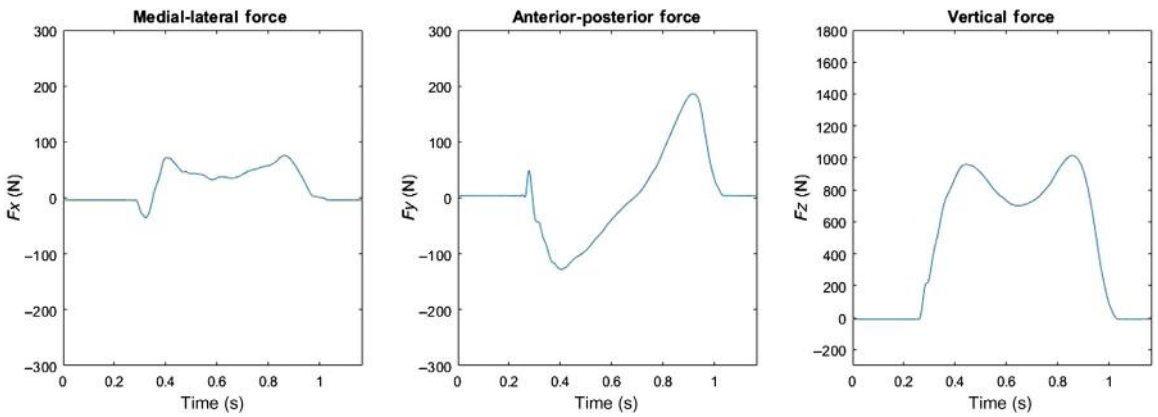

FIGURE 7.1

The three separate components of the resultant ground reaction force vector during the gait cycle; medial–lateral, anterior–posterior, and vertical (in Newtons).

4. Terminal stance (31%–50% of the GC). This is the second part of the single-leg support period. Stability is still a concern as well as the heel strike of the opposite foot. The center of gravity "falls" from its highest point and potential energy transfers to kinetic energy.
5. Preswing (50%–60% of the GC). This is the terminal double-leg support period and it is our second loading period. In terms of the vertical ground reaction force, we have the occurrence of the second loading peak or the second local maximum or the second "hump." During this phase, we also have our maximum propulsion peak in terms of the anterior–posterior force as we prepare to propel our foot off the ground (Fig. 7.1).
6. Initial swing (60%–73% of the GC). This is the first part of the swing period and our major concerns are to clear the floor by flexing the entire leg. This overall flexion decreases the leg's moment of inertia and increases the angular velocity of the swinging leg.
7. Midswing (74%–87% of the GC). This is the second part of the swing period and our major concern is that our opposite/contralateral leg is in single support with a small base of support and thus stability is a concern. We are also getting ready for the upcoming foot contact at the end of our swing.
8. Terminal swing (85%–100% of the GC). This is the third and last part of the swing period and our major concern is our upcoming foot contact.

A most recent approach to divide the CG in phases is based on mechanical power produced (Zelik, Takahashi, & Sawicki, 2015). From this approach, we have the following phases:

1. Collision (0%–15% of the GC). This phase starts with the initial foot contact and is described by a negative individual leg center of mass (COM) power. However, it also includes a positive power transient right after heel strike.
2. Rebound (15%–30% of the GC). This phase is described by a positive individual leg COM power.
3. Preload (30%–45% of the GC). This phase is described by a negative individual leg center of mass power.
4. Push off (45%–65% of the GC). This phase is described by a positive individual leg COM power.
5. Swing (65%–100% of the GC). This phase is described by zero individual leg COM power as the ipsilateral leg is not in contact with the ground. Thus, stance is the phase of gait when the ipsilateral foot is on the ground and consists of the collision, rebound, preload, and push-off phases of gait.

7.5 Spatiotemporal parameters of gait

The above periods and phases of the GC are evaluated with the use of a variety of different measures. The most commonly used such measures are several elementary spatiotemporal parameters that are fairly straightforward and easy to acquire in the laboratory and the hospital. These parameters are listed below.

Step length. This is defined as the distance between the point of initial contact of the ipsilateral foot and the point of initial contact of the contralateral foot. Here is an example of using step length in gait analysis research. Recently, Lim, Lin, and Pandy (2017) used gait data in conjunction with musculoskeletal modeling techniques to evaluate muscle function over a range of walking speeds using prescribed combinations of step length and step frequency. They found that changes in step length had a greater influence on lower-limb joint motion, net joint moments, and muscle function than step frequency. These authors also identified that peak forces developed by the hip and knee extensors correlated more closely with changes in step length than step frequency. Specifically, increases in step length resulted in larger contributions from the hip and knee extensors. The authors suggested that this may be why older people with weak hip and knee extensors walk more slowly by reducing step length rather than step frequency.

Stride length. This is defined as the distance between successive ground contacts of the same foot. Here is an example of using stride length in gait analysis research. In a recent study, Hak, Houdijk, Beek, and Van Dieën (2013) reported that backward margins of stability became larger as stride length decreased. Informationally, it has been suggested that the concept of margin of stability can provide a better understanding of mechanical stability during gait (Hof, Gazendam, & Sinke, 2005). Margin of stability is defined as the distance between the base of support and the extrapolated COM, with the extrapolated COM accounting for both COM position and velocity. The margin of stability can be calculated in both the medial–lateral and backward directions. Changes in the medial–lateral margin of stability are related to deviations from the straight walking trajectory, while changes in the backward margin of stability are related to interruptions of the forward progression.

Stride time (i.e., GC duration). This is defined as the time elapsed between foot contact of a leg to the following foot contact of the same leg. The stride time is a very popular measure in gait analysis research and especially with respect to gait variability; the variability that exists between consecutive strides (Goldberger et al., 2003; Hausdorff et al., 1997; Hausdorff, Cudkowicz, Firtion, Wei, & Goldberger, 1998;

Hausdorff, Rios, & Edelberg, 2001). In gait rehabilitation, research has been performed on continuous stride times to investigate the efficiency of different external cueing methods (Hunt, McGrath, & Stergiou, 2014; Kaipust, McGrath, Mukherjee, & Stergiou, 2013).

Cadence. This is defined as the rate at which an individual walks. It is expressed in steps per minute. In terms of gait analysis research, cadence provides information about the gait rhythm (Hollman, McDade, & Peterson, 2011; Oh-Park, Holtzer, Xue, & Verghese, 2010; Verghese, Wang, Lipton, Holtzer, & Xue, 2007) and can influence the magnitude of ground reaction forces (Castro et al., 2015).

Gait speed. This is defined as the rate of change in distance with respect to time (speed = distance/time). It is a scalar quantity and informs us only about how fast we move (see also Chapter 2: Basic biomechanics). In gait analysis research, gait speed is used extensively and most recently has been associated with mortality in older adults (Studenski, Perera, & Patel, 2011). This is why gait speed has been recommended as a simple and accessible indicator of the health of the older person (Studenski et al, 2011).

Foot progression angle. This is defined as the angle between the line from the calcaneus to the second metatarsal and the line of progression averaged from heel strike to toe off during the stance phase of walking for each step (toe-in angle is positive and toe-out angle is negative). In gait analysis, research shows that toeing-in increases lateral loading in the midfoot and forefoot approximately 61% and 49%, respectively, whereas toeing-out increases medial loading 72% and 52%, respectively (Rosenbaum, 2013).

Step width. This is defined as the distance between the centers of the feet during double-leg support when both feet are in contact with the ground. In gait analysis research, Yentes, Rennard, Schmid, Blanke, and Stergiou (2017) have shown that patients with chronic obstructive pulmonary disease (COPD) walk with a narrower step width in which the variability of the step widths from step to step is decreased. The authors suggested that this result may explain the increased prevalence of falls in patients with COPD. This is because step width has been associated with lateral stability (Bauby & Kuo, 2000). Maintaining lateral stability during walking is a challenge to the motor control system (Kuo & Donelan, 2010). It has been suggested that step width variability reflects the amount of active control that is required for lateral stabilization (Bauby & Kuo, 2000). Based on this theoretical framework, when lateral foot placement becomes more stable the required amount of active control decreases, resulting in a consonant decrease in step width variability (Bauby & Kuo, 2000; Donelan, Shipman, Kram, & Kuo, 2004). Accordingly, it appears that the age-related decreased capabilities in active

control result in higher step width variability (Kuo & Donelan, 2010). Furthermore, evidence has surfaced to support the link between increased step width variability and risk of falling in older adults (Maki, 1997). Step width variability was able to predict falls (Brach, Berlin, Van Swearingen, Newman, & Studenski, 2005; Brach, Studenski, Perera, Van Swearingen, & Newman, 2007; Hausdorff et al., 2001; Maki, 1997), and to differentiate older adults who fell from those who did not fall after a slip (Yang & Pai, 2014).

7.5.1 Step width and lateral stepping gait: a special case

A passive walker is a bipedal walking model that can successfully emulate human gait with only input from the passive mechanics of motion (Kuo, 1999). When extended into three-dimensions, the model becomes passively stable only in the anterior–posterior direction and requires an artificial neural network to retain stability in the medial–lateral direction. By comparing step length and step width variability of the passive walker in three dimensions, Bauby and Kuo (2000) concluded that the greater step width variability compared to step length variability meant that the medial–lateral direction requires active control from the central nervous system, whereas the anterior–posterior direction is passively stabilized from the dynamics of motion (Fig. 7.2A). Findings of greater medial–lateral variability during walking have led to the belief that the different control mechanisms for medial–lateral and anterior–posterior foot placement are "hard-wired." It has been suggested that the Bauby and Kuo (2000) approach to medial–lateral control strategy has potential rehabilitation aids (Kuo & Donelan, 2010). These aids could take the form of external stabilization mechanisms during

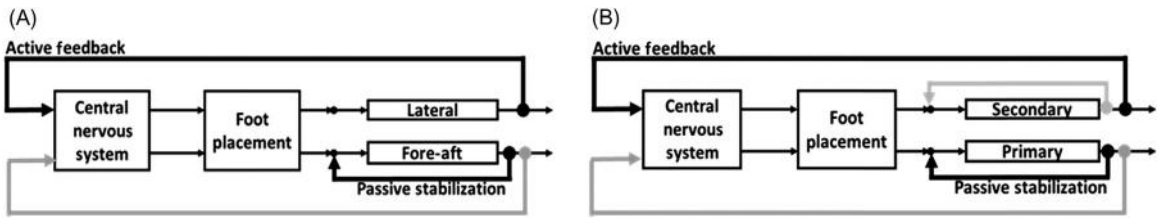

FIGURE 7.2

(A) Bauby and Kuo's theoretical perspective for motor control of gait. Note that the Bauby and Kuo (2000) model shows a distinct division between the anatomical planes with no potential for passive stabilization in the lateral direction. (B) Proposed modifications of Bauby and Kuo's theoretical perspective for motor control of gait. In the proposed modified model the anatomical planes are no longer divided, rather planes are organized according to the direction of progression resulting in primary and secondary planes (Wurdeman & Stergiou, 2013; Wurdeman et al., 2012). There is also now potential for both directions to benefit from both active and passive stabilization. The primary plane of progression will benefit most from the mechanics of motion and thus have greater passive control. The secondary plane has less (although not absent) influence from passive stabilization, thus requiring increased active control.

treadmill walking to reduce step width and step width variability. Therefore simple spring or more sophisticated mechanisms of external lateral stabilization have been constructed for balance rehabilitation interventions in different clinical and subclinical populations (Chang & Ulrich, 2008).

The Bauby and Kuo (2000) approach has been put into question through a series of studies from Wurdeman and colleagues investigating a lateral stepping gait (Wurdeman, Huben, & Stergiou, 2012; Wurdeman & Stergiou, 2013). In a lateral stepping gait (Fig. 7.3), the direction of progression is aligned with the medial–lateral direction. By aligning the direction of progression with the medial–lateral direction, the anterior–posterior direction no longer benefits from the mechanics of motion to provide passive stabilization. Lateral stepping gait permitted Wurdeman et al. to directly test the control model proposed by Bauby and Kuo. Wurdeman et al. found greater anterior–posterior variability and less medial–lateral variability in the lateral stepping gait, which is the exact opposite of what is found in typical walking. These findings have led Wurdeman et al. to propose a modification to Bauby and Kuo's theoretical perspective (Fig. 7.2B) (Wurdeman & Stergiou, 2013). They proposed that motor control in gait is not divided by anatomical planes but rather influenced by the direction of progression (i.e., no longer "lateral" and "fore–aft" divisions, but rather "primary" and "secondary" planes). They also proposed that all planes can benefit from both active and passive control properties. The amount of active control depends on the task. Moreover, the amount of passive control can reduce the need for active control. Their refinement may seem minor at first glance. However, their modifications to Bauby and Kuo's model could allow for improved walking balance training interventions. According to the Bauby and Kuo model, the interventions

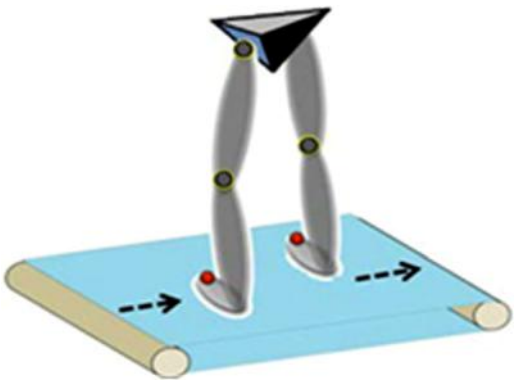

FIGURE 7.3

Body is oriented orthogonal to typical forward walking during lateral stepping gait to alter the influence from passive mechanics of motion.

attempting to improve medial–lateral stabilization during typical walking would need to target always the medial–lateral direction during such typical walking. The modified model allows targeting the direction orthogonal to the progression (i.e., the secondary plane), while not necessarily limiting progression to the forward anterior–posterior direction. This is crucial because the thousands of daily steps in the typical forward-walking direction will strongly reinforce any possible incorrect control mechanisms. Therefore any intervention with the individual walking in the typical forward direction requires the person to attempt to learn a new control strategy while simultaneously reinforcing the old habit. The modified model permits implementation of a motor learning task that could improve stabilization of the secondary plane (which would be the medial–lateral direction during typical forward walking) without simultaneously reinforcing the individual's old motor control strategy. Wurdeman and colleagues' findings of similar control during a lateral stepping gait compared to traditional forward walking make this task a promising gait-based task to improve walking balance. It is a dynamic gait task that requires the individual to place the foot for each step in a position that stabilizes the primary and secondary planes of progression, like typical forward walking. The novelty of a lateral stepping gait task is that it requires individuals with lateral stabilization problems to completely reorganize the control mechanisms for maintaining walking balance without the need for any external stabilization device. With the lateral stepping gait, individuals with lateral stabilization problems have the opportunity to completely reorganize their motor control over the lateral stepping task and thus "relearn" how to walk. Importantly, they are doing this without adding any bias from previous motor control mechanisms.

7.5.2 Stride time and variability: a special case

One parameter of increasing importance is stride time due to the study of gait variability. Gait variability refers to the natural stride-to-stride fluctuations that are inherent in normal, healthy gait (Delignières & Torre, 2009; Hausdorff et al., 1997; Stergiou et al., 2006). These stride-to-stride fluctuations are thought to arise from interconnected, nonlinear processes that enable us to expand and maintain a large repertoire of movement strategies, allowing for robust gait in dynamic, unpredictable environments (Cavanaugh et al., 2017; Harrison & Stergiou, 2015). The pattern of variability found in stride-to-stride fluctuations has been identified as fractal (see also Chapter 10: A tutorial on fractal analysis of human movements). Such fractal patterns are also observed in the cycle-to-cycle fluctuations of other biological signals like heart rate (Goldberger et al., 2003), respiration (Peng et al., 2002), and brain activity (Harrison, Hough, Schmid, Groff, & Stergiou, 2018). Being fractal means that, in a healthy system, these physiological

processes have time intervals between events that are neither equal nor independent. Rather, there is a relationship between these intervals that extends far forward and backward in time exhibiting long-range correlations. The presence of these fractal patterns has been suggested as a theoretical marker of biological complexity (Goldberger et al., 2003; Stergiou & Decker, 2011). The evaluation of the stride-to-stride fluctuations is performed with nonlinear analysis tools (see Chapter 8: Gait variability: a theoretical framework for gait analysis and biomechanics and Chapter 10: A tutorial on fractal analysis of human movements) that will allow you to identify if such patterns exist. Practically, the time series of the stride time intervals is subjected to rigorous examination with tools such as detrended fluctuation analysis, entropy, and others that are metrics of complexity (Stergiou, 2017).

Furthermore, complexity is recognized as an inherent attribute of healthy biological systems, whereas the loss of complexity with aging and disease is thought to reduce the adaptive capabilities of the individual (Cavanaugh et al., 2017; Goldberger et al., 2003; Harrison & Stergiou, 2015; Stergiou & Decker, 2011; Stergiou et al, 2006). A loss of complexity can refer to either an overly constrained, periodic system, or an overly random, incoherent system. Increasingly, abnormal gait patterns can be characterized by a loss of complexity and have been associated with a variety of disorders ranging from joint and skeletal problems (Decker, Moraiti, Stergiou, & Georgoulis, 2011; Myers et al., 2009; Myers, Pipinos, Johanning, & Stergiou, 2011) to Huntington disease (Hausdorff et al., 1998), Parkinson disease (Hove, Suzuki, Uchitomi, Orimo, & Miyake, 2012), multiple sclerosis (Kaipust, Huisinga, Filipi, & Stergiou, 2012), and falls (Hausdorff, 2007).

Gait variability has also been explored with the dynamic walking method. This method refers to passive dynamic walkers that descend a slope, and active dynamic robotic walkers that walk on level ground (Kuo, 2007). Kurz and Stergiou have used passive dynamic walker models as templates to explore if gait variability has a structure that resembles mathematical chaos (Fig. 7.4; Kurz & Stergiou, 2005, 2007a, 2007b; Kurz et al., 2005). Their work was inspired by previous simulation studies that have revealed parameterizations of simple template models of bipedal gait that exhibit chaotic modes of behavior. Specifically, Garcia, Chatterjee, Ruina, and Coleman (1998) observed that even a quite simple passive dynamic walking model can exhibit a cascade of period doublings in their gait variability as a function of changes in slope angle (γ in Fig. 7.4). Garcia et al. noted that the distances between consecutive period doublings appeared to converge to the Feigenbaum constant (4.669201...). This suggested the possibility that even passive dynamic walking models may exhibit modes of chaotic gait variability (Alligood, Sauer, & Yorke, 1996).

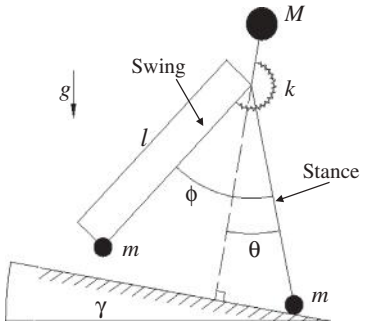

FIGURE 7.4

Simplest passive dynamic walking model composed of a point mass hip and two massless legs. This model also includes a hip joint actuator which was used in some of the Kurz and Stergiou experiments.

Kurz et al. (2005) tested this possibility with numerical simulations that confirmed that the gait variability of the model had chaotic dynamics. The authors performed analyses of the gait variability of the model from 5000 footfalls with the first 500 footfalls removed to be certain that the model converged to the given attractor. In the first stage of the analysis, bifurcations in the model's gait variability were noted with Poincaré maps composed from the step time interval of the right leg of the model. The Poincaré maps provided a way to simplify the dynamics of the system by viewing the behavior of the system stroboscopically (Baker & Gollub, 1996). Step time interval from heel contact to toe-off of the right leg was utilized to construct the Poincaré map because this interval can be taken to represent the global outcome of the gait dynamics of the model. This approach was chosen in part due to the potential to generally apply the method irrespective of the complexity of the underlying system dynamics. Furthermore, previous investigations that have demonstrated that human gait exhibits chaotic dynamics have similarly analyzed step time intervals (Hausdorff et al., 1997; Hausdorff, 2007). The Poincaré maps revealed that a period one gait attractor was present in the simple passive walker model for $\gamma < 0.0169$ rad. This indicated that the model selected the same step time interval for every step of the continuous gait pattern. At $\gamma = 0.017$ rad, the gait pattern bifurcated from period one to period two Poincaré map. A period two Poincaré map indicated that the gait pattern alternated between two different step time intervals. Beyond $\gamma = 0.017$ rad there was a cascade of bifurcations in the step time interval that led to a strange attractor in the model's gait. At $\gamma = 0.0180$ rad, the model exhibited a period four gait pattern. This indicated that the model utilized four different step time intervals for gait. As γ was increased to 0.01823 rad, the gait pattern bifurcated from a period four to a

period eight gait pattern. These results indicate that the gait pattern utilized eight different step time intervals as it traversed down the surface. Additional increases in γ resulted in further bifurcations in the step time intervals chosen by the walking model. These bifurcations appeared to lead to a strange gait attractor where multiple step time intervals are chosen for a stable walking pattern.

In the second stage of the analysis performed by Kurz and Stergiou (2005), tools from mathematical chaos theory were used to classify the data that composed the Poincaré map as representing a chaotic gait pattern (Alligood et al., 1996; Wurdeman et al., 2012; Baker & Gollub, 1996; Stergiou, 2017). Two methods were employed, the calculation of Lyapunov exponents, and the calculation of Hurst exponents. Lyapunov exponents were calculated to quantify the exponential separation of nearby trajectories in the reconstructed state space of the simulated gait pattern at the respective γ. This information was necessary to classify the stability of the gait pattern and determine if the pattern was chaotic. Positive Lyapunov exponents were present from $0.01839 \text{ rad} < \gamma < 0.0189 \text{ rad}$ (Lyapunov exponent range from 0.002 to 0.158), indicating the presence of stable chaotic modes in a finite region of the parameter space. This interpretation was further confirmed by determining the Hurst exponent for each of the simulated step interval data time series (Stergiou, 2017). A Hurst exponent greater than 0.5 indicates that the positive Lyapunov exponent is due to a persistent chaotic gait pattern, conversely, a Hurst exponent less than 0.5 indicates that the positive Lyapunov exponent was related to random noise in the model, not chaos. Analysis of the Hurst exponents indicated chaotic behaviors in the model's gait pattern ($H = 0.98$ for all $\gamma > 0.01839$). In sum, the numerical simulations of the model indicated that as the slope angle (γ) increased, the model's gait pattern showed a cascade of bifurcations which led to a chaotic attractor. These results provided evidence that such a model can be used as a template (Full & Koditschek, 1999) for exploring the dynamics and the control parameters responsible for chaos in human gait variability.

7.6 Determinants of gait

The major determinants of gait were introduced by Saunders, Inman, and Eberhart (1953), based on the concept that the ideal locomotion is when the translation of the COM through space will require the least energy expenditure while walking. This is accomplished by decreasing the vertical displacement of the COM and subsequently decreasing the exchange of kinetic and potential energy, thus reducing metabolic cost. Essentially, the COM rises and falls about 2 inches during walking (Inman, 1966); however, a mechanical model rises and falls 3 inches (Fenn, 1930). The explanation of these

differences, as well as of the shape of the COM curve, arises from the six determinants of gait which are as follows (Saunders et al., 1953):

1 Transverse pelvic rotation. While both feet rest on the ground after the step, the pelvis is at its lowest point. Therefore the COM has made a drop across an arc, and the pelvis is perpendicular to the line of progression. Rotation of the body forward with the swinging leg will elevate and rotate forward the COM. This rotation cuts the angle of the femur with the floor. If we lengthen the femur toward its lowest point by lengthening the segment, we can then save the COM drop at its lowest point. Thus we save 3/8 of an inch of the COM drop at its lowest point.
2 Pelvic tilt. The pelvis drops on the side of the swinging leg. This leads to a depression of the COM apex at the highest point by shortening the swinging leg, which saves a COM elevation of 3/16 of an inch at the highest point.
3 Knee flexion. The knee flexes about 15° during support phase. If we had a rigid leg, at the middle of stance, the COM will be at its highest point. With knee flexion, the COM drops and its apex will be depressed. That saves 7/16 of an inch from COM's elevation.

So, the first three determinants save an inch and explain the drop from 3 to 2 inches. This, as we mentioned before, will diminish energy expenditure.

4 Foot and ankle motion. At heel strike the foot is dorsiflexed. The ankle's center of rotation rises and then falls at foot flat. During flat foot, there is no rise or fall of the center of rotation. When heel-off starts, the center of rotation starts rising and keeps rising until toe-off. As the COM is dropping and the leg flexes, this center of rotation rise might slow the drop a small amount. This would then tend to smooth the terms on the graphic representation. Actually, the ankle, foot, and knee smooth the COM by acting as a cushion to the heel strike.
5 Knee motion. At heel strike, when the center of rotation of the ankle is high, the knee joint begins to flex. During midstance when the ankle center is low the knee joint flexes a second time. The net effect of this close relation between the motions of the foot, ankle, and knee is to smooth the pathway of the COM.
6 Lateral motion of the pelvic. The pelvic tilt is 6–8 inches. The COM must be directly above the support point on the ground in order to balance on one leg. If the leg segments are parallel, the COM will shift from 8 to 12 inches. However, the femurs are adducted and the tibias are in slight valgus, and this narrows the support joint. The base is narrowed about 2 inches.

The six determinants of gait were generally accepted without, however, any rigorous testing regarding their validity. More recently, Gard and Childress (1999) found that the knee flexion during stance does not decrease the magnitude of

the trunk's vertical displacement and occurs before its peak. They concluded that the function of the knee flexion during stance is related to shock absorption. Gard and Childress (2001) also used a rocker-based inverted pendulum model and concluded that the vertical displacement of the COM is determined by variables such as step length and foot and leg geometry. The inverted pendulum assumes the body with the ankle as the axis and a counterclockwise movement in the sagittal plane. This model is based on the assumption that gravity continuously acts on the pendulum to produce a forward-tumbling torque with the COM in front of the ankle joints and the attached ankle extensor muscles acting backwards to prevent falling. The dynamic equation of this pendulum can be briefly described and simplified as follows (Nakazawa et al., 2012):

$$I\ddot{\theta} = mgh\theta - T_{\alpha} \tag{7.2}$$

where I is the moment of inertia of the body around the axis formed by the ankle, θ the angle of the COM with the vertical, m the body mass with the exception of the feet, g is the gravitational acceleration, h the distance between the ankle joint and the CoM, and T_{α} the ankle extensor torque (Fig. 7.5).

Gard and Childress (2001), in their rocker-based inverted pendulum model, analyzed vertical excursion of the body (h). The step length (S_l), anatomical leg length (L), foot rocker radius (r), and virtual leg length (L_v) were related by the following equation:

$$L_v = \frac{L^2}{L-r} = L\left(\frac{1}{1-r/L}\right) = L_{\rho} \tag{7.3}$$

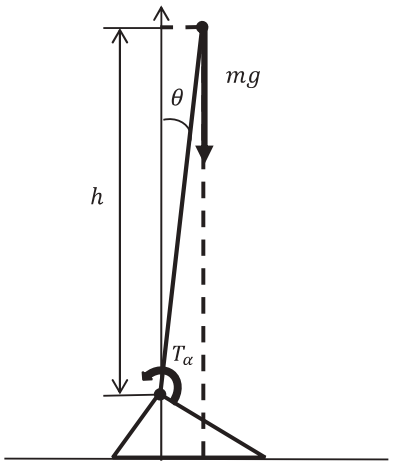

FIGURE 7.5
Simplified inverted pendulum model in the sagittal plane.

where ρ is the "roll factor" (usually between 1.7 and 1.9 for normal gait). It represents the effective lengthening of the leg that is used to smooth the trajectory of the trunk while walking. Eq. (7.4) is used to predict the vertical excursion (h):

$$h = \frac{S_l^2}{8L_\rho} = \frac{S_l^2}{8L_v} \tag{7.4}$$

They found that the magnitude of vertical displacement of the COM is practically unchanged by pelvic obliquity and knee flexion during stance. The vertical displacement of the trunk varied 25−85 mm over a range of walking speeds between 0.9 and 2.3 m/s. The authors confirmed that both pelvic obliquity and knee flexion during stance are related to shock absorption during the loading response. Furthermore, Kerrigan, Della Croce, Marciello, and Riley (2000) initially identified that heel rise from a foot being flat has a considerable role in vertical displacement. Subsequently, this research team also found that pelvic rotation contributes about 12% to the reduction of the COM vertical displacement (Della Croce, Riley, Lelas, & Kerrigan, 2001). In addition, they showed that heel rise is a major determinant contributing almost two-thirds of the total reduction of the COM vertical displacement. Lastly, Kuo (2007) examined the six determinants of gait and their premise of minimizing the energetic cost of locomotion by reducing the vertical displacement of the COM, as well as the inverted pendulum model of gait and its premise of the stance leg behaving like a pendulum, prescribing a more circular arc rather than a horizontal path for the COM. Kuo used a different method to explore these two models described above, the dynamic walking method. Based on this method, Kuo (2007) suggested that a better perspective to identify the determinants of gait is to focus on mechanical work rather than the kinematics or forces of gait.

7.7 Conclusions

In this chapter we have covered the basic principles of gait analysis. We discussed gait as a skill along with the definition of motor skill, more generally; we defined gait analysis; presented the periods and phases of gait; identified the most important spatiotemporal parameters to evaluate during gait analysis where we explored two special cases, the first being step width and lateral stepping and the second stride/step time and gait variability; and we examined the determinants of gait. In addition, we presented a few more advanced principles with respect to modeling such as the dynamic walking method and the inverted pendulum. There are many more topics with respect to gait analysis, but to include them here we would need a book and not just a chapter. However, we wanted to give a solid foundation and to cultivate a desire to dive deeper into the research performed in this exciting area of gait analysis.

References

Adams, J. A. (1987). Historical review and appraisal of research on the learning, retention, and transfer of human motor skills. *Psychological Bulletin*, *101*(1), 41–74.

Alligood, K. T., Sauer, T. D., & Yorke, J. A. (1996). *Chaos*. New York, NY: Springer.

Arutyunyan, G., Gurfinkel, V., & Mirskii, M. (1968). Investigation of aiming at a target. *Biophysics*, *13*, 536–538.

Arutyunyan, G., Gurfinkel, V., & Mirskii, M. (1969). Organization of movements on execution by man of an exact postural task. *Biophysics*, *14*, 1162–1167.

Baker, G. L., & Gollub, J. P. (1996). *Chaotic dynamics: An introduction* (2nd ed.). Cambridge, England: Cambridge University Press.

Baker, R. (2006). Gait analysis methods in rehabilitation. *Journal of Neuroengineering and Rehabilitation*, *3*(4), 1–10.

Baker, R., Esquenazi, A., Benedetti, M. G., & Desloovere, K. (2016). Gait analysis: Clinical facts. *European Journal of Physical and Rehabilitation Medicine*, *52*(4), 560–574.

Bauby, C. E., & Kuo, A. D. (2000). Active control of lateral balance in human walking. *Journal of Biomechanics*, *33*, 1433–1440.

Berstein, N. (1967). *The coordination and regulation of movement*. Oxford, UK: Pergamon Press.

Blanc, Y., Balmer, C., Landis, T., & Vingerhoets, F. (1999). Temporal parameters and patterns of the foot roll over during walking: Normative data for healthy adults. *Gait & Posture*, *10*(2), 97–108.

Brach, J. S., Berlin, J. E., Van Swearingen, J. M., Newman, A. B., & Studenski, S. A. (2005). Too much or too little step width variability is associated with a fall history in older persons who walk at or near normal gait speed. *Journal of Neuroengineering and Rehabilitation*, *2*, 21.

Brach, J. S., Studenski, S. A., Perera, S., Van Swearingen, J. M., & Newman, A. B. (2007). Gait variability and the risk of incident mobility disability in community-dwelling older adults. *The Journals of Gerontology, Series A, Biological Sciences and Medical Sciences*, *62*, 983–988.

Castro, M. P., Figueiredo, M. C., Abreu, S., Sousa, H., Machado, L., Santos, R., & Vilas-Boas, J. P. (2015). The influence of gait cadence on the ground reaction forces and plantar pressures during load carriage of young adults. *Applied Ergonomics*, *49*, 41–46.

Cavanaugh, J. T., Kelty-Stephen, D. G., & Stergiou, N. (2017). Multifractality, interactivity, and the adaptive capacity of the human movement system: A perspective for advancing the conceptual basis of neurologic physical therapy. *Journal of Neurologic Physical Therapy*, *41*(4), 245–251.

Chambers, H. G., & Sutherland, D. H. (2002). A practical guide to gait analysis. *The Journal of the American Academy of Orthopaedic Surgeons*, *10*(3), 222–231.

Chang, C. L., & Ulrich, B. D. (2008). Lateral stabilization improves walking in people with myelomeningocele. *Journal of Biomechanics*, *41*(6), 1317–1323.

Decker, L. M., Moraiti, C., Stergiou, N., & Georgoulis, A. D. (2011). New insights into anterior cruciate ligament deficiency and reconstruction through the assessment of knee kinematic variability in terms of nonlinear dynamics. *Knee Surgery, Sports Traumatology, Arthroscopy*, *19*(10), 1620–1633.

Delignières, D., & Torre, K. (2009). Fractal dynamics of human gait: A reassessment of the 1996 data of Hausdorff et al. *Journal of Applied Physiology*, *106*(4), 1272–1279.

Della Croce, U., Riley, P. O., Lelas, J. L., & Kerrigan, D. C. (2001). A refined view of the determinants of gait. *Gait & Posture*, *14*(2), 79–84.

Donelan, J. M., Shipman, D. W., Kram, R., & Kuo, A. D. (2004). Mechanical and metabolic requirements for active lateral stabilization in human walking. *Journal of Biomechanics*, *37*, 827–835.

Fenn, W. O. (1930). Work against gravity and work due to velocity changes in running. *American Journal of Physiology*, *93*, 433–462.

Full, R. J., & Koditschek, D. E. (1999). Templates and anchors: Neuromechanical hypotheses of legged locomotion on land. *Journal of Experimental Biology*, *202*(23), 3325–3332.

Garcia, M., Chatterjee, A., Ruina, A., & Coleman, M. (1998). The simplest walking model: Stability, complexity, and scaling. *Journal of Biomedical Engineering—Transactions of the ASME*, *120*(2), 281–288.

Gard, S. A., & Childress, D. S. (1999). The influence of stance-phase knee flexion on the vertical displacement of the trunk during normal walking. *Archives of Physical Medicine and Rehabilitation*, *80*(1), 26–32.

Gard, S. A., & Childress, D. S. (2001). What determines the vertical displacement of the body during normal walking? *Journal of Prosthetics and Orthotics*, *13*(3), 64–67.

Gentile, A. M., Higgins, J. R., Miller, E. A., & Rosen, B. M. (1975). The structure of motor tasks. *Movement*, *7*, 11–28.

Gleick, J. (1987). *Chaos: Making a new science*. New York, NY: Viking Books.

Goldberger, A. L., Amaral, L. A. N., Hausdorff, J. M., Ivanov, P. C., Peng, C.-K., & Stanley, H. E. (2003). Fractal dynamics in physiology: Alterations with disease and aging. *Proceedings of the National Academy of Sciences of the United States of America*, *19*(2), 282–289.

Hak, L., Houdijk, H., Beek, P. J., & Van Dieën, J. H. (2013). Steps to take to enhance gait stability: The effect of stride frequency, stride length, and walking speed on local dynamic stability and margins of stability. *PLoS ONE*, *8*(12), e82842.

Harkema, S., Dobkin, B., & Edgerton, V. R. (2000). Pattern generators in locomotion: Implications for recovery of walking after spinal cord injury. *Topics in Spinal Cord Injury Rehabilitation*, *6*(2), 82–96.

Harrison, S. J., Hough, M., Schmid, K., Groff, B. R., & Stergiou, N. (2018). When coordinating finger tapping to a variable beat the variability scaling structure of the movement and the cortical BOLD signal are both entrained to the auditory stimuli. *Neuroscience*, *10*(392), 203–218.

Harrison, S. J., & Stergiou, N. (2015). Complex adaptive behavior and dexterous action. *Nonlinear Dynamics, Psychology, and Life Sciences*, *19*(4), 345–394.

Hausdorff, J. M. (2007). Gait dynamics, fractals and falls: Finding meaning in the stride-to-stride fluctuations of human walking. *Human Movement Science*, *26*(4), 555–589.

Hausdorff, J. M., Cudkowicz, M. E., Firtion, R., Wei, J. Y., & Goldberger, A. L. (1998). Gait variability and basal ganglia disorders: Stride-to-stride variations of gait cycle timing in Parkinson's disease and Huntington's disease. *Movement Disorders*, *13*(3), 428–437.

Hausdorff, J. M., Mitchell, S. L., Firtion, R., Peng, C. K., Cudkowicz, M. E., Wei, J. Y., & Goldberger, A. L. (1997). Altered fractal dynamics of gait: Reduced stride-interval correlations with aging and Huntington's disease. *Journal of Applied Physiology*, *82*(1), 262–269.

Hausdorff, J. M., Rios, D. A., & Edelberg, H. K. (2001). Gait variability and fall risk in community-living older adults: A 1-year prospective study. *Archives of Physical Medicine and Rehabilitation*, *82*, 1050–1056.

Higgins, J. R. (1977). *Human movement: An integrated approach*. St. Louis, MO: C.V. Mosby.

Higgins, S. (1985). Movement as an emergent form: Its structural limits. *Human Movement Science*, *4*, 119–148.

Hof, A. L., Gazendam, M. G., & Sinke, W. E. (2005). The condition for dynamic stability. *Journal of Biomechanics*, *38*, 1–8.

Hollman, J. H., McDade, E. M., & Peterson, R. C. (2011). Normative spatiotemporal gait parameters in older adults. *Gait & Posture*, *34*(1), 111–118.

Hove, M. J., Suzuki, K., Uchitomi, H., Orimo, S., & Miyake, Y. (2012). Interactive rhythmic auditory stimulation reinstates natural 1/f timing in gait of parkinson's patients. *PLoS One*, *7*(3), e32600.

Hunt, N., McGrath, D., & Stergiou, N. (2014). The influence of auditory-motor coupling on fractal dynamics in human gait. *Scientific Reports*, *4*, 1–6.

Inman, V. T. (1966). Human locomotion. *The Canadian Medical Association Journal*, *94*, 1047–1054.

Inman, V. T., Ralston, H. J., & Todd, F. (1981). *Human walking*. Baltimore, MD: Williams & Wilkins.

Jeng, B., Sandroff, B. M., & Motl, R. W. (2018). Energetic cost of walking and spasticity in persons with multiple sclerosis with moderate disability. *NeuroRehabilitation*, *43*(4), 483–489.

Kaipust, J., Huisinga, J., Filipi, M., & Stergiou, N. (2012). Gait variability measures reveal differences between multiple sclerosis patients and healthy controls. *Motor Control*, *16*(2), 229–244.

Kaipust, J. P., McGrath, D., Mukherjee, M., & Stergiou, N. (2013). Gait variability is altered in older adults when listening to auditory stimuli with differing temporal structures. *Annals of Biomedical Engineering*, *41*(8), 1595–1603.

Kelso, J. A. S., & Ding, M. (1993). Fluctuations, intermittency, and controllable chaos in biological coordination. In K. M. Newell, & D. M. Corcos (Eds.), *Variability and motor control* (pp. 291–316). Champaign, IL: Human Kinetics.

Kerrigan, D. C., Della Croce, U., Marciello, M., & Riley, P. O. (2000). A refined view of the determinants of gait: Significance of heel rise. *Archives of Physical Medicine and Rehabilitation*, *81*(8), 1077–1080.

Kuo, A. D. (1999). Stabilization of lateral motion in passive dynamic walking. *The International Journal of Robotics Research*, *18*(9), 917–930.

Kuo, A. D. (2007). The six determinants of gait and the inverted pendulum analogy: A dynamic walking perspective. *Human Movement Science*, *26*(4), 617–656.

Kuo, A. D., & Donelan, J. M. (2010). Dynamic principles of gait and their clinical implications. *Physical Therapy*, *90*(2), 157–174.

Kurz, M. J., & Stergiou, N. (2005). An artificial neural network that utilizes hip joint actuations to control bifurcations and chaos in a passive dynamic bipedal walking model. *Biological Cybernetics*, *93*(3), 213–221.

Kurz, M. J., & Stergiou, N. (2007a). Do horizontal propulsive forces influence the nonlinear structure of locomotion? *Journal of Neuroengineering and Rehabilitation*, *4*, 30.

Kurz, M. J., & Stergiou, N. (2007b). Hip actuations can be used to control bifurcations and chaos in a passive dynamic walking model. *Journal of Biomechanical Engineering*, *129*, 216–222.

Kurz, M. J., Stergiou, N., Heidel, J., & Terry Foster, E. (2005). A template for the exploration of chaotic locomotive patterns. *Chaos, Solutions & Fractals*, *23*(2), 485–493.

Levine, D., Richards, J., & Whittle, M. W. (2012). *Whittle's gait analysis* (5th ed.). London, UK: Elsevier.

Lim, Y. P., Lin, Y. C., & Pandy, M. G. (2017). Effects of step length and step frequency on lower-limb muscle function in human gait. *Journal of Biomechanics*, *57*, 1–7.

Maki, B. E. (1997). Gait changes in older adults: Predictors of falls or indicators of fear? *Journal of the American Geriatric Society*, *45*, 313–320.

Marteniuk, R. G. (1974). Individual differences in motor performance and learning. In J. H. Wilmore (Ed.), *Exercise and sport sciences reviews*. New York: Academic Press.

McDonald, P. V., van Emmerik, R. E. A., & Newell, K. M. (1989). The effects of practice on limb kinematics in a throwing task. *Journal of Motor Behavior*, *21*, 245–264.

Merriam-Webster's Collegiate Dictionary (11th ed.). (2003). Springfield, MA: Merriam-Webster Incorporated.

Muro-de-la-Herran, A., García-Zapirain, B., & Méndez-Zorrilla, A. (2014). Gait analysis methods: An overview of wearable and non-wearable systems, highlighting clinical applications. *Sensors (Switzerland)*, *14*(2), 3362–3394.

Murray, M. P., Drought, A. B., & Kory, R. C. (1964). Walking patterns of normal men. *The Journal of Bone and Joint Surgery*, *46*(A), 335–360.

Murray, M. P., Mollinger, L. A., Gardner, D. G. M., & Sepic, S. B. (1984). Kinematic and EMG patterns during slow, free, and fast walking. *Journal of Orthopaedic Research*, *2*(3), 272–280.

Myers, S. A., Johanning, J. M., Stergiou, N., Celis, R. I., Robinson, L., & Pipinos, I. I. (2009). Gait variability is altered in patients with peripheral arterial disease. *Journal of Vascular Surgery*, *49*(4), 924–931.

Myers, S. A., Pipinos, I. I., Johanning, J. M., & Stergiou, N. (2011). Gait variability of patients with intermittent claudication is similar before and after the onset of claudication pain. *Clinical Biomechanics*, *26*(7), 729–734.

Nakazawa, K., Obata, H., & Sasagawa, S. (2012). Neural control of human gait and posture. *The Journal of Physical Fitness and Sports Medicine*, *1*(2), 263–269.

Newell, K. M., & van Emmerik, R. E. A. (1989). The acquisition of coordination: Preliminary analysis of learning to write. *Human Movement Science*, *8*, 17–32.

Oh-Park, M., Holtzer, R., Xue, X., & Verghese, J. (2010). Conventional and robust quantitative gait norms in community-dwelling older adults. *Journal of the American Geriatric Society*, *58*, 1512–1518.

Peng, C. K., Mietus, J. E., Liu, Y., Lee, C., Hausdorff, J. M., Stanley, H. E., & Lipsitz, L. A. (2002). Quantifying fractal dynamics of human respiration: Age and gender effects. *Annals of Biomedical Engineering*, *30*(5), 683–692.

Perry, J., & Burnfield, J. M. (2010). *Gait analysis. Normal and pathological function* (2nd ed.). Thorofare, NJ: Slack Incorporated.

Pirker, W., & Katzenschlager, R. (2017). Gait disorders in adults and the elderly: A clinical guide. *Wiener Klinische Wochenschrift*, *129*(3–4), 81–95.

Rose, J., & Gamble, J. G. (2005). *Human walking* (3rd ed.). Philadelphia, PA: Lippincott Williams & Wilkins.

Rosenbaum, D. (2013). Foot loading patterns can be changed by deliberately walking with in-toeing or out-toeing gait modifications. *Gait & Posture*, *38*(4), 1067–1069.

Saunders, J., Inman, V., & Eberhart, H. (1953). The major determinants in normal and pathological gait. *The Journal of Bone & Joint Surgery*, *35*(3), 543–558.

Schmidt, R. C., Treffner, P. J., Shaw, B. K., & Turvey, M. T. (1992). Dynamical aspects of learning an interlimb rhythmic movement pattern. *Journal of Motor Behavior*, *24*, 67–83.

Sebastião, E., Bollaert, R. E., Hubbard, E. A., & Motl, R. W. (2018). Gait variability and energy cost of oveground walking in persons with multiple sclerosis. *American Journal of Physical Medicine & Rehabilitation*, *97*(9), 646–650.

Silva, M. P. T., & Ambrósio, J. A. C. (2002). Kinematic data consistency in the inverse dynamic analysis of biomechanical systems. *Multibody System Dynamics*, *8*(2), 219–239.

Stergiou, N. (2017). *Nonlinear analysis for human movement variability*. Boca Raton, FL: CRC Press, Taylor & Francis Group.

Stergiou, N., & Decker, L. M. (2011). Human movement variability, nonlinear dynamics, and pathology: Is there a connection? *Human Movement Science*, *30*(5), 869–888.

Stergiou, N., Harbourne, R., & Cavanaugh, J. (2006). Optimal movement variability: A new theoretical perspective for neurologic physical therapy. *Journal of Neurologic Physical Therapy*, *30*(3), 120–129.

Studenski, S., Perera, S., Patel, K., et al. (2011). Gait speed and survival in older adults. *JAMA*, *305*(1), 50–58.

Sugi, T., Kawana, F., & Nakamura, M. (2009). Automatic EEG arousal detection for sleep apnea syndrome. *Biomedical Signal Processing and Control*, *4*(4), 329–337.

Takakusaki, K. (2017). Functional neuroanatomy for posture and gait control. *Journal of Movement Disorders*, *10*(1), 1–17.

Van Rossum, J. H. A. (1990). Schmidt's schema theory: The empirical base of the variability of practice hypothesis. *Human Movement Science*, *9*, 387–435.

Vaughan, C. L., Davis, B. L., & O'Connor, J. C. (1999). In C. L. Vaughan (Ed.), *Dynamics of human gait* (2nd ed.). Howard Place, Western Cape: Kiboho Publishers.

Verghese, J., Wang, C., Lipton, R. B., Holtzer, R., & Xue, X. (2007). Quantitative gait dysfunction and risk of cognitive decline and dementia. *Journal of Neurology, Neurosurgery, and Psychiatry*, *78*, 929–935.

Wurdeman, S. R., Huben, N. B., & Stergiou, N. (2012). Variability of gait is dependent on direction of progression: Implications for active control. *Journal of Biomechanics*, *45*(4), 653–659.

Wurdeman, S. R., & Stergiou, N. (2013). Temporal structure of variability reveals similar control mechanisms during lateral stepping and forward walking. *Gait & Posture*, *38*(1), 73–78.

Yang, F., & Pai, Y.-C. (2014). Can stability really predict an impending slip-related fall among older adults? *Journal of Biomechanics*, *47*, 3876–3881.

Yentes, J. M., Rennard, S. I., Schmid, K. K., Blanke, D., & Stergiou, N. (2017). Patients with COPD walk with altered step time and step width variability as compared to healthy controls. *Annals of the American Thoracic Society*, *14*(6), 858–866.

Zelik, K. E., Takahashi, K. Z., & Sawicki, G. S. (2015). Six degree-of-freedom analysis of hip, knee, ankle and foot provides updated understanding of biomechanical work during human walking. *Journal of Experimental Biology*, *218*(6), 876–886.

Further reading

Perry, J. (1992). *Gait analysis: Normal and pathological function*. Thorofare, NJ: Slack Incorporated.

CHAPTER 8

Gait variability: a theoretical framework for gait analysis and biomechanics

James T. Cavanaugh[1] **and Nick Stergiou**[2]

[1]University of New England, Portland, ME, United States, [2]University of Nebraska at Omaha, Omaha, NE, United States

CONTENTS

> We have now to consider the parts which are useful to animals for movement in place (locomotion); first, why each part is such as it is and to what end they possess them; and second, the differences between these parts both in one and the same creature, and again by comparison of the parts of creatures of different species with one another. First then let us lay down how many questions we have to consider.
>
> **The opening sentence from the book *On the Gait of Animals* by Aristotle (384–322 BCE)**

8.1 Introduction

Human walking is a necessarily adaptable motor behavior. Its fundamental form (i.e., forward progression at a comfortable pace along a straight path across an uncluttered, level surface) is frequently adjusted from moment to moment to meet fluctuating task demands or to accommodate changing environmental conditions. Humans typically adjust their walking behavior without necessarily stopping: they speed up and slow down; they shorten or lengthen their strides; they increase foot clearance or step sideways when traversing obstacles; they narrow or widen their base of support; they alter the orientation of their head and torso when their visual or auditory attention is otherwise occupied; and they routinely engage in a variety of superimposed movement strategies with arms, legs, and torso to carry objects or recover from a slip, trip, or other perturbation. Normal biomechanical variations in the fundamental form of walking allow humans to produce effective walking behavior under real-world conditions.

Gait variability, or fluctuations in gait characteristics from one step to the next (Gabell & Nayak, 1984), is evident even when task demands and environmental

Biomechanics and Gait Analysis. DOI: https://doi.org/10.1016/B978-0-12-813372-9.00008-7

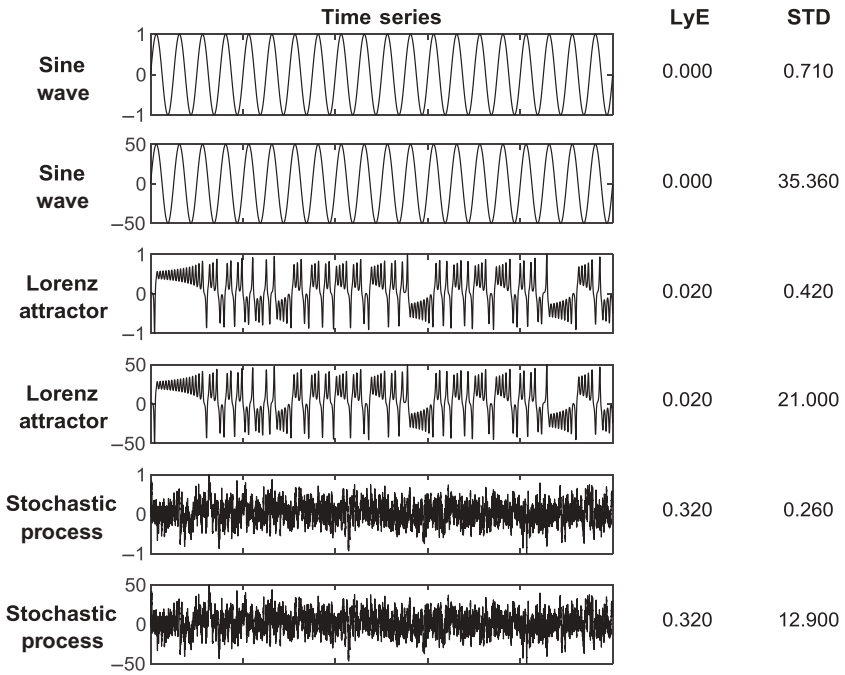

FIGURE 8.1

Six hypothetical time series with differing amounts and complexities of variability. The sinusoidal time series featured in the upper two panels contain patterns of fluctuation that differ in amount but are entirely predictable (i.e., not complex). The time series in the lower two panels contain patterns of fluctuation that differ in amount but are much more random (i.e., also not particularly complex). The center two time series differ in amount and contain a complex temporal sequence that appears to include approximately but not precisely repeating patterns that are neither entirely predictable nor random. *LyE*, Largest Lyapunov exponent (see Section 8.3.4).

conditions are constant and impose minimal constraints on the performer. Like motor performance in general, gait characteristics (e.g., step length or stride duration) naturally vary across multiple cycles in two distinct yet complementary ways: in terms of (1) the *amount* or magnitude of their fluctuations, and (2) the *complexity* of their fluctuations over time (Fig. 8.1). Complex patterns of fluctuation by definition are neither entirely predictable nor random; instead their temporal sequence appears to mix repetition with variation (Fig. 8.1, center two panels).

The amount and complexity of gait variability each depend on a performer's health, state of learning, and the conditions under which their gait is measured. In healthy adults walking in a closed (i.e., static, uncluttered) environment at their preferred speed, the *amount* of variability associated with many biomechanical measures is very low, consistent with the idea that the fundamental form of adult human gait is a well-learned, highly

repeatable movement pattern (Winter, 1983). The amount of gait variability typically increases with age (Gabell & Nayak, 1984), pathology (Rosano, Brach, Studenski, Longstreth, & Newman, 2007), and/or as task and environmental demands are added (Smith, Cusack, Cunningham, & Blake, 2017; Tamburini et al., 2018). It is typically measured with traditional linear statistical tools [i.e., standard deviation (SD), range, and variance]. The *complexity* of fluctuations in a given gait parameter also changes with pathology, state of learning, and the conditions under which it is measured. It is typically measured with nonlinear tools (i.e., entropy, Lyapunov Exponent, and fractal indices). In healthy adults walking in a closed environment at their preferred speed, the complexity of gait variability generally is relatively high, consistent with the idea that the system is maximally capable of responding to unexpected perturbations (Goldberger et al., 2002; Manor & Lipsitz, 2013). The amount and complexity of gait variability are most reliably quantified using relatively long series of gait cycles recorded with electronic data capture technology, something that has been possible only in the last few decades.

A growing body of movement science literature suggests that the amount and complexity of gait variability reflect different facets of the "on-demand" adaptability of the system. In this context, adaptability refers not only to the ability to select from a repertoire of walking-related movement patterns and behaviors to meet a given set of task demands and environmental conditions, but also to the ability to make relatively subtle adjustments to a gait pattern to maximize efficiency and/or ensure the successful completion of a specific task goal. Both aspects of adaptability are thought to emerge from continuous, complex physiologic interactions across multiple time scales (milliseconds, seconds, minutes, hours, etc.) (Cavanaugh, Kelty-Stephen, & Stergiou, 2017). Internal constraints (e.g., pathology; stage of learning) and externally imposed task and environmental constraints typically alter the dynamics of physiologic interactions, and therefore, the amount and complexity of variability evident in a series of gait cycles (Harrison & Stergiou, 2015; Morrison & Newell, 2015).

Based on these ideas, we proposed over a decade ago that variability is a natural, often beneficial, feature of human movement that can be optimized with skill development and healthy physiologic systems (Stergiou, Harbourne, & Cavanaugh, 2006). Indeed, clinical studies of gait variability have provided support for its utility as a biological marker of pathology (see Section 8.4.1) that presumably is associated with the diminished adaptability of the movement system. More recent literature (see Section 8.4.2) suggests that interventions incorporating exercise or complex sequences of stimulation may improve the amount and/or complexity of a patient's gait variability, and by extension, the adaptability of their walking behavior in general. These exciting clinical developments have opened new avenues for studying human gait and applying gait variability analyses to health care.

The purpose of this chapter is to provide biomechanists or clinical gait analysts with a contemporary, clinically oriented primer on gait variability concepts and methods. The chapter begins with a review of conceptual approaches to understanding gait variability, followed by considerations for its measurement and analysis. Thereafter, selected examples of gait variability analyses and interventions are described to illustrate a variety of practical common applications. Finally, the chapter concludes with a look to future directions for clinical research and practice.

8.2 Conceptual approaches to gait variability

As stated above, the amount and complexity of gait variability are influenced by the health of the performer, their state of learning, and the external (i.e., task and environmental) constraints present during walking. The extent to which gait variability might be considered beneficial or detrimental depends on the theoretical perspective adopted to explain the underlying control of movement. While an individual theory might apply more convincingly in a specific situation, multiple motor control mechanisms are likely to coexist in the real-life circumstances of individual clinical settings. For this reason, this chapter adopts an eclectic theoretical approach to help the biomechanist/gait analyst to consider what factors might be most at play with each individual performer.

8.2.1 Amount of variability

Two well-recognized motor control theories, generalized motor program theory (GMPT) (Schmidt, 2003) and dynamic systems theory (DST) (Warren, 2006), provide distinctly different yet complementary explanations as to why the fundamental form of gait, when produced under familiar and unchallenging conditions, is highly repeatable. Both theories also provide a useful method for interpreting what might account for increases or decreases in the amount of gait variability under a variety of clinical scenarios.

GMPT frames motor control as arising from motor programs embedded in the central nervous system for the purpose of executing relatively rapid skilled movement (i.e., too fast to be controlled through feedback mechanisms) (Schmidt, 2003). Accordingly, a healthy, adult performer performing a well-learned task like walking in familiar and unchallenging conditions should be able to efficiently and accurately employ a motor program that allows gait cycles to be generated consistently, with minimal variations in the amplitude and timing of stepping from one gait cycle to the next. Any increase in the amount of gait variability is considered in GMPT to be either an error in the ongoing selection of a motor program for gait

(i.e., a central command error), an error in the scaling of force parameters during the execution of the program (i.e., central and/or peripheral error), or random error as the movement is executed (Schmidt, 2003; Schmidt, Zelaznik, Hawkins, Frank, & Quinn, 1979). Regardless of its source, an increase in the amount of gait variability is considered to be detrimental to skilled performance.

GMPT provides a plausible interpretation for how health conditions, stage of learning, and external constraints might produce an increase in the amount of gait variability for a given performer—suggesting that their skill level is less than optimal. For example, a performer with central nervous system pathology (e.g., stroke) might present with perceptual, motor, or cognitive impairments that predictably would result in motor programming and/or execution errors leading to more variable foot placement or stride duration. A healthy performer first learning to walk while carrying a full cup of water without spilling may make frequent motor program and/or execution errors when attempting to adopt a less familiar, much-smoother-than-usual gait pattern. Even normally skilled adult performers may produce more variable gait patterns as a result of motor programming or execution errors as they attempt to adjust to challenging task demands (e.g., carrying a heavy or awkward load) or environmental conditions (e.g., walking in the dark) that alter gait biomechanics or sensory inputs. In each of these cases, motor learning interventions presumably could be used to reduce programming and execution errors through repetitive practice and augmented feedback, thereby resulting in lower, more optimal amounts of gait variability.

DST stands in sharp contrast to GMPT. DST fames motor control as emerging at any given moment from nonlinear interactions among relevant internal physiologic subsystems (i.e., neuromuscular, musculoskeletal, cardiopulmonary, metabolic) in the context of specific internal (i.e., physiologic capacity) and external (i.e., task and environmental) constraints (Lipsitz & Goldberger, 1992; Morrison & Newell, 2015; Vaillancourt & Newell, 2002; Warren, 2006). Physiologic interactions and their resulting motor output, therefore, are largely determined by the initial internal and external conditions under which movement production is organized. As the functioning or capacity of internal physiologic systems changes, and/or external constraints change, their collective dynamic interactions reorganize in an ongoing attempt to meet context-specific movement goals as efficiently as possible (Harrison & Stergiou, 2015). Accordingly, the low amount of gait variability emerging from a healthy, adult performer performing a well-learned task like walking in familiar and unchallenging conditions would be interpreted to reflect stable system dynamics. Larger amounts of gait variability, if present, would be consistent with system dynamics that are relatively unstable and perhaps transitioning to a more dramatic reorganization that ultimately would produce a fundamentally different gait pattern more suitable for the internal and external conditions.

According to DST, an increase in the amount of gait variability (i.e., reflecting at least some degree of system instability) is not necessarily detrimental to performance (James, 2004). In fact, the amount of variability is thought to reflect flexibility within the neuromotor system to optimize the parameters for a given gait pattern. The amount of gait variability also can reflect the flexibility of the system to transition to a new movement pattern at any moment. Finally, the amount of gait variability may reflect constant sampling of different variations in a gait pattern as a form of exploratory behavior, so that the gait pattern being produced is always the most appropriate one for the conditions.

DST provides alternative interpretations for how health conditions, stage of learning, and external constraints might produce an increase in the amount of gait variability for a given performer—by providing insight into the stability of underlying physiologic system dynamics. For the performer with a recent stroke, perceptual, motor, or cognitive impairments initially would destabilize system dynamics and increase the amount of gait variability by reducing the number of internal neural connections between systems (i.e., nerve cell death) or the strength of their interaction (i.e., nerve cell injury). For the healthy performer first learning to walk while carrying a full cup of water without spilling, the amount of gait variability would increase while underlying system dynamics go through a learning (i.e., adaptive) process of reorganization in an attempt to find a new stable state from which the new movement goal can be successfully achieved. For the healthy adult performer encountering challenging task demands (e.g., carrying a heavy or awkward load) or environmental conditions (e.g., walking in the dark), altered gait biomechanics or sensory inputs would impose additional external constraints that also cause the system dynamics to operate closer to a relatively destabilized point of transition to a new gait pattern more appropriate for the conditions. In each of these cases, motor learning interventions presumably could be used to facilitate the development of stable system dynamics needed for the consistent performance (i.e., low amount of variability) of a given walking task under a specific set of environmental conditions.

8.2.2 Complexity of variability

DST complements GMPT by expanding the theoretical arena in which the interpretation of gait variability can occur. Whereas GMPT is useful for interpretations of the extent to which walking performance matches a single skillful gait pattern (i.e., one that is smooth, fluid, efficient, and error-free), DST allows for the possibility that (1) multiple variations of a gait pattern can be similarly efficient under a single set of task demands and environmental conditions and (2) multiple variations of a gait pattern can be employed

effectively across a continuum of task demands and environmental conditions. Taken together, these ideas suggest that the concept of "walking skill" more accurately encompasses a repertoire of motor behavior that provides a pool of "solutions" to the problem of needing to continuously maximize gait efficiency in ever-changing real-world situations (Hess, Brach, Piva, & VanSwearingen, 2010; Stergiou et al., 2006).

The ability to adjust the basic gait pattern in real time to meet task demands and environmental conditions relies on a movement system characterized by robustness and degeneracy (Harrison & Stergiou, 2015). Robustness refers to the system's broad adaptive ability to reliably produce walking behavior across changes in context. Degeneracy refers to the system's adaptive ability to employ multifunctional elements to produce walking behavior, such as when different sets of muscle groups are employed to produce forward, backward, and sideways stepping under various conditions. Degeneracy identifies a special case of the term "flexibility," in which multiple solutions to a given motor problem are available for use. The coexistence of robustness and degeneracy (i.e., system stability and flexibility) is a hallmark of the complex, adaptive movement system from which adjustable and variable walking behaviors emerge (Harrison & Stergiou, 2015; Warren, 2006).

In this context, complexity refers not only to the compositional nature of the movement system, with its collection of mutually interacting physiologic subsystems (Rickles, Hawe, & Shiell, 2007), but also to the multiple time scales over which physiologic interactions occur (Cavanaugh et al., 2017). For example, nerve impulses interact with motor units in milliseconds to produce instantaneous control of the gait pattern. Similarly, cardiovascular functioning enables oxygen and energy transport to meet immediate walking needs. Over longer time scales (i.e., minutes, hours, days, months, and years), however, sensory feedback from gait-related muscle activity influences the neuroplastic organization of cortical areas, and repeated brisk walking enhances the functioning of cardiopulmonary and metabolic systems. These types of nonlinear, repeated, multidirectional, multiscale interactions among physiologic systems contribute to the richness of the system's adaptive capacity across both short (i.e., immediate) and long (i.e., life span) periods of time (Cavanaugh et al., 2017).

Given the aforementioned system complexity, and the ever-present potential for changes in task demands and environmental conditions, it should be apparent that the many influences on a performer's gait pattern at any given moment are in a perpetual state of flux. Thus, mirroring the compositional complexity and adaptive capacity of the movement system, gait parameters also vary in complex, adaptive ways from one cycle to the next (Harrison & Stergiou, 2015; Hausdorff, Mitchell, & Firtion, 1997).

Although no one method for measuring complexity captures all the ways in which gait variability can be considered complex, suffice it to say that the complexity of gait variability is determined by analyzing the extent to which the pattern of fluctuations in a given gait parameter tends to approximately (but not precisely) repeat itself, either when measured on a single time scale or across progressively longer time scales. Such "self-similarity" across time scales is often referred to as a form of "temporal structure" (Stergiou, Buzzi, Kurz, & Heidel, 2004). Indeed, gait variability emerging over a long series of continuous cycles collected from the fundamental form of walking typically contains a self-similar temporal structure (Hausdorff et al., 1997). The structure provides evidence that variations in gait parameters from one cycle to the next are not purely independent errors, as proposed in GMPT. Rather, cycle-to-cycle fluctuations are in large part related to one another in nonlinear ways over multiple time scales as a result of time-evolving internal and external influences (Cavanaugh et al., 2017). The notion that patterns of fluctuations are approximately similar but do not precisely repeat themselves is indicative of the stable yet flexible (i.e., robust and degenerate) nature of complex adaptive systems (Harrison & Stergiou, 2015).

8.2.3 Optimal movement variability

The GMPT and DST frameworks provide a theoretical foundation for understanding that mature motor skills and healthy states are associated with an optimal state of movement variability (Fig. 8.2) (Cavanaugh et al., 2017;

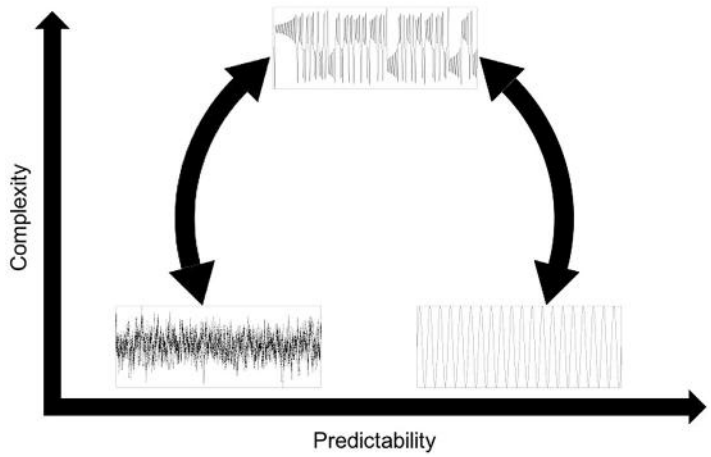

FIGURE 8.2

Theoretical model of optimal movement variability. Less than optimal variability can be either too random and unstable or too predictable and overly rigid. Optimal variability is associated with greater adaptive capacity.

Harrison & Stergiou, 2015; Stergiou et al., 2006). According to the theory, less than optimal movement variability characterizes biological systems that are overly predictable and unchanging, indicative of inflexibly constrained degrees of freedom and behavioral rigidity. Greater than optimal variability characterizes systems that are unconstrained to the point of behavioral instability. Both situations characterize systems that are less adaptable to perturbations, such as those associated with abnormal development or pathology. Optimal movement variability, in contrast, characterizes an adaptive "middle ground" diagnostic of healthy states and skill mastery.

The theory of optimal movement variability proposes that optimal or skilled action should be self-organized at the border between system stability and flexibility, as indexed by complex patterns of variability. A more recent theory of complex adaptive behavior, in which complexity measures are revealing of robustness and degeneracy, also has been proposed (Harrison & Stergiou, 2015). Together these frameworks have helped to fuel the rapid development of clinically applicable tools for assessing gait variability diagnostic and intervention contexts.

8.2.4 Summary: sources of gait variability

Theoretical descriptions of gait variability provide biomechanists and gait analysts with a variety of potential factors to consider when interpreting the gait variability of a given performer. The performer's health and stage of learning for the task of interest, combined with the walking task demands and environmental conditions, all influence the amount and complexity of gait variability detected in a given trial of walking. Random sources of variability, or those associated with measurement error on the part of the equipment or examiner, are also worthy of consideration.

The coexistence of multiple sources of variability (Table 8.1) gives rise to a global conceptual model of the total variability associated with gait. The model, which has been adapted from previous work (James, 2004), can be represented by the following equation:

$$V_{\text{Total}} = V_{\text{nonlinear}} + V_{\text{error}} \tag{8.1}$$

where V_{Total} is the total variability that exists within a system and is detectable in a long series of gait cycles, $V_{\text{nonlinear}}$ is the variability emerging from nonlinear interactions among physiologic systems, task demands, and environmental conditions as described in DST and extended by the theory of optimal movement variability, and V_{error} is the variability due to error. V_{error} can be partitioned further into

$$V_{\text{error}} = V_{\text{physiological error}} + V_{\text{methodological error}} + V_{\text{external error}} \tag{8.2}$$

Table 8.1 Theoretical sources of gait variability and their conceptual constructs.

Facet of variability	Theoretical source	Conceptual constructs

Amount	• Random, inability to properly select and execute a motor program and related schema (GMPT)
	• Extent to which system dynamics are destabilized and nearing a transition to a new stable state (DST)
	• Methodological error
	• Pathology-generated errors
		• Reflects physiologic system capacity for finely tuned control over gait pattern related to
		  ◦ Health of one or more physiologic systems
		  ◦ Task demand
		  ◦ Environmental conditions
		• Reflects system adjustment and/or exploration of alternative gait parameters to maximize efficiency

Complexity	• Motor output with detectable levels of complexity reflects the dexterity and adaptability of the underlying system (OMV) • Task and environmental conditions constrain gait patterns (DST)	• Reflects the number and/or strength of internal physiologic inputs to movement • Reflects alternation in multidirectional and multiscale influences of physiologic interactions on movement • Reflects system adjustment and/or exploration of alternative gait parameters to maximize efficiency • Reflects the degree of task and environmental constraint on performance

GMPT, *Generalized motor program theory;* DST, *dynamic systems theory;* OMV, *optimal movement variability.*

where $V_{\text{physiological error}}$ is the internal error associated with the functioning of individual physiologic systems that may or may not be affected by pathology (i.e., motor programming, execution, or random error as described in GMPT), $V_{\text{methodological error}}$ is the error contributed by methodological processes involving equipment or an examiner, and $V_{\text{external error}}$ is the error associated with all other sources of error external to the organism (e.g., variations due to task demands, environmental changes). The fully partitioned global conceptual model

$$V_{\text{Total}} = V_{\text{nonlinear}} + V_{\text{physiological error}} + V_{\text{methodological error}} + V_{\text{external error}} \tag{8.3}$$

is intended simply to convey the idea that the meaningful interpretation of gait variability data as relating to the stability of physiological system dynamics, system complexity, and/or errors in execution depends on strict adherence to proper experimental design and methodological controls (i.e., data collection and processing procedures, equipment operation, and the environmental conditions in which data collection occurs). These issues are discussed in greater detail in Section 8.3.

For a given performer, therefore, the approach taken to measuring and interpreting gait variability depends on the nature of the clinical or research question under consideration. When the health of the individual is of interest,

the amount of variability can be used to infer physiologic capacity to perform a given task under a given set of conditions and the stability of underlying system dynamics. Additionally, the complexity of gait variability can be used to make inferences about the adaptability of the underlying system. When the mastery of a specific walking skill is of interest, the amount of variability can be used to quantify a performer's stage of learning in terms of the magnitude of errors produced (i.e., novice performers produce more error than expert performers). Additionally, complexity measures can be used to make inferences about the extent to which moment-to-moment gait pattern adjustments reflect fine tuning of movement control. When the impact of task demand or environmental conditions on healthy human performance is of interest, the amount of gait variability can be used to infer the extent to which the conditions exceed capacity or destabilize system dynamics. The complexity of gait variability can indicate the degree of constraints imposed by the task and environmental conditions (i.e., greater constraints often lower movement complexity). Table 8.2 lists examples of hypothetical clinical interpretations for the amount and complexity of gait variability in various situations.

Importantly, the interpretation of gait variability for a given performer will depend on the specific mix of health status, stage of learning, task demands, and environmental conditions. In addition, the interpretation may be linked to the aspect of movement control that a specific gait parameter is thought to represent. For example, an impaired performer with a recent stroke who is relearning how to walk across a quiet room at their own pace may display a relatively large amount of variability in step length and/or stride duration, suggesting diminished control over gait progression (Lord, Howe, Greenland, Simpson, & Rochester, 2011). Assuming that the performer's postural control during gait is similarly impaired, their step width variability may, in fact, be

Table 8.2 Examples of clinical interpretations of gait variability.

	Relatively high/increase	Relatively low/decrease
Amount	• Diminished physiologic capacity and/or control of movement • Task and/or environmental conditions exceed physiologic capacity • Destabilized system dynamics • Earlier/novice stage of learning	• Robust physiologic capacity and/or control of movement • Physiologic capacity adequate for task demands/environmental conditions • Stable system dynamics • Later/expert stage of learning
Complexity	• Robust/complex physiological systems • Adaptable and dexterous physiologic systems • Task and/or environmental conditions minimally constraining	• Diminished physiologic interactivity • Diminished adaptability of physiologic systems • Task and/or environmental conditions are relatively constraining

either excessively high or low (Brach, Berlin, VanSwearingen, Newman, & Studenski, 2005). At the same time, the complexity of the stride-to-stride time series for each parameter may be reduced due to impairments in the adjustability of foot placement and timing. In contrast, a healthy individual performing the same task may display small amounts of stride-to-stride variability, a moderate amount of step width variability, and a relatively more complex pattern of stride-to-stride fluctuations, indicating that the nondemanding task and environmental conditions were well within the capability of their relatively more robust and adaptive physiologic systems. The latter result could change, however, if the task demands and environmental constraints were altered to force the healthy performer to operate closer to the limit of their physiologic capacity, dynamic system stability, or fine movement adjustability. For example, raising the speed and accuracy requirements of the task could be accomplished by asking the performer to walk as quickly as possible along a narrow walkway. Compared to the original conditions, the performer's gait pattern predictably would display a relative increase in the amount but decrease in the complexity of gait variability.

8.3 Gait analysis and biomechanical measurements for gait variability

The conceptual examples above provide a starting point for understanding basic considerations for measuring and analyzing gait variability. Most important among them are the health status of the performer, their stage of learning, and the degree of demand or constraint imposed by the task and environment. In addition, the gait variability facet of interest (i.e., amount and complexity) dictates the choice of measurement equipment, measurement protocol, and data analysis tool(s). As will be apparent in the discussion below, current methods for measuring and analyzing the amount of gait variability generally impose fewer technical requirements than measuring its complexity. However, future technological developments are anticipated to alleviate such problems.

8.3.1 Equipment options for data collection

8.3.1.1 Visual observation

Methods of gait analysis familiar to rehabilitation professionals are rooted in the visual observation of steady-state walking behavior over a short distance. In one way or another, however, visual observation methods have limited use for assessing gait variability. The short distance alone prohibits the assessment of complexity, which requires a much longer series of gait cycles and instrumented technology. *Traditional biomechanical tools like the well-known Rancho Los Amigos Observational Gait Analysis method*

(Pathokinesiology Service and Physical Therapy Department, 2001; Perry & Burnfield, 2010) *or Winter's framework for understanding atypical gait patterns* (Winter, 1983), *do not include gait variability as part of the assessment.* Only clinical performance measures like the Gait Assessment Rating Scale (Wolfson, Whipple, Amerman, & Tobin, 1990), the Dynamic Gait Index (Shumway-Cook, Baldwin, Polissar, & Gruber, 1997; Shumway-Cook, Taylor, Matsuda, Studer, & Whetten, 2013), and the Functional Gait Assessment (Wrisley, Marchetti, Kuharsky, & Whitney, 2004) capture the amount of gait variability, either as a specific element of analysis (Wolfson et al., 1990) or as observed gait deviations and unsteadiness produced when performing a specific walking task (Shumway-Cook et al., 1997, 2013; Wrisley et al., 2004). In a typical protocol, a performer completes one or more trials over a short distance under one or more walking conditions. A standardized ordinal rating scale provides only a coarse level of measurement. The clinical advantage of these tools is that they are relatively quick and simple to use, have established reliability and validity for various populations, are freely available, allow performers to walk unencumbered by measurement devices, and require only a few pieces of commonly available equipment (tape, chair, stop watch, cones, etc.) to conduct.

The clinical value of visual observation notwithstanding, technology-assisted gait analysis methods have evolved substantially in recent decades. Motion analysis hardware and associated software now allow multiple gait cycles to be captured and stored, often at high frequencies. Data subsequently can be analyzed within short time periods to obtain an in-depth view of the fluctuations present between gait cycles. This dramatic technological revolution has created a "movement microscope" that facilitates scientific discovery, similar to what happened in the 20th century by placing blood samples under a medical microscope. The following technologies have begun to provide biomechanists, gait analysts, and clinicians with a deeper understanding of the manner in which movement emerges over time.

8.3.1.2 Instrumented gait walkways

Commercially available instrumented walkway systems are used to assess the fundamental form of walking over a short distance. Walkways are typically several meters in length and contain embedded pressure sensors that open and close as a performer walks across them. No user-worn equipment is required. Using an attached computer along with manufacturer software, the systems reliably quantify spatial and temporal variables (e.g., step length, width, and time; swing and stance time; double support time). Instrumented walkways are suitable for assessing the amount of gait variability (Almarwani, Perera, VanSwearingen, Sparto, & Brach, 2016; Beauchet et al., 2013; Brach et al., 2005, 2010; Vergara-Diaz, Osypiuk, & Hausdorff, 2018;

Verghese, Holtzer, Lipton, & Wang, 2009; Wang et al., 2015; Wittwer, Webster, & Hill, 2013), but are too short for collecting the large number of gait cycles needed to assess the complexity of gait variability.

8.3.1.3 Foot-switch systems

Ultrathin, user-worn, pressure-sensitive shoe insoles or similar foot-switch systems are designed to capture selected gait characteristics over relatively long distances within a clinical or laboratory setting (Fig. 8.3) (Gow, Hausdorff, & Manor, 2017; Hausdorff et al., 1997; Hausdorff, Rios, & Edelberg, 2001; Herman, Giladi, Gurevich, & Hausdorff, 2005; Hove, Suzuki, Uchitomi, Orimo, & Miyake, 2012; Marmelat, Delignieres, Torre, Beek, & Daffertshofer, 2014; Rhea, Kiefer, D'Andrea, Warren, & Aaron, 2014; Turcato, Godi, & Giardini, 2018; Wayne, Hausdorff, & Lough, 2015). Rather than being constrained to walk along an instrumented walkway, the performer wears a data collection device or transmitter and walks continuously in a

FIGURE 8.3

Pressure-sensitive insole for a left shoe. Sensors can be used to transmit stride time data to a nearby computer. This example product is manufactured by TekScan, Inc., South Boston, Massachusetts.

large open area or on a treadmill at a pace determined by the examiner. When Bluetooth technology is used, the performer must remain within range of the data collection device during walking. In a typical gait variability protocol, at least several hundred gait cycles are collected during a single trial. The total number of cycles collected is limited only by the data collection capacity of the equipment. Most commonly, the systems are used to capture a single gait parameter, namely, the duration of each gait cycle (i.e., the "stride time" or "stride-to-stride" interval). Given the large number of cycles collected, the temporal series of stride-to-stride intervals can be analyzed for both the amount and complexity of variability.

8.3.1.4 Inertial sensors

Commercially available inertial sensors (i.e., accelerometers) offer another user-worn equipment option for capturing long time series of kinematic gait characteristics. Depending on their design, inertial sensors are suitable for capturing data in clinic, laboratory, and/or natural "free-living" environments (Cavanaugh, Kochi, & Stergiou, 2010; Del Din, Galna, & Godfrey, 2017; Esser, Dawes, Collett, & Howells, 2013; Hausdorff, Hillel, & Shustak, 2018; Hollman et al., 2016; Ihlen, Weiss, Bourke, Helbostad, & Hausdorff, 2016; Warlop et al., 2017; Warlop, Detrembleur, Stoquart, Lejeune, & Jeanjean, 2018; Yu, Acharya, Lim, & Low, 2009). The anatomical placement (e.g., ankle, wrist, low back, and sternum) of the sensor and the gait parameter(s) selected for analysis depend on the device and protocol used. Unlike foot-switch systems used in gait variability analysis, many inertial sensors record data at a relatively high sampling frequency, allowing more precise measurement and potentially longer time series. In protocols involving free-living walking activity, inertial sensors can be used to capture how gait cycles accumulate naturally over time (e.g., daily steps taken; number of bouts of walking; intensity of walking activity). Given the large number of gait cycles recorded, accelerometer data also can be analyzed for both the amount and complexity of gait variability.

8.3.1.5 Three-dimensional motion capture systems

Due to their small data collection volumes, three-dimensional (3D) motion capture systems are best suited for the gait variability analysis of performers walking on a treadmill (Fig. 8.4) (Davies & Kurz, 2013; Estep, Morrison, Caswell, Ambegaonkar, & Cortes, 2018; Kaipust, McGrath, Mukherjee, & Stergiou, 2013; Karmakar, Khandoker, Begg, & Palaniswami, 2013; Kempski, Awad, Buchanan, Higginson, & Knarr, 2018; Powell, Blackmore, & Puppa, 2018; Raffalt et al., 2018; Zampeli et al., 2010). Performers are fitted with reflective markers placed on bony landmarks of interest, but otherwise are not encumbered by data collection equipment. As with typical measurement protocols using foot-switch systems, a performer walks for several minutes

FIGURE 8.4
Performer walking on a treadmill wearing reflective markers for three-dimensional (3D) motion capture data collection.

on the treadmill at a pace determined by the examiner until at least hundreds of gait cycles have been collected. Similar to inertial sensors, 3D motion capture systems permit a relatively wide variety of kinematic gait parameters to be calculated and operate at much higher sampling frequencies. Once again, given the large number of cycles collected, gait parameters of interest can be analyzed for both the amount and complexity of their variability.

8.3.1.6 Force plate systems

Similar to 3D motion capture systems, instrumented treadmills with embedded force plates can be used to collect gait cycle time series data at a high sampling frequency to produce a variety of kinematic (e.g., stride interval

and length, step interval and length) and/or kinetic (vertical ground reaction force) parameters (Jordan, Challis, & Newell, 2007; Marmelat, Torre, Beek, & Daffertshofer, 2014). Several minutes of continuous walking typically are used to collect hundreds of gait cycles, allowing for the analysis of both the amount and complexity of gait variability.

8.3.2 Selection of task demands and environmental conditions

The fundamental form of walking (i.e., forward progression at a comfortable pace along a straight path across an uncluttered, level, firm, surface) is the traditional focus of biomechanical gait analysis. Rehabilitation professionals and medical practitioners, however, increasingly are seeking to understand more than fundamental gait mechanics; their goal is to understand the extent to which a performer can adapt their walking. A thorough examination of walking, therefore, whether done for clinical or research purposes, should assess performance under a variety of task demands and environmental conditions (Table 8.3) (Earhart, 2013). Examples of alternative task demands include walking to the side or backward, slower or faster than preferred speed, along a curved path (e.g., turning or along a "figure of 8"), while looking side to side or up and down, with a narrow base of support (e.g., tandem walk), and with a secondary cognitive (e.g., counting backward from 100 by 7) or manual (e.g., carrying a cup of water or a tray) task. Examples of alternative environmental conditions include objects placed in the walking path, an inclined or compliant surface, and reduced lighting (e.g., eyes closed). Although not all combinations of task demand and environmental conditions may be feasible or safe for even healthy performers

Table 8.3 Task demands and environmental conditions for gait assessment.

	Fundamental form of walking	Options
Task demand		
Progression	Forward	Side-stepping, backward
Speed	Preferred	Slower, faster
Trajectory	Straight ahead	Curved
Head orientation	Straight ahead	Horizontal, vertical head motion
Base of support	Preferred	Narrow, wide
Secondary task	None	Cognitive, manual
Environmental condition		
Path	Clear	Obstacles
Incline	Flat	Uphill, downhill, and tilted
Surface	Firm	Compliant, uneven
Lighting	Well-lit	Dark

(e.g., tandem walking as fast as possible with eyes closed), when considered as a group the conditions mimic many of the task demands and environmental conditions common to daily adult walking. Virtual reality systems [e.g., Computer Assisted Rehabilitation Environment (CAREN)] also are utilized to combine several of the abovementioned constraints, immersing the performer in a variety of environments.

The array of demands and conditions featured in Table 8.3 has the potential to produce varying amounts and degrees of difficulty to affect the gait variability of a given performer. Demands and conditions typically are chosen based on a performer's health status, stage of learning, or the experimental design being employed. In addition, rehabilitation professionals and medical practitioners may be interested in evaluating performance under more demanding or constrained conditions when the goal is to assess the amount and complexity of gait variability emerging from system dynamics that may be operating closer to a relatively destabilized point of transition to a new, more effective gait pattern.

8.3.3 Analyzing the amount of gait variability

Mathematical tools used to analyze the amount of variability in a given gait parameter quantify how widely the data points collected during a given trial are dispersed around their mean value. Such tools commonly include the SD, coefficient of variation (CV) [i.e., the SD relative to the mean; CV], and range of values (James, 2004). The statistical assumption of these tools is that the parameter values in the time series are random, independent from one another (i.e., their time-evolving relationships over the course of the trial are irrelevant), and normally distributed. The tools are derived from a branch of mathematics known as linear statistical modeling, for which gait parameter values (i.e., the output of the system) eventually converge to a mean value, are assumed to be generally predictable, and are proportional to the contributions of their various underlying sources (i.e., physiologic systems, measurement error, etc.) (Katerndahl, 2005).

In practical terms, there are several considerations for applying linear tools to reliably quantify the amount of gait variability in a given trial. Perhaps most importantly, collecting relatively fewer gait cycles is associated with lower test–retest reliability. Indeed, many gait variability studies have produced reliability estimates from gait data collected in relatively short, discontinuous trials. As a result, reliability estimates have varied, depending on the gait parameter being analyzed, the equipment used to collect the data, performer gait speed, and sample characteristics (Byun, Han, Kim, & Kim, 2016; Faude, Donath, Roth, Fricker, & Zahner, 2012; Galna, Lord, & Rochester, 2013; Grimpampi et al., 2015; Hamacher, Hamacher, Taylor, Singh, & Schega,

2014; Hars, Herrmann, & Trombetti, 2013; Kiss, 2010; Konig, Singh, von Beckerath, Janke, & Taylor, 2014; Lord et al., 2011; Najafi, Helbostad, Moe-Nilssen, Zijlstra, & Aminian, 2009; Rennie et al., 2018; Riva, Bisi, & Stagni, 2014; Roche, Simon, & Guilmin-Crepon, 2018; Wittwer et al., 2013). For example, Hartmann, Luzi, Murer, de Bie, and de Bruin (2009) used discontinuous gait data to recommended a minimum of 20 m or 25 steps when using a triaxial accelerometer to assess step duration and step length variability in older adults. In contrast, Hollman et al. (2010) recommended collecting hundreds of strides to generate reliable estimates for the amount of gait velocity variability in healthy individuals. Step width variability has been found to be less reliable in younger adults than step length variability, but the reverse may be true in older adults (Almarwani et al., 2016). In older adults, meaningful change values, which are derived from test−retest reliability estimates, have varied with gait parameter (Brach et al., 2010). Reliability estimates under dual-task conditions have been comparable to single-task conditions (Hollman et al., 2010; Lord et al., 2011).

While best practice guidelines are not yet available, current literature suggests that as many strides as is practical should be collected from an individual performer to generate reliable estimates for the amount of variability in a given gait parameter. From a statistical perspective, at least 25 trials are recommended to generate reliable parameter estimates when single-subject data are collected in a discontinuous manner (i.e., in a series of short trials) (Bates, Dufek, & Davis, 1992; Dufek, Bates, & Davis, 1995). Pooling right and left step data to increase the number of data points entered into an SD or CV calculation is not recommended due to the possibility of underlying spatiotemporal asymmetries (Lord et al., 2011). Additional information is available to assist the interested reader with the development of standardized gait variability measurement protocols (Lord, Galna, & Rochester, 2013).

8.3.4 Analyzing the complexity of gait variability

Unlike tools derived from linear dynamics, tools derived from the mathematical field of nonlinear dynamics are used to describe the complex, time-evolving structure and organization of stride-to-stride fluctuations present in gait parameters collected during walking. As previously discussed, the complexity inherent in these fluctuations provides an indication of the interactions occurring among the underlying physiologic systems, task demands, and environmental constraints. There are a variety of complexity measures, which differ in their mathematic manipulation of the available time series. The algorithms are applied to time series data using computer programming languages such as Matlab (Mathworks, Natick, Massachusetts) or R (R Foundation for Statistical Computing, Vienna, Austria). Importantly,

no one measure provides a complete picture of complexity. The selection of a specific complexity measure depends on the clinical or research question under consideration and the number of data points available for the analysis of a given gait trial. Furthermore, the evidence of the test–retest reliability of nonlinear measures (and their accompanying minimal detectable change estimates) for human gait variability data is relatively scant in comparison to the reliability literature for linear measures. The following methods commonly have been applied to evaluate the complexity of gait variability. The featured methods, as well as others, are described elsewhere in greater detail (Stergiou, 2016; Stergiou et al., 2004).

8.3.4.1 Largest Lyapunov exponent

The largest LyE is a nonlinear measure used to quantify how the movement trajectories of the biomechanical variable under study are related with each other in time. It is best suited for gait data that are inherently periodic (e.g., continuous kinematic joint angle data). To calculate the LyE, the time series data first must be used to construct a "phase space" (or "phase plane") plot (Stergiou et al., 2004). Such plots define the behavior of a dynamic system in its "state space," that is, the space in which the system can be defined mathematically at any point. Phase space plots are created by plotting the value of each data point in the time series against at least one time-delayed copy. In a three-dimensional phase space plot (Fig. 8.5), each time series value is plotted against its first and second derivatives to produce a composite, time-evolving behavioral picture of (1) every parameter value produced by the dynamical system in its state space, (2) its change in value compared to the immediate neighboring value, and (3) the change in the change value from the previous change value. For purely sinusoidal and completely repeatable time series data, the phase space plot appears as a closed orbit with complete overlapping (i.e., no divergence) of the movement trajectories (Fig. 8.5, upper panel). The phase plot of data containing a complex temporal structure (e.g., data from a known time series that exhibits mathematical chaos) provides an elegant picture of approximately but not precisely overlapping trajectories that diverge in a specific organized fashion from one another (Fig. 8.5, center panel). The phase plot of the randomly sequenced data exhibits no clear pattern of evolving behavior and divergence is completely erratic (Fig. 8.5, lower panel).

In mathematical terms, the LyE is a measure of the exponential rate at which the nearby trajectories in the phase space plot diverge in state space. Specifically, LyE is calculated as the slope of the average logarithmic divergence of the neighboring trajectories. As nearby points separate, they diverge rapidly and produce instability. LyE requires more than 10,000 data points to calculate (Stergiou et al., 2004). Its values range from 0 (no divergence) to

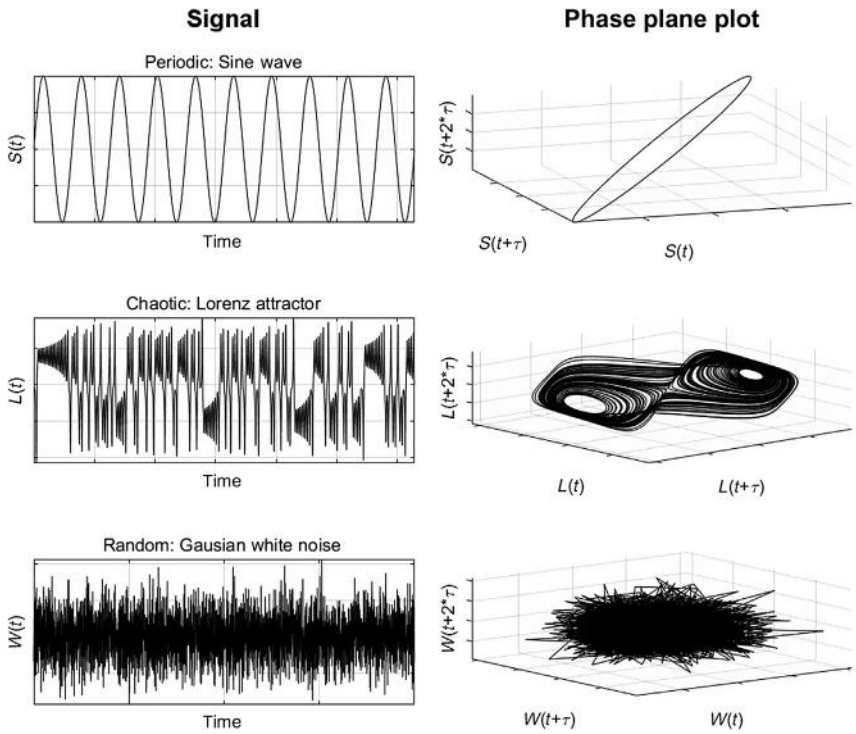

FIGURE 8.5

Periodic (*upper panel*), chaotic (*center panel*), and random (*lower panel*) time series from Fig. 8.1 and their corresponding three-dimensional phase space plots. LyE values were calculated using an algorithm developed by Wolf, Swift, Swinney, and Vastano (1985) and implemented using the Chaos Data Analyzer software (Sprott & Rowlands, 1995).

greater than 0.4 (rapid divergence). In DST terms, the periodic data sequence in the upper panel of Fig. 8.5 (LyE $\sim$ 0) could be interpreted as emerging from a noncomplex, rigidly stable dynamic system with no potential for adaptation; the randomly sequenced data in the lower panel (LyE $>$ 0.4) could be interpreted as emerging from a completely destabilized, noncomplex system, also with no potential for adaptation. The data with complex temporal structure ($0 <$ LyE $0 < 0.4$), however, could be interpreted as emerging from a stable yet flexible, complex, adaptive dynamic system.

In studies of human gait, LyE has been used to examine the sensitivity of the dynamical system to the types of small perturbations produced by the natural stride-to-stride fluctuations present in gait parameters. Given the large amount of data needed for calculation, LyE is best suited for data collected with 3D motion analysis equipment and inertial sensors, rather than

instrumented walkways, foot-switch systems, or force plates. This is not to say, however, that a large number of gait cycles are needed. For example, 7000 data points are produced with 35 gait cycles sampled at 180 Hz (Stergiou et al., 2004).

8.3.4.2 Approximate entropy

Approximate entropy (ApEn) is a nonlinear measure that quantifies the regularity (i.e., predictability) of the fluctuations present in a time series on a given time scale (Stergiou et al., 2004). Specifically, ApEn determines the probability that short sequences of consecutive values in the time series repeat, at least approximately, throughout the entire time series. In mathematical terms, ApEn is calculated as the logarithmic probability that a series of data points a certain distance apart will exhibit similar relative characteristics on the next incremental comparison within the state space. ApEn generates a unitless real number between 0 and 2, with zero values corresponding to maximum regularity (Fig. 8.5, upper panel) and values of 2 corresponding to maximum irregularity (i.e., randomness) (Fig. 8.5, lower panel). As with LyE, ApEn values at either extreme end of the scale (entirely predictable or random) indicate a relative lack of complexity in the time series, whereas values in the center of the scale indicate that the time series contains a complex pattern of fluctuation.

Several input parameters are needed to run the ApEn calculation: the length of the short sequence of points to be compared (m), a lag value indicating the separation of the points in the short sequence, an error tolerance (r) indicating the closeness of the match to other short sequences, and the total length of the time series (N). The number of data points needed for ApEn computations is typically between 50 and 5000. The relatively smaller size of the required data set makes ApEn practical for use with a variety of gait data types, from stride-to-stride intervals collected with foot-switch systems or inertial sensors to frequently sampled kinematic data collected with inertial sensor or 3D motion analysis systems.

One weakness of ApEn is that it can generate inconsistent results for a given time series over a range of m, r, and N values. Sample entropy (SampEn) is a related complexity measure which provides more consistent results than ApEn (Richman & Moorman, 2000). SampEn (m, r, N) is exactly equal to the negative logarithm of conditional probability that two sequences of similar m points remain similar at the next point, where self-matches are not included in calculating the probability. SampEn is largely independent of N values, displays relative consistency in circumstances where ApEn does not, and is better suited for shorter time series (Richman & Moorman, 2000; Yentes et al., 2013). Both ApEn and SampEn have been applied to various forms of gait cycle data, as will be illustrated in the next section.

8.3.4.3 Detrended fluctuation analysis

Unlike LyE and ApEn, which quantify the complexity of a time series on a given time scale, detrended fluctuation analysis (DFA) analyzes fractal-like (i.e., self-similar) relationships between patterns of fluctuation across progressively longer time scales (Cavanaugh et al., 2017). As a first step in DFA, a "random walk series" (i.e., cumulative sum series) is constructed by adding, in order, the value of each point in the original time series to the sum of all previous data points in a given trial. Next, the root mean square (RMS) of values in the random walk series is evaluated for its rate of growth over time as each new data point is added. When the data points in the original time series are uncorrelated, RMS values in the random walk series grow relatively slowly. When the data points in the original series are correlated to some extent (i.e., the value of a given point is dependent on the value of previous points), RMS values in the random walk series grow relatively more quickly. Because the statistical properties (e.g., mean, variance, autocorrelation, etc.) of many types of time series data are not constant, it is important to evaluate the rate of growth in RMS values above and beyond nonstationary trends. DFA, therefore, assesses the growth rate of detrended RMS values over many different time scales of measurement. The resulting detrended "fluctuation function" depicts what is called a power-law relationship between the rate of growth in RMS values and measurement scale. Statistical self-similarity is quantified using a scaling exponent, α, to estimate inherent long-range correlations within the time series over multiple time scales. A power-law exponent of 0.5 indicates a pattern of temporally uncorrelated fluctuations, whereas values anywhere in the range of 0.75−1.25 are commonly interpreted as indicating a self-similar, fractal-like pattern of positive correlations across time scales.

Similar to LyE and ApEn, DFA requires relatively large amounts of time series data to generate reliable estimates of its specific form of complexity. Previous studies of gait variability that employed DFA suggested that time series data collected from continuous walking of at least 600 strides are required (Damouras, Chang, Sejdic, & Chau, 2010) however, methods for using shorter time series have been proposed (Kuznetsov & Rhea, 2017; Pierrynowski et al., 2005). Like ApEn, DFA is practical for use with a variety of gait data types, from stride-to-stride intervals collected with foot-switch systems or inertial sensors to frequently sampled kinematic data collected with inertial sensor or 3D motion analysis systems.

Surrogation. Regardless of the chosen measure, an important procedure to ensure the validity of the nonlinear analysis is to compare the complexity value derived from a given gait parameter time series with the complexity value derived from a surrogate version that has been experimentally stripped of its temporal structure (Stergiou et al., 2004). Removing the inherent temporal structure is accomplished by randomizing the sequence of parameter values in the series, which when reentered into the nonlinear analysis procedure, should

return a value indicating the complete absence of complexity (i.e., entirely random sequences are not complex, as described earlier). Because the original and surrogate versions of the time series contain the same data points, albeit in different order, they should share the same mean, variance, and power spectra according to the algorithm used to perform the surrogation (Stergiou, 2016). Statistically significant differences in complexity between the original and surrogate time series validate that the gait parameter sequence in the original time series did not emerge randomly, and indeed, contained a sequential order that to some extent was determined by an underlying cause.

8.4 Examples from clinical research

The rapidly growing clinical research literature on gait variability contains studies that generally fall into one of two areas: (1) using gait variability as a clinical biomarker of aging or pathology, in some cases when a type 2 error is made with traditional diagnostic tools and (2) using gait variability as an outcome measure following a clinical intervention. In this section, we highlight examples from each clinical area simply to illustrate the selection of gait variability parameters, data collection equipment, and measurement protocols for various purposes. It is important to recognize that some older studies were published before contemporary understanding of the complex, adaptive human movement system had been fully articulated. The interested reader is encouraged to further explore and critically analyze the rapidly expanding literature, which includes many foundational studies of gait variability methodology and motor control and a large number of recent papers that improve our understanding of the reliability and validity of gait variability assessment.

8.4.1 Gait variability as a biomarker of aging or pathology

Here we highlight several studies that utilize analysis of gait variability as a biomarker of aging or pathology.

Wittwer, Webster, and Menz (2010) used an 8.3 m long instrumented mat to investigate changes in spatiotemporal gait characteristics over 1 year in community-dwelling people with Alzheimer's disease (AD) walking at their self-selected speed. Gait characteristics at baseline were compared with age-matched, healthy control participants. As part of the analysis, the authors applied CV and SD statistics to quantify the amount of variability in gait velocity, cadence, stride length, step time, double support time, and support base. Their results revealed that compared to healthy participants at baseline, the AD group had larger amounts of gait velocity, cadence, and step time variability. Over the subsequent year, stride length variability significantly increased in the AD group in comparison to baseline, concurrently with

decreased gait speed, decreased stride length, and increased double support time. Of all the gait performance declines, the largest effect size was found for the change in stride length variability.

Brach et al. (2005) used a 4 m instrumented walkway to examine associations between 12-month fall history and amount of gait variability, as measured by CV, in step width, step length, stance time, and step time in older adults walking at their self-selected speed. They were specifically interested in whether or not step width variability was associated with falls in highly mobile older persons as well as in those who walk slowly. Their results revealed that across the entire sample, the amount of gait variability for all parameters did not differ between participants who reported a fall and those who did not report a fall in the previous year. When stratifying the sample by gait speed, highly mobile individuals who walked >1.0 m/s and reported a fall had more variable step width than individuals who had not fallen. Furthermore, after controlling for age, gender, and gait speed, the highly mobile subset of participants who had extremely large or small amounts of step width variability were 4.38 (95% CI: 1.79−10.72) times more likely to report a fall in the past year than highly mobile individuals with moderate step width variability. In individuals who walked more slowly (<1.0 m/s), there was no association between step width variability and fall history.

In a prospective study of community-dwelling older adults, Hausdorff et al. (2001) examined the predictive validity of using the amount of gait variability to predict future falls over 1 year. Stride time and swing time data were collected at baseline with user-worn force-sensitive insoles during 6 minutes of walking at their normal pace. The amount of variability in stride time data was quantified using SD. The authors also examined the consistency of the magnitude of the SD across 20 segments of a normalized time series created by subtracting the mean of the time series from each data point. The results revealed a greater amount of stride time variability, swing time variability, and inconsistency of the SD variance among participants who reported falling over the course of the year compared to participants who reported not falling. The likelihood of falling was increased approximately fivefold with only a moderate increase in stride time variability. Importantly, fallers and nonfallers did not differ significantly with respect to demographic, health status, mental health, physical activity, or physical performance test measures. Gait parameters based on mean values rather than variability also were similar between those who reported and did not report falling. Increased stride time and swing time variability, in particular, were associated with many factors, including poor health status, lower mental status, diminished vitality, weakness, and decreased physical performance. The authors concluded that the amount of gait variability provided a sensitive "assay" of neurodynamic function that could be useful for detecting underlying disease.

In a related study, Herman et al. (2005) used measures of both the amount and complexity of variability to examine the altered, cautious gait of older adults without well-defined chronic disease, lower extremity impairment, or other peripheral dysfunction (i.e., individuals with "high-level gait disorder") in comparison to healthy participants. Participants walked over level ground wearing force-sensitive insoles for 2 minutes at their normal pace in a 25 m long hallway under usual lighting conditions. They were told to turn around and continue walking when they reached the end of the hallway. Stride time data were filtered to remove outliers greater or less than the median value of the time series (e.g., data collected during turns at the ends of the hallway). The amount of variability in stride time data was calculated using SD and CV. The complexity of gait variability was quantified using DFA. The results revealed that the amount of gait variability was significantly greater in older adults with cautious gait compared to healthy participants. Among participants with cautious gait, the amount of variability was significantly associated with a greater number of depressive symptoms and fear of falling but was not associated with a variety of demographic and clinical measures. Furthermore, among all measures collected, only the DFA fractal scaling index was significantly different between fallers and nonfallers.

Zampeli et al. (2010) compared the complexity of stride-to-stride variability of individuals with deficient anterior cruciate ligaments (ACLs) with healthy participants during backward walking on a treadmill. Knee angular displacement data were captured using 3D motion analysis technology at 100 Hz and LyE was used to quantify complexity. Each time series consisted of 12,000 unfiltered data points. The results revealed that the ACL-deficient knees of injured participants exhibited significantly lower ($P < .001$) LyE values (mean = 0.142) as compared to the healthy knees of control subjects (mean = 0.125). Similarly, the contralateral intact knees of patients with ACL injury also produced significantly lower LyE values as compared to the healthy participants ($P < .001$). Finally, the intact knees of ACL-deficient participants produced significantly lower LyE values compared to the ACL-deficient knees ($P = .01$) and healthy participant knees. The authors interpreted the results as indicating that individuals with ACL-deficient knees exhibit more rigid (i.e., less divergent, more periodic) kinematic patterns that had less capability of responding to perturbations and adapting to a changing environment. Moreover, the presence of relatively more rigid kinematic patterns in the contralateral, intact knee was consistent with previous studies of individuals who have more generalized difficulty adapting their lower extremity kinematic patterns following ACL injury (i.e., "noncopers").

Karmakar et al. (2013) compared the amount and complexity of minimum toe clearance (MTC) time series collected from healthy young, healthy elderly, and balance-impaired elderly at risk for falls walking on a treadmill

at a comfortable pace. MTC data were collected using a two-dimensional motion analysis system. SD was used to calculate the amount of variability in the MTC time series, while SampEn was used to calculate its complexity over a range of m and r values. The results revealed that the amount of variability in MTC increased significantly with aging and fall risk. For all values of m and r, the mean SampEn values were lower in the fall risk elderly group compared to the healthy young and healthy elderly groups and higher in the healthy young than in the healthy elderly group. Only the difference in mean SampEn values between healthy young and fall risk elderly groups was statistically significant. The authors concluded that although the amount of MTC variability increases with age, MTC regulation appears to remain intact with healthy aging, as indicated by the relatively automatic and less constrained gait of healthy elderly participants compared to the fall risk elderly group. They suggested that the disparate results between the amount and complexity of gait variability suggested that locomotor control with advanced age may be conceptually different from pathological conditions that produce balance impairments.

Cavanaugh et al. (2010) studied patterns of free-living ambulatory activity of community-dwelling older adults wearing an ankle-worn accelerometer for 2 weeks. The device recorded the number of strides taken in 1-minute intervals. In a post hoc analysis, participants were grouped according to their average daily number of steps taken: highly active (steps $\geq$ 10,000), moderately active (5000 $\leq$ steps $\leq$ 10,000), and inactive (steps $\leq$ 5000). The amount of variability in daily patterns of 1-minute step counts was quantified using CV. DFA and ApEn were used to examine the complexity of step count variability. The results revealed that whereas the amount of variability in 1-minute step counts was similar across the groups, highly active participants had more complex patterns of ambulatory activity than less active participants. The results were used to support the idea that the lower complexity of daily activity patterns in chronically inactive individuals might result in reduced ability to adapt walking function to various task demands and environmental conditions.

8.4.2 Gait variability as an outcome measure following intervention

Can the amount and complexity of gait variability be improved through intervention? Studies designed to answer this question have been published relatively recently and have focused on populations for which abnormal gait variability had been previously identified [e.g., older adults and individuals with Parkinson disease (PD)]. Taken together, these studies suggest that gait variability indeed can be positively influenced under certain intervention conditions.

Studies that have focused on reducing abnormally high amounts of gait variability generally have employed exercise-based interventions. For example, Beauchet et al. (2013) used a 12-week physical training program to demonstrate reductions in the amount (i.e., CV) of stride time variability of older adults walking alone but not when walking while counting backward from 50 or while enumerating animal names. Data were captured using a foot-switch system while participants walked along a 10 m walkway. Importantly, the results were apparent only in participants with relatively higher amounts of gait variability at baseline. Wang et al. (2015) used a 12-week combined strength, balance, and endurance exercise intervention to demonstrate significant reductions in the CV of stride time and length variability as recorded on an instrumented mat. Vergara-Diaz et al. (2018) used a 6-month Tai Chi intervention to demonstrate a trend toward reducing the amount (i.e., CV) of dual-task stride time variability in a small sample of individuals with early-stage PD. Data were collected using a foot-switch system as participants walked along a 15 m path. The results confirmed that the amount of dual-task stride time variability is a promising discriminating metric for predicting falls and understanding PD progression (Wayne et al., 2015).

Most studies to date that were designed to influence the complexity of gait variability employed a form of external rhythmical stimulation to alter gait dynamics. For example, Hove et al. (2012) measured the complexity of stride time variability in individuals with PD who walked under three rhythmic auditory stimulation (RAS) conditions: no auditory stimulus, fixed-tempo stimulus, and an interactive stimulus embedded with nonlinear temporal structure. Data were collected with a foot-switch system. The results revealed that the diminished baseline fractal scaling properties of gait dynamics were restored to healthy levels only with exposure to the interactive, nonlinear RAS. Interestingly, participants reported greater perceived stability when walking with the nonlinear RAS compared with a fixed-tempo RAS.

Kaipust et al. (2013) compared the effects of listening to white noise (i.e., a randomly organized stimulus), a complex rhythm based on mathematical chaos, a fixed-tempo metronome, and no auditory stimulation on the gait dynamics of young and elderly participants. Stride time, length, and step width data were collected using 3D motion analysis system as participants walked on a treadmill for 5 minutes. The results revealed that in comparison to white noise, fixed-tempo, or no stimulation, the complex stimulation produced the highest degree of fractal scaling in the older adult group. For younger adults, however, none of the stimulation conditions appeared to influence the complexity of gait variability. Conceptually similar results in healthy young adults have been found with fractal-based auditory cues (Marmelat et al., 2014), human paced walking stimulus (Marmelat et al., 2014), and a visual metronome stimulus (Rhea et al., 2014).

One exception to the trend in stimulation interventions was an exercise-based intervention employed by Gow et al. (2017), who studied the effect of a 6-month program of Tai Chi on the complexity of gait variability in older adults. Participants included individuals who were new to Tai Chi, those who had some expertise with Tai Chi, and a group of nonexercising older adults for comparison. Stride time data were collected using a foot-switch system as participants walked for 10 minutes in a hallway. DFA was used to quantify complexity of gait variability. Cross-sectional results revealed that the gait patterns of Tai Chi experts displayed a higher degree of complexity than naïve participants. Longitudinal results revealed a small but not statistically significant increase in the complexity of gait variability for Tai Chi participants compared to nonexercising participants. The authors concluded that Tai Chi is associated with healthy gait dynamics and that long-term Tai Chi training shows promise for helping to enhance the adaptability of physiologic systems. We speculate that the lack of significant increase in complexity is due to the fact that the Tai Chi intervention did not include specifically gait-related tasks. Compared to the more discrete, dynamic postural control movements of Tai Chi, gait involves more continuous movements that require ongoing adjustments by the neuromuscular system.

8.5 Future directions

The expanding clinical implications of gait variability analysis have paralleled contemporary developments in the understanding of the complex, adaptive human movement system. No longer is variability viewed solely in terms of its amount and as an error to be minimized or eliminated. Variability now is clearly recognized as having two distinct facets that provide complementary insights into gait production and execution. That being said, several important challenges will influence the future direction of gait variability implementation as a routine component of gait analysis. First, there remains no strong clinical evidence that restoring healthy levels of gait variability, either in terms of its amount or complexity, prepares individuals to cope more effectively with unpredictable changes in walking task demands or environmental conditions. Second, clinically expedient methods for collecting and analyzing long series of gait cycles are not routinely available in contemporary clinical practice settings. Finally, the psychometric properties of gait variability metrics (e.g., SD, CV, LyE, ApEn, SampEn, and DFA values) are not well understood. In particular, the responsiveness of parameters to change and what constitutes clinically meaningful change require elucidation. These challenges are not insignificant and will require the collective efforts of variability-minded biomechanists, gait analysts, and rehabilitation professionals to be overcome. Nevertheless, we are extremely optimistic that the

amount and complexity of gait variability will be widely valued in the future as a fundamental aspect of clinical evaluation, and that rapid improvements in biotechnologies soon will allow for the utilization of this approach in rudimentary fashion simply through the use of wearable devices.

References

Almarwani, M., Perera, S., VanSwearingen, J. M., Sparto, P. J., & Brach, J. S. (2016). The test–retest reliability and minimal detectable change of spatial and temporal gait variability during usual over-ground walking for younger and older adults. *Gait & Posture*, *44*, 94–99. Available from https://doi.org/10.1016/j.gaitpost.2015.11.014.

Bates, B. T., Dufek, J. S., & Davis, H. P. (1992). The effect of trial size on statistical power. *Medicine & Science in Sports & Exercise*, *24*(9), 1059–1065.

Beauchet, O., Launay, C., Annweiler, C., Fantino, B., Allali, G., & De Decker, L. (2013). Physical training-related changes in gait variability while single and dual tasking in older adults: Magnitude of gait variability at baseline matters. *European Journal of Physical and Rehabilitation Medicine*, *49*(6), 857–864. Available from https://doi.org/R33Y9999N00A0268, [pii].

Brach, J. S., Berlin, J. E., VanSwearingen, J. M., Newman, A. B., & Studenski, S. A. (2005). Too much or too little step width variability is associated with a fall history in older persons who walk at or near normal gait speed. *Journal of NeuroEngineering and Rehabilitation*, *2*, 21. Available from https://doi.org/1743-0003-2-21, [pii].

Brach, J. S., Perera, S., Studenski, S., Katz, M., Hall, C., & Verghese, J. (2010). Meaningful change in measures of gait variability in older adults. *Gait & Posture*, *31*(2), 175–179. Available from https://doi.org/10.1016/j.gaitpost.2009.10.002.

Byun, S., Han, J. W., Kim, T. H., & Kim, K. W. (2016). Test–retest reliability and concurrent validity of a single tri-axial accelerometer-based gait analysis in older adults with normal cognition. *PLoS One*, *11*(7), e0158956. Available from https://doi.org/10.1371/journal.pone.0158956.

Cavanaugh, J. T., Kelty-Stephen, D. G., & Stergiou, N. (2017). Multifractality, interactivity, and the adaptive capacity of the human movement system: A perspective for advancing the conceptual basis of neurologic physical therapy. *Journal of Neurologic Physical Therapy*, *41*(4), 245–251. Available from https://doi.org/10.1097/NPT.0000000000000199.

Cavanaugh, J. T., Kochi, N., & Stergiou, N. (2010). Nonlinear analysis of ambulatory activity patterns in community-dwelling older adults. *Journal of Gerontology Series A, Biological Sciences and Medical Sciences*, *65*(2), 197–203. Available from https://doi.org/10.1093/gerona/glp144.

Damouras, S., Chang, M. D., Sejdic, E., & Chau, T. (2010). An empirical examination of detrended fluctuation analysis for gait data. *Gait & Posture*, *31*(3), 336–340. Available from https://doi.org/10.1016/j.gaitpost.2009.12.002.

Davies, B. L., & Kurz, M. J. (2013). Children with cerebral palsy have greater stochastic features present in the variability of their gait kinematics. *Research in Developmental Disabilities*, *34*(11), 3648–3653. Available from https://doi.org/10.1016/j.ridd.2013.08.012.

Del Din, S., Galna, B., Godfrey, A., et al. (2017). Analysis of free-living gait in older adults with and without Parkinson's disease and with and without a history of falls: Identifying generic and disease specific characteristics. *Journal of Gerontology Series A, Biological Sciences and Medical Sciences*. Available from https://doi.org/10.1093/gerona/glx254.

Dufek, J. S., Bates, B. T., & Davis, H. P. (1995). The effect of trial size and variability on statistical power. *Medicine & Science in Sports & Exercise*, *27*(2), 288–295.

Earhart, G. M. (2013). Dynamic control of posture across locomotor tasks. *Movement Disorders*, *28*(11), 1501–1508. Available from https://doi.org/10.1002/mds.25592.

Esser, P., Dawes, H., Collett, J., & Howells, K. (2013). Insights into gait disorders: Walking variability using phase plot analysis, Parkinson's disease. *Gait & Posture*, *38*(4), 648–652. Available from https://doi.org/10.1016/j.gaitpost.2013.02.016.

Estep, A., Morrison, S., Caswell, S., Ambegaonkar, J., & Cortes, N. (2018). Differences in pattern of variability for lower extremity kinematics between walking and running. *Gait & Posture*, *60*, 111–115. Available from https://doi.org/S0966-6362(17)31017-2, [pii].

Faude, O., Donath, L., Roth, R., Fricker, L., & Zahner, L. (2012). Reliability of gait parameters during treadmill walking in community-dwelling healthy seniors. *Gait & Posture*, *36*(3), 444–448. Available from https://doi.org/10.1016/j.gaitpost.2012.04.003.

Gabell, A., & Nayak, U. S. (1984). The effect of age on variability in gait. *Journal of Gerontology*, *39*(6), 662–666.

Galna, B., Lord, S., & Rochester, L. (2013). Is gait variability reliable in older adults and Parkinson's disease? Towards an optimal testing protocol. *Gait & Posture*, *37*(4), 580–585. Available from https://doi.org/10.1016/j.gaitpost.2012.09.025.

Goldberger, A. L., Amaral, L. A., Hausdorff, J. M., Ivanov, P. C., Peng, C. K., & Stanley, H. E. (2002). Fractal dynamics in physiology: Alterations with disease and aging. *Proceedings of the National Academy of Sciences of the United States of America*, *99*(Suppl. 1), 2466–2472. Available from https://doi.org/10.1073/pnas.012579499.

Gow, B. J., Hausdorff, J. M., Manor, B., et al. (2017). Can tai chi training impact fractal stride time dynamics, an index of gait health, in older adults? Cross-sectional and randomized trial studies. *PLoS One*, *12*(10), e0186212. Available from https://doi.org/10.1371/journal.pone.0186212.

Grimpampi, E., Oesen, S., Halper, B., Hofmann, M., Wessner, B., & Mazza, C. (2015). Reliability of gait variability assessment in older individuals during a six-minute walk test. *Journal of Biomechanics*, *48*(15), 4185–4189. Available from https://doi.org/10.1016/j.jbiomech.2015.10.008.

Hamacher, D., Hamacher, D., Taylor, W. R., Singh, N. B., & Schega, L. (2014). Towards clinical application: Repetitive sensor position re-calibration for improved reliability of gait parameters. *Gait & Posture*, *39*(4), 1146–1148. Available from https://doi.org/10.1016/j.gaitpost.2014.01.020.

Harrison, S. J., & Stergiou, N. (2015). Complex adaptive behavior and dexterous action. *Nonlinear Dynamics, Psychology and Life Sciences*, *19*(4), 345–394.

Hars, M., Herrmann, F. R., & Trombetti, A. (2013). Reliability and minimal detectable change of gait variables in community-dwelling and hospitalized older fallers. *Gait & Posture*, *38*(4), 1010–1014. Available from https://doi.org/10.1016/j.gaitpost.2013.05.015.

Hartmann, A., Luzi, S., Murer, K., de Bie, R. A., & de Bruin, E. D. (2009). Concurrent validity of a trunk tri-axial accelerometer system for gait analysis in older adults. *Gait & Posture*, *29*(3), 444–448. Available from https://doi.org/10.1016/j.gaitpost.2008.11.003.

Hausdorff, J. M., Hillel, I., Shustak, S., et al. (2018). Everyday stepping quantity and quality among older adult fallers with and without mild cognitive impairment: Initial evidence for new motor markers of cognitive deficits? *Journal of Gerontology Series A, Biological Sciences and Medical Sciences*, *73*(8), 1078–1082. Available from https://doi.org/10.1093/gerona/glx187.

Hausdorff, J. M., Mitchell, S. L., Firtion, R., et al. (1997). Altered fractal dynamics of gait: Reduced stride-interval correlations with aging and Huntington's disease. *Journal of Applied Physiology (1985)*, *82*(1), 262–269. Available from https://doi.org/10.1152/jappl.1997.82.1.262.

Hausdorff, J. M., Rios, D. A., & Edelberg, H. K. (2001). Gait variability and fall risk in community-living older adults: A 1-year prospective study. *The Archives of Physical Medicine and Rehabilitation*, *82*(8), 1050–1056. Available from https://doi.org/S0003-9993(01)63215-5, [pii].

Herman, T., Giladi, N., Gurevich, T., & Hausdorff, J. M. (2005). Gait instability and fractal dynamics of older adults with a "cautious" gait: Why do certain older adults walk fearfully? *Gait & Posture*, *21*(2), 178–185. Available from https://doi.org/S0966636204000438, [pii].

Hess, R. J., Brach, J. S., Piva, S. R., & VanSwearingen, J. M. (2010). Walking skill can be assessed in older adults: Validity of the figure-of-8 walk test. *Physical Therapy*, *90*(1), 89–99. Available from https://doi.org/10.2522/ptj.20080121.

Hollman, J. H., Childs, K. B., McNeil, M. L., Mueller, A. C., Quilter, C. M., & Youdas, J. W. (2010). Number of strides required for reliable measurements of pace, rhythm and variability parameters of gait during normal and dual task walking in older individuals. *Gait & Posture*, *32*(1), 23–28. Available from https://doi.org/10.1016/j.gaitpost.2010.02.017.

Hollman, J. H., Watkins, M. K., Imhoff, A. C., Braun, C. E., Akervik, K. A., & Ness, D. K. (2016). Complexity, fractal dynamics and determinism in treadmill ambulation: Implications for clinical biomechanists. *Clinical Biomechanics (Bristol, Avon).*, *37*, 91–97. Available from https://doi.org/S0268-0033(16)30096-1, [pii].

Hove, M. J., Suzuki, K., Uchitomi, H., Orimo, S., & Miyake, Y. (2012). Interactive rhythmic auditory stimulation reinstates natural 1/f timing in gait of Parkinson's patients. *PLoS One.*, *7*(3), e32600. Available from https://doi.org/10.1371/journal.pone.0032600.

Ihlen, E. A. F., Weiss, A., Bourke, A., Helbostad, J. L., & Hausdorff, J. M. (2016). The complexity of daily life walking in older adult community-dwelling fallers and non-fallers. *Journal of Biomechanics*, *49*(9), 1420–1428. Available from https://doi.org/S0021-9290(16)30254-8, [pii].

James, C. (2004). Considerations of movement variability in biomechanics research. In N. Stergiou (Ed.), *Innovative analyses of human movement.* (pp. 29–62). Champaign, IL: Human Kinetics.

Jordan, K., Challis, J. H., & Newell, K. M. (2007). Walking speed influences on gait cycle variability. *Gait & Posture*, *26*(1), 128–134. Available from https://doi.org/S0966-6362(06)00184-6, [pii].

Kaipust, J. P., McGrath, D., Mukherjee, M., & Stergiou, N. (2013). Gait variability is altered in older adults when listening to auditory stimuli with differing temporal structures. *Annals of Biomedical Engineering*, *41*(8), 1595–1603. Available from https://doi.org/10.1007/s10439-012-0654-9.

Karmakar, C., Khandoker, A., Begg, R., & Palaniswami, M. (2013). Understanding ageing effects using complexity analysis of foot-ground clearance during walking. *Computer Methods in Biomechanics and Biomedical Engineering*, *16*(5), 554–564. Available from https://doi.org/10.1080/10255842.2011.628943.

Katerndahl, D. A. (2005). Is your practice really that predictable? Nonlinearity principles in family medicine. *Journal of Family Practice*, *54*(11), 970–977. Available from https://doi.org/jfp_1105_5411f, [pii].

Kempski, K., Awad, L. N., Buchanan, T. S., Higginson, J. S., & Knarr, B. A. (2018). Dynamic structure of lower limb joint angles during walking post-stroke. *Journal of Biomechanics*, *68*, 1–5. Available from https://doi.org/S0021-9290(17)30728-5, [pii].

Kiss, R. M. (2010). Effect of walking speed and severity of hip osteoarthritis on gait variability. *Journal of Electromyography and Kinesiology*, *20*(6), 1044–1051. Available from https://doi.org/10.1016/j.jelekin.2010.08.005.

Konig, N., Singh, N. B., von Beckerath, J., Janke, L., & Taylor, W. R. (2014). Is gait variability reliable? An assessment of spatio-temporal parameters of gait variability during continuous overground walking. *Gait & Posture*, *39*(1), 615–617. Available from https://doi.org/10.1016/j.gaitpost.2013.06.014.

Kuznetsov, N. A., & Rhea, C. K. (2017). Power considerations for the application of detrended fluctuation analysis in gait variability studies. *PLoS One*, *12*(3), e0174144. Available from https://doi.org/10.1371/journal.pone.0174144.

Lipsitz, L. A., & Goldberger, A. L. (1992). Loss of 'complexity' and aging. Potential applications of fractals and chaos theory to senescence. *JAMA*, *267*(13), 1806–1809.

Lord, S., Galna, B., & Rochester, L. (2013). Moving forward on gait measurement: Toward a more refined approach. *Movement Disorders*, *28*(11), 1534–1543. Available from https://doi.org/10.1002/mds.25545.

Lord, S., Howe, T., Greenland, J., Simpson, L., & Rochester, L. (2011). Gait variability in older adults: A structured review of testing protocol and clinimetric properties. *Gait & Posture*, *34*(4), 443–450. Available from https://doi.org/10.1016/j.gaitpost.2011.07.010.

Manor, B., & Lipsitz, L. A. (2013). Physiologic complexity and aging: Implications for physical function and rehabilitation. *Progress in Neuropsychopharmacology & Biological Psychiatry*, *45*, 287–293. Available from https://doi.org/10.1016/j.pnpbp.2012.08.020.

Marmelat, V., Delignieres, D., Torre, K., Beek, P. J., & Daffertshofer, A. (2014). 'Human paced' walking: Followers adopt stride time dynamics of leaders. *Neuroscience Letters*, *564*, 67–71. Available from https://doi.org/10.1016/j.neulet.2014.02.010.

Marmelat, V., Torre, K., Beek, P. J., & Daffertshofer, A. (2014). Persistent fluctuations in stride intervals under fractal auditory stimulation. *PLoS One*, *9*(3), e91949. Available from https://doi.org/10.1371/journal.pone.0091949.

Morrison, S., & Newell, K. M. (2015). Dimension and complexity in human movement and posture. *Nonlinear Dynamics, Psychology and Life Sciences*, *19*(4), 395–418.

Najafi, B., Helbostad, J. L., Moe-Nilssen, R., Zijlstra, W., & Aminian, K. (2009). Does walking strategy in older people change as a function of walking distance? *Gait & Posture*, *29*(2), 261–266. Available from https://doi.org/10.1016/j.gaitpost.2008.09.002.

Pathokinesiology Service and Physical Therapy Department. (2001). *Observational gait analysis* (4th ed.). Downey, CA: Los Amigos Research and Education Institute, Inc., Rancho Los Amigos National Rehabilitation Center.

Perry, J., & Burnfield, J. M. (2010). *Gait analysis, normal and pathological function* (2nd ed.). Thorofare, NJ: Charles B. Slack.

Pierrynowski, M. R., Gross, A., Miles, M., Galea, V., McLaughlin, L., & McPhee, C. (2005). Reliability of the long-range power-law correlations obtained from the bilateral stride intervals in asymptomatic volunteers whilst treadmill walking. *Gait & Posture*, *22*(1), 46–50. Available from https://doi.org/S0966-6362(04)00115-8, [pii].

Powell, D. W., Blackmore, S. E., Puppa, M., et al. (2018). Deep brain stimulation enhances movement complexity during gait in individuals with Parkinson's disease. *Neuroscience Letters*. Available from https://doi.org/S0304-3940(18)30337-9, [pii].

Raffalt, P. C., Alkjaer, T., Brynjolfsson, B., Jorgensen, L., Bartholdy, C., & Henriksen, M. (2018). Day-to-day reliability of nonlinear methods to assess walking dynamics. *Journal of Biomechanical Engineering*, *140*(12), 10. Available from https://doi.org/10.1115/1.4041044.

Rennie, L., Lofgren, N., Moe-Nilssen, R., Opheim, A., Dietrichs, E., & Franzen, E. (2018). The reliability of gait variability measures for individuals with Parkinson's disease and healthy older adults—The effect of gait speed. *Gait & Posture*, *62*, 505–509. Available from https://doi.org/S0966-6362(18)30352-7, [pii].

Rhea, C. K., Kiefer, A. W., D'Andrea, S. E., Warren, W. H., & Aaron, R. K. (2014). Entrainment to a real time fractal visual stimulus modulates fractal gait dynamics. *Human Movement Science*, *36*, 20–34. Available from https://doi.org/10.1016/j.humov.2014.04.006.

Richman, J. S., & Moorman, J. R. (2000). Physiological time-series analysis using approximate entropy and sample entropy. *American Journal of Physiology-Heart and Circulatory Physiology*, *278*(6), 2039. Available from https://doi.org/10.1152/ajpheart.2000.278.6.H2039.

Rickles, D., Hawe, P., & Shiell, A. (2007). A simple guide to chaos and complexity. *Journal of Epidemiology and Community Health*, *61*(11), 933–937. Available from https://doi.org/61/11/933, [pii].

Riva, F., Bisi, M. C., & Stagni, R. (2014). Gait variability and stability measures: Minimum number of strides and within-session reliability. *Computers in Biology and Medicine*, *50*, 9–13. Available from https://doi.org/10.1016/j.compbiomed.2014.04.001.

Roche, B., Simon, A. L., Guilmin-Crepon, S., et al. (2018). Test–retest reliability of an instrumented electronic walkway system (GAITRite) for the measurement of spatio-temporal gait parameters in young patients with Friedreich's ataxia. *Gait & Posture*, *66*, 45–50. Available from https://doi.org/S0966-6362(18)31429-2, [pii].

Rosano, C., Brach, J., Studenski, S., Longstreth, W. T., Jr, & Newman, A. B. (2007). Gait variability is associated with subclinical brain vascular abnormalities in high-functioning older adults. *Neuroepidemiology.*, *29*(3-4), 193–200. Available from https://doi.org/000111582, [pii].

Schmidt, R. A. (2003). Motor schema theory after 27 years: Reflections and implications for a new theory. *Research Quarterly for Exercise and Sport*, *74*(4), 366–375. Available from https://doi.org/10.1080/02701367.2003.10609106.

Schmidt, R. A., Zelaznik, H., Hawkins, B., Frank, J. S., & Quinn, J. T., Jr. (1979). Motor-output variability: A theory for the accuracy of rapid motor acts. *Psychological Review*, *47*(5), 415–451.

Shumway-Cook, A., Baldwin, M., Polissar, N. L., & Gruber, W. (1997). Predicting the probability for falls in community-dwelling older adults. *Physical Therapy*, *77*(8), 812–819.

Shumway-Cook, A., Taylor, C. S., Matsuda, P. N., Studer, M. T., & Whetten, B. K. (2013). Expanding the scoring system for the dynamic gait index. *Physical Therapy*, *93*(11), 1493–1506. Available from https://doi.org/10.2522/ptj.20130035.

Smith, E., Cusack, T., Cunningham, C., & Blake, C. (2017). The influence of a cognitive dual task on the gait parameters of healthy older adults: A systematic review and meta-analysis. *Journal of Aging and Physical Activity*, *25*(4), 671–686. Available from https://doi.org/10.1123/japa.2016-0265.

Sprott, J. C., & Rowlands, G. (1995). *Chaos data analyzer*. New York: American Institute of Physics.

Stergiou, N. (2016). *Nonlinear analysis for human movement variability*. Boca Raton, FL: CRC Press.

Stergiou, N., Buzzi, U. H., Kurz, M. J., & Heidel, J. (2004). Nonlinear tools in human movement. In N. Stergiou (Ed.), *Innovative analyses of human movement*. (pp. 63–90). Champaign, IL: Human Kinetics.

Stergiou, N., Harbourne, R., & Cavanaugh, J. (2006). Optimal movement variability: A new theoretical perspective for neurologic physical therapy. *Journal of Neurologic Physical Therapy*, *30*(3), 120–129.

Tamburini, P., Storm, F., Buckley, C., Bisi, M. C., Stagni, R., & Mazza, C. (2018). Moving from laboratory to real life conditions: Influence on the assessment of variability and stability of gait. *Gait & Posture*, *59*, 248–252. Available from https://doi.org/S0966-6362(17)30981-5, [pii].

Turcato, A. M., Godi, M., Giardini, M., et al. (2018). Abnormal gait pattern emerges during curved trajectories in high-functioning Parkinsonian patients walking in line at normal speed. *PLoS One.*, *13*(5), e0197264. Available from https://doi.org/10.1371/journal.pone.0197264.

Vaillancourt, D. E., & Newell, K. M. (2002). Changing complexity in human behavior and physiology through aging and disease. *Neurobiology of Aging*, *23*(1), 1–11. Available from https://doi.org/S0197458001002470, [pii].

Vergara-Diaz, G., Osypiuk, K., Hausdorff, J. M., et al. (2018). Tai chi for reducing dual-task gait variability, a potential mediator of fall risk in Parkinson's disease: A pilot randomized controlled trial. *Global Advances in Health and Medicine*, *7*. Available from https://doi.org/10.1177/2164956118775385, 2164956118775385.

Verghese, J., Holtzer, R., Lipton, R. B., & Wang, C. (2009). Quantitative gait markers and incident fall risk in older adults. *The Journal of Gerontology Series A, Biological Sciences and Medical Sciences*, *64*(8), 896–901. Available from https://doi.org/10.1093/gerona/glp033.

Wang, R. Y., Wang, Y. L., Cheng, F. Y., Chao, Y. H., Chen, C. L., & Yang, Y. R. (2015). Effects of combined exercise on gait variability in community-dwelling older adults. *Age (Dordrecht, The Netherlands).*, *37*(3), 2. Available from https://doi.org/10.1007/s11357-015-9780-2, Epub 2015 Apr 25.

Warlop, T., Detrembleur, C., Buxes Lopez, M., Stoquart, G., Lejeune, T., & Jeanjean, A. (2017). Does Nordic walking restore the temporal organization of gait variability in Parkinson's disease? *Journal of Neuroengineering and Rehabilitation*, *14*(1), 1. Available from https://doi.org/10.1186/s12984-017-0226-1.

Warlop, T., Detrembleur, C., Stoquart, G., Lejeune, T., & Jeanjean, A. (2018). Gait complexity and regularity are differently modulated by treadmill walking in Parkinson's disease and healthy population. *Frontiers in Physiology*, *9*, 68. Available from https://doi.org/10.3389/fphys.2018.00068.

Warren, W. H. (2006). The dynamics of perception and action. *Psychological Review*, *113*(2), 358–389. Available from https://doi.org/2006-04733-006, [pii].

Wayne, P. M., Hausdorff, J. M., Lough, M., et al. (2015). Tai chi training may reduce dual task gait variability, a potential mediator of fall risk, in healthy older adults: Cross-sectional and randomized trial studies. *Frontiers in Human Neuroscience*, *9*, 332. Available from https://doi.org/10.3389/fnhum.2015.00332.

Winter, D. A. (1983). Biomechanical motor patterns in normal walking. *Journal of Motor Behavior*, *15*(4), 302–330.

Wittwer, J. E., Webster, K. E., & Hill, K. (2013). Reproducibility of gait variability measures in people with Alzheimer's disease. *Gait & Posture*, *38*(3), 507–510. Available from https://doi.org/10.1016/j.gaitpost.2013.01.021.

Wittwer, J. E., Webster, K. E., & Menz, H. B. (2010). A longitudinal study of measures of walking in people with Alzheimer's disease. *Gait & Posture*, *32*(1), 113–117. Available from https://doi.org/10.1016/j.gaitpost.2010.04.001.

Wolf, A., Swift, J. B., Swinney, H. L., & Vastano, J. A. (1985). Determining Lyapunov exponents from a time series. *Physica D: Nonlinear Phenomena*, *16*(3), 285–317. Available from https://doi.org/10.1016/0167-2789(85)90011-9. Available from http://www.sciencedirect.com/science/article/pii/0167278985900119.

Wolfson, L., Whipple, R., Amerman, P., & Tobin, J. N. (1990). Gait assessment in the elderly: A gait abnormality rating scale and its relation to falls. *Journal of Gerontology*, *45*(1), 12.

Wrisley, D. M., Marchetti, G. F., Kuharsky, D. K., & Whitney, S. L. (2004). Reliability, internal consistency, and validity of data obtained with the functional gait assessment. *Physical Therapy, 84*(10), 906–918.

Yentes, J. M., Hunt, N., Schmid, K. K., Kaipust, J. P., McGrath, D., & Stergiou, N. (2013). The appropriate use of approximate entropy and sample entropy with short data sets. *Annals of Biomedical Engineering, 41*(2), 349–365. Available from https://doi.org/10.1007/s10439-012-0668-3.

Yu, W. W., Acharya, U. R., Lim, T. C., & Low, H. W. (2009). Non-linear analysis of body responses to functional electrical stimulation on hemiplegic subjects. *Proceedings of the Institution of Mechanical Engineers, Part H., 223*(6), 653–662. Available from https://doi.org/10.1243/09544119JEIM535.

Zampeli, F., Moraiti, C. O., Xergia, S., Tsiaras, V. A., Stergiou, N., & Georgoulis, A. D. (2010). Stride-to-stride variability is altered during backward walking in anterior cruciate ligament deficient patients. *Clinical Biomechanics (Bristol, Avon)., 25*(10), 1037–1041. Available from https://doi.org/10.1016/j.clinbiomech.2010.07.015.

CHAPTER 9

Coordination and control: a dynamical systems approach to the analysis of human gait

Aaron D. Likens and Nick Stergiou
University of Nebraska at Omaha, Omaha, NE, United States

The entire creation is synthesized by essence and attributes, and has the need of Divine Providence, because it is not free of variability

Saint Maximus the Confessor (580–662)

CONTENTS

9.1 Introduction

Coordination is defined as the mastery of the overwhelming number of degrees of freedom inherent to the human neuromuscular system, while healthy patterns of functional movement are thought to emerge from the skillful organization of these degrees of freedom (Bernstein, 1967; Turvey, 1990; Turvey, Fitch, & Tuller, 1982). These powerfully general ideas have led to the introduction and application of dynamical systems theory (DST) as a general approach to movement science (Haken, Kelso, & Bunz, 1985; Kelso, 1995; Kugler & Turvey, 1987; Stergiou, 2004, 2016; Thelen & Smith, 1994). There are many advantages to undertaking the DST approach to the analysis of human movement. Notably, the DST approach often simplifies the task of selecting and analyzing the "correct" multidimensional biomechanical variables measured during activities such as walking and running. Simplification comes from focusing on the so-called *collective variables*, low-dimensional variables that capture the overall state of a system (Gilmore, 1981; Kelso, 1995), rather than on the vast number of biomechanical variables used in more traditional lines of research (Hamill & Knutzen, 2009). This chapter explores this and other benefits of a DST approach to human gait and its application to clinical populations.

The remainder of this chapter is organized into four main sections. In Section 9.2, we discuss eight hallmark properties of a dynamical system and their identifying features in human movement. In Section 9.3, we cover

Biomechanics and Gait Analysis. DOI: https://doi.org/10.1016/B978-0-12-813372-9.00009-9

practical matters in applying DST to the study of gait, including details about computations and recent developments. In Section 9.4, we present two examples from the literature that highlight the generality of the DST approach in applying DST in clinical settings. Finally, Section 9.5 presents a brief chapter summary along with concluding remarks and some suggestions for future research in this area.

9.2 Hallmark properties of a dynamical system

Early work on DST often focused on identifying a set of particular features expected to be observed from dynamical systems (Gilmore, 1981; Thelen & Smith, 1994; Thelen, Ulrich, & Wolff, 1991). We have found these early treatments invaluable in thinking about human movement from a DST perspective. In particular, those and other authors set forth a formula for applying DST to problems as diverse as engineering and development of locomotion in infants. The formula involves the identification and study of several key features that signal the presence and behavior of a dynamical system. This section presents eight such hallmark characteristics, both in the abstract and (especially) with specific application to movement. Doing so develops a vocabulary often missing from the contemporary application of the dynamical systems analysis toolbox. This vocabulary provides the bedrock for applying and interpreting DST within the context of human movement.

The following section largely describes these hallmark properties within the context of a prominent model of bimanual coordination known as the Haken–Kelso–Bunz (HKB) model (Haken et al., 1985). This approach was chosen for a few reasons. First, the HKB model stands as the prime example for applying the DST framework to the study of human movement. Second, the HKB model is quite general in that it describes rhythmic patterns of coordination that bear similarity to those involved in walking (Diedrich & Warren, 1995; Kelso, 1995; Kugler & Turvey, 1987; Kurz & Stergiou, 2004a; Russell, Haworth, & Martinez-Garza, 2016; Thelen et al., 1991; Turvey, 1990). Lastly, the coordinated patterns inherent to the HKB model are relatively simple, making them concrete candidates to discuss otherwise abstract and difficult concepts.

9.2.1 State space

The state space is the fundamental property of a dynamical system because it represents the space in which dynamics unfold over time and trace out a trajectory. Simply stated, a *state space* is a coordinate system (e.g., Cartesian, polar), whose axes are defined by the collective variables that capture the moment-by-moment state of a system. *Collective variables* are

one-dimensional variables that capture the overall state of a potentially complicated system. A classic example from the motor coordination literature helps solidify these concepts (Haken et al., 1985; Kelso, 1984, 1995) and build a foundation to introduce other important DST concepts. Imagine arranging and rhythmically moving one's fingers in the transverse plane as depicted by the curved arrows in Fig. 9.1A. This rhythmic pattern of coordination can be captured with a single collective variable, ϕ, which represents the relative phasing of the fingers throughout their respective cycles. When $\phi = 0$ degrees, this represents the symmetric (i.e., inphase) activation of homologous muscles across the limbs (Fig. 9.1A). When $\phi = 180$ degrees or -180 degrees, this indicates an antisymmetric (i.e., antiphase) pattern of coordination (Fig. 9.1B). Note that the inphase/antiphase relationship distinctions refer to muscle activation and not the spatial relationship. There are a vast number of neuromuscular degrees of freedom that must be controlled in order to perform even this seemingly simple pattern of coordination (Bernstein, 1967; Turvey, 1990; Turvey et al., 1982). Remarkably, though, this one-dimensional collective variable, ϕ, captures these complex system

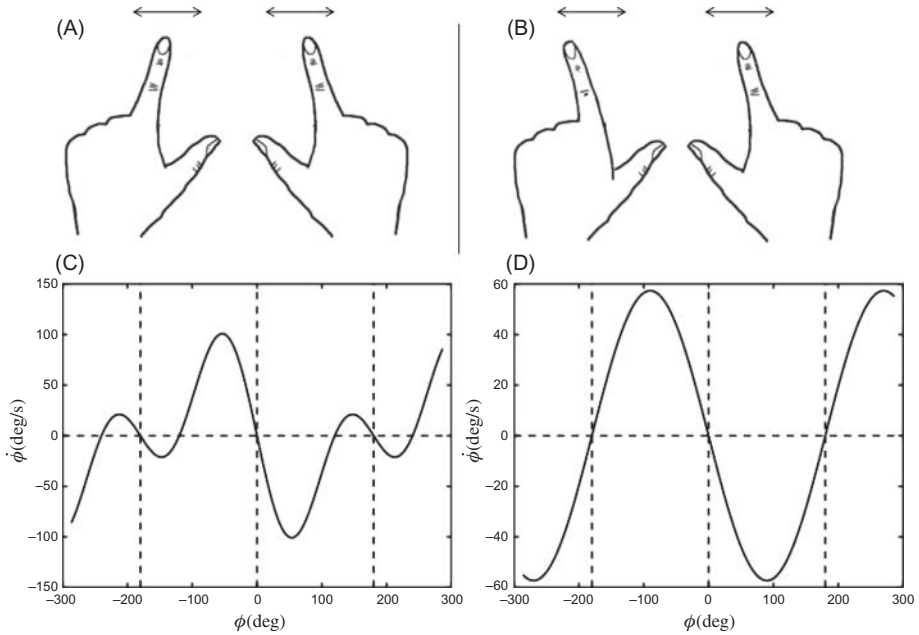

FIGURE 9.1

(A) Inphase preparation of fingers in bimanual coordination task. (B) Antiphase preparation of fingers in a bimanual coordination task. (C) Phase portrait derived from the Haken—Kelso—Bunz (HKB) model when fingers are oscillating at a slow frequency. (D) Phase portrait derived from the HKB model when the fingers are oscillating at collective frequency beyond the critical value.

dynamics. A full appreciation of ϕ as a suitable collective variable for rhythmic bimanual coordination follows from examining the predictions of a now famous and successful model of interlimb coordination, known as the HKB model (Amazeen, Amazeen, & Turvey, 1998; Haken et al., 1985). In what follows, we present the model graphically to reduce the technical burden on the reader but point to foundational references for more detailed and technical treatments (Amazeen et al., 1998; Haken et al., 1985).

Perhaps the most used concept from DST is the concept of a stable state or *attractor*. Attractors take on many forms and reflect the tendency for a system to behave in certain, bounded ways. The simplest form is a *point attractor* or stable *set point* and describes a system whose collective variable tends toward a specific value over time. An illustration of this behavior appears in Fig. 9.1C. This graph, called a *phase portrait* or *phase plane*, is framed by the collective variable on the horizontal axis and its velocity on the vertical axis (Rosen, 1970). The use of phase portraits in depicting dynamical systems originates in the fact that dynamical systems are modeled by differential equations; however, phase portraits are often used to study processes like human locomotion where the governing equations may be unknown. Here we have constructed a phase portrait using ϕ and its velocity, $d\phi/dt$ as related in the HKB model referenced above (Haken et al., 1985). In the vicinity of $\phi = 0$ degrees, the slope of the line is negative. This means that $d\phi/dt$ is positive when immediately to the left of $\phi = 0$ degrees, which pushes the system toward $\phi = 0$ degrees. Similarly, a negative velocity to the right of $\phi = 0$ degrees implies that the system is pulled back toward that value. In short, the system is attracted to $\phi = 0$ degrees; $\phi = 0$ degrees is an attractor of the system, with the slope of the line at the zero crossing being proportional to the strength of attraction. Other prototypical attractors such as *limit cycle attractors* (Fig. 9.2B) and *strange/chaotic attractors* (Fig. 9.2C) are also commonly discussed within the context of movement (Kelso, 1995; Kugler & Turvey, 1987; Stergiou, 2004).

The *limit cycle attractor* captures periodic forms of behavior and has been frequently used to model movement of lower limb segments involved in human locomotion such as walking and running (Clark & Phillips, 1993; Kelso, 1995; Kugler & Turvey, 1987; Stergiou, Jensen, Bates, Scholten, & Tzetzis, 2001; Stergiou, Scholten, Jensen, & Blanke, 2001; Whitall & Getchell, 1995; Winstein & Garfinkel, 1989). A simple example of a limit cycle involves a sinusoidal signal. Fig. 9.2A depicts the phase portrait obtained by plotting $\sin(x)$ with a period of $0.5/\pi$ against its first derivative. The result is the unit circle and implies that the system described by this phase portrait is attracted to the set of points circumscribed by the circle. As will become evident in Section 9.3, limit cycles are especially important in the study of human locomotion as they characterize the rhythmic movement of limb

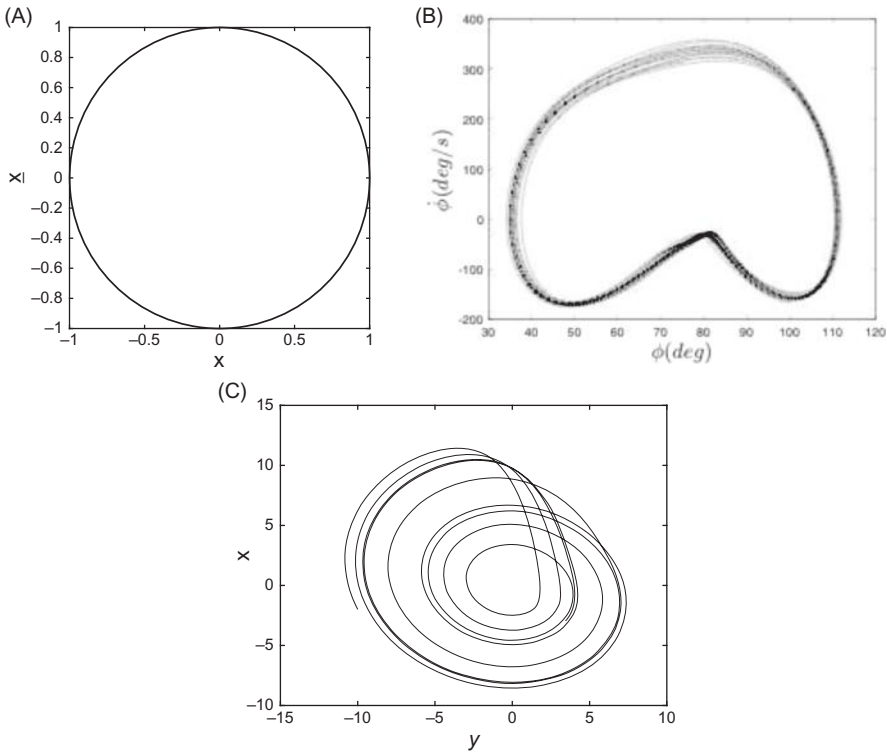

FIGURE 9.2

(A) Phase portrait of a simple sinusoid. The horizontal axis has arbitrary units and the vertical axis depicts its time derivative. (B) Phase portrait of a lower limb segment captured from several walking cycles on a treadmill. (C) Simulation of a strange attractor, the Rössler equation, projected into the x—y plane. Panel (C) also has arbitrary units.

segments. In fact, the HKB model itself is a model of two coupled limit cycle oscillators. As a preview, Fig. 9.2B depicts the phase portrait formed from the lower limb of a healthy adult during several walking cycles. From this picture, it is easy to appreciate an essential feature of a limit cycle, namely, that its trajectory is attracted to specific regions of state space. *Strange attractors*, like the one depicted in Fig. 9.2C, at first glance, seem similar to a limit cycle in that they are bounded and appear to orbit around some region of state space. A principal difference between these attractor types relates to the idea of *equifinality*. For a range of initial conditions, systems that exhibit equifinality tend toward the same pattern over time. Systems with point attractors and limit cycles exhibit this property, that is, point attractors tend toward a single value and limit cycles tend toward a set of points in state space. When perturbed by external noise, these systems return to their attractive state.

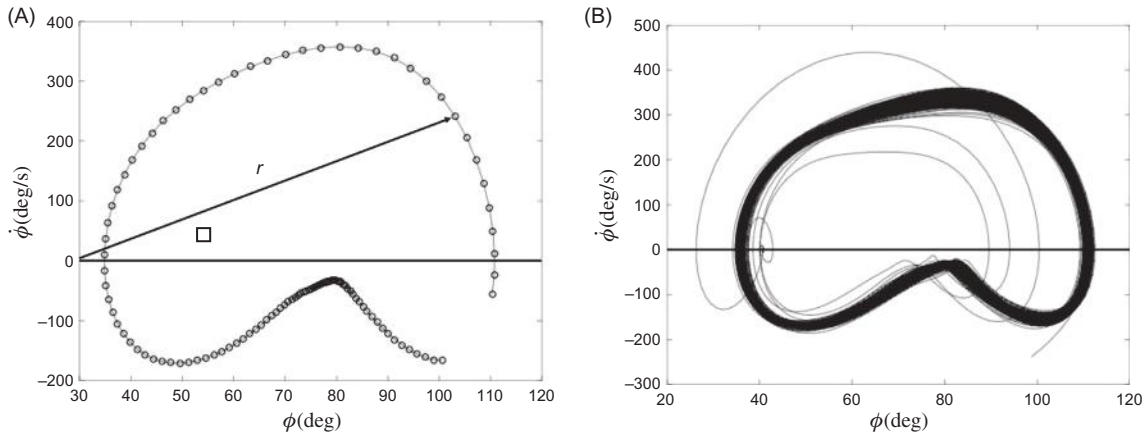

FIGURE 9.3

(A) Demonstration of right thigh phase angle calculation for approximately one stride of treadmill walking. The phase portrait traces out its trajectory in a clockwise fashion. (B) Phase portrait of right thigh angle over several cycles of treadmill walking. Deviations from limit cycle behavior resulted from a brief halt of the treadmill belts.

Fig. 9.3B provides an example of this behavior involving treadmill walking. That figure depicts the phase portrait from a single participant while talking on a treadmill. Similar to the phase portrait depicted in Fig. 9.2B, the limit cycle behavior is evident from the concentration of trajectories in what appears to be a closed orbit; however, Fig. 9.3B also shows that a few orbits deviate from the typical pattern. These trajectories originated from a brief stall of the treadmill belt, providing a mechanical perturbation. Evident from this graph is that, although gait trajectory temporarily deviates from its limit cycle behavior after perturbation, it gradually returns to its attractor as the walker overcomes the perturbation and stabilizes their gait.

In contrast, systems with chaotic attractors are sensitive to initial conditions, meaning that even small differences in initial conditions result in the system tracing out very different trajectories in state space. This sensitivity to initial conditions gives strange attractors the complicated trajectories demonstrated in Fig. 9.2C, the phase portrait of a system known to possess a strange attractor, the so-called Rössler system (Rössler, 1976). A natural question to ask is: Can systems have more than one attractor? This answer to this question leads to a discussion of the *modality* and *inaccessibility*.

9.2.2 Modality, inaccessibility, and sudden jumps

Modality refers to the observation that dynamical systems may have two or more attractors (Gilmore, 1981). This property is evident from the phase portrait found in Fig. 9.1C. The preceding section noted that the HKB model

possessed an inphase attractor at $\phi = 0$ degrees, and this was apparent from the negatively sloped zero crossing at that point (Haken et al., 1985). Further examination of Fig. 9.1C reveals additional negative zero crossings at $\phi = 180$ degrees and -180 degrees (symmetry is a property of the HKB model), implying that the modeled system is also attracted to an antiphase pattern of coordination. The sign of ϕ simply refers to which finger leads the other in their respective cycles. In addition, there are many values of the collective variable that are *inaccessible* to the system, that is, there are many values of the collective variable in which the system does not reside.

Importantly, the presence of two or more attractors often depends on the particular value of a *control parameter* (Gilmore, 1981). Conceptually similar to an independent variable, control parameters alter the dynamics a given system exhibits, often in a discontinuous way. In the HKB system (Haken et al., 1985), the control parameter is the collective frequency of finger oscillation. At low movement frequencies, both $\phi = 0$ degrees and $\phi = 180$ degrees are stable attractors; however, at higher frequencies, the negative zero crossing at $\phi = 180$ degrees disappears and becomes a positive zero crossing, implying that $\phi = 180$ degrees is no longer a stable state in bimanual coordination. In DST terminology, tuning the control parameter to some *critical value* results in a *phase transition* or *sudden jump*, a sudden, discrete change in the collective variable. What, though, might the interpretation be of positively sloped zero crossings like those observed in Fig. 9.1C and D? Positively sloped zero crossings are evidence of a *repellor*, that is, a single point in state space from which the system diverges over time. Similar to attractors, this behavior may be understood from characterizing the velocity profile in the phase portrait near the location of a repellor. Fig. 9.1D depicts the phase portrait of the HKB (Haken et al., 1985) model after having undergone a phase transition. Note that $d\phi/dt$ is positive to the right of $\phi = 180$ degrees and negative to the left of the attractor, both pushing the system toward the only remaining stable attractor, the inphase attractor at $\phi = 0$ degrees (Vignette 9.1).

9.2.3 Divergence

Every attractor (e.g., $\phi = 0$ degrees and $\phi = 180$ degrees) has an associated *basin of attraction*, a region of state space in which all initial conditions converge to a single attractor. These regions are delineated in Fig. 9.1C by the positively sloped zero crossings. The repellor implied by the positive slope that separates the attractors at $\phi = 180$ degrees and $\phi = 0$ degrees acts as a *separatrix*, defining each attractor's basin of attraction. This separatrix simultaneously defines the property of *divergence*. Trajectories that are initially very close to one another may rapidly separate over time as each trajectory converges toward its respective attractor.

VIGNETTE 9.1 A simple experiment to try yourself.

The hallmark properties of dynamical systems are frequently observed in laboratory settings and in everyday life. We encourage the reader to take part in a simple experiment that has become a bit of a party trick for DST practitioners. Place your hands flat on a table in front of you in the antiphase configuration depicted in Fig. 9.1B. Next, at some slow frequency (<1 Hz), begin laterally oscillating each finger at the same speed while maintaining this antiphase configuration. Over the course of several seconds, gradually increase the frequency of finger oscillations. At some critical frequency of oscillation, you may find it difficult to maintain this antiphase pattern. If so, no longer attempt to maintain the antiphase pattern but keep oscillating your fingers. The expected result is that you will shift to an inphase coordination pattern. That is, you will have tuned a control parameter (movement frequency) to some critical value, resulting in a nonlinear phase transition to a stable attractive state.

9.2.4 Critical fluctuations, critical slowing down, and hysteresis

The development of the HKB model was largely motivated by the empirical observation of phase transitions in bimanual coordination tasks like those described in Section 9.2.1. Three other hallmark DST properties aid in the detection of phase transitions in other patterns of coordination as well. *Critical fluctuations* are instabilities that arise from a weakening attractor (e.g., HKB phase transition). Empirically, critical fluctuations are revealed by incrementally increasing a control parameter and looking for increases in the variability of the collective variable. In empirical tests of the HKB model (Haken et al., 1985; Kelso, 1995), procedures like those in Section 9.2.2 reveal increases in the standard deviation of ϕ just prior to the phase transition from $\phi = 180$ degrees to $\phi = 0$ degrees. Weakening of attractors near phase transitions has another consequence, the appearance of *critical slowing down* (Scholz, Kelso, & Schöner, 1987). This refers to the fact that a system takes longer to return to its attractor after being momentarily perturbed by external forces. Referring again to Fig. 9.3B, recovering from the mechanical perturbation might take longer to return if the perturbation occurred near the walk–run transition point.

Post phase transition, *hysteresis* is revealed by tuning the control parameter in the opposite direction. Hysteresis refers to the fact that phase transitions and their reciprocals do not occur at the same value of the control parameter. In the HKB model, hysteresis is observed by decreasing the collective frequency of finger oscillation after transitioning from antiphase to inphase. Remarkably, the system maintains the inphase pattern and does not return to antiphase coordination. Hysteresis has also been observed in human gait, where the transition from a walk to a run takes place at a higher speed than the reverse run to walk transition (Diedrich & Warren, 1995).

9.2.5 Interim summary

Preceding subsections have presented a brief, yet comprehensive overview of eight hallmark properties that characterize dynamical systems. These eight properties provide for a rich collection of dynamics observable from human movements. As has been shown, each of these properties has a telltale signature, putatively allowing for its identification in laboratory data. Identification of these properties led to the earliest applications of DST within human movement science (Amazeen et al., 1998; Haken et al., 1985; Kelso, 1984, 1995; Kugler & Turvey, 1987; Stergiou, 2004; Thelen & Smith, 1994; Thelen et al., 1991; Whitall, 1989; Whitall & Getchell, 1995). The coming sections direct attention more fully toward applying DST to human gait, an area of research where the DST approach has been particularly successful.

9.3 A dynamical systems approach to gait analysis

The theoretical discussion appearing in Section 9.2 made considerable reference to the collective variable ϕ, meant to capture the relative phase of two limbs producing a coordinated pattern of movement (e.g., inphase, antiphase). While ϕ is but one of an infinite number of potential collective variables characterizing a dynamical system, it is also a very useful quantity for studying human gait (Clark & Phillips, 1993; Stergiou, Scholten, et al., 2001; Thelen et al., 1991; Whitall, 1989; Whitall & Getchell, 1995). This section comprises the various details pertinent to the computation of relative phase from data obtained in a gait analysis laboratory.

9.3.1 Phase portraits and phase angles

In the study of gait, the lower limb segments involved in locomotion have traditionally been modeled as limit cycles (Byrne et al., 2002; Clark & Phillips, 1993; Donker & Beek, 2002; Kelso & Tuller, 1984; Kugler & Turvey, 1987; Kurz & Stergiou, 2004a; Roerdink, Bank, Peper, & Beek, 2011; Roerdink et al., 2009; Thelen et al., 1991). The rationale for this approach is based on the idea that the state of the locomotor system depends on the exchange of energy that occurs within each oscillatory movement (Clark & Phillips, 1993; Kurz & Stergiou, 2004a). As the legs move throughout the gait cycle, they dissipate energy when the feet come into contact with the ground, and this energy is put back into the system at push off. The implication is that this oscillatory motion of the limbs constitutes a limit cycle attractor like those described in Section 9.2.1 (Clark & Phillips, 1993). This implication has received much empirical support from the literature cited above.

Further rationale for modeling the limb segments as limit cycles derives from the very organization of the human neuromuscular system. In a very general sense, all movements are actually rotations (oscillations) around a joint. These rotations eventually lead to more holistic translations of our body. We are equipped with muscles that come in pairs (agonists and antagonists) to further facilitate these rotations. Even the nervous system assists in cyclical behavior by providing the means to relax or rapidly contract one's musculature through the presence of the muscle spindles and the Golgi tendon organs.

The limit cycle character of lower limb motion is further revealed by examining the phase portrait (Section 9.2) of individual limb segments (Figs. 9.2B and 9.3A, B). As a reminder, phase portraits are constructed by plotting some collective variable (e.g., ϕ in the HKB model) on the horizontal axis along with its first derivative on the vertical axis (e.g., $d\phi/dt$). A suitable collective variable for a single limb is its angular displacement throughout the gait cycle. This was demonstrated in Fig. 9.2B, as an example of a phase portrait constructed from absolute angular displacement of the thigh segment relative to a fixed horizontal axis. Section 9.2 largely dealt with point attractors, illustrating the importance of zero crossings. Zero crossings are also important within the context of the limit cycle dynamics governing lower limb movements (Winstein & Garfinkel, 1989). These points indicate instances at which the angular velocity of the segment is zero, that is, the minima and maxima of the angular displacement series. Zero crossings index transitions in movement patterns during the gait cycle. Furthermore, the presence of cusps in the phase portrait indicates sudden interruptions to the movement patterns, and a nearly vertical slope at zero crossings suggests the presence of ballistic-like movements like those involved in reaching (Zaal, Bootsma, & van Wieringen, 1999). A larger number of zero crosses and cusps is a sign of many changes to the limb segment's dynamics during the gait cycle.

A *phase angle* quantifies the motion of the lower limb segment as it traverses the phase portrait and is necessary for computing relative phase (Fig. 9.3A). Calculation of the phase angle involves transforming phase portrait trajectories from Cartesian to polar coordinates, with a radius, r, and phase angle, θ (Clark & Phillips, 1993). The following equation estimates the angle formed by the radius and the horizontal axis at each point on the phase trajectory:

$$\Phi_{\text{Segment}}(t) = \tan^{-1}\frac{\gamma(t)}{x(t)} \tag{9.1}$$

where $\gamma(t)$ represents the angular velocity and $x(t)$ is the angular displacement at each moment in time. The sign of $\Phi_{\text{Segment}}(t)$ depends on the quadrant the trajectory occupies as depicted in Fig. 9.3A.

9.3.2 Continuous and point estimate relative phase

After computing the phase angle for each limb segment, computation of the so-called *continuous relative phase* (CRP) is straightforward such that

$$\text{CRP} = \phi_{\text{Distal}}(t) - \phi_{\text{Proximal}}(t) \tag{9.2}$$

where $\phi_{\text{Distal}}(t)$ and $\phi_{\text{Proximal}}(t)$ are the respective phase angles of two limb segments at each point in time. The computation of relative phase is relatively simple; however, selection of variables to use in the computation is not trivial. In this chapter, we use and advocate the use of segment angles (e.g., absolute angles: thigh, shank) in favor of joint angles (e.g., relative angles: knee, hip). The former treats the two variables (e.g., thigh and shank) as discrete pendula, leading to correct and meaningful interpretation of CRP values. The use of relative angles, however, introduces interpretive difficulty. Consider, for example, using hip and knee angles in the computation of CRP. This would entail using the angle of the thigh twice in the CRP computation, directly inhibiting any meaningful description of the relative motion of limb segments during movement. Thus great care should be taken in selecting variables for use in the computation of CRP.

In keeping with the theoretical concepts developed earlier, CRP acts as the collective variable describing the complex neuromuscular system implied by the motion of the lower limbs during walking. At a minimum, CRP reduces two measures of absolute angular displacement (one for each limb segment) and two measures of velocity (also one for each limb segment) to a single collective variable that is far easier to interpret than examining the phase portrait of each limb segment and then extrapolating the relationship between them (Clark & Phillips, 1993). At an extreme, CRP reduces the vast number of neuromuscular degrees of freedom that rapidly fluctuate through passage of time and changing of task to a single collective variable that reflects the overall state of the neuromuscular system constraints (Kelso, Buchanan, DeGuzman, & Ding, 1993).

Interpretation of CRP is identical to interpretation of ϕ from Section 9.2. A CRP = 0 degrees (or radians) indicates that two limb segments have an inphase pattern of coordination; a CRP = 180 degrees or π radians suggests that the limb segments have an antiphase relationship (Diedrich & Warren, 1995; Haken et al., 1985; Kelso, 1984). The arrangement of proximal versus distal segments in Eq. (9.2) is not arbitrary and must be maintained throughout interpretation because the sign of relative phase carries meaning about limb segment coordination. Given the convention expressed Eq. (9.2), positive values indicate that the distal segment (e.g., shank) is ahead of the proximal segment (e.g., thigh) in phase space; negative values imply that the proximal segment is ahead of the distal segment.

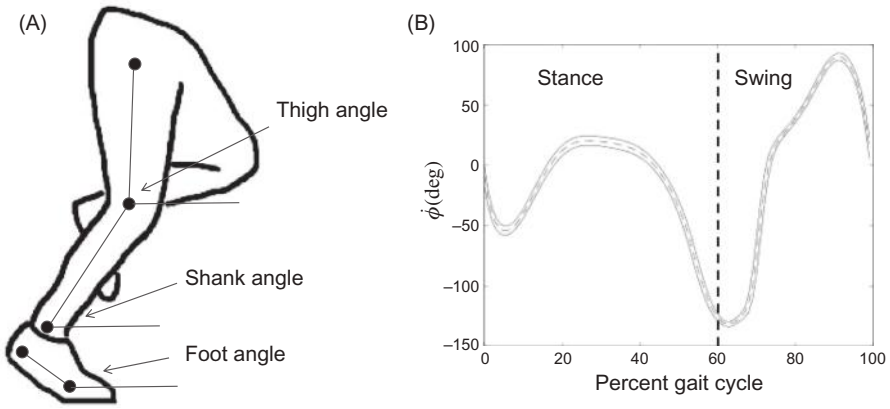

FIGURE 9.4

(A) Graphical representations of the segment angles. (B) Mean ensemble continuous relative phase (CRP) curve showing coordination patterns between shank and thigh segments during several minutes of walking performed by a single healthy exemplar subject. The dashed line reflects the mean ensemble curve. Solid lines represent ± 1 standard deviation from the mean. The dashed vertical line separates the stance and swing phases of the gait cycle.

Fig. 9.4B depicts the mean ensemble CRP curve relating the thigh and shank of one healthy adult, averaged over several gait cycles defined by successive right heel strikes. The horizontal axis has been time normalized to percent of gait cycle using a quintic spline algorithm (Wood & Jennings, 1979). Like instantaneous measures of relative phase, the slope of the relative phase curve also carries meaning. Again, given our convention in Eq. (9.2), positive slopes indicate that the shank is moving faster in phase space and vice versa. Further inspection of Fig. 9.4B reveals that the relationship between the thigh and shank is highly dynamic throughout the gait cycle with thigh leading the shank early in the gait cycle before reversing at the first local minima ($\sim$10%) and then reversing again at the local maxima ($\sim$30%), and reversing again at the end of the stance phase. It is also evident that coordination tends to be more inphase near this point in the stance phase. Another reversal is evident near the end of the swing phase ($\sim$90%). A common practice is to analyze the stance and swing phases separately (Kurz & Stergiou, 2004a).

In addition to the continuous measure of relative phase discussed so far, discrete forms of relative phase have also been used extensively in the literature to study the coordination of two oscillating segments (Diedrich & Warren, 1995; Thelen et al., 1991; van Emmerik & Wagenaar, 1996). As its name implies, the *point estimate relative phase* (PRP) examines relative phase at specific points in the gait cycle. More specifically, PRP is based on the relative times it takes each segment to reach a local maximum or minimum. These extrema represent important events in the gait cycle such as maximum knee extension or initiation

of the stance phase. Using gait velocity as a control parameter, researchers have used PRP to document several properties (e.g., critical fluctuations, hysteresis) inherent to the phase transition that occurs when switching from walking to running modes of gait (Diedrich & Warren, 1995; van Emmerik & Wagenaar, 1996). Computation of PRP is accomplished using Eq. (9.3):

$$\text{PRP} = 180 \text{ degrees} \frac{(t_1 - t_2)}{T} \tag{9.3}$$

where t_1 is the time to a local minimum/maximum angle for segment one, t_2 is the time to local minimum/maximum for segment two, and T is the period of segment one relating similar, consecutive extrema. Segment one is usually taken to be the slower oscillating segment. Interpretation of PRP is similar to its continuous counterpart with 0 and 180 degrees, respectively, indicating inphase and antiphase coordination patterns between segments.

A remaining issue concerns the choice between PRP and CRP measures. Some authors have argued that PRP should be the coordination measure of choice, as compared with CRP (Diedrich & Warren, 1995; Kelso, 1995; Peters, Haddad, Heiderscheit, Van Emmerik, & Hamill, 2003). Some motivation for this suggestion originates in underlying arguments about the nature of the control of movement (Kelso, 1995; Torre, Delignières, & Lemoine, 2007), while the remainder has a more practical origin (Peters et al., 2003). Others have argued that overreliance on a discrete relative phase in favor of a CRP may also be problematic because the discrete relative phase ignores potentially important intracycle gait dynamics (Kurz & Stergiou, 2004a; Li, van den Bogert, Caldwell, van Emmerik, & Hamill, 1999). Ultimately, the choice of PRP or CRP may depend on the specific research question at hand. For example, CRP may be inappropriate when measuring coordination of segments with pulse-like external stimuli, a popular area of research in the context of gait rehabilitation (Kaipust, McGrath, Mukherjee, & Stergiou, 2013; Thaut & Abiru, 2010; Thaut, McIntosh, & Hoemberg, 2015). Thus we contend that both measures have a place in the literature. Moreover, Section 9.3.4 discusses an alternative approach to computation of relative phase that may satisfy proponents of both PRP and CRP.

9.3.3 Phase portrait normalization

Matters related to normalization are a common aspect of gait analysis. Analysis of CRP is no different in that regard and remains an area of active research (Kurz & Stergiou, 2002; Lamb & Stöckl, 2014; Mehdizadeh & Glazier, 2018; Peters et al., 2003; Varlet & Richardson, 2011). Early concerns about the use of CRP originated in the observation that its power spectrum contained multiple peaks when two limb segments were not maintaining a 1:1 frequency ratio, a problem magnified by increasing disparity between the segments' oscillatory frequencies (Schmidt, Beek, Treffner, & Turvey, 1991). Those authors further

suggested that measures of relative phase may not be sufficient for characterizing intersegmental coordination. However, Fuchs, Jirsa, Haken, and Kelso (1996) provided a mathematical proof that CRP does, in fact, measure coordination between two segments. The multiple peaks in the power spectrum were a function of the phase portrait coordinate system used to examine the oscillators. They further demonstrated a nonlinear normalization technique to remedy this issue but noted this was likely an unnecessary step given that power spectral peaks tended to differ by at least an order of magnitude.

Another set of CRP-related criticism targeted studies that failed to normalize phase portrait coordinates before computation of the relative phase (Burgess-Limerick, Abernethy, & Neal, 1993; Hamill, Haddad, & Mcdermott, 2000; Hamill, van Emmerik, Heiderscheit, & Li, 1999; Li et al., 1999; Peters et al., 2003; van Emmerik & Wagenaar, 1996). The argument was that the segment producing the largest amplitude would dominate the relative phase computation, rendering relative phase an inaccurate measure of coordination. Normalization techniques aimed at producing scalar multiples of originating phase portraits, while leaving the dynamic qualities of limb segments intact. However, later research demonstrated amplitude normalization tends to distort phase portraits, resulting in erroneous CRP calculations (Kurz & Stergiou, 2002). In general, three primary methods have appeared in the literature. The first method entails normalizing the velocity by a factor of $2\pi/p$, where p is the period of oscillation (Peters et al., 2003). This method is problematic in practice because it is only appropriate for sinusoidal signals and may require knowing the governing equations, two conditions often not met within the context of human gait analysis. Two other methods have received the bulk of the attention in the literature and have been labeled Method A and Method B (Kurz & Stergiou, 2002), although these labels are not consistent across the literature (Lamb & Stöckl, 2014). These methods make various use of the two following equations:

$$f(\gamma(t)) = \frac{\gamma(t)}{\max(|\gamma(t)|)} \tag{9.4}$$

and

$$g(\gamma(t)) = \frac{\gamma(t) - \min(\gamma(t))}{\max(\gamma(t)) - \min(\gamma(t))} \tag{9.5}$$

Following the convention in Kurz and Stergiou (2002), Method A requires normalizing both limb segment angular displacement and velocity by application of Eq. (9.4). Method B requires normalizing displacement by Eq. (9.5) and velocity by Eq. (9.4). At issue, though, is that phase portrait amplitude normalization techniques like these do not address frequency differences between limb

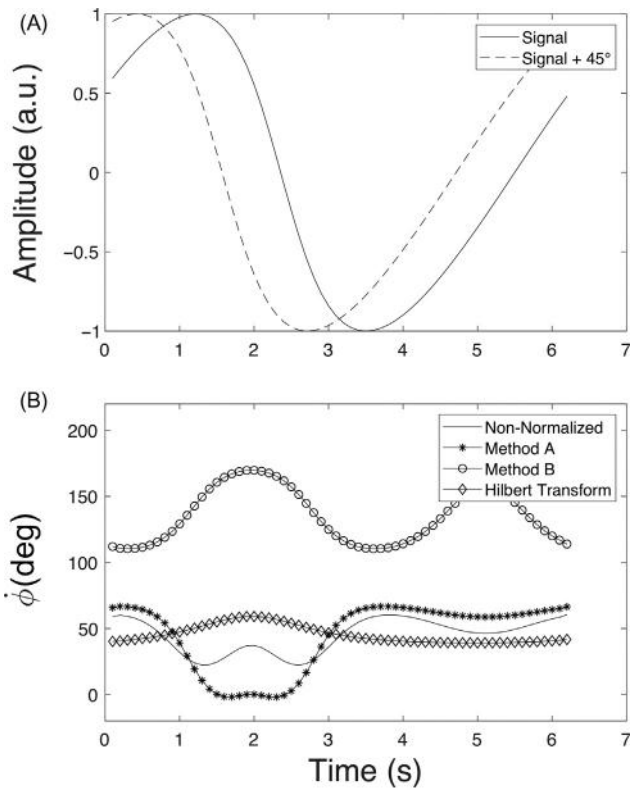

FIGURE 9.5

(A) Time series plots of nonsinusoidal signals. The signals are identical, but one is shifted by 45 degrees. (B) Comparison of normalization techniques with the Hilbert transform method of continuous relative phase (CRP) estimation.

segments that ultimately give rise to artifacts in relative phase. These artifacts are clearly demonstrated in Fig. 9.5 within the context of a more contemporary measure of CRP involving the Hilbert transform.

9.3.4 The Hilbert transform for estimating relative phase

As discussed, there are a number of issues surrounding the estimation of relative phase from angular displacement time series. In addition to amplitude and frequency nonstationarities inherent to human gait, these computations raise a number of issues related to measurement noise and the estimation of time derivatives. An alternative approach for estimating CRP, involving the *Hilbert transform*, has recently received a resurgence of interest from the movement science community (Lamb & Stöckl, 2014; Mehdizadeh & Glazier, 2018; Rosenblum & Kurths, 1998; Varlet & Richardson, 2011). Although

additional empirical work is needed, the Hilbert transform shows great promise as this method simultaneously addresses all of the above problems as well as another recently raised issue concerning so-called order errors in the calculation of CRP (Mehdizadeh & Glazier, 2018).

The phase angles of a time series, $x(t)$, can be calculated from the time series itself and its Hilbert transform, $H(t) = H(x(t))$. The Hilbert transform of $x(t)$ results in the complex analytical signal:

$$\zeta(t) = x(t) + iH(t) \tag{9.6}$$

such that $H(t)$ serves as the imaginary part of the analytical signal and i is the square root of the negative one (Gabor, 1946). Based on this transform, the phase angle for a time series at a given point in time, $\phi(t)$ is calculated as

$$\phi(t) = \tan^{-1}\frac{H(t)}{x(t)} \tag{9.7}$$

The CRP based on the Hilbert transform, $\mathrm{CRP}_{H(t)}$, is then estimated as the difference between two phase angle series (e.g., ϕ_{Thigh} and ϕ_{Shank}) where

$$\mathrm{CRP}_{H(t)} = \phi_1(t) - \phi_2(t) \tag{9.8}$$

or, equivalently,

$$\mathrm{CRP}_{H(t)} = \tan^{-1}\frac{H_1(t)x_2(t) - H_2(t)x_1(t)}{x_1(t)x_2(t) - H_1(t)H_2(t)} \tag{9.9}$$

where $H_1(t)$ and $H_2(t)$ are the Hilbert transforms obtained from each limb segment angular displacement time series, $x_1(t)$ and $x_2(t)$, respectively. In demonstrating this technique, we follow a previous simulation example in the literature comparing $\mathrm{CRP}_{H(t)}$ with CRP obtained using phase portraits and the normalization methods listed above (Fuchs et al., 1996; Lamb & Stöckl, 2014; Peters et al., 2003; Varlet & Richardson, 2011). The Hilbert transform is particularly useful for series with nonstationary frequencies like those often observed in the case of human locomotion.

Consider the two series depicted in the top panel of Fig. 9.5. These signals were generated by the following equation:

$$x(t) = \frac{\cos(t - 0.25\pi)}{\sqrt{1 + 0.41418^2 - 2 \times 0.41418\sin(t - 0.25\pi)}}$$

The two signals are identical except that they are shifted by 45 degrees. The nonsinusoidal nature of the two signals implies that their relative phase continuously increases and decreases around the 45 degrees phase shift. Hence, the expectation is that the observed CRP phase should fluctuate near that value. Fig. 9.5 shows that the Hilbert transform reproduces the expected

result, whereas the normalized and nonnormalized signals deviate considerably from the true value, as expected when applying normalization to nonsinusoidal signals (Kurz & Stergiou, 2002). Interestingly, the nonnormalized relative phase better estimates the expected relationship than either of the two standard normalization techniques. Additional suggestions have been made regarding centering and normalizing empirical time series, but additional research may be needed to understand the effects of those approaches (Lamb & Stöckl, 2014; Varlet & Richardson, 2011).

9.3.5 Statistical summaries of relative phase dynamics

Unsurprisingly, human locomotion tends to be highly variable from one person, and even one cycle, to the next. This is what Bernstein (1967) referred to as "repetition without repetition." Thus it becomes necessary to assess relative phase dynamics in statistical terms. Standard measures used in the literature are those that relate to mean relative phase and the variability around that value (Amazeen et al., 1998; Kelso, 1995). These statistical measures allow for identification of the dominant modes of coordination along with their stability. Mean absolute relative phase (MARP) serves the first of those two goals, identification of dominant modes such as inphase or antiphase attractors (Armitano, Morrison, & Russell, 2018; Byrne et al., 2002; Eslami, Begon, Farahpour, & Allard, 2007; Ghanavati et al., 2014; Kurz & Stergiou, 2004a, 2004b; Stergiou, Jensen, et al., 2001; Stergiou, Scholten, et al., 2001). Computation of MARP involves averaging the absolute values of mean ensemble curve points according to Eq. (9.10):

$$\text{MARP} = \frac{1}{N}\sum_{i=1}^{N}|\phi_i| \tag{9.10}$$

where ϕ_i is relative phase and N is the number of points in the relative phase mean ensemble. Values of MARP closer to zero indicate a tendency toward an inphase attractor. Larger values imply a tendency toward an out-of-phase coordination mode. Deviation phase (DP) provides a measure of the stability of an attractor mode for a particular configuration of the neuromuscular system. That is, it provides a measure of how stable a particular coordination pattern is between two limb segments (Stergiou, Jensen, et al., 2001; Stergiou, Scholten, et al., 2001; van Emmerik & Wagenaar, 1996). The computation of DP involves averaging the standard deviations of the ensemble relative phase curve as given by Eq. (9.11):

$$\text{DP} = \frac{1}{N}\sum_{i=1}^{N}|SD_i| \tag{9.11}$$

where N is the number of points in the relative phase ensemble curve and SD_i is the standard deviation of the ensemble curve at each point, i. Lower

values of DP indicate a more stable coordination pattern; higher values indicate less stability.

9.4 Applications of relative phase dynamics to human gait

Almost since its introduction into the field of movement science (Kelso, 1984; Kelso, Holt, Rubin, & Kugler, 1981; Kugler & Turvey, 1987; Turvey, 1990), the DST approach has appealed to researchers interested in characterizing human gait (Clark & Phillips, 1993; Thelen et al., 1991). The theoretical constructs discussed in Section 9.2 are a natural fit for a process like human locomotion that demands the control of many neuromuscular degrees of freedom within an ever-changing context. Thus it is not surprising that many early applications of DST to human locomotion were from a developmental perspective (Clark & Phillips, 1993; Thelen et al., 1991). The DST approach advocated in this chapter, involving the study of collective variable dynamics, is remarkably general, and in this section, we summarize a few examples from the literature that capture the essence of that generality. These examples serve as basic templates for DST-oriented approaches to gait analysis (as well as other forms of human behavior). We also encourage interested readers to consult the many references in this chapter for excellent worked out examples (Kurz & Stergiou, 2004a).

As we have noted, the DST approach to intersegmental coordination implies that gait patterns arise from the collective dynamics of the neuromuscular system. The ongoing organization of this system depends on numerous constraints that span multiple spatial and temporal scales inherent to the person, environment, and task. Coordinated patterns of walking obviously depend on factors like walking surface and speed but also on factors related to injury and disease.

9.4.1 Relative phase dynamics after anterior cruciate ligament reconstruction surgery

Anterior cruciate ligament (ACL) injury is a common pathology that often requires surgical intervention, and from a DST perspective, one might speculate that the change in context resulting from reconstruction of the ACL might alter the dynamics of intersegmental coordination. These differences are thought to emerge from loss of proprioceptive information about the knee joint (Kiefer et al., 2013; Kurz, Stergiou, Buzzi, & Georgoulis, 2005). Several studies have been conducted that support this general idea (Kiefer et al., 2013; Kurz et al., 2005; Leporace et al., 2013; Nematollahi et al., 2016; Pollard, Stearns, Hayes, & Heiderscheit, 2015).

Kurz et al. (2005) explored the idea that alterations to the ACL by surgical intervention would lead to altered relative phase dynamics of the foot, shank, and thigh. They collected walking and running kinematic data from 10 healthy controls and 10 participants that had recently undergone ACL reconstruction surgery using the patellar tendon. The average time since surgery was 10 months. Participants from both the surgical and control groups walked and ran at a self-selected pace until they were comfortable, at which point, data from an additional 15 consecutive foot falls was collected for analysis. CRP was estimated between both foot–shank and shank–thigh relationships during the stance phase. Consistent with expectations, several notable findings emerged both in terms of graphical inspection of ensemble relative phase curves and statistical characteristics (e.g., MARP).

Those authors noted that, although the timing of reversal points in the foot–shank ensemble CRP curve was similar for surgical patients and controls during walking, the magnitudes of minima and maxima differed (Kurz et al., 2005). They also found that the typical thigh phase lead over the shank toward the end of the stance phase was greater for surgical patients than controls (see Fig. 9.4B for an example of phase lead during walking). Graphical inspection of CRP curves also provided evidence of surgical alterations to joint dynamics during running, suggesting profound differences in both the timing and magnitude of CRP in both joints. For example, during the initiation of stance surgical patients exhibited out-of-phase behavior ($\sim$80 degrees), whereas statistical analysis of MARP corroborated the graphical results, suggesting surgery-related differences in both walking and running conditions. Collectively, these results suggest that ACL reconstruction alters joint dynamics and make a strong case for the use of CRP in the laboratory and clinical settings.

9.4.2 Relative phase dynamics and aging

The preceding section highlighted the differential dynamics of people who have undergone ACL reconstruction compared with matched healthy controls. Moreover, these results highlight the generality of the DST approach in its translation to clinical settings. We should also mention that, in the previous example, ACL reconstruction was the control parameter. Importantly, and from a statistical standpoint, the DST's control parameter doubles as the independent variable of the study, while the DST's collective variable is the dependent variable. This is another considerable advantage of this approach that allows the gait analyst, the researcher, and the biomechanist, to utilize this framework in order to think from the perspective of constructing appropriate experimental designs for probing collective variable dynamics.

The generality of DST is further emphasized in understanding age-related alterations to locomotion (Byrne et al., 2002). Several early studies on DST and gait analysis have focused on age as a control parameter (Clark & Phillips, 1993; Whitall, 1989; Whitall & Getchell, 1995). That is, one might hypothesize that qualitative changes in gait dynamics (i.e., phase transitions) take place over the lifespan as the age control parameter is tuned. This phenomenon has been well documented with respect to infant acquisition of locomotive skill (Clark & Phillips, 1993; Thelen & Smith, 1994; Thelen et al., 1991) and, more recently, within the context of older adults (Byrne et al., 2002; Kyvelidou, Kurz, Ehlers, & Stergiou, 2008; McGibbon & Krebs, 2001; Ogaya, Iwata, Higuchi, & Fuchioka, 2016; Terrier & Reynard, 2015). That is, a number of authors have demonstrated differences in the gait dynamics expressed by older adults as compared with young people. Some studies have found differences in the coordination patterns emerging between body segments (Byrne et al., 2002; Ogaya et al., 2016), while others have found differences emerging in higher order dynamical variables (Kyvelidou et al., 2008) and the statistical structure of gait kinematics (Hausdorff, 2007; Hausdorff et al., 1997; Kaipust et al., 2013).

For example, in one recent study, 91 older female adults walked on a 7 m walkway, while their movements were recorded using a motion-tracking system (Ogaya et al., 2016). Similar to the experiment reported in Section 9.4.1 (Kurz et al., 2005), foot−shank and thigh−shank CRP were computed but this time using the Hilbert transform method discussed in Section 9.3.4. Several standard measures of gait (gait speed, step length, and cadence) were also recorded and correlated with mean relative phase measured over different portions of the gait cycle. The authors reported several, expected correlations between mean relative phase and participant characteristics such as age and weight. Relative phase dynamics are known to differ between younger and older adults (Byrne et al., 2002). More interestingly, they found moderately strong correlations ($|\text{Pearson's } r| \geq 0.5$) between mean relative phase and other measured gait parameters after controlling for participant characteristics (Ogaya et al., 2016). In late stance, negative correlations emerged between gait speed, step length, and cadence and mean relative phase, although correlations involving gait speed and cadence were much stronger. Similar to previous studies (Byrne et al., 2002), these results supported the hypothesis that gait dynamics change as a function of age but also suggest that age-related alterations to other important gait parameters may be related to joint angle coordination dynamics. Clearly, the generality of the DST approach translates to important clinical and developmental settings.

9.5 Summary and concluding remarks

This chapter has presented the application of DST to the study of human movement, with particular attention paid to gait and gait analysis. This

presentation addressed matters of both theory and practice, with practical suggestions concerning the analysis and interpretation of results. Moreover, we have demonstrated a major benefit in applying DST to human gait—simplicity. We revisit a claim from the introductory paragraph: Simplification comes from focusing on collective variables, these low-dimensional variables that capture the overall state of a system (Gilmore, 1981; Kelso, 1995), in favor of the seemingly innumerable biomechanical variables found in more traditional lines of research (Hamill & Knutzen, 2009). The supporting literature for both this claim and this chapter is quite large and spans several decades, and we encourage interested practitioners to explore this literature in detail. Despite several decades of research on modeling the limit cycle and control properties of human gait, there is still much work to be done both from basic science and clinical perspectives. Our intention in compiling this chapter is to facilitate research in those domains, as we feel there is much revolutionary science yet to come from applying DST to the analysis of gait. Furthermore, we strongly advocate the use of this powerful investigative approach by scientists and clinicians who work in gait analysis laboratories or utilize gait analysis to understand the effects of various pathologies on human gait.

References

Amazeen, P. G., Amazeen, E. L., & Turvey, M. T. (1998). Dynamics of human intersegmental coordination: Theory and research. *Timing of Behavior: Neural, Psychological, and Computational Perspectives*, 237–259.

Armitano, C. N., Morrison, S., & Russell, D. M. (2018). Coordination stability between the legs is reduced after anterior cruciate ligament reconstruction. *Clinical Biomechanics*, *58*, 28–33. Available from https://doi.org/10.1016/j.clinbiomech.2018.07.003.

Bernstein, N. (1967). *The co-ordination and regulation of movements*. New York: Pergamon.

Burgess-Limerick, R., Abernethy, B., & Neal, R. J. (1993). Relative phase quantifies interjoint coordination. *Journal of Biomechanics*, *26*(1), 91–94. Available from https://doi.org/10.1016/0021-9290(93)90617-N.

Byrne, J. E., Stergiou, N., Blanke, D., Houser, J. J., Kurz, M. J., & Hageman, P. A. (2002). Comparison of gait patterns between young and elderly women: An examination of coordination. *Perceptual and Motor Skills*, *94*(1), 265–280. Available from https://doi.org/10.2466/pms.2002.94.1.265.

Clark, J. E., & Phillips, S. J. (1993). A longitudinal study of intralimb coordination in the first year of independent walking: A dynamical systems analysis. *Child Development*, *64*(4), 1143–1157. Available from https://doi.org/10.1111/j.1467-8624.1993.tb04192.x.

Diedrich, F. J., & Warren, W. H. (1995). Why change gaits? Dynamics of the walk-run transition. *Journal of Experimental Psychology: Human Perception and Performance*, *21*(1), 183–202. Available from https://doi.org/10.1037/0096-1523.21.1.183.

Donker, S. F., & Beek, P. J. (2002). Interlimb coordination in prosthetic walking: Effects of asymmetry and walking velocity. *Acta Psychologica*, *110*(2), 265–288. Available from https://doi.org/10.1016/S0001-6918(02)00037-9.

Eslami, M., Begon, M., Farahpour, N., & Allard, P. (2007). Forefoot–rearfoot coupling patterns and tibial internal rotation during stance phase of barefoot versus shod running. *Clinical Biomechanics*, *22*(1), 74–80. Available from https://doi.org/10.1016/j.clinbiomech.2006.08.002.

Fuchs, A., Jirsa, V. K., Haken, H., & Kelso, J. A. S. (1996). Extending the HKB model of coordinated movement to oscillators with different eigenfrequencies. *Biological Cybernetics*, *74*(1), 21–30. Available from https://doi.org/10.1007/BF00199134.

Gabor, D. (1946). Theory of communication. Part 1: The analysis of information. *Journal of the Institution of Electrical Engineers – Part III: Radio and Communication Engineering*, *93*(26), 429–441. Available from https://doi.org/10.1049/ji-3-2.1946.0074.

Ghanavati, T., Salavati, M., Karimi, N., Negahban, H., Ebrahimi Takamjani, I., Mehravar, M., & Hessam, M. (2014). Intra-limb coordination while walking is affected by cognitive load and walking speed. *Journal of Biomechanics*, *47*(10), 2300–2305. Available from https://doi.org/10.1016/j.jbiomech.2014.04.038.

Gilmore, R. (1981). *Catastrophe theory for scientists and engineers*. North Chelmsford, MA: Courier Corporation.

Haken, H., Kelso, J. A. S., & Bunz, H. (1985). A theoretical model of phase transitions in human hand movements. *Biological Cybernetics*, *51*(5), 347–356. Available from https://doi.org/10.1007/BF00336922.

Hamill, J., Haddad, J. M., & Mcdermott, W. J. (2000). Issues in quantifying variability from a dynamical systems perspective. *Journal of Applied Biomechanics*, *16*, 407–418.

Hamill, J., & Knutzen, K. (2009). *Biomechanical basis of human movement* (3rd ed.). Philadelphia, PA: Wolters Kluwer Health/Lippincott Williams and Wilkins.

Hamill, J., van Emmerik, R. E. A., Heiderscheit, B. C., & Li, L. (1999). A dynamical systems approach to lower extremity running injuries. *Clinical Biomechanics*, *14*(5), 297–308. Available from https://doi.org/10.1016/S0268-0033(98)90092-4.

Hausdorff, J. M. (2007). Gait dynamics, fractals and falls: Finding meaning in the stride-to-stride fluctuations of human walking. *Human Movement Science*, *26*(4), 555–589. Available from https://doi.org/10.1016/j.humov.2007.05.003.

Hausdorff, J. M., Mitchell, S. L., Firtion, R., Peng, C. K., Cudkowicz, M. E., Wei, J. Y., & Goldberger, A. L. (1997). Altered fractal dynamics of gait: Reduced stride-interval correlations with aging and Huntington's disease. *Journal of Applied Physiology*, *82*(1), 262–269. Available from https://doi.org/10.1152/jappl.1997.82.1.262.

Kaipust, J. P., McGrath, D., Mukherjee, M., & Stergiou, N. (2013). Gait variability is altered in older adults when listening to auditory stimuli with differing temporal structures. *Annals of Biomedical Engineering*, *41*(8), 1595–1603. Available from https://doi.org/10.1007/s10439-012-0654-9.

Kelso, J. A. S. (1984). Phase transitions and critical behavior in human bimanual coordination. *American Journal of Physiology – Regulatory, Integrative and Comparative Physiology*, *246*(6), R1000–R1004. Available from https://doi.org/10.1152/ajpregu.1984.246.6.R1000.

Kelso, J. A. S. (1995). *Dynamic patterns: The self-organization of brain and behavior*. Cambridge, MA: The MIT Press.

Kelso, J. A. S., Buchanan, J. J., DeGuzman, G. C., & Ding, M. (1993). Spontaneous recruitment and annihilation of degrees of freedom in biological coordination. *Physics Letters A*, *179*(4), 364–371. Available from https://doi.org/10.1016/0375-9601(93)90692-S.

Kelso, J. A. S., Holt, K. G., Rubin, P., & Kugler, P. N. (1981). Patterns of human interlimb coordination emerge from the properties of non-linear, limit cycle oscillatory processes. *Journal of Motor Behavior*, *13*(4), 226–261. Available from https://doi.org/10.1080/00222895.1981.10735251.

Kelso, J. A. S., & Tuller, B. (1984). *A dynamical basis for action systems. Handbook of cognitive neuroscience* (pp. 321–356). Springer.

Kiefer, A. W., Ford, K. R., Paterno, M. V., Schmitt, L. C., Myer, G. D., Riley, M. A., ... Hewett, T. E. (2013). Inter-segmental postural coordination measures differentiate athletes with ACL reconstruction from uninjured athletes. *Gait & Posture*, *37*(2), 149–153. Available from https://doi.org/10.1016/j.gaitpost.2012.05.005.

Kugler, P. N., & Turvey, M. T. (1987). *Information, natural law, and the self-assembly of rhythmic movement*. London: Routledge.

Kurz, M. J., & Stergiou, N. (2002). Effect of normalization and phase angle calculations on continuous relative phase. *Journal of Biomechanics*, *35*(3), 369–374. Available from https://doi.org/10.1016/S0021-9290(01)00211-1.

Kurz, M. J., & Stergiou, N. (2004a). Applied dynamic systems theory for the analysis of movement. In N. Stergiou (Ed.), *Innovative analyses of human movement: Analytical tools for human movement research* (pp. 93–119). Champaign, IL: Human Kinetics.

Kurz, M. J., & Stergiou, N. (2004b). Does footwear affect ankle coordination strategies? *Journal of the American Podiatric Medical Association*, *94*(1), 53–58. Available from https://doi.org/10.7547/87507315-94-1-53.

Kurz, M. J., Stergiou, N., Buzzi, U. H., & Georgoulis, A. D. (2005). The effect of anterior cruciate ligament recontruction on lower extremity relative phase dynamics during walking and running. *Knee Surgery, Sports Traumatology, Arthroscopy*, *13*(2), 107–115. Available from https://doi.org/10.1007/s00167-004-0554-0.

Kyvelidou, A., Kurz, M. J., Ehlers, J. L., & Stergiou, N. (2008). Aging and partial body weight support affects gait variability. *Journal of NeuroEngineering and Rehabilitation*, *5*(1), 22. Available from https://doi.org/10.1186/1743-0003-5-22.

Lamb, P. F., & Stöckl, M. (2014). On the use of continuous relative phase: Review of current approaches and outline for a new standard. *Clinical Biomechanics*, *29*(5), 484–493. Available from https://doi.org/10.1016/j.clinbiomech.2014.03.008.

Leporace, G., Metsavaht, L., Oliveira, L. P., Nadal, J., Batista, L. A., Leporace, G., ... Batista, L. A. (2013). Motor coordination during gait after anterior cruciate ligament injury: A systematic review of the literature. *Revista Brasileira de Ortopedia*, *48*(4), 293–299. Available from https://doi.org/10.1016/j.rbo.2012.07.008.

Li, L., van den Bogert, E. C. H., Caldwell, G. E., van Emmerik, R. E. A., & Hamill, J. (1999). Coordination patterns of walking and running at similar speed and stride frequency. *Human Movement Science*, *18*(1), 67–85. Available from https://doi.org/10.1016/S0167-9457(98)00034-7.

McGibbon, C. A., & Krebs, D. E. (2001). Age-related changes in lower trunk coordination and energy transfer during gait. *Journal of Neurophysiology*, *85*(5), 1923–1931.

Mehdizadeh, S., & Glazier, P. S. (2018). Order error in the calculation of continuous relative phase. *Journal of Biomechanics*, *73*, 243–248. Available from https://doi.org/10.1016/j.jbiomech.2018.03.032.

Nematollahi, M., Razeghi, M., Mehdizadeh, S., Tabatabaee, H., Piroozi, S., Shirazi, Z. R., & Rafiee, A. (2016). Inter-segmental coordination pattern in patients with anterior cruciate ligament deficiency during a single-step descent. *PLoS One*, *11*(2), e0149837. Available from https://doi.org/10.1371/journal.pone.0149837.

Ogaya, S., Iwata, A., Higuchi, Y., & Fuchioka, S. (2016). The association between intersegmental coordination in the lower limb and gait speed in elderly females. *Gait & Posture*, *48*, 1–5. Available from https://doi.org/10.1016/j.gaitpost.2016.04.018.

Peters, B. T., Haddad, J. M., Heiderscheit, B. C., Van Emmerik, R. E. A., & Hamill, J. (2003). Limitations in the use and interpretation of continuous relative phase. *Journal of Biomechanics*, *36*(2), 271–274. Available from https://doi.org/10.1016/S0021-9290(02)00341-X.

Pollard, C. D., Stearns, K. M., Hayes, A. T., & Heiderscheit, B. C. (2015). Altered lower extremity movement variability in female soccer players during side-step cutting after anterior cruciate ligament reconstruction. *The American Journal of Sports Medicine*, *43*(2), 460–465. Available from https://doi.org/10.1177/0363546514560153.

Roerdink, M., Bank, P. J. M., Peper, C. L., & Beek, P. J. (2011). Walking to the beat of different drums: Practical implications for the use of acoustic rhythms in gait rehabilitation. *Gait & Posture*, *33*(4), 690–694. Available from https://doi.org/10.1016/j.gaitpost.2011.03.001.

Roerdink, M., Lamoth, C. J. C., van Kordelaar, J., Elich, P., Konijnenbelt, M., Kwakkel, G., & Beek, P. J. (2009). Rhythm perturbations in acoustically paced treadmill walking after stroke. *Neurorehabilitation and Neural Repair*, *23*(7), 668–678. Available from https://doi.org/10.1177/1545968309332879.

Rosen, R. (1970). *Dynamical system theory in biology*. New York: Wiley-Interscience.

Rosenblum, M., & Kurths, J. (1998). *Analysing synchronization phenomena from bivariate data by means of the Hilbert transform. Nonlinear analysis of physiological data* (pp. 91–99). Springer.

Rössler, O. E. (1976). An equation for continuous chaos. *Physics Letters A*, *57*(5), 397–398. Available from https://doi.org/10.1016/0375-9601(76)90101-8.

Russell, D. M., Haworth, J. L., & Martinez-Garza, C. (2016). Coordination dynamics of (a)symmetrically loaded gait. *Experimental Brain Research*, *234*(3), 867–881. Available from https://doi.org/10.1007/s00221-015-4512-5.

Schmidt, R. C., Beek, P. J., Treffner, P. J., & Turvey, M. T. (1991). Dynamical substructure of coordinated rhythmic movements. *Journal of Experimental Psychology: Human Perception and Performance*, *17*(3), 635–651. Available from https://doi.org/http://dx.doi.org.ezproxy1.lib.asu.edu/10.1037/0096-1523.17.3.635.

Scholz, J. P., Kelso, J. A. S., & Schöner, G. (1987). Nonequilibrium phase transitions in coordinated biological motion: Critical slowing down and switching time. *Physics Letters A*, *123*(8), 390–394. Available from https://doi.org/10.1016/0375-9601(87)90038-7.

Stergiou, N. (Ed.), (2004). *Innovative analyses of human movement*. Champaign, IL: Human Kinetics.

Stergiou, N. (2016). *Nonlinear analysis for human movement variability*. Boca Raton, FL: Taylor & Francis.

Stergiou, N., Jensen, J. L., Bates, B. T., Scholten, S. D., & Tzetzis, G. (2001). A dynamical systems investigation of lower extremity coordination during running over obstacles. *Clinical Biomechanics*, *16*(3), 213–221. Available from https://doi.org/10.1016/S0268-0033(00)00090-5.

Stergiou, N., Scholten, S. D., Jensen, J. L., & Blanke, D. (2001). Intralimb coordination following obstacle clearance during running: The effect of obstacle height. *Gait & Posture*, *13*(3), 210–220.

Terrier, P., & Reynard, F. (2015). Effect of age on the variability and stability of gait: A cross-sectional treadmill study in healthy individuals between 20 and 69 years of age. *Gait & Posture*, *41*(1), 170–174. Available from https://doi.org/10.1016/j.gaitpost.2014.09.024.

Thaut, M. H., & Abiru, M. (2010). Rhythmic auditory stimulation in rehabilitation of movement disorders: A review of current research. *Music Perception: An Interdisciplinary Journal*, *27*(4), 263–269. Available from https://doi.org/10.1525/mp.2010.27.4.263.

Thaut, M. H., McIntosh, G. C., & Hoemberg, V. (2015). Neurobiological foundations of neurologic music therapy: Rhythmic entrainment and the motor system. *Frontiers in Psychology*, *5*, 1185. Available from https://doi.org/10.3389/fpsyg.2014.01185.

Thelen, E., & Smith, L. B. (1994). A dynamic systems approach to the development of cognition and action *(5 print)*. Cambridge, MA: MIT Press.

Thelen, E., Ulrich, B. D., & Wolff, P. H. (1991). Hidden skills: A dynamic systems analysis of treadmill stepping during the first Year. *Monographs of the Society for Research in Child Development*, *56*(1), 1–103. Available from https://doi.org/10.2307/1166099.

Torre, K., Delignières, D., & Lemoine, L. (2007). 1/fβ fluctuations in bimanual coordination: An additional challenge for modeling. *Experimental Brain Research*, *183*(2), 225–234. Available from https://doi.org/10.1007/s00221-007-1035-8.

Turvey, M. T. (1990). Coordination. *American Psychologist*, *45*(8), 938.

Turvey, M. T., Fitch, H. L., & Tuller, B. (1982). *The Bernstein perspective: I. The problems of degrees of freedom and context-conditioned variability. Human motor behavior: An introduction* (pp. 239–252). Hillsdale, NJ: Lawrence Erlbaum Associates.

van Emmerik, R. E. A., & Wagenaar, R. C. (1996). Effects of walking velocity on relative phase dynamics in the trunk in human walking. *Journal of Biomechanics*, *29*(9), 1175–1184. Available from https://doi.org/10.1016/0021-9290(95)00128-X.

Varlet, M., & Richardson, M. J. (2011). Computation of continuous relative phase and modulation of frequency of human movement. *Journal of Biomechanics*, *44*(6), 1200–1204. Available from https://doi.org/10.1016/j.jbiomech.2011.02.001.

Whitall, J. (1989). A developmental study of the interlimb coordination in running and galloping. *Journal of Motor Behavior*, *21*(4), 409–428. Available from https://doi.org/10.1080/00222895.1989.10735492.

Whitall, J., & Getchell, N. (1995). From walking to running: Applying a dynamical systems approach to the development of locomotor skills. *Child Development*, *66*(5), 1541–1553. Available from https://doi.org/10.2307/1131663.

Winstein, C. J., & Garfinkel, A. (1989). Qualitative dynamics of disordered human locomotion. *Journal of Motor Behavior*, *21*(4), 373–391. Available from https://doi.org/10.1080/00222895.1989.10735490.

Wood, G. A., & Jennings, L. S. (1979). On the use of spline functions for data smoothing. *Journal of Biomechanics*, *12*(6), 477–479. Available from https://doi.org/10.1016/0021-9290(79)90033-2.

Zaal, F. T., Bootsma, R. J., & van Wieringen, P. C. (1999). Dynamics of reaching for stationary and moving objects: Data and model. *Journal of Experimental Psychology: Human Perception and Performance*, *25*(1), 149.

CHAPTER 10

A tutorial on fractal analysis of human movements

Aaron D. Likens and Nick Stergiou
University of Nebraska at Omaha, Omaha, NE, United States

My life seemed to be a series of events and accidents. Yet when I look back, I see a pattern.

Benoît B. Mandelbrot (1924–2010).

10.1 Introduction

Fractal analysis and its derivatives have become common fixtures in physiological and psychological time series analysis. Their application has revealed deep truths about the underlying structure present in the moment-to-moment variability of human behavior. Far from just a theoretical exercise, fractal analysis has also promoted new technologies that hold tremendous promise for diagnosis and treatment of a range of diseases including those related to human gait. This chapter is a "how to guide" on performing fractal analysis on time series data collected from a human movement laboratory. The chapter begins with the relevant theoretical background, which focuses on the development of fractal geometry and its relation to human time series data. Next, we present a step-by-step tutorial of the basic concepts involved in fractal analysis. We then provide an in-depth tutorial on the most common form of fractal analysis and its generalization, providing a number of best practice recommendations. Finally, we provide two complete worked out examples from experiments involving human movement.

10.2 Fractal theory and its connection to human movement

Mandelbrot (1967, 1975, 1982) codified fractal geometry in order to describe natural patterns that cannot be accurately described using Euclidean forms such as circles, squares, cylinders, and cubes. Euclidean surfaces and

CONTENTS

Biomechanics and Gait Analysis. DOI: https://doi.org/10.1016/B978-0-12-813372-9.00010-5

solids fail to describe the rich variability inherent in nature because, as Mandelbrot noted, nature is rough and irregular. The terms *rough* and *irregular* are also appropriate in many contexts related to human movement. Even movements that are notoriously rhythmic reveal their roughness upon closer inspection.

Consider an experiment where a participant is asked to coordinate an upper limb with an external stimulus (Likens, 2016). Fig. 10.1 represents just such an experiment. In this experiment, participants were asked to maintain an *inphase* coordination pattern with a stimulus over the course of 15 minutes. An inphase pattern means that both the stimulus and the participant moved from left to right at the same time and at the same speed. The stimulus was a red dot that oscillated from side to side on a computer screen at a frequency of about 1 Hz. The three-dimensional position (with respect to camera origin) of the participant's hand was captured via motion-tracking equipment at a sampling rate of 100 Hz. Participant movements were transformed to linear motion (the blue dot) on the same computer screen as the stimulus and in real time. Performance feedback was provided to the participants by way of visual representation of coordination. When the participant and the computer dot were in the same vicinity, the participant-controlled dot partially or completely covered the stimulus, depending on how accurately the participant followed along with the stimulus. Perfect performance meant that the red dot was invisible, that is, the red dot was completely obscured by the blue dot.

There are, of course, many ways in which one could assess performance on the task. One could define and compute error in terms of distance, or one could estimate relative phase characteristics (see Chapter 9: Coordination and control: a dynamical systems approach to the analysis of human gait). However, the present interest is not in defining performance as such but rather uncovering less-than-obvious (and nontrivial!) structure present in

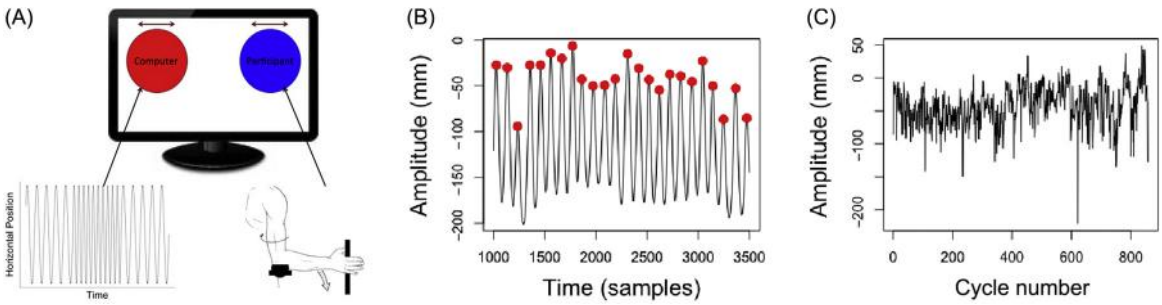

FIGURE 10.1

(A) Experimental setup for a visual-motor tracking experiment. (B) Lateral position time series obtained for several cycles from the experiment in depicted in (A). (C) Time series of oscillation amplitudes obtained from the time series partially depicted in (B).

what seems to be an otherwise periodic movement pattern. Fig. 10.1B depicts a single representative time series captured from the experiment described above. This represents the horizontal position of the hand during repetitive rotation of the forearm about the elbow. Clearly, there appears to be a very regular pattern. By visual inspection, one can observe that this participant seems to be rotating their forearm at a frequency near the required frequency of ~ 1 Hz. That is, there are roughly five peaks for every 500 samples. However, the movement is not a perfect sinusoid. As depicted by the red dots superimposed on the series in Fig. 10.1B, the amplitude of external rotations changes, sometimes dramatically, from one cycle to the next. This amplitude variability is captured in full detail in Fig. 10.1C, which illustrates successive amplitudes as points in a rather messy-looking time series. Resolving the structure from Fig. 10.1C, however, strains the limits of visual inspection. Clearly missing from this figure is the striking rhythmicity present in Fig. 10.1B. Movement patterns that upon first inspection seem smooth and predictable, produce structure that is better described in terms of its roughness.

One might speculate, as many have done in the past, that the variability in amplitude might represent some form of error (Schmidt & Lee, 2011). That is, the time series found in Fig. 10.1B may be represented by an equation of the form: Observed = Signal + Noise, where Noise is taken to be random variation, a nuisance variable to be ignored. The signal, on the other hand, might be the result of a motor program uncorrupted by the presence of motor noise or measurement error. The concepts underlying this equation should be familiar to most anyone who has taken even an introductory statistics course. However, a number of studies over the last couple of decades have revealed time series like the one in Fig. 10.1C often deviate considerably from simple random noise (Cavanaugh, Kelty-Stephen, & Stergiou, 2017; Ding, Chen, & Scott Kelso, 2002; Diniz et al., 2011; Fine, Likens, Amazeen, & Amazeen, 2015; Gilden, 2001; Gilden, Thornton, & Mallon, 1995; Hunt, McGrath, & Stergiou, 2014; Kaipust, McGrath, Mukherjee, & Stergiou, 2013; Kello et al., 2010; Likens, Fine, Amazeen, & Amazeen, 2015; Thornton & Gilden, 2005; Torre & Delignières, 2008; Torre, Delignières, & Lemoine, 2007; Van Orden, Holden, & Turvey, 2003, 2005; Wijnants, Cox, Hasselman, Bosman, & Van Orden, 2012). In all those many but nonexhaustive instances, the general result is that variability in human movements is meaningful and deserving of intense investigation.

Noisy-looking time series like those depicted in Fig. 10.1C are at the very core of this chapter. Quantifying these noisy processes is essential for making a strong connection between human movements and fractal theory. Later in this chapter, we will revisit this and similar series when discussing techniques for quantifying the fractal properties of a time series. In the coming sections,

though, we take a step back and explore some basic concepts from fractal theory, both from geometrical and statistical standpoints. We then use these basic concepts to characterize the hidden structure found in physiological processes recorded over time and investigate its relationship to health and disease.

10.2.1 A geometrical interpretation

The purpose of this section is to introduce the reader to the basic ideas behind fractal geometry and theory. This background provides the theoretical foundation on which to characterize the fractal properties in human movements. This section is not meant to be a complete explication of fractal geometry. We refer the reader to the classic text for a more complete discussion (Mandelbrot, 1982). Instead, our goal is to give the reader an intuitive (i.e., nontechnical) level of understanding of fractal properties for the purpose of translating these ideas to the study of movement. By way of example, we show that fractal shapes differ from ordinary shapes (e.g., squares and circles) in terms of their roughness and regularity.

A stroll through the grocery store can be an exciting scientific adventure when you stop to appreciate the amazing variety of shapes and colors in the produce section. Consider Fig. 10.2, a photograph of *Brassica oleracea*, aka Romanesco broccoli. The vegetable has several striking features, ranging from its bright green color to its swirling texture. Its most striking feature, though, is that Romanesco broccoli seems to exhibit a fundamental property of fractals, *self-similarity*. Self-similarity refers to the fact that small parts of an object resemble the shape formed by the entire object. Self-similarity is readily observed in Fig. 10.2 when contrasting some small portion of the Romanesco to the entire vegetable. The same rough, swirling pattern is observed at smaller and smaller spatial scales. This characterization suggests another key property of fractals: fractals are *scale-free*. This means that fractals do not exist at any privileged scale of measurement. Mandelbrot (1967) famously discussed the scale-free property of fractals within the context of coastlines.

Fig. 10.3 depicts three different drawings of Great Britain. In each panel, going from left to right, the island is circumscribed by a different ruler, with each successive ruler being half the length of the previous one. If one were to measure the length of the coastline with the largest ruler, the result would be very different than if one instead used the shortest ruler. The "length" would increase in a systematic away as the ruler shortened. The word "length" was placed in quotes in this and the preceding sentence in order to emphasize that the meaning of words like length or area when measuring rough, irregular shapes like the coastline of Great Britain often depart from common understanding.

FIGURE 10.2

Brassica oleracea (aka Romanesco broccoli). This vegetable is famous for its characteristic fractal shape. The entire vegetable is composed of a unique spiraling texture such that small portions of the bud look like the entire thing. Source*: https://en.wikipedia.org/wiki/Romanesco_broccoli#/media/File:Romanesco_broccoli_(3).jpg*.

FIGURE 10.3

Three drawings of Great Britain, with the length of its coastline measured using three different rulers. Each successive ruler is one-half the length of the previous one. This demonstrates the *scale-free* property of fractals: changing ruler size changes the length measurement. Hence, the coastline of Great Britain has no characteristic length. Source*: https://commons.wikimedia.org/wiki/File:Britain-fractal-coastline-combined.jpg*.

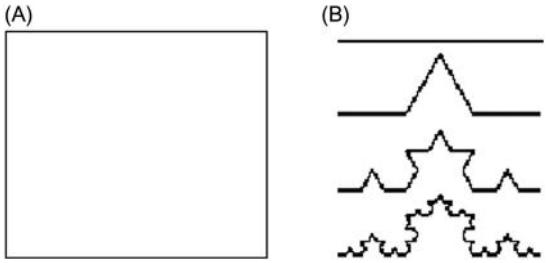

FIGURE 10.4

(A) Line drawing of a square. The area of the square does not change as a function of the ruler used to measure it. Measuring the perimeter with increasingly smaller rulers does not alter the result of measurement. (B) The von Koch curve after 0—3 iterations (*top to bottom*). The von Koch curve is defined over an infinite number of iterations, with the length of the curve also increasing upon each iteration. Hence the von Koch curve has no characteristic measurement of length.

To understand this distinction, first consider the square depicted in Fig. 10.4A. Each side of the square has a length of 1 m. One way to find the perimeter of the square is to use this known information and geometrical formula for the perimeter of a square: perimeter = 4 × side length. If we did not have this information, we could still find the area by using some sort of ruler with known dimensions. For example, one could measure the square with a ruler that has a length such as 1, 1/2, 1/4, or 1/8 m, and add up the lengths of all the measurements with known length that fit around the square. In this case, unlike the coastline of Great Britain, changing the size of the measurement tool does not change the measured area. The square has a perimeter equal to four, regardless of how one measures it. Thus the square is not scale-free.

Now consider a second line drawing in Fig. 10.4B. This is known as the von Koch curve, named after Swedish mathematician Helge von Koch. The von Koch curve is constructed by *iterating* a simple algorithm: (1) Take a line segment and remove the middle third and (2) replace the segment with two vertices of an equilateral triangle. (3) Repeat the process on all line segments resulting from (2). *Iteration* generally refers to the process of performing an operation on an object, then repeating the operation on the output of the original operation. Iteration of simple rules is a fundamental method for generating fractal objects. The result after three iterations is illustrated in Fig. 10.4B (bottom curve), but the process can be continued an infinite number of times resulting in finer and finer detail. The length, L_n, of the von Koch curve,

$$L_n = (4/3)^n, \tag{10.1}$$

increases upon each iteration such that as $n \to \infty$, $L_n \to \infty$, therefore, L_n has no characteristic measurement of length. This means that if we applied the same process to the von Koch curve as was applied to the square, the length of the von Koch curve would depend on the size of the ruler used to measure it. Thus the von Koch curve, like the coastline of Great Britain is scale-free.

The preceding examples have demonstrated important, defining features of fractal objects. Fractals are self-similar and scale-free, and it is these qualities that give fractals their inherent roughness and irregularity. Importantly, Eq. (10.1) implies a means to quantify these qualities that will carry through to the investigation of fractal properties in human movement time series data. Eq. (10.1) has the general form of a power law, $Y = x^m$, where Y is some measurement (e.g., length), x is a scaling factor, and m is a real number representing the characteristic exponent of the power law. Essentially, m determines how fast a measure changes as a function of scale. A useful feature of power laws is that they appear as straight lines when plotted on double logarithmic axes, and we will return to this point in Section 10.2.2. Thus Eq. (10.1) elegantly captures another defining feature of fractals: fractal characteristics tend to follow power laws. More succinctly, characteristic properties such as length and area, when measured at small scales, are proportional to those properties measured at large scales. This is what is meant in the literature by *fractal scaling*.

At this point in the discussion, the reader may be formulating questions about the relevance of vegetables and coastlines for the study of human movement. In the foregoing examples, our intention was to provide an approachable, intuitive introduction to fractal concepts. In doing so, we focused on geometrical objects. In order to translate these ideas to the study of human movement variability as depicted in Fig. 10.1B, we revisit the concept of fractal scaling within a statistical framework.

10.2.2 A statistical interpretation: demystifying fractal analysis

In writing this chapter, we were tempted to use just a single sentence for this entire section because once you understand the basic tenets, fractal analysis actually becomes relatively simple. Therefore here is the sentence: *All fractal time series analyses amount to measuring how some form of variability changes a function of scale.* If you have tried your hand at reading foundational papers on fractal analysis (Eke, Herman, Kocsis, & Kozak, 2002; Kantelhardt, Koscielny-Bunde, Rego, Havlin, & Bunde, 2001; Peng et al., 1994), you may think otherwise. Many primary papers tend to be fairly technical, often seeming to contain more equations than words, and thereby, adding to the mystique surrounding fractal analysis. Our goal in this section is to convince the reader of the veracity of the above italicized sentence.

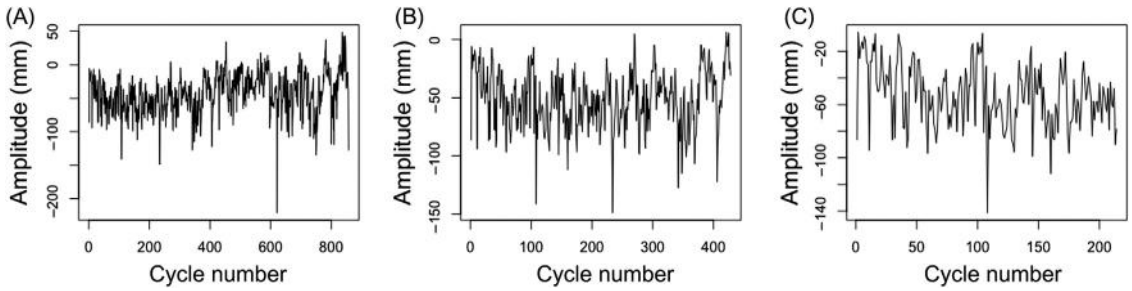

FIGURE 10.5

Zooming into the amplitude time series from Fig. 10.1C. (A) The entire time series. (B, C) Plots half and one-fourth of that time series, respectively. Plotting the data in this way suggests that, consistent with fractal theory, smaller portions of the time series bear a striking resemblance to the entire series.

In Section 10.2.1, we introduced the basic concepts underlying the roughness observed in geometrical fractals (e.g., self-similarity), both naturally occurring and mathematically derived. Here we translate those ideas to statistical fractals. Fig. 10.5A plots again the movement amplitude time series presented in Section 10.2. Subsequent panels plot the first half (Fig. 10.5B) and fourth (Fig. 10.5C) of that time series, respectively. Doing so reveals the first clue that movement time series may exhibit fractal properties. Though not as immediately vivid as Romanesco, one gets the sense that there is something similar about these smaller windows when compared to their larger predecessors. The similarity lies in the variability of the series. The same slow undulating pattern is present in all three panels. That is, *a similar pattern of variability* is observed regardless of the scale of observation.

This is the basic idea behind fractal analysis. Of interest is investigating how variability changes according to differing timescales. When variability changes proportionally from one timescale to the next, this provides statistical evidence that a time series exhibits fractal properties. That is, variability may also be scale-free in that its magnitude depends on the scale of measurement. Scale-free variability is the statistical equivalent to scale-free length or area typical of geometrical fractals and is the primary focus in fractal analysis of movement data. Is it possible that the movement amplitudes also exhibit fractal scaling, as anticipated in Fig. 10.5?

To explore that idea, we conducted a form of fractal analysis called detrended fluctuation analysis (DFA) on the time series in Fig. 10.5A and then plotted the output of that method in Fig. 10.6A. The technical details of that approach are explained in great detail in Section 10.3. For now, we simply note that Fig. 10.6A demonstrates how a measure of variance [called fluctuation, $F(s)$], depends on scale, s. In Section 10.2.2, we noted a convenience,

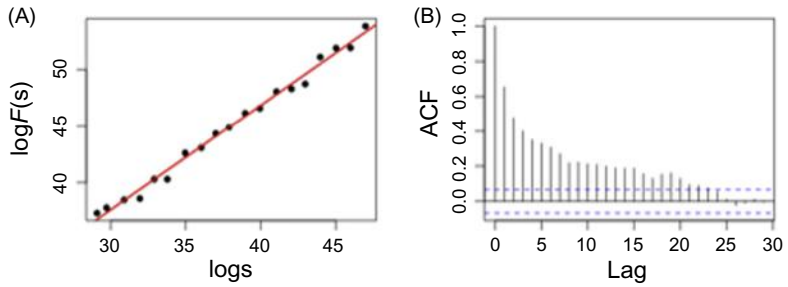

FIGURE 10.6

(A) Results of applying detrended fluctuation analysis (DFA) to the time series depicted in Fig. 10.5A. (B) Autocorrelation of the time series depicted in Fig. 10.5A.

namely, that power laws appear as straight lines on double logarithmic axes. Visual inspection suggests that this is a fitting description of Fig. 10.6A. That is, $\log F(s)$ appears to increase at a constant proportion as the timescale is stretched by a constant factor, as expected in the case of a power law. To test that hypothesis, a simple linear regression was fit to these data (red trend line in Fig. 10.6A) and provided an excellent fit ($R^2 = 0.99$) from the following regression equation, $\log F(s) = 0.93 \times \log s + 9.83$. Hence, results from the linear regression suggest that a power law may indeed be the underlying statistical model relating $F(s)$ and s. The regression coefficient, $m = 0.93$, represents the characteristic power law exponent relating variability and scale.

In the DFA literature, this exponent is termed α and is directly related to the measure Mandelbrot called the Hurst exponent in honor of Harold Edwin Hurst for his pioneering work related to hydrology (Hurst, 1951). Mandelbrot suggested H as a means to measure and quantify roughness typical of fractal time series (Mandelbrot & Hudson, 2006). H varies from 0 to 1, with roughness decreasing with increasing H. H is also related to the autocorrelation function depicted in Fig. 10.6B and is discussed in more detail in Section 10.3.1. The autocorrelation provides yet additional clues about the underlying fractal nature of the movement amplitude series. This is because the autocorrelation seems to decay quite slowly. This relationship is no coincidence. The autocorrelation function at a given lag, k, depends on the Hurst exponent in the following way:

$$\gamma(k) = 1/2|k+1|^{2H} - 2|k|^{2H} + |k-1|^{2H} \tag{10.2}$$

In Sections 10.2.1 and 10.2.2, we have provided the basic, theoretical underpinnings necessary for understanding the goal of applying fractal analysis to human movement data. As stated, the basic goal is to quantify how human movement variability changes as a function of timescale. In Section 10.3, we

provide an in-depth tutorial on the DFA method introduced in this section as well as a generalization of fractal analysis that has figured prominently in more recent work on human movement (Cavanaugh et al., 2017; Ihlen & Vereijken, 2013; Kelty-Stephen, Palatinus, Saltzman, & Dixon, 2013; Stephen et al., 2012). Despite a minor increase in technical detail, we think the reader will agree that the basic lessons explored in this section will hold: *Fractal analysis amounts to measuring how some measure of variability changes as a function of scale.*

10.2.3 Fractals in physiology and psychology

Before making the transition from theory to practice, we provide some insight into the important role fractals have played to-date in the study of human physiology and movement. There is an ever-growing list of processes that have been observed to produce fractal characteristics (Goldberger et al., 2002; Harrison & Stergiou, 2015; Peng, Havlin, Stanley, & Goldberger, 1995; Stergiou & Decker, 2011; Stergiou, Kent, & McGrath, 2016). The classic example is related to the human heartbeat, that is, fractal fluctuations of the heart are associated with cardiac health, while other patterns are associated with disease states like cardiac arrhythmia. Other examples abound and suggest that fractal behavior may distinguish healthy and unhealthy patients with Huntington's disease (Hausdorff et al., 1997), Parkinson's disease (Hausdorff, 2009), Alzheimer's disease (Woyshville & Calabrese, 1994), and attention-deficit/hyperactivity disorder (Anderson, Lowen, & Renshaw, 2006; Gilden & Hancock, 2007). Moreover, a number of other studies have shown fractal behavior is more prominent in the gait pattern of young adults than older adults or children (Hausdorff et al., 1997, 2001). Together, those findings suggest that fractal behavior may be a marker of health and also a measure of adaptability or smooth performance.

A natural question to follow this list of interesting results is: Why would biological systems exhibit fractal patterns to begin with? Over the years, a number of hypotheses have been suggested for the presence of fractal scaling in human movements (Diniz et al., 2011; Harrison & Stergiou, 2015; Ihlen & Vereijken, 2010; Kello et al., 2010; Thornton & Gilden, 2005; Van Orden et al., 2003). One particular hypothesis that has appeared to gain ground is the so-called *optimal movement variability* hypothesis (Hunt et al., 2014; Kaipust et al., 2013; Stergiou & Decker, 2011; Stergiou, Harbourne, & Cavanaugh, 2006; Stergiou, Yu, & Kyvelidou, 2013). This hypothesis suggests that human movement strikes a balance between predictability and complexity. Fractal processes inherently capture those qualities because fractals reflect complex structure that deviates from randomness without being overly predictable (Van Orden, Kloos, & Wallot, 2011). This hypothesis,

then, provides a reason why the presence of fractal scaling has been repeatedly discovered to be a marker of health and its absence a marker of disease. Situating the correlation between fractal scaling and health in terms of complexity has important consequences for the diagnosis and treatment of movement disorders. In Section 10.4, we present experiments that suggest ways in which to selectively alter the fractal characteristics of human movements.

10.3 Fractal analysis of time series data

It is not an exaggeration to say that one could devote an entire volume to the various techniques that fall under the umbrella of fractal analysis (Brown & Liebovitch, 2010). The purpose of this section, however, is not to provide an exhaustive treatment of all forms of fractal analysis. Instead, our goal is to provide a tutorial of one particular method of fractal analysis and its generalization. This method, *DFA*, is arguably the most common form of fractal analysis, and it is used by researchers in many scientific domains (Alvarez-Ramirez, Alvarez, & Rodriguez, 2008; Alvarez-Ramirez, Rodriguez, & Echeverria, 2009; Fayyaz et al., 2018; Hunt et al., 2014; Kaipust, Huisinga, Filipi, & Stergiou, 2012; Kaipust et al., 2013; Kantelhardt et al., 2001; Likens et al., 2015; Peng et al., 1994; Wang & Liu, 2010). There are many reasons for this popularity, not least of which is the method's simplicity, as will be demonstrated in the next section. To ease the technical burden of the reader, our presentation of the method is graphical and algorithmic in nature, but see Kantelhardt et al. (2001) for a more technical treatment.

10.3.1 Detrended fluctuation analysis

DFA was not the first method of fractal analysis introduced but has become the methodological workhorse (cf. Hurst, 1951). The method's rise in popularity originates from several sources: (1) As we will show in this section, the method is relatively simple. You can perform the analysis with virtually any programming language; the method has even been implemented in Microsoft Excel (Arsac & Deschodt-Arsac, 2018). (2) The method is versatile. It was developed specifically to address many common issues also encountered in movement science such as *nonstationarity*. Nonstationarity has many potential meanings, but here we use this term to refer to the tendency for the mean and variance of a time series to fluctuate over time.

DFA was originally introduced in the application of random walk theory to DNA nucleotide sequences (Peng et al., 1994). Those authors were interested in whether sequences of DNA nucleotides exhibited slowly decaying autocorrelation functions like those depicted in Fig. 10.6B. The authors based their approach on the observation of "patchiness" in nucleotide sequences where,

for example, purine was found to exist in relative abundance over pyrimidine in different parts of a sequence. To explore this idea, they assigned a value of −1 or 1 to each nucleotide, respectively, and then integrated the resulting binary increment time series to create a one-dimensional walker. In the absence of autocorrelation, one expects $F(s)$ describing a random walker to grow as a power law such that $F(s) \sim s^{0.5}$. Deviations from the proportion where $\alpha = 0.5$ signify the presence of autocorrelation that decays slower than a simple random walk with independent increments. Consistent with predictions, the authors found that the "patchiness" observed in nucleotide sequences seemed to indicate the presence of fractal scaling. In the remainder of this section, we describe the DFA algorithm in considerable detail to illustrate its use on human movement data.

The DFA algorithm is composed of five essential steps. *Step 1* involves creating a *profile* of a time series by subtracting its mean from each data point and then integrating the series. This step is absolutely critical because it converts the observed time series to a random walk-like process that meets the theoretical assumptions of DFA. Integrating the series simply involves creating a new time series where each point is the sum of all preceding points of the original time series. As an example, consider the simple time series. $X(t) = \{3,1,2,4\}$, where $t = 1, 2, 3, 4$. Integrating $X(t)$ results in a time series $X'(t) = \{3, 4, 6, 10\}$. Again, these operations have the effect of creating a random walk-like process. Our analysis is concerned with how this profile deviates from a genuine random walk (i.e., a walk with increments that are uncorrelated noise), revealing any underlying fractal characteristics of the time series in question. This toy example also illustrates the importance of mean-centering. Without first centering, we run the risk of the integral tending toward infinity and again obscuring underlying structure. Now, consider Fig. 10.7A, which represents a time series collected over a period of 10 seconds. We have intentionally given this series arbitrary units because we want to emphasize the generality of DFA as a time series tool. Fig. 10.7A could represent any number of physiological processes such as postural sway or neural activity. Transitioning from Fig. 10.7A to B is a more realistic presentation of step 1 mentioned earlier in this paragraph. The difference is striking; Fig. 10.7B bears a remarkable similarity to the random walks such as those observed in stock prices (Mandelbrot & Hudson, 2006). Note that the series drifts for long periods of time in one direction before changing direction and drifting in the opposite direction.

Step 2 of the DFA algorithm is illustrated in Fig. 10.7C. As this figure implies, step 2 involves dividing the series into a sequence of nonoverlapping windows. Here we have separated the series into four windows. In practice, four windows are not sufficient to obtain unbiased estimates of fluctuation discussed later in step 4 of the algorithm. We use four windows here for ease of

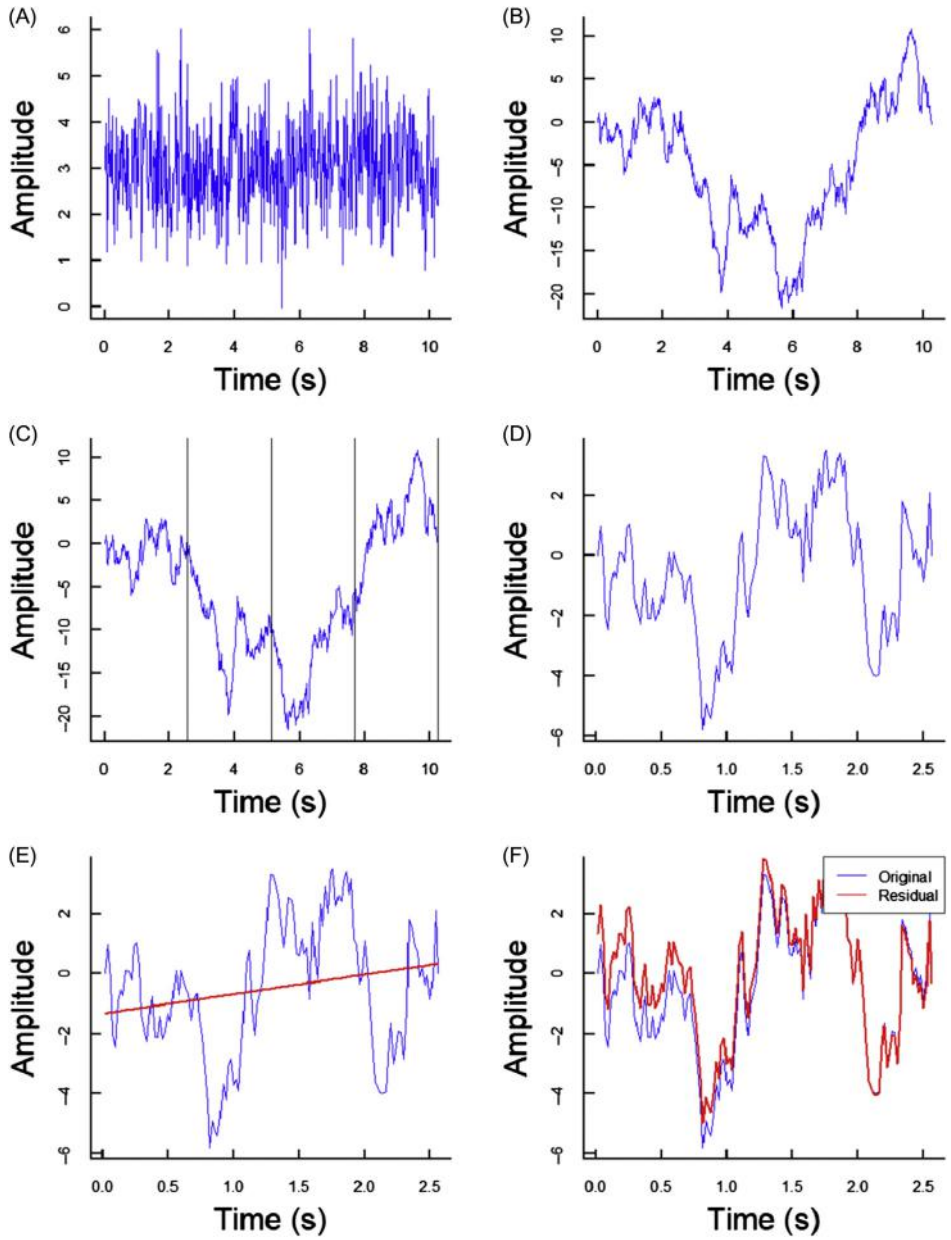

FIGURE 10.7

Demonstration of the first three steps of DFA. Starting with the time series in (A), we create the profile in (B) by mean-centering and summing over the series in (A). Next, in (C) we divide the series into four windows. In practice, more windows are needed for stable estimates of the fluctuation function, $F(s)$. Panel (D) "zooms in" to the first window of (C) to better emphasize the linear regression conducted within each window as depicted in (D). Panel (E) depicts fitting a local trend line via ordinary least squares. Finally, (F) illustrates removal of the local trend estimated in (E).

visualization. For better understanding of how the algorithm works, Fig. 10.7D zooms in to the first window of Fig. 10.7C. *Step 3* is the *detrending* step that gives DFA its name and entails fitting a regression line within each of the windows depicted in Fig. 10.7E, before subtracting the fitted trend line from the data in each window as depicted in Fig. 10.7F.

Step 4 of the DFA algorithm is depicted in Fig. 10.8A–E and involves finding the average fluctuation, $F(s)$, which is defined as the root mean square of local residuals. That is, $F(s)$ represents the average distance of each point in a time series from a local trend line estimated at a given scale, s. In this sense, it is a standardized measure of deviation. This process is repeated for several s as depicted in Fig. 10.8B–E.

Finally, in *step 5*, a regression is performed as depicted in Fig. 10.8F in order to estimate the scaling exponent, α, which provides a measure of how fast the standard deviation changes as a function of the timescale. When α sits on the interval (0,1), it is equivalent to the Hurst exponent, H, and has important interpretative ranges. When $\alpha = H = (0, 0.5)$, the time series is said to be *antipersistent* and has a negative autocorrelation that dampens to zero quickly over time (Beran, 1994). In contrast, $\alpha = H = (0.5, 1.0)$ reflects a *persistent* time series with a positive autocorrelation that dampens slowly over time. An example of this sort of autocorrelation function was presented in Fig. 10.6B.

10.3.1.1 Best practices suggestions for applying detrended fluctuation analysis to human movement data

Plot your data

One of the most important steps in performing fractal analysis (or any analysis, for that matter) is plotting and visually inspecting your data. The example time series presented in this chapter are prototypical examples of time series that are appropriate for conducting fractal analysis. The time series in Fig. 10.1C, for example, is a very noisy-looking time series without any obvious polynomial (e.g., linear, quadratic, cubic) or periodic (e.g., sinusoidal) trends. Visual inspection is no guarantee that one's time series actually is a good candidate, but it can help identify some obvious problems present in one's data. For example, your time series may have a general upward or downward linear trend, indicating the need for at least a quadratic polynomial detrend (detrending order is discussed in more detail in the section "Choosing a polynomial order").

Time series length

Students of statistics are keenly aware of the relationship between statistical power and the number of participants in one's study. In general, more participants mean a more powerful research design, holding effect size constant.

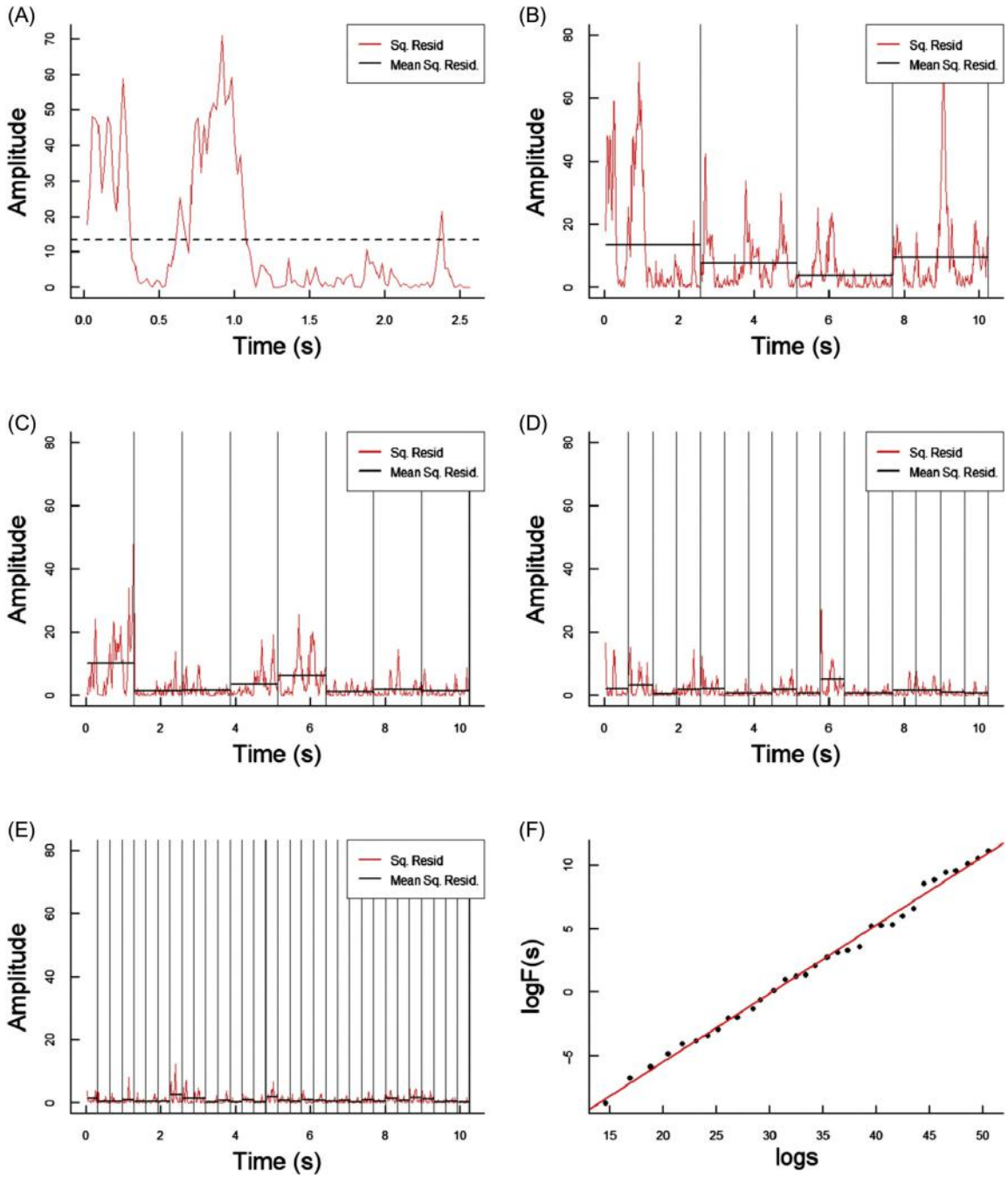

FIGURE 10.8

This figure depicts steps 4 and 5 of the DFA algorithm. Panel (A) zooms into the first window depicted in Fig. 10.7 and shows the computation of both the squared residuals as well as their average (*black line*). Panels (B)—(E) show this process of squaring and averaging repeated for each of four scales ranging from 4 to 32 bins. Panel (F) shows step 5 of DFA, which regresses the square root of the average squared residual as a function of timescale. The logarithmic scale in that panel is based on a power of 11/10 rather than a power of 2 as depicted in (B)—(E).

A similar situation emerges within the context of time series methods such as DFA. Fortunately, researchers have investigated the performance of DFA with time series of different lengths to investigate its performance in various contexts (Delignieres et al., 2006; Stroe-Kunold, Stadnytska, Werner, & Braun, 2009). The general rule with this and all other fractal analysis methods is that more is always better. Standard errors associated with DFA become almost trivial with several thousand observations. However, this general rule is cold comfort for the gait analyst limited to only a few hundred strides, for example. Instead, we follow precedent in the literature and make the following recommendation. In general, ≥ 500 data points is considered necessary for stable estimates of α. A caveat to this advice, however, pertains to instances when it is possible to obtain several, identical short trials in succession (Delignieres et al., 2006). This is because, in those instances, the *average* α seems to remain unbiased. We note, though, that one recent study questions this suggestion (Marmelat & Meidinger, 2019), indicating the need for additional research. In addition, a newer modified version of DFA, called unbiased DFA, has recently been introduced that shows excellent performance with as few 300 data points (Yuan, Gu, Weng, & Yang, 2018). We test this new method in Section 10.4.2 in order to investigate movement amplitude time series similar to those depicted in Figs. 10.1 and 10.5.

Choosing a polynomial order

One of the least discussed and reported parameters of DFA is the polynomial order chosen for detrending. Even when discussed, the advice given is rarely much beyond something like "choose the appropriate detrending order" without any definition of what the word "appropriate" means in this context. Here, we recapitulate concrete suggestions for performing DFA that have been present in the literature for some time (Kantelhardt et al., 2001). In that study, the recommendation involves visual inspection for *crossovers*. A crossover reflects a sharp change in slope of $\log F(s)$ against s. Crossovers stem from two possible sources.

First, the crossovers may reflect two different scaling regions, that is, different scaling behaviors over short and long timescales. In the center of pressure data, for example, crossovers have been suggested as evidence of two different control strategies involved in maintenance of upright posture (Collins & De Luca, 1993). Second, crossovers may stem from strong time trends (e.g., linear, quadratic, cubic, quartic) superimposed on a signal and may be masking scaling behavior. In the latter case, the scale at which the crossover is observed (i.e., the *inflection point*) will shift to larger timescales as a function of increasing detrending order. In fact, when the DFA detrending order is larger than the polynomial order of the time trend, artificial crossovers are completely eliminated (Kantelhardt et al., 2001). Hence, applying increasing

detrending orders in DFA simultaneously provide a means to distinguish real from artificial crossovers and identify the order of polynomial time trends, if they exist.

The recommendation then is to compute DFA with the lowest detrending order, say a linear detrending order, and inspect the log$F(s)$ by s plot for evidence of crossovers. If no crossovers are present, the linear detrending function is sufficient. If a crossover is present, repeat DFA with higher and higher order detrending functions and investigate the effect on the crossover. If the inflection point changes very little as a function of increasing order, then a linear detrending function is sufficient and the researcher may then investigate the two scaling regions separately (Likens et al., 2015). If the inflection point does change, continue increasing the detrending order until the crossover disappears and proceed to estimate the slope of the log$F(s)$ by s plot.

Which timescales should you use?

Selecting the number of timescales over which to compute DFA remains somewhat unclear, despite the method's long history. One problem is that at the smallest timescales, it is easy to overfit the local regressions in the smaller windows. This matter is further complicated by the presence of crossovers that require higher order polynomials to resolve. A second issue concerns the estimate of $F(s)$ at large timescales. The number of windows becomes small as timescales become large. This is problematic because the variance of the estimate of $F(s)$ also increases in an undesirable way, as the number of bins involved in the average becomes fewer and fewer. One recommendation from the gait analysis literature is to use 16 data points as a minimum and $T/9$ as a maximum where T is the length of the series in question. However, maintaining even spacing of scales on a logarithm scale may allow for higher upper limits on the maximum scale (Almurad & Delignières, 2016; Likens et al., 2015; Yuan et al., 2018). Additional research needs to be conducted in order to answer this question more definitively, especially with respect to crossover phenomena (Collins & De Luca, 1993; Kantelhardt et al., 2001).

10.3.2 Multifractal detrended fluctuation analysis: It's still that simple (almost)

10.3.2.1 An intuitive introduction to multifractals

The term *multifractal* has a somewhat intuitive quality to it. It seems to refer to the idea of multiple fractals. The preceding sections discussed the concept of a fractal in some detail. This discussion revealed interesting, naturally occurring properties like self-similarity and scale-invariance, roughness, and irregularity. Our discussion thus far, however, may have painted an overly simplistic picture. The reader may have noted that some natural structures are not perfectly self-similar. Reinvestigating the swirling pattern of

Romanesco broccoli in Fig. 10.2 at finer and finer scales eventually gives way to a stalk. Performing DFA on a time series of movement amplitudes eventually gives way to a line, revealing the absolute limit of its timescale resolution (Section 10.3.1.1; Kantelhardt et al., 2001). The implication of these lower limits is that natural processes are limited in their exhibition of self-similarity and scale-invariance. Furthermore, these limits raise additional questions about other ways in which naturally occurring time series differ from perfect fractal forms.

As a means to addressing that latter point, consider an experiment where participants are asked to walk on a treadmill for a relatively long period of time, say 20 minutes. Additional details about this experiment will be given in Section 10.4.1, but for now we will keep things simple. The researchers collected kinematic data across the body and used that data to estimate a series of step lengths for the left leg while walking. Fig. 10.9 depicts one of these time series. Immediately, the impression is that the time series has something in common with the amplitude time series in Fig. 10.1C. Fig. 10.9 has a similar undulating structure with trends that seem to span timescales ranging from tens to hundreds of steps. Thus a natural inclination is to apply DFA to this time series in order to investigate whether it has the same self-similar structure found in so many naturally occurring time series. This seems reasonable enough, and, in fact, many studies have performed this analysis on various features of gait (Hausdorff, 2007, 2009; Hausdorff & Peng, 1996; Hunt et al., 2014; Kaipust et al., 2012; Marmelat & Meidinger, 2019; Rhea, Wittstein, Kiefer, & Haran, 2013; Terrier & Dériaz, 2011). Thus results supporting the presence of fractal scaling in human gait span decades.

A tacit assumption in applying DFA to those gait time series (e.g., stride time, step length), though, is that DFA is a one-size-fits-all modeling

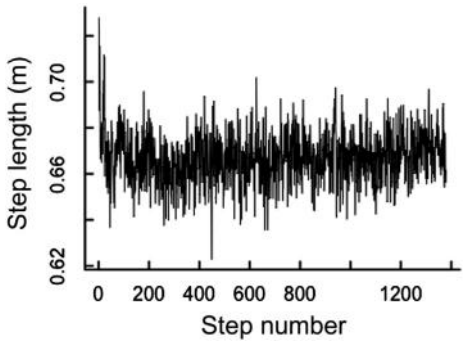

FIGURE 10.9
Sample step length time series.

approach. Furthermore, DFA carries with it the assumption that the series in question follows one—and only one—power law. That is, DFA assumes a time-invariant process, a process that does not change as a function of time. As variable and dynamic as Fig. 10.9 appears, DFA assumes it reflects one and only one control strategy. Gait is a highly dynamic process, perfectly embodying what Bernstein called repetition without repetition (Bernstein, 1967). Hence, we raise the question: Is it reasonable to assume that gait reflects one—and only one—control strategy? Results from studies of scaling behavior of gait have suggested the contrary (Scafetta, Griffin, & West, 2003). For instance, scaling behavior appears strongly related to the age of the walker (Hausdorff et al., 1997), implying that gait control strategies change over the lifespan. Moreover, several studies have produced evidence that scaling behavior is sensitive to a range of experimental manipulations and contexts (Anastas, Stephen, & Dixon, 2011; Fine et al., 2015; Hunt et al., 2014; Kaipust et al., 2012; Likens, Amazeen, Stevens, Galloway, & Gorman, 2014; Likens et al., 2015; Stephen & Anastas, 2011; Stephen, Arzamarski, & Michaels, 2010). In the remainder of this section, we will demonstrate another method of analysis, a generalization of DFA called multifractal detrended fluctuation analysis (MFDFA) that allows one to investigate time-varying fractal properties where they exist (Kantelhardt et al., 2002).

10.3.2.2 A brief tutorial on multifractal detrended fluctuation analysis

Much like the literature on DFA, the primary literature on multifractal analysis is often very challenging. Most original work is published in statistical mechanics journals (Kantelhardt et al., 2002), and as such, can be difficult for many researchers to digest. In this section, we follow the same format as is used in Section 10.3.1. In fact, most of the algorithm has already been covered in that section. Here, we simply point out modifications to the original steps in DFA. We again present the steps involved in a graphical manner. That is, we present the steps in descriptive, algorithmic form rather than in equation form. We encourage the reader to keep in mind the statement made at the outset of Section 10.3—we are measuring how some form of variability changes as a function of scale.

Performing MFDFA on a time series follows the same basic steps presented in Section 10.3.1. Differences appear in *steps 4* and *5*. Focusing first on *step 4* (Fig. 10.8A–E), recall that the step involved computing the root mean *squared* deviation of each point from a local trend line at a given scale, *s*. Squaring the residuals implies that we are working with the second statistical moment, that is, *variance*. If we were to cube the residuals and then take the cubed root of the average cubed residual, we would be dealing instead with the third statistical moment, *skewness*. If we were to raise the residuals to the

fourth power and take the fourth root, we would be dealing with the fourth statistical moment, *kurtosis*. These moments will be familiar to students in introductory statistics courses. It turns out, though, that just as there are higher order, albeit less common, derivatives (e.g., snap, crackle, and pop), there are also higher and lower statistical moments. Analyzing the scaling behavior of these statistical moments in relation to one another reveals the presence of *monofractality* (i.e., a single power law) or *multifractality* (i.e., more than one power law).

This works because different statistical moments, ranging between negative and positive real numbers, act as microscopes capable of emphasizing fluctuations of different sizes (Cavanaugh et al., 2017; Ihlen, 2012; Ihlen & Vereijken, 2010; Kelty-Stephen et al., 2013). To illustrate this point, consider Fig. 10.10A that represents the squared residuals obtained in *step 4* in Section 10.3.1 within a single window. This panel is identical to that in Fig. 10.8A. Now consider Fig. 10.10B, in which we have cubed the residuals instead of squaring them. This has the effect of magnifying large fluctuations like those between 0 and 1.0 seconds, while minimizing smaller fluctuations like those found later in that window. Looking at the *y*-axis, the scale increases by one order of magnitude! In contrast, Fig. 10.10C shows the effect of raising the residuals to the power of -3. The dramatic difference is that raising the residuals to increasingly negative values has the effect of emphasizing small fluctuations while minimizing large fluctuations. This is the difference between step 4 in DFA and step 4 in MFDFA. Rather than simply estimating root mean squared residuals as in DFA, MFDFA involves finding the qth root mean q-order residual, $F^{(q)}(s)$, where q is the order of the statistical moment that theoretically ranges from negative infinity to positive infinity. The original DFA procedure is equivalent to the case when $q = 2$. As the reader might have anticipated, *step 5* in MFDFA simply entails measuring how $F^{(q)}(s)$ varies as a function of scale, s, via ordinary least squares regression as depicted in Fig. 10.10D for q ranging from -3 to 3 in integer increments.

The result of step 5 in MFDFA is a spectrum of scaling exponents called the *multifractal spectrum* depicted in Fig. 10.10E. The multifractal spectrum provides a summary of time-varying scaling exponents present in the data known as the *generalized Hurst exponent*, $H(q)$. In the case of a monofractal, all the regression lines are parallel (i.e., a single exponent), as depicted in Fig. 10.10D, and relatively constant $H(q)$, as seen in Fig. 10.10E. In the case of a multifractal, the expectation would be that the q-order regression lines have different slopes, reflecting differing scaling behavior for different statistical moments. Many authors prefer to transform the spectrum to the parabolic form depicted in Fig. 10.10F. We include it here for completeness sake but refer readers to other texts for further details and interpretation

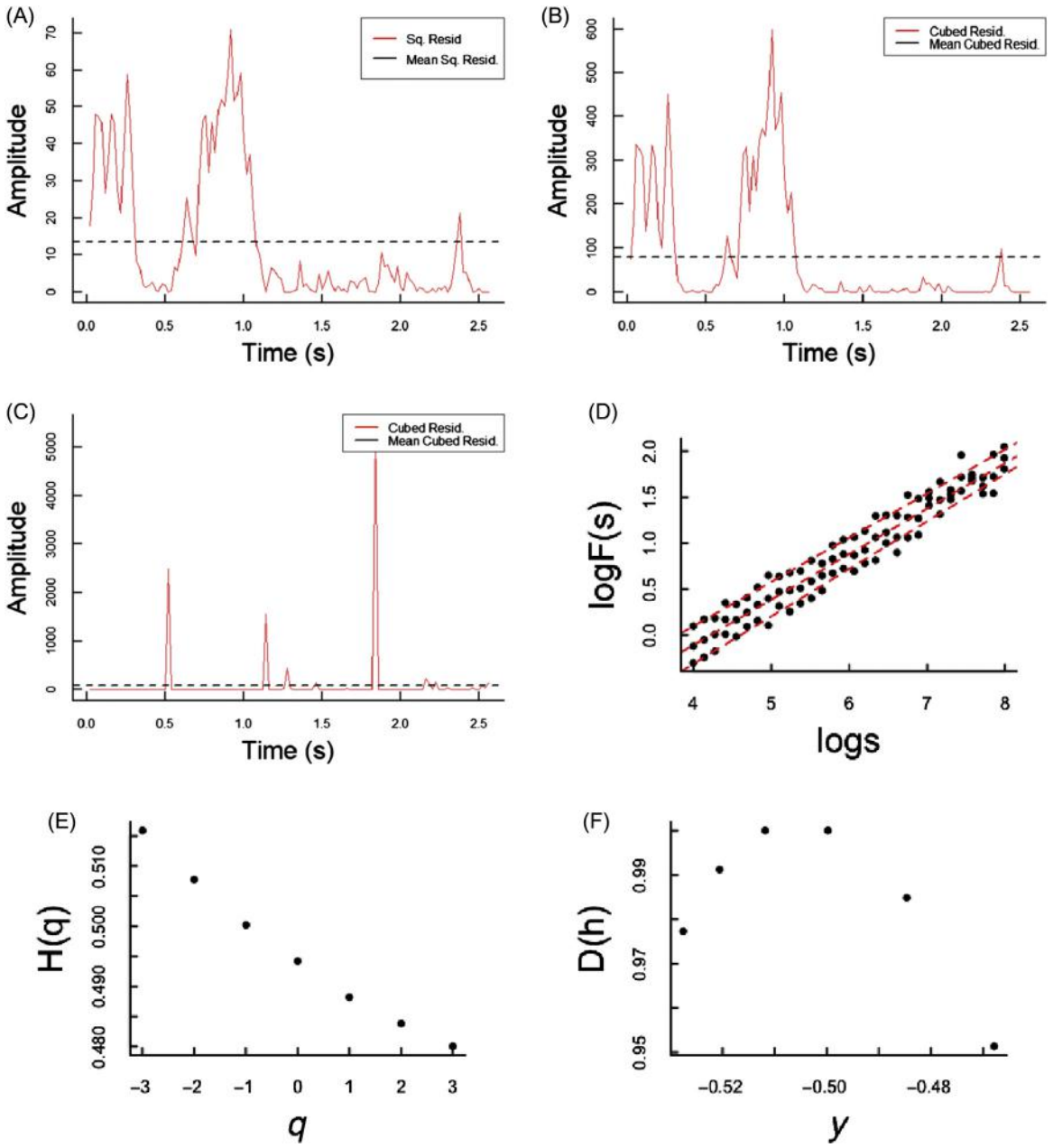

FIGURE 10.10

Steps 4 and 5 in MFDFA. Panel (A) shows the familiar DFA step of squaring and averaging residuals. Panels (B) and (C) show the alteration of step 4 in MFDFA which involves larger positive values (e.g., 3 in B) or negative values (e.g., −3 in C). Panel (D) shows step 5 in MFDFA, fitting $F^{(q)}(s)$ with a linear regression where scale is once again the predictor. Panel (E) shows the spectrum of generalized Hurst exponents, $H(q)$. Panel (F) shows an alternative representation of the spectrum found in (E).

(Kantelhardt et al., 2002). We do this for two reasons: (1) Our goal is to make this presentation as simple as possible and we felt that including these computational details was contrary to that goal. (2) We prefer to think in terms of the Hurst exponent with its convenient interpretive ranges, related to the relative roughness and persistence of the time series under investigation. For those reasons, we prefer the spectrum presented in Fig. 10.10E. The width of the multifractal spectrum will be a matter of further study in Section 10.4.

10.3.2.3 Practical considerations

All of the practical considerations concerning MFDFA translate directly from DFA with a few exceptions. The length of time series needed to properly estimate the multifractal spectrum is less straightforward than in the case of DFA because the needed length depends heavily on the range of q inspected. In addition, far less work has been done evaluating MFDFA's performance in various contexts. There have been some efforts made, but more work is needed in this regard (López & Contreras, 2013). That study found that, across a range of time series lengths, the accuracy of MFDFA depended more on the range of q than the series length. Indeed, they found good agreement between theoretical and observed values when q ranged between small negative values (e.g., -1, -2) and small positive values (e.g., 1, 2) and the time series was as short as 1024 data points in length. However, others have successfully used MFDFA with relatively shorter time series, having only about 500 data points (Delignières, Almurad, Roume, & Marmelat, 2016). Therefore as a general recommendation, we suggest that practitioners strive to collect series as long as allowed by theoretical and practical concerns for use with MFDFA. However, we would strongly advise against using the method on fewer than 500 data points. In any case, we also recommend using MFDFA with only a small range of q (e.g., -2 to 2). Future simulation work should focus on the performance of MFDFA on short time series typical of human movement data.

10.4 Applications to laboratory data

The preceding discussions were meant to alleviate some of the technical burden associated with conducting fractal analysis of human movements. Our presentation has been largely graphical and descriptive, and we have tried, where possible, to make concrete suggestions regarding the parameter selection and conducting fractal analysis. In Section 10.4, we present complete examples demonstrating the use of fractal analysis on studies involving human movement.

10.4.1 Example 1: Application to human gait

A number of recent studies have shown that walking in time with various pacing signals may have a dramatic effect on fractal scaling patterns observed from various features of gait (Hunt et al., 2014; Kaipust et al., 2012). The basic message implied by these studies is that fractal characteristics of gait are sensitive to experimental manipulations involving both visual and auditory stimuli. Studies of this nature have important consequences for developing treatments for a broad range of motor disorders that affect walking. In this section, we report results from a simple experiment that involves walking in time to one of four metronomes and demonstrates how monofractal and multifractal characteristics depend on the act of paced walking.

In this study, 31 healthy young subjects were asked to perform two walking tasks: (1) a baseline task in which they walked at a comfortable, self-selected pace on a treadmill, and (2) a pacing task in which they coordinated their steps with the onset of auditory metronome beeps. Participants walked with one of four metronome conditions that were labeled: None, Pink, White, and Periodic. The None condition simply involved participants walking at a self-selected speed on a treadmill. The Pink noise condition involved participants waking to a metronome where the intervals between beeps had a Hurst exponent near 1.0. In the White noise condition, interbeat intervals had a Hurst exponent near 0.5. In the Periodic condition, participants attempted to walk in sync with a standard metronome with interbeat intervals that were constant over time. Participant's movements were tracked during both tasks using motion-tracking equipment. These kinematic data were used to compute time series of step lengths, the distance in meters between successive heel strikes of the left foot. Each task lasted approximately 20 minutes.

Both DFA and MFDFA were applied to these data in order to investigate how the fractal properties characterizing participants step length depend on the metronomes used in this experiment. Results from this experiment are depicted in Fig. 10.11.

10.4.1.1 Monofractal results and discussion

Focusing Fig. 10.11A, several interesting patterns may be observed. First, and as expected, Hurst exponents for the various metronome conditions clustered tightly together during the Baseline task. A second, rather mundane result is that participants in the None condition produced the same scaling patterns in the Pacing task as in the Baseline task. In contrast, the Hurst exponent for both the White noise condition and the Periodic condition seem to be lower during the Pacing task than during the Baseline task. One might be tempted to conclude that the mere act of synchronizing with an external pacing signal

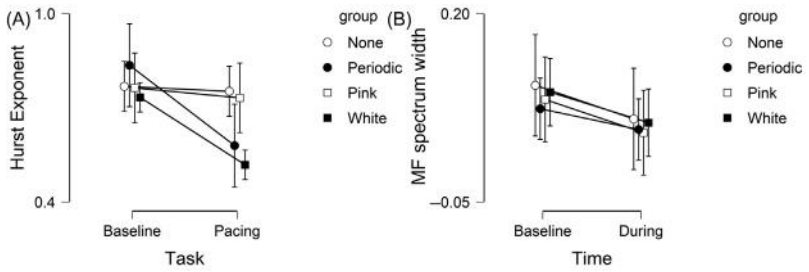

FIGURE 10.11

(A) The Hurst exponent as a function of time and metronome type. (B) The multifractal spectrum width as a function of both time and metronome type. In both panels, error bars reflect 95% confidence intervals.

is sufficient to disturb fractal patterning in gait. That conclusion may be premature, however, because walking in time with the Pink noise metronome did not seem to alter the natural fractal characteristics of gait, consistent with previous findings (Hunt et al., 2014; Kaipust et al., 2012).

We investigated these implied trends by conducting a 4_B(Metronome) × 2_W(Task) mixed design analysis of variance (ANOVA) with the Hurst exponent derived from DFA as the dependent variable. The analysis revealed both a main effect of metronome condition, $F(3,23) = 4.808$, $P = .01$, $\omega^2 = 0.297$, and a main effect of task, $F(1,23) = 22.93$, $P < .001$, $\omega^2 = 0.297$; however, those main effects were modified by a two-way interaction, $F(3,23) = 5.32$, $P = .006$, $\omega^2 = 0.115$. The nature of that interaction was revealed by exploring simple main effects, by comparing Pacing task at each level of metronome type. Consistent with trends implied in Fig. 10.11A, both the Periodic, $F(1,23) = 23.914$, $P < .001$, and the White noise, $F(1,23) = 19.317$, $P < .001$, metronomes reduced the fractal scaling that is naturally observed across many consecutive step lengths.

10.4.1.2 Multifractal results and discussion

We now switch focus to Fig. 10.11B, which represents the average multifractal spectrum width as a function of task and metronome type. The multifractal spectrum width was obtained by applying MFDFA (Section 10.3.2) to time series of successive step lengths captured in the experiment described in Section 10.4. Similar to the results regarding the Hurst exponent described in Section 10.4.1.1, the average multifractal spectrum width for all Pacing conditions tends to cluster during the Baseline condition. In contrast, though, no interaction is apparent between Task and Pacing condition, implying a uniform decrease in multifractal spectrum width across all Pacing conditions.

We statistically investigated the effects of task and metronome on multifractal spectrum width using a $4_B(\text{metronome}) \times 2_W(\text{task})$ mixed ANOVA. Results from the ANOVA supported those from visual inspection. That is, the analysis revealed a relatively weak main effect of task, $F(1,23) = 6.46$, $P = .018$, $\omega^2 = 0.12$, resulting from the fact that, on average, the Pacing task produced more narrow multifractal spectra than did the Baseline task. One might be tempted to explain these results in terms of the task constraints. Walking in time with a metronome is an arguably more attention-demanding task than simply walking at a self-selected speed. However, this conclusion would also be premature as participants in the None condition also showed the decline in spectrum width during the metronome condition. Hence, contrary to our hypothesis, the multifractal spectrum width was not differentially perturbed by the various metronome conditions used in this experiment. Instead, the observed decrease in multifractal spectrum width may be better explained by some other source of unexplained influence such as fatigue or simple passage of time. We reserve further interpretation as a matter of future investigation.

10.4.1.3 General discussion

In this example, we explored the idea that the fractal characteristics of step lengths observed during treadmill walking are sensitive to experimental manipulations involving auditory synchronization. Specifically, we investigated the extent to which various metronome types alter the naturally occurring fractal patterns observed during walking. In doing so, we replicated known findings concerning alteration of monofractal scaling from periodic and white noise metronomes (Hunt et al., 2014; Kaipust et al., 2012). A surprise was the lack of an effect for the multifractal spectrum width. Future work will investigate, in depth, how resistant multifractal gait characteristics are to manipulations similar to those currently investigated.

10.4.2 Example 2: Detrended fluctuation analysis applied to visual-motor tracking

Referring back to the example first discussed in Section 10.2, this section presents a complete worked out example where we apply fractal analysis to movement time series recorded in an experimental setting. Eleven participants performed a simple visuomotor task wherein they coordinated their right arms with on on-screen oscillating stimuli (see Fig. 10.1). Additional details about the task are given in Section 10.2. In that earlier section, we partially described an experiment in which participants coordinated their right arm (through external rotation about the elbow) with an on-screen oscillatory stimulus. Section 10.2.2 described only one condition of the complete experiment, the control condition, in which participants simply attempted to

coordinate with a stimulus with constant frequency, in the absence of perturbations. In actuality, the experiment described here had three conditions: a control condition, a movement perturbation condition, and a respiratory perturbation condition. The movement perturbation condition contained three distinct time segments: 5 minutes at 1 Hz, 5 minutes at 1.4 Hz, and another 5 minutes at 1 Hz, corresponding to Pre, During, and Post perturbation. The respiratory perturbation condition also had three segments. The first and third segments (5 minutes each) were identical to the control condition. In the second segment, however, participants were instructed to slow their breathing. Interpretation of what "slow" meant was left to the participants. The purpose of this exploratory study was to investigate how different perturbation types affect the fractal scaling of amplitude series.

We applied DFA to the maximum amplitude time series as described in Section 10.2 (see Fig. 10.1) using the unbiased DFA algorithm that has been suggested recently for short time series (Yuan et al., 2018). This algorithm differs from the one presented in Section 10.3.2 in two ways: (1) The algorithm uses overlapping windows instead of nonoverlapping windows, and (2) the algorithm has an alternative approach to estimating the fluctuations in each window. The technical details of that approach are beyond the scope of this chapter, but the method essentially involves estimating variance via evaluating autocorrelation with only a few data points.

10.4.2.1 Results and discussion

Results from this experiment are depicted in Fig. 10.12, which suggests that the Hurst exponent in the speed perturbation was varied over the course the trial, decreasing considerably post perturbation. Fig. 10.12 also suggests a decrease in the Hurst exponent in the speed condition after the perturbation. In order to explore those trends, we conducted a 3(time) × 3(condition) repeated measures ANOVA. The ANOVA found no evidence of main effects of either time or condition; however, the analysis did reveal an interaction between time and condition, $F(4,\ 40) = 3.27$, $P = .021$, $\omega^2 = 0.071$, a weak effect by conventional standards. Simple effects tests were then conducted by comparing change over time while holding condition constant. No differences were present in either the control or breathing perturbation conditions; however, a significant simple effect was found for the speed perturbation condition, $F(2,\ 40) = 5.38$, $P = .009$. Follow-up tests revealed that only the post perturbation period in the speed condition differed from baseline, $t(18) = 2.95$, $P = .04$.

The results from this experiment clearly demonstrate that movement amplitudes exhibited evidence of fractal scaling as all observed Hurst exponents were in the region considered typical for persistent fractal series. However, the results from this experiment provide little support for the idea that fractal scaling of movement amplitudes is altered by perturbations of speed or

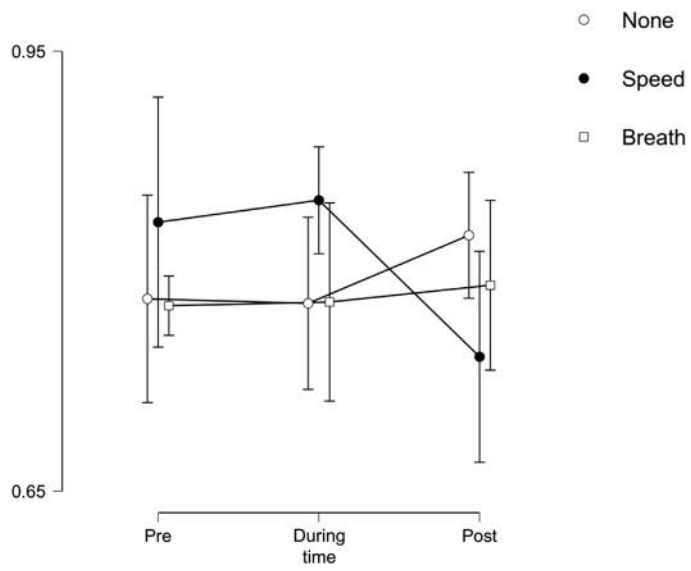

FIGURE 10.12
Hurst exponent as a function of time and condition. Error bars reflect 95% confidence intervals.

respiration. If anything, participants in the speed perturbation may have experienced some sort of residual effect, given the decrease in scaling present post perturbation. This interpretation should be taken with a grain of salt, though, because the interaction effect size was rather small. There are several possible reasons for the collective lack of results. First, it is possible that the perturbations used in this study were not sufficient in magnitude to elicit a significant response. Second, we analyzed movement amplitudes. It is possible, given the task, that amplitude was not a relevant control variable and there is evidence in the literature that task-irrelevant aspects of movement are unaffected by task constraints (Kello, Beltz, Holden, & Van Orden, 2007). A third possibility is that our time series were simply not long enough to promote precise measurement of the Hurst exponent. Future research will be needed in order to determine how well the modified version of DFA used for these short time series performs is in settings similar the present one.

10.5 Conclusion

Our goal in constructing this chapter was to present a simplified introduction to fractal analysis of human movement data by avoiding heavy-handed mathematics and confusing jargon. Instead, we have presented the material in plain language and taken care to define terms unique to fractal theory and analyses.

To that end, we have presented basic ideas related to fractal theory and translated those ideas to fractal characteristics typical of human movement variability. In addition, we have presented an in-depth tutorial on one of the most common methods of fractal and multifractal analysis. Lastly, we presented two complete examples demonstrating how to use these techniques in laboratory studies, in biomechanics and gait analysis. One of those experiments replicated known findings from the literature, while the other found that fractal dynamics may, in some cases, be resistant to experimental manipulations. All in all, we believe that our presentation will provide newcomers to fractal movement science with an easy way to contribute to an exciting line of research.

References

Almurad, Z. M. H., & Delignières, D. (2016). Evenly spacing in detrended fluctuation analysis. *Physica A: Statistical Mechanics and Its Applications*, *451*, 63–69. Available from https://doi.org/10.1016/j.physa.2015.12.155.

Alvarez-Ramirez, J., Alvarez, J., & Rodriguez, E. (2008). Short-term predictability of crude oil markets: A detrended fluctuation analysis approach. *Energy Economics*, *30*(5), 2645–2656.

Alvarez-Ramirez, J., Rodriguez, E., & Echeverria, J. C. (2009). Using detrended fluctuation analysis for lagged correlation analysis of nonstationary signals. *Physical Review E*, *79*(5), 057202.

Anastas, J. R., Stephen, D. G., & Dixon, J. A. (2011). The scaling behavior of hand motions reveals self-organization during an executive function task. *Physica A: Statistical Mechanics and Its Applications*, *390*(9), 1539–1545.

Anderson, C. M., Lowen, S. B., & Renshaw, P. F. (2006). Emotional task-dependent low-frequency fluctuations and methylphenidate: Wavelet scaling analysis of 1/f-type fluctuations in fMRI of the cerebellar vermis. *Journal of Neuroscience Methods*, *151*(1), 52–61. Available from https://doi.org/10.1016/j.jneumeth.2005.09.020.

Arsac, L. M., & Deschodt-Arsac, V. (2018). Detrended fluctuation analysis in a simple spreadsheet as a tool for teaching fractal physiology. *Advances in Physiology Education*, *42*(3), 493–499. Available from https://doi.org/10.1152/advan.00181.2017.

Beran, J. (1994). *Statistics for long-memory processes*. New York: Chapman & Hall.

Bernstein, N. (1967). *The co-ordination and regulation of movements*. New York: Pergamon.

Brown, C. T., & Liebovitch, L. S. (2010). *Fractal analysis*. Los Angeles, CA: SAGE.

Cavanaugh, J. T., Kelty-Stephen, D. G., & Stergiou, N. (2017). Multifractality, interactivity, and the adaptive capacity of the human movement system: A perspective for advancing the conceptual basis of neurologic physical therapy. *Journal of Neurologic Physical Therapy*, *41*(4), 245–251.

Collins, J. J., & De Luca, C. J. (1993). Open-loop and closed-loop control of posture: A random-walk analysis of center-of-pressure trajectories. *Experimental Brain Research*, *95*(2), 308–318. Available from https://doi.org/10.1007/BF00229788.

Delignières, D., Almurad, Z. M. H., Roume, C., & Marmelat, V. (2016). Multifractal signatures of complexity matching. *Experimental Brain Research*, *234*(10), 2773–2785. Available from https://doi.org/10.1007/s00221-016-4679-4.

Delignieres, D., Ramdani, S., Lemoine, L., Torre, K., Fortes, M., & Ninot, G. (2006). Fractal analyses for 'short' time series: A re-assessment of classical methods. *Journal of Mathematical Psychology*, *50*(6), 525–544. Available from https://doi.org/10.1016/j.jmp.2006.07.004.

Ding, M., Chen, Y., & Scott Kelso, J. A. (2002). Statistical analysis of timing errors. *Brain and Cognition*, *48*(1), 98–106. Available from https://doi.org/10.1006/brcg.2001.1306.

Diniz, A., Wijnants, M. L., Torre, K., Barreiros, J., Crato, N., Bosman, A. M. T., ... Delignières, D. (2011). Contemporary theories of 1/f noise in motor control. *Human Movement Science*, *30*(5), 889–905. Available from https://doi.org/10.1016/j.humov.2010.07.006.

Eke, A., Herman, P., Kocsis, L., & Kozak, L. R. (2002). Fractal characterization of complexity in temporal physiological signals. *Physiological Measurement*, *23*(1), R1.

Fayyaz, Z., Bahadorian, M., Doostmohammad, J., Davoodnia, V., Khodadadian, S., & Lashgari, R. (2018). Multifractal detrended fluctuation analysis of continuous neural time series in primate visual cortex. *Journal of Neuroscience Methods*, *312*, 84–92. Available from https://doi.org/10.1016/j.jneumeth.2018.10.039.

Fine, J. M., Likens, A. D., Amazeen, E. L., & Amazeen, P. G. (2015). Emergent complexity matching in interpersonal coordination: Local dynamics and global variability. *Journal of Experimental Psychology: Human Perception and Performance*, *41*(3), 723.

Gilden, D. L. (2001). Cognitive emissions of 1/f noise. *Psychological Review*, *108*(1), 33.

Gilden, D. L., & Hancock, H. (2007). Response variability in attention-deficit disorders. *Psychological Science*, *18*(9), 796–802. Available from https://doi.org/10.1111/j.1467-9280.2007.01982.x.

Gilden, D. L., Thornton, T., & Mallon, M. W. (1995). 1/f noise in human cognition. *Science*, *267*(5205), 1837–1839.

Goldberger, A. L., Amaral, L. A. N., Hausdorff, J. M., Ivanov, P. C., Peng, C.-K., & Stanley, H. E. (2002). Fractal dynamics in physiology: Alterations with disease and aging. *Proceedings of the National Academy of Sciences of the United States of America*, *99*(suppl 1), 2466–2472. Available from https://doi.org/10.1073/pnas.012579499.

Harrison, S. J., & Stergiou, N. (2015). Complex adaptive behavior and dexterous action. *Nonlinear Dynamics, Psychology, and Life Sciences*, *19*(4), 345–394.

Hausdorff, J. M. (2007). Gait dynamics, fractals and falls: Finding meaning in the stride-to-stride fluctuations of human walking. *Human Movement Science*, *26*(4), 555–589. Available from https://doi.org/10.1016/j.humov.2007.05.003.

Hausdorff, J. M. (2009). Gait dynamics in Parkinson's disease: Common and distinct behavior among stride length, gait variability, and fractal-like scaling. *Chaos: An Interdisciplinary Journal of Nonlinear Science*, *19*(2), 026113. Available from https://doi.org/10.1063/1.3147408.

Hausdorff, J. M., & Peng, C.-K. (1996). Multiscaled randomness: A possible source of 1/*f* noise in biology. *Physical Review E*, *54*(2), 2154–2157. Available from https://doi.org/10.1103/PhysRevE.54.2154.

Hausdorff, J. M., Mitchell, S. L., Firtion, R., Peng, C. K., Cudkowicz, M. E., Wei, J. Y., & Goldberger, A. L. (1997). Altered fractal dynamics of gait: Reduced stride-interval correlations with aging and Huntington's disease. *Journal of Applied Physiology*, *82*(1), 262–269. Available from https://doi.org/10.1152/jappl.1997.82.1.262.

Hausdorff, J. M., Rios, D. A., & Edelberg, H. K. (2001). Gait variability and fall risk in community-living older adults: a 1-year prospective study. *Archives of physical medicine and rehabilitation*, *82*(8), 1050–1056.

Hunt, N., McGrath, D., & Stergiou, N. (2014). The influence of auditory-motor coupling on fractal dynamics in human gait. *Scientific Reports*, *4*, 5879. Available from https://doi.org/10.1038/srep05879.

Hurst, H. E. (1951). Long-term storage capacity of reservoirs. *Transactions of American Society of Civil Engineers*, *116*, 770–799.

Ihlen, E. A., & Vereijken, B. (2013). Identifying multiplicative interactions between temporal scales of human movement variability. *Annals of Biomedical Engineering*, *41*(8), 1635–1645.

Ihlen, E. A. F. (2012). Introduction to multifractal detrended fluctuation analysis in Matlab. *Frontiers in Physiology*, *3*, 141. Available from https://doi.org/10.3389/fphys.2012.00141.

Ihlen, E. A. F., & Vereijken, B. (2010). Interaction-dominant dynamics in human cognition: Beyond $1/f\alpha$ fluctuation. *Journal of Experimental Psychology: General*, *139*(3), 436–463. Available from https://doi.org/10.1037/a0019098.

Kaipust, J. P., Huisinga, J. M., Filipi, M., & Stergiou, N. (2012). Gait variability measures reveal differences between multiple sclerosis patients and healthy controls. *Motor Control*, *16*(2), 229–244. Available from https://doi.org/10.1123/mcj.16.2.229.

Kaipust, J. P., McGrath, D., Mukherjee, M., & Stergiou, N. (2013). Gait variability is altered in older adults when listening to auditory stimuli with differing temporal structures. *Annals of Biomedical Engineering*, *41*(8), 1595–1603. Available from https://doi.org/10.1007/s10439-012-0654-9.

Kantelhardt, J. W., Koscielny-Bunde, E., Rego, H. H. A., Havlin, S., & Bunde, A. (2001). Detecting long-range correlations with detrended fluctuation analysis. *Physica A: Statistical Mechanics and Its Applications*, *295*(3), 441–454. Available from https://doi.org/10.1016/S0378-4371(01)00144-3.

Kantelhardt, J. W., Zschiegner, S. A., Koscielny-Bunde, E., Havlin, S., Bunde, A., & Stanley, H. E. (2002). Multifractal detrended fluctuation analysis of nonstationary time series. *Physica A: Statistical Mechanics and Its Applications*, *316*(1), 87–114. Available from https://doi.org/10.1016/S0378-4371(02)01383-3.

Kello, C. T., Beltz, B. C., Holden, J. G., & Van Orden, G. C. (2007). The emergent coordination of cognitive function. *Journal of Experimental Psychology: General*, *136*(4), 551.

Kello, C. T., Brown, G. D. A., Ferrer-i-Cancho, R., Holden, J. G., Linkenkaer-Hansen, K., Rhodes, T., & Van Orden, G. C. (2010). Scaling laws in cognitive sciences. *Trends in Cognitive Sciences*, *14*(5), 223–232. Available from https://doi.org/10.1016/j.tics.2010.02.005.

Kelty-Stephen, D. G., Palatinus, K., Saltzman, E., & Dixon, J. A. (2013). A tutorial on multifractality, cascades, and interactivity for empirical time series in ecological science. *Ecological Psychology*, *25*(1), 1–62.

Likens, A. D. (2016). Multiscale interactions in psychological systems (Ph.D. Dissertation). Arizona State University, 2010.

Likens, A. D., Amazeen, P. G., Stevens, R., Galloway, T., & Gorman, J. C. (2014). Neural signatures of team coordination are revealed by multifractal analysis. *Social Neuroscience*, *9*(3), 219–234.

Likens, A. D., Fine, J. M., Amazeen, E. L., & Amazeen, P. G. (2015). Experimental control of scaling behavior: What is not fractal? *Experimental Brain Research*, *233*(10), 2813–2821.

López, J. L., & Contreras, J. G. (2013). Performance of multifractal detrended fluctuation analysis on short time series. *Physical Review E*, *87*(2), 022918. Available from https://doi.org/10.1103/PhysRevE.87.022918.

Mandelbrot, B. B. (1967). How long is the coast of Britain? Statistical self-similarity and fractional dimension. *Science*, *156*(3775), 636–638. Available from https://doi.org/10.1126/science.156.3775.636.

Mandelbrot, B. B. (1975). Stochastic models for the Earth's relief, the shape and the fractal dimension of the coastlines, and the number-area rule for islands. *Proceedings of the National Academy of Sciences*, *72*(10), 3825–3828. Available from https://doi.org/10.1073/pnas.72.10.3825.

Mandelbrot, B. B. (1982). *The fractal geometry of nature*. San Francisco, CA: W.H. Freeman.

Mandelbrot, B. B., & Hudson, R. L. (2006). *The (mis)behavior of markets: A fractal view of risk, ruin, and reward*. New York: Basic Books. (1. publ. paperback).

Marmelat, V., & Meidinger, R. L. (2019). Fractal analysis of gait in people with Parkinson's disease: Three minutes is not enough. *Gait & Posture*, *70*, 229–234. Available from https://doi.org/10.1016/j.gaitpost.2019.02.023.

Peng, C.-K., Buldyrev, S. V., Havlin, S., Simons, M., Stanley, H. E., & Goldberger, A. L. (1994). Mosaic organization of DNA nucleotides. *Physical Review E*, *49*(2), 1685–1689. Available from https://doi.org/10.1103/PhysRevE.49.1685.

Peng, C.-K., Havlin, S., Stanley, H. E., & Goldberger, A. L. (1995). Quantification of scaling exponents and crossover phenomena in nonstationary heartbeat time series. *Chaos: An Interdisciplinary Journal of Nonlinear Science*, *5*(1), 82–87. Available from https://doi.org/10.1063/1.166141.

Rhea, C. K., Wittstein, M. W., Kiefer, A. W., & Haran, F. J. (2013). Retaining fractal gait patterns learned in virtual environments. In *2013 International conference on virtual rehabilitation (ICVR)* (pp. 264–269). https://doi.org/10.1109/ICVR.2013.6662069.

Scafetta, N., Griffin, L., & West, B. J. (2003). Hölder exponent spectra for human gait. *Physica A: Statistical Mechanics and Its Applications*, *328*(3–4), 561–583.

Schmidt, R. A., & Lee, T. D. (2011). *Motor control and learning: A behavioral emphasis* (5th ed.). Champaign, IL: Human Kinetics.

Stephen, D. G., & Anastas, J. (2011). Fractal fluctuations in gaze speed visual search. *Attention, Perception, & Psychophysics*, *73*(3), 666–677.

Stephen, D. G., Arzamarski, R., & Michaels, C. F. (2010). The role of fractality in perceptual learning: Exploration in dynamic touch. *Journal of Experimental Psychology: Human Perception and Performance*, *36*(5), 1161–1173. Available from https://doi.org/10.1037/a0019219.

Stephen, D. G., Hsu, W.-H., Young, D., Saltzman, E. L., Holt, K. G., Newman, D. J., … Goldfield, E. C. (2012). Multifractal fluctuations in joint angles during infant spontaneous kicking reveal multiplicativity-driven coordination. *Chaos, Solitons & Fractals*, *45*(9–10), 1201–1219. Available from https://doi.org/10.1016/j.chaos.2012.06.005.

Stergiou, N., & Decker, L. M. (2011). Human movement variability, nonlinear dynamics, and pathology: Is there a connection? *Human Movement Science*, *30*(5), 869–888. Available from https://doi.org/10.1016/j.humov.2011.06.002.

Stergiou, N., Harbourne, R. T., & Cavanaugh, J. T. (2006). Optimal movement variability: A new theoretical perspective for neurologic physical therapy. *Journal of Neurologic Physical Therapy*, *30*(3), 120. Available from https://doi.org/10.1097/01.NPT.0000281949.48193.d9.

Stergiou, N., Kent, J. A., & McGrath, D. (2016). Human movement variability and aging. *Kinesiology Review*, *5*(1), 15–22. Available from https://doi.org/10.1123/kr.2015-0048.

Stergiou, N., Yu, Y., & Kyvelidou, A. (2013). A perspective on human movement variability with applications in infancy motor development. *Kinesiology Review*, *2*(1), 93–102. Available from https://doi.org/10.1123/krj.2.1.93.

Stroe-Kunold, E., Stadnytska, T., Werner, J., & Braun, S. (2009). Estimating long-range dependence in time series: An evaluation of estimators implemented in R. *Behavior Research Methods*, *41*(3), 909–923. Available from https://doi.org/10.3758/BRM.41.3.909.

Terrier, P., & Dériaz, O. (2011). Kinematic variability, fractal dynamics and local dynamic stability of treadmill walking. *Journal of Neuro Engineering and Rehabilitation*, *8*(1), 12. Available from https://doi.org/10.1186/1743-0003-8-12.

Thornton, T. L., & Gilden, D. L. (2005). Provenance of correlations in psychological data. *Psychonomic Bulletin & Review*, *12*(3), 409–441. Available from https://doi.org/10.3758/BF03193785.

Torre, K., & Delignières, D. (2008). Unraveling the finding of 1/f β noise in self-paced and synchronized tapping: A unifying mechanistic model. *Biological Cybernetics*, *99*(2), 159–170. Available from https://doi.org/10.1007/s00422-008-0247-8.

Torre, K., Delignières, D., & Lemoine, L. (2007). 1/fβ fluctuations in bimanual coordination: An additional challenge for modeling. *Experimental Brain Research*, *183*(2), 225–234. Available from https://doi.org/10.1007/s00221-007-1035-8.

Van Orden, G. C., Holden, J. G., & Turvey, M. T. (2003). Self-organization of cognitive performance. *Journal of Experimental Psychology: General*, *132*(3), 331.

Van Orden, G. C., Holden, J. G., & Turvey, M. T. (2005). Human cognition and 1/f scaling. *Journal of Experimental Psychology: General*, *134*(1), 117.

Van Orden, G. C., Kloos, H., & Wallot, S. (2011). *Living in the pink: Intentionality, wellbeing, and complexity*. *Philosophy of complex systems* (pp. 629–672). Elsevier.

Wang, Y., & Liu, L. (2010). Is WTI crude oil market becoming weakly efficient over time?: New evidence from multiscale analysis based on detrended fluctuation analysis. *Energy Economics*, *32*(5), 987–992.

Wijnants, M. L., Cox, R. F. A., Hasselman, F., Bosman, A. M. T., & Van Orden, G. (2012). A trade-off study revealing nested timescales of constraint. *Frontiers in Physiology*, *3*. Available from https://doi.org/10.3389/fphys.2012.00116.

Woyshville, M. J., & Calabrese, J. R. (1994). Quantification of occipital EEG changes in Alzheimer's disease utilizing a new metric: The fractal dimension. *Biological Psychiatry*, *35*(6), 381–387. Available from https://doi.org/10.1016/0006-3223(94)90004-3.

Yuan, Q., Gu, C., Weng, T., & Yang, H. (2018). Unbiased detrended fluctuation analysis: Long-range correlations in very short time series. *Physica A: Statistical Mechanics and Its Applications*, *505*, 179–189. Available from https://doi.org/10.1016/j.physa.2018.03.043.

CHAPTER 11

Future directions in biomechanics: 3D printing

Jorge M. Zuniga and Nick Stergiou
University of Nebraska at Omaha, Omaha, NE, United States

"Nature is the source of all true knowledge. She has her own logic, her own laws, she has no effect without cause nor invention without necessity."
Leonardo Da Vinci (1452–1519)

11.1 Introduction

Applications for three-dimensional (3D) printing are increasing rapidly and are expected to revolutionize health care. The biomedical uses of 3D printing can be summarized into three categories: (1) tissue and organ fabrication, (2) creation of customized wearable devices, and (3) anatomical models for surgical planning. This chapter focuses on categories 2 and 3 due to their direct impact in the field of biomechanics.

The introduction of 3D printing for the manufacture of orthoses and prostheses has resulted in the development of new cost reduction strategies as well as better accessibility and customization of such devices (Burn, Ta, & Gogola, 2016; Tanaka & Lightdale-Miric, 2016; Ten Kate, Smit, & Breedveld, 2017; Zuniga, Carson et al., 2016; Zuniga, Katsavelis, & Peck, 2015; Zuniga, Peck, & Srivastava, 2015; Zuniga, Peck, Srivastava, Katsavelis, & Carson, 2016). The existence of 3D printing prosthetic and orthotic designs allows clinicians and researchers, such as biomechanists, to manufacture their own devices (Burn et al., 2016; Tanaka & Lightdale-Miric, 2016; Ten Kate et al., 2017). For example, biomechanists have manufactured upper limb 3D printed prostheses that can be customized as the child grows, reducing cost and weight, improving fit and comfort, while also maximizing quality of life (Figs. 11.1 and 11.2) (Walbran, Turner, & McDaid, 2016). These customizations can also allow improved esthetics (Fig. 11.3A) and function adapting and instrumenting the prosthesis for a specific activity (Fig. 11.3B). Children are encouraged to use these devices, thus allowing data collection during activities of daily living, helping biomechanists to better understand movement control and learning.

CONTENTS

Biomechanics and Gait Analysis. DOI: https://doi.org/10.1016/B978-0-12-813372-9.00011-7

11.2 Lower extremity applications

11.2.1 Foot orthoses

Custom foot orthoses have been used to reduce the risk of recurrence of injury through patient-specific placement of soft and rigid support features. The standard customization of foot orthoses is recognized as the gold standard of treatment for foot and lower limb gait disorders (Allan, Woodburn, Telfer, Abbott, & Steultjens, 2017). 3D printing has the potential to greatly enhance the clinical effectiveness of foot orthoses (Allan et al., 2017; Dombroski, Balsdon, & Froats, 2014; Telfer, Abbott, Steultjens, & Woodburn, 2013). It can also enable instrumentation that can quantitatively assess a wide range of parameters from pressure points to temperature control.

A previous investigation (Allan et al., 2017) tested a personalized approach using 3D printed foot orthotics to assess knee joint kinetics when modifying

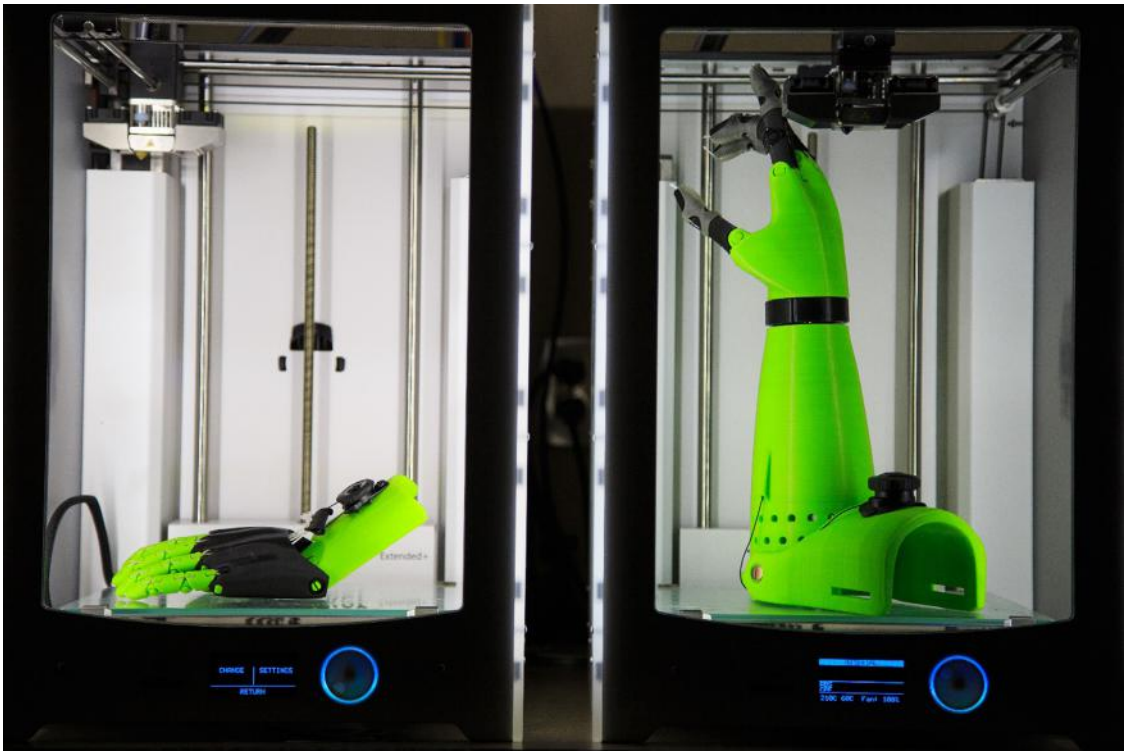

FIGURE 11.1

Upper limb 3D printed prostheses manufactured at the University of Nebraska Omaha, Department of Biomechanics. A partial hand prosthesis (*left*) and a trans-radial arm prosthesis (*right*). *3D*, three-dimensional.

FIGURE 11.2
Pediatric patient performing a bimanual coordination assessment using a trans-radial 3D printed prosthesis. The device was manufactured at the University of Nebraska Omaha, Department of Biomechanics. *3D*, three-dimensional.

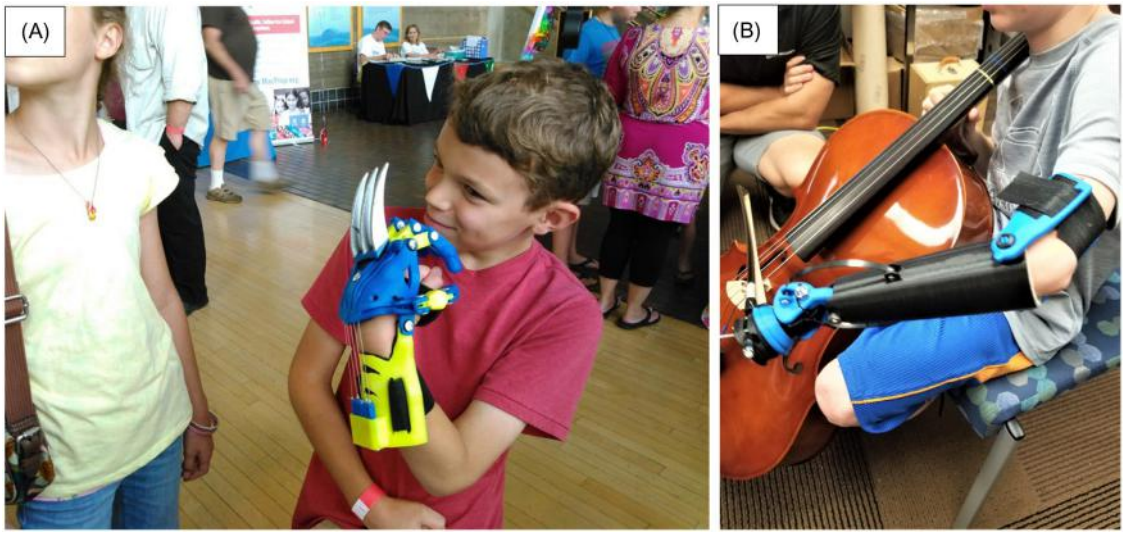

FIGURE 11.3
(A) Wolverine 3D printed hand design. (B) Activity-specific modular 3D printed prosthesis. The activity-specific device was manufactured at the University of Nebraska Omaha, Department of Biomechanics. *3D*, three-dimensional.

orthotic length and lateral wedging. Knee joint kinetics were assessed in response to multiple customized 3D printed foot orthoses used for the treatment of medial compartment knee osteoarthritis. Ten individuals with symptomatic medial knee osteoarthritis and 10 controls participated in the study. Four full-length and four three-quarter-length 3D printed foot orthoses were designed and manufactured for each participant. The full-length and three-quarter-length 3D printed foot orthoses had different variations of lateral postings. Lateral posting of 0 degrees "neutral," 5 degrees rearfoot, 10 degrees rearfoot, and a combination of 5 degrees forefoot with 10 degrees rearfoot were tested. Peak knee adduction moment, second peak knee adduction moment, first knee flexion moment, and knee adduction moment impulse were evaluated.

The above study (Allan et al., 2017) found that full-length foot orthoses provided greater reductions in first peak knee adduction moment, second peak knee adduction moment, and knee adduction moment impulse compared to three-quarter-length foot orthoses. Greater lateral wedging significantly reduced first peak knee adduction moment, second peak knee adduction moment, and knee adduction moment impulse. These findings indicate that 3D printing the foot orthoses provides the ability to customize the device affecting crucial biomechanical parameters that can improve the treatment of medial compartment knee osteoarthritis. In general, additive manufacturing has been shown to facilitate a personalized clinical approach to examine the dose–response effects of different interventions aimed to improve lower limb kinematics and kinetics in abnormal gait (Allan et al., 2017; Telfer et al., 2013).

The creation of a dynamic structure, with patient-specific parameters controlling flexibility and rigidity, provides an opportunity to examine gait parameter changes and improvements in gait of pathological conditions (Dombroski et al., 2014). In a number of domains, 3D printing technology facilitates using a mixture of materials within a single orthotic device, providing a previously unrealizable level of customization (Allan et al., 2017; Dombroski et al., 2014; Telfer et al., 2013). In sports, 3D printing technology affords the opportunity to design lighter, stronger, and more durable foot orthoses, customized to each athlete, shoe type (i.e., cleats), and environmental condition. This level of customization effectively lessens the burden on the athlete's feet and maximizes performance. For a diabetic patient, the ability to customize the pressure and shear forces in different regions of the foot has the potential to prevent limb amputation. The effects of customized 3D foot orthoses (Fig. 11.4) on the biomechanics of gait of patients and athletes have many applications (Telfer et al., 2013). These applications include pain relief due to excessive pressure, increased heel cushion to diminish impact forces during landing, increased foot

FIGURE 11.4
Antimicrobial 3D printed foot orthosis manufactured at the University of Nebraska Omaha, Department of Biomechanics. *3D*, three-dimensional.

stability by increasing arch stiffness, and prevention of skin breakdowns, such as ulcerations (Dombroski et al., 2014). All these applications have profound implications in human gait (Allan et al., 2017; Dombroski et al., 2014; Telfer et al., 2013).

11.2.2 Ankle foot orthoses

Devices such as ankle foot orthoses (AFOs) can provide support for the ankle during daily activities and improve gait during rehabilitation. There are two main categories of AFO in the market: (1) standard off-the-shelf and (2) custom-fabricated models. A newer method of orthosis production involves 3D printing. The combination of digital surface capture, 3D printing, and the thermoforming capabilities of 3D printing filament offer the possibility of greatly simplifying production of the AFO and facilitate customization (Walbran et al., 2016). A preliminary study from Creylman, Muraru, Pallari, Vertommen, and Peeraer (2013) performed a gait assessment during the initial fitting using a traditionally manufactured AFO and a 3D printed AFO (Fig. 11.5) in patients experiencing dropped foot. Both AFOs showed

FIGURE 11.5
3D printed AFO manufactured at the University of Nebraska Omaha, Department of Biomechanics. *3D*, three-dimensional; *AFO*, ankle foot orthosis.

significant improvements for spatial-temporal gait parameters (i.e., stride duration, stride length, and stance phase duration) and ankle kinematic parameters (i.e., ankle plantar-flexion at initial foot–floor contact and maximum plantar flexion) when compared to barefoot gait of patients with drop foot. However, no statistically significant difference was found between the two AFOs for the same parameters. The study concluded that the 3D-printed AFOs show performances that are at least equivalent to the traditionally manufactured AFOs commonly prescribed in current clinical practice (Creylman et al., 2013).

11.3 Upper extremity applications

It is estimated that in the United States, more than 541,000 individuals lived with upper limb deficiencies in 2005 (Behrend, Reizner, Marchessault, & Hammert, 2011). Worldwide estimates for upper limb reductions range

from 4–5 to 10 of 10,000 live births (Bethge, von Groote, Giustini, & Gutenbrunner, 2014). In other parts of the world, such as Australia, Finland, and Canada, reports indicate that 3.4–5.3 of 10,000 live births experience upper limb abnormalities. Despite this prevalence, however, only 1 in 9400 children is considered for a prosthesis due to a number of factors, such as the complexity of the reduction and fitting process, lack of interest from the pediatric patient, and the prohibitive cost of upper limb prostheses (Resnik, Meucci, & Lieberman-Klinger, 2012). Furthermore, many children with upper limb deficiencies from resource-limited countries are not being fitted with a prosthesis due to a lack of trained technicians able to provide these services and a local shortage of the necessary components for the fabrication of proper devices (ISPO, 2001).

Advancements in computer-aided design (CAD) software and 3D printing hardware offer the possibility of circumventing the above problems by designing, printing, and fitting prosthetic hands and other assistive devices at a very low cost. Previous studies (Gretsch et al., 2016; Zuniga, Carson et al., 2016; Zuniga, Katsavelis et al., 2015; Zuniga, Peck et al., 2015; Zuniga, Peck et al., 2016) have described how low-cost prosthetic hands, arms, and shoulders with practical and easy-fitting procedures can be performed remotely. Importantly, in children, the durability of their prostheses is challenged continuously due to relatively higher activity levels and outgrowth of the prostheses (Tanaka & Lightdale-Miric, 2016). Therefore, the cost effectiveness of 3D printing makes repairs and upgrades of prostheses substantially more affordable (Tanaka & Lightdale-Miric, 2016). In general, previous publications (Burn et al., 2016; Tanaka & Lightdale-Miric, 2016; Ten Kate et al., 2017; Zuniga, Carson et al., 2016; Zuniga, Katsavelis et al., 2015; Zuniga, Peck et al., 2015; Zuniga, Peck et al., 2016) have presented different aspects of the development of 3D printed prostheses for children, and the consensus is that 3D printing is a promising manufacturing method for the development of these devices.

11.4 Methods for three-dimensional printing assistive devices

The most common method for 3D-printed prostheses is fused deposition modeling. Fused deposition modeling is a form of additive manufacturing that involves melting thin layers of plastic over each other to form a 3D structure (McLaughlin, 2013). The two most common 3D printed filament materials used to manufacture upper limb prostheses are polylactic acid filament and acrylonitrile butadiene styrene filament (McLaughlin, 2013). Polylactic acid filament has similar properties to a thermoplastic and permits

minor modifications through targeted heating once the device has been 3D printed. Acrylonitrile butadiene styrene filament, however, does not offer homogeneous thermoplastic properties, making postprocessing modifications difficult (McLaughlin, 2013). Thus, the preferred material for 3D-printed prostheses is polylactic acid filament, given the ability to perform postprocessing modifications that may be required during assembly or clinical fitting.

Other forms of polylactic acid, such as Raptor polylactic acid filament (Maker Geeks, Springfield, MO, USA), withstand the sanitizing heat of a dishwasher without deforming and have promising applications in clinical settings. The development of new 3D printing materials using high-quality polylactic acid, combined with nanoparticles of copper using the latest nanotechnology, has the potential to revolutionize the manufacturing of medical devices. PLACTIVE (PLACTIVE AN[1] 1% Antibacterial Nanoparticles additive, Copper3D, Santiago, Chile) is a high-quality polylactic acid polymer containing copper nanoparticles. Copper nanoparticles have been shown to be effective in eliminating fungi, viruses, and bacteria, but are harmless to humans (Palza, 2015; Palza, Nunez, Bastias, & Delgado, 2018; Palza, Quijada, & Delgado, 2015). PLACTIVE is widely used in the medical industry. It provides a sound and proven antibacterial mechanism, is a low-cost material that is biodegradable, and possesses thermoforming characteristics that facilitate postprocessing and final adjustments of 3D printed prostheses (Fig. 11.6B and C) (Zuniga, 2018). All these technological advances in the durability and antibacterial properties of 3D printing filaments, along with expertise in the development of 3D-printed medical devices, will allow biomechanists and clinicians to work together in developing durable and medical grade 3D-printed prostheses for their patients (Fig. 11.6) (Young, Pierce, & Zuniga, 2019; Zuniga, 2018).

11.5 Anatomical modeling for surgical planning

The efficacy of a joint replacement depends on the ability to identify gait adaptations specific to design features of the orthopedic implant and the surgical procedures used. The use of 3D-printed orthopedic implants, customized and developed from patient-specific medical imaging, then, can have a major impact on changes in gait and human locomotion. This impact further depends on the ability of 3D printing to replicate internal pathology and allow the surgeon to prepare and plan highly complex surgeries (Fig. 11.7) (Ripley, Levin, & Kelil, 2016). In some cases, 3D-printed models have proven to be more intuitive and desirable than the magnetic resonance imaging (MRI) or computed tomography (CT) data that are typically provided. The technique to convert a medical image into a 3D-printed model can be

FIGURE 11.6

Example of upper limb 3D printed prostheses. (A) 3D printed prosthetic shoulder using dishwasher-safe 3D printed filament. (B) 3D printed partial hand prosthesis using antibacterial filament. (C) 3D printed partial finger prosthesis using antibacterial 3D printed filament. *3D*, three-dimensional.

performed in a very short period of time (i.e., within a day) and at a very low cost (Fig. 11.7). Clinical applications of 3D printing include creating tracheobronchial splints for pediatric patients suffering from excessive collapse of the airways (Morrison, Hollister, & Niedner, 2015), improving preoperative sizing of instruments, constructing custom implants and surgical cutting guides, enhancing procedural training of surgical residents, and promoting better patient education (Ripley et al., 2016; Vodiskar, Kutting, Steinseifer, Vazquez-Jimenez, & Sonntag, 2016). In many cases, the end result is decreased operating room time and improved surgical technique leading to significantly improved clinical outcomes (Wulf, Vitt, Erben, Bill, & Busch, 2003).

The process of developing a 3D-printed anatomical model involves the acquisition of the medical images, segmentation of the region of interest using a slicing software, rendering of the 3D model using a CAD program, and 3D printing of the anatomical model using a 3D printer (Fig. 11.7). Medical imaging is the process of creating visual representations of the interior of a body for clinical analysis and medical intervention (Ripley et al., 2016). The most commonly used medical imaging techniques are CT scans,

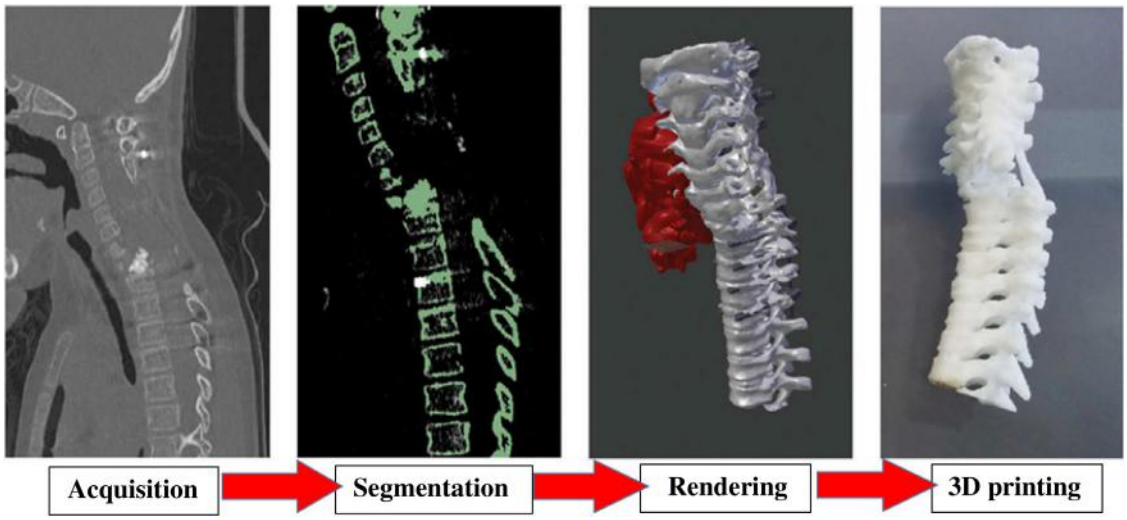

FIGURE 11.7
Overall process for the development of an anatomical model of a spine segment for surgical planning. *3D*, three-dimensional.

MRI, and ultrasonography (Ripley et al., 2016). A CT scan utilizes computer-processed combinations of many X-ray images taken from different angles to produce cross-sectional (tomographic) images of specific areas of a scanned object (Ripley et al., 2016). An MRI uses powerful magnets to polarize and excite hydrogen nuclei of water molecules in human tissue, producing a detectable signal, which is spatially encoded, resulting in images of the body. An ultrasound uses high-frequency sound waves that are reflected by tissue to varying degrees to produce 2D and 3D images. These medical imaging modalities (CT, MRI, and ultrasound) are stored in a standard digital file named Digital Imaging and Communication in Medicine (Huff, Ludwig, & Zuniga, 2018; Ripley et al., 2016). These digital files allow the exchange of medical images for 3D visualization and the development of physical models (Ripley et al., 2016). 3D printing offers a significant overall improvement over traditional two-dimensional (2D) medical imaging. A physical model can be held, inspected, and manipulated before any procedure begins and used as a tool to verify anatomical orientation, ultimately reducing errors that might arise from misreading radiologic images (Huff et al., 2018). The main advantage of 3D-printed anatomical models over traditional 2D medical imaging is that they improve surgeons' visualization of complex anatomical structures (Huff et al., 2018). These personalized anatomical models can also be taken into the operating room to help the clinical staff to visualize the surgery, train new surgeons, and educate patients (Huff et al., 2018).

The ability to develop physical anatomical models from existing medical imaging files can expedite and improve clinical outcomes (Ripley et al., 2016). However, the main barrier for the massive implementation of this technology in clinical settings is the lack of evidence demonstrating cost-effectiveness when used to improve patient outcomes (Ripley et al., 2016). The cost of equipment, materials, proprietary-segmentation software, and specialized personnel, can be prohibitive for many medical institutions. Preliminary data from our laboratory has shown the combination of using small desktop 3D printers (less that US $1000), low-cost polymers, and open-source software can significantly reduce the overall cost of each anatomical model (Fig. 11.8).

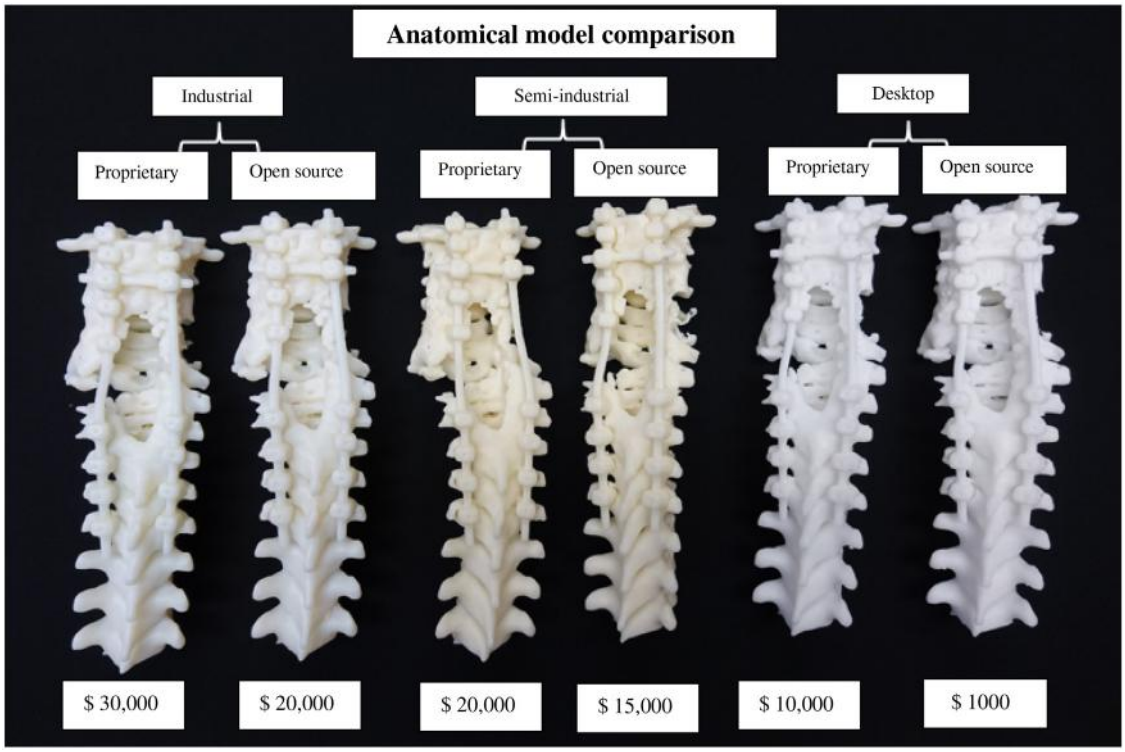

FIGURE 11.8

Low-cost methodology for the development of anatomical models for presurgical planning. *From left to right*: Anatomical models of a section of the spine using proprietary versus open source software and industrial 3D printers, semi-industrial, and desktop (low-cost) 3D printers. Our methodology resulted in a significant cost reduction from $30,000 to $1000. The cost estimations are rough approximations of the software and equipment cost. Engineering time is included. *3D*, three-dimensional.

11.6 Fracture casting

The conventional method to develop fracture casting, the plaster-casting method, is essentially an additive process. The advantage of 3D printing is that it provides more control in the additive manufacturing process. 3D printing provides the ability to create complex shapes customized to each patient using plastic materials that are breathable, lightweight, washable, and antimicrobial.

Distal radius fractures are common skeletal injuries and occurred at all ages of the general population. These types of fractures are reported as having one of the highest incidences, accounting for over 15% of bone fractures (Chen et al., 2017). The medical management of these types of fracture includes plaster casting, a strap, and a molded synthetic material cast to immobilize the injured upper extremity for 4–6 weeks. The main problem with conventional fracture casting is poor ventilation, discomfort, and improper fit. As a result, patients often suffer from cutaneous diseases, bone and joint injuries, or malunion (Chen et al., 2017). Malunion is a clinical term used to indicate that a fracture has healed, but that it has healed in less than an optimal position. The rate of plaster casting-related complications is 31% (Chen et al., 2017). 3D printing can decrease these complications and can be used to develop patient-specific features with an appropriate fit and a ventilated structure.

In a recent publication by Chen et al. (2017), the authors developed 3D-printed and conventional plaster casts for the treatment of distal radius fractures. Ten patients participated in a clinical trial using a 3D-printed cast with a 6-week follow-up to examine clinical outcomes. The authors reported that all 10 patients opted for the 3D-printed cast instead of the conventional plaster cast and concluded that the 3D-printed cast offered a proper fit to immobilize an injured arm and hold the fracture reduction appropriately. Graham et al. (2018) found no significant differences for function and dexterity using the Jebsen Hand Function Test between 3D-printed and standard fiberglass short arm casts. Furthermore, 42% of the patients using the fiberglass cast reported cutaneous complications compared to only 8% for the 3D-printed cast. It was concluded that a custom-fitted structure reduces the risk of pressure-related complications due to the high and concentrated local stress. The ventilated and lightweight design of the 3D-printed casts have been shown to diminish interference with a patient's activities of daily living and reduce the risk of cutaneous complications.

Previous investigations have also reported that patients using orthoses and socket-based prostheses face multiple skin disorders and are susceptible to bacterial and fungal infections (Bowker & Michael, 1992). These skin disorders have a significant detrimental impact on patient daily living quality of

FIGURE 11.9
Antimicrobial 3D printed surgical instruments manufactured at the University of Nebraska Omaha, Department of Biomechanics. *3D*, three-dimensional.

life (Biddiss & Chau, 2007). 3D printing and the development of an antibacterial 3D printing filament with thermoforming capabilities has the potential to revolutionize patient care in the orthotic and prosthetic industry. The addition of copper nanoparticles to polymers, and the resulting antimicrobial properties have promising applications in the development of medical devices associated with bacterial development (Palza, 2015). These applications are not limited to postoperative prostheses (Palza, 2015; Zuniga, Peck et al., 2016), but can also be used for other types of medical devices, such as wound dressings (Muwaffak et al., 2017) and surgical instruments (Fig. 11.9) (Rankin et al., 2014). Another advantage of 3D-printed casts is the ability to use 3D printing to embed electronics to accelerate bone healing. Commonly used upper limb orthoses, such as a hand wrist orthosis (Fig. 11.10), can be instrumented for delivery of low-intensity pulsed ultrasonic bone stimulation that could help accelerate bone healing.

11.7 Upper extremity three-dimensional printed exoskeleton for stroke patients

Additive manufacturing could be used to develop wearable devices, such as upper limb exoskeletons for stroke patients, and used to assist these patients

FIGURE 11.10
Antimicrobial hand wrist orthosis. Manufactured by Copper3D Inc.

to regain mobility during functional tasks (Kopowski, Rojek, Mikołajewski, & Macko, 2019). Stroke has a large impact on disability and loss of motor function (Michielsen, Selles, Stam, Ribbers, & Bussmann, 2012). When the cerebral cortex is injured, motor deficits are usually seen on the opposite side of where the stroke occurred (Michielsen et al., 2012). When the brain tissue is damaged, the associated pathways and the neuromuscular junction are compromised. As a result, the affected upper limb becomes spastic with a predominant flexor tone (Michielsen et al., 2012). Due to this permanently flexed hand, the stroke patient has reduced hand dexterity (Michielsen et al., 2012). Wearable devices, such as exoskeletons are useful in that they offer patients the ability to regain mobility in their own environment (Takahashi, Lewek, & Sawicki, 2015).

Upper limb exoskeletons are typically designed to interact independently with the user, while assisting and promoting movement of the affected hand

(Knorr et al., 2005). Our research team developed an inexpensive and simple 3D-printed hand exoskeleton which is designed to assist in keeping the fingers of the paretic side extended and allowing a functional grasp (Fig. 11.11). The exoskeleton incorporates elastic and tension control of the nonelastic components (Fig. 11.11). The tensioners to control the nonelastic components are located on the dorsal side of the body of the exoskeleton. The body of the exoskeleton is attached to the forearm of the user through straps on the ventral side. The elastic cords connect with the nonelastic component midway between the tensioners and the wrist of the user. The elastic cords run through guides at the distal end of the body of the exoskeleton. These guides separate the elastic cord to direct them to a specific finger. The elastic cords attach on the dorsal side of each finger enclosure. Extension of the fingers occurs at this attachment point. Each finger has its own enclosure that fits snugly around the distal and intermediate phalanges of each finger. The exoskeleton was designed so that the user was able to tighten the tensioner system to shorten the length of the elastic cords in order to control the tension and thus extending the user's fingers. Due to the elastic properties of the cords, once the user's fingers are extended, the user is able to flex their fingers in order to stretch the elastic cords and grasp an object. This 3D-printed exoskeleton allows for an object to be grasped by utilizing the elasticity of the cords and the active control of flexion by the user.

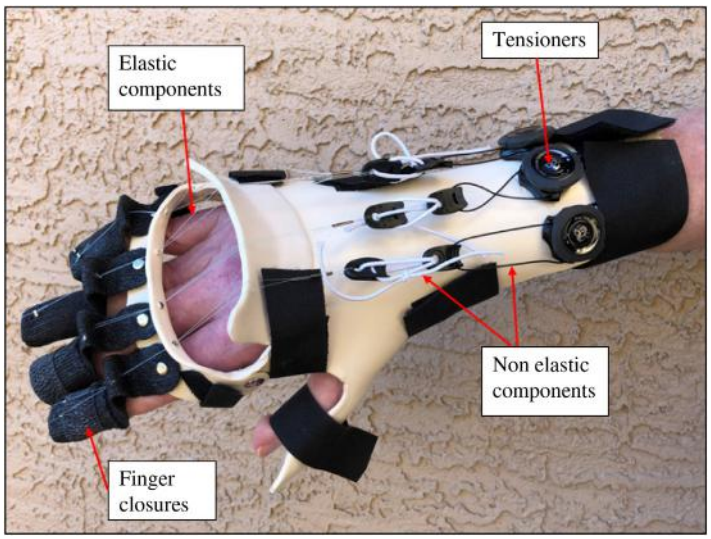

FIGURE 11.11

A 3D printed hand exoskeleton developed by researchers at the University of Nebraska at Omaha. The device was manufactured at the University of Nebraska Omaha, Department of Biomechanics. *3D*, three-dimensional.

To test the effectiveness of this device we collected information from a stroke patient. It was hypothesized that our custom-designed 3D-printed exoskeleton would increase the function of the stroke patient's affected hand by showing an improvement in functional tests. Our subject was a 66-year-old male who was more than 6 months post-stroke that occurred in his left hemisphere. To assess hand function, a trained hand therapist evaluated the subject using the Fugl–Meyer assessment of physical performance. To assess hand gross dexterity, the Box and Block test was performed. The Box and Block test required the subject to move 1-inch blocks one at a time from one box, over a partition, and to drop the blocks in the adjacent box. The subject was fitted with a 3D-printed exoskeleton (Fig. 11.11) to assist with extension of his hand. The results of the investigation showed that without the hand exoskeleton, the subject was unable to perform any of the tasks from the Fugl–Meyer assessment. While wearing the exoskeleton, however, the subject improved in flexion, extension, and successfully performed three of the four different grasps described in the Fugl–Meyer assessment. Furthermore, the subject reported that while wearing the exoskeleton he was able to increase the number of activities of daily living that he could perform with his paretic right hand. During the Box and Block test, the subject doubled the number of blocks moved with the exoskeleton compared to not wearing it (five blocks per minute without the exoskeleton versus 10 blocks per minute with the exoskeleton). In addition, the hand exoskeleton also assisted the subject in pinching the blocks between his index finger and thumb. Without the exoskeleton, the subject used a rudimentary palmar pinch to move the blocks. Finally, the hand exoskeleton improved grasping biomechanics by assisting the subject to extend his index finger to properly pinch the block with his thumb, instead of inefficiently wedging each block between his thumb and index finger.

11.8 Implementation of a three-dimensional printing research laboratory

The implementation of a 3D printing laboratory will include basic knowledge handling different types of digital files, specialized slicing software, and hardware. The Standards for the Exchange of Product (STEP) model data files are the most common source files used in 3D printing and seem to be the most appropriate format for transferring CAD data. STEP files are able to contain all the parametric data required to read and modify the size and geometry of the overall prosthesis model contained in the digital file and simplify mesh-editing procedures. Typical mesh editing is

required to adjust the medical device through modification of mesh facets. Mesh facets are the face unit of a digital structure and can be smoothed, split, collapsed, and extruded to change the morphology of the overall structure of the device (Ripley et al., 2016). This type of file is the preferred option, if extensive modifications to the mesh of the prosthesis are required. STEP files can be also converted to stereolithographic files, providing great versatility when sharing files with collaborators. Having a digital file, such as STEP or stereolithographic files that can be modified or scaled to fit the residual limbs of an amputee patient, facilitates a number of activities such as the development of remote prosthetic fitting procedures (Zuniga, Young, & Peck, 2019). However, the procedures can be cumbersome and may require a multidisciplinary team with experience using this software to manipulate these types of files. As 3D modeling and printing procedures have become more mainstream, the industry and the open-source community have committed significant effort to simplify the procedures for editing and modifying different file formats for research applications (Zuniga et al., 2019).

3D printing can provide great benefits to biomechanists who want to design and investigate the effectiveness of customized upper and lower limb prostheses, orthoses, or other assistive devices to restore human motion and/or improve movement performance. Thus, 3D printing can effectively complement a gait analysis laboratory. Due to the use of advanced technology and materials, 3D printing can be expensive. As with any other research setting, creating a 3D printing laboratory can represent a significant capital investment (Figs. 11.12 and 11.13). However, there are low-cost approaches that can be used when implementing 3D printing in a laboratory setting. The cost of a desktop 3D printer ranges from $200 for a basic model to $6000 for an advanced model. Currently, the most cost-effective method of additive manufacturing is fusion deposition modeling and the most common 3D printing filament is polylactic acid. 3D filaments made of polylactic acid melt at a temperature of 175°C and have a glass transition temperature of 57°C. Unlike most thermoplastics that use distillation and polymerization of nonrenewable petroleum reserves, polylactic acid is derived from renewable resources such as cornstarch and sugar cane, making this bioplastic cost effective and environmentally friendly (McLaughlin, 2013). The cost of 1 kg spool of polylactic acid filament ranges from $20 for standard filament to $92 for specialty filament such as antibacterial filament. For a total of $11,071.78 a researcher could implement a fully equipped 3D printing laboratory with the capabilities of printing class I medical devices (Table 11.1).

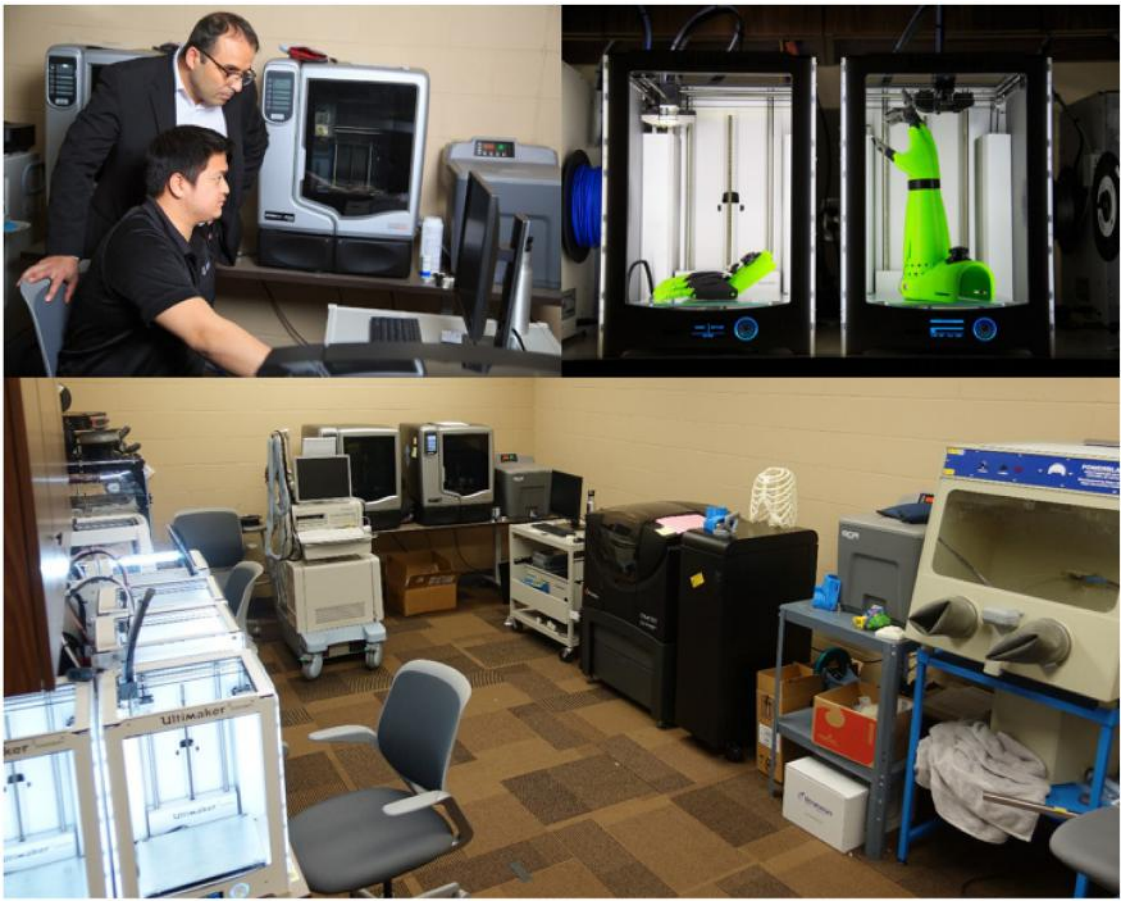

FIGURE 11.12
3D printing laboratory at the University of Nebraska Omaha, Department of Biomechanics. The *top left picture* shows a researcher and a student inspecting a digital model before printing. The *top right picture* shows a desktop 3D printer set up used to manufacture prosthetic devices. The *bottom picture* shows a general view of the 3D printing laboratory. *3D*, three-dimensional.

11.9 Current Food and Drug Administration recommendations of three-dimensional printed medical devices

One of the most useful and groundbreaking features of 3D printing is its ability to produce complex geometries quickly and at low cost for the medical device manufacturer. As 3D printing technology matures and continues to permeate varied industries and products, it is apparent that some level of regulation must be developed to ensure consistent quality and reproducibility across fabrication types, manufacturers, and materials. According to 21

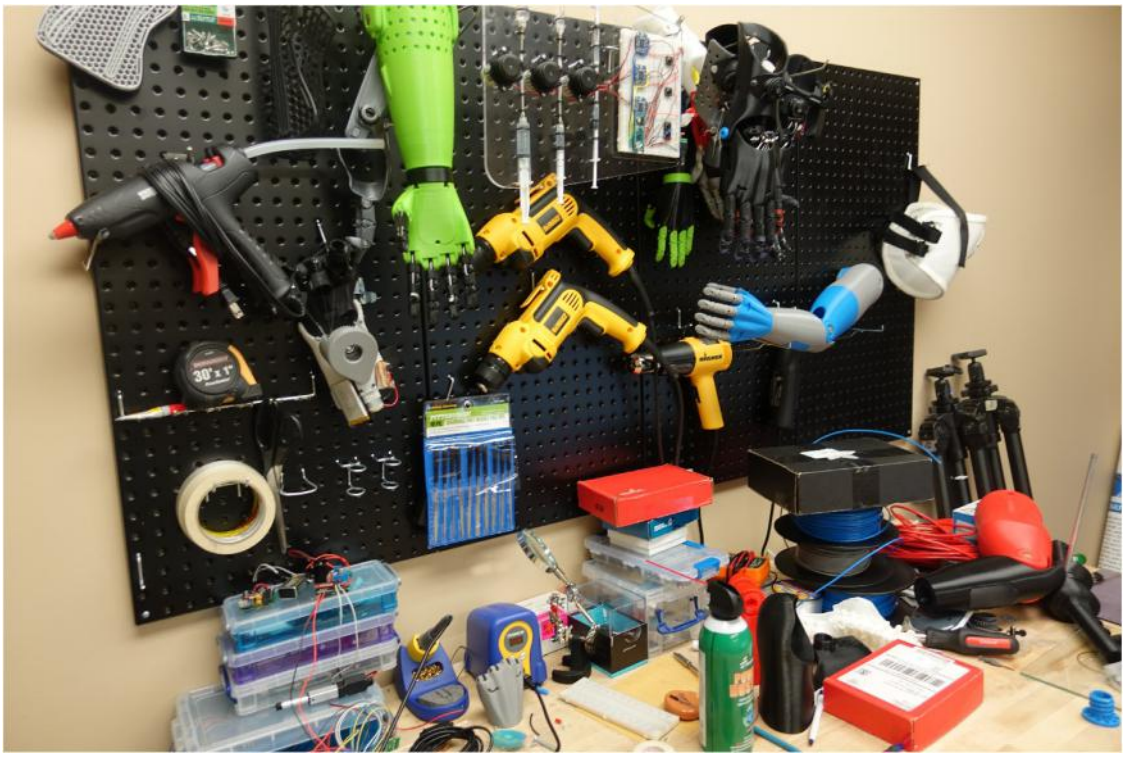

FIGURE 11.13
Example of 3D printed medical devices at the University of Nebraska Omaha, Department of Biomechanics. *3D*, three-dimensional.

CFR Part 812 (Part 890.3420), the FDA's product classification listings, external limb prosthetic components and accessories are defined as physical medical devices and are generally considered class I devices. Class I devices are considered low risk (FDA, 2017). The use of upper limb 3D-printed prostheses for research purposes may or may not require an investigational device exemption, depending upon whether the FDA-approved device is used within approved labeling use or not. If used outside of labeling use, an abbreviated investigational device exemption is required as described in Title 21 of the Code of Federal Regulations Part 812. The FDA indicates that abbreviated investigational device exemption requirements under §812.2 (b) are the following:

- *Labeling*—The device must be labeled in accordance with the labeling provisions of the IDE regulations (§812.5) and must bear the statement "CAUTION—Investigational Device. Limited by Federal (or United States) law to investigational use";

Table 11.1 Resources for the limplementation of 3D printing in a research setting.

Item	Quantity and cost	Resources
Ultimaker Extended PLUS Desktop 3D printers	2 × $2999 = $5998	Vendors: ultimaker.com shop3duniverse.com www.dynamism.com
CAD software	Open-sourced (free)	Open-sourced software for mesh editing: Blender (https://www.blender.org/), FreeCAD (https://www.freecadweb.org/), SketchUp (https://www.sketchup.com/), MeshMixer (http://www.meshmixer.com/), MeshLab (http://www.meshlab.net/), 3D Slash (https://www.3dslash.net/index.php), SculptGL (https://stephaneginier.com/sculptgl/)
Sense 3D Scanners	2 × $697.39 = $1394.78	Vendors: www.3dsystems.com www.amazon.com www.matterhackers.com
Desktop computer with double monitor	1 × $2500 = $2500	Vendors: www.amazon.com
Spools of standard 3D printing filament (polylactic acid)	10 × $20 = $200	shop3duniverse.com
Spools of specialized filament	5 × $92 = $460	Vendors:
PLACTIVE AN (antibacterial)	5 × $74 = $370	http://copper3d.com/
Nylon 680 (durable)		www.matterhackers.com
CURAs software	Free with printer	Vendor: ultimaker.com
Slicing software (custom supports)	1 × $149 = $149	Vendor: www.simplify3d.com
STL files for devices and G-code	Open-sourced (free)	Sources: 3dprint.nih.gov www.thingiverse.com https://www.unomaha.edu/college-of-education/biomechanics-core-facility/research/cyborg-beast/index.php
Total expense	**$11,071.78**	

3D, *Three-dimensional;* CAD, *computer-aided design;* STL, *stereolithographic.*

- *IRB approval*—The sponsor must obtain and maintain Investigational Review Board (IRB) approval throughout the investigation as a nonsignificant risk device study;
- *Informed consent*—The sponsor must assure that investigators obtain and document informed consent from each subject according to 21 CFR 50, Protection of Human Subjects, unless documentation is waived by an IRB in accordance with §56.109(c);
- *Monitoring*—All investigations must be properly monitored to protect the human subjects and assure compliance with approved protocols (§812.46);
- *Records and reports*—Sponsors are required to maintain specific records and make certain reports as required by the IDE regulations;
- *Investigator records and reports*—The sponsor must assure that participating investigators maintain records and make reports as required (see Responsibilities of Investigators); and
- *Prohibitions*—Commercialization, promotion, test marketing, misrepresentation of an investigational device, and prolongation of the study are prohibited (§812.7).

A recent FDA guidance document titled *Technical Considerations for Additive Manufactured Devices* (FDA, 2017) serves as a first step toward defining government policy regarding the use of 3D printing for medical devices. In general, the FDA recommends (FDA, 2017) that all medical devices fabricated using additive manufacturing processes (either entirely or in part) be validated and tested with similar procedures as performed on traditionally manufactured devices with adaptation of protocols to ensure proper functionality. The overall requirements, described by the FDA, depend almost entirely on the intended end-use of the product; some common factors listed include whether it is an implant, load bearing, and/or available in prespecified standard sizes or patient-matched. Based on these parameters, a series of recommendations for design, production, and testing are then provided. These recommendations stem from areas of importance to the additive manufacturing process, such as materials, design, printing, and postprinting validation; printing characteristics and parameters; physical and mechanical assessment of final devices; and biological considerations of final devices (including cleaning, sterility, and biocompatibility). For example, an external assistive device would require far less material regulation, biocompatibility testing, and dimensional accuracy than an additive manufacturing-produced vascular stent. Despite the lesser requirements placed on prostheses, there are still a number of intensive and important inspection tools and process tasks that are recommended for all design and manufacturing stages.

11.9.1 Design

Starting with the design of a device, the FDA recommends (FDA, 2017) that a full production flow diagram be created to ensure repeatability in the process of product development and engineering. This flow diagram would include all critical steps from device design to the postprocessing of the final part identified and documented. During design, it is also highly recommended to specify feasible size ranges and feature sizes based on the end-user requirements as well as the additive manufacturing machine capabilities. Because the relative scale of additive manufacturing medical devices can be modified so easily, as compared to traditionally manufactured parts, it is important that versioning history be recorded in a digital folder. It is likewise important to store specific device scales and other identifying information on the device itself. This policy prevents future third parties from improperly modifying or adapting the additive manufacturing device due to lack of information.

11.9.2 Materials

Once a design has been completed, it is important to properly characterize and select suitable materials for fabricating the device. As with any type of manufacturing method, the FDA recommends (FDA, 2017) documenting safety procedures, and chemical, mechanical and physical properties of the materials used in a laboratory log. For 3D-printed prostheses, necessary material properties include chemical composition, molecular formula, purity, chemical structure, molecular weight, molecular weight distribution, glass transition temperature, and melting temperature. Because material recycling is not commonly used with fused deposition of 3D printing processes, no additional analysis into material properties should be required.

11.9.3 Printing characteristics/parameters

Equally as important as material properties, the printer and parameters used in the production of 3D-printed prostheses could also affect durability, surface finish, interlayer adhesion, strength-to-weight ratio, and many other part characteristics. Due to the anisotropic mechanical properties of nearly all additive manufacturing processes (McLaughlin, 2013), it is important to optimize physical part orientation when printing. Additionally, the infill density (the density of the interior reinforcing lattice structure in fused deposition modeling) can significantly affect the strength, flexibility, and opacity of finished parts (FDA, 2017). Many additive manufacturing machines incorporate a supporting external lattice (or support structure) to aid in the creation of "floating" geometries which could not otherwise be produced. If not carefully placed, these supplementary supports can cause structural damage and

issues with surface finish. Finally, layer thickness can significantly affect surface finish (causing pronounced interlayer striations), interlayer adhesion, and production speed. By justifying the print parameter choices for a balance between speed, strength, and quality, the opportunity exists to create optimized additive manufacturing devices and workflows (FDA, 2017).

11.9.4 Physical/mechanical assessment

The FDA (2017) suggests that a series of mechanically destructive and nondestructive tests be performed to determine ideal printing parameters. The results of such an analysis can be used to optimize parameters. To test additive manufacturing parts nondestructively, many potential tests have been proposed (FDA, 2017), including ultrasound, CT, radiography (for simple geometry), confocal microscopy, and hyperspectral imaging. Each of these methods can return valuable information such as part porosity, structural integrity, dimension accuracy, and density. In addition to this battery of assessments, the FDA recommends that tensile test coupons be destructively analyzed to document the impact of the additive manufacturing process on mechanical properties. Parts can also be manually inspected for conformance to the intended design constraints.

11.9.5 Biological considerations

Because the focus of the FDA Draft Guidance (FDA, 2017) is to determine additive manufacturing requirements of medical devices, the interactions that parts have (mechanically, chemically, etc.) with the patients' physiology must be documented and verified before use. Cleaning protocols must also be established, especially for devices with complex geometries, such as engineered porosity, honeycomb structures, channels, and internal voids or cavities that cannot be produced by traditional manufacturing methods. The FDA (2017) recommends that the cleaning process should account for the complex geometry of the device under worst-case conditions (e.g., greatest amount of residual manufacturing materials for cleaning validation, and a combination of largest surface area, greatest porosity, and most internal voids for sterilization validation). In general, the cleaning protocols should follow similar precautions to those already established by the FDA (2017) and used for standard prostheses and orthoses.

11.10 Limitations

The durability of 3D-printed devices is a major limitation. Specifically, it is the main obstacle for the development of weight-bearing prostheses or orthoses. 3D printing technology advances quickly, and the development of

new filaments allows the manufacturing of devices with high durability, similar to injection molding manufacturing. In the last few years, the 3D printing industry has released several new materials for desktop 3D printers that provide the strength necessary to develop durable and weight-bearing devices. Polylactic acid filaments have addressed biocompatibility issues, but lack durability. Taulman 3D is a company that specializes in developing high-strength materials for desktop 3D printers. Several filaments produced by this company, such as Nylon 618 and Nylon 680, are being used to develop medical-grade biomedical devices with promising results (Hyde, MacNicol, Odle, & Garcia-Rill, 2014). Nylon 680 is an FDA-registered polymer that offers injection-molded strength when printed at 40% infill (tensile modulus stress of 28.6 psi or 197 MPa). Several other emerging companies, such as Carbon3D, the developers of Continuous Liquid Interface Production, and RepRapper Tech, the developers of high-strength aluminum-filled PLA, are constantly improving their materials and revolutionizing the 3D printing industry. Recently, Stratasys, one of the leading companies in the 3D printing industry, created Nylon 12CF, which is a carbon-fiber-reinforced thermoplastic that meets the demanding needs of the production environment, allowing the replacement of metal tooling for applications such as forming and end-of-arm tooling for robotic applications. Furthermore, specialty filaments such as Raptor filaments have the ability to withstand the sanitizing heat of a dishwasher without deforming, offering increased durability. PLACTIVE filaments offer antibacterial properties with all the thermoplastic characteristics of polylactic acid. All these new 3D printing materials offer promising applications in clinical and research settings.

Other areas of improvement of 3D printing technology are with respect to surface finish and accuracy. Component anisotropy often depends on layer thickness and orientation of a surface, resulting in ridges appearing in the final component as a result of the layer-building process (stair stepping). Although part finish is improving, it is still not comparable to that of subtractive systems.

The speed of the manufacturing process can also be an important limitation for the development of wearable devices. Depending on the resolution, building layer by layer can be a time-consuming process, especially for larger devices, such as adult orthoses and prostheses. The size of the device is limited to the size of the machine's building platform. Other technical considerations, such as the software used for slicing and developing a digital file that is ready for printing, can be complex and often require technical expertise.

Cost can also be a limitation. This is due to the use of advanced technology and materials that can make 3D printing an expensive proposition. As with other new technologies, 3D printing machines can represent a significant capital investment.

Finally, there is a need for international standards and practices for 3D printing of biomedical devices that will allow standard performance measurements and monitoring of manufacturing.

11.11 Future perspectives

The rapid and fast-growing field of 3D printing is revolutionizing the industry of medical devices and providing biomechanists with new research tools to restore and improve human function. Due to the relatively low cost of implementing a 3D printing laboratory and the wide range of digital files available online, biomechanists and rehabilitation specialists will have the unique opportunity to use wearable devices as effective research tools. A good example of the impact 3D printing is having in the field of biomechanics is the development and testing of 3D-printed prostheses for pediatric patients. Recent technological advances in CAD programs and 3D printing offer the unique possibility of designing and manufacturing customized upper limb prostheses that can improve performance of daily activities and be used as a rehabilitation tool (Zuniga, Peck, & Srivastava, 2017). The research team at the University of Nebraska at Omaha is pioneering the development and testing of 3D-printed prostheses for children (Zuniga, Katsavelis et al., 2015; Zuniga, Peck et al., 2015; Zuniga, Peck et al., 2016; Zuniga et al., 2017, 2019). The primary function of these 3D-printed prostheses is to provide children with congenital or acquired reductions the opportunity to perform bimanual and unilateral activities with a functional grasp (Zuniga, Katsavelis et al., 2015; Zuniga, Peck et al., 2016; Zuniga et al., 2017). 3D printing technology allows full customization of these prostheses designed to fulfill most of the functional and esthetic needs of each child as they grow, including appearance based on fictional characters and color selection (Zuniga et al., 2015). These devices can also be cost-effective and lightweight, potentially encouraging and facilitating use (Zuniga et al., 2016). The ability to design prostheses that encourage use and that can be easily modified (i.e., instrumented) offers the opportunity to examine several unanswered research questions regarding pediatric subjects with upper limb loss. The main unanswered research questions in this population are related to the length of time of prosthetic use and the type of activities the child performs at home. Up until now, this simple information has not been described or reported in a quantitative manner. The time and type of activities can inform prosthetic design and rehabilitation programs for children aimed at increasing the functional use of the prosthesis at home. Unlike standard prostheses, 3D-printed prostheses allow for the embedment of inertial measurement units to quantitatively monitor the length and type of activity performed during the day. Accelerometers, magnetometers, and gyroscopes

can collect positional data points that will indicate the relative location of the prosthesis. Additionally, movement data from the accelerometer can be used to visualize arm asymmetry during upper limb performance in activities of daily living. This is made possible when data from the affected limb are combined with an inertial measurement unit mounted on the unaffected limb. Accelerometer-based movement data may also be used to confirm wear time, activity, and frequency of use implied from survey data (Bailey, Klaesner, & Lang, 2014; Bailey, Klaesner, & Lang, 2015).

Another aspect of 3D printing that is opening new opportunities for biomechanics is the development of new durable 3D printing filaments for the development of medical devices. Such filaments will be able to better facilitate the implementation of additive manufacturing in research and clinical settings. Antimicrobial 3D printing materials, such as emerging thermoplastic polyurethane-based flexible materials, will also play a major role in the development of biomedical devices and tissue-engineered scaffolds (Zuniga & Thompson, 2019). The combination of 3D printing technology and the development of antimicrobial materials has several applications for "on-demand" and "on-site" manufacturing of medical devices in austere environments, such as military applications. Sterilization and biocidal technology in combat support hospitals and emergency humanitarian relief settings must be capable of providing a wide range of "on-demand" medical devices. Currently, the sterilization of medical devices depends on large-chamber sterilizers introducing a significant logistical burden. Treatment of battlefield trauma presents the unique logistical challenge of providing sterile medical devices to medical personnel. Transport and supply constraints limit the quantity and variety of medical devices available in the field and sterilization equipment is often not available to support the instruments required. Thus, additive manufacturing can address the current supply chain problems involving medical care in austere medical environments.

References

Allan, R., Woodburn, J., Telfer, S., Abbott, M., & Steultjens, M. P. (2017). Knee joint kinetics in response to multiple three-dimensional printed, customised foot orthoses for the treatment of medial compartment knee osteoarthritis. *Proceedings of the Institution of Mechanical Engineers. Part H, Journal of Engineering in Medicine*, *231*(6), 487–498.

Bailey, R. R., Klaesner, J. W., & Lang, C. E. (2014). An accelerometry-based methodology for assessment of real-world bilateral upper extremity activity. *PLoS One*, *9*(7), e103135.

Bailey, R. R., Klaesner, J. W., & Lang, C. E. (2015). Quantifying real-world upper-limb activity in nondisabled adults and adults with chronic stroke. *Neurorehabilitation and Neural Repair*, *29*(10), 969–978.

Behrend, C., Reizner, W., Marchessault, J. A., & Hammert, W. C. (2011). Update on advances in upper extremity prosthetics. *The Journal of Hand Surgery*, *36*(10), 1711–1717.

Bethge, M., von Groote, P., Giustini, A., & Gutenbrunner, C. (2014). The world report on disability: A challenge for rehabilitation medicine. *American Journal of Physical Medicine & Rehabilitation/Association of Academic Physiatrists*, *93*(1 Suppl 1), S4–11.

Biddiss, E. A., & Chau, T. T. (2007). Upper limb prosthesis use and abandonment: A survey of the last 25 years. *Prosthetics and Orthotics International*, *31*(3), 236–257.

Bowker, J. H., Michael, J. W., & Surgeons A.A.o.O. (1992). *Atlas of limb prosthetics: Surgical, prosthetic, and rehabilitation principles*. Mosby Year Book.

Burn, M. B., Ta, A., & Gogola, G. R. (2016). Three-dimensional printing of prosthetic hands for children. *The Journal of Hand Surgery*, *41*(5), 103–109.

Chen, Y. J., Lin, H., Zhang, X., Huang, W., Shi, L., & Wang, D. (2017). Application of 3D-printed and patient-specific cast for the treatment of distal radius fractures: Initial experience. *3D Printing in Medicine*, *3*(1), 11.

Creylman, V., Muraru, L., Pallari, J., Vertommen, H., & Peeraer, L. (2013). Gait assessment during the initial fitting of customized selective laser sintering ankle foot orthoses in subjects with drop foot. *Prosthetics and Orthotics International*, *37*(2), 132–138.

Dombroski, C. E., Balsdon, M. E., & Froats, A. (2014). The use of a low cost 3D scanning and printing tool in the manufacture of custom-made foot orthoses: A preliminary study. *BMC Research Notes*, *7*(1), 443.

FDA. (2017). Technical considerations for additive manufactured devices. Available from <http://www.fda.gov/downloads/medicaldevices/deviceregulationandguidance/guidancedocuments/ucm499809.pdf>.

Graham, J., Wang, M., Frizzell, K., Watkins, C., Beredjiklian, P., & Rivlin, M. (2018). Conventional vs 3-dimensional printed cast wear comfort. *Hand (New York, N.Y.)*. Available from https://doi.org/10.1177/1558944718795291.

Gretsch, K. F., Lather, H. D., Peddada, K. V., Deeken, C. R., Wall, L. B., & Goldfarb, C. A. (2016). Development of novel 3D-printed robotic prosthetic for transradial amputees. *Prosthetics and Orthotics International*, *40*(3), 400–403.

Huff, T. J., Ludwig, P. E., & Zuniga, J. M. (2018). The potential for machine learning algorithms to improve and reduce the cost of 3-dimensional printing for surgical planning. *Expert Review of Medical Devices*, *15*(5), 349–356.

Hyde, J., MacNicol, M., Odle, A., & Garcia-Rill, E. (2014). The use of three-dimensional printing to produce in vitro slice chambers. *Journal of Neuroscience Methods*, *238*, 82–87.

ISPO. (2001). Consensus conference on appropriate orthopaedic technology for low-income countries: Conclusions and recommendations. International Society for Prosthetics and Orthotics. *Prosthetics and Orthotics International*, *25*(3), 168–170.

Knorr, B., Hughes, R., Sherrill, D., Stein, J., Akay, M., & Bonato, P. (2005). *Quantitative measures of functional upper limb movement in persons after stroke*. Paper presented at Proceedings of 2nd international IEEE EMBS conference on neural engineering, 16–19 March 2005.

Kopowski, J, Rojek, I, Mikołajewski, D., Macko, M. (2019). *3D printed hand exoskeleton – own concept*. Paper presented at Advances in manufacturing II, 2019, Cham.

McLaughlin, P. (2013). Testing agreement between a new method and the gold standard—how do we test? *Journal of Biomechanics*, *46*(16), 2757–2760.

Michielsen, M. E., Selles, R. W., Stam, H. J., Ribbers, G. M., & Bussmann, J. B. (2012). Quantifying nonuse in chronic stroke patients: A study into paretic, nonparetic, and bimanual upper-limb use in daily life. *Archives of Physical Medicine and Rehabilitation*, *93*(11), 1975–1981.

Morrison, R. J., Hollister, S. J., Niedner, M. F., et al. (2015). Mitigation of tracheobronchomalacia with 3D-printed personalized medical devices in pediatric patients. *Science Translational Medicine*, *7*(285), 285ra264.

Muwaffak, Z., Goyanes, A., Clark, V., Basit, A. W., Hilton, S. T., & Gaisford, S. (2017). Patient-specific 3D scanned and 3D printed antimicrobial polycaprolactone wound dressings. *International Journal of Pharmaceutics*, *527*(1-2), 161–170.

Palza, H. (2015). Antimicrobial polymers with metal nanoparticles. *International Journal of Molecular Sciences*, *16*(1), 2099–2116.

Palza, H., Nunez, M., Bastias, R., & Delgado, K. (2018). In situ antimicrobial behavior of materials with copper-based additives in a hospital environment. *International Journal of Antimicrobial Agents*, *51*(6), 912–917.

Palza, H., Quijada, R., & Delgado, K. (2015). Antimicrobial polymer composites with copper micro- and nanoparticles: Effect of particle size and polymer matrix. *Journal of Bioactive and Compatible Polymers*, *30*(4), 366–380.

Rankin, T. M., Giovinco, N. A., Cucher, D. J., Watts, G., Hurwitz, B., & Armstrong, D. G. (2014). Three-dimensional printing surgical instruments: Are we there yet? *The Journal of Surgical Research*, *189*(2), 193–197.

Resnik, L., Meucci, M. R., Lieberman-Klinger, S., et al. (2012). Advanced upper limb prosthetic devices: Implications for upper limb prosthetic rehabilitation. *Archives of Physical Medicine and Rehabilitation*, *93*(4), 710–717.

Ripley, B., Levin, D., Kelil, T., et al. (2016). 3D printing from MRI data: Harnessing strengths and minimizing weaknesses. *Journal of Magnetic Resonance Imaging: JMRI*, *45*(3), 635–645.

Takahashi, K. Z., Lewek, M. D., & Sawicki, G. S. (2015). A neuromechanics-based powered ankle exoskeleton to assist walking post-stroke: A feasibility study. *Journal of Neuroengineering and Rehabilitation*, *12*, 23.

Tanaka, K. S., & Lightdale-Miric, N. (2016). Advances in 3D-printed pediatric prostheses for upper extremity differences. *Journal of Bone and Joint Surgery American Volume*, *98*(15), 1320–1326.

Telfer, S., Abbott, M., Steultjens, M. P., & Woodburn, J. (2013). Dose-response effects of customised foot orthoses on lower limb kinematics and kinetics in pronated foot type. *Journal of Biomechanics*, *46*(9), 1489–1495.

Ten Kate, J., Smit, G., & Breedveld, P. (2017). 3D-printed upper limb prostheses: A review. *Disability and Rehabilitation: Assistive Technology*, *12*(3), 300–314.

Vodiskar, J., Kutting, M., Steinseifer, U., Vazquez-Jimenez, J. F., & Sonntag, S. J. (2016). Using 3D physical modeling to plan surgical corrections of complex congenital heart defects. *The Thoracic and Cardiovascular Surgeon*, *65*(1), 31–35.

Walbran, M., Turner, K., & McDaid, A. J. (2016). Customized 3D printed ankle-foot orthosis with adaptable carbon fibre composite spring joint. *Cogent Engineering*, *3*, 1227022.

Wulf, J., Vitt, K. D., Erben, C. M., Bill, J. S., & Busch, L. C. (2003). Medical biomodelling in surgical applications: Results of a multicentric European validation of 466 cases. *Studies in Health Technology and Informatics*, *94*, 404–406.

Young, K. J., Pierce, J. E., & Zuniga, J. M. (2019). Assessment of body-powered 3D printed partial finger prostheses: A case study. *3D Printing in Medicine*, *5*(1), 7.

Zuniga, J. (2018). 3D printed antibacterial prostheses. *Applied Sciences*, *8*(9), 1651.

Zuniga, J. M., Carson, A. M., Peck, J. M., Kalina, T., Srivastava, R. M., & Peck, K. (2016). The development of a low-cost three-dimensional printed shoulder, arm, and hand prostheses for children. *Prosthetics and Orthotics International*, *41*(2), 205–209.

Zuniga, J. M., Katsavelis, D., Peck, J., et al. (2015). Cyborg beast: A low-cost 3D-printed prosthetic hand for children with upper-limb differences. *BMC Research Notes*, *8*(1), 10.

Zuniga, J. M., Peck, J., & Srivastava, R. (2015). Anthropometric, range of motion and strength changes after 6 months of using the cyborg beast, an open source wrist driven 3D-printed

prosthetic hand for children. In: *Midwest Chapter American Academy of Orthotists & Prosthetists*: American Academy of Orthotist & Prosthetist Annual Meeting, March 9–12, 2016. Orlando, FL.

Zuniga, J. M., Peck, J., Srivastava, R., Katsavelis, D., & Carson, A. (2016). An open source 3D-printed transitional hand prosthesis for children. *JPO: Journal of Prosthetics and Orthotics*, *28*(3), 103–108.

Zuniga, J. M., Peck, J. L., Srivastava, R., et al. (2017). Functional changes through the usage of 3D-printed transitional prostheses in children. *Disability and Rehabilitation: Assistive Technology*, *14*(1), 68–74.

Zuniga, J. M., & Thompson, M. (2019). Applications of antimicrobial 3D printing materials in space. *Journal of 3D Printing in Medicine*, *3*(1), 5–9.

Zuniga, J. M., Young, K. J., Peck, J. L., et al. (2019). Remote fitting procedures for upper limb 3D printed prostheses. *Expert Review of Medical Devices*, *16*(3), 257–266.

Index

Note: Page numbers followed by "*f*," "*t*," and "*b*" refer to figures, tables, and boxes, respectively.

C

D

E

F

G

M

N

O

P

Q

R

S

T

U

V

Biomechanics and Gait Analysis

Nick Stergiou

A go-to resource both to understand fundamental concepts and how to collect, analyze, and interpret data for research, industry, clinical research, and sport.

Biomechanics and Gait Analysis is a comprehensive biomechanics book with a focus on gait analysis, written by a leading expert in this field and his team. It is written primarily for biomedical engineering students and professionals and biomechanists with a strong emphasis on medical devices and assistive technology, but is also of interest to clinicians and physiologists. It allows novice readers to acquire the basis of gait analysis and expert readers to update their knowledge in the area.

This reference book covers the most up-to-date acquisition and computational methods and advances in the field. Key topics included are:

- Muscle mechanics and modelling
- Motor control and coordination
- Measurements and assessments

Key Features:

- Details the fundamental issues leading to biomechanical analyses of gait and posture
- Covers the theoretical basis and practical aspects associated with gait analysis
- Discusses methods and tools used in this field including: electromyography, signal processing and spectral analysis amongst others

Dr. Nick Stergiou is the Founding Chair of the Department of Biomechanics and a Distinguished Community Research Professor as well as the Founder and the Director of the Biomechanics Research Building and the Center for Research in Human Movement Variability at the University of Nebraska at Omaha where his primary appointment is. He is also a Professor of the Department of Environmental, Agricultural, and Occupational Health of the College of Public Health at the University of Nebraska Medical Center. His research focuses on understanding variability inherent in human movement. Dr. Stergiou's research spans from infant development to older adult fallers, and has impacted training techniques of surgeons and treatment and rehabilitation techniques of pathologies, such as peripheral artery disease. He has received more than 40 million dollars in personal funding from NIH, NASA, NSF, the NIDRR/US Department of Education, and many other agencies and foundations. He is an international authority in the study of Nonlinear Dynamics and has published more than 250 peer reviewed articles as well as three books.

ACADEMIC PRESS
An imprint of Elsevier
elsevier.com/books-and-journals